

ISSET JOURNAL OF EARTHQUAKE TECHNOLOGY

Vol. 44

No. 1

March 2007

SPECIAL ISSUE: RESPONSE SPECTRA
Guest Editor: Professor Mihailo D. Trifunac

CONTENTS

Foreword	(iii)
Guest Editor's Note	(v)

No.	Paper	Page
474	The Early Entrance of Dynamics in Earthquake Engineering: Arturo Danusso's Contribution Luigi Sorrentino	1
475	Response Spectra as a Useful Design and Analysis Tool for Practicing Structural Engineers Sigmund A. Freeman	25
476	Empirical Scaling and Regression Methods for Earthquake Strong-Motion Response Spectra—A Review Vincent W. Lee	39
477	On the Regional Dependence of Earthquake Response Spectra John Douglas	71
478	A Note on Spatial Variations in Response Spectra of Earthquake Ground Motions Hideji Kawakami, Hidenori Mogi and Eric Augustus J. Tingatinga	101
479	Effect of System Initial Conditions on Seismic Design of Long-Period Structures Carlos E. Ventura and Rafael Blázquez	111
480	Probabilistic Seismic Hazard Analysis Method for Mapping of Spectral Amplitudes and Other Design-Specific Quantities to Estimate the Earthquake Effects on Man-Made Structures I.D. Gupta	127
481	A Response Spectrum-Based Nonlinear Assessment Tool for Practice: Incremental Response Spectrum Analysis (IRSA) M. Nuray Aydinoglu	169
482	An Earthquake Response Spectrum Method for Linear Light Secondary Substructures Giuseppe Muscolino and Alessandro Palmeri	193

483	A Modal Combination Rule for Peak Floor Accelerations in Multistoried Buildings	213
	Rashmi Kumari and Vinay K. Gupta	
484	Spatial Seismic Excitations and Response Spectra	233
	Zbigniew Zembaty	
485	Multi-Component Ground Motion Response Spectra for Coupled Horizontal, Vertical, Angular Accelerations, and Tilt	259
	Erol Kalkan and Vladimir Graizer	
486	Strength-Reduction Factors for Structures Subjected to Near-Source Differential Strong Ground Motions	285
	Reza S. Jalali and Mihailo D. Trifunac	
487	Energy and Power of Nonlinear Waves in a Seven-Story Reinforced Concrete Building	305
	V. Gicev and Mihailo D. Trifunac	

<p>Financial Assistance from AICTE and DST, New Delhi for the Publication of ISET Journals for 2006–2007 is duly acknowledged.</p>

FOREWORD

The concept of response spectrum method has evolved to become a backbone of essentially all aspects of earthquake-resistant design. It describes in a compact manner how a structure vibrating in its fundamental mode would respond to the earthquake ground motion. The method continues to be popular among practicing earthquake engineers, despite some of the critical information it does not provide and the limited extent to which it is applicable to more complex design situations. It dominates the earthquake engineering practice so much that several concepts and methods of analysis have been developed around it, sometimes at the cost of physics of the problem and realism. Generation of accelerograms compatible with a given response spectrum is one such example. It is therefore topical to take a stock of how the earthquake engineering profession now looks at this concept and the methods based on it, and to consider future directions based on the current needs. This special issue is planned with this spirit and to commemorate the 75th anniversary of the birth of the response spectrum method. It is hoped that this issue will help sensitize the earthquake engineering research to continue to contribute simple solutions for the practicing engineers and, at the same time, will remind us that simple solutions are not always best for special situations.

This special issue is guest-edited by Professor Mihailo D. Trifunac, University of Southern California, U.S.A. Professor Trifunac has been serving on the editorial board of the Journal for the past nine years. He has made significant and pioneering contributions to the use of response spectrum in seismic design and in extending the response spectrum concept to specialized situations. Besides guest-editing the issue, he has also contributed two papers with two of his former students. Each paper included in this special issue has undergone a rigorous review by three experts. On behalf of ISET, and on my own behalf, I thank Professor Trifunac for his efforts and time. I also thank all those who responded to our invitation to submit papers and to all the reviewers who contributed comprehensive and critical reviews.

Vinay K. Gupta
Editor

GUEST EDITOR'S NOTE

Mihailo D. Trifunac

Department of Civil Engineering
University of Southern California
Los Angeles, CA 90089, U.S.A.

A comprehensive review of the conditions that prepared the key players to create the concept of the response spectrum method is beyond the scope of this brief introduction. Thus, I will mention only a few examples. First, the teaching of physics, and, in particular, of engineering mechanics and applied mathematics, started to expand in Europe around the end of 19th and the beginning of 20th century (Timoshenko, 1968; von Karman and Edson, 1967; Cornwell, 2003). Second, several earthquake disasters (in 1906, 1908, and 1923) in densely populated areas made it clear that defensive mechanisms needed to be developed to prevent future loss of life and property from destructive earthquakes. Third, the arrival of leading scientists and engineers in earthquake-prone areas (e.g., Milne in Japan; Compté de Montessus de Ballore in Chile; Millikan, Gutenberg, and von Karman in Southern California), and their organizational abilities, interest, and curiosity to examine yet another challenging group of physical phenomena, created new critical mass and organization, which in turn attracted the next generation of talented students.

The first practical steps which initiated the engineering work on the design of earthquake-resistant structures accompanied the introduction of the seismic coefficient (*shindo* in Japan, and *rapporto sismico* in Italy, for example), which started to appear following the destructive earthquakes in San Francisco, California, in 1906, Messina-Reggio, Italy, in 1908 (Sorrentino, 2007), and Tokyo, Japan, in 1923. The first seismic design code was introduced in Japan in 1924 following the 1923 earthquake. In California, the work on developing a code started in 1920s, but it was not until after the Long Beach earthquake in 1933 that the Field Act was finally adopted in 1934 (Reitherman, 2006).

In early 1900s, at most American universities engineering curricula did not include advanced mathematics and mechanics, both essential for teaching analysis of the dynamic response of structures. This lack of theoretical preparation is reflected in the views of C. Derleth (1874–1956), a civil engineering professor and Dean of the College of Engineering at University of California Berkeley, who commented after the 1906 earthquake: “Many engineers with whom the writer has talked appear to have the idea that earthquake stresses in framed structures can be calculated, so that rational design to resist earthquake destruction can be made, just as one may allow for dead and live loads, or wind and impact stresses. Such calculations lead to no practical conclusions of value” (Derleth, 1907).

A comment made three decades later by A. Ruge, the first professor of engineering seismology at the Massachusetts Institute of Technology (Ruge, 1940), that “the natural tendency of the average design engineer is to throw up his hands at the thought of making any dynamical analysis at all” shows that progress was slow (Reitherman, 2006).

In 1929, at University of Michigan in Ann Arbor, the first lectures were organized in the Summer School of Mechanics by S. Timoshenko (1878–1972), with the participation of A. Náday, R.V. Southwell, and H.M. Westergaard. “After the first session of the summer school in 1929”, Timoshenko wrote later, “the number of doctoral students in mechanics ... started rapidly to increase” (Timoshenko, 1968). In the summer of 1933, M.A. Biot was among the young post-doctoral students who took part in Timoshenko’s summer school (Mindlin, 1989; Boley, 2005; Biot, 2007).

In Southern California, studies of earthquakes and research in theoretical mechanics were expanded and energized by R. Millikan (1868–1953), who became the first president (chair of the executive council) of the California Institute of Technology (Caltech) in 1921. Millikan completed his Ph.D. studies in physics at Columbia University in 1895, and following recommendation of his advisor M. Pupin (1854–1935) spent a year in Berlin and Göttingen. This visit to Europe appears to have influenced many of Millikan’s later decisions when he recruited the leading Caltech faculty members two decades later. In 1921, H.O. Wood (1879–1958) invited Millikan to serve on the Advisory Committee in Seismology (Geschwind, 1996). The work on that committee and Millikan’s interest in earthquakes were also significant for several subsequent events. In 1926, J. Buwalda (1886–1954) was asked to set up the division of geological sciences at Caltech, and in 1926 C. Richter (1900–1985), and then in 1930 B. Gutenberg (1889–1960), joined the seismological laboratory. In the area of applied mechanics, Millikan

invited Theodor von Karman (1881–1963) to join the Caltech faculty, and in 1930 von Karman became the first director of the Guggenheim Aeronautical Laboratory. It was Millikan's vision and his ability to anticipate future developments that brought so many leading minds to a common place of work, creating an environment that made the first theoretical formulation of the concept of the response spectrum method (RSM) possible.

This issue of the ISET Journal commemorates the 75th anniversary of the formulation of the concept in 1932. Since then, RSM has evolved into an essential tool and the central theoretical framework—in short, a *conditio sine qua non*—for earthquake engineering. The mathematical formulation of the RSM first appeared in the doctoral dissertation of M.A. Biot (1905–1985) in 1932, and in two of his papers (Biot, 1932, 1933, 1934). Biot defended his Ph.D. thesis in June 1932 (Biot, 2007) and presented a lecture on the method to the Seismological Society of America meeting, which was held at Caltech the same month. Theodore von Karman, Biot's advisor, played the key role in guiding his student and in promoting his accomplishments. After the method of solution was formulated, Biot and von Karman searched for an optimal design strategy. A debate at the time was whether, to better resist earthquake forces, a building should be designed with a soft first floor or be stiff throughout its height. An excerpt from New York Herald Tribune in June 1932 illustrates this:

**Shock Proof Buildings Sought by Scientists.
Rigid or Flexible Materials, Their Difference in Theory**

A building proof against earthquakes is the goal of Dr. Theodor von Karman and Dr. M. Biot, of California Institute of Technology. Dr. von Karman described to the American Society of Mechanical Engineers, whose convention was held recently at Yale, studies of the amount of shock, which various types of buildings have undergone in Japan, South America and California. Their researches are being conducted at the Institute's Guggenheim Aeronautical Laboratory.

One of the principal problems is to decide whether a rigid or flexible structure is better. Some scientists contend the first is preferable; others would make the ground floor of tall buildings flexible.

Pointing out that reinforced concrete is superior to steel in absorbing the shocks, Dr. von Karman's personal belief is that buildings should be constructed to shake "with the rhythm of the earth's movements".

Another newspaper article, describing the same meeting, stated:

**QUAKE STRAINS DISCUSSED
Von Karman Tells New Haven Meeting Engineers Are Divided between Rigid and Flexible
Buildings**

The most interesting piece of research now being conducted at the California Institute of Technology by Dr. M. Biot on the calculation of stresses occurring in buildings during an earthquake was described informally this morning by Dr. T.H. von Karman, director of the Guggenheim Aeronautical Laboratory at the school, under whose direction Dr. Biot is doing the work.

Seek "Quake-Proof" Building

By a study of past earthquakes in California and Japan and along the Pacific Coast of Central America, engineers interested in building problems have accumulated a record on which they believe they can calculate the rhythm or characteristic of the earth movement in these particular regions. They have sought to evolve an "earthquake proof" building on the basis of this data.

As a result of this research, said Dr. von Karman, there have arisen two schools of thought. One asserts only the most rigid structures should be built in the earthquake regions and the second, which Dr. von Karman supports, contends a flexible type of building, which can swing with the earthquake, is the better.

Biot's interest in the maxima of the transient response in solids and fluids preceded, and extended beyond earthquake engineering. After he formulated the concept of the RSM, he extended it to other vibrational problems, such as the analysis of aircraft landing gear. Biot briefly returned to the subject of earthquake engineering almost ten years later, presenting response spectral amplitudes of several earthquakes, which he calculated using the torsional pendulum at the Columbia University (Biot, 1941). In 1942, he presented a review of RMS, discussed the effects of flexible soil on the rocking period of a rigid block (Biot, 2006), and described the spectrum superposition method based on the sum of absolute modal maxima (Biot, 1942). After 1942, Biot moved on to other subjects, making fundamental contributions to many other fields. He did not write papers on earthquake engineering (Trifunac, 2005), but he followed closely and with interest the work of others.

The principal areas of Biot's opus and his exceptional talent and technical views have been described by Mindlin (1989) and Tolstoy (2006), who wrote: "While Biot's contributions to science owed much to his command of the sophisticated mathematical tools of theoretical mechanics, they were always rooted in concrete problems of engineering and geophysics. His solutions were firmly based on physical insight. He

understood the pitfalls of formalism, but at the same time he appreciated the creative role of mathematical elegance upon which he laid much stress. He was one of the twentieth century's true masters of Lagrangian techniques". A complete list of Biot's publications can be found in Trifunac (2006), and of his patents and awards in the introduction to Volume 14 of the *Journal of Mathematical and Physical Sciences*, published in Madras, India, in 1980, on the occasion of his 70th birthday anniversary.



Theodor von Karman (left) and Maurice A. Biot (right) at Professor von Karman's house in Pasadena, California (circa 1932)

RSM remained in the academic sphere of research for almost 40 years, gaining engineering acceptance during the early 1970s. There were two main reasons for this. First, the computation of response to earthquake ground motion led to "certain rather formidable difficulties" (Housner, 1947), and, second, there were only a few well-recorded accelerograms that could be used for response studies. This started to change in the 1960s with the arrival of digital computers and with the commercial availability of strong-motion accelerographs. Before the digital computer age, the computation of response was time-consuming, and the results were unreliable (Trifunac, 2003). By the late 1960s and early 1970s, the digitization of analog accelerograph records and the digital computation of ground motion and of the response spectra were developed completely and tested for accuracy. Then, in 1971, with the occurrence of the San Fernando, California, earthquake, the modern era of RSM was launched. This earthquake was recorded by 241 accelerographs. By combining the data from the San Fernando earthquake with all previous strong-motion records, it became possible to launch the first comprehensive empirical scaling analyses of response spectral amplitudes (Lee, 2002, 2007).

This special issue of the ISET Journal presents examples of the use and extensions of RSM in earthquake engineering. It begins with a historical review of the early studies of dynamic response, following the Messina-Reggio earthquake of 1908 in Italy, and it includes the period that preceded the formulation of the concept of RSM in 1932. Sorrentino describes the pioneering work of Arturo Danusso, who recognized the need to account for the dynamic properties of the building responding to earthquake shaking and to understand how the linear elastic n -degree of freedom can be considered as equivalent to n single-degree-of-freedom oscillators. Arturo Danusso presented a paper in Liege, Belgium at the first international conference on concrete and reinforced concrete (1–6 September 1930), at the time when Biot was a student at Louvain and von Karman was in the process of moving from Germany to Pasadena. In his last paper on earthquake-resistant structures in 1946, Danusso reviews the results he had obtained previously and references the works of Levi-Civita and Rayleigh, but he was apparently not aware of Biot's papers on RSM written in 1933 and 1934.

The paper by Freeman in this issue outlines the design aspects of RSM. Freeman describes the role Biot's standard acceleration spectrum played in the proposed design curve, $C = K/T$, in the seismic codes in California.

Papers by Lee, Douglas, and Kawakami et al. describe empirical scaling of spectral amplitudes and the regional differences in attenuation. The paper by Ventura and Blázquez reminds us of the effect of the initial ground velocity on the RMS amplitudes.

Different uses of spectral amplitudes in mapping the geographical distribution of seismic hazard are reviewed by Gupta, and the paper by Aydınoğlu describes the use of push-over analyses in earthquake-resistant design. The response of secondary structures and the estimation of the peak floor accelerations are addressed in the papers by Muscolino and Palmeri, and Kumari and Gupta.

The last four papers explore the possibilities for extending RSM to more complex excitations and describe the nature of the strength-reduction factors for impulsive and large near-fault strong-motion pulses. Zembaty reviews the role of differential motions and describes extensions of RSM that incorporate those additional effects. Kalkan and Graizer describe the role of rotational excitations, and Jalali and Trifunac examine the behavior of the response-reduction factors for an extreme excitation at the earthquake source.

Finally, Gicev and Trifunac discuss limitations of Biot's RSM, which is based on the vibrational solution of the linear differential equations of motion, and which does not explicitly consider the duration of the forcing function. They describe the power of strong-motion waves in a building, in search of a new design tool in the near-field of strong earthquakes.

ACKNOWLEDGMENTS

I am grateful to all the authors and anonymous reviewers who contributed their time generously in making this special issue of ISET journal possible. I thank the Chief Editor whose outstanding organization and meticulous attention to details during various stages of this effort made my role easy and almost effortless.

I am indebted and most grateful to the Mrs. Nady Biot, wife of M.A. Biot (1905–1985), who generously contributed old newspaper clippings from 1932 and a photograph of von Karman and Biot in von Karman's house in Pasadena, and who gave me a copy of her Biographical Sketch of Maurice A. Biot (Biot, 2007). Without her help, the inclusion in this preface of many of the details and specific dates would not have been possible. *Merci, trois fois merci.*

REFERENCES

1. Biot, M.A. (1932). "Transient Oscillations in Elastic Systems", Ph.D. Thesis No. 259, Aeronautics Department, California Institute of Technology, Pasadena, U.S.A.
2. Biot, M.A. (1933). "Theory of Elastic Systems Vibrating under Transient Impulse with an Application to Earthquake-Proof Buildings", Proceedings of the National Academy of Sciences of the United States of America, Vol. 19, No. 2, pp. 262–268.
3. Biot, M.A. (1934). "Theory of Vibration of Buildings during Earthquake", Zeitschrift für Angewandte Mathematik und Mechanik, Vol. 14, No. 4, pp. 213–223.
4. Biot, M.A. (1941). "A Mechanical Analyzer for the Prediction of Earthquake Stresses", Bulletin of the Seismological Society of America, Vol. 31, No. 2, pp. 151–171.
5. Biot, M.A. (1942). "Analytical and Experimental Methods in Engineering Seismology", ASCE Transactions, Vol. 108, pp. 365–408.
6. Biot, M.A. (2006). "Influence of Foundation on Motion of Blocks", Soil Dynamics and Earthquake Engineering, Vol. 26, No. 6–7, pp. 486–490.
7. Biot, N. (2007). "Maurice Anthony Biot—A Biographical Sketch" in "Early History of the Response Spectrum Method (edited by M.D. Trifunac)", Report CE 07-01, University of Southern California, Los Angeles, U.S.A.
8. Boley, B.A. (2005). "Maurice Biot—He is One of Us", in "Poro-Mechanics III: Biot Centennial (1905–2005) (edited by Y.N. Abousleiman, A.H.-D. Cheng and F.-J. Ulm)", A.A. Balkema, London, U.K.
9. Cornwell, J. (2003). "Hitler's Scientists", Penguin Books, New York, U.S.A.

10. Derleth, C., Jr. (1907). "The Destructive Extent of the California Earthquake. Its Effect upon Structures and Structural Materials within the Earthquake Belt", A.M. Robertson, San Francisco, U.S.A.
11. Geschwind, C.-H. (1996). "Earthquakes and Their Interpretation: The Campaign for Seismic Safety in California, 1906–1933", Ph.D. Dissertation, Johns Hopkins University, Baltimore, U.S.A.
12. Housner, G.W. (1947). "Characteristics of Strong Motion Earthquakes", Bulletin of the Seismological Society of America, Vol. 37, No. 1, pp. 19–31.
13. Lee, V.W. (2002). "Empirical Scaling of Strong Earthquake Ground Motion—Part I: Attenuation and Scaling of Response Spectra", ISET Journal of Earthquake Technology, Vol. 39, No. 4, pp. 219–254.
14. Lee, V.W. (2007). "Empirical Scaling and Regression Methods for Earthquake Strong-Motion Response Spectra—A Review", ISET Journal of Earthquake Technology, Vol. 44, No. 1, pp. 39–69.
15. Mindlin, R.D. (1989). "Maurice Anthony Biot: 1905–1985" in "Memorial Tributes", National Academy of Engineering, Vol. 3, pp. 31–35.
16. Reitherman, R. (2006). "The Effects of the 1906 Earthquake in California on Research and Education", Earthquake Spectra, Vol. 22, No. S2, pp. S207–S236.
17. Ruge, A. (1940). "Ruge on Earthquakes and Structures", ASCE Transactions, Vol. 105, p. 307.
18. Sorrentino, L. (2007). "The Early Entrance of Dynamics in Earthquake Engineering: Arturo Danusso's Contribution", ISET Journal of Earthquake Technology, Vol. 44, No. 1, pp. 1–24.
19. Timoshenko, S.P. (1968). "As I Remember", Van Nostrand Company, Princeton, U.S.A.
20. Tolstoy, I. (2006). "M.A. Biot: Applied Mathematician and Engineering Scientist", Soil Dynamics and Earthquake Engineering, Vol. 26, No. 6-7, pp. 484–485.
21. Trifunac, M.D. (2003). "23rd ISET Annual Lecture: 70-th Anniversary of Biot Spectrum", ISET Journal of Earthquake Technology, Vol. 40, No. 1, pp. 19–50.
22. Trifunac, M.D. (2005). "Scientific Citations of M.A. Biot" in "Poro-Mechanics III: Biot Centennial (1905–2005) (edited by Y.N. Abousleiman, A.H.-D. Cheng and F.-J. Ulm)", A.A. Balkema, London, U.K.
23. Trifunac, M.D. (2006). "Biographical Sketch and Publications of M.A. Biot", Soil Dynamics and Earthquake Engineering, Vol. 26, No. 6-7, pp. 718–724.
24. von Karman, T. and Edson, L. (1967). "The Wind and Beyond", Little, Brown and Company, Boston, U.S.A.

THE EARLY ENTRANCE OF DYNAMICS IN EARTHQUAKE ENGINEERING: ARTURO DANUSSO'S CONTRIBUTION

Luigi Sorrentino

Structural and Geotechnical Engineering Department
Sapienza University, via Antonio Gramsci, 53
00197 Rome, Italy

ABSTRACT

In 1908, a 7.1 equivalent magnitude earthquake struck Southern Italy. During the following year, the scientific community produced a considerable number of contributions, which were also encouraged by two competitions. In both competitions, the highest recognition was given to a Piedmont engineer—Arturo Danusso. Danusso derived the closed form equation of the response of an undamped linear elastic single-degree-of-freedom system to harmonic excitation. Thus, he suggested how to design a one-storey structure in order to minimize the amplification of its ground acceleration. In addition, he studied the case of a two-degree-of-freedom system, determining its two eigenfrequencies and concluding that the motion of each of the two masses can be reduced to the linear combination of the motions of two ideal simple systems subjected to given base motions. Danusso was probably the first to propose a dynamic analysis method rather than static lateral force analysis method and, possibly for the first time in earthquake engineering, he stated that seismic demand does not depend upon the ground motion characteristics alone. Danusso correctly solved the equations, and made some correct statements without writing any equations, as given in this paper. In addition, a brief account on Danusso's life, Italian research after the 1908 earthquake, and Danusso's influence on later Italian earthquake engineering will be presented.

KEYWORDS: Modal Analysis, Southern Calabria-Messina 1908 Earthquake, Early Earthquake Engineering, Arturo Danusso

INTRODUCTION: THE 1908 SOUTHERN CALABRIA-MESSINA EARTHQUAKE AND SUBSEQUENT INITIATIVES

On December 28, 1908, a 7.1 equivalent magnitude earthquake (XI Mercalli Cancani Sieberg Intensity) hit Messina, Reggio Calabria, and Southern Calabria (CPTI04¹), causing extensive damage and tens of thousands of deaths (Baratta, 1910). On January 12, 1909, the Italian Parliament issued Law No. 12 (Giuffrè, 1987), following which, on 15 January a Royal Decree appointed a panel to single out and suggest earthquake-resistant construction techniques (MLLPP, 1909a). The panel was made up of fourteen engineers, five of which were professors at Italian universities, and an English synopsis of the panel's report can be found on Pages 556–581 of Freeman (1932). It is not possible to follow here all of the committee's work, which spanned damage interpretation, examination of available literature, and, finally and most important, development of one of the first quantitative procedures for the design of earthquake-resistant structures. The procedure became mandatory through the Royal Decree of April 18, 1909 (RI, 1909) and a ministerial memorandum (MLLPP, 1909b).

Concise accounts can be found in Freeman (1932), Housner (1984), Giuffrè (1987), and Bertero and Bozorgnia (2004). It is perhaps significant that this procedure, which was largely a contribution of Modesto Panetti (at that time Professor at the Royal Naval Upper School in Genoa and later key figure at the Technical University in Turin), started from the assumption that any dynamic analysis would be impractical. Therefore, the panel proposed to conventionally substitute dynamic actions with purely static ones in representing seismic effects. This preliminary decision had great impact on subsequent early earthquake engineering in Italy, because it simplified the design procedures but ruled out from the code any dynamic consideration until mid-seventies (MLLPP, 1975), when a design spectrum was introduced (Di Pasquale et al., 2000).

¹ Website of CPTI04, <http://emidius.mi.ingv.it/CPTI04/>

It is perhaps hard to believe that almost contemporary to this original code was an early significant contribution to the use of dynamics for the design of earthquake-resistant structures. As a matter of fact, the Southern Calabria-Messina disaster raised an incredible reaction in public opinion, and specifically in the technical community, and a wealth of contributions was published in scientific journals. For example, whereas in the preceding years only a few communications, notes, or papers followed significant seismic events, in 1909 alone 5 publications were published in “Giornale del Genio Civile”, 6 in “Rivista di Ingegneria Sanitaria”, 19 in “Annali della Società degli Ingegneri e degli Architetti Italiani”, 20 in “Il Cemento”, and 26 in “Il Monitore Tecnico”. Two competitions also contributed to the flood of publications.

The first competition was called by the Società Cooperativa Lombarda di Lavori Pubblici, under the patronage of the Milan Institution of Engineers and Architects (Manfredini, 1909a, 1909b, 1909c; Anonymous, 1909a, 1909b, 1909c, 1909d, 1909g, 1909h, 1909i). The aim of the contest was to “achieve and apply construction types and systems for civil, rural, and industrial buildings to be adopted in the Italian regions most subjected to seismic shaking and most seismologically dangerous” (Anonymous, 1909g). The deadline for the presentation of the projects was March 31, barely three months after the main shock and prior to the release of the Royal Decree. Two hundred and fourteen proposals were presented (Novelli, 1909), and the panel delivered its decision (Anonymous, 1909h). It is interesting to note that two out of three money prizes went to A. Danusso and G. Revere (the latter together with V. Gianfranceschi), both associate editors of the journal “Il Cemento” (Anonymous, 1909c). The criteria followed by the panel can be found in Manfredini (1909c), Anonymous (1909i), and in Danusso (1960). Danusso's proposal met many of them, with its round raft foundation, centroid kept low by means of lighter infills in the upper storey, and overall good connection through a reinforced concrete two-way frame, which was easier to build in Southern Italy than steel or timber frames. The panel appreciated the calculations accompanying some of the projects because “it is of the outmost interest to give to the builder a guide more rigorous than a simple intuitive criterion, in order to allow the application to this branch of the construction art those calculation and verification methods that form the base of structural mechanics” (Anonymous, 1909i). However, they praised Danusso's contribution much more than any other. Although criticising the modelling of the ground motion through a harmonic function and the small importance attached to the vertical component, the members appreciated the engineer's account of the building deformations under the shaking, something that made him capable of explaining why “an excessive building stiffness does not contribute to its stability” (Anonymous, 1909i). The proposal by Danusso was published in several journal papers (Danusso, 1909c, 1909e).

During the same year, a second competition was called by the Tuscany Institution of Engineers and Architects, on the occasion of the 12th Institution National Conference held in Florence at the beginning of October (Manfredini, 1909d; Losio, 1909; Anonymous, 1909e, 1909f, 1909j, 1909k). The deadline was June 30, but it was later extended to August 31. The impact of this contest was much smaller than the one in Milan, since only 18 projects were submitted. The committee this time was made up by nine engineers designated by local institutions and one delegate of the Agriculture Industry and Trade Ministry. Only two members had been part of the first competition panel. The committee criticized the lack of adequate calculations in many proposals, although the Royal Decree No. 193 was now in force, and the use in a few cases of a steel frame, was considered too expensive to be widely exploited. On this occasion again, Danusso's proposal was the most praised because it was based “on the laws and principles of rational mechanics and theory of elasticity and on the strength of the materials data” (Anonymous, 1909k). During a special “seismological” session, Danusso made also an oral presentation to the conference, “On Earthquake Resistant Constructions”, without submitting a written memory (Anonymous, 1909k). This was later published separately in journals (Danusso, 1909d, 1909f, 1910a) and in a 45-page stand-alone volume (Danusso, 1910b). Compared with the Milan proposal, this was widened on the theoretical side (Anonymous, 1909f). Danusso's recommendation of the use of reinforced concrete structures met resistance from many engineers as being a non-local technique that was highly dependent upon the quality of the workmanship (Anonymous, 1909k). However, the Southern Calabria-Messina earthquake and the subsequent Royal Decree, even though it was soon watered down to some extent (RI, 1912; Danusso, 1912a, 1912b; MLLPP, 1921), proved major reasons for the spread of reinforced concrete structures in Italy (Pages 86–93 of Iori (2001)).

ARTURO DANUSSO (1880–1968): BIOGRAPHICAL NOTES

Who was this engineer, whom the Milan Committee addressed with the words: “lucky holder, at the same time, of the most powerful calculation means and of the most effective artifices of the building art” (Anonymous, 1909i)?

Contrary to what is sometimes believed (Page 580 of Freeman (1932); Housner, 1984), when Danusso won the Milan competition, he was not a professor.



Fig. 1 Arturo Danusso (1880–1968) in his office, early 1960s (courtesy: Professor Marco Locatelli)

Born on September 9, 1880 in Priocca d’Alba (Piedmont region, in Northern Italy), Arturo Danusso (Figure 1) lived his first years in Genoa, where his father Ferdinando taught mathematics and physics in a technical high school. At the age of four, he lost his father and moved with his mother, Paolina Dotta, to Turin. He attended Catholic schools (his high school was run by Jesuits), then thanks to a scholarship enrolled in the Civil Engineering College, where he graduated “cum laude” on August 29, 1902. His master, C. Guidi (Vice-President of the Milan competition committee), offered him a position as an assistant. Danusso reluctantly declined because his family’s finances were not flourishing (Danusso, 1978; Cristina Danusso, personal communication). Adhering to his mother’s wishes, he moved to Koblenz for a long stay, thus polishing his German (D’Aquino, 1986; Cristina Danusso, personal communication). His cultural ties with that country always remained strong, even when Italy was at war against it (Danusso, 1916). In 1903, he returned to Turin. After an initial post at the Southern Italy Railway Company in Benevento (Southern Italy), he moved back to Turin in 1905, where he obtained a

position in the Porcheddu Enterprise, Italian licensee of the Hennebique reinforced concrete patent (Danusso, 1937). This was the occasion of his first practical experiences and theoretical works, many of which he published in the journal “Il Cemento”, established in 1905, where he was associate editor (Anonymous, 1968).

In 1912, Danusso patented the two-way clay reinforced concrete floor “Duplex” (Page 230 of Iori (2001)). In 1915, he won the competition for the chair in Structural Mechanics at the Royal Upper Institute (later Technical University) in Milan, to which he moved (Anonymous, 1915a; Danusso, 1915b). His academic career proceeded jointly with the consulting work. He was also frequently involved in the assessment and the retrofitting of historical constructions, such as the Pisa Tower, the Milan Sant’Ambrogio Belltower, the Turin Mole Antonelliana, the Novara (Piedmont) San Gaudenzio Dome, and the Milan and Pavia cathedrals. He took part also in the design of many large structures such as bridges, dams, power lines, and skyscrapers. Just after the end of World War II, he was elected Milan town councillor and contributed to the reconstruction of the city, and between 1955 and 1959 he was consultant for the Pirelli centre designed by G. Ponti and P.L. Nervi (Page 62 of Desideri et al. (1979); Page 231 of Iori (2001)), carrying out static and dynamic tests on a model.

His research interests were in the field of reinforced concrete structures, investigating their static and dynamic behaviour, which involved testing originally in the Technical University laboratory and then at the Istituto Sperimentale Modelli e Strutture (ISMES, Models and Structures Experimental Institute), which he helped to establish in Bergamo (Lombardy region) in 1951, the year after he retired. He understood the importance of the plastic features of reinforced concrete and exploited them in the design of his buildings (D’Aquino, 1986).

He also developed an initial interest in the theoretical aspects of pre-stressing, recommending (against the risks of a wrong measuring out of the induced forces and their change through time) the resort to the plasticity of reinforced concrete as a natural resource of statically indeterminate structures (Pages 216, 218, 227 of Iori (2001)). Further references on Danusso’ scientific publications can be found in D’Aquino (1986) and on Pages 243–248, 250, 261 of Iori (2001), while a selection of more meditative writings—which give testimony of a deep religious feeling—is collected in Danusso (1978). He was member of the Turin Science Academy, of the Lombardy Institution of Science, Literature, and Arts, of the Italian Research National Council (Danusso, 1957), of the Milan Mathematics and Physics Seminary (Danusso, 1927), within which he helped to establish a course on Mechanics of Vibrations in 1949 (Finzi, 1952; Tibiletti Marchionna, 1997). As a matter of fact, Danusso has had the chance to apply his work in the field of structural dynamics such as machine-induced vibrations and wind-induced vibrations (Danusso, 1919, 1952, 1954a, 1954b). In 1967, when he was seriously ill, the “International Center of Earthquake Engineering” was established by the Technical University of Milan and ISMES, under the auspices of UNESCO (United Nations Educational, Scientific and Cultural Organization) and the National Research Council. The centre was named “Arturo Danusso” (Grandori, 1967). Danusso died in Milan on 5 December 1968.

DANUSSO’S 1909–1910 PAPERS

Although the deadline for the Milan competition was barely three months after the Southern Calabria-Messina earthquake, Danusso’s proposal was not his first attempt to solve the problem of the “houses that do not collapse” during earthquakes. In a paper with such a title (Danusso, 1909a), published less than twenty days after the shock, he presented many of the ideas that would grant him the highest recognition in the two 1909 contests, and which highlighted the importance of studying the damages caused by severe earthquakes. He had already shown great confidence in two-way reinforced concrete frames, emphasizing which details should be adopted (raft foundation—which he studied in the same year (Danusso, 1909g), columns with increased panel zone height, beams with top and bottom reinforcement, infills growing lighter for the higher storey), and recommending the avoidance of excessive stiffness, a topic on which he would focus later.

The papers related to the two 1909 competitions are Danusso (1909c, 1909d, 1909e, 1909f, 1910a, 1910b). The most comprehensive ones are the Danusso (1910a, 1910b) papers, which are nearly identical to and use almost all of the text from the previous ones.

In Danusso (1909c, 1909e), which followed right after the Milan contest, no equations are to be found. Even so, there must have been some in the submitted contribution, for otherwise the Committee

would have complained about the lack of calculations, as they did in other cases. There is, however, a plot (Figure 4(a)), later presented in every one of Danusso's earthquake engineering papers (Danusso, 1909d, 1909f, 1910a, 1910b, 1928, 1931, 1932, 1952, 1954b; on Page 533 of Danusso and Ceruti (1935)) and also to be found, with minor differences, on Page 583 of Freeman (1932). This plot will be discussed later, when the equations at its base are presented. The Danusso (1909c, 1909e) papers conclude with recommendations about buildings' number of storeys and maximum plan size.

The two Danusso (1909c, 1909e) papers are identical, with the latter also having an additional section devoted to the proposed residential building (Figure 2), whose longitudinal cross-section shows the influence of designs by previous practitioners (Danusso, 1909b).

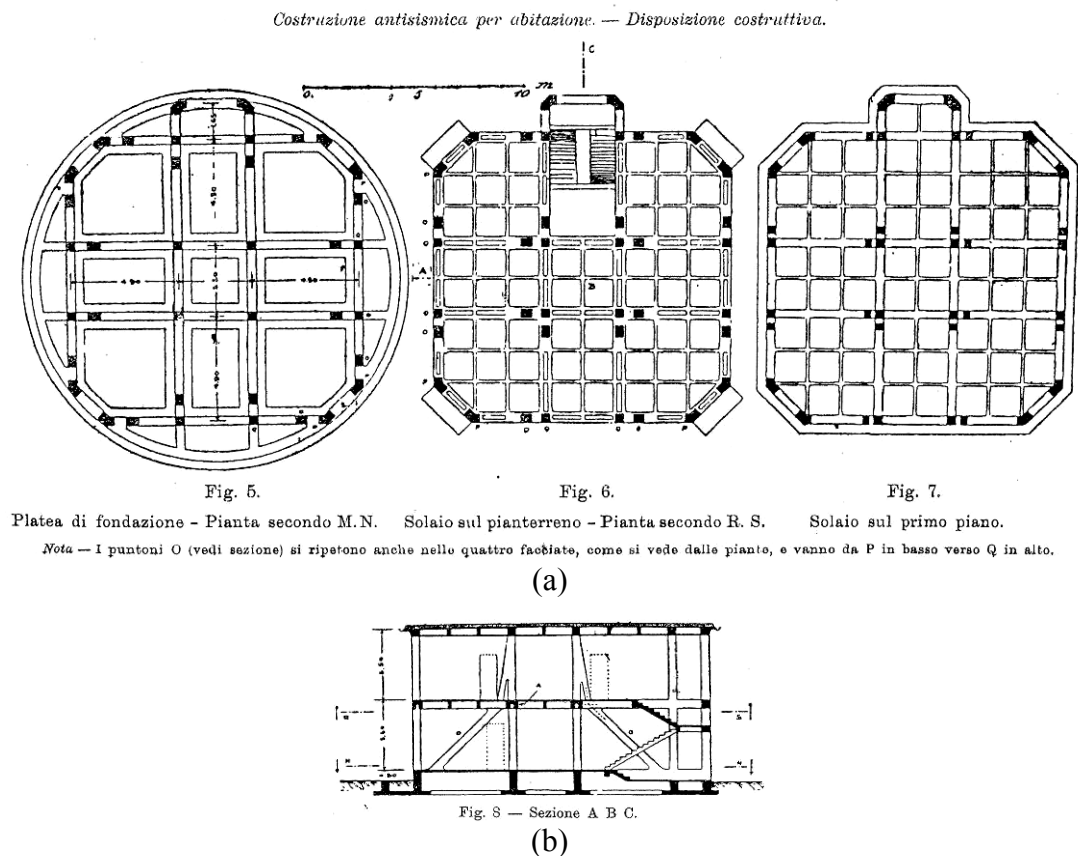


Fig. 2 Danusso's earthquake-resistant building, a reinforced concrete frame: (a) Plans at foundation, at first and second level (from Danusso, 1910b); (b) Section

The two Danusso (1909d, 1909f) papers following the Florence competition are again identical. They present the mathematics at the base of Danusso's statements, which will be discussed shortly with reference to the more complete papers published in 1910. The only material not included in the latter is a brief reference to some "in situ" dynamic measurements (Alfani, 1909a, 1909b, 1909c, 1915a), which precede those quoted in Bertero and Bozorgnia (2004).

The two papers published in 1910 are identical, the latter being a reprint of the former in a stand-alone volume. Both are addressed as the "report presented at the 12th Engineers and Architects Conference in Florence in October 1909".

Danusso begins his presentation by stating that he will focus his attention on the ground motions without permanent and severe soil deformation because such ground motions "are beyond the remedies of science. To try to save the building against them would be as to study the safety of trains against the possible collapse of railway bridges" (Danusso, 1910b).

Even without breaking the soil, seismic ground motion is mostly dangerous because it induces vertical and horizontal actions usually not considered, which severely affect the response of columns designed for axial loads only. Already in Danusso (1909c, 1909e) papers there are two key assertions: (1) the intensity of horizontal inertia forces is not governed by ground motion acceleration alone but depends

also on the “elastic flexibility of the building skeleton” (Danusso, 1909c); (2) such flexibility strongly influences the intensity of such forces and has some bearing on a rational and cost-effective design. Danusso is aware that “every building is a system of masses more or less stiffly connected” (Danusso, 1909c), with those masses belonging to the superstructure subjected to an acceleration differing from the ground one, due to their inertia and to their connection to the base. It is possible to take advantage of the structure flexibility to attenuate the shaking’s sudden effects. “To cut as much as possible this (seismic) energy that will be transferred to the construction—here is, in my opinion, the fundamental standard of seismic building. This will be obeyed by letting the built organ follow the shaking action docilely, not by opposing it stiffly” (Danusso, 1909c).

DYNAMIC CONSIDERATIONS

1. One-Degree-of-Freedom “Elastic Pendulum”

Danusso was keen to leave intuitive suggestions and to compute scientifically the elastic response of a building under a ground shaking. Of the whole edifice, he considers only the structure made up by columns and horizontal floors, constituted by materials reacting to both tension and compression. The columns have no mass, and this is concentrated at floor levels. The vertical component can be separately addressed because, according to Danusso, it induces only a pounding effect that is easy to tackle. The horizontal motion at the base of the building will generate inertia forces at the floor levels.

Danusso’s goal is “to determine the laws of motion of the whole superstructure under the combined action of the shake, the inertia of the masses and the elasticity related to the shape of the structure and its materials” (Danusso, 1910b). Once such motion is known it will be possible to look for the “molecular inner stresses in the resisting material” (Danusso, 1910b).

He initially considers a one-storey building, which he assimilates to an “elastic pendulum”—i.e., a mass resting on a vertical massless column clamped to a foundation undergoing horizontal motion.

Following Figure 3(a), he writes (Danusso, 1910b)

$$ds + (f_1 - f) = dx = ds + df \quad (1)$$

with s defined as total displacement of the mass from the initial position, x as ground displacement, $f = kN$ as deflection, k as the flexibility of the pendulum, N as the product of the mass m with its “instantaneous acceleration during its own motion” (Danusso, 1910b).

This leads to

$$N = m \frac{d^2s}{dt^2} \quad (2)$$

with t being time. Therefore, after integrating once, Danusso gets from Equation (1) the following differential equation (Danusso, 1910b) (also see Appendix II):

$$km \frac{d^2s}{dt^2} + s = x(t) \quad (3)$$

Danusso writes Equation (3) without quoting previous works. He simply states that he made use of “the principle of inertia which dominates the entire dynamics” (Danusso, 1909f), exploited “rational mechanics, and precisely the dynamics of elastic systems” (Danusso, 1909c), and resorted to the “simple combination of D’Alembert’s principle with the law of elastic deformations” (Danusso, 1910b). Elsewhere, he states: “the fundamental principle of dynamics informs us that no motion of the building can be thought to be without a system of forces applied to the building elements and such as to resist the motion” (Danusso, 1910b).

No damping is considered. Apparently, this will be considered for the first time in the Italian earthquake engineering literature on Pages 120, 192, 206–207 of Giannelli (1932), who however quotes R. Sano, “On the Vibration of Steel Frame Buildings”, without adding a more complete reference. Viscous damping had already been considered on Pages 45–46 of Rayleigh (1877), and possibly even before, who presented the equation of motion in terms of relative displacements. Moreover, Rayleigh (1877) obtained the equation of motion using potential and kinetic energies, in a Lagrange approach (on

Pages 43–45). In contrast, Danusso gets his equation by writing a compatibility equation. Therefore, Danusso probably did not consider this precedent.

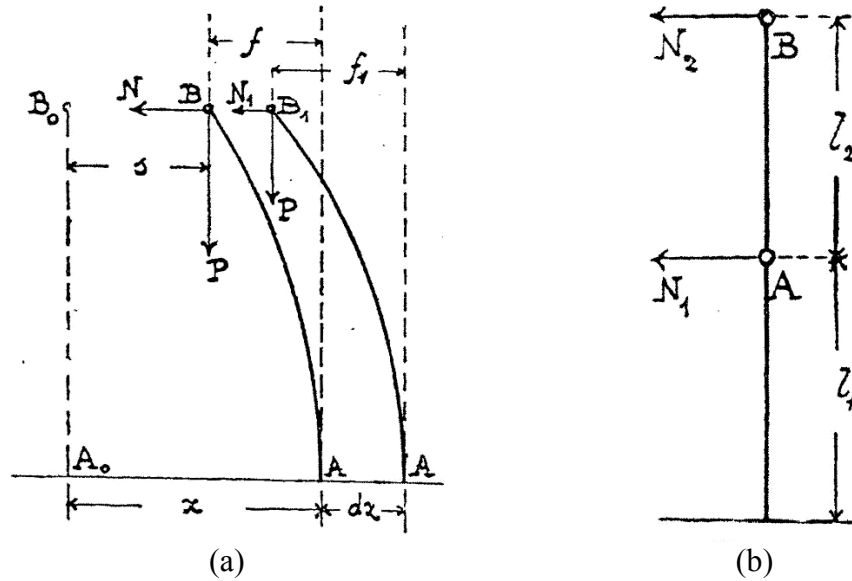


Fig. 3 (a) Simple elastic pendulum; (b) Double elastic pendulum (Danusso, 1910b)

Whereas today it is more common to write the equation of motion using relative displacements and accelerations, a chance that Danusso suggested elsewhere (Danusso, 1928), he preferred to make reference to total (absolute) parameters. The reason for such a choice lies in the fact that Danusso is looking for a force to be used in a static design of the structure. Therefore, inertia force, related to total and not relative accelerations, is what he is interested in. By the way, the advantage of using total quantities has been highlighted also more recently (Uang and Bertero, 1990). Furthermore, at that time only seismograms (i.e., displacement time histories) were available. The first acceleration time history was recorded in 1933, during the Long Beach (California, USA) earthquake (Marletta, 1934; Hudson, 1983).

Danusso (1910b) presents the solution for a generic ground motion as follows (also see Appendix II):

$$s = -\omega \cos \omega t \int_0^t x(t) \sin \omega t \, dt + \omega \sin \omega t \int_0^t x(t) \cos \omega t \, dt \quad (4)$$

with $\omega = 1/\sqrt{km}$, a natural circular frequency that he calls “elastic constant”, obtained after setting “at rest” initial conditions. Thus,

$$s(t=0) = \frac{ds}{dt}(t=0) = 0 \quad (5)$$

He then considers a ground displacement (Danusso, 1910b)

$$x(t) = r(1 - \cos \alpha t) \quad (6)$$

with r being amplitude and α being the exciting circular frequency. Danusso denotes this ground motion “without initial impact” since initial ground velocity is zero. Probably Danusso selected this ground motion instead of $x(t) = r \cos \alpha t$ so that both ground displacement and velocity are initially equal to zero (compared to Equation (10)).

The correct solution, he wrote, is (Danusso, 1910b)

$$s = r \left[1 + \frac{\cos \omega t - \rho^2 \cos \alpha t}{\rho^2 - 1} \right] \quad (7)$$

with $\rho = \omega / \alpha$. Therefore, the acceleration undergone by the mass is (Danusso, 1910b)

$$\frac{d^2s}{dt^2} = \frac{r\omega^2}{\rho^2 - 1} (\cos \alpha t - \cos \omega t) \quad (8)$$

Considering a time t_1 when $\cos \omega t_1 = -1$ and $\cos \alpha t_1 = 1$, the ratio μ of maximum inertia acceleration to the maximum ground acceleration $r\alpha^2$ is indeed (Danusso, 1910b)

$$\mu = \frac{2\rho^2}{\rho^2 - 1} \quad (9)$$

Danusso (1928) will later call the ratio of Equation (9) the “rapporto sismico” (seismic ratio). Because ρ is the only parameter governing μ , Danusso (1910b) calls it “characteristic”. Absolute value of Equation (9) is the one represented in Figure 4(a) with a dashed line.

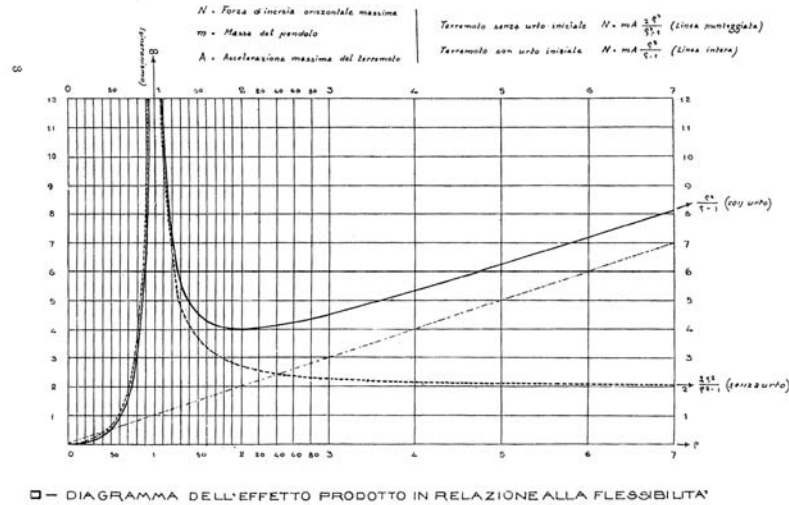


Fig. 1.

(a)

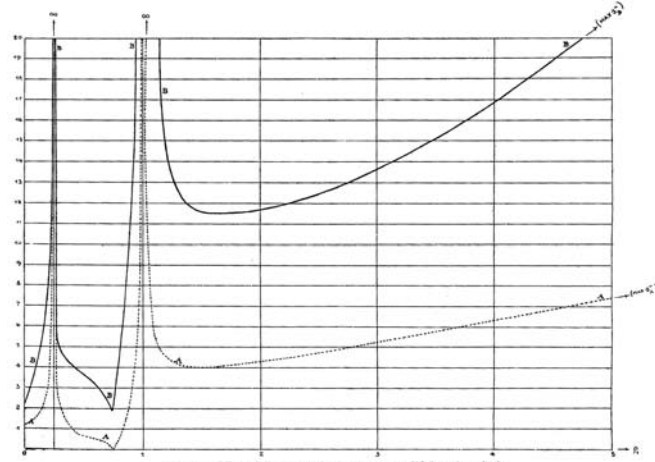


Fig. 2 — Effetto della scossa sismica sopra un edificio a due piani.

(b)

Fig. 4 (a) Seismic ratio under harmonic excitations (Danusso, 1910b) (on the horizontal axis is the “characteristic” ρ , and on the vertical axis is the “seismic ratio” μ ; the original caption means: “diagram of the effect [of the ground shaking] in relation to the flexibility”); (b) Shake effect on a two-storey building (Danusso, 1910b)

If the ground displacement is the function

$$x(t) = r \sin \alpha t \quad (10)$$

which Danusso (1910b) denotes as “with an initial maximum impact”, the solution he rightly worked out is (Danusso, 1910b)

$$s = \frac{r\omega}{\omega^2 - \alpha^2} (-\alpha \sin \omega t + \omega \sin \alpha t) \quad (11)$$

Differentiating s two times with respect to time and considering similarly a time t_1 when $\sin \omega t_1 = 1$ and $\sin \alpha t_1 = -1$, μ is indeed (Danusso, 1910b)

$$\mu = \frac{\rho^2}{\rho - 1} \quad (12)$$

Absolute value of Equation (12) is the one represented in Figure 4(a) with a solid line.

To understand why sinusoidal ground displacement induces such amplifications for increasing ρ , let us consider the now customary equation of motion of a mass-spring system to be found in textbooks (e.g., Pages 1–19 of Timoshenko (1928); Pages 113–115, 130–139 of von Kármán and Biot (1940)). Such an equation is

$$\frac{d^2 y}{dt^2} + \omega^2 y = r\alpha^2 \cos \alpha t \quad (13)$$

with $y = s - x$ taken as the relative displacement and with excitation obtained by differentiating two times the ground displacement in Equation (6). In this case, the “at rest” initial conditions for the total mass displacement equation of motion involve the “at rest” initial conditions for the relative mass displacement equation of motion as well. Therefore, it is easy to show that the solution is of the form:

$$y = \frac{r\alpha^2}{\omega^2 - \alpha^2} (-\cos \omega t + \cos \alpha t) \quad (14)$$

Hence, the “seismic ratio,” with symbols consistent with those previously used, is

$$\mu = \frac{\max|\ddot{y}|}{\max|\ddot{x}|} + 1 = \left| \frac{\rho^2 + 1}{\rho^2 - 1} \right| + 1 = \left| \frac{2\rho^2}{\rho^2 - 1} \right| \quad (15)$$

with the dots representing the derivatives with respect to time. This is coincident with Equation (5).

However, if one considers the sinusoidal excitation of Equation (10), the equation of motion becomes

$$\frac{d^2 y}{dt^2} + \omega^2 y = r\alpha^2 \sin \alpha t \quad (16)$$

Anyway, in this case the initial conditions are

$$\begin{aligned} y(0) &= s(0) - x(0) = 0 \\ \dot{y}(0) &= \dot{s}(0) - \dot{x}(0) = -r\alpha \end{aligned} \quad (17)$$

Therefore, the solution is

$$y = \frac{r\alpha^2}{\omega^2 - \alpha^2} (-\rho \sin \omega t + \sin \alpha t) \quad (18)$$

Hence, the “seismic ratio” is

$$\mu = \left| \frac{\rho^3 + 1}{\rho^2 - 1} \right| + 1 = \left| \frac{\rho^2}{\rho - 1} \right| \quad (19)$$

which is coincident with Equation (12).

A mass-spring-damper system, in which transient response is neglected, has the same (relative) acceleration response factors, R_a , whether the excitation is cosinusoidal or sinusoidal (e.g., refer to Pages 75–78 of Chopra (1995) where, with symbols consistent with those here previously used, $\mu = 1/(\rho^2 - 1)$). On the contrary, the mass-spring system considered by Danusso has two different response factors. These are

$$\begin{aligned}
 R_{a, \cos} &= \left| \frac{\rho^2 + 1}{\rho^2 - 1} \right| \\
 R_{a, \sin} &= \left| \frac{1}{\rho - 1} \right|
 \end{aligned}
 \tag{20}$$

which are plotted in Figure 5(a).

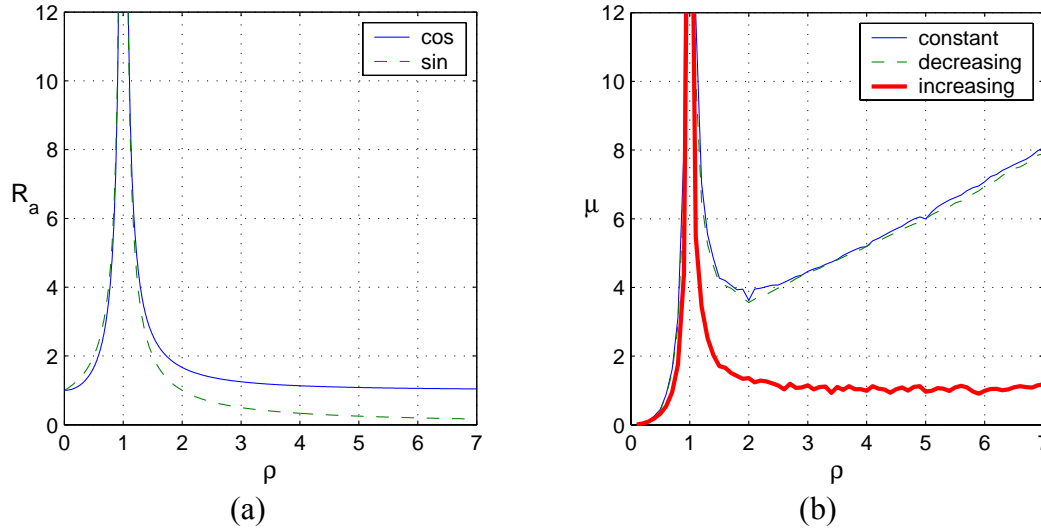


Fig. 5 (a) Relative acceleration response factor for an undamped linear elastic single-degree-of-freedom oscillator subjected to harmonic excitation; (b) Danusso's "seismic ratio" μ as a function of system natural frequency to excitation frequency ratio ρ , for an undamped linear elastic single-degree-of-freedom oscillator initially at rest subjected to sinusoidal excitations of constant, linearly increasing and linearly decreasing amplitudes

Danusso comments on the plot of Figure 4(a) at length, and it is perhaps noteworthy that no analogous plot is to be found in Rayleigh (1877, 1894). The caption under the plot is "Diagram of the effect [of the ground shaking] in relation to the flexibility". On the horizontal axis is the "characteristic" ρ , and on the vertical axis is the "seismic ratio" μ .

Danusso notes that the system, due to its proper characteristics, can reduce or increase the ground acceleration. This is of the utmost interest—possibly for the first time in earthquake engineering it is stated, based on a mathematical demonstration, that the seismic demand does not depend upon the ground motion characteristics alone but also on those of the structure. For Danusso, this is also the explanation of the very wide differences observed in the behaviour of buildings after severe earthquakes. He discusses the "synchronism" (Danusso, 1909c) condition $\rho = 1$, stating that although it is theoretically very worrying it is actually rather unlikely because earthquake "shakings are all short and moreover changing" (Danusso, 1909c).

As a practical example, Danusso then assumes an amplitude of 2.5 m/s^2 and a period of $1/3 \text{ s}$. He also states that the range of ρ from 0 to $1/2$ is virtually not obtainable because this would be valid for a steel frame with columns that are designed for buckling but therefore are unable to carry any load when displaced from rest. Therefore, only values greater than 1 should be considered, and only such values are plotted in the figure to be found on Page 583 of Freeman (1932), and the case $\rho = 2$ should be preferred because a local minimum is located in the "impact" case. Higher values of the "characteristic" would be theoretically better for the ground motion "without impact", but they would involve significant amplifications in the other case which, even if resisted by means of the higher resistance, can involve global lack of equilibrium of the system. Based on this plot, Danusso maintains that an excessively stiff building "would be truncated by the actions of an impact", and that he does "not believe that absolute stiffness is the goal toward which every earthquake-resistant construction should tend" (Danusso, 1909c). Moreover, such a solution would bear unnecessarily higher costs. Values around 2 can be gained even

with the more (compared to steel) stiff reinforced concrete frame, which is Danusso's preferred solution. The recommended design procedure is to assume an acceleration that is four times the ground ones, to dimension the structure, and then to verify whether the value of ρ is reasonably close to 2. Otherwise, a second attempt should be sufficient.

Danusso (1910b) says that he also considered the case of "an initial impact with given velocity and a steady-state motion continuing with the same velocity. The pendulum oscillates regularly with a constant period, depending not upon the impact velocity (on this only the amplitude is dependent) but uniquely on the elastic properties of the column—i.e., on the material nature, its shape, and the borne load. And if, while pursuing the analogy with an ordinary compound pendulum, the reduced length of an elastic pendulum is sought, it is easy to prove that this is equal to the elastic deflection that the column would undergo when the top load is applied horizontally".

Danusso (1910b) also studies the response to a generic ground motion displacement time history, recorded by a seismograph. He is persuaded that "any motion, even if complex, can be reduced to the superposition of simpler elementary motions". Considering the time history as a series of sinusoidal "waves", the response to each can be obtained by means of Equation (11) and by determining the values of the constants of integration in order to match the position and velocity condition at the end of the previous wave. For example, at the end of the first full sine "wave", the position, S_1 , and velocity, V_1 , of the system are (Danusso, 1910b)

$$\begin{aligned} S_1 &= -\frac{r_1 \omega^2}{\omega^2 - \alpha_1^2} \frac{\alpha_1}{\omega} \sin\left(2\pi \frac{\omega}{\alpha_1}\right) \\ V_1 &= \frac{r_1 \omega^2 \alpha_1}{\omega^2 - \alpha_1^2} \left[1 - \cos\left(2\pi \frac{\omega}{\alpha_1}\right)\right] \end{aligned} \quad (21)$$

Then Danusso says: "In order to simplify the expressions, it is convenient to take a new time origin at the beginning of every wave".

Danusso (1910b) writes also that he considered the response of the system to sinusoidal motions of increasing or decreasing amplitudes, and he states that in the first case he found "a lesser effect" compared with that of a constant amplitude, while in the second he found "a not greater and sometimes equal effect". He does not add any equation. However, if the ground motions are

$$\begin{aligned} x(t) &= \frac{t}{t_2} r \sin \alpha t \\ x(t) &= \left(1 - \frac{t}{t_2}\right) r \sin \alpha t \end{aligned} \quad (22)$$

with t_2 being the end of the time interval considered and with "at rest" initial conditions being considered, it is possible to prove that the solutions are

$$\begin{aligned} s &= \frac{r \omega^2 \{2\alpha(\cos \omega t - \cos \alpha t) + (\omega^2 - \alpha^2)t \sin \alpha t\}}{t_2 (\alpha - \omega)^2 (\alpha + \omega)^2} \\ s &= \frac{-r \omega^2 \left\{2\alpha(\cos \omega t - \cos \alpha t) + (\omega^2 - \alpha^2) \left[(t - t_2) \sin \alpha t + \frac{\alpha}{\omega} t_2 \sin \omega t \right] \right\}}{t_2 (\alpha - \omega)^2 (\alpha + \omega)^2} \end{aligned} \quad (23)$$

respectively. By deriving the expressions in Equation (23) two times and by normalizing with respect to ground acceleration amplitude, the "seismic ratios" are obtained as

$$\mu_{\text{incr}} = \left| \frac{\rho^2 \left\{ \frac{4}{n} \rho^2 + (1 - \rho^2) \right\}}{(1 - \rho)^2 (1 + \rho)^2} \right|$$

$$\mu_{\text{decr}} = \left| \frac{\rho^2 \left\{ \frac{4}{n} \rho^2 + (1 - \rho^2) \left[\left(1 - \frac{t_1}{t_2} \right) + \rho \right] \right\}}{(1 - \rho)^2 (1 + \rho)^2} \right| \quad (24)$$

with $n = \alpha t_2$. Hence, for $t_2 \gg 1/\alpha$ the first term in the curly braces vanishes, and for $t_2 \gg t_1$ the “seismic ratios” reduce to

$$\mu_{\text{incr}} \cong \left| \frac{\rho^2}{\rho^2 - 1} \right|$$

$$\mu_{\text{decr}} \cong \left| \frac{\rho^2}{\rho - 1} \right| \quad (25)$$

which are indeed minor or equal, respectively, to Equation (12). The “seismic ratios” have also been computed numerically, again verifying Danusso's statement (Figure 5(b)).

2. Two-Degree-of-Freedom, Two-Storey Building

Probably in the framework of the newly issued seismic code, which limited to two, the number of stories of any building, Danusso (1910b) then considers a two-storey structure as a two-degree-of-freedom system (Figure 3(b)). He writes two coupled differential equations, analogous to Equation (3) (also see Appendix I and Appendix II):

$$k_1 m_1 \frac{d^2 s_A}{dt^2} + k_2 m_2 \frac{d^2 s_B}{dt^2} + s_A = x(t)$$

$$k_2 m_1 \frac{d^2 s_A}{dt^2} + k_3 m_2 \frac{d^2 s_B}{dt^2} + s_B = x(t) \quad (26)$$

with k_1, k_2 and k_3 being constants to be determined by means of “Virtual Works Theory” or “Elasticity Ellipse” and the “Reciprocity Law, whatever the degree of restraint granted by the column in A and B ”, so that (Danusso, 1910b)

$$f_A = k_1 N_1 + k_2 N_2$$

$$f_B = k_2 N_1 + k_3 N_2 \quad (27)$$

Danusso (1910b) then presents, without intermediate development, the two “elastic constants (similar to ω)” ξ and η (also see Appendix I):

$$\xi^2 = \frac{B - \sqrt{B^2 - 4A}}{2A}$$

$$\eta^2 = \frac{B + \sqrt{B^2 - 4A}}{2A} \quad (28)$$

with

$$A = m_1 m_2 (k_1 k_3 - k_2^2)$$

$$B = k_1 m_1 + k_3 m_2 \quad (29)$$

ξ and η are the roots of the polynomial, quadratic in ω_n^2 , of the eigenvalue problem:

$$\left([km] - \frac{1}{\xi_n^2} [I] \right) \{ \phi_n \} = 0 \quad (30)$$

with ξ_n and $\{ \phi_n \}$ being the n th eigenvalue and (right) eigenvector, respectively (in today's, not Danusso's, terminology); square brackets being used for the square matrices; $[I]$ as the identity matrix; and curly braces indicating a column vector. The $[km]$ matrix is equal to

$$[km] = \begin{bmatrix} k_1 m_1 & k_2 m_2 \\ k_2 m_1 & k_3 m_2 \end{bmatrix} \quad (31)$$

It is important to stress that the orthogonality of modes does not hold with respect to the $[km]$ matrix. This is due to the fact that the problem is not self-adjoint. Danusso (1910b) does not present the matrix of (right) eigenvectors. However, he writes that the two functions s_A and s_B are expressed in finite terms as follows:

$$s_A = \frac{1}{\eta^2 - \xi^2} \left[\frac{(R_A)}{\xi^2} - \frac{(S_A)}{\eta^2} \right] \quad (32)$$

$$s_B = \frac{1}{k_2 m_2 (\eta^2 - \xi^2)} \left[\left(m_2 k_3 - \frac{1}{\eta^2} \right) \frac{(R_A)}{\xi^2} + \left(\frac{1}{\xi^2} - m_2 k_3 \right) \frac{(S_A)}{\eta^2} \right] \quad (33)$$

with (R_A) and (S_A) , respectively, being the expressions of the distance of two equivalent pendulum masses from the initial position in any instant. Therefore, from the last two equations, Danusso's matrix $[\phi]$ of right eigenvectors, never explicitly presented, is

$$[\phi] = \frac{1}{\eta^2 - \xi^2} \begin{bmatrix} \frac{1}{\xi^2} & -\frac{1}{\eta^2} \\ k_3 m_2 - \frac{1}{\eta^2} & k_3 m_2 - \frac{1}{\xi^2} \\ \frac{k_2 m_2}{\xi^2} & -\frac{k_2 m_2}{\eta^2} \end{bmatrix} \quad (34)$$

which is indeed the eigenvector matrix associated with the matrix in round brackets in Equation (30). According to Danusso (1910b), (R_A) and (S_A) can be determined as the total displacements of two simple pendulums with "elastic constants (similar to ω)" ξ and η , dragged at the foot, respectively, by the motions (also see Appendix I and Appendix II):

$$\begin{aligned} F_1(t) &= \frac{1}{A} [1 - \xi^2 m_2 (k_3 - k_2)] x(t) \\ F_2(t) &= \frac{1}{A} [1 - \eta^2 m_2 (k_3 - k_2)] x(t) \end{aligned} \quad (35)$$

Therefore, Danusso (1910b) clearly uncoupled the two expressions in Equation (26), without explaining how he acted. In order to uncouple the problem and diagonalize $[km]$, it is necessary to compute the matrix of the left eigenvectors—i.e., the eigenvectors of the transpose of the matrix in round brackets in Equation (30), or, equivalently, the columns of $[\phi]^{-1}$. Therefore, the matrix $[\psi]$ of left eigenvectors is equal to

$$[\psi] = \eta^2 \xi^2 \begin{bmatrix} -(\xi^2 k_3 m_2 - 1) & -(\eta^2 k_3 m_2 - 1) \\ \xi^2 k_2 m_2 & \eta^2 k_2 m_2 \end{bmatrix} \quad (36)$$

Let us consider the variable transformation

$$\{s\} = [\phi] \{R\} \quad (37)$$

with $\{R\}$ being the vector of new coordinates, and then pre-multiply by $[\psi]^T$ each term in Equation (26). Thus,

$$[\psi]^T [km] [\phi] \frac{d^2 R}{dt^2} + [\psi]^T [I] [\phi] R = [\psi]^T \{1\} x(t) \quad (38)$$

with $\{1\}$ being the vector of ones. The expressions in Equation (26) thus become

$$\begin{aligned} \frac{d^2 R_A}{dt^2} + \xi^2 R_A &= \xi^2 \eta^2 \xi^2 [1 - \xi^2 m_2 (k_3 - k_2)] x(t) \\ \frac{d^2 S_A}{dt^2} + \eta^2 S_A &= \eta^2 \eta^2 \xi^2 [1 - \eta^2 m_2 (k_3 - k_2)] x(t) \end{aligned} \quad (39)$$

Because $\eta^2 \xi^2 = 1/A$, the manipulation presented in Equation (35) is correct, and indeed Equation (39) can be regarded as equivalent to the already solved Equation (3). That is why Danusso (1910b) concluded that “the motion of each of the two masses of the double pendulum can be reduced to the linear combination of the motions of two ideal simple pendulums subjected to given base motions and characterised by given elastic constants”. Such a procedure falls fully within what is defined as modal analysis in standard textbooks (Page 159 of Meirovitch (1986)).

Danusso (1910b) did not quote any reference about how he solved the problem. The solution for self-adjoint problems had already been presented on Pages 360–365 of Kelvin and Tait (1867) and on Page 107 of Rayleigh (1877). Moreover, a German translation of both books, probably easier for Danusso to understand, was available (Kelvin and Tait, 1871; Rayleigh, 1879). Besides, the study of a three-degree-of-freedom system was already available in the Italian literature (Levi-Civita, 1896). As for problems that are not self-adjoint, at least from a mathematical point of view, the solution must have been known. Probably Danusso was more aware of the mathematics of the problem (Pages 327–366 of Lie (1888)) than of the previous treatments by Kelvin and Rayleigh; otherwise, he would have adopted a more synthetic and efficient symbolism, already present in the two Britons' very comprehensive treatises. He also did not develop any further a method in the direction of the response spectrum method. In any case, the methodology of Danusso was probably the first application of modal analysis to earthquake engineering.

Danusso (1910b) did not study explicitly the response of the double pendulum to the kind of ground motions previously considered. However, he presented a plot (Figure 4(b)), without specifying the values of the parameters and the ground motion he assumed. He stressed that “synchronism” happened for two different values of the abscissa and that “the curves of maximum accelerations of masses m_1 and m_2 reach a secondary minimum and then climb up again slowly, leaving to the designer of two-storey houses that freedom that we asked for since the beginning”.

Several attempts have been made to reproduce Figure 4(b). Defining

$$\rho_1 = \frac{\xi}{\alpha} ; \quad \rho_2 = \frac{\eta}{\alpha} \quad (40)$$

and

$$\mu_1 = \left| \frac{\ddot{S}_{A, \max}}{r\alpha^2} \right| ; \quad \mu_2 = \left| \frac{\ddot{S}_{B, \max}}{r\alpha^2} \right| \quad (41)$$

and considering a ground displacement time history $x(t) = r \sin \alpha t$, plots of Equation (41) have been computed, and some are presented in Figure 6. Although similar to Figure 4(b), they do not match it. These curves have been numerically worked out because the problem is undamped and seemingly it is impossible to calculate in closed form the response factors. It is perhaps noteworthy that Danusso did not present this plot again in his later papers, as he did with that in Figure 4(a).

DANUSSO'S LATER PAPERS AND HIS INFLUENCE

During September 1–6, 1930, Danusso attended the first international conference on concrete and reinforced concrete in Liege, Belgium. At the conference, he presented a paper on earthquake-resistant

constructions. A brief paper in French is included in the proceedings (Danusso, 1932), while a longer one was published in a volume containing the full version of all the Italian manuscripts (Danusso, 1931), which is the same as a previously published paper (Danusso, 1928) quoted on Page 580 of Freeman (1932).

In the 1928 paper, Danusso presents again the results obtained in 1909–1910 using a more effective symbolism and adding new results. In particular, he studies the case of a mass-spring system under an excitation that is the product of two sines or of a sine and a cosine function, showing that they are less dangerous than the ones previously studied. He then considers a system with n degrees of freedom, generalising the solution already found for the two degrees of freedom already shown and stressing again that “it is easy to recognise in the motion of any mass of an n -tuple pendulum a linear combination of the motions of n simple pendulums” (Danusso, 1928). Finally, he studies the case of an elastic prismatic and homogenous tower, which was later developed by Bertolini (1935).

In his last paper on earthquake-resistant constructions (Danusso, 1946), Danusso reconsiders the results previously obtained, uses a terminology more customary today when he writes of “eigenvalues”, and makes references to the works by T. Levi-Civita, Rayleigh, and G. Krall, but there are no significant new results. Apparently Danusso was not aware of the research developed in the meantime by Biot (1932, 1933, 1934) (Trifunac, 2003). This is proved also by his last study on building vibrations induced by machines, wind and earthquakes (Danusso, 1952), where he has summarized his and other researchers’ results.

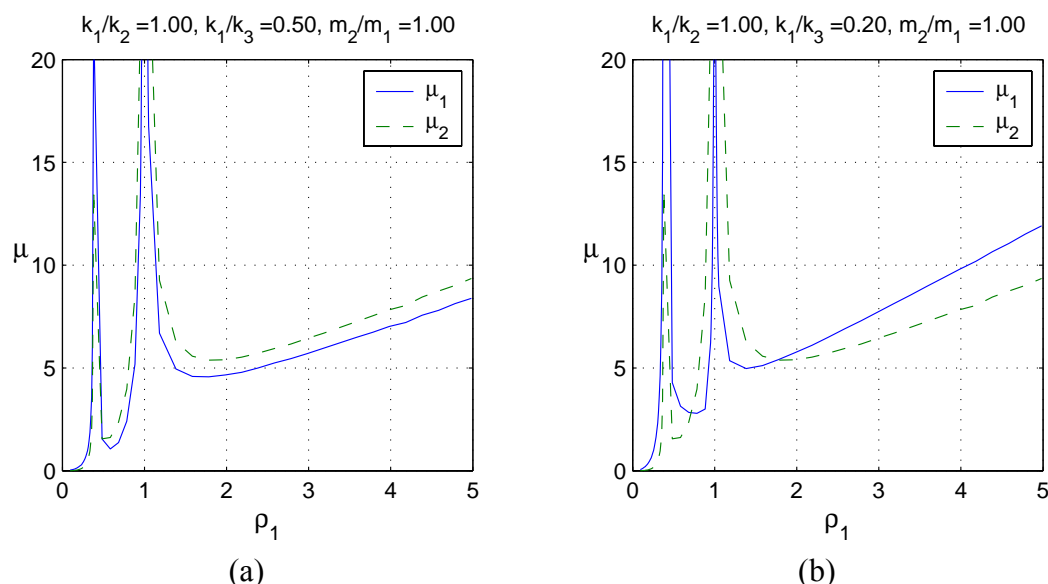


Fig. 6 Plot of Equation (41) for a shear-type frame with (a) floors with the same height, mass, and columns, and (b) with the lower floor stiffer than the other (in comparison with Figure 3(b))

All these papers show the continuous recurrence of a sincere interest in the topic, which was still something episodic in the Italian landscape of those years.

Danusso’s proposal, backed at the 12th Conference of Italian Engineers and Architects, to establish a permanent institute on “seismotecnica” studies (Anonymous, 1909f, 1909k) was not listened to (Danusso, 1912a, 1912b, 1915a). Similarly, his proposal to visit Yokohama after the 1923 Kanto earthquake was not funded (Cristina Danusso, personal communication). In contrast, after the 1923 event the Earthquake Research Institute was established in Japan (Reitherman, 2006a, 2006b). This partially explains the decay of studies on earthquake engineering in Italy for many decades. Other reasons were

- The death of some key figures: in 1914, Italo Maganzini (Luigi, 1914), President of the Committee appointed to write what then became the 1909 Royal Decree No. 193; and in 1918, Silvio Canevazzi (Revere, 1918a, 1918b), who worked with Modesto Panetti on that Decree (MLLP, 1909a) and then developed a simplified design method (Canevazzi, 1913a, 1913b; Page 579 of Freeman (1932)).

- The switch of interest of some others: Panetti was more and more attracted by aeronautics—probably he found that there was more glory there (Marzolo, 1957).
- The occurrence of the large January 15, 1915 Avezzano (Central Italy) earthquake when World War I had already started and a few months before Italy joined it. This event again raised some interest, resulting in some bulky publications (Masciari-Genoese, 1915; Alfani, 1915b; Anonymous, 1915b), but without the scientific impetus observed in 1909 (Danusso, 1915c, 1915d, 1915e, 1915f) and without the same extension as in 1909. As a matter of fact, in 1915 two papers were published in “Giornale del Genio Civile”, two in “Rivista di Ingegneria Sanitaria”, four in “Annali della Società degli Ingegneri e degli Architetti Italiani”, three in “Il Cemento”, and four in “Il Monitore Tecnico”.
- The appointment of a committee after that 1915 event with only one academic, Roman Cesare Ceradini, who was a member also of the 1909 committee (MLLPP, 1915).

Isolated papers or textbooks on earthquake engineering can be found during the 1920s and 1930s. For example, the July 23, 1930 Vulture earthquake (Pages 513–555 of Freeman (1932)) helped to revive attention to the subject.

Camillo Guidi showed a constant interest in earthquake-resistant construction, both studying earthquake effects (Guidi, 1925, 1926a), including applications to elastic frames in his textbooks (Guidi, 1926b, 1930), and performing possibly the first experimental tests in Italy on a reinforced concrete frame (Guidi, 1927), subjected to horizontal forces.

Danusso's work was certainly known. In his very successful reinforced concrete textbook, Santarella (1926) made reference on Pages 398–400 to Danusso's 1909 papers, although the examples presented in the case studies used the approach proposed in the code developed by Panetti.

Panetti (Page 157 of MLLPP (1913); Panetti, 1914, 1916) praises the achievements the Piedmont engineer made by means of dynamics. Panetti, commenting on a lightly amended version of Royal Decree 1909 (RI, 1913), suggested assuming a higher seismic coefficient for higher stiffness (Page 163 of MLLPP (1913)), but such an indication did not become part of the code and, therefore, its influence on practical design was negligible.

Priolo (1930, 1931) was aware of Danusso's 1909 papers and quotes his conclusions, although he states that at that time there was no experimental definition of the inertia acceleration as a function of the ratio between building frequency and ground motion frequency. Therefore, in the design examples in his works he follows the equivalent static procedure of the Italian seismic code. It was only after World War II that Priolo (1951) made reference to the dynamic behaviour of structures to guide their earthquake-resistant design. However, his work was then influenced by American literature.

Giannelli, in his textbook, briefly quotes Danusso's research and notes the importance of the dynamic issues in earthquake-resistant design (Page 120 of Giannelli (1932)). Although he presents the study of multi-degrees-of-freedom plane frames with an approach similar to that in Danusso (1928) and discusses the role of damping on the building periods, finding also the solution for damped vibrations under harmonic excitation, he does not present any example among the many numerical exercises he carries out.

Krall (1940) mentioned Danusso's work on Page xvi of Volume 1 and Page 422 of Volume 2, and considered explicitly earthquake-induced inertia forces in his proposed design of two steel power line pylons on the Messina strait (Krall, 1947, 1948; Priolo, 1948). However, the open competition for the final design and the construction of those towers was won by the Società Anonima di Elettificazione, whose leading consultant was Danusso (Anonymous, 1952, 1955, 1956; Toscano, 1958, 1960). The towers, built between 1952 and 1955, have a height of 224 m and a span of 3646 m, which was the world's largest at the time. In 1958 the public work was awarded by the Italian National Institution of Engineers and Architects (Anonymous, 1958).

Danusso started the design process in 1945. As for earthquake related issues, he modelled the structure as a two lumped masses system. Although a dominant period between 0.25 and 1.5 s was expected, Danusso designed the structure to withstand a transient harmonic excitation, lasting five pulses, with same period as that of the tower (2.5 s), and amplitude of 2.5 m/s^2 . He also performed shake-table tests on a 1:25 scale model.

As a recognition to Danusso's work in the field, he was asked to deliver the introductory keynote lecture in the Conference held in Messina for the 50th anniversary of the 1908 earthquake (Danusso,

1960; Anonymous, 1960a, 1960b). The conference was attended, among others, by G.W. Housner, L. Jacobsen, H. Kawasumi, K. Kubo, and K. Takeyama.

Danusso also used to hold lectures on earthquake-resistant constructions for a wider, not necessarily technical, audience, such as at Rotary meetings (Cristina Danusso, personal communication). However, as already mentioned, it was only in the mid-1970s that the stiffness of the structure was taken into account in the Italian seismic code, when a simplified design spectrum was introduced.

Even smaller was probably Danusso's international influence. Although Freeman was aware of the outline of his research, there is no evidence that M.A. Biot, at the time of Liege 1930 conference studying at Louvain (Belgium), had any knowledge (Biot, 1932, 1933, 1934). During the discussion following the Liege conference session in which Danusso's paper was presented, no reference was made to it, and apparently the only U.S. participant at the conference was C.C. Fishburn from the Bureau of Standards, Department of Commerce, Washington, D.C.

CONCLUSIONS

In the introduction to his 1910 papers, Arturo Danusso writes that "the studies on earthquake-resistant buildings until now, and with very few exceptions, produced a series of personal criteria, more or less empirical, which deserve nonetheless great respect, since a good building relies for three quarters on the designer's common sense and experience, but they do not suffice to solve scientifically the problem that nowadays interests all the Italians" (Danusso, 1910b). The research conducted by him after the 1908 Southern Calabria-Messina earthquake represents a major turning point in the field of earthquake engineering: Danusso was probably the first to propose a dynamic analysis method rather than static lateral force analysis method and to apply modal analysis. Moreover, he proved scientifically that seismic demand does not depend upon the ground motion characteristics alone. He showed that he possessed the mathematical knowledge to solve differential equations and their linear systems. His considerations about the need to account for the dynamic properties of a building in its design, and the fact that a linear elastic n -degrees-of-freedom system can be considered as equivalent to n single-degree-of-freedom oscillators, are right and of the greatest interest. However, his quantitative design recommendation suffered from the lack of reliable, strong ground motion recordings. Danusso's consideration of a ground motion "with an initial impact" perhaps looks as too severe, unless it is very close to the fault where the detailed nature of the ground motion cannot be predicted and large velocities can develop. Thus, his design recommendations already seemed exaggerated to Panetti (MLLPP, 1913) and Bertolini (Bertolini, 1935). Apparently the lack of systematic experimental research, both on buildings and on seismic ground motion, as well as the absence of interest within the academic community and the lack of practical applications of his mathematical results, caused the most advanced results of his research to be forgotten. All of these aspects show the importance of a constant and widespread effort to gain higher results, and how isolated, although excellent, achievements can be forgotten.

ACKNOWLEDGEMENTS

I would like to thank Professor Cristina Danusso De Pol, who kindly has given me access to her grandfather's biographical notes ("A Little History of Arturo"), the 45 pages typewritten by his daughter Eleonora, probably around 1963 and 1966. She also brought to my attention some of Danusso's late works I was not aware of. Moreover, I am deeply indebted to Professor Mihailo D. Trifunac, who kindly encouraged me to write this paper.

APPENDIX I: POSSIBLE MISPRINTS IN DANUSSO'S PAPERS

In the following are reported actual equations found in Danusso's papers. In this paper they have been interpreted as affected by misprints. The first expression in Equation (28) (also in Danusso, 1910a) was actually written as

$$\xi^2 = B - \frac{\sqrt{B^2 - 4A}}{2A} \quad (\text{A.1})$$

In Equation (26) (also in Danusso, 1910a) Danusso actually wrote

$$k_2 m_1 \frac{d^2 s_A}{dt_2} + \dots \quad (\text{A.2})$$

In Equation (35) (contrary to Danusso, 1910a) the second expression actually is

$$F_2(t) = \frac{1}{A} [1 - \eta^2 m_2 (k_3 - k_2) x(t)] \quad (\text{A.3})$$

APPENDIX II: CHANGES IN DANUSSO'S ORIGINAL SYMBOLS

Danusso's presentation has been retained herein almost every time, in order to make a complete assessment of his work possible. In particular, this makes it apparent how sometimes a much simpler and concise symbolism was still lacking.

However, in a few cases presented in this appendix his original symbols have been changed in order to avoid confusion or to translate them into English style.

On the right-hand side of Equation (3), Danusso writes $f(t)$ instead of $x(t)$. However, since he previously used the symbol f to indicate the deflection and previously referred to the ground displacement by means of symbol x , the latter has been preferred.

In Equations (4), (26), and (35), Danusso actually writes “sen” instead of “sin”, as is customary in the Italian language. In the spirit of an English presentation of his work, this has been translated as the other text quotations presented.

REFERENCES

1. Alfani, G. (1909a). “Riassunto delle Comunicazioni fatte al Congresso degli Ingegneri ed Architetti Italiani, Tenutosi a Firenze nell'Ottobre 1909”, *Giornale dei Lavori Pubblici e delle Strade Ferrate*, Vol. 36, No. 47, pp. 773–778 (in Italian).
2. Alfani, G. (1909b). “Le Vibrazioni e le Oscillazioni nei Fabbricati. Studi e Ricerche”, *Il Monitore Tecnico*, Vol. 15, No. 35, pp. 683–686; No. 36, pp. 704–707 (in Italian).
3. Alfani, G. (1909c). “Alcuni Studj sulle Vibrazioni Meccaniche dei Fabbricati”, *Proceedings of XII Congresso degli Ingegneri e Architetti Italiani*, Firenze, Italy, Vol. 1, p. 37, p. 131; Vol. 2, pp. 344–385 (in Italian).
4. Alfani, G. (1915a). “Le Vibrazioni nei Fabbricati Prodotte da Macchine in Movimento”, *Il Monitore Tecnico*, Vol. 21, No. 14, pp. 238–241 (in Italian).
5. Alfani, G. (1915b). “Ing. F. Masciari-Genoese—Trattato di Costruzioni Antisismiche, Preceduto da un Corso di Sismologia. (Ulrico Hoepli, Milano, 1915, Prezzo L. 24)”, *Il Monitore Tecnico*, Vol. 21, No. 28, p. 434 (in Italian).
6. Anonymous (1909a). “Programma del Concorso per Costruzioni Edilizie nelle Regioni Italiane Soggette a Movimenti Sismici”, *Il Cemento*, Vol. 5, No. 2, pp. 17–18 (in Italian).
7. Anonymous (1909b). “Concorso per Costruzioni Edilizie nelle Regioni Italiane Soggette a Movimenti Sismici”, *Il Cemento*, Vol. 5, No. 10, p. 158 (in Italian).
8. Anonymous (1909c). “L'esito del Concorso di Costruzioni per Regioni Sismiche”, *Il Cemento*, Vol. 5, No. 12, pp. 181–182 (in Italian).
9. Anonymous (1909d). “Relazione della Giuria del Concorso per Costruzioni Edilizie nelle Regioni Italiane Soggette a Movimenti Sismici Indetto dalla Società Cooperativa Lombarda di Lavori Pubblici sotto gli Auspici del Collegio degli Ingegneri ed Architetti di Milano”, *Il Cemento*, Vol. 5, No. 18, pp. 273–277; No. 19, pp. 292–297 (in Italian).
10. Anonymous (1909e). “XII Congresso degli Ingegneri e degli Architetti in Firenze nel 1909”, *Il Cemento*, Vol. 5, No. 10, pp. 158–160 (in Italian).
11. Anonymous (1909f). “Il XII Congresso degli Ingegneri e degli Architetti in Firenze (Ottobre 1909)”, *Il Cemento*, Vol. 6, No. 21, pp. 333–335 (in Italian).
12. Anonymous (1909g). “Programma del Concorso per Costruzioni Edilizie nelle Regioni Italiane Soggette a Movimenti Sismici”, *Il Monitore Tecnico*, Vol. 15, No. 2, p. 36 (in Italian).

13. Anonymous (1909h). "Le Deliberazioni della Giuria del Concorso per le Costruzioni Antisismiche Bandito dalla Cooperativa Lombarda dei Lavori Pubblici", *Il Monitore Tecnico*, Vol. 15, No. 18, p. 348 (in Italian).
14. Anonymous (1909i). "Relazione della Giuria del Concorso per Costruzioni Edilizie nelle Regioni Italiane Soggette a Movimenti Sismici Indetto dalla Società Cooperativa Lombarda di Lavori Pubblici sotto gli Auspici del Collegio degli Ingegneri ed Architetti di Milano", *Il Monitore Tecnico*, Vol. 15, No. 26, pp. 501–504; No. 27, pp. 522–526; No. 28, pp. 543–546 (in Italian).
15. Anonymous (1909j). "XII Congresso degli Ingegneri e Architetti Italiani, Firenze 1909. Concorso per Costruzioni Antisismiche", *Il Monitore Tecnico*, Vol. 15, No. 36, pp. 709–711 (in Italian).
16. Anonymous (1909k). "Concorso per Costruzioni Antisismiche Indetto dal Collegio Toscano degli Ingegneri e Architetti", *Proceedings of XII Congresso degli Ingegneri e Architetti Italiani, Firenze, Italy*, Vol. 1, pp. 9–10, p. 37, pp. 131–134; Vol. 2, p. 344, pp. 450–455 (in Italian).
17. Anonymous (1915a). "Congratulazioni a Danusso", *Il Cemento*, Vol. 12, No. 5, p. 65 (in Italian).
18. Anonymous (1915b). "Rivista di Libri. F. Masciari-Genoese. Trattato di Costruzioni Antisismiche", *Annali della Società degli Ingegneri e degli Architetti Italiani*, Vol. 30, No. 10, p. 234 (in Italian).
19. Anonymous (1952). "L'Inizio dei Lavori per l'Attraversamento dello Stretto di Messina con Elettrodotto a 220 kV", *L'Ingegnere*, Vol. 26, No. 3, pp. 269–277 (in Italian).
20. Anonymous (1955). "L'attraversamento dello Stretto di Messina di una linea a 220 kW", *Acciaio e Costruzioni Metalliche*, Vol. 7, No. 4, pp. 45 (in Italian).
21. Anonymous (1956). "L'attraversamento elettrico dello Stretto di Messina", *Acciaio e Costruzioni Metalliche*, Vol. 8, No. 3, pp. 118–122 (in Italian).
22. Anonymous (1958). "Le Giornate Siciliane dell'ANIAI. Il Premio ANIAI 1957 per l'Ingegneria Elettrotecnica Assegnato all'Elettrodotto sullo Stretto di Messina", *L'Ingegnere*, Vol. 32, No. 5, pp. 445–446 (in Italian).
23. Anonymous (1960a). "Convegno di Studi di Ingegneria Sismica Messina", *Costruzioni Metalliche*, Vol. 12, No. 1, p. 31 (in Italian).
24. Anonymous (1960b). "Resoconto del Convegno di Studi di Ingegneria Sismica (Messina, 10–13 Dicembre 1959)", *Il Cemento*, Vol. 57, No. 2, pp. 27–29 (in Italian).
25. Anonymous (1968). "Arturo Danusso Ingegnere", *Il Cemento*, Vol. 65, No. 11–12, p. 242 (in Italian).
26. Baratta, M. (1910). "La Catastrofe Sismica Calabro Messinese (28 Dicembre 1908)", *Società Geografica Italiana, Rome, Italy* (in Italian).
27. Bertero, V.V. and Bozorgnia, Y. (2004). "The Early Years of Earthquake Engineering and Its Modern Goal" in "Earthquake Engineering: From Engineering Seismology to Performance-Based Engineering (edited by Y. Bozorgnia and V.V. Bertero)", CRC Press, London, U.K.
28. Bertolini, I. (1935). "Sulla Statica Sismica delle Torri. Degli Spostamenti Sismici nelle Torri a Sezione Costante", *Il Politecnico*, Vol. 83, No. 6, pp. 341–352; No. 7, pp. 407–416; No. 10, pp. 569–580 (in Italian).
29. Biot, M.A. (1932). "Transient Oscillations in Elastic System", Ph.D. Thesis No. 259, Aeronautics Department, California Institute of Technology, Pasadena, U.S.A.
30. Biot, M.A. (1933). "Theory of Elastic Systems Vibrating under Transient Impulse with an Application to Earthquake-Proof Buildings", *Proceedings of the National Academy of Sciences of the United States of America*, Vol. 19, No. 2, pp. 262–268.
31. Biot, M.A. (1934). "Theory of Vibration of Buildings during Earthquakes", *Zeitschrift für Angewandte Mathematik und Mechanik*, Vol. 14, No. 4, pp. 213–223.
32. Canevazzi, S. (1913a). "Note di Edilizia Antisismica", *Il Cemento*, Vol. 10, No. 13, pp. 195–197; No. 14, pp. 211–215; No. 15, pp. 228–231; No. 17, pp. 260–262; No. 18, pp. 275–277 (in Italian).
33. Canevazzi, S. (1913b). "Note di Edilizia Antisismica", *Gamberini e Parmeggiani, Bologna, Italy* (in Italian).
34. Chopra, A.K. (1995). "Dynamics of Structures: Theory and Applications to Earthquake Engineering", Prentice Hall, Upper Saddle River, U.S.A.
35. Danusso, A. (1909a). "Le Case che non Crollano (A Proposito del Terremoto Calabro-Siculo)", *Il Cemento*, Vol. 5, No. 1, pp. 4–9 (in Italian).

36. Danusso, A. (1909b). "Il Problema delle Case nei Paesi del Terremoto", *Il Cemento*, Vol. 5, No. 2, pp. 18–19 (in Italian).
37. Danusso, A. (1909c). "I Progetti Premiati al Concorso per Costruzioni Edilizie nelle Regioni Italiane Soggette a Movimenti Sismici. Le Costruzioni Antisismiche (Ing. A. Danusso)", *Il Monitore Tecnico*, Vol. 15, No. 22, pp. 423–428 (in Italian).
38. Danusso, A. (1909d). "La Statica delle Costruzioni Antisismiche", *Il Monitore Tecnico*, Vol. 15, No. 33, pp. 641–645 (in Italian).
39. Danusso, A. (1909e). "I Progetti Premiati al Concorso per Costruzioni Edilizie nelle Regioni Italiane Soggette a Movimenti Sismici. Le Costruzioni Antisismiche", *Il Cemento*, Vol. 6, No. 16, pp. 241–249 (in Italian).
40. Danusso, A. (1909f). "La Statica delle Costruzioni Antisismiche", *Il Cemento*, Vol. 6, No. 24, pp. 369–373 (in Italian).
41. Danusso, A. (1909g). "Contributo al Calcolo delle Fondazioni Continue in Cemento Armato", *Il Cemento*, Vol. 5, No. 3, pp. 36–41; No. 4, pp. 51–55; No. 5, pp. 68–71; No. 7, pp. 100–103; No. 8, pp. 116–119; No. 10, pp. 145–147 (in Italian).
42. Danusso, A. (1910a). "La Statica delle Costruzioni Antisismiche", *Giornale dei Lavori Pubblici e delle Strade Ferrate*, Vol. 37, No. 6, pp. 94–97; No. 7, pp. 113–114; No. 8, pp. 131–132; No. 9, pp. 148–151 (in Italian).
43. Danusso, A. (1910b). "La Statica delle Costruzioni Antisismiche: Comunicazione Svolta nel 12 Congresso degli Ingegneri ed Architetti in Firenze nell'Ottobre del 1909", *Tipografia dell'Unione Editrice*, Rome, Italy (in Italian).
44. Danusso, A. (1912a). "La Revisione delle Norme Asismiche Ministeriali", *Il Monitore Tecnico*, Vol. 18, No. 10, pp. 183–184 (in Italian).
45. Danusso, A. (1912b). "La Revisione delle Norme Asismiche Ministeriali", *Il Cemento*, Vol. 9, No. 8, pp. 114–115 (in Italian).
46. Danusso, A. (1915a). "Il Terremoto", *Il Cemento*, Vol. 12, No. 2, pp. 17–19 (in Italian).
47. Danusso, A. (1915b). "Lettera al Direttore", *Il Cemento*, Vol. 12, No. 6, p. 81 (in Italian).
48. Danusso, A. (1915c). "F. Masciari-Genoese. Trattato di Costruzioni Antisismiche. Preceduto da un Corso di Sismologia—con 900 Figure nel Testo e 1002 Pagine. U. Hoepli—Milano", *Il Cemento*, Vol. 12, No. 6, pp. 92–93 (in Italian).
49. Danusso, A. (1915d). "Bibliografia", *Il Monitore Tecnico*, Vol. 21, No. 30, pp. 463–464 (in Italian).
50. Danusso, A. (1915e). "Per la Dignità della Letteratura Scientifica", *Giornale del Genio Civile*, Vol. 53, pp. 488–489 (in Italian).
51. Danusso, A. (1915f). "Per la Dignità della Letteratura Scientifica", *Il Cemento*, Vol. 12, No. 11, pp. 145–146 (in Italian).
52. Danusso, A. (1916). "Noi e i Tedeschi", *Il Monitore Tecnico*, Vol. 22, No. 9, pp. 125–127 (in Italian).
53. Danusso, A. (1919). "Sul Calcolo delle Ossature che Sopportano Macchinari e Trasmissioni. Un Caso di Sincronismo", *Il Cemento*, Vol. 16, No. 2, pp. 8–11 (in Italian).
54. Danusso, A. (1927). "Notizie Sull'Impiego della Matematica negli Ordinari Problemi della Scienza delle Costruzioni", *Rendiconti del Seminario Matematico e Fisico di Milano*, Vol. 1, pp. 91–116 (in Italian).
55. Danusso, A. (1928). "Sulla Statica delle Costruzioni Antisismiche", *Rendiconti del Seminario Matematico e Fisico di Milano*, Vol. 2, pp. 175–199 (in Italian).
56. Danusso, A. (1931). "Sulla Statica delle Costruzioni Asismiche", *Proceedings of La Partecipazione Italiana al Primo Congresso Internazionale del Beton Semplice ed Armato, Liegi settembre 1930*, *Tipografia del Senato*, Rome, Italy, pp. 55–78 (in Italian).
57. Danusso, A. (1932). "Le Calcul Statique des Constructions Asismiques", *Proceedings of Premier Congrès International du Béton et du Béton Armé, Liege, Belgium*, Vol. 1, pp. 310–312 (in French).
58. Danusso, A. (1937). "In Memoria di G.A. Porcheddu", *Il Cemento Armato*, Vol. 34, No. 11, p. 185 (in Italian).
59. Danusso, A. (1946). "Costruzioni Asismiche" in "Tecnica del Cemento Armato (edited by G. Albenga)", *Edizioni della Bussola*, Rome, Italy (in Italian).

60. Danusso, A. (1952). "Vibrazioni degli Edifici" in "Lezioni sulle Vibrazioni Meccaniche (edited by B. Finzi)", Tamburini, Milan, Italy, pp. 133–152 (in Italian).
61. Danusso, A. (1954a). "Sul Calcolo delle Ossature che Sopportano Macchinari e Trasmissioni. Un Caso di Sincronismo", *Il Cemento*, Vol. 51, No. 10, pp. 2–5 (in Italian).
62. Danusso, A. (1954b). "Vibrazioni degli Edifici", *Il Cemento*, Vol. 51, No. 12, pp. 2–11 (in Italian).
63. Danusso, A. (1957). "Inaugurazione del Symposium su la Plasticità nella Scienza delle Costruzioni in Onore di Arturo Danusso. Milano, 25 Settembre 1956", Zanichelli, Bologna, Italy (in Italian).
64. Danusso, A. (1960). "Nel Cinquantenario del Terremoto di Messina", *Il Cemento Armato*, Vol. 57, No. 1, pp. 3–6 (in Italian).
65. Danusso, A. (1978). "La Scienza e lo Spirito negli Scritti di Arturo Danusso", Morcelliana, Brescia, Italy (in Italian).
66. Danusso, A. and Ceruti, G. (1935). "Costruzioni: Concetti Teorici Fondamentali e Criteri di Pratica Applicazione", Principato, Messina, Italy (in Italian).
67. D'Aquino, U. (1986). "Danusso Arturo" in "Dizionario Biografico degli Italiani (edited by G. Alessi)", Istituto dell'Enciclopedia Italiana, Rome, Italy (in Italian).
68. Desideri, P., Nervi, P., Jr. and Positano, G. (editors) (1979). "Pier Luigi Nervi", Zanichelli, Bologna, Italy (in Italian).
69. Di Pasquale, G., Fralleone, A., Pizza, A.G. and Serra, C. (2000). "L'evoluzione della Normativa Sismica" in "La Classificazione e la Normativa Sismica dal 1909 al 1984 (edited by R. De Marco)", Istituto Poligrafico e Zecca dello Stato, Rome, Italy (in Italian).
70. Finzi, B. (editor) (1952). "Lezioni sulle Vibrazioni Meccaniche", Tamburini, Milano, Italy (in Italian).
71. Freeman, J.R. (1932). "Earthquake Damage and Earthquake Insurance", McGraw-Hill, New York, U.S.A.
72. Giannelli, A. (1932). "Lezioni sui Telai Elastici Piani", Tipografia del Senato, Rome, Italy (in Italian).
73. Giuffrè, A. (1987). "Cento Anni di Norme Sismiche Italiane", *Ingegneria Sismica*, Vol. 4, No. 2, pp. 13–18 (in Italian).
74. Grandori, G. (1967). "Theory of Earthquake Engineering", International Center of Earthquake Engineering, Milan, Italy; ISMES, Bergamo, Italy.
75. Guidi, C. (1925). "Costruzioni Antisismiche", *Annali dei Lavori Pubblici*, Vol. 63, No. 3, pp. 263–264 (in Italian).
76. Guidi, C. (1926a). "Costruzioni Antisismiche", *Il Cemento Armato*, Vol. 23, No. 3, pp. 32–33 (in Italian).
77. Guidi, C. (1926b). "Esercizi Sulla Scienza delle Costruzioni. Quarta Edizione con Appendice", Tip. V. Bona, Turin, Italy (in Italian).
78. Guidi, C. (1927). "Studi Sperimentali su Costruzioni in Cemento Armato", *Il Cemento Armato*, Vol. 24, No. 2, pp. 9–14; No. 3, pp. 23–30 (in Italian).
79. Guidi, C. (1930). "Telai Antisismici", Tipografia del Senato, Rome, Italy (in Italian).
80. Housner, G.W. (1984). "Historical View of Earthquake Engineering", *Proceedings of the Eighth World Conference on Earthquake Engineering*, San Francisco, U.S.A., Post-Conference Volume, pp. 25–39.
81. Hudson, D.E. (1983). "Golden Anniversary Workshop on Strong-motion Seismometry, March 30–31", Department of Civil Engineering Report, University of Southern California, Los Angeles, U.S.A.
82. Iori, T. (2001). "Il Cemento Armato in Italia: dalle Origini alla Seconda Guerra Mondiale", EdilStampa, Rome, Italy (in Italian).
83. Kelvin, W.T. and Tait, P.G. (1867). "Treatise on Natural Philosophy", Oxford University Press, Oxford, U.K.
84. Kelvin, W.T. and Tait, P.G. (1871). "Handbuch der Theoretischen Physik", Vieweg, Braunschweig, Germany (in German).
85. Krall, G. (1940). "Meccanica Tecnica delle Vibrazioni", Eredi V. Veschi, Rome, Italy (in Italian).

86. Krall, G. (1947). "Meccanica Asismica delle Torri", Rendiconti dell'Accademia Nazionale dei Lincei. Classe di Scienze Fisiche, Matematiche e Naturali, Ser. 8, Vol. 3, No. 2, pp. 3–11 (in Italian).
87. Krall, G. (1948). "Un Progetto di Torri-Piloni alte 200 m. per l'Attraversamento dello Stretto di Messina con Linea Aerea a 200 kV. e Questioni Generali di Asismica", Ingegneria Ferroviaria, Vol. 3, No. 2, pp. 89–100 (in Italian).
88. Levi-Civita, T. (1896). "Sul Moto dei Sistemi con Tre Gradi di Libertà", Rendiconti dell'Accademia dei Lincei, Ser. 5, Vol. 5, No. 2, pp. 164–171 (in Italian).
89. Lie, S. (1888). "Theorie der Transformationsgruppen", BG Teubner, Leipzig, Germany (in German).
90. Losio, C. (1909). "XII Congresso Degli Ingegneri e Architetti in Firenze", Rivista di Ingegneria Sanitaria, Vol. 5, No. 20, pp. 319–325 (in Italian).
91. Luiggi, L. (1914). "Necrologio del Prof. Ing. Comm. Italo Maganzini", Annali della Società degli Ingegneri e degli Architetti Italiani, Vol. 29, No. 9, pp. 201–206 (in Italian).
92. Manfredini, A. (1909a). "I Danni del Terremoto e le Nuove Costruzioni nelle Zone Colpite. Una Lodevolissima Iniziativa della Cooperativa Lombarda delle Opere Pubbliche", Il Monitore Tecnico, Vol. 15, No. 1, pp. 1–2 (in Italian).
93. Manfredini, A. (1909b). "Due Concorsi Tecnici a Milano: L'Esposizione dei Modelli di Agganciato Automatico ai Veicoli Ferroviari e l'Esposizione dei Progetti per le Costruzioni Antisismiche—Il Concorso per il Nuovo Palazzo Municipale di Messina e quello per la Nuova Facciata della Stazione di Milano", Il Monitore Tecnico, Vol. 15, No. 12, pp. 221–223 (in Italian).
94. Manfredini, A. (1909c). "Deliberazioni della Giuria nel Concorso delle Costruzioni Antisismiche Bandito dalla Cooperativa Lombarda dei Lavori Pubblici", Il Monitore Tecnico, Vol. 15, No. 18, pp. 341–342 (in Italian).
95. Manfredini, A. (1909d). "XII Congresso degli Ingegneri e Architetti in Firenze", Il Monitore Tecnico, Vol. 15, No. 28, pp. 542–543 (in Italian).
96. Marletta, R. (1934). "Il Terremoto del 10 Marzo 1933 a Long Beach", Annali dei Lavori Pubblici, Vol. 12, No. 9, pp. 745–778 (in Italian).
97. Marzolo, F. (1957). "Modesto Panetti: Commemorazione", Ministero della Pubblica Istruzione, Consiglio Superiore della P.I., Tip. S. Pancrazio, Rome, Italy (in Italian).
98. Masciari-Genoese, F. (1915). "Trattato di Costruzioni Antisismiche Preceduto da un Corso di Sismologia", Hoepli, Milan, Italy (in Italian).
99. Meirovitch, L. (1986). "Elements of Vibration Analysis", McGraw-Hill, New York, U.S.A.
100. MLLPP (1909a). "Relazione della Commissione Incaricata di Studiare e Proporre Norme Edilizie Obbligatorie per i Comuni Colpiti dal Terremoto del 28 Dicembre 1908 e da Altri Anteriori", Report, Ministero dei Lavori Pubblici, Rome, Italy; Giornale del Genio Civile, Vol. 47, No. 4, pp. 197–294 (in Italian).
101. MLLPP (1909b). "Circolare Esplicativa delle Norme Inviata ai Prefetti, ai Sindaci, ai Presidenti delle Deputazioni Provinciali, agli Ingegneri del Genio Civile e agli Uffici Tecnici di Finanza", Circolare No. 2664, Ministero dei Lavori Pubblici, Direzione Generale dei Servizi Speciali—Sezione Terremoto, Div. 13, Rome, Italy; Bollettino Ufficiale del Ministero dei Lavori Pubblici, Vol. 10, No. 13, pp. 593–623; L'Ingegneria Ferroviaria, Vol. 6, No. 9, pp. 12–14 (in Italian).
102. MLLPP (1913). "Seconda Relazione della Commissione Incaricata di Rivedere le Norme Edilizie Obbligatorie per i Comuni Colpiti dal Terremoto del 28 Dicembre 1908 e da Altri Anteriori: Istruzioni Tecniche, Metodi di Calcolo, Applicazioni", Report, Ministero dei Lavori Pubblici, Rome, Italy; Giornale del Genio Civile, Vol. 51, No. 10, pp. 545–697 (in Italian).
103. MLLPP (1915). "Relazione del Comitato Speciale del Consiglio dei Lavori Pubblici Incaricato di Studiare e Proporre Norme Edilizie Obbligatorie per i Comuni Colpiti dal Terremoto del 13 Gennaio 1915", Report, Ministero dei Lavori Pubblici, Rome, Italy (in Italian).
104. MLLPP (1921). "Comitato Speciale per le Costruzioni nei Paesi Colpiti dal Terremoto. Esempi di Calcolo di Edifici a Tre Piani nelle Regioni Sismiche", Report, Ministero dei Lavori Pubblici, Rome, Italy; Bollettino Ufficiale del Ministero dei Lavori Pubblici, Vol. 22, No. 25, pp. 1596–1608 (in Italian).

105. MLLPP (1975). "Approvazione delle Norme Tecniche per le Costruzioni in Zone Sismiche", Decreto Ministeriale No. 39, Ministero dei Lavori Pubblici, Rome, Italy; Gazzetta Ufficiale della Repubblica Italiana, Vol. 116, No. 93, pp. 1–7 (in Italian).
106. Novelli, L. (1909). "Impressioni sul Concorso per Costruzioni Antisismiche di Milano", *L'Ingegneria Ferroviaria*, Vol. 6, No. 20, pp. 344–347 (in Italian).
107. Panetti, M. (1914). "Sulla Tecnica delle Costruzioni Asismiche. Comunicazione dell'ing. Modesto Panetti Fatta nella Seduta del 26 Giugno 1914. Estratto dagli Atti della Società degli Ingegneri e degli Architetti di Torino", Tip. P. Celanza e C., Turin, Italy (in Italian).
108. Panetti, M. (1916). "I Progressi della Dinamica nella Tecnica dell'Ingegnere. Estratto dagli Atti della Società Italiana per il Progresso delle Scienze. VIII Riunione—Roma, Marzo 1916", Società Italiana per il Progresso delle Scienze, Rome, Italy (in Italian).
109. Priolo, D.A. (1930). "Le Costruzioni Antisismiche: Manuale Pratico con Esempi Numerici Completi di Calcolo per Edifici Ordinari, Chiese ad Una e Tre Navate", G. Principato, Messina, Italy (in Italian).
110. Priolo, D.A. (1931). "Cenni sulle Costruzioni Antisismiche", *Il Politecnico*, Vol. 79, No. 10, pp. 601–610 (in Italian).
111. Priolo, D.A. (1948). "Sui Criteri più Idonei per il Progetto di Alti Piloni Metallici in Zone Sismiche. Strutture Geodetiche", *Giornale Genio Civile*, Vol. 86, No. 9, pp. 488–501 (in Italian).
112. Priolo, D.A. (1951). "Dinamica delle Costruzioni Antisismiche", Ed. del Giornale del Genio Civile, Rome, Italy (in Italian).
113. Rayleigh, J.W.S. (1877). "The Theory of Sound", MacMillan, London, U.K.
114. Rayleigh, J.W.S. (1879). "Die Theorie des Schalles", Vieweg, Braunschweig, Germany (in German).
115. Rayleigh, J.W.S. (1894). "The Theory of Sound", MacMillan, London, U.K.
116. Reitherman, R. (2006a). "The Effects of the 1906 Earthquake in California on Research and Education", *Earthquake Spectra*, Vol. 22, No. S2, pp. S207–S236.
117. Reitherman, R. (2006b). "Earthquakes That Have Initiated the Development of Earthquake Engineering", *Bulletin of the New Zealand Society for Earthquake Engineering*, Vol. 39, No. 3, pp. 145–147.
118. Revere, G. (1918a). "Prof. Ing. Silvio Canevazzi", *Il Monitore Tecnico*, Vol. 24, No. 8, p. 63 (in Italian).
119. Revere, G. (1918b). "Necrologio [Silvio Canevazzi]", *Il Cemento*, Vol. 15, No. 4, pp. 37–38 (in Italian).
120. RI (1909). "Norme Tecniche ed Igieniche Obbligatorie per le Riparazioni, Ricostruzioni e Nuove Costruzioni degli Edifici Pubblici e Privati nei Comuni Colpiti dal Terremoto del 28 Dicembre 1908 e da Altri Precedenti", Regio Decreto No. 193, Regno d'Italia, Rome, Italy; Gazzetta Ufficiale del Regno d'Italia, Vol. 50, No. 95, pp. 1957–1962 (in Italian).
121. RI (1912). "Norme Obbligatorie per le Riparazioni, Ricostruzioni e Nuove Costruzioni degli Edifici nei Comuni Colpiti dal Terremoto, in Sostituzione di Quelle Approvate col R. D. 18 Aprile 1909, N. 193", Regio Decreto No. 1080, Regno d'Italia, Rome, Italy; Gazzetta Ufficiale del Regno d'Italia, Vol. 53, No. 247, pp. 6037–6042 (in Italian).
122. RI (1913). "Testo Unico delle Leggi Emanate in Conseguenza del Terremoto del 28 Dicembre 1908", Regio Decreto No. 1261, Regno d'Italia, Rome, Italy; Gazzetta Ufficiale del Regno d'Italia, Vol. 54, No. 290, pp. 1–33 (in Italian).
123. Santarella, L. (1926). "Il Cemento Armato nelle Costruzioni Civili ed Industriali", Hoepli, Milan, Italy (in Italian).
124. Tibiletti Marchionna, C. (1997). "Il Seminario Matematico e Fisico di Milano (1927–1996)", *Rendiconti del Seminario Matematico e Fisico di Milano*, Vol. 67, pp. 27–47 (in Italian).
125. Timoshenko, S.P. (1928). "Vibration Problems in Engineering", Van Nostrand, New York, U.S.A.
126. Toscano, A.M. (1958). "L'Attraversamento Elettrico dello Stretto di Messina", Dedalo, Rome, Italy (in Italian).
127. Toscano, A.M. (1960). "Le Torri di Messina", *Costruzioni Metalliche*, Vol. 12, No. 5, pp. 205–225 (in Italian).

128. Trifunac, M.D. (2003). "23rd ISET Annual Lecture: 70-th Anniversary of Biot Spectrum", ISET Journal of Earthquake Technology, Vol. 40, No. 1, pp. 19–50.
129. Uang, C.M. and Bertero, V.V. (1990). "Evaluation of Seismic Energy in Structures", Earthquake Engineering & Structural Dynamics, Vol. 19, No. 1, pp. 77–90.
130. von Kármán, T. and Biot, M.A. (1940). "Mathematical Methods in Engineering", McGraw-Hill, New York, U.S.A.

RESPONSE SPECTRA AS A USEFUL DESIGN AND ANALYSIS TOOL FOR PRACTICING STRUCTURAL ENGINEERS

Sigmund A. Freeman

Wiss, Janney, Elstner Associates, Inc.
2200 Powell Street, Suite 925
Emeryville, CA 94608, U.S.A.

ABSTRACT

Although response spectra have been in general use for decades by researchers, academics, and geotechnical professionals, their use by structural design professionals has generally been limited. However, as response spectra and dynamic analysis are being included within the newer building codes and as performance-based design (PBD) techniques are becoming acceptable, there is a need for the design professional to more clearly understand the meaning and usefulness of response spectra. The purpose of this paper is to review the concept of response spectra for design engineers not familiar with their significance and to summarize a variety of uses that can be applied for purposes such as rapid evaluation for a large inventory of buildings, performance verification of new construction, evaluation of existing structures for seismic vulnerability, and post earthquake estimates of potential damage of buildings.

KEYWORDS: Response Spectra, Building Codes, Performance-Based Design, Seismic Vulnerability, Earthquake Intensity

INTRODUCTION

The concept of response spectra was first incorporated into the United States building codes in the late 1950's by means of the coefficient C in the lateral force equation $V = KCW$ by the Structural Engineers Association of California (SEAO, 1960), where V is the total lateral force, K is a structural systems coefficient of 1.33, 1.0 or 0.67, and W is the total dead load. Over the decades, response spectra have been playing an increasing role in the development of earthquake design criteria. Much of this is due to research and the vast data obtained from recording earthquake motion from earthquakes in California, such as 1971 San Fernando, 1989 Loma Prieta, and 1994 Northridge, as well as from earthquakes worldwide.

The paper traces the development of building code provisions and the relationship to response spectra. Response spectra used for design tend to be smooth curves, whereas response spectra obtained from ground motion recordings are generally very ragged with sharp spikes and valleys. The effects of these differences are discussed along with recommendations on how to graphically smooth out the curves. In general, response spectra are used to analyze structures that respond within elastic-linear limits. The paper presents methods of using response spectra to evaluate structural response in the inelastic-nonlinear range. This includes easy to use graphical methods that compare the seismic demand represented by a response spectrum to the capacity of the structure represented by pushover force-displacement curves. Such methods are the capacity spectrum method (CSM) developed by the author (Freeman et al., 1975) as well as modifications (ATC, 1996; FEMA, 2005; Freeman, 2006), and procedures presented by others (Fajfar, 1998; Priestley et al., 1996). Other uses of response spectra include the development of an earthquake engineering intensity scale (EEIS) that extends the TriNet instrumental intensity scale (Wald et al., 1999) to estimate damage levels for a variety of building types.

INTRODUCTION TO RESPONSE SPECTRA

Response spectra provide a very handy tool for engineers to quantify the demands of earthquake ground motion on the capacity of buildings to resist earthquakes. Data on past earthquake ground motion is generally in the form of time-history recordings obtained from instruments placed at various sites that are activated by sensing the initial ground motion of an earthquake. The amplitudes of motion can be

expressed in terms of acceleration, velocity and displacement. The first data reported from an earthquake record is generally the peak ground acceleration (PGA) which expresses the tip of the maximum spike of the acceleration ground motion (Figure 1).

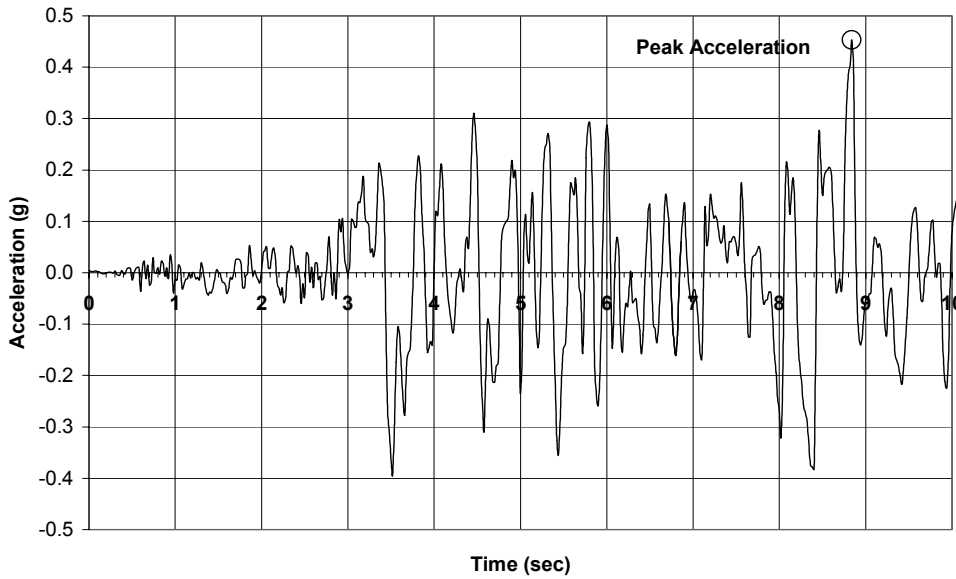


Fig. 1 Recorded ground motion (Holiday Inn, Van Nuys 1994, 270 degrees: 0–10 sec)

Although useful to express the relative intensity of the ground motion (i.e., small, moderate or large), the PGA does not give any information regarding the frequency (or period) content that influences the amplification of building motion due to the cyclic ground motion. In other words, tall buildings with long fundamental periods of vibration will respond differently than short buildings with short periods of vibration. Response spectra provide these characteristics. Picture a field of lollipop-like structures of various heights and sizes stuck in the ground. The stick represents the stiffness (K^*) of the structure and the lump at the top represents the mass (M^*). The period of this idealized single-degree-of-freedom (SDOF) system is calculated by the equation:

$$T = 2\pi(M^* / K^*)^{1/2} \quad (1)$$

If the peak acceleration (S_a) of each of these SDOF systems, when subjected to an earthquake ground motion, is calculated and plotted with the corresponding period of vibration (T), the locus of points will form a response spectrum for the subject ground motion. Thus, if the period of vibration is known, the maximum acceleration can be determined from the plotted curve. When calculating response spectra, a nominal percentage of critical damping is applied to represent viscous damping of a linear-elastic system, typically five-percent.

Response spectra can be plotted in a variety of formats. A format commonly used in the 1960s was the tripartite logarithmic plot, where the vertical scale is spectral velocity (S_v) and the horizontal scale is T in seconds or frequency (f) in Hertz. On diagonal lines are designated S_a and spectral displacement (S_d). An example is shown in Figure 2.

Mathematical relationships between the components of response spectra are given by the following equations:

$$S_v = (T / 2\pi) S_a \quad (2)$$

$$S_a = (2\pi / T) S_v \quad (3)$$

$$S_d = (T / 2\pi) S_v = S_a (T / 2\pi)^2 \quad (4)$$

$$f = 1 / T \quad (5)$$

Figure 3 shows other graphical formats used to represent response spectra. Figure 3(a) is known as the ADRS format (Mahaney et al., 1993) that plots S_a versus S_d and shows the period, T , as radial lines. Curved lines representing S_v can also be added (not shown, see Figure 4(b)). ADRS is essentially the

tripartite format in a rotated linear coordinate system. Figure 3(b) is the commonly used S_a versus T coordinate system. When S_d is the unit of interest, the S_d versus T format can be used (Figure 3(c)). The relationships among these curves are consistent with the equations listed above, which define S_v as a pseudo velocity.

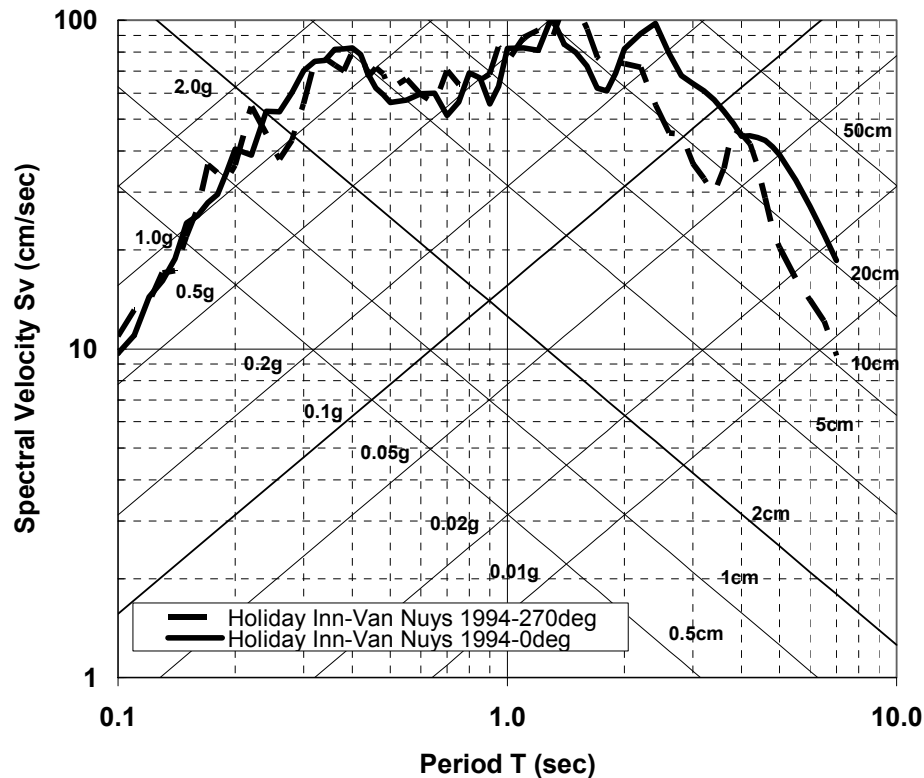
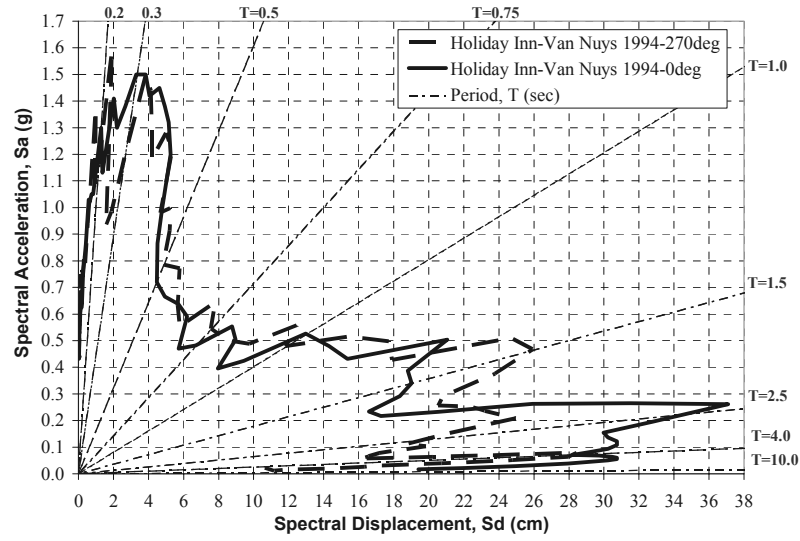


Fig. 2 Tripartite (logarithmic) response spectra

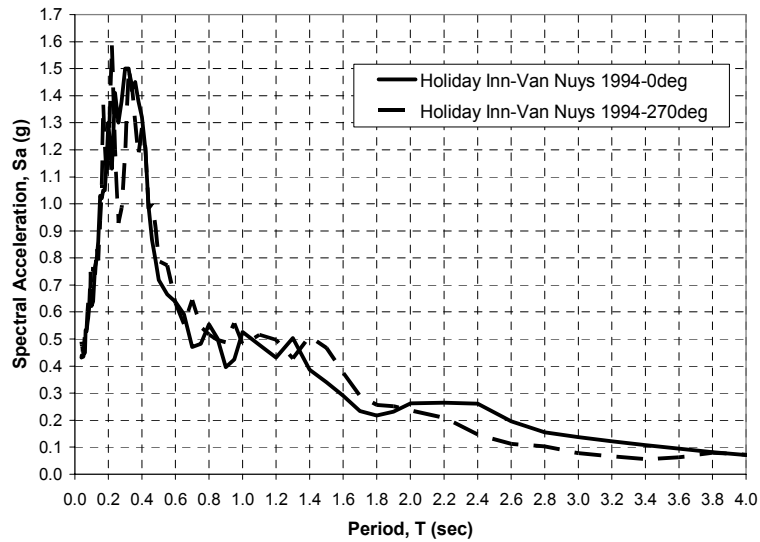
The response spectra shown in Figures 2 and 3 represent the ground motion recorded at the ground level of the Holiday Inn hotel structure during the Northridge earthquake of January 1994 in California, U.S.A. The continuous curves represent the horizontal motion in the 0-degree direction and the dashed curves represent the horizontal orthogonal motion in the 270-degree direction. Vertical motion was also recorded (not shown). Ground motion, as well as building motion, was recorded for many other locations during the Northridge event. Response spectra have also been obtained during the 1971 San Fernando earthquake as well as from other earthquakes in the Los Angeles, California area. This data bank, as well as data from earthquakes from all over the world, provides useful tools for studying the effects of earthquake ground motion on building structures and for the development of code provisions for the design of buildings.

It is observed that the response spectra shown in Figures 2 and 3 are rather jagged with sharp peaks and valleys; and there are significant variations in the two directions of motion. It can also be shown that there are large variations in ground motion characteristics at other sites for the same earthquake, as well as for the same site from other earthquakes. The peaks and valleys illustrate the sensitivity of the response of structures to a slight variation in the natural period of vibration. The large variations in ground motion characteristics illustrate the difficulties in accurately predicting demands of future earthquakes. This leads us to the challenge to develop standard response spectra that give a reasonable probability of having credible design provisions.

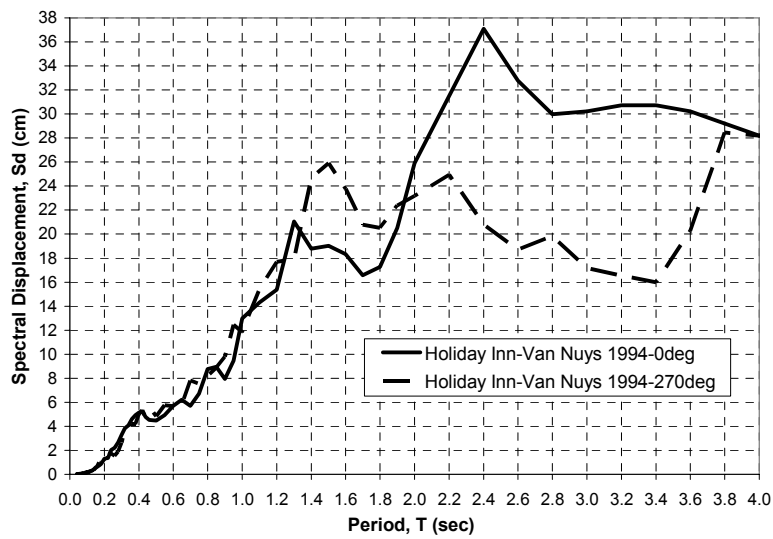
Methods of constructing smooth response spectra for design purposes have been developed to compensate for the peaks, valleys, and shape variations in actual response spectra; for example, the use of a constant S_a for short periods of response, constant S_v for the mid range, and constant S_d for long period response to develop probabilistic design spectra (Newmark and Hall, 1982; Newmark et al., 1973). An example of smooth spectra is shown in Figure 4 based on a building code design response spectrum for a site of high seismicity.



(a)



(b)



(c)

Fig. 3 Response spectra formats (Holiday Inn, Van Nuys 1994): (a) ADRS format, (b) S_a versus T format, (c) S_d versus T format

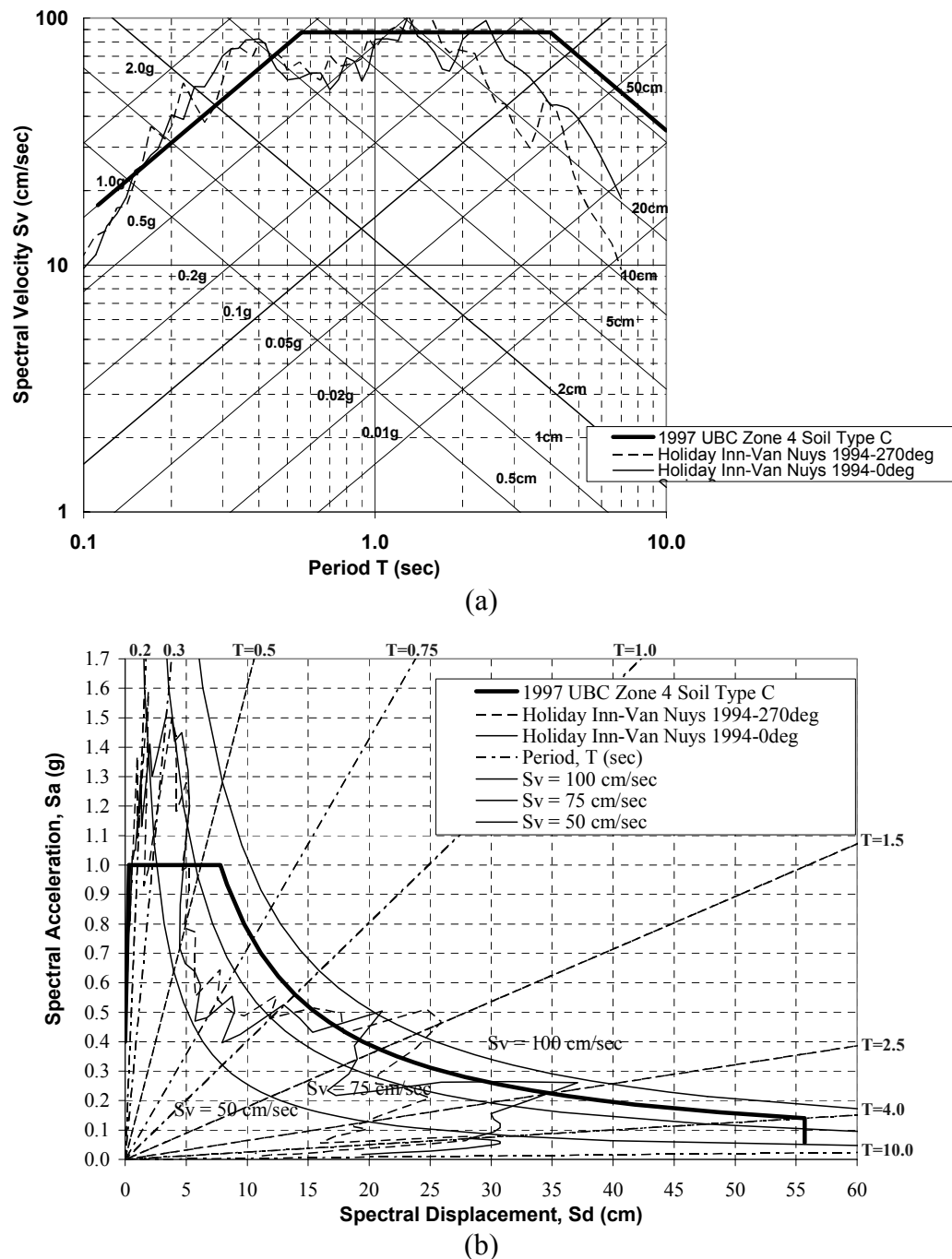


Fig. 4 Building code type smooth response spectra: (a) Tripartite format, (b) ADRS format

The example shown is for a 1997 Uniform Building Code criterion for seismic zone 4 at a soil category C site. The PGA is $0.4g$ (i.e., 40% of gravity), the constant S_a is 2.5 times the PGA ($= 1.0g$). Constant velocity is based on S_a at one second that equals 1.4 times PGA ($= 0.56g$). This translates to a S_v equal to 87 cm/sec (using Equation (2)). Assuming a cut-off period of 4 sec, the constant displacement becomes 56 cm (using Equation (4)).

Once design response spectra are established, it is fairly simple to establish seismic design forces for a building. For low-rise buildings, where the fundamental mode of vibration (in each direction) is predominant, we estimate the period of vibration of the building and find the corresponding S_a . This may be used as a base shear coefficient for determining the lateral forces on the building or adjustments may be made for dynamic participation factors. For tall buildings, where the dynamic effects of higher modes of vibration are significant, spectral accelerations for each of the several modes may be quickly determined using the estimated periods. If the period estimates are revised, the lateral forces can be easily adjusted proportionally to the revised spectral accelerations.

INFLUENCE OF RESPONSE SPECTRA ON BUILDING CODE PROVISIONS

The basis for the development of current seismic building code provisions had their beginnings in the 1950s. A joint committee of the San Francisco section of ASCE and the Structural Engineers Association of Northern California prepared a “model lateral force provision” based on a dynamic analysis approach and response spectra (Anderson et al., 1952). The proposed design curve, $C = K/T$, was based on a compromise between a standard acceleration spectrum by M.A. Biot (Biot, 1941, 1942) and an El Centro analysis by E.C. Robison (Figure 5). It is interesting to note that the PGA of 0.2g in the Biot curve has a peak spectral acceleration of 1.0g at a period of 0.2 sec. The curve then descends in proportion to $1/T$ (i.e., constant velocity). If the peak spectral acceleration is limited to 2.5 times the PGA, the Biot spectrum is very close to the 1997 UBC design spectrum for a PGA of 0.2g (dashed line without symbols in Figure 5). The proposed design lateral force coefficient was $C = 0.015/T$, with a maximum of 0.06 and a minimum of 0.02 (line with dots in Figure 6). These values were considered consistent with the current practice, and the weight of the building included a percentage of live load.

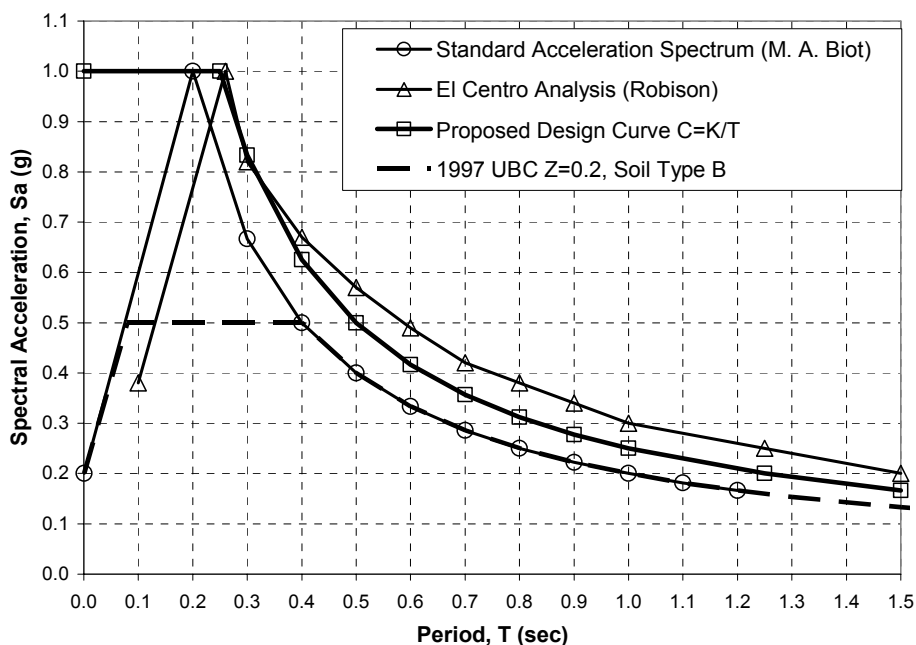


Fig. 5 1952 Joint Committee Response Spectra (Anderson et al., 1952)

In 1959, the Seismology Committee of the Structural Engineers Association of California published “Recommended Lateral Force Requirements” (generally referred to as the SEAOC bluebook) and included “Commentary” in 1960 (SEAOC, 1960). Influenced by the Joint Committee (many of the members were on both committees), recommendations were proposed that were adopted for the 1961 Uniform Building Code (UBC) (ICBO, 1961). The new recommended design lateral force coefficient was $C = 0.05/T^{1/3}$, and the live loads were not included in the weight (except for a percentage in storage facilities). By using T to the one-third power, the equation could account for higher modal participation and give a larger load factor for tall buildings. In addition it avoided the need for a minimum cut-off. The maximum was set at $C = 0.10$ (Figure 6). Also shown in Figure 6 is a comparably adjusted version of the 1997 UBC.

Over the years, the SEAOC bluebook and the UBC went through many revisions, generally influenced by some events such as the 1971 San Fernando, 1989 Loma Prieta, and 1994 Northridge earthquakes, and by data relating to soil effects. The comparable curves shown in Figure 7 have been adjusted to represent strength design response spectra and include factors representing soil classification type D. At this level of design, the structures would be expected to remain linear-elastic with some reserve capacity before reaching yield. In order to survive a major earthquake ground motion (e.g., PGA = 0.4g) the structure is expected to experience nonlinear post-yielding response.

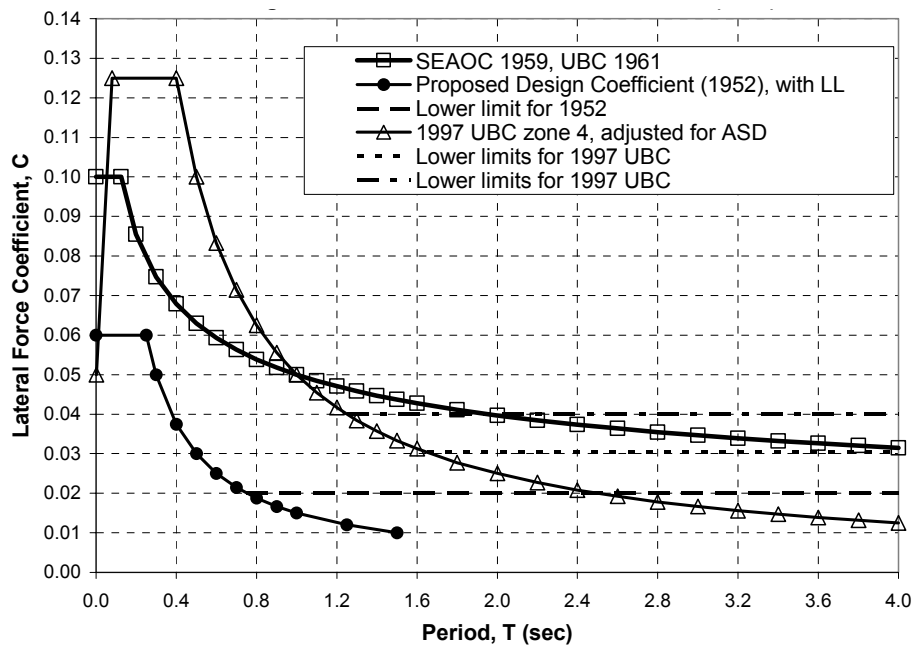


Fig. 6 1959 design lateral force coefficients (SEAOC, 1960)

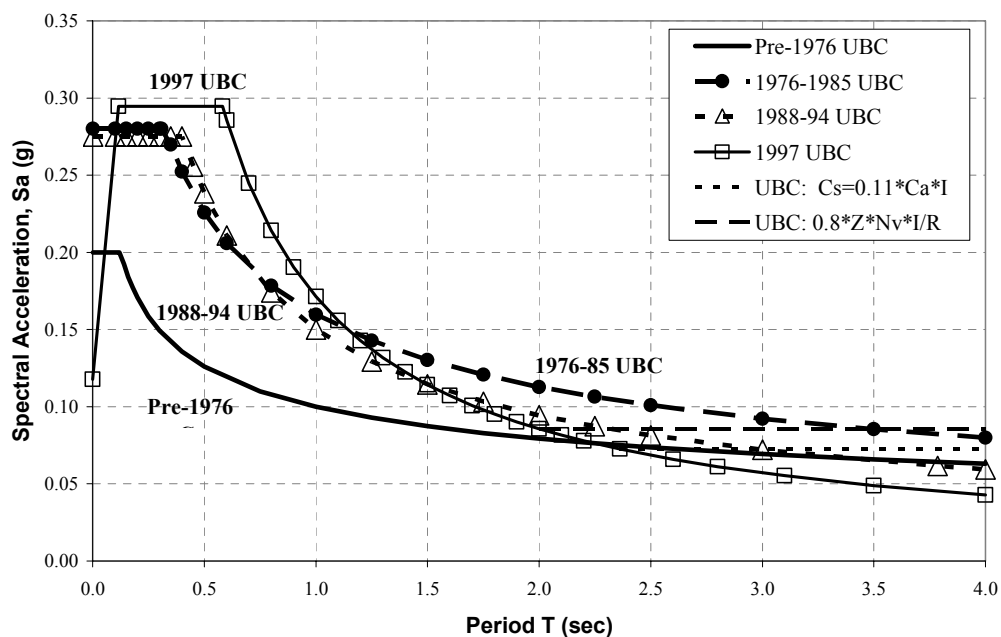


Fig. 7 UBC strength design response spectra (Zone 4, Soil D equivalents)—1961 to 1997

RESPONSE SPECTRA FROM GROUND MOTION RECORDINGS

It is convenient for design to have smooth response spectra; however, in the real world response spectra come in a large variety of sizes and shapes. Therefore, data on PGA and intensity do not give the full picture of an earthquake event. Examples of response spectra from three locations in the Los Angeles, California area from the 1994 Northridge earthquake are shown in Figure 8. The locations are Santa Monica, Newhall and Sylmar, which experienced PGAs greater than 0.6g (code's maximum probable PGAs are generally considered to be 0.4g). The ADRS format is used and, for scale, constant spectral velocity is shown for 150 and 75 cm/sec by double-dot-dash curves. For Santa Monica the demand is great for very short period buildings ($T < 0.3$ sec) and moderate for tall buildings ($T > 1.5$ sec). In the mid-period range the demands are relatively small. On the other hand, Newhall has a huge demand in the mid-period range with a broad double hump (T from 0.6 to 1.5 sec). The Sylmar spectrum has moderate

demands in the mid-period range, but has a very large displacement demand for long periods (T from 2 to 4 sec). It is tempting to envelope these and a whole family of response spectra to illustrate that the ground motion was about twice the expected average 475-year event, but that would be misleading. For each of the locations, buildings would respond differently, and because of energy absorption (in soil and in the building), nonlinearity and changing periods, many buildings avoided catastrophic results.

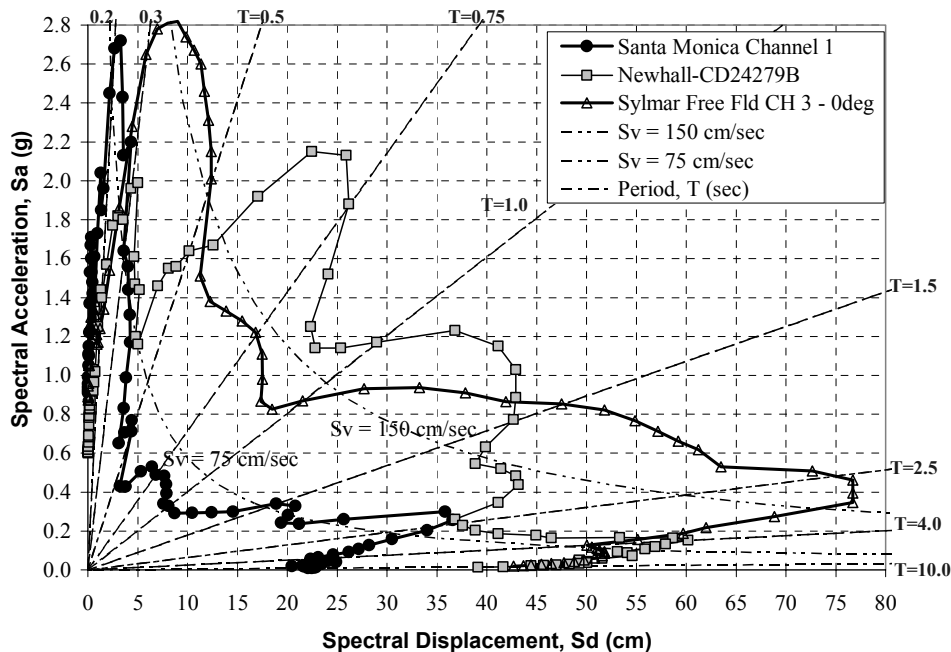


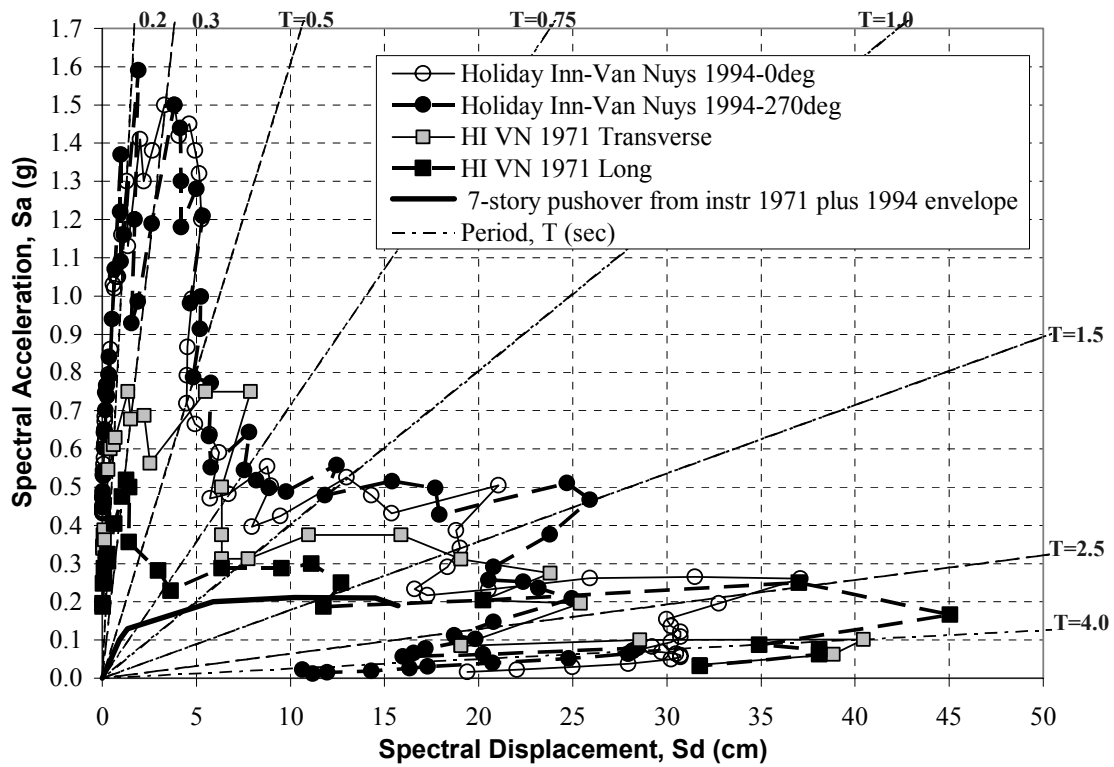
Fig. 8 Three Northridge, 1994 response spectra (5% damped)

In Figure 9, response spectra are shown for the Holiday Inn hotel structure, which experienced damage from both the 1971 San Fernando and 1994 Northridge earthquakes. The spectra with circles show two directions for 1994 and the curves with squares show 1971. The building experienced damage and was softened up by the 1971 earthquake (Murphy, 1973). The initial period was about 0.5 sec; after the earthquake it was about 1 sec. The 7-story pushover curve represents the capacity of the structure (e.g., lateral force versus roof displacement, transformed to S_a versus S_d). The curve shown in Figure 9 was obtained by an evaluation of the recorded building motion (Gilmartin et al., 1998) and is consistent with calculations. Figure 9(a) shows 5% damped spectra and Figure 9(b) shows 20% damped spectra. The structure is overwhelmed by the 5% damped spectra; however, the use of 20% damped spectra to represent inelastic-nonlinear response spectra (Freeman, 2004), illustrates how the building survived without total collapse (i.e., the capacity curve breaks through the response spectra envelopes). In this example 20% damping represents roughly a displacement ductility of 2.5 (Freeman, 2006).

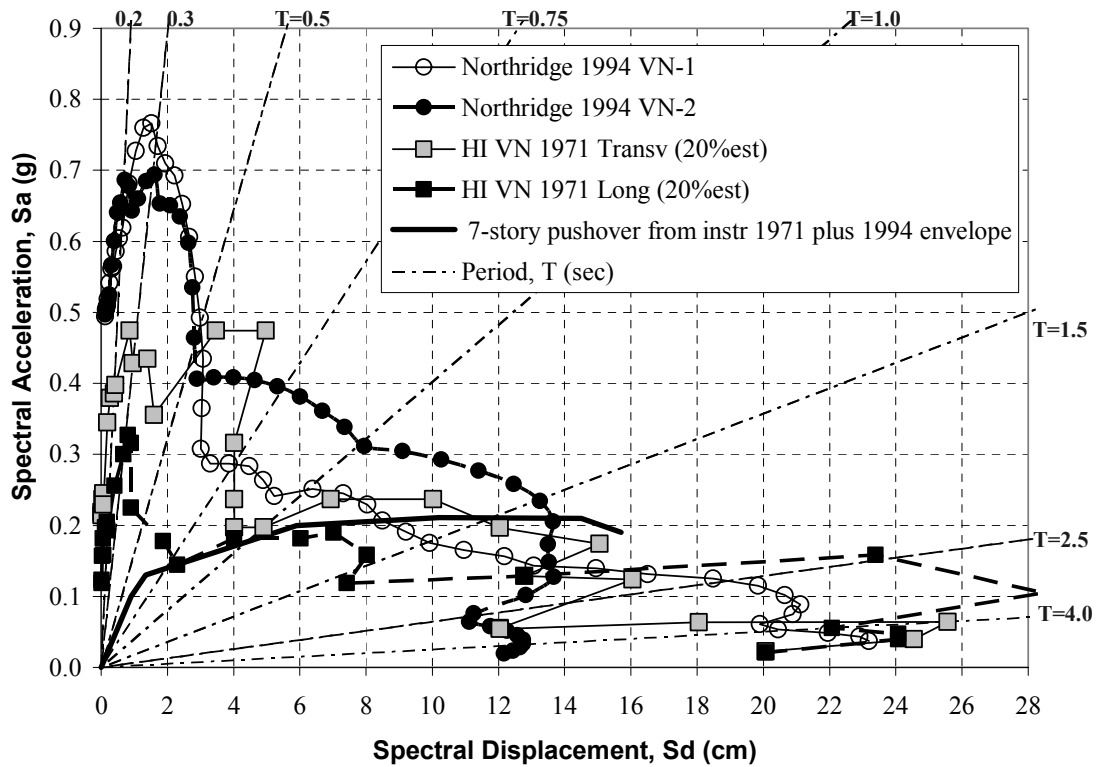
SMOOTHING RESPONSE SPECTRA

If there is a desire to construct a smooth spectrum from a jagged response spectrum Figure 10(a) illustrates a very simple method. Using the ADRS format, we identify the peak spectral acceleration and draw a horizontal line (constant acceleration). We do the same for the peak spectral displacement, drawing a vertical line for the maximum constant displacement. Then, moving out along radial lines from the origin, we locate the maximum spectral velocity (this may be more visually clear on the tripartite graph in Figure 10(b)). Connecting the lines forms a maximum smooth spectrum. A similar procedure is used to form the minimum smooth spectrum (for the minimum acceleration we use the spectral acceleration at $T = 0.1$ sec to avoid selecting the peak ground acceleration). Taking an average of the maximum and minimum curves will result in a reasonable estimation of a smooth spectrum. Also shown on the Figure 10 graphs are peak ground motion (PGM) spectra, which are formed using the measured peak acceleration, velocity and displacement. An interesting use of these graphs is to estimate dynamic amplification factors (DAFs) by dividing spectral values by ground motion values. For example, if

average constant acceleration (1.05g) is divided by the peak ground acceleration (0.4g) the DAF is about 2.5. For velocity the DAF is about 1.7, and for displacement the DAF is about 2.3.



(a)



(b)

Fig. 9 Holiday Inn, Van Nuys response spectra for 1971 and 1994 earthquakes: (a) 5% damped, and (b) 20% damped

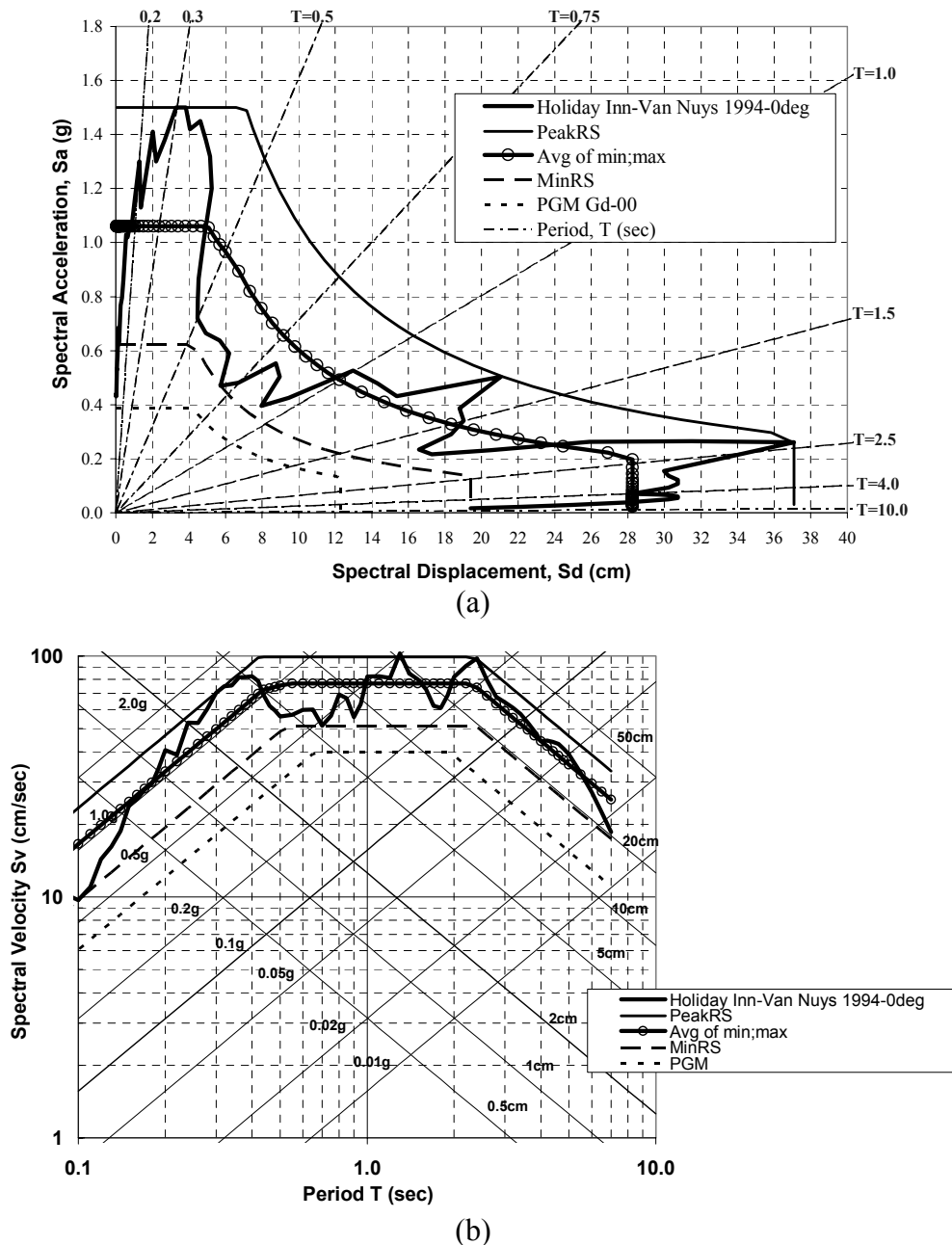


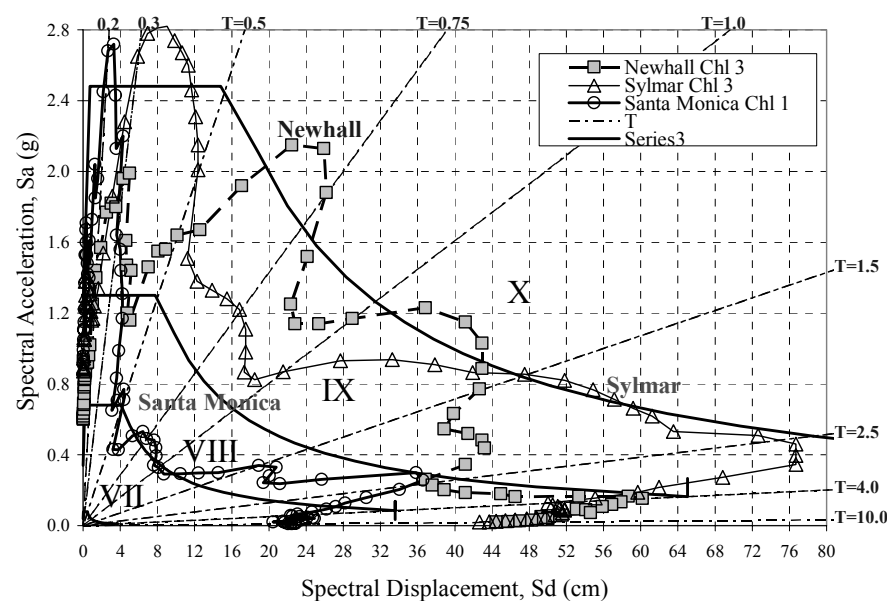
Fig. 10 Smoothing response spectra and ground motion spectra (Holiday Inn, Van Nuys 1994): (a) ADRS format, (b) Tripartite format

AN EARTHQUAKE ENGINEERING INTENSITY SCALE

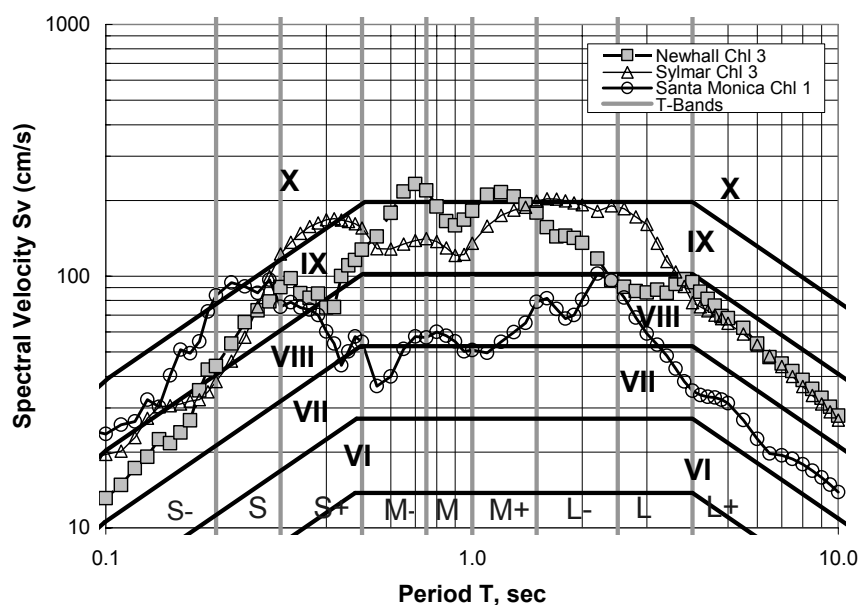
Emergency response after an urban area earthquake requires incorporation of data from various sources. Main sources of data for engineering use are the so-called free-field instruments, as used in TriNet ShakeMap, and strong-motion instruments installed in buildings. The TriNet system is capable of providing a rapid instrumental intensity map for strong motion earthquakes on the basis of an array of recording instruments. The instrumental intensity scale (I_{mm}) is based on recorded peak ground accelerations (PGAs) and peak ground velocities (PGVs). Both are calibrated against historical Modified Mercalli Intensity (MMI) data, and are related to two parallel scales describing potential damage and perceived shaking (Wald et al., 1999). To improve emergency response, an Earthquake Engineering Intensity Scale (EEIS), built on a scale initially developed by the late John A. Blume in 1970s (Blume, 1970), is presented (Freeman et al., 2004). EEIS allows translation of ground shaking information in the form of response spectra at a site into response/shaking intensity for different kinds of buildings. When this translation is presented in Acceleration-Displacement Response Spectrum (ADRS) format, spectrum

levels for different period ranges can be graded into various EEIS levels by relating them to the Instrumental Intensity (I_{mm}) scale developed for TriNet ShakeMap.

To construct the link, response spectra corresponding to the I_{mm} scale can be approximated by applying dynamic amplification factors to the TriNet PGA and PGV values. Studies dating back from the 1970s to the present have provided recommendations for these amplification factors (Newmark et al., 1973; Newmark and Hall, 1982). By multiplying the PGA values by the acceleration amplification factor for the short periods (i.e., constant acceleration range) and by multiplying the PGV values by the velocity amplification factor for the medium-to-long periods (i.e., constant velocity range), smooth response spectra can be formed into a structural response intensity scale. Amplification factors of 2.0 for the PGA and 1.7 for the PGV were selected as illustrated in Figure 11. The response spectra shown in Figure 8 are shown superimposed on transformed I_{mm} scales VII through X. Note that they have small bumps into X, but generally lie in intensity IX. Santa Monica lies in intensity VIII except at very short periods. The EEIS is also shown on the tripartite format (Figure 11(b)). Note the period bands that designate zones of short-, medium- and long-period buildings.



(a)



(b)

Fig. 11 Earthquake Engineering Intensity Scale (EEIS): (a) ADRS format, (b) Tripartite format

CLOSING

An introduction to response spectra has been presented, illustrating procedures that may be useful to professional engineers as an aid to design and evaluation of buildings and other structures. When earthquake ground motion data is available, the use of response spectra can be very useful in understanding how buildings perform and to identify deficiencies and damage potential.

However, response spectra, as in any other technique, must be used with caution and a good understanding of the process. For single-degree-of-freedom systems responding in a linearly elastic manner, response spectra give good credible results, assuming that the data is credible. For a measured earthquake response spectrum with sharp peaks and valleys, the variations due to uncertainty in actual structural period of vibration is visually apparent. For multi-modal systems, the combination of modes is generally done by SRSS (square root of the sum of the squares) or CQC (complete quadratic combination) rule. Although these rules are based on probability approximations, the results are generally reasonable. The more technical time-history method is generally considered more exact; however, due to sensitivity to small variations in accuracy of structural periods of vibration, there are also uncertainties in this procedure. When analysis is extended into the inelastic nonlinear realm of structural response, complexities of analysis multiply. Response spectrum techniques allow engineers to visually imagine how buildings will perform during major damaging earthquakes.

It is recommended that researchers and design professionals put more effort into detailed examinations of individual building response records. By deconstructing individual recorded floor motions into individual modes of vibration, there is the potential of better understanding how buildings perform during earthquake ground motions. This could lead to developing better methods of using response spectra.

REFERENCES

1. Anderson, A.W., Blume, J.A., Degenkolb, H.J., Hammill, H.B., Knapik, E.M., Marchand, H.L., Powers, H.C., Rinne, J.E., Sedgwick, G.A. and Sjoberg, H.O. (1952). "Lateral Forces of Earthquake and Wind", Transactions of the ASCE, Vol. 117, pp. 716–780.
2. ATC (1996). "Seismic Evaluation and Retrofit of Concrete Buildings: Volume 1", Report ATC-40, Applied Technology Council, Redwood City, California, U.S.A.
3. Biot, M.A. (1941). "A Mechanical Analyzer for the Prediction of Earthquake Stresses", Bulletin of the Seismological Society of America, Vol. 31, No. 2, pp. 151–171.
4. Biot, M.A. (1942). "Analytical and Experimental Methods in Engineering Seismology", Transactions of the ASCE, Vol. 108, pp. 365–408.
5. Blume, J.A. (1970). "An Engineering Intensity Scale for Earthquakes and other Ground Motion", Bulletin of the Seismological Society of America, Vol. 60, No. 1, pp. 217–229.
6. Fajfar, P. (1998). "Capacity Spectrum Method Based on Inelastic Demand Spectra", Report EE-3/98, IKPIR, Ljubljana, Slovenia.
7. FEMA (2005). "Improvement of Nonlinear Static Seismic Analysis Procedures", Report FEMA 440, Federal Emergency Management Agency, Washington, DC, U.S.A.
8. Freeman, S.A. (2004). "Review of the Development of the Capacity Spectrum Method", ISET Journal of Earthquake Technology, Vol. 41, No. 1, pp. 1–13.
9. Freeman, S.A. (2006). "A Penultimate Proposal of Equivalent Damping Values for the Capacity Spectrum Method", Proceedings of the Eighth US National Conference on Earthquake Engineering, San Francisco, U.S.A., Paper No. 161 (on CD).
10. Freeman, S.A., Nicoletti, J.P. and Tyrell, J.V. (1975). "Evaluations of Existing Buildings for Seismic Risk—A Case Study of Puget Sound Naval Shipyard, Bremerton, Washington", Proceedings of the US National Conference on Earthquake Engineering, Berkeley, U.S.A., pp. 113–122.
11. Freeman, S.A., Irfanoglu, A. and Paret, T.F. (2004). "Earthquake Engineering Intensity Scale: A Template with Many Uses", Proceedings of the 13th World Conference on Earthquake Engineering, Vancouver, Canada, Paper No. 1667 (on CD).
12. Gilmartin, U.M., Freeman, S.A. and Rihal, S.S. (1998). "Using Earthquake Strong Motion Records to Assess the Structural and Nonstructural Response of the 7-Story Van Nuys Hotel to the Northridge

- Earthquake of January 17, 1994”, Proceedings of the Sixth US National Conference on Earthquake Engineering, Seattle, U.S.A., Paper No. 268 (on CD).
13. ICBO (1961). “Uniform Building Code (UBC)”, International Conference of Building Officials, Whittier, U.S.A.
 14. Mahaney, J.A., Paret, T.F., Kehoe, B.E. and Freeman, S.A. (1993). “The Capacity Spectrum Method for Evaluating Structural Response during the Loma Prieta Earthquake”, Proceedings of the 1993 National Earthquake Conference on Earthquake Hazard Reduction in the Central and Eastern United States: A Time for Examination and Action, Oakland, U.S.A., Vol. 1, pp. 501–510.
 15. Murphy, L.M. (1973). “San Fernando, California, Earthquake of February 9, 1971” in “Effects on Building Structures: Volume 1 (edited by L.M. Murphy)”, National Oceanic and Atmospheric Administration, Washington, DC, U.S.A.
 16. Newmark, N.M. and Hall, W.J. (1982). “Earthquake Spectra and Design”, Earthquake Engineering Research Institute, Oakland, U.S.A.
 17. Newmark, N.M., Blume, J.A. and Kapur, K.K. (1973). “Seismic Design Spectra for Nuclear Power Plants”, Journal of the Power Division, Proceedings of ASCE, Vol. 99, No. PO2, pp. 287–303.
 18. Priestley, M.J.N., Kowalsky, M.J., Ranzo, G. and Benzoni, G. (1996). “Preliminary Development of Direct Displacement-Based Design for Multi-Degree of Freedom Systems”, Proceedings of the 65th Annual SEAOC Convention, Maui, U.S.A., pp. 47–66.
 19. SEAOC (1960). “Recommended Lateral Force Requirements and Commentary”, Structural Engineers Association of California, San Francisco, U.S.A.
 20. Wald, D.J., Quitoriano, V., Heaton, T.H., Kanamori, H., Scrivner, C.W. and Worden, C.B. (1999). “TriNet “ShakeMaps”: Rapid Generation of Peak Ground Motion and Intensity Maps for Earthquakes in Southern California”, Earthquake Spectra, Vol. 15, No. 3, pp. 537–555.

EMPIRICAL SCALING AND REGRESSION METHODS FOR EARTHQUAKE STRONG-MOTION RESPONSE SPECTRA—A REVIEW

Vincent W. Lee

Department of Civil & Environmental Engineering
University of Southern California
Los Angeles, CA 90089-2531, U.S.A.

ABSTRACT

Spectral regression studies of four selected research groups, namely, Boore and co-workers at the U.S. Geological Survey (USGS) in Menlo Park, California, Abrahamson and Silva at the Pacific Gas and Electric Company (PG&E) in California, Trifunac and co-workers at the Strong-Motion Group of the University of Southern California (USC) in Los Angeles, and Ambraseys and co-workers at the Imperial College of Science, Technology and Medicine in London, England. Their scaling procedures are described, and their approaches are compared. All regression equations reviewed depend upon magnitude, distance, and local site conditions, though different groups used different database, definitions of magnitude, distance and site conditions. Among the many differences, one stands out: Boore and co-workers in 1997, Abrahamson and Silva in 1997, and later Ambraseys and co-workers in 2005 considered using fault-type scaling variables to differentiate among the motions from different fault mechanisms, while the USC Strong-Motion Group introduced a source-to-station path-type term.

KEYWORDS: PSV Spectra, Strong Earthquake Motions, Empirical Scaling of Spectra

INTRODUCTION

In this paper a review of the selected regression equations for estimation of pseudo relative velocity (PSV) response spectral amplitudes by various groups and organizations will be presented. The response spectrum concept was first introduced by Biot (1932, 1933, 1934). Until the mid-1960s, when modern digital computers became available, empirical regression analyses of spectral amplitudes were not possible because there were only a few significant processed earthquake records (e.g., those recorded during the 1933 Long Beach, the 1940 Imperial Valley, the 1952 Kern County, the 1966 Parkfield, and the 1968 Borrego Mountain earthquakes). Also, the digitization and processing of strong-motion records from analog instruments was a slow, manual process, requiring many hours of hand digitization (Trifunac, 2006).

The San Fernando earthquake of February 9, 1971 changed all that. More than 250 analog accelerometers in Southern California were triggered and recorded many excellent acceleration traces. The earthquake strong-motion data processing program at the California Institute of Technology in Pasadena, California, led by D.E. Hudson, then started to select, digitize, and process all significant records, and by 1975 all of the records had been processed. The data were then distributed on magnetic tapes and computer cards. A series of reports were published detailing the corrected and processed acceleration, velocity, and displacement of each record, and the corresponding response spectral amplitudes were calculated at 91 periods between 0.04 to 15 s for damping ratios of 0.0, 0.02, 0.05, 0.10, and 0.20 (Hudson et al., 1970, 1971, 1972a, 1972b).

During the following 30 years, many well-recorded strong-motion earthquakes occurred worldwide, including the three in California: the 1987 Whittier-Narrows, the 1989 Loma-Prieta, and the 1994 Northridge earthquakes. With an ever-increasing digitized database, various groups started to develop regression equations for the empirical scaling of response spectral amplitudes. These equations were later used for the computation of uniform hazard PSV spectra in the probabilistic site-specific analyses for seismic micro- and macro-zonation (Trifunac, 1988, 1989d, 1990b). Those equations were also needed in the probabilistic determination of the envelopes of shear forces and of bending moments in engineering design (Amini and Trifunac, 1985; Gupta and Trifunac, 1988a, 1988b, 1990a, 1990b; Todorovska, 1994a, 1994b, 1995), and in the estimation of losses for buildings exposed to strong shaking (Jordanovski et al., 1992a, 1992b).

In this paper, we review the contributions of four groups that performed systematic regression analyses of the response spectral amplitudes. Three of these groups are in the U.S., and one is in Europe. The three U.S. groups are all in California: the group at U.S. Geological Survey (USGS) in Menlo Park, California (D. Boore and colleagues); N.A. Abrahamson at the Pacific Gas and Electric Company (PG&E); and the Strong-Motion Group at the University of Southern California (USC) in Los Angeles. The fourth group works in Europe, at the Imperial College of Science, Technology, and Medicine in London. A summary of the main contributions of each group will be presented next, followed by a comparison of their scaling equations. We will examine the following categories:

- the database and data processing procedures,
- site classification,
- distance definitions used for attenuation relations, and
- the regression equations.

There are many other groups and individuals in the world who have worked on the same and related topics, but a comprehensive review of all of their contributions is beyond the scope of this paper.

SUMMARY OF THE WORKS OF THE USGS GROUP

1. The Database and Data Processing Procedures

The first set of equations by this group was for estimating the horizontal response spectra from strong-motion data recorded before 1981 in western North America (Joyner and Boore, 1981, 1982). The authors referred to these studies as JB8182. These data were later expanded to include the recordings from the 1989 Loma Prieta, the 1992 Petrolia, and the 1992 Landers earthquakes. The data set was restricted to shallow earthquakes in western North America with moment magnitudes greater than 5.0. Shallow earthquakes are those with fault ruptures that lie mainly above a depth of 20 km. Most of the data used by this group have been collected by the Strong-Motion Instrumentation Program (SMIP) of the California Division of Mines and Geology (CDMG), and the National Strong-Motion Program of the USGS. This database was also used in the subsequent work by Boore et al. (1993, 1994a, 1994b) and is referred to as BJF93, BJF94a, BJF94b, or collectively as BJF9394. A summary of this work is presented in the paper by Boore et al. (1997). The following points were emphasized in their work:

1. To avoid bias due to soil-structure interaction, the authors did not include data from structures three floors or higher, from dam abutments, or from the bases of bridge columns.
2. No more than one station with the same site condition within a circle of 1-km radius was included, and the station with the lowest database code number was chosen, while others were excluded.
3. A systematic effort was made to exclude records from instruments triggered by the S wave because it was felt that in such cases a part of the strong motion might be missed.
4. To avoid bias toward larger response values, a distance cutoff for each earthquake was imposed, beyond which all data from that earthquake were ignored. This was done to eliminate any bias by any circumstance that might cause high values of ground motion. The cutoff distance was determined by the geological conditions and the trigger level of the recording instrument.

The 1993 studies, as well as all previous studies, used the values for peak acceleration scaled directly from the recorded accelerograms, rather than from the processed, instrument-corrected data. The authors did this to avoid “bias” in the peak values from the “sparsely sampled” older data. This bias is not a problem with the densely sampled data after the late 1960s. With few exceptions, the response data used were all PSV response spectra data.

2. Site Classification

Originally, a binary classification, “rock” and “soil”, was used to characterize the site by Joyner and Boore (1981, 1982) (JB8182). Later, Boore et al. (1993) (BJF93) used a site classification based on the shear velocity averaged over the upper 30 m, as shown in Table 1.

The measurements from boreholes at a site, if available, were used. In most cases when such measurements were not available the site classifications were estimated by analogy with borehole measurements at similar sites. This information was usually obtained from site visits, consultations with geologists familiar with the area, and from various geological maps. Of the four site classes listed below,

Class D is poorly represented in the data and thus was not included in the analyses here. Following points may be noted:

- The authors pointed out that such classification was similar to the one that was incorporated into the 1994 edition of the code provisions of the National Earthquake Hazard Reduction Program (NEHRP) (Boore et al., 1997), with 5 site classes (see Table 2). The two site classifications were referred to as BJT93 and NEHRP, respectively.
- These two site classifications were modified again by Boore et al. (1994a, 1994b) (BJT94a, BJT94b) when the site effects were changed from being a constant for each site class to a continuous function of V_s (shear-wave velocity at the site) averaged over the depth of the top 30 m. The authors recommended that the values of V_s given in Table 3 be used for the NEHRP site classes B, C, and D, and for typical rock and soil sites (Boore et al., 1997).

Table 1: Boore et al. (1993) Site Class versus Range of Shear Wave Velocities

Site Class	Range of Shear Wave Velocities
A	> 750 m/s
B	360–750 m/s
C	180–360 m/s
D	< 180 m/s

Table 2: NEHRP Site Class versus Range of Shear Wave Velocities

NEHRP Site Class	Range of Shear Wave Velocities
A	> 1500 m/s
B	760–1550 m/s
C	360–760 m/s
D	180–360 m/s
E	< 180 m/s

Table 3: Boore et al. (1997) Site Class versus Average Shear Velocity

Site Class	Average Shear Velocity Used
NEHRP Site Class B	1070 m/s
NEHRP Site Class C	520 m/s
NEHRP Site Class D	250 m/s
Rock	620 m/s
Soil	310 m/s

3. Distance Definition Used for Attenuation Relation

In the work of Boore et al. (1993) (BJT93), the “hypocentral” distance term used, r , was defined as $r = \sqrt{d^2 + h^2}$, where d is the measured epicentral distance in km from the earthquake source to the site, and h is a fictitious depth to be determined. Instead of using the actually estimated focal depth of the earthquake focus, Boore et al. (1993) treated h as an unknown parameter to be determined by regression. They performed a two-stage linear regression, where, in a departure from Joyner and Boore (1993), the sum of square errors in the first stage was minimized with respect to the parameter h by a simple numerical search, using the subroutine GOLDEN of Press et al. (1992). Note that at all spectral periods used, this fitted fictitious depth h would be a constant for all records and earthquakes.

The regression equation of Boore et al. (1993, 1997) used the attenuation term $b_4 r + b_5 \ln r$. The two terms represent, respectively, anelastic and geometric attenuation. This was subsequently replaced by $b_5 \ln r$, which is just the geometric attenuation term. The authors pointed out that regressions that included the anelastic $b_4 r$ term resulted in values of b_4 greater than zero, which would lead to

unreasonable estimates at large distances. The remaining geometric term, $b_5 \ln r$, is thus the only term used by Boore et al. (1993, 1997) to characterize the attenuation of the spectral amplitudes from the source to the recording site.

4. The Regression Equation

4.1 The 1993 Regression (Boore et al., 1993, 1997)

In their early studies (JB8182), Boore et al. (1993) presented equations for horizontal peak ground acceleration, velocity, and response spectra as functions of earthquake magnitude, distance from the earthquake source, and the type of material underlying the site. The regression equation of Boore et al. (1993, 1997) takes the form:

$$\log Y = b_1 + b_2(M - 6) + b_3(M - 6)^2 + b_4r + b_5 \log r + b_6G_B + b_7G_C + \epsilon_r + \epsilon_e \quad (1)$$

where Y is the ground motion parameter (in cm/s for response spectra, g for peak acceleration); M is the moment magnitude; $r = \sqrt{d^2 + h^2}$; d is the distance in km; h is a fictitious depth to be determined, as described in the previous section; G_B , G_C are the site classification variables; $G_B = 1$ for Class B and 0 otherwise; $G_C = 1$ for Class C and 0 otherwise (for Class A sites, both would be zero); ϵ_r is an independent random variable that takes on a specific value for each record; and ϵ_e is an independent random variable that takes on a specific value for each earthquake.

The coefficients to be determined are b_1 through b_7 , h , and the variance of ϵ_r , and ϵ_e : σ_r^2 and σ_e^2 , respectively. Those are determined using a weighted, two-stage regression procedure. In the first stage, the distance dependence is determined along with a set of amplitude factors, one for each earthquake. In the second stage, the amplitude factors are regressed against magnitude using a weighting matrix to determine the magnitude dependence (Joyner and Boore, 1993).

4.2 The Revised Equation (Boore et al., 1994a, 1994b, 1997)

In addition to the site classification revision, as described in the previous section, Boore et al. (1994b) modified the equations to take into consideration different ground-motion estimates for strike-slip and reverse-slip earthquakes. The revised ground-motion equation is

$$\log Y = b_1 + b_2(M - 6) + b_3(M - 6)^2 + b_5 \ln r + b_v \ln \frac{V_s}{V_A} \quad (2)$$

where the same variables are used as in BJJF93, except that

$$b_1 = \begin{cases} b_{1SS} & \text{for strike-slip earthquakes;} \\ b_{1RS} & \text{for reverse-slip earthquakes;} \\ b_{1ALL} & \text{for unspecified mechanism for earthquakes;} \end{cases} \quad (3)$$

and V_s in m/s is the average shear-wave velocity to 30 m depth below surface. It is now scaled relative to a “fictitious” wave velocity variable V_A to be determined by regression.

The coefficients to be determined are b_{1SS} , b_{1RS} , b_{1ALL} , b_2 , b_3 , b_5 , h , b_v and V_A . It may be noted that the term $b_4r + b_5 \log r$ ($= b_4r + b_5 \ln r$ in BJJF93) is now replaced by $b_5 \ln r$. Also, Boore et al. (1994a, 1994b, 1997) considered only the horizontal response spectra in their regression analyses.

SUMMARY OF THE WORKS OF ABRAHAMSON AND SILVA

1. The Database and Data Processing Procedures

The strong ground motion data used by Abrahamson and Silva (1997) is from shallow crustal events worldwide, in seismically active tectonic regions. Subduction zones are excluded. The events included are up through the 1994 Northridge earthquake in Southern California. The data set starts out with 853 recordings from 98 earthquakes and aftershocks with magnitudes above 4.5. All of the recordings with either unknown or poor estimates of magnitude, source mechanism, distance, or site conditions are excluded from the regression analysis. In the end, the final data used in the regressions is a set of 655 recordings from 58 earthquakes, starting with the 1940 Imperial Valley earthquake and ending with the 1994 Northridge earthquake. The majority of the earthquakes are from the western U.S., with not more than ten events from Armenia, Canada, Iran, Italy, Mexico, and Russia. As in the studies by Boore et al. (1997), it was pointed out that the data set is biased toward the larger motions because those have a higher likelihood of being recorded.

Abrahamson and Silva (1997) summarize the procedures they used to reprocess all the records as follows:

1. Interpolation of uncorrected, non-uniformly sampled data to evenly spaced data at 400 samples/s. This should not be interpreted as implying a Nyquist frequency of 200 Hz, since most of the data are from analog recordings with reliable frequency resolution up to about 25 Hz (Trifunac et al., 1973).
2. Low-pass filtering of the data using a causal 5-pole Butterworth filter. The corner cut-off frequency for each record is selected by visual examination of the Fourier amplitude spectrum.

It may be noted that

- The Butterworth filter is an infinite impulse response (IIR) filter, which produces the output data only from the input of past (earlier time) and present data. It is known that such filters distort the phase of the filtered output data (Rabiner and Gold, 1975; Lee and Trifunac, 1984). Unlike finite impulse response (FIR) filters, which can be implemented to have zero phase shift, these IIR filters create phase distortions, so corrections to zero-phase output must be made. It seems that no discussion is presented by Abrahamson and Silva (1997 or elsewhere) on whether their data were corrected for this phase distortion.
 - The selection of the cut-off frequency by visual examination of the Fourier spectra could be subjective. The authors present no discussion on whether this was done by one or several analysts, nor what the criteria of the selection process were.
3. Removing the instrument response (instrument correction).
It may be noted that no detailed information is included to describe this procedure. It can thus only be assumed that this is similar to the “instrument correction” procedure outlined by Trifunac (1972) and Trifunac and Lee (1973).
 4. Decimating to 100 or 20 samples/s, depending upon the low-pass filter corner frequency.
 5. Applying a time-domain baseline-correction procedure and a final high-pass filter. The baseline correction procedure uses a polynomial of 0 or up to 10 degrees depending upon the initial displacements obtained by integration. The high-pass filter used is that proposed by Grazier (1979), based on an over-damped oscillator. This filter is applied in the time domain twice, forward and in reverse time to produce an end result with zero phase shift. The high-pass filtering parameters are selected by visual inspection.

It may be noted that

- As noted by the authors, correction of the phase shift created by the IIR filter is an important step in the processing. Unfortunately, again no such phase correction appears to have been made in the second step of processing above, where the IIR Butterworth filter was used for low-pass filtering of the data.
- With the useful bandwidth of each record separately evaluated, it was found that there are more above-average records than smaller records in the database. The smaller records are also often contaminated with noise. The authors preferred to have some biased data rather than have no data (for higher frequencies and longer periods) at all.

2. Site Classification

Following the guidelines for the Geomatrix site classification, Abrahamson and Silva (1997) used the classification given in Table 4. It may be noted that for most of their sites, they point out that the quantitative information for soil velocity profiles is not available. Those sites were assigned a site classification subjectively, using the table as a guide, rather than a scheme. This classification might be misleading to some readers, with A, B as rock or shallow soil, and C, D, E as simply deep soil.

Table 4: Abrahamson and Silva (1997) Site Classification

Site Classification	Description
A	Rock ($V_s > 600$ m/s) or very thin soil (< 5 m) over rock
B	Shallow soil; Soil 5–20 m thick over rock
C	Deep soil in narrow canyon; Soil > 20 m thick; Canyon < 2 km wide
D	Deep soil in broad canyon; Soil > 20 m thick; Canyon > 2 km wide
E	Soft soil ($V_s < 150$ m/s)

3. Distance Definition Used for Attenuation Relation

Abrahamson and Silva (1997) adopted the definition of distance used by Idriss (1991) and Sadigh et al. (1993)—namely, r_{rup} , the closest distance from the site to the rupture plane. They illustrated the distribution of the data in terms of magnitude, M , and rupture distance, r_{rup} , for two soil types, deep soil, and rock or shallow soil, at four natural periods, $T = 0.075, 0.2, 1.0$, and 5.0 s.

4. The Regression Model

The regression model used by Abrahamson and Silva (1997) is of the form

$$\ln Sa(g) = f_1(M, r_{rup}) + Ff_3(M) + HWf_4(M, r_{rup}) + Sf_5(\widehat{pga}_{rock}) \quad (4)$$

where

$Sa(g)$ is the spectral acceleration in g;

M is the moment magnitude;

r_{rup} is the closest distance to the rupture plane in km;

F is the fault type: 1 for reverse, 0.5 for reverse/oblique, and 0 otherwise;

HW is the dummy variable for hanging wall sites;

S is a dummy variable for the site class: 0 for rock or shallow soil, 1 for deep soil; and

f_1, f_3, f_4 and f_5 are the functions for attenuation, style-of-faulting factor, hanging wall effect, and site response, respectively, with each being described below.

It may be noted that

- Abrahamson and Silva (1997) do not justify or explain how or why the fault type numbers of 1, 0.5, and 0 were assigned respectively to reverse, reverse/oblique, and other fault types.
- Abrahamson and Silva (1997) considered the horizontal and vertical response spectra separately in their regression analyses.

4.1 Attenuation Function, $f_1(M, r_{rup})$

The function $f_1(M, r_{rup})$ for attenuation has the following form:

$$f_1(M, r_{rup}) = \begin{cases} a_1 + a_2(M - c_1) + a_{12}(8.5 - M)^n + [a_3 + a_{13}(M - c_1)] \ln R & M \leq c_1 \\ a_1 + a_4(M - c_1) + a_{12}(8.5 - M)^n + [a_3 + a_{13}(M - c_1)] \ln R & M > c_1 \end{cases} \quad (5)$$

where $R = \sqrt{r_{rup}^2 + c_4^2}$ is a distance (similar to what is used by Boore et al. (1993, 1997)), at which the $c_4 = h$ term can be interpreted as a representative depth. As in Boore et al. (1993), $c_4 = h$ is determined by regression. What is different here from Boore et al. (1993, 1997) is that the coefficient for “ $\ln R$ ” is now magnitude-dependent. It may be noted that Abrahamson and Silva (1997) do not describe the procedure used to define the parameter c_1 and the exponent n in the above equation.

4.2 Style-of-Faulting Factor, $f_3(M)$

Abrahamson and Silva (1997) try to differentiate among the ground motions from strike-slip and reverse faults, arguing that those show a difference in attenuation relations and they characterize this difference using the style-of-faulting factor. Originally, a constant style-of-faulting factor was used, but later, as in Sadigh et al. (1993), Campbell and Bozorgnia (1994), the authors included a magnitude and distance dependence of this factor for peak acceleration. Boore et al. (1997) also included a period dependence in the faulting factor. Combining all of these, the authors allow for a magnitude and period dependence of the faulting factor:

$$f_3(M) = \begin{cases} a_5 & \text{for } M \leq 5.8 \\ a_5 + \frac{(a_6 - a_5)}{c_1 - 5.8} & \text{for } 5.8 < M < c_1 \\ a_6 & \text{for } M > c_1 \end{cases} \quad (6)$$

It may be noted that

- The authors give no explanation on how or why the style-of-faulting factor is of the above form.
- The authors point out that the style-of-faulting factor has a strong magnitude dependence. For rock sites, this effect is about 30% for large-magnitude events but almost a factor of 2 for small ($M < 5.8$) events. Such strong magnitude dependence is driven by the sequence of Coalinga aftershocks, for which 8 of the 11 reverse and reverse/oblique events with magnitudes $M < 5.8$ were considered. Those produced above-average response motions at high frequencies, and the authors concluded that this resulted in a large style-of-faulting factor for small-magnitude events.

4.3 Hanging Wall Effect, $f_4(M, r_{rup})$

Here, Abrahamson and Silva (1997) followed the approach of Somerville and Abrahamson (2000) to model the differences in motions on a “hanging wall” and a “foot wall” of dipping faults. The functional form is assumed to be separable into a magnitude and a distance term. Their functional forms are given in Somerville and Abrahamson (2000) as

$$f_4(M, r_{rup}) = f_{HW}(M) f_{HW}(r_{rup}) \quad (7)$$

where

$$f_{HW}(M) = \begin{cases} 0 & \text{for } M \leq 5.5 \\ M - 5.5 & \text{for } 5.5 < M < 6.5 \\ 1 & \text{for } M \geq 6.5 \end{cases} \quad (8)$$

and

$$f_{HW}(r_{rup}) = \begin{cases} 0 & \text{for } r_{rup} < 4 \\ a_9 \left(\frac{r_{rup} - 4}{4} \right) & \text{for } 4 \leq r_{rup} \leq 8 \\ a_9 & \text{for } 8 < r_{rup} \leq 18 \\ a_9 \left(1 - \frac{r_{rup} - 18}{7} \right) & \text{for } 18 < r_{rup} \leq 25 \\ 0 & \text{for } r_{rup} > 25 \end{cases} \quad (9)$$

This means that

- Data from earthquakes with magnitudes below 5.5 are not affected by the hanging wall effect.
- Only data from earthquakes with known rupture sizes between 4 and 25 km are included; all others are not affected by the hanging wall effect.

4.4 Site Response, $f_5(\widehat{PGA}_{rock})$

Following Youngs (1993), Abrahamson and Silva (1997) used the following functional form of site response to accommodate non-linear soil response:

$$f_5(\widehat{PGA}_{rock}) = a_{10} + a_{11} \ln(\widehat{PGA}_{rock} + c_5) \quad (10)$$

where \widehat{PGA}_{rock} is the expected peak acceleration on rock in units of g , as predicted by the median attenuation relation with $S = 0$.

It is pointed out that the site response factor is dependent only upon the expected peak acceleration on rock. This is an improvement over the models that have only a constant scale factor for the site effects. The authors note that this does not include a magnitude dependence, and thus the model does not include all of the effects that may be found in the detailed site-specific studies.

SUMMARY OF THE WORK OF AMBRASEYS ET AL. (1996, 2005a, 2005b)

1. The Database and Data Processing Procedures

Ambraseys et al. (1996) state that a large and uniform dataset was used. Their database consists of a total of 422 records from 157 earthquakes in Europe and the Middle East, with surface wave magnitude M_S between 4.0 and 7.9 and focal depth ≤ 30 km. The smaller earthquakes are excluded because the authors said that they are generally not of “engineering significance”.

All acceleration records available were first preprocessed (plotted and visually inspected, with spurious points from bad digitization removed). A correction procedure was applied to all of the records that involved reducing the noise in the high- and low-frequency ranges. For short records not exceeding 5 s, a parabolic baseline adjustment was made using a least-squares fit. For records longer than 10 s, the data was re-sampled at 100 points/s, and an elliptical filter was applied, using a filter design proposed by Sunder and Connor (1982). For records between 5 and 10 s long, both procedures were applied, and the more effective correction was selected. However, this does not include instrument correction because a large portion of the data are from accelerometers with no reliable information on natural frequencies and damping. The authors claim that “...the instrument characteristics only significantly distort the recorded amplitude at frequencies > 25 Hz, and since the smallest response period considered is 0.1 s (10 Hz), this contamination is not important...”.

The local magnitude, M_L , which is the common magnitude scale used in California, was avoided because the authors claimed that local magnitudes either were not used in some of the study areas (Algeria, Iran, Turkey, and the former USSR), or if they were used the values were either unavailable or not reliably determined because of differences in the calibration methods. The moment magnitude, M_W , defined by Kanamori (1977), $M_W = \frac{2}{3} \log M_0 - 6$, where M_0 is the seismic moment in N-m, was discussed, but the authors pointed out that Kanamori intended only to use this for large earthquakes of magnitudes ≥ 7.2 . It was thus decided to use the surface wave magnitude, M_S , instead.

Ambraseys et al. (2005a, 2005b) updated their earlier work to include 595 triaxial (three-component) strong-motion records, from 135 earthquakes and 338 different stations in seismically active parts of Europe and the Middle East. The magnitude scale used in this recent work is the moment magnitude, M_W . They implemented the Basic Strong-Motion Accelerogram Processing (BAP) software (Converse and Brady, 1992) for all time histories, which included the bi-directional, elliptical Butterworth filter to low-pass the acceleration time histories after padding the data with zeros.

2. Site Classification

As in Boore et al. (1993, 1997) and Abrahamson and Silva (1997), the site classification in Ambraseys et al. (1996) uses the local soil conditions. Using shear wave velocity data available at 207 of the 212 sites, for 416 of 422 records, they use four categories of soil given in Boore et al. (1993) (see Table 5). The R, A, S, L soil classification used here is identical to the A, B, C, D site classification in Boore et al. (1993, 1997). The same site classification was used in Ambraseys et al. (2005a, 2005b).

Table 5: Ambraseys et al. (1996) Site Class versus Range of Shear Velocities & Number of Records

Site Class	Range of Shear Velocities	Number of Records
R (rock)	> 750 m/s	106
A (stiff soil)	360 to 750 m/s	226
S (soft soil)	180 to 360 m/s	81
L (very soft soil)	< 180 m/s	3

3. Distance Definition Used for Attenuation Relation

As in the work of Boore et al. (1993), the “hypocentral” distance term used, r , is defined as $r = \sqrt{d^2 + h_0^2}$, where d in km is defined as the shortest distance from the station to the surface projection of the fault rupture, and h_0 is a fictitious depth to be determined. Instead of using the seismologically determined focal depth, Ambraseys et al. (1996) treated, as in Boore et al. (1993), h_0 as an unknown parameter to be determined by regression. They explained that h_0 is a term that accounts for the fact that the source of the peak motion is not necessarily at the closest point on the surface projection of the fault, or at the hypocenter.

The attenuation versus distance used in the regression, as in Boore et al. (1993), is of the form, $\dots C_3 r + C_4 \log r + \dots$, which includes the anelastic and geometric distance terms, both of which are magnitude independent. Here $r = \sqrt{d^2 + h_0^2}$, where h_0 is determined in the first of the two-stage regressions. h_0 is assumed to be a constant for all records of all earthquakes. As in Boore et al. (1993), the authors found that the distribution of the data is not sufficiently large to allow determination of both the anelastic and geometric attenuation coefficients in “ $\dots C_3 r + C_4 \log r + \dots$ ” because a positive value of C_3 is obtained. Furthermore, for some choices of h_0 the coefficient C_3 can be less than zero, and hence permissible, but it is too small to make any difference. The same distance definition was used in Ambraseys et al. (2005a, 2005b).

4. The Regression Equation

Ambraseys et al. (1996) use a two-stage regression equation:

$$\log(y) = C_1 + C_2 M + C_4 \log r + C_5 S_R + C_6 S_A + C_7 S_S + \sigma P \quad (11)$$

where y is the parameter being predicted, which is either the peak ground acceleration in g or the spectral amplitudes for 5% critical damping for periods in the range, 0.1 to 2.0 s. $M = M_S$ is the surface wave magnitude.

At first, the term $C_3 r$ was included in the regression equation. However, it was found to be insignificant and was subsequently deleted. The first stage of regression determines the coefficients C_1 , C_2 and C_4 (without C_3), together with the term h_0 in $r = \sqrt{d^2 + h_0^2}$, and the same h_0 for “all” records of “all” the earthquakes. In the second stage of regression, the residues

$$\varepsilon_i = \log(y_i) - C_1 - C_2 M_i - C_4 \log(r_i) \quad (12)$$

are fitted with the local site soil classification

$$\varepsilon_i = C_5 S_R + C_6 S_A + C_7 S_S \quad (13)$$

where S_R , S_A and S_S are, respectively, the indicator variables for the three soil sites: rock, stiff, and soft soil sites, being 1 when the site is of the representative type and 0 otherwise. The standard deviation of $\log(y)$ is σ , and the constant P takes on the value of 0 for mean estimates and 1 for 84-percentile values of $\log(y)$. The σ term is calculated using the residuals at the second stage of regression. It may be noted that

- Ambraseys et al. (1996) considered only the horizontal response spectra in the above regression analyses. Ambraseys et al. (2005a, 2005b), in their recent regression work, switched back to the one-stage maximum-likelihood method of Joyner and Boore (1993). The equation takes the form,

$$\log(y) = a_1 + a_2 M_W + (a_3 + a_4 M_W) \log \sqrt{d^2 + a_5^2} + a_6 S_S + a_7 S_A + a_8 F_N + a_9 F_T + a_{10} F_O \quad (14)$$

where S_S and S_A are, respectively, the indicator variables for the two soil sites: soft and stiff sites. As in Boore et al. (1993) and Abrahamson and Silva (1997), Ambraseys et al. (2005a, 2005b) updated their regression equation to include fault types. The last three terms are for the faulting mechanism, and F_N , F_T and F_O are, respectively, the indicator variables for the three fault types: normal, thrust, and odd faults. F_N is equal to 1 for normal faulting earthquakes and 0 otherwise; $F_T = 1$ for thrust faulting earthquakes and 0 otherwise; and $F_O = 1$ for odd faulting earthquakes and 0 otherwise.

- Ambraseys et al. (2005a, 2005b) considered both the horizontal and vertical response spectra in the above regression analyses. As in Abrahamson and Silva (1997), they considered the horizontal and vertical response spectra in separate equations in the above regression analyses.

SUMMARY OF THE WORKS OF THE STRONG-MOTION GROUP AT USC

The Strong-Motion Earthquake Research Group at the University of Southern California contributed many papers and reports on the empirical scaling of strong-motion spectra. The examples include

1. 1970s: Trifunac (1973, 1976a, 1976b, 1976c, 1977a, 1977b, 1977c, 1977d, 1978, 1979), Trifunac and Anderson (1977, 1978a, 1978b, 1978c), Trifunac and Brady (1975a, 1975b, 1975c, 1975d, 1975e), Trifunac and Lee (1978, 1979a);
2. 1980s: Trifunac and Lee (1980, 1985a, 1985b, 1985c, 1987, 1989a, 1989b), Lee and Trifunac (1985), Lee (1989), Trifunac (1989a, 1989b, 1989c, 1989d), Trifunac and Todorovska (1989a, 1989b), Trifunac et al. (1988);
3. 1990s: Lee (1990, 1991, 1993), Trifunac (1990a, 1990b, 1991a, 1991b), Trifunac and Lee (1990, 1992), Trifunac and Novikova (1994), Lee and Trifunac (1993, 1995a, 1995b), Lee et al. (1995), Todorovska (1994a, 1994b, 1995), Trifunac and Zivcic (1991), Trifunac et al. (1991);
4. 2000s: Trifunac and Todorovska (2001a, 2001b).

They developed three generations of empirical regression equations for the scaling and attenuation of spectral amplitudes. Semi-theoretical extrapolation functions for extension of these empirical equations to both high and low frequencies had also been presented (Trifunac, 1993a, 1993b, 1994a, 1994b, 1994c, 1994d, 1994e, 1995a, 1995b). A review of and further details on the contributions of this group can be found in Lee (2002). The following is a brief summary of all their work on the empirical scaling of response spectral amplitudes only.

1. The Database and Data Processing Procedures

The database for the first generation of scaling equations of spectral amplitudes in the 1970s consisted of 186 free-field recordings. This corresponds to 558 acceleration components of data from 57 earthquakes in the western U.S. The data had been selected, digitized, and processed while M.D. Trifunac and V.W. Lee were at the Engineering Research Laboratory of the California Institute of Technology in Pasadena. The earthquakes included in the list of contributing events started with the 1933 Long Beach earthquake and ended with the San Fernando earthquake of 1971. The magnitudes of the earthquakes in

the database ranged from 3.0 to 7.7, and all data were hand-digitized from analog records using a manually operated digitizer (Hudson et al., 1970, 1971, 1972a, 1972b).

In 1976, the Strong-Motion Group moved to the University of Southern California in Los Angeles. The automatic digitization and data processing of strong-motion records by a mini-computer were developed and introduced in 1979 (Trifunac and Lee, 1979b; Lee and Trifunac, 1979), and the work on the collection of strong-motion records (Anderson et al., 1981; Trifunac and Todorovska, 2001a) continued. By the early 1980s, the second-generation database was expanded to 438 free-field records from 104 earthquakes. Most of the contributing earthquakes were from northern and southern California, and all were from the western U.S. All of these strong-motion records are documented in the first of a series of USC reports entitled the Earthquake Strong-Motion Data Information System (EQINFOS) (Trifunac and Lee, 1987).

By late 1994, the strong-motion database (third generation) grew to over 1,926 free-field records from 297 earthquakes and aftershocks. Those included the records from the main shock and aftershocks of both the 1987 Whittier Narrows and the 1994 Northridge earthquakes in Southern California, and from the 1989 Loma Prieta earthquake in Northern California. Many accelerograms in Southern California were recorded by the USC strong-motion array (Trifunac and Todorovska, 2001b). If the analog records were available, they were digitized and processed by the automatic digitization system using a PC in the strong-motion laboratory at USC (Lee and Trifunac, 1990). Other records included were mainly those from the Strong-Motion Instrumentation Program (SMIP) of the California Division of Mines and Geology and from the United States Geological Survey. At each stage of the database processing, all data were treated uniformly, using the standard software for image processing developed at USC (Trifunac and Lee, 1979b; Lee and Trifunac, 1979, 1984).

2. Site Classification

The first geological site classification was introduced (Trifunac and Brady, 1975b) to describe the broad environment of the recording station and was based on geologic maps. The recording sites were to be viewed on a scale measured in terms of kilometers, in contrast to the geotechnical site characterization viewed for the top several tens of meters only (Trifunac, 1990a). This geological site classification is given in Table 6. Ideally, according to this approach, a site should be classified either as being on sediments ($s = 0$) or on the basement rock ($s = 2$). However, for some sites having a complex environment, an “intermediate” classification ($s = 1$) was assigned. Trifunac and Lee (1979a) later refined the above classification and used the depth of sediments beneath the recording site, h , in km, as a site characteristic. This new parameter was used in the second generation of empirical scaling equations in the 1980s.

Table 6: USC Strong-Motion Group Geological Site Classification

Geological Site Classification	Description
0	Alluvial and Sedimentary Deposits
1	Intermediate Sites
2	Basement Rock

In the 1980s, additional parameters were introduced to refine the characterization of the local site beyond the geological site condition, s , and the depth of sediments, h . The first such parameter is the local soil type, s_L , which is representative of the top 100–200 m of soil (Trifunac, 1990a) (see Table 7).

Table 7: USC Strong-Motion Group Soil Type, s_L

Soil Type, s_L	Description
0	“Rock” Soil Site
1	Stiff Soil Site
2	Deep Soil Site

The second parameter added to site characterization was the average shear wave velocity, V_L , of the soil in the top 30 m. The soil velocity type variable, S_T , was used as described in Table 8. In the scaling equations, the velocity type was represented by indicator variables.

Table 8: USC Strong-Motion Group Soil Velocity Type, S_T

Soil Velocity Type, S_T	Description
A	$V_L > 0.75$ km/s
B	$0.75 \text{ km/s} \geq V_L > 0.36$ km/s
C	$0.36 \text{ km/s} \geq V_L > 0.18$ km/s
D	$V_L \leq 0.18$ km/s

3. Distance Definition Used for Attenuation Relation

In the 1970s, the functional form of the attenuation with epicentral distance R followed the definition of local magnitude scale (Trifunac, 1976b), which states that the logarithm of the corrected peak amplitude on a standard instrument is equal to the earthquake magnitude (Richter, 1958; Trifunac, 1991b). Hence, the functional form of attenuation,

$$\log A_0(R) + \dots - g(T)R \quad (15)$$

was used, where $\log A_0(R)$ together with a term linear in epicentral distance at each period was intended to account for the average correction for anelastic attenuation. A detailed description of this attenuation function can be found in Trifunac (1976b).

In 1980s, Trifunac and Lee (1985a, 1985b) developed the first magnitude-frequency-dependent attenuation function, $\mathcal{Att}(\Delta, M, T)$, a function of the “representative” distance Δ from the source to the site, for magnitude M and for period T of strong motion. For a complete, detailed physical description of such a function, the reader is referred to the above reference. Briefly,

$$\mathcal{Att}(\Delta, M, T) = \mathcal{A}_0(T) \log_{10} \Delta$$

where

$$\mathcal{A}_0(T) = \begin{cases} a + b \log_{10} T + c (\log_{10} T)^2 & T < 1.8 \text{ s} \\ -0.732025 & T \geq 1.8 \text{ s} \end{cases} \quad (16)$$

with $\mathcal{A}_0(T)$, a function in T , approximated by a parabola for $T < 1.8$ s and by a constant beyond that, where $a = -0.767$, $b = 0.272$ and $c = -0.526$. The source-to-station distance Δ , was defined as in Gusev (1983):

$$\Delta = S \left(\ln \frac{R^2 + H^2 + S^2}{R^2 + H^2 + S_0^2} \right) \quad (17)$$

where R is the surface distance from epicenter to the site, H is the focal depth, $S = 0.2 + 8.51(M - 3)$ is the size of the earthquake source at magnitude M , and S_0 is the correlation radius of the source function. It was approximated by $S_0 = c_s T / 2$, where c_s is the shear wave velocity in the rocks surrounding the fault.

In the 1990s, Lee and Trifunac (1990) modified this attenuation function to the following form:

$$\mathcal{Att}(\Delta, M, T) = \begin{cases} \mathcal{A}_0(T) \log_{10} \left(\frac{\Delta}{L} \right) & R \leq R_{\max} \\ \mathcal{A}_0(T) \log_{10} \left(\frac{\Delta_{\max}}{L} \right) - \frac{(R - R_{\max})}{200} & R > R_{\max} \end{cases} \quad (18)$$

with Δ and R defined as above. Δ_{\max} and R_{\max} represent the distances beyond which $\mathcal{A}tt(\Delta, M, T)$ has a slope defined by the Richter's local magnitude scale M_L . The new parameter, $L = L(M)$, was introduced to model the length of the earthquake fault. It was approximated by $L = .01 \times 10^{0.5M}$ km (Trifunac, 1993a, 1993b). Δ/L is thus a dimensionless representative source-to-station distance.

4. The Source-to-Station Path Types

In the third generation of regression studies of spectral amplitudes in the 1990s, a new term (Lee et al., 1995; Lee and Trifunac, 1995a, 1995b), r , $0 \leq r \leq 1$ (or $100r$, as a percentage) was introduced. In this, r is the ratio (or percentage) of wave path through geological basement rock relative to the total path, measured along the surface from the earthquake epicenter to the recording site. Alternately, a generalized path type classification was also used. It describes the characteristic types of wave paths between the sources and stations for the strong-motion data available up to the early 1990s in the western U.S. At that time, due to the limited amount of data, only eight such categories could be identified with a sufficient number of recordings to be included in the regression analyses (see Table 9). Figure 1 shows a schematic representation of the "geometry" of these path types. The eight path types in Figure 1 can further be grouped into four path groups: "1", "2", "3", and "4", as described in Table 10.

Table 9: USC Strong-Motion Group Source-to-Station Path Type

Path Type	Description
1	Sediments-to-sediments (100%)
2	Rock-to-sediments, almost vertically
3	Rock-to-sediments, almost horizontally
4	Rock-to-rock (100%)
5	Rock-to-rock through sediments, almost vertically
6	Rock-to-sediments through rock and sediments, almost vertically
7	Rock-to-sediments through rock and sediments, almost horizontally
8	Rock-to-rock through sediments, almost horizontally

5. The Scaling Equations

Only the most recent (the third generation) scaling equations (Lee and Trifunac, 1995a, 1995b) for spectral amplitudes will be illustrated here. A description of the complete set of scaling relations of all three generations can be found in Lee (2002). The following regression equations illustrate the four scaling models.

Model (i): Mag-site + soil + % rock path multi-step model

$$\log PSV(T) = \frac{M + \mathcal{A}tt(\Delta, M, T) + b_1(T)M + b_2(T)s + b_3(T)v + b_4(T) + b_5(T)M^2}{+ \sum_i b_6^{(i)}(T)S_6^{(i)} + (b_{70}(T)r + b_{71}(T)(1-r))R_{<}} \quad (19)$$

where $R_{<} = \min(R, R_{\max})$, and $\mathcal{A}tt(\Delta, M, T)$ were defined in the previous section (Equation (18)). Substituting $\mathcal{A}tt(\Delta, M, T)$ into Equation (19) gives

$$\log PSV(T) = \begin{cases} M + \mathcal{A}_0(T) \log_{10} \left(\frac{\Delta}{L} \right) + b_1(T)M + b_2(T)s + b_3(T)v + b_4(T) + b_5(T)M^2 \\ \quad + \sum_i b_6^{(i)}(T)S_6^{(i)} + (b_{70}(T)r + b_{71}(T)(1-r))R & R \leq R_{\max} \\ M + \mathcal{A}_0(T) \log_{10} \left(\frac{\Delta_{\max}}{L} \right) + b_1(T)M + b_2(T)s + b_3(T)v + b_4(T) + b_5(T)M^2 \\ \quad + \sum_i b_6^{(i)}(T)S_6^{(i)} + (b_{70}(T)r + b_{71}(T)(1-r))R_{\max} - \frac{(R - R_{\max})}{200} & R > R_{\max} \end{cases} \quad (20)$$

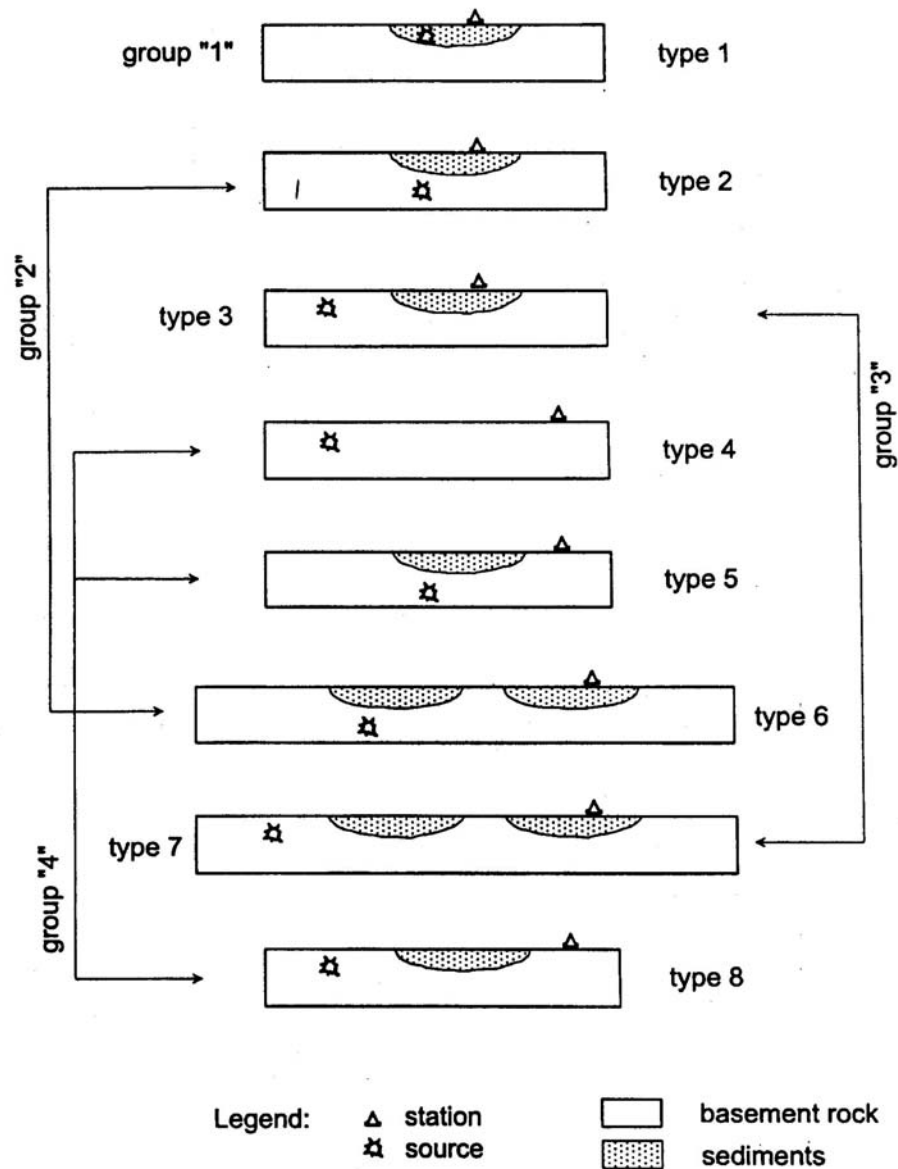


Fig. 1 Eight path types from source to recording station

Table 10: USC Strong-Motion Group Source-to-Station Path Groups

Path Group	Path Types Included	Description
"1"	1	Earthquake source and recording site within the same sediment
"2"	2, 6	Earthquake source in basement rock, recording site almost vertically above
"3"	3, 7	Earthquake source in basement rock close to the surface; Recording site on nearby sediment, almost horizontally
"4"	4, 5, 8	Earthquake source in basement rock, recording site on the same basement rock, with or without sediments in between

Model (ii): Mag-depth + soil + % rock path multi-step model

$$\log PSV(T) = M + \mathcal{A}tt(\Delta, M, T) + b_1(T)M + b_2(T)h + b_3(T)v + b_4(T) + b_5(T)M^2 + \sum_i b_6^{(i)}(T)S_6^{(i)} + (b_{70}(T)r + b_{71}(T)(1-r))R_{\zeta} \quad (21)$$

Model (iii): Mag-site + no soil + % rock path multi-step model

$$\log PSV(T) = M + \mathcal{A}tt(\Delta, M, T) + b_1(T)M + b_2(T)s + b_3(T)v + b_4(T) + b_5(T)M^2 + (b_{70}(T)r + b_{71}(T)(1-r))R_z \quad (22)$$

Model (iv): Mag-site + no soil + % rock path multi-step model

$$\log PSV(T) = M + \mathcal{A}tt(\Delta, M, T) + b_1(T)M + b_2(T)h + b_3(T)v + b_4(T) + b_5(T)M^2 + (b_{70}(T)r + b_{71}(T)(1-r))R_z \quad (23)$$

A description of the detailed steps required for the development of these regression equations, and illustration of the results and comparison with the actual data can be found in Lee and Trifunac (1995a, 1995b), a brief summary of which can also be found in Lee (2002).

It may be noted that the equations of Lee and Trifunac (1995a, 1995b) (as with all previous USC equations) considered the horizontal and vertical response spectral amplitudes simultaneously in the same equation. These are differentiated by the term $b_3(T)v$, where $v = 0$ for the horizontal components and $v = 1$ for the vertical component.

6. Scaling with Modified Mercalli Intensity (MMI)

Instead of using magnitude and distance to describe the strong earthquake motions, another alternate scaling parameter used is the site intensity. In the U.S., the Modified Mercalli Intensity (MMI) scale is used. To scale PSV spectra in terms of MMI, I_{MM} , the (first generation) scaling equations can take the following form (Trifunac and Lee, 1979a):

$$\log_{10} [PSV(T)] = b(T)I_{MM} + c(T) + d(T)h + e(T)v \quad (24)$$

with I_{MM} being the discrete levels of the MMI scale at the recording site, and all other scaling parameters, h and v , being the same as before. In the second generation, in the 1980s, the analysis was carried out on the database of 438 free-field records from 104 earthquakes. For some of the free-field sites, the reported MMI levels were not available, so estimated MMI levels were used instead. These estimated MMI levels were calculated using the equation (Lee and Trifunac, 1985),

$$\hat{I}_{MM} = 1.5M - A - B \ln \Delta - C\Delta/100 - Ds \quad (25)$$

\hat{I}_{MM} was then used in place of I_{MM} in Equation (24).

SUMMARY: COMPARISONS AND CONCLUSIONS

The scaling models of the four groups are next compared, and their differences and similarities are discussed. Since a typical scaling model involves the database, the regression parameters, the dependent scaling variables, and the scaling equation used in the regression, all these for all the groups will be examined.

1. The Database

The main sources of earthquake records used in the regressions by Boore et al. (1993, 1997) are from the Strong-Motion Instrumentation Program of the California Division of Mines and Geology and the United States Geological Survey. The authors did not digitize and process any of the analog records themselves, and the data collected (Boore et al., 1993, 1997) were restricted to shallow earthquakes with moment magnitudes greater than 5.0. As stated in Boore et al. (1997), 271 two-component recordings from 20 earthquakes were used to develop the equations for peak acceleration, and 112 two-component recordings from 14 earthquakes were used for the response spectral equations. Of the 112 records, 109 were all from 11 earthquakes in California. Three earthquakes outside the continental U.S. that were also used in the regression were in Alaska and Nicaragua (Boore et al., 1993), as shown in Table 11.

The sources of earthquake records used by Abrahamson and Silva (1997) are more “international”. The final data used in their regression analysis consists of a set of 655 recordings from 58 earthquakes. While the majority of the earthquakes are from the western U.S., the database does include 9 (of the 58) events from other countries, including Armenia, Canada, Iran, Italy, Mexico, and Russia. In the order of

occurrence, these non-U.S. earthquakes are given in Table 12 (Abrahamson and Silva, 1997). It may be noted that all of these non-U.S. earthquakes, except for Event # 62, the Taiwan (SMART # 5: $M = 5.7$) earthquake, have magnitudes > 6 .

Table 11: Boore et al. (1993, 1997) Earthquake Database

Western U.S. (California) Earthquakes				
Event No.	Earthquake	Year	Magnitude	Number of Records
8	Imperial Valley	1940	7.0	1
4	Kern Country	1952	7.4	4
32	Daly City	1957	5.3	1
50	Parkfield	1966	6.1	5
58	Borrego Mountain	1968	6.6	1
65	San Fernando	1971	6.6	4
146	Coyote Lake	1979	5.8	5
147	Imperial Valley	1979	6.5	19
328	Loma Prieta	1989	6.92	49
349	Petrolia	1992	7.1	6
352	Landers	1992	7.3	14
Total of 11 (all California) earthquakes with 109 records				
All Other (Non-California) Earthquakes				
Event No.	Earthquake	Year	Magnitude	Number of Records
76	Sitka, Alaska	1972	7.7	1
79	Managua, Nicaragua	1972	6.2	1
144	St. Elias, Alaska	1979	7.6	1
Total of 3 (non-California) earthquakes with 3 records				

Table 12: Abrahamson and Silva (1997) Non-U.S. Earthquakes

Event No.	Earthquake	Year	Magnitude
38	Friuli, Italy	1976	6.5
39	Gazli, USSR	1976	6.8
41	Friuli, Italy	1976	6.1
43	Tabas, Iran	1978	7.4
59	Victoria, Mexico	1980	6.4
62	Taiwan (SMART # 5)	1981	5.7
79	Nahanni, Canada	1985	6.8
82	Taiwan (SMART # 40)	1986	6.4
93	Spitak, Armenia	1988	6.8

The sources of earthquake records studied by the Strong-Motion Group at USC are numerous, but so far come from only four countries. The regression in the 1990s used 1,926 free-field records from 297 earthquakes and aftershocks, all from western U.S. Records from other parts of the world have also been collected, processed, and documented in a series of USC reports referred to as EQINFOS, which were later used in regression studies for scaling strong-motion amplitudes within the region contributing the data (see Table 13).

Table 13: USC Strong-Motion Group EQINFOS Reports for Different Countries

Country	EQINFOS Report Reference
USA	Trifunac and Lee, 1987; Lee et al., 1995
Yugoslavia	Jordanovski et al., 1987
Bulgaria	Nenov et al., 1990
India	Gupta et al., 1993; Chandrasekaran et al., 1993

In all of the USC studies, the records from different parts of the world were kept separately and were never used together in one regression. This is because the records in different countries are on sites situated on different tectonic regions and are from earthquakes with different fault characteristics. Earthquake magnitudes in different countries are also defined differently (Trifunac, 1991a; Trifunac and Živčić, 1991; Trifunac et al., 1991), and therefore it is impossible to have a uniform database worldwide. In general, no single attenuation law or common regression equation can satisfactorily be used to estimate strong motions in different seismic regions. It is, thus, appropriate that different regression equations be established for sites from different parts of the world. Readers interested in the regression equations for different countries, using homogeneous data recorded within that country, will find such examples as those listed in Table 14. The regression equations for the western U.S., developed at USC, used the available data “from, and only from”, earthquakes in the western U.S.

Table 14: USC Strong-Motion Group Regression Work on Earthquakes in Other Countries

Country	Regression Work
Yugoslavia	Novikova et al. (1993), Lee and Trifunac (1992), Lee and Manic (1994)
India	Das et al. (2002)

The data used in the regression of spectral amplitudes by the above three groups can be summarized as given in Table 15. The sources of earthquake records used by Ambraseys et al. (1996) were in Europe and the Middle East. A breakdown in percentage from various countries is shown in Table 16(a). The sources of earthquake records used by Ambraseys et al. (2005a, 2005b) were again in Europe and the Middle East. A breakdown in percentage from various countries is shown in Table 16(b).

Trifunac and Todorovska (1989a), and Trifunac et al. (1988), in their studies of the attenuation of seismic intensities in Albania and Yugoslavia, described the differences in the attenuation of the intensities for natural seismological zones of the Balkan Peninsula in southeastern Europe, as proposed by Shebalin et al. (1974). The observed differences for these regions are significant, and are neither adequately studied nor fully understood. It is, thus, unlikely that the attenuation of strong motions and response spectral amplitudes in Italy, Greece, the former Yugoslavia, and the former Soviet Union, for example, can all be described satisfactorily by just one common regression equation (Lee, 1997).

Having said all this, it is noted that there are many regions of the world where little or no recorded strong-motion acceleration data exist. For those regions, it is natural to use the equations developed for other regions. Care must be taken in doing so, and scaling equations may be considered from other similar tectonic regions and with similar path and local site conditions.

Table 15: Summary of Regression Database of the Three Groups

Group	Number of Earthquakes	Number of Recordings	Number of Earthquakes outside Continent U.S.
Boore et al. (1993)	14	112	3
Abrahamson and Silva (1997)	58	655	9
Lee and Trifunac (1995a, 1995b)	297	1,926	0

Table 16(a): Ambraseys et al. (1996) Earthquake Database for Different Countries

Earthquakes in Europe and Adjacent Regions	
Country	Percentage (%)
Italy	42
Greece	19
Former Soviet Union	13
Former Yugoslavia, Algeria, Azores, Bulgaria	12
Iran, Portugal, Turkey	14

Table 16(b): Ambraseys et al. (2005a, 2005b) Earthquake Database for Different Countries

Earthquakes in Europe and the Middle East		
Country	Number	Percentage (%)
Italy	174	29
Turkey	128	22
Greece	112	19
Iceland	69	12
Other	112	19
“Other” represents other countries contributing the records: Albania (1 record), Algeria (3), Armenia (7), Bosnia and Herzegovina (4), Croatia (1), Cyprus (4), Georgia (14), Iran (17), Israel (5), Macedonia (1), Portugal (4), Serbia & Montenegro (24), Slovenia (15), Spain (6), Syria (5), and Uzbekistan (1).		

2. Data Processing Procedures

As already noted, the sources of earthquake records used in the regression studies by Boore et al. (1993, 1997) are mostly from CDMG and USGS. Different agencies use slightly different methods of digitization and data processing, but any such differences usually cannot be taken into account in the regression studies. Up to 1993, Boore and co-workers used the values for peak acceleration scaled directly from the recorded accelerograms, rather than the peaks from the processed, instrument-corrected data. They did this to avoid “bias” in the peak values from the sparsely sampled older data. Thus, the peak values they used are from uncorrected, raw scaled data. The question that needs to be addressed, then, is what the systematic differences are in the peak values, and what percentages of data come from accelerographs that are known to have different natural frequencies (e.g., MO-2, AR-240, RFT-250, SMA-1, etc.) (Trifunac and Todorovska, 2001a, 2001b).

Abrahamson and Silva (1997) used a common procedure to reprocess all of the records, which included low-pass filtering of the data using a causal five-pole Butterworth filter to remove the long-period noises. As stated above, this filter is an infinite impulse response (IIR) filter, which produces the output data from past (earlier time) and present inputs, with no participation from future inputs. Such filters distort the phase in the output-filtered data (Rabiner and Gold, 1975; Lee and Trifunac, 1984). Obviously, if the acceleration data after filtering is phase-distorted and then used as input for calculations, the output response spectra will also be affected by those phase distortions, thus changing the shapes and amplitudes of the spectra.

In the work of Ambraseys et al. (1996), for the records not longer than 5 s, a parabolic baseline adjustment was made using a least-squares fit. For records longer than 10 s, an elliptical filter was applied. An elliptical (Chebyshev-typed) filter, like a Butterworth filter, is also an IIR filter, which means that the phase of the output data is distorted. IIR filters with these causal characteristics are useful in communication theory, where the outputs need to be obtained concurrently (instantaneously) with the inputs but are not suitable for processing of strong-motion accelerograms. Ambraseys et al. (2005a, 2005b) also used elliptical filters for low-pass filtering in the BAP software (Converse and Brady, 1992).

Ambraseys et al. (1996), like Boore et al. (1993, 1997), omitted instrument correction in their data processing procedure. They claim: “the instrument characteristics only significantly distort the recorded amplitudes at frequencies above 25 Hz, and their smallest response period included is from 0.1 s (10 Hz or below), thus this contamination is not important”. However, as pointed out in the discussion by Lee (1997), “The natural frequency of AR-240 accelerographs, for example, is $f_N \sim 18$ Hz (natural period of $T_N \sim 0.556$ s)”. The absolute acceleration spectral amplitudes are not affected significantly by the instrument transfer function for $f \ll f_N$, or $T \gg T_N$, but the slope of the regression coefficients C_1 , C_2 and C_4 in their regression equation (see Equation (11) above), versus period T would be affected near the period $T = 0.1$ s. This type of systematic bias becomes important and will lead to problems for other studies, which start from the empirically scaled spectral amplitudes (e.g., Trifunac, 1995a, 1995b), especially at high frequencies. The response spectral amplitudes predicted by Ambraseys et al. (1996), as

calculated from uncorrected acceleration data, have biased trends and large residuals at high frequencies due to the differences in the transfer functions of the recording instruments.

All of the data processing procedures of the Strong-Motion Group at USC used finite-impulse-response (FIR) filters for band-pass filtering to remove the high-frequency noise and long-period errors (Trifunac, 1972; Lee and Trifunac, 1984, 1990). The very first filter used, the Ormsby filter, was one such filter (Trifunac, 1972). For these FIR filters, each point of the output data is determined from past, present, and future inputs. In routine data processing for earthquake engineering, the entire input acceleration is available in a computer file memory, and so the dependence of filters on future inputs poses no problem.

The use of low-pass IIR filters was suggested by Sunder and Conner (1982), who claimed that the elliptical-type filters have the unique characteristics of being optimal, in the sense that, for a given order and ripple specifications, no other filters achieve a faster transition between the pass band and the stop band. However, the filters they proposed cause phase distortion of the input acceleration, and thus they are not acceptable in earthquake engineering (Lee and Trifunac, 1984). Note that the Ormsby-type (FIR) filter used by the USC group performs a perfect phase-distortionless transmission between the input and output data.

3. Site Classification

As stated in BJJ93, Boore et al. (1993) performed the regression analysis using a site classification scheme based on the average shear-wave velocity in the upper 30 m below the surface (see Table 1). Boore et al. (1993) point out that such a classification is similar to, “but different from” the one incorporated into the 1994 edition of the National Earthquake Hazard Reduction Program’s code provisions (Boore et al., 1997), which has five site classifications. Boore et al. (1993) refer to that site classification as the “NEHRP Site Class”. The possible confusion of the two site classifications was avoided in their subsequent work, BJJ94a and BJJ94b, and in their revised reports (Boore et al., 1994a, 1994b), in which the site effect was changed from being a constant for each site class to a continuous function of shear-wave velocity V_s , averaged to a depth of 30 m (Boore et al., 1997) (see Table 3). This suggests that a discrete value of shear wave velocity may be used in the regression. In summary, the site classification parameter used by Boore et al. (1993, 1997) is based completely, and only, on the shear-wave velocity at the site, averaged to a depth of 30 m. No information on the overall geological classification or on the depth of the soil and sediments below the site was included in their classification.

Abrahamson and Silva (1997) used the site classification given in Table 4. For most of their sites, however, the quantitative information for the velocity of shear waves in the soil is not available, so the sites are assigned a site classification subjectively, using the table as a guide, rather than being determined through some quantitative analysis. Their classification is similar to that of Boore et al. (1993, 1997), which is based only on the soil and not on the geological information below the surface.

Ambraseys et al. (1996, 2005a, 2005b) use a site scheme that is identical to that of Boore et al. (1993), using soil site classification. They may confuse the reader by renaming the categories A, B, C, and D, which are defined in Boore et al. (1993), as R, A, S, and L, respectively. This can become even more confusing when the terms “rock” and “stiff soil” are associated with their categories R and A. These terms were originally proposed and used by Seed et al. (1974) and were also adopted by the Strong-Motion Group at USC (Trifunac, 1990a). The terms “rock” and “stiff soil” belong to a very different type of classification from the A, B, C, and D classification in Boore et al. (1993). The latter are based only on the average shear wave velocity in the top 30 m. The terms “rock” and “stiff soil”, in contrast, also involve the size (depth) of soil deposits, as in Seed (1974) (see Table 17).

Table 17: Seed (1974) Soil Type Characterization

Soil Type, s_L	Characterization
0 (Rock)	Soil with shear wave velocity > 800 m/s and depth $< \sim 10$ m
1 (Stiff Soil)	Soil with shear wave velocity > 800 m/s and depth < 75 – 100 m
2 (Deep Soil)	Soil with shear wave velocity < 800 m/s and depth ~ 100 – 200 m

The Strong-Motion Group at USC first started with a completely different site classification. The first, in the 1970s (Trifunac and Brady, 1975b), was proposed to characterize roughly the geological environment of the recording station, using geologic maps. The geological sites were grouped as shown in Table 6. This geological site classification was intended to be measured in “thousands (not hundreds), of feet, or in kilometers (not meters)”. Thus, this is totally different from the soil classifications later proposed by Boore et al. (1993, 1997) and Abrahamson and Silva (1997), which are for the soil deposits below the surface, measured to only about “a hundred feet (not thousands) or meters (not kilometers)”. In the late 1970s, Trifunac and Lee (1979a) refined their site classification and used the “depth of sedimentary deposits beneath the recording site, h , in km, as a geological site characteristic”. The continuous parameter h , and the discrete geological classification s , were subsequently both used at USC in the second and third generations of regression analyses in the 1980s and 1990s.

This was the trend in the 1980s—the groups of Boore, Abrahamson, and Ambraseys were all using the surface soil information as a site characteristic, while the Strong-Motion Group at USC was using the geological information below the surface and surrounding the site.

In the 1990s, the above differences in site classification and their effects on spectral amplitudes were addressed in the third generation analyses of spectral regressions, in the reports by the Strong-Motion Group at USC (Lee and Trifunac, 1993, 1995a, 1995b; Lee et al., 1995). It is conjectured that the geological characteristics below a site affect the long-to-intermediate periods, or small-to-intermediate frequencies of waves arriving at the site, while the surface soil characteristic at a site affects the short periods (high frequencies) of motions. In the third generation of regressions at USC, two additional parameters were introduced to characterize the local soil site in addition to the geological site effects. The first one is the local soil type, s_L , representative of the top 100–200 m beneath the surface (Trifunac, 1990a), defined as in Table 7. A second parameter used was the average soil velocity, V_L , in the top 30 m beneath the surface. This is the same parameter as was used by Boore et al. (1994a, 1994b) in their revised site characterization. When this information was not available, a soil velocity type, S_T , was adopted, defined as in Table 8. In each case, an indicator variable representing the velocity type is assigned.

Thus, the Strong-Motion Group at USC is the only group that has used both geological and soil site classifications in their latest generation of regressions of spectral amplitudes. They argued that both classifications must be included “simultaneously” in the characterization of site-specific spectra because ignoring the local geological conditions may lead to exaggerated factors “representing” the local soil conditions.

A study of the response spectral amplitudes of recorded strong motions in California (Lee and Trifunac, 1995b) concluded that the A, B, C, and D local soil classification based only on the average shear wave velocity in the top 30 m, as proposed by Boore et al. (1993), becomes statistically insignificant when used as a third parameter simultaneously with the soil ($s_L = 0, 1$ and 2) and geological ($s = 0, 1$ and 2) classifications. This suggests that when the depth of the soil deposit at a site is included in the soil classification, this will out-perform the scaling equations based only on the soil information close to the surface. Finally, we note that the systematic gathering of many of these site soil parameters is often very expensive, difficult, and time consuming, but the geological site description in terms of $s = 0, 1$ and 2 is simple and easy to perform.

The site characterizations used in the spectral regressions in the 1990s for the four groups are summarized in Tables 18(a) and 18(b).

Table 18(a): Comparison of Soil Site Characterizations Used by the Four Groups

Group	Soil Classification		
	Site Class	Soil Velocity	Reference
Boore et al. (1993)	A, B, C, D	average 30 m V_L	Table 1
Abrahamson and Silva (1997)	A, B, C, D, E	—	Table 4
Ambraseys et al. (1996, 2005a, 2005b)	R, A, S, L	—	Table 5
Lee and Trifunac (1995a, 1995b)	$s_L : 0, 1, 2$	average 30 m V_L	Table 7

Table 18(b): Comparison of Geological Site Characterizations Used by the Four Groups

Group	Geological Classification	
	Site, <i>s</i>	Alluvial Depth, <i>h</i>
Boore et al. (1993)	No	No
Abrahamson and Silva (1997)	No	No
Ambraseys et al. (1996, 2005a, 2005b)	No	No
Lee and Trifunac (1995a, 1995b)	Yes	Yes (see Table 6)

4. Distance Definition Used in Attenuation Relations

In the work of Boore et al. (1993), BJS93, the epicentral distance term used, r , is defined as $r = \sqrt{d^2 + h^2}$, where d is the measured epicentral distance in km from the earthquake source to the site, and h is a fictitious depth to be determined. Instead of using the actual measured depth of the earthquake source, Boore et al. (1993) treated h as an unknown parameter to be determined by regression. They first used the attenuation term, $b_4 r + b_5 \ln r$, in their regression equation, but this was subsequently replaced by $b_5 \ln r$. It was pointed out that a regression including the $b_4 r$ term resulted in values of b_4 greater than zero, which would lead to unreasonable behavior at large distances, and so the term was deleted. The remaining term, $b_5 \ln r$, is thus the only term used by Boore et al. (1993, 1997) to characterize the attenuation of the spectral amplitudes from the source to the recording site.

In the work of Abrahamson and Silva (1997), the distance introduced by Idriss (1991) and Sadigh et al. (1993)—namely, r_{rup} , is the closest distance from the site to the rupture plane. The distance term is then $R = \sqrt{r_{rup}^2 + c_4^2}$, which is the same as in Boore et al. (1993), where c_4 is again a fictitious term to be determined by regression. Unlike Boore et al. (1993), where the term c_4 is interpreted as a fictitious depth term, Abrahamson and Silva (1997) pointed out that in their model the rupture distance r_{rup} may include the depth for dipping faults and for faults that do not reach the surface. It is not clear if c_4 can be interpreted as a fictitious depth, but it is included in their distance definition. The attenuation term used is $[a_3 + a_{13}(M - c_1)] \ln R$, which is similar to that used by Boore et al. (1993), except that the coefficient is taken to be dependent upon earthquake magnitude, M .

From the seismological and earthquake engineering points of view, the definition of the distance from the earthquake source to the site is not as simple as it may seem. This is because the earthquake source is not a point but a three-dimensional surface, which is often empirically correlated with the magnitude and size of the earthquake. To execute a regression analysis, one has to decide on how to define a distance between a rupture surface area and a recording site. The attenuation of the spectral amplitudes is, thus, even more complicated because the attenuation will also depend upon the frequency of the motions.

In the 1980s, Trifunac and Lee (1985a, 1985b) developed the first frequency-dependent attenuation function, $\mathcal{A}tt(\Delta, M, T)$ (see Equation (16)), a function of the “representative” distance Δ from the source to the site, for magnitude M and period T of strong motion. For a complete, detailed description of this function, the reader is referred to the above references. Here, Δ is the source-to-station distance of Gusev (1983), selected to include the rupture size of the earthquake (see Equation (17)). In the 1990s, Lee and Trifunac (1990) refined and modified the attenuation function to the form given in Equation (18). This attenuation function aims to account for the complicated nature of the attenuation from the rupture area to the site and is magnitude-, period-, and distance-dependent. Compared with the works of the other three groups—Boore et al. (1993, 1997), Abrahamson and Silva (1997), and Ambraseys et al. (1996)—this is a more detailed description of the attenuation from the source to the site.

5. Differences between the Models: Fault Type and Path Type

Boore et al. (1994a, 1994b, 1997), in their updated regression equation, introduced an earthquake-fault term (see Equation (3)), as an indicator variable, which defines a constant term, one each for strike-slip, reverse-slip, and unknown-slip earthquakes. This distinction of ground motions that result from

strike-slip and reverse-slip faults is a feature that has been studied by others as well (Idriss, 1991; Sadigh et al., 1993; Boore et al., 1993, 1997; Campell and Bozorgnia, 1994; Abrahamson and Silva, 1997).

Abrahamson and Silva (1997) introduced a similar term in their regression equation, which they called the style-of-faulting factor, $Ff_3(M)$, where F is the fault type. It is 1 for reverse, 0.5 for reverse/oblique, and 0 otherwise, and $f_3(M)$ is as defined in Equation (6) and fitted for each period T . They, thus, allowed for magnitude and period dependence of the faulting factor. Following Somerville and Abrahamson (2000), they introduced another term to account for the differences in motions from the hanging wall and foot wall of dipping faults; they called this term, $f_4(M, r_{rup})$, as the “hanging wall effect” (see Equations (7)-(9)).

Ambraseys et al. (1996) did not consider any fault-type parameters in their regression. Ambraseys et al. (2005a, 2005b) did include the fault mechanism terms in their regression equations, as in Boore et al. (1994a, 1994b, 1997).

The above indicates that different fault geometries and slip directions could generate different motions at the site, which no one would dispute. If the motions that originate from the fault travel directly to the site without scattering and diffraction, the resulting motions at the site should depend upon the type of faulting and the type of motions at the source. In reality, however, the waves will not travel directly from the source to the site because the medium between the source and the site is almost always very irregular. The waves arriving at the site are thus a combination of waves traveling between different parts of the source and the site along multiple paths, and, therefore, they have undergone significant changes as a result of scattering and diffraction along the path. The arriving signals, besides being attenuated, can thus be very different in phase and amplitude from those at the source.

It may be argued and conjectured that such source and fault mechanism factors may have influence mainly on the near-source records and, hence, on the resulting spectra. Further away from the source with increasing distance, such kind of influence may become weaker and weaker. Up till now, there are very few near-field records available in the database worldwide. In the future when more near-field records become available, the question of whether to include a source-mechanism term in regression will be determined by the data.

The strong-motion group at USC thus far did not consider earthquake fault-type terms in their regression. Lee and Trifunac (1993, 1995a, 1995b), and Lee et al. (1995) conjectured that, instead, the spectral motions are more dependent on the complicated path between the source and the site. They introduced a generalized path type classification, which describes the different types of wave paths between the source and stations (see Figure 1). As confirmed by the regressions, the path types are significant factors for the resulting motions at the site. Therefore, a new term (Lee et al., 1995a, 1995b), r , with $0 \leq r \leq 1$ (or $100r$, in percentage) was introduced. r is the ratio (or percentage) of wave path through geological basement rock to the total path, measured along the surface from the earthquake epicenter to the recording site.

In summary, the use of fault type and path type parameters in the regressions of the four different group is as given in Table 19.

Table 19: Fault Type versus Source-to-Station Path Type

Group	Fault Type	Source-to-Station Path Type
Boore et al. (1993)	Yes	No
Abrahamson and Silva (1997)	Yes	No
Ambraseys et al. (1996)	No	No
Ambraseys et al. (2005a, 2005b)	Yes	No
Lee and Trifunac (1995a, 1995b)	No	Yes

6. Other Differences between the Models

6.1 Frequency Band of Analysis

One additional difference among the various studies of spectral amplitudes has to do with the period range of data in the regression. As noted by many in this field (Trifunac, 2005), the spectral amplitudes are available only for a limited frequency range. This is because the input acceleration data recorded by analog instruments are affected by the recording and digitization noise (Lee et al., 1982). In the 60's and early 70's, the digitization process had to be performed manually. In fact, up to 1975, all the recorded accelerograms from the 1933 Long Beach to the 1971 San Fernando earthquakes were processed in this way.

The digitized data was not available at many points per second, and the high frequency data beyond 25 Hz (< 0.04 s) was out of reach. At the long period end, the Fourier and spectral data were dependent on the amplitudes of the recorded acceleration, i.e., more dependent on the magnitude of the earthquake, the location of the recording site relative to the earthquake source, and the level of digitization noise associated with the frequency content of the input data. Figure 2 (Lee, 2002) is the PSV spectra for 5% damping and 0.5 probability of exceedance for a site at epicentral distance $R = 10$ km and on rock ($h = 0$), the source at depth $H = 5$ km, and for magnitudes $M = 4, 5, 6$ and 7. It shows the plot of the usable frequency range of the spectral amplitudes for various amplitudes of the recorded data. The figure shows that the uniformly processed high quality strong-motion data is available at periods from 0.04 second (at or below 25 Hz) up to several seconds, and no more than 10 s (or no less than 0.10 Hz). The figure also indicates the domain (see the lightly shaded area) where the empirical scaling equation can be used.

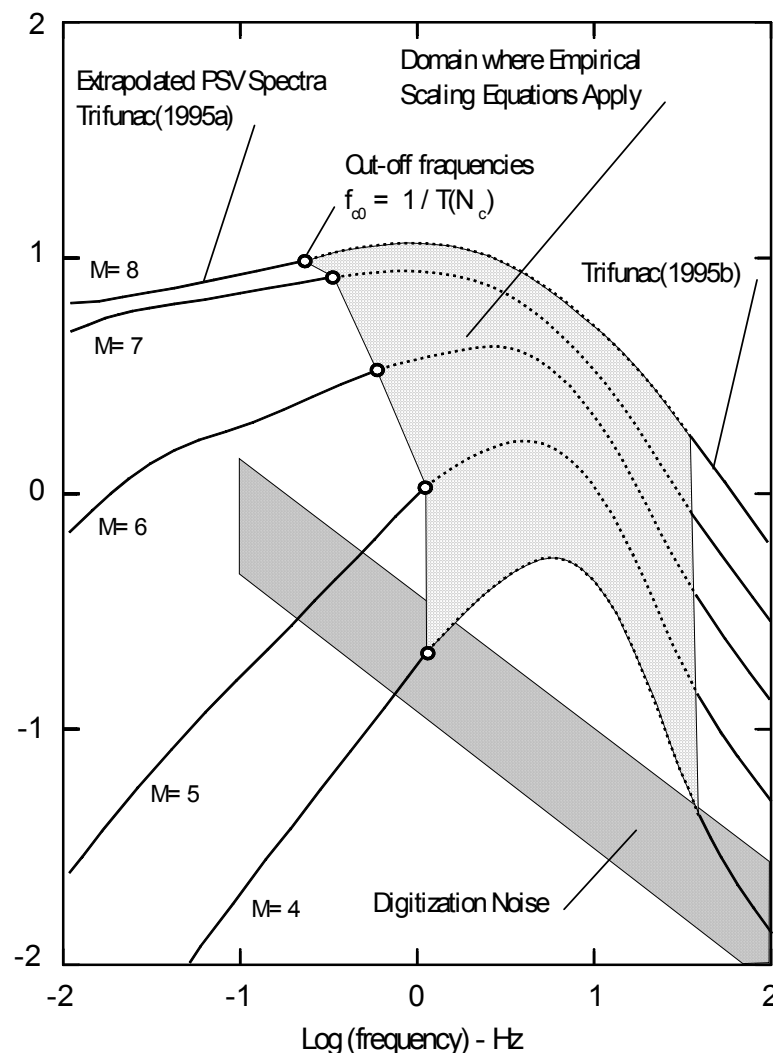


Fig. 2 PSV spectra for 5% damping (from Lee (2002))

This area is bounded by the spectra for $M = 4$ and $M = 7$, and is between the period $T = 0.04$ s and the cut-off period, T_c , increasing from $T_c = 0.90$ s for $M = 3$ and 4 to $T_c = 7.5$ s for $M = 7$ (Trifunac, 1993a). In the figure, the dark shaded zone, extending from $PSV \sim 0.1$ in/s around $T = 0.04$ s to $PSV \sim 1$ in/s around $T = 10.0$ s, represents the amplitudes of the recording and processing noise (Trifunac and Todorovska, 2001a).

In many engineering applications, the spectral amplitudes need to be specified in a broad frequency band, which is broader than the available band shown above, where the empirical regression equations are valid. Trifunac (1993a, 1993b, 1994a) presented a method for extension of the regression equations of spectral amplitudes to periods at both ends, namely, to the periods beyond just several seconds, and to periods shorter than 0.04 s.

6.2 Component Orientation: Horizontal and Vertical Response Spectra

The regression equations of Boore et al. (1997) (see Equations (1) and (2)) have no terms indicating the component orientation of the spectral amplitudes. This is because they considered only the response spectra from the two horizontal components of recorded acceleration at each site. In a similar fashion, Ambraseys et al. (1996) did the regression analyses only on the response spectra from the horizontal components of motions.

Abrahamson and Silva (1997) did perform the regression analyses for both the horizontal and vertical response spectra. The vertical components use the same functional form and multiple step procedure as for the horizontal components. The authors listed the coefficients for the horizontal and vertical components in their work. Since the regression procedure is performed separately for the horizontal and vertical components at each period, the coefficients for them are different at each period, even though the scaling equations used have the same form for both components. This means that the dependence of spectral amplitudes on magnitude, distance, local site effects and fault type is different for the horizontal and vertical components in their regression model. Ambraseys et al. (2005a, 2005b), as in Abrahamson and Silva (1997), considered the horizontal and vertical response spectra in separate equations.

The strong-motion group at USC considered both the horizontal and vertical components of response spectra in all their studies, the only difference being that the regression for both the horizontal and vertical components were not performed separately, but together simultaneously in one equation (see Equations (19)–(23)). In each of the scaling model, the horizontal and vertical components were differentiated by the term, $b_3(T)^v$, where $v = 0$ for the horizontal component, and $v = 1$ for the vertical component. Since both of the components use the same scaling equation, the dependence of the spectral amplitudes on magnitude, distance, path type and site effects are the same for both the horizontal and vertical components of each recorded motion. The only difference between them is just one scaling factor $b_3(T)^v$. This approach is more physical since the horizontal and vertical motions of the recorded accelerations are just components of the total resultant motion at the site. They should thus have the same dependence on magnitude, distance, path type and site effects.

A summary of the above is given in Table 20.

Table 20: Summary of Regression Works on Horizontal and Vertical Components of Motions

Group	Horizontal	Vertical	Together?
Boore et al. (1993)	Yes	No	—
Abrahamson and Silva (1997)	Yes	Yes	No
Ambraseys et al. (1996)	Yes	No	—
Ambraseys et al. (2005a, 2005b)	Yes	Yes	No
Lee and Trifunac (1995a, 1995b)	Yes	Yes	Yes

6.3 Scaling in Terms of Earthquake Intensity

Of the four groups, the strong-motion group at USC is the only group that has developed scaling equations of response spectra in terms of earthquake intensity. The other three groups used only earthquake magnitude in their regression analyses.

ACKNOWLEDGEMENTS

The author would like to thank the anonymous reviewers for their critical and constructive comments that resulted in numerous improvements in the final version of this paper.

REFERENCES

1. Abrahamson, N.A. and Silva, W.J. (1997). "Empirical Response Spectral Attenuation Relations for Shallow Crustal Earthquakes", *Seismological Research Letters*, Vol. 68, No. 1, pp. 94–127.
2. Ambraseys, N.N., Simpson, K.A. and Bommer, J.J. (1996). "Prediction of Horizontal Response Spectra in Europe", *Earthquake Engineering & Structural Dynamics*, Vol. 25, No. 4, pp. 371–400.
3. Ambraseys, N.N., Douglas, J., Sarma, S.K. and Smit, P.M. (2005a). "Equations for the Estimation of Strong Ground Motions from Shallow Crustal Earthquakes Using Data from Europe and the Middle East: Horizontal Peak Ground Acceleration and Spectral Acceleration", *Bulletin of Earthquake Engineering*, Vol. 3, No. 1, pp. 1–53.
4. Ambraseys, N., Douglas, J., Sarma, S.K. and Smit, P. (2005b). "Equations for the Estimation of Strong Ground Motions from Shallow Crustal Earthquakes Using Data from Europe and the Middle East: Vertical Peak Ground Acceleration and Spectral Acceleration", *Bulletin of Earthquake Engineering*, Vol. 3, No. 1, pp. 55–73.
5. Amini, A. and Trifunac, M.D. (1985). "Statistical Extension of Response Spectrum Superposition", *International Journal of Soil Dynamics and Earthquake Engineering*, Vol. 4, No. 2, pp. 54–63.
6. Anderson, J.G., Trifunac, M.D., Teng, T.L., Amini, A. and Moslem, K. (1981). "Los Angeles Vicinity Strong Motion Accelerograph Network", Report CE 81-04, University of Southern California, Los Angeles, U.S.A.
7. Biot, M.A. (1932). "Transient Oscillations in Elastic Systems", Ph.D. Thesis No. 259, Aeronautics Department, California Institute of Technology, Pasadena, U.S.A.
8. Biot, M.A. (1933). "Theory of Elastic Systems Vibrating under Transient Impulse with an Application to Earthquake-Proof Buildings", *Proceedings of the National Academy of Sciences of the United States of America*, Vol. 19, No. 2, pp. 262–268.
9. Biot, M.A. (1934). "Theory of Vibration of Buildings during Earthquake", *Zeitschrift für Angewandte Mathematik und Mechanik*, Vol. 14, No. 4, pp. 213–223.
10. Boore, D.M., Joyner, W.B. and Fumal, T.E. (1993). "Estimation of Response Spectra and Peak Accelerations from Western North American Earthquakes: An Interim Report", Open-File Report 93-509, United States Geological Survey, Denver, U.S.A.
11. Boore, D.M., Joyner, W.B. and Fumal, T.E. (1994a). "Estimation of Response Spectra and Peak Accelerations from Western North American Earthquakes: An Interim Report, Part 2", Open-File Report 94-127, United States Geological Survey, Denver, U.S.A.
12. Boore, D.M., Joyner, W.B. and Fumal, T.E. (1994b). "Ground Motion Estimates for Strike- and Reverse-Slip Faults", Insert in "Estimation of Response Spectra and Peak Accelerations from Western North American Earthquakes: An Interim Report, Part 2 (by D.M. Boore, W.B. Joyner and T.E. Fumal)" for the Southern California Earthquake Center, Open-File Report 94-127, United States Geological Survey, Denver, U.S.A.
13. Boore, D.M., Joyner, W.B. and Fumal, T.E. (1997). "Equations for Estimating Horizontal Response Spectra and Peak Acceleration from Western North American Earthquakes: A Summary of Recent Work", *Seismological Research Letters*, Vol. 68, No. 1, pp. 128–153.
14. Campbell, K.W. and Bozorgnia, Y. (1994). "Near-Source Attenuation of Peak Horizontal Acceleration from Worldwide Accelerograms Recorded from 1957 to 1993", *Proceedings of the 5th National Conference of Earthquake Engineering*, Chicago, U.S.A., Vol. 1, pp. 283–292.
15. Chandrasekaran, A.R., Das, J.D., Trifunac, M.D., Todorovska, M.I. and Lee, V.W. (1993). "Strong Earthquake Ground Motion Data in EQINFOS for India: Part IB", Report CE 93-04, University of Southern California, Los Angeles, U.S.A.
16. Converse, A.M. and Brady, A.G. (1992). "BAP, Basic Strong-Motion Accelerogram Processing Software; Version 1.0", Open-File Report 92-296A, United States Geological Survey, Denver, U.S.A.

17. Das, S., Gupta, I.D. and Gupta, V.K. (2002). "A New Attenuation Model for North-East India", Proceedings of the 12th Symposium on Earthquake Engineering, Roorkee, pp. 151–158.
18. Grazier, V.M. (1979). "Determination of the True Ground Displacement by Using Strong Motion Records", Physics of the Solid Earth, Izvestiya Academy of Sciences, U.S.S.R., Vol. 15, No. 12, pp. 875–885 (English edition published by the American Geophysical Union).
19. Gupta, I.D. and Trifunac, M.D. (1988a). "Order Statistics of Peaks in Earthquake Response", Journal of Engineering Mechanics, ASCE, Vol. 114, No. 10, pp. 1605–1627.
20. Gupta, I.D. and Trifunac, M.D. (1988b). "Attenuation of Intensity with Epicentral Distance in India", Soil Dynamics and Earthquake Engineering, Vol. 7, No. 3, pp. 162–169.
21. Gupta, I.D. and Trifunac, M.D. (1990a). "Probabilistic Spectrum Superposition for Response Analysis Including the Effects of Soil-Structure Interaction", Probabilistic Engineering Mechanics, Vol. 5, No. 1, pp. 9–18.
22. Gupta, V.K. and Trifunac, M.D. (1990b). "Response of Multistoried Buildings to Ground Translation and Rocking during Earthquakes", Probabilistic Engineering Mechanics, Vol. 5, No. 3, pp. 138–145.
23. Gupta, I.D., Rambabu, V. and Joshi, R.G. (1993). "Strong Earthquake Ground Motion Data in EQINFOS for India: Part 1A (edited by M.D. Trifunac, M.I. Todorovska and V.W. Lee)", Report CE 93-03, University of Southern California, Los Angeles, U.S.A.
24. Gusev, A.A. (1983). "Descriptive Statistical Model of Earthquake Source Radiation and Its Application to an Estimation of Short-Period Strong Motion", Geophysical Journal of the Royal Astronomical Society, Vol. 74, No. 3, pp. 787–808.
25. Hudson, D.E., Trifunac, M.D. and Brady, A.G. (1970). "Strong-Motion Earthquake Accelerograms, Digitized and Plotted Data, Vol. I", Report EERL 70-20, California Institute of Technology, Pasadena, U.S.A.
26. Hudson, D.E., Trifunac, M.D., Brady, A.G. and Vijayaraghavan, A. (1971). "Strong-Motion Earthquake Accelerograms, II, Corrected Accelerograms and Integrated Velocity and Displacement Curves", Report EERL 71-50, California Institute of Technology, Pasadena, U.S.A.
27. Hudson, D.E., Trifunac, M.D. and Brady, A.G. (1972a). "Strong-Motion Accelerograms, III, Response Spectra", Report EERL 72-80, California Institute of Technology, Pasadena, U.S.A.
28. Hudson, D.E., Trifunac, M.D., Udawadia, F.E. and Vijayaraghavan, A. (1972b). "Strong-Motion Earthquake Accelerograms, IV, Fourier Spectra", Report EERL 72-100, California Institute of Technology, Pasadena, U.S.A.
29. Idriss, I.M. (1991). "Selection of Earthquake Ground Motions at Rock Sites", Report prepared for National Institute of Standards and Technology, Department of Civil Engineering, University of California, Davis, U.S.A.
30. Jordanovski, L.R., Lee, V.W., Manic, M.I., Olumceva, T., Sinadinovski, C., Todorovska, M.I. and Trifunac, M.D. (1987). "Strong Earthquake Ground Motion Data in EQINFOS: Yugoslavia, Part I", Report CE 87-05, University of Southern California, Los Angeles, U.S.A.
31. Jordanovski, L.R., Todorovska, M.I. and Trifunac, M.D. (1992a). "Total Loss in a Building Exposed to Earthquake Hazard, Part I: The Model", European Earthquake Engineering, Vol. VI, No. 3, pp. 14–25.
32. Jordanovski, L.R., Todorovska, M.I. and Trifunac, M.D. (1992b). "Total Loss in a Building Exposed to Earthquake Hazard, Part II: A Hypothetical Example", European Earthquake Engineering, Vol. VI, No. 3, pp. 26–32.
33. Joyner, W.B. and Boore, D.M. (1981). "Peak Horizontal Acceleration and Velocity from Strong-Motion Records Including Records from the 1979 Imperial Valley, California, Earthquake", Bulletin of the Seismological Society of America, Vol. 71, No. 6, pp. 2011–2038.
34. Joyner, W.B. and Boore, D.M. (1982). "Prediction of Earthquake Response Spectra", Open-File Report 82-977, United States Geological Survey, Denver, U.S.A.
35. Joyner, W.B. and Boore, D.M. (1993). "Methods for Regression Analysis of Strong-Motion Data", Bulletin of the Seismological Society of America, Vol. 83, No. 2, pp. 469–487.

36. Kanamori, H. (1977). "The Energy Release in Great Earthquakes", *Journal of Geophysical Research*, Vol. 82, No. 20, pp. 2981–2988.
37. Lee, V.W. (1989). "Empirical Scaling of Pseudo Relative Velocity Spectra of Recorded Strong Earthquake Motion in Terms of Magnitude and Both Local Soil and Geologic Site Classifications", *Earthquake Engineering and Engineering Vibrations*, Vol. 9, No. 3, pp. 9–29.
38. Lee, V.W. (1990). "Scaling PSV Spectra in Terms of Site Intensity, and Both Local Soil and Geological Site Classifications", *European Earthquake Engineering*, Vol. IV, No. 1, pp. 3–12.
39. Lee, V.W. (1991). "Correlation of Pseudo Relative Velocity Spectra with Site Intensity, Local Soil Classification and Depth of Sediments", *Soil Dynamics and Earthquake Engineering*, Vol. 10, No. 3, pp. 141–151.
40. Lee, V.W. (1993). "Scaling PSV from Earthquake Magnitude, Local Soil, and Geologic Depth of Sediments", *Journal of Geotechnical Engineering, ASCE*, Vol. 119, No. 1, pp. 108–126.
41. Lee, V.W. (1997). "Discussion: Prediction of Horizontal Response Spectra in Europe", *Earthquake Engineering & Structural Dynamics*, Vol. 26, No. 2, pp. 289–293.
42. Lee, V.W. (2002). "Empirical Scaling of Strong Earthquake Ground Motion—Part I: Attenuation and Scaling of Response Spectra", *ISSET Journal of Earthquake Technology*, Vol. 39, No. 4, pp. 219–254.
43. Lee, V.W. and Manic, M. (1994). "Empirical Scaling of Response Spectra in Former Yugoslavia", *Proceedings of the Tenth European Conference on Earthquake Engineering, Vienna, Austria*, Vol. IV, pp. 2567–2572.
44. Lee, V.W. and Trifunac, M.D. (1979) "Automatic Digitization and Processing of Strong-Motion Accelerograms, Part II: Computer Processing of Accelerograms", Report CE 79-15 II, University of Southern California, Los Angeles, U.S.A.
45. Lee, V.W. and Trifunac, M.D. (1984). "Current Developments in Data Processing of Strong-Motion Accelerograms", Report CE 84-01, University of Southern California, Los Angeles, U.S.A.
46. Lee, V.W. and Trifunac, M.D. (1985). "Attenuation of Modified Mercalli Intensity for Small Epicentral Distances in California", Report CE 85-01, University of Southern California, Los Angeles, U.S.A.
47. Lee, V.W. and Trifunac, M.D. (1990). "Automatic Digitization and Processing of Accelerograms Using PC", Report CE 90-03, University of Southern California, Los Angeles, U.S.A.
48. Lee, V.W. and Trifunac, M.D. (1992). "Frequency Dependent Attenuation of Strong Earthquake Ground Motion in Yugoslavia", *European Earthquake Engineering*, Vol. VI, No. 1, pp. 3–13.
49. Lee, V.W. and Trifunac, M.D. (1993). "Empirical Scaling of Fourier Amplitude Spectra in Former Yugoslavia", *European Earthquake Engineering*, Vol. VII, No. 2, pp. 47–61.
50. Lee, V.W. and Trifunac, M.D. (1995a). "Frequency Dependent Attenuation Function and Fourier Amplitude Spectra of Strong Earthquake Ground Motion in California", Report CE 95-03, Department of Civil Engineering, University of Southern California, Los Angeles, California, 355pp.
51. Lee, V.W. and Trifunac, M.D. (1995b). "Pseudo Relative Velocity Spectra of Strong Earthquake Ground Motion in California", Report No. CE 95-04, University of Southern California, Los Angeles, U.S.A.
52. Lee, V.W., Trifunac, M.D. and Amini, A. (1982). "Noise in Earthquake Accelerograms", *Journal of the Engineering Mechanics Division, Proceedings of ASCE*, Vol. 108, No. EM6, pp. 1121–1129.
53. Lee, V.W., Trifunac, M.D., Todorovska, M.I. and Novikova, E.I. (1995). "Empirical Equations Describing Attenuation of the Peaks of Strong Ground Motion, in Terms of Magnitude, Distance, Path Effects, and Site Conditions", Report CE 95-02, University of Southern California, Los Angeles, U.S.A.
54. Nenov, D., Georgiev, G., Paskaleva, I., Lee, V.W. and Trifunac, M.D. (1990). "Strong Earthquake Ground Motion Data in EQINFOS: Accelerograms Recorded in Bulgaria between 1981 and 1987", Report CE 90-02, Bulgarian Academy of Sciences, Sofia, Bulgaria, and University of Southern California, Los Angeles, U.S.A.
55. Novikova, E.I., Todorovska, M.I. and Trifunac, M.D. (1993). "A Preliminary Study of the Duration of Strong Earthquake Ground Motion on the Territory of Former Yugoslavia", Report CE 93-09, University of Southern California, Los Angeles, U.S.A.

56. Press, W.H., Teukolsky, S.A., Vetterling, W.T. and Flannery, B.P. (1992). "Numerical Recipes", Cambridge University Press, London, U.K.
57. Rabiner, L.R. and Gold, B. (1975). "Theory and Application of Digital Signal Processing", Prentice-Hall, Englewood Cliffs, U.S.A.
58. Richter, C.F. (1958). "Elementary Seismology", W.H. Freeman & Company, San Francisco, U.S.A.
59. Sadigh, K., Chang, C.-Y., Abrahamson, N.A., Chiou, S.J. and Power, M. (1993). "Specification of Long Period Motions: Updated Attenuation Relations for Rock Site Conditions and Adjustment Factors for Near-Fault Effects" in "Proceedings of a Seminar on Seismic Isolation, Passive Energy Dissipation and Active Control", Report ATC-17-1, Applied Technology Council, Redwood City, California, U.S.A.
60. Seed, H.B., Ugas, C. and Lysmer, J. (1974). "Site-Dependent Spectra for Earthquake-Resistant Design", Report UCB/EERC-74/12, University of California, Berkeley, U.S.A.
61. Shebalin, N.V., Karnik, V. and Hadžievski, D. (editors) (1974). "Catalogue of Earthquakes (Part I, 1901–1970; Part II, Prior to 1901)", UNDP/UNESCO Survey of the Seismicity of the Balkan Region, UNESCO, Skopje, Yugoslavia.
62. Somerville, P. and Abrahamson, N. (2000). "Prediction of Ground Motions for Thrust Earthquakes", Data Utilization Report CSMIP/00-01, California Department of Conservation, Sacramento, U.S.A.
63. Sunder, S.S. and Conner, J.J. (1982). "A New Procedure for Processing Strong-Motion Earthquake Signals", Bulletin of the Seismological Society of America, Vol. 72, No. 2, pp. 643–661.
64. Todorovska, M.I. (1994a). "Order Statistics of Functionals of Strong Motion", Soil Dynamics and Earthquake Engineering, Vol. 13, No. 3, pp. 149–161.
65. Todorovska, M.I. (1994b). "Comparison of Response Spectrum Amplitudes from Earthquakes with Lognormally and Exponentially Distributed Return Period", Soil Dynamics and Earthquake Engineering, Vol. 13, No. 2, pp. 97–116.
66. Todorovska, M.I. (1995). "A Note on Distribution of Amplitudes of Peaks in Structural Response Including Uncertainties of the Exciting Ground Motion and of the Structural Model", Soil Dynamics and Earthquake Engineering, Vol. 14, No. 3, pp. 211–217.
67. Trifunac, M.D. (1972). "A Note on Correction of Strong-Motion Accelerograms for Instrument Response", Bulletin of the Seismological Society of America, Vol. 62, No. 1, pp. 401–409.
68. Trifunac, M.D. (1973). "Analysis of Strong Earthquake Ground Motion for Prediction of Response Spectra", Earthquake Engineering & Structural Dynamics, Vol. 2, No. 1, pp. 59–69.
69. Trifunac, M.D. (1976a). "Preliminary Analysis of the Peaks of Strong Earthquake Ground Motion—Dependence of Peaks on Earthquake Magnitude, Epicentral Distance, and Recording Site Conditions", Bulletin of the Seismological Society of America, Vol. 66, No. 1, pp. 189–219.
70. Trifunac, M.D. (1976b). "Preliminary Empirical Model for Scaling Fourier Amplitude Spectra of Strong Ground Acceleration in Terms of Earthquake Magnitude, Source-to-Station Distance, and Recording Site Conditions", Bulletin of the Seismological Society of America, Vol. 66, No. 4, pp. 1343–1373.
71. Trifunac, M.D. (1976c). "A Note on the Range of Peak Amplitudes of Recorded Accelerations, Velocities and Displacements with Respect to the Modified Mercalli Intensity", Earthquake Notes, Vol. 47, No. 1, pp. 9–24.
72. Trifunac, M.D. (1977a). "Statistical Analysis of the Computed Response of Structural Response Recorders (S.R.R.) for Accelerograms Recorded in the United States of America", Proceedings of the Sixth World Conference on Earthquake Engineering, New Delhi, Vol. III, pp. 2956–2961.
73. Trifunac, M.D. (1977b). "Forecasting the Spectral Amplitudes of Strong Earthquake Ground Motion", Proceedings of the Sixth World Conference on Earthquake Engineering, New Delhi, Vol. I, pp. 139–152.
74. Trifunac, M.D. (1977c). "An Instrumental Comparison of the Modified Mercalli (M.M.I.) and Medvedev-Karnik-Sponheuer (M.K.S.) Intensity Scales", Proceedings of the Sixth World Conference on Earthquake Engineering, New Delhi, Vol. I, pp. 715–721.

75. Trifunac, M.D. (1977d). "Uniformly Processed Strong Earthquake Ground Accelerations in the Western United States of America for the Period from 1933 to 1971: Pseudo Relative Velocity Spectra and Processing Noise", Report CE 77-04, University of Southern California, Los Angeles, U.S.A.
76. Trifunac, M.D. (1978). "Response Spectra of Earthquake Ground Motion", Journal of the Engineering Mechanics Division, Proceedings of ASCE, Vol. 104, No. EM5, pp. 1081–1097.
77. Trifunac, M.D. (1979). "Preliminary Empirical Model for Scaling Fourier Amplitude Spectra of Strong Motion Acceleration in Terms of Modified Mercalli Intensity and Geologic Site Conditions", Earthquake Engineering & Structural Dynamics, Vol. 7, No. 1, pp. 63–74.
78. Trifunac, M.D. (1988). "Seismic Microzonation Mapping via Uniform Risk Spectra", Proceedings of the Ninth World Conference on Earthquake Engineering, Tokyo-Kyoto, Japan, Vol. VII, pp. 75–80.
79. Trifunac, M.D. (1989a). "Dependence of Fourier Spectrum Amplitudes of Recorded Strong Earthquake Accelerations on Magnitude, Local Soil Conditions and on Depth of Sediments", Earthquake Engineering & Structural Dynamics, Vol. 18, No. 7, pp. 999–1016.
80. Trifunac, M.D. (1989b). "Empirical Scaling of Fourier Spectrum Amplitudes of Recorded Strong Earthquake Accelerations in Terms of Magnitude and Local Soil and Geologic Conditions", Earthquake Engineering and Engineering Vibration, Vol. 9, No. 2, pp. 23–44.
81. Trifunac, M.D. (1989c). "Scaling Strong Motion Fourier Spectra by Modified Mercalli Intensity, Local Soil and Geologic Site Conditions", Structural Engineering/Earthquake Engineering, JSCE, Vol. 6, No. 2, pp. 217–224.
82. Trifunac, M.D. (1989d). "Threshold Magnitudes Which Exceed the Expected Ground Motion during the Next 50 Years in a Metropolitan Area", Geofizika, Vol. 6, No. 1, pp. 1–12.
83. Trifunac, M.D. (1990a). "How to Model Amplification of Strong Earthquake Motions by Local Soil and Geologic Site Conditions", Earthquake Engineering & Structural Dynamics, Vol. 19, No. 6, pp. 833–846.
84. Trifunac, M.D. (1990b). "A Microzonation Method Based on Uniform Risk Spectra", Soil Dynamics and Earthquake Engineering, Vol. 9, No. 1, pp. 34–43.
85. Trifunac, M.D. (1991a). "Empirical Scaling of Fourier Spectrum Amplitudes of Recorded Strong Earthquake Accelerations in Terms of Modified Mercalli Intensity, Local Soil Conditions and Depth of Sediments", Soil Dynamics and Earthquake Engineering, Vol. 10, No. 1, pp. 65–72.
86. Trifunac, M.D. (1991b). " M_L^{SM} ", Soil Dynamics and Earthquake Engineering, Vol. 10, No. 1, pp. 17–25.
87. Trifunac, M.D. (1993a). "Long Period Fourier Amplitude Spectra of Strong Motion Acceleration", Soil Dynamics and Earthquake Engineering, Vol. 12, No. 6, pp. 363–382.
88. Trifunac, M.D. (1993b). "Broad Band Extension of Fourier Amplitude Spectra of Strong Motion Acceleration", Report CE 93-01, University of Southern California, Los Angeles, U.S.A.
89. Trifunac, M.D. (1994a). "Fourier Amplitude Spectra of Strong Motion Acceleration: Extension to High and Low Frequencies", Earthquake Engineering & Structural Dynamics, Vol. 23, No. 4, pp. 389–411.
90. Trifunac, M.D. (1994b). " Q and High-Frequency Strong Motion Spectra", Soil Dynamics and Earthquake Engineering, Vol. 13, No. 3, pp. 149–161.
91. Trifunac, M.D. (1994c). "Earthquake Source Variables for Scaling Spectral and Temporal Characteristics of Strong Ground Motion", Proceedings of the Tenth European Conference of Earthquake Engineering, Vienna, Austria, Vol. 4, pp. 2585–2590.
92. Trifunac, M.D. (1994d). "Response Spectra of Strong Motion Acceleration: Extension to High and Low Frequencies", Proceedings of the Tenth European Conference of Earthquake Engineering, Vienna, Austria, Vol. 1, pp. 203–208.
93. Trifunac, M.D. (1994e). "Broad Band Extension of Pseudo Relative Velocity Spectra of Strong Motion", Report CE 94-02, University of Southern California, Los Angeles, U.S.A.
94. Trifunac, M.D. (1995a). "Pseudo Relative Velocity Spectra of Earthquake Ground Motion at Long Periods", Soil Dynamics and Earthquake Engineering, Vol. 14, No. 5, pp. 331–346.

95. Trifunac, M.D. (1995b). "Pseudo Relative Velocity Spectra of Earthquake Ground Motion at High Frequencies", *Earthquake Engineering & Structural Dynamics*, Vol. 24, No. 8, pp. 1113–1130.
96. Trifunac, M.D. (2005). "The Role of the Brune Spectrum in Earthquake Engineering", *Journal of Seismology and Earthquake Engineering*, Vol. 7, No. 2, pp. 63–82.
97. Trifunac, M.D. (2006). "Brief History of Computation of Earthquake Response Spectra", *Soil Dynamics and Earthquake Engineering*, Vol. 26, No. 6-7, pp. 501–508.
98. Trifunac, M.D. and Anderson, J.G. (1977). "Preliminary Empirical Models for Scaling Absolute Acceleration Spectra", Report CE 77-03, University of Southern California, Los Angeles, U.S.A.
99. Trifunac, M.D. and Anderson, J.G. (1978a). "Preliminary Empirical Models for Scaling Pseudo Relative Velocity Spectra", Report CE 78-04, University of Southern California, Los Angeles, U.S.A.
100. Trifunac, M.D. and Anderson, J.G. (1978b). "Preliminary Models for Scaling Relative Velocity Spectra", Report CE 78-05, University of Southern California, Los Angeles, U.S.A.
101. Trifunac, M.D. and Anderson, J.G. (1978c). "Estimation of Relative Velocity Spectra", *Proceedings of the Sixth Symposium on Earthquake Engineering*, Roorkee, Vol. I, pp. 9–18.
102. Trifunac, M.D. and Brady, A.G. (1975a). "A Study on the Duration of Strong Earthquake Ground Motion", *Bulletin of the Seismological Society of America*, Vol. 65, No. 3, pp. 581–626.
103. Trifunac, M.D. and Brady, A.G. (1975b). "On the Correlation of Seismic Intensity Scales with the Peaks of Recorded Strong Ground Motion", *Bulletin of the Seismological Society of America*, Vol. 65, No. 1, pp. 139–162.
104. Trifunac, M.D. and Brady, A.G. (1975c). "On the Correlation of Seismoscope Response with Earthquake Magnitude and Modified Mercalli Intensity", *Bulletin of the Seismological Society of America*, Vol. 65, No. 2, pp. 307–321.
105. Trifunac, M.D. and Brady, A.G. (1975d). "Correlations of Peak Acceleration, Velocity and Displacement with Earthquake Magnitude, Epicentral Distance and Site Conditions", *Earthquake Engineering & Structural Dynamics*, Vol. 4, No. 5, pp. 455–471.
106. Trifunac, M.D. and Brady, A.G. (1975e). "On the Correlation of Peak Accelerations of Strong-Motion with Earthquake Magnitude, Epicentral Distance and Site Conditions", *Proceedings of the U.S. National Conference on Earthquake Engineering*, Ann Arbor, U.S.A., pp. 43–52.
107. Trifunac, M.D. and Lee, V.W. (1973). "Routine Computer Processing of Strong-Motion Accelerograms", Report EERL 73-03, California Institute of Technology, Pasadena, U.S.A.
108. Trifunac, M.D. and Lee, V.W. (1978). "Dependence of Fourier Amplitude Spectra of Strong Motion Acceleration on the Depth of Sedimentary Deposits", Report CE 78-14, University of Southern California, Los Angeles, U.S.A.
109. Trifunac, M.D. and Lee, V.W. (1979a). "Dependence of Pseudo Relative Velocity Spectra of Strong Motion Acceleration on the Depth of Sedimentary Deposits", Report CE 79-02, University of Southern California, Los Angeles, U.S.A.
110. Trifunac, M.D. and Lee, V.W. (1979b). "Automatic Digitization and Processing of Strong-Motion Accelerograms, Part I: Automatic Digitization", Report CE 79-15 I, University of Southern California, Los Angeles, U.S.A.
111. Trifunac, M.D. and Lee, V.W. (1980). "Fourier Amplitude Spectra of Strong Motion Acceleration", *The Bulletin of the European Association for Earthquake Engineering*, Vol. 6, No. 1, pp. 2–18.
112. Trifunac, M.D. and Lee, V.W. (1985a). "Frequency Dependent Attenuation of Strong Earthquake Ground Motion", Report CE 85-02, University of Southern California, Los Angeles, U.S.A.
113. Trifunac, M.D. and Lee, V.W. (1985b). "Preliminary Empirical Model for Scaling Fourier Amplitude Spectra of Strong Ground Acceleration in Terms of Earthquake Magnitude, Source to Station Distance, Site Intensity and Recording Site Conditions", Report CE 85-03, University of Southern California, Los Angeles, U.S.A.
114. Trifunac, M.D. and Lee, V.W. (1985c). "Preliminary Empirical Model for Scaling Pseudo Relative Velocity Spectra of Strong Earthquake Accelerations in Terms of Magnitude, Distance, Site Intensity and Recording Site Conditions", Report CE 85-04, University of Southern California, Los Angeles, U.S.A.

115. Trifunac, M.D. and Lee, V.W. (1987). "Direct Empirical Scaling of Response Spectral Amplitudes from Various Site and Earthquake Parameters", Report NUREG/CR-4903, Vol. 1, United States Nuclear Regulatory Commission, Washington, DC, U.S.A.
116. Trifunac, M.D. and Lee, V.W. (1989a). "Empirical Models for Scaling Fourier Amplitude Spectra of Strong Ground Acceleration in Terms of Earthquake Magnitude, Source to Station Distance, Site Intensity and Recording Site Conditions", *Soil Dynamics and Earthquake Engineering*, Vol. 8, No. 3, pp. 110–125.
117. Trifunac, M.D. and Lee, V.W. (1989b). "Empirical Models for Scaling Pseudo Relative Velocity Spectra of Strong Earthquake Accelerations in Terms of Magnitude, Distance, Site Intensity and Recording Site Conditions", *Soil Dynamics and Earthquake Engineering*, Vol. 8, No. 3, pp. 126–144.
118. Trifunac, M.D. and Lee, V.W. (1990). "Frequency Dependent Attenuation of Strong Earthquake Ground Motion", *Soil Dynamics and Earthquake Engineering*, Vol. 9, No. 1, pp. 3–15.
119. Trifunac, M.D. and Lee, V.W. (1992). "A Note on Scaling Peak Acceleration, Velocity and Displacement of Strong Earthquake Shaking by Modified Mercalli Intensity (MMI) and Site Soil and Geologic Conditions", *Soil Dynamics and Earthquake Engineering*, Vol. 11, No. 2, pp. 101–110.
120. Trifunac, M.D. and Novikova, E.I. (1994). "State of the Art Review of Strong Motion Duration", *Proceedings of the Tenth European Conference on Earthquake Engineering*, Vienna, Austria, Vol. 1, pp. 131–140.
121. Trifunac, M.D. and Todorovska, M.I. (1989a). "Attenuation of Seismic Intensity in Albania and Yugoslavia", *Soil Dynamics and Earthquake Engineering*, Vol. 18, No. 5, pp. 617–631.
122. Trifunac, M.D. and Todorovska, M.I. (1989b). "Methodology for Selection of Earthquake Design Motions for Important Engineering Structures", Report CE 89-01, University of Southern California, Los Angeles, U.S.A.
123. Trifunac, M.D. and Todorovska, M.I. (2001a). "A Note on the Useable Range in Accelerographs Recording Translation", *Soil Dynamics and Earthquake Engineering*, Vol. 21, No. 4, pp. 275–286.
124. Trifunac, M.D. and Todorovska, M.I. (2001b). "Evolution of Accelerographs, Data Processing, Strong Motion Arrays and Amplitude and Spatial Resolution in Recording Strong Earthquake Motion", *Soil Dynamics and Earthquake Engineering*, Vol. 21, No. 6, pp. 537–555.
125. Trifunac, M.D. and Zivcic, M. (1991). "A Note on Instrumental Comparison of the Modified Mercalli Intensity (MMI) in the Western United States and the Mercalli-Cancani-Sieberg (MCS) Intensity in Yugoslavia", *European Earthquake Engineering*, Vol. V, No. 1, pp. 22–26.
126. Trifunac, M.D., Udawadia, F.E. and Brady, A.G. (1973). "Analysis of Errors in Digitized Strong-Motion Accelerograms", *Bulletin of the Seismological Society of America*, Vol. 63, No. 1, pp. 157–187.
127. Trifunac, M.D., Lee, V.W., Cao, H. and Todorovska, M.I. (1988). "Attenuation of Seismic Intensity in Balkan Countries", Report CE 88-01, University of Southern California, Los Angeles, U.S.A.
128. Trifunac, M.D., Lee, V.W., Zivcic, M. and Manic, M. (1991). "On the Correlation of Mercalli-Cancani-Sieberg Intensity Scale in Yugoslavia with the Peaks of Recorded Strong Earthquake Ground Motion", *European Earthquake Engineering*, Vol. V, No. 1, pp. 27–33.
129. Youngs, R.R. (1993). "Soil Amplification and Vertical to Horizontal Ratios for Analysis of Strong Motion Data from Active Tectonic Regions" in "Guidelines for Determining Design Basis Ground Motions, Vol. 2: Appendices for Ground Motion Estimation", Report TR-102293, Electric Power Research Institute, Palo Alto, U.S.A.

ON THE REGIONAL DEPENDENCE OF EARTHQUAKE RESPONSE SPECTRA

John Douglas
ARN/RIS, BRGM
3 avenue C. Guillemin, BP 36009
45060 Orléans Cedex 2, France

ABSTRACT

It is common practice to use ground-motion models, often developed by regression on recorded accelerograms, to predict the expected earthquake response spectra at sites of interest. An important consideration when selecting these models is the possible dependence of ground motions on geographical region, i.e., are median ground motions in the (target) region of interest for a given magnitude and distance the same as those in the (host) region where a ground-motion model is from, and are the aleatoric variabilities of ground motions also similar? These questions can be particularly difficult to tackle in many regions of the world where little observed strong-motion data is available since there are few records to validate the choice of model. Reasons for regionally dependent ground motions are discussed and possible regional dependence of earthquake response spectra is examined using published ground-motion models, observed accelerograms and also by using ground motions predicted by published stochastic models. It is concluded that although some regions seem to show considerable differences in spectra it is currently more defensible to use well-constrained models, possibly based on data from other regions, rather than use predicted motions from local, often poorly-constrained, models.

KEYWORDS: Ground-Motion Estimation, Attenuation Relationships, Regional Dependence, Analysis of Variance, Stochastic Method

INTRODUCTION

The selection of ground-motion estimation equations (e.g., Douglas, 2003) for use in estimating elastic earthquake response spectra at sites in most regions of the world, such as many parts of Europe and India, is a challenging task due to the relatively short histories of quantitative recording of ground motions of engineering significance by strong-motion networks in these areas. For example, the French accelerometric network (the Réseau Accélérométrique Permanent, RAP) is only about ten years old and the seismicity level of metropolitan France is moderate; therefore, there are only a handful of records from earthquakes of magnitudes greater than $M_w = 5.0$ and at source-to-site distances less than 100 km. Two recent empirical ground-motion models have been published based on French data (Marin et al., 2004; Souriau, 2006). However, these equations are only for the estimation of peak ground acceleration (PGA) and, in addition, are based on data from small earthquakes. Due to the observation that ground motions from small and large earthquakes scale differently with magnitude and distance (e.g., Pousse et al., 2007), these equations cannot be used for the estimation of ground motions from damaging earthquakes. In addition, as shown by Trifunac and Todorovska (2000), the extrapolation of ground-motion estimates for soil sites derived from weak motions may not be appropriate for large events due to nonlinear site amplifications.

Although the study of Douglas (2003) lists over 120 equations for the estimation of PGA (this list was updated in two recent reports (Douglas, 2004a, 2006) to over 200 equations), most of the equations in the literature have: (a) been superseded by more recent equations from the same authors or by other studies for the region, (b) fail one or more of the criteria listed by Cotton et al. (2006), or (c) cannot be used for near-source distances or for moderate or large earthquakes due to the distribution with respect to magnitude and distance of the data used to derive the equation. After removing these equations the seismic hazard analyst is left with a choice of possibly 20–30 equations.

Criteria for the further narrowing down and weighting of these possible ground-motion models have been discussed by Scherbaum et al. (2004) and Scherbaum et al. (2005), specifically with respect to the selection of models for seismic hazard analysis in Switzerland, a country where the choice of ground-

motion models is challenging for similar reasons to those discussed above (short history of quantitative observation and relatively low seismicity). Even following these articles there is still much debate over the selection of ground-motion estimation equations, especially for regions with limited observational data (e.g., Klügel, 2005; Musson et al., 2005).

An important consideration when selecting ground-motion models for seismic hazard analysis is the possible dependence of earthquake ground motions on geographical region, i.e., are average ground motions in the (target) region of interest for a given magnitude and distance the same as those in the (host) region where a ground-motion model is from, and are the aleatoric variabilities of ground motions also similar? This article investigates this problem mainly with respect to empirical ground-motion estimation. Estimated response spectra based on physically based simulations explicitly model regional dependence by the choice of input parameters. Therefore, the goal of such studies is to use input parameters that are appropriate for the considered region. The selection of such input parameters is not considered here.

The following section discusses possible reasons for a regional dependence of elastic earthquake response spectra. The next section of the article investigates regional dependence based on published empirical ground-motion estimation equations. In the following section, the method proposed by Douglas (2004b) based on analysis of variance is applied to two Italian regions (Umbria-Marche and Molise) where recent studies have suggested a large difference in ground motions. Due to the difficulty in developing robust empirical ground-motion models for many parts of the world a number of studies have investigated whether ground motions in one region are comparable to those in another region, see for example, Douglas (2004b) and the references therein. However, many of the proposed methods rely on the availability of observed ground motion data from moderate and large earthquakes, which is often lacking. Therefore, later a different approach is taken that is less reliant on such data. The article ends with some conclusions and suggestions.

For many of the analyses presented PGA is used because of the greater availability of predictive models and observation data for this strong-motion intensity measure. Since PGA equals elastic response spectral acceleration (SA) for an infinitely stiff single-degree-of-freedom system, it is often used as a basis of seismic design response spectra (e.g., CEN, 2005). Note that some of the results presented here for PGA may not be directly applicable to the estimation of response spectra because of differences in the frequency range of the ground motions sampled by PGA and SAs. Regional dependence, or independence, of PGA may not imply the same conclusion for SA at a given period.

REGIONAL DEPENDENCE

Earthquake response spectra are dependent on various factors that are commonly divided into source, path and site factors, and include the following: earthquake magnitude, epicentral intensity, faulting mechanism, source depth, fault geometry, stress drop and direction of rupture; source-to-site distance, crustal structure, geology (e.g., sedimentary basins) along wave paths, radiation pattern and directionality; and site geology, topography, soil-structure interaction, nonlinear soil behaviour and site intensity. Within models for the prediction of response spectra the dependence of spectra on some of these factors (mainly magnitude, source-to-site distance, site geology and faulting mechanism) is considered, albeit often only simply (e.g., Douglas, 2003). The unmodelled effects, that can be important, are ignored and consequently predictions from the ground-motion models contain a bias due to the (unknown) distribution of records used to construct the model with respect to these variables. Therefore, if the ground-motion model was used to estimate the response spectra in another region where the distribution of scenarios was different to the one used to create the model, the predictions would be biased.

An example of an unmodelled factor that can lead to an implicit inclusion of regional dependence within ground-motion models is focal depth. The depth at which an earthquake occurs can significantly influence the resultant ground motions. The fact that the earthquake source is closer (for shallow events) or further (for deep events) away from a site is important due to differences in decay especially for small and moderate earthquakes, which are approximately point sources (e.g., Ambraseys and Bommer, 1991). This effect can be modelled by the use of a distance metric that includes a consideration of the depth of the earthquake source, such as hypocentral distance or the distance metric proposed by Gusev (1983) and used by, for example, Lee and Trifunac (1995) for the development of empirical ground-motion models. Models using a distance metric, such as distance to the surface projection of rupture (commonly known as

Joyner-Boore distance) (Joyner and Boore, 1981), cannot model variations in ground motions due to focal depth. Therefore, if they are applied in a target region where the distribution of source depths is different from that in the host region, the predicted ground motions could be incorrect. However, the scaling of ground motions with focal depth is more complicated than that simply explainable by increased source-to-site distance for deep earthquakes. McGarr (1984) shows that for the same hypocentral distance, ground motions from deep earthquakes can be higher than those from shallow earthquakes due to differences in stress conditions.

Another factor, that until recently was commonly unmodelled but can have an impact on ground motions, is faulting mechanism (often called style of faulting). Ground motions from reverse-faulting earthquakes are, on average, slightly higher (about 10-30% for PGA and for SAs at short periods) than those from strike-slip and normal-faulting earthquakes (e.g., Bommer et al., 2003). Therefore, if, for example, within a region only reverse-faulting earthquakes occur, a ground-motion model developed using data from this region will overpredict, on average, the shaking in a region where only strike-slip earthquakes occur (other effects being equal). The correction of this possible bias is the basis of the method developed by Bommer et al. (2003).

Similarly, another important effect that could lead to apparent regional dependence of strong ground motions is differences in average site conditions between host and target regions. For example, sites classified into a common soft soil category in the two regions may be underlain by, on average, deeper soil deposits in one region than in the other, thereby leading to differences in average site response. As an example of this, Atkinson and Boore (2003) find that ground-motion amplitudes differ from those in Japan by more than a factor of two for the same magnitude, distance and site class, which they relate to differences in the depth of soil profiles in the two regions. This type of regional difference could be modelled by using more sophisticated methods for capturing site effects, such as considering the depth of soil profiles (e.g., Seed et al., 1976; Trifunac, 1990) rather than only the average near-surface shear-wave velocity. Another factor that contributes to differences in the response of otherwise similar sites is geological age (e.g., Novikova et al., 1994). Such methods, however, rely on having sufficient high-quality data on site conditions, which is unfortunately often unavailable.

If much more complex ground-motion models were developed that explicitly include all the factors affecting response spectra then these models could be applied throughout the world without introducing regional bias, as long as the correct input parameters were used. A proposal of how empirical ground-motion models could be developed to incorporate the possibly important effect of regional differences in crustal structure is discussed by Douglas et al. (2004) and Douglas et al. (2007).

It is common practice within Europe to combine data from different countries together in order to obtain sufficiently large datasets for regression analysis (e.g., Berge-Thierry et al., 2003; Ambraseys et al., 2005). Due to increasing regional datasets from sensitive digital seismic networks there is a growing move towards the development of empirical ground-motion models developed using data from small geographical regions, e.g., north-eastern Italy (Bragato and Slejko, 2005; Costa et al., 2006), north-western Italy (Frisenda et al., 2005), Umbria-Marche (Zonno and Montaldo, 2002; Bindi et al., 2006), Molise (Luzi et al., 2006), France (Marin et al., 2004; Souriau, 2006) and north-western Turkey (Özbey et al., 2004). An idea of the difference in geographical scale between these small regions and the broader areas otherwise used as source of data is given by comparing the surface area of the State of California (410,000 km²) to the surface area of the Region of Molise (4,400 km²): a factor of almost 100. This comparison is not completely fair since models developed using Californian data have mainly employed data from well-instrumented relatively small zones (e.g., the Los Angeles Basin, San Francisco Bay Area and Imperial Valley). However, these models are usually applied for the prediction of motions at all sites in California (and often beyond).

Political boundaries do not usually follow seismotectonic boundaries: many countries feature various tectonic regimes (e.g., Greece includes extensional, compressional, volcanic and subduction regimes) and numerous countries share one tectonic regime (e.g., the extensional Upper Rhine Graben straddles the borders of France, Germany and Switzerland). Therefore, the number of countries that are the source of data for a ground-motion model is not important but rather whether the data come from similar tectonic regions. As is discussed below, lack of observed data and uncertainties and simplifications within empirical and stochastic ground-motion models mean that variations in ground motions from different tectonic regimes have not yet been clearly demonstrated.

If the practice of only using data from small geographical zones in order to develop more applicable ground-motion models was justified it could be expected that such models would be associated with lower aleatoric variabilities (standard deviations, σ) than models developed by combining records from many different areas, since regional dependence would be contributing to the scatter. However, this is not observed (see Table 1 comparing σ from regional models to those derived using data from larger areas). One reason that current equations developed based on data from small regions do not have lower σ is that they are mainly based on motions from small earthquakes ($M < 5$), which have been shown to be more variable than motions from larger earthquakes (e.g., Youngs et al., 1995). Although Youngs et al. (1995) and others find that σ are relatively constant for magnitudes below 5, recently derived models from the PEER Next Generation Attenuation (NGA) project (Boore and Atkinson, 2007; Campbell and Bozorgnia, 2007; Chiou and Youngs, 2006) do not show magnitude-dependent σ . The previously reported dependence could have been due to a lack of strong-motion data from large events and also errors in the associated parameters (e.g., magnitudes and distances) of the strong-motion data for small earthquakes. The NGA models, however, are mainly based on data from earthquakes with $M > 5.5$, therefore σ could be magnitude-dependent for small events.

One possible way of investigating possible regional dependence is to compare recorded ground motions in one region with those predicted by models from other regions. In the past this type of comparison has often been made by visually comparing observations and predictions or through analyses of residuals (e.g., Boore, 2001); however, Scherbaum et al. (2004) suggest a statistically more rigorous method to undertake this task than has been applied. They compare recordings of the 2003 St Dié (France) earthquake at 13 rock stations to predicted motions from various models. This study has recently been extended by Hintersberger et al. (2007) and the same method has been applied by Drouet et al. (2007) for the Pyrenees. Douglas et al. (2006a) investigate the ground motions observed on the French Antilles from both shallow crustal and subduction earthquakes (considered separately) using this approach and find that these motions are not well-predicted by published equations developed for other regions. One difficulty with this method, which was faced by Douglas et al. (2006a), is that the available observations from the target region often are from magnitudes and distances that require extrapolation of the ground-motion models beyond their ranges of assumed applicability, creating uncertainties over the comparisons.

Table 1: Standard Deviations in Common Logarithms (σ) of Selected Empirical Ground-Motion Models for Prediction of PGA from Strike-Slip Shallow-Crustal Earthquakes at Rock Sites, the Regions Used as Sources of Accelerograms and the Number of Accelerograms (T) and Earthquakes (E) and the Magnitude and Distance Ranges (d_e is epicentral distance, d_f is distance to surface projection of rupture, d_h is hypocentral distance, d_r is distance to rupture, and d_s is distance to seismogenic rupture) of Data Used for the Deviation of the Model (standard deviations given for Abrahamson and Silva (1997), Ambraseys et al. (2005), Campbell and Bozorgnia (2003) and Sadigh et al. (1997) are for $5.0 \leq M_w \leq 7.5$ since the authors report magnitude-dependent σ s)

Reference	Region	T	E	M Range	d Range (km)	σ
Small Regions						
Bindi et al. (2006)	Umbria-Marche	239	45	$4.0 \leq M_L \leq 5.9$	$1 \leq d_e \leq 100$	0.27
Bragato and Slejko (2005)	Eastern Alps	1402	240	$2.5 \leq M_L \leq 6.3$	$0 \leq d_f \leq 130$	0.36
Costa et al. (2006)	Friuli	900	123	$3.0 \leq M_L \leq 6.5$	$1 \leq d_e \leq 100$	0.34
Frisenda et al. (2005)	NW Italy	6899	1152	$0.0 \leq M_L \leq 5.1$	$0 \leq d_h \leq 300$	0.32
Kalkan and Güllkan (2004)	Mainly NW Turkey	112	57	$4.0 \leq M_w \leq 7.4$	$1 \leq d_f \leq 250$	0.27
Luzi et al. (2006)	Molise	886	—	$2.6 \leq M_L \leq 5.7$	$5 \leq d_h \leq 55$	0.35
Marin et al. (2004)	France	63	14	$2.6 \leq M_L \leq 5.6$	$5 \leq d_h \leq 700$	0.55
Özbey et al. (2004)	NW Turkey	195	17	$5.0 \leq M_w \leq 7.4$	$5 \leq d_f \leq 300$	0.26
Sabetta and Pugliese (1987)	Italy	95	17	$4.6 \leq M_s, M_L \leq 6.8$	$1 \leq d_f \leq 179$	0.17
Zonno and Montaldo (2002)	Umbria-Marche	161	15	$4.5 \leq M_L \leq 5.9$	$2 \leq d_e \leq 100$	0.28

Broad Regions

Abrahamson and Silva (1997)	Mainly California	655	58	$4.4 \leq M_w \leq 7.4$	$0 \leq d_r \leq 220$	0.19–0.31
Ambraseys et al. (1996)	Europe & Middle East	422	157	$4.0 \leq M_S \leq 7.9$	$0 \leq d_f \leq 260$	0.25
Ambraseys et al. (2005)	Europe & Middle East	595	135	$5.0 \leq M_w \leq 7.6$	$0 \leq d_f \leq 99$	0.19–0.36
Berge-Thierry et al. (2003)	Europe & Middle East	802	403	$4.0 \leq M_S \leq 7.9$	$4 \leq d_h \leq 330$	0.29
Boore et al. (1997)	Mainly California	271	20	$5.1 \leq M_w \leq 7.7$	$0 \leq d_f \leq 118$	0.23
Campbell and Bozorgnia (2003)	Mainly California	443	36	$4.7 \leq M_w \leq 7.7$	$2 \leq d_s \leq 60$	0.17–0.25
Joyner and Boore (1981)	Mainly California	182	23	$5.0 \leq M_w \leq 7.7$	$0 \leq d_f \leq 370$	0.26
Lussou et al. (2001)	Japan	3011	102	$3.7 \leq M_{JMA} \leq 6.3$	$4 \leq d_h \leq 600$	0.32
Sadigh et al. (1997)	Mainly California	960	119	$3.8 \leq M_w \leq 7.4$	$0 \leq d_r \leq 305$	0.17–0.30
Spudich et al. (1999)	Worldwide Extensional Regimes	142	39	$5.1 \leq M_w \leq 7.2$	$0 \leq d \leq 99$	0.20

INVESTIGATION USING EMPIRICAL MODELS

It is common practice when presenting a new ground-motion model to compare its predicted ground motions to those estimated by earlier published models, both for same region and for other geographical areas. These comparisons are invariably made by graphically plotting the predicted levels of shaking (characterised, for example, by the elastic response spectra) for a number of magnitudes and distances. Then it is often stated that the predictions are similar or different without much statistical justification. Some researchers believe that there is clear evidence for regional dependence while others doubt that a clear conclusion can currently be drawn. For example, Sokolov (2000) states during a discussion of empirical models, ‘at present, there is no doubt that these relations are different for different seismic regions, and “region and site-specific” models should be developed on the basis of available strong ground motion records’, whilst Bommer (2006) believes, when presenting comparisons between empirical models developed for different European datasets, ‘these plots do not suggest that there are strong regional differences and this leads to the conclusion that it is not only acceptable but in fact desirable to ignore national borders when compiling datasets for the derivation of ground-motion prediction equations’. Previous discussions on this issue are those by Lee (1997) and Ambraseys et al. (1997) following the publication of the empirical ground-motion estimation equations of Ambraseys et al. (1996), who combined together data from numerous European, Middle Eastern and north African countries in order to derive their model.

Bommer (2006) compares ground motion predictions from various empirical models derived solely from Turkish data and finds larger differences between predicted median ground-motions from these models than between models derived from databanks containing data from many parts of Europe and the Middle East. Figure 1 shows a comparison between simple empirical models (Aman et al., 1995; Singh et al., 1996; Jain et al., 2000; Sharma, 1998; Sharma and Bungum, 2006) for the prediction of PGA based on data from the Indian Himalayas. These five studies basically used the same sparse poorly-distributed dataset (see Figure 2) but chose different functional forms and regression techniques. An earlier study that showed the large variations in median predictions possible simply by changing the functional form is that by McCann, Jr. and Echezwia (1984). Figure 1 shows a similar finding to that for the Turkish models reported by Bommer (2006): a large dispersion in predicted median ground motions even between models derived for the same region. PGA estimates from the different models become slightly more coherent at 50-200 km where most of the available observations are located (Figure 2). This example shows that reaching conclusions on regional dependence of ground motions based solely on comparisons between empirical ground-motion models is difficult because of the large epistemic uncertainty in the models due to limited data. Many published empirical models could be rejected from consideration in a seismic hazard assessment due to problems in their underlying data, weaknesses in the analysis performed and since they are too simple with respect to the underlying physics.

One important question that is rarely asked when making these comparisons of curves derived through regression analysis on sets of data with differing underlying distributions is: what is the uncertainty in the prediction of the median ground motion? Note that this is different than asking: what is the uncertainty of a single ground-motion estimate (for which the answer is given by the reported standard deviations of the model)? For example, the standard deviation of a mean is given by σ/\sqrt{n} where σ is the standard deviation and n is the number of samples, showing that the mean becomes more precisely defined when more data is used (e.g., Moroney, 1990). The uncertainty in the median is due to the lack of sufficient data to precisely define the coefficients of the regression model whereas the uncertainty of a single ground-motion estimate is mainly caused by the simplicity of the physical model assumed (e.g., Douglas and Smit, 2001). Given a very large well-distributed dataset, the uncertainty in the prediction of the median ground motion will tend to zero but the uncertainty of a single ground-motion estimate will tend to a constant non-negligible value unless additional independent parameters are included. This difference is related to that between epistemic uncertainty and aleatoric variability. The uncertainty in the median is important when comparing ground motions in two different regions.

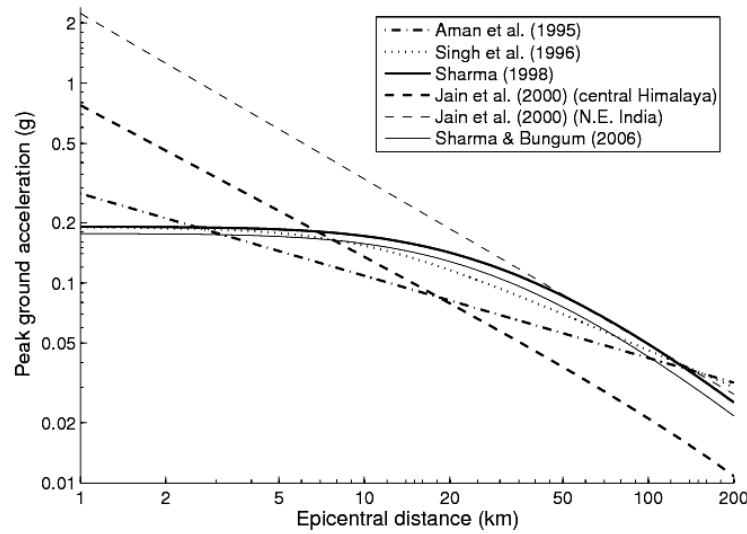


Fig. 1 Comparison of horizontal PGA predicted by various empirical ground-motion models developed using Indian strong-motion data for an $M_w = 6.0$ ($m_b = 5.6$, using the magnitude-conversion formula of Castellaro et al. (2006): $m_b = (M_w + 1.272)/1.291$) earthquake with a focal depth of 10 km

In his survey of empirical ground-motion estimation Campbell (1985) estimates the confidence limits for the mean of n_0 observations for linear models as $\hat{y} \pm t_{\alpha/2, \nu} \sigma \sqrt{\frac{1}{n_0} + X_0' C X_0}$, where \hat{y} is the mean predicted ground-motion (in logarithms), $t_{\alpha/2, \nu}$ is the absolute value of the t -statistic associated with an exceedance probability $\alpha/2$ and $\nu = n - p - 1$ degrees of freedom, n is the number of records used to derive the model, p is the number of coefficients in the model, σ is the standard deviation, X_0 is a vector containing specified values of model parameters (e.g., M and $\log R$), and C is the covariance matrix of the model coefficients. He notes that the usual assumption of simply multiplying the median ground motion by the antilogarithm of differing numbers of standard deviations in order to obtain the confidence limits (e.g., the 84% percentile by multiplying with the antilogarithm of one σ) is inappropriate since it is only valid for many degrees of freedom (not too serious for the most recent ground-motion models for which many hundreds of records are used) and also since it neglects uncertainty in the mean prediction of \hat{y} , which is only true near the centroid of the data. Applying this formula in place of the usual formula for the computation of confidence limits leads to marginally broader limits that are curved at short and long distances and small and large magnitudes (points distant from the centroid of the data). These types of curved confidence limits are shown by Boore et al. (1980) for

predictions from their models but in very few other articles. McGuire (1977) reports that the consideration of these correctly computed confidence limits does not significantly affect the hazard computed by probabilistic seismic hazard analysis compared with the standard approach. However, this was for a site 40 km from a single line source, hence it may not be true for real situations where near-source events are important.

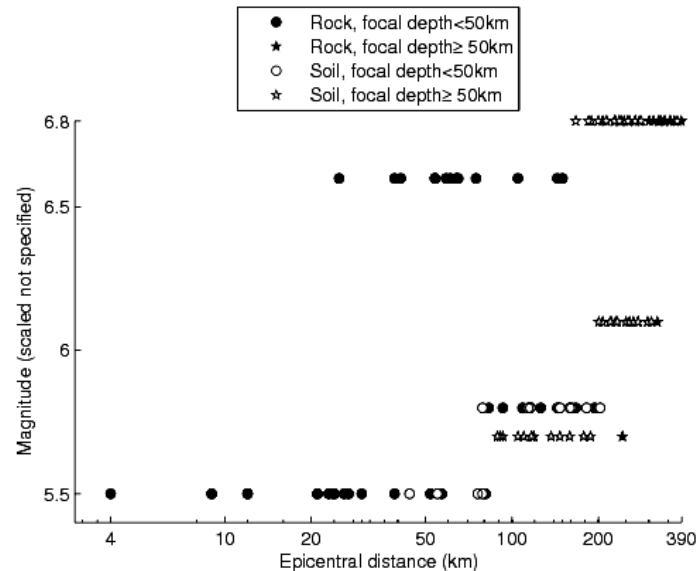


Fig. 2 Distribution with respect to magnitude, epicentral distance, focal depth and site class of Indian strong-motion data (113 records from seven earthquakes) used by Sharma (1998) to derive his empirical ground-motion model; data used by the other authors of ground-motion models for the Indian Himalayas (Aman et al., 1995; Singh et al., 1996; Jain et al., 2000; Sharma and Bungum, 2006) are almost identical

In order to compute confidence limits of the median ground motion, the covariance matrix, C , is required (as shown above) and, within the formula above, $n_0 \rightarrow \infty$. To the knowledge of the writer, the complete covariance matrix of a published ground-motion model has never been publicly reported (the diagonal elements of these matrices, the standard errors of the coefficients are, however, occasionally reported). Therefore a number of published PGA datasets that have been used to derive ground-motion models have been re-regressed here using the standard one-stage regression method and a simple linear functional form in order to obtain and plot confidence limits on the median curves. The equations used for this analysis were selected from those that published their datasets. In total, following seven models published in peer-reviewed journals for the prediction of PGA from shallow crustal earthquakes were recomputed: Joyner and Boore (1981) and Boore et al. (1993, 1997) (western USA); Ambraseys et al. (1996) and Ambraseys et al. (2005) (Europe and Middle East); Ulusay et al. (2004) and Kalkan and Güllkan (2004) (Turkey); and Sabetta and Pugliese (1987) (Italy). Equations were derived for the larger horizontal component, M_w (derived by conversion from M_s using Equation 6.2 of Ambraseys and Free (1997) with $P = 0$ for Ambraseys et al. (1996)) and distance to the surface projection of rupture (except for Ulusay et al. (2004) for which epicentral distance was used). The simple functional form adopted was $\log y = a_1 + a_2 M + a_3 \log \sqrt{d^2 + 5^2} + a_{3+i} S_i$ where S_i equals unity for site class i and zero otherwise (the same site classes as in the original equation were used). A fixed coefficient of 5 km (a rough average value for this coefficient for most models that adopt this functional form) inside the square root has been assumed in order to make the function linear. This functional form has been commonly adopted in the past and models the major dependencies on magnitude, distance and site class. In addition, the model is linear; therefore, it allows easy computation of the confidence limits using the formula above. Note that the effects of style-of-faulting and other factors have been neglected. The idea of this analysis is not to develop ground-motion estimation equations to be used for seismic hazard assessments but to derive confidence limits on the median PGA and thereafter to examine possible regional dependence. The 95% confidence limits are computed since it is common to examine the rejection of a null hypothesis (in this

case that there is no regional dependence) at a 5% significance level (e.g., Moroney, 1990). Note that it is assumed here that PGAs are log-normally distributed, which was shown to be a valid hypothesis by Douglas and Smit (2001); however, for response spectral amplitudes a log-normal distribution may not be appropriate (Lee and Trifunac, 1995).

Figure 3 displays the predicted median PGAs at rock sites and their 95% confidence limits from the various re-derived models for $M_w = 5.0, 6.5$ and 8.0 events and for distances up to 200 km. Note that events of magnitude 5 and 8 are often outside the limits of the data used to derive these models but they are included in order to show how the median becomes less precisely defined when extrapolation is required. Similarly most dataset have few records from distances greater than 100 km; therefore, again this shows the effect of extrapolation. In order to emphasize the imprecision in the median ground motions, the median is plotted using a dashed line and the 95% confidence limits as solid lines.

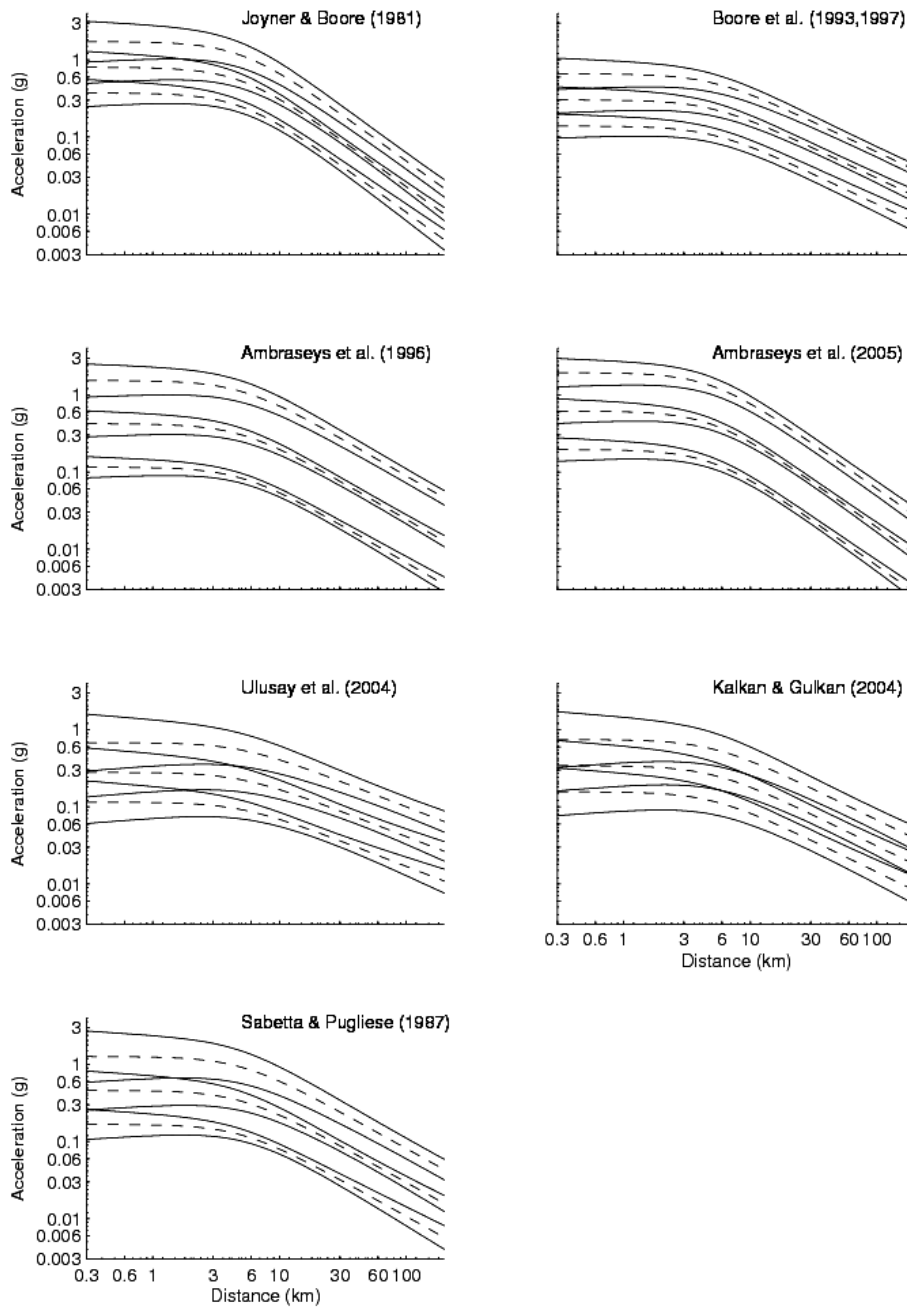


Fig. 3 Predicted median PGAs (dashed lines) at rock sites for $M_w = 5.0, 6.5$ and 8.0 earthquakes and their 95% confidence limits (solid lines) for ground-motion models derived using various datasets (the names in this figure refer to the datasets, not to the equations, of the respective authors)

The confidence limits on the median ground-motion predictions for equations derived with limited data, especially when it is poorly distributed with respect to magnitude and distance (Ulusay et al., 2004; Kalkan and Gülkan, 2004; Sabetta and Pugliese, 1987), are much wider than those of the models based on large well-distributed datasets (Joyner and Boore, 1981; Boore et al., 1993, 1997; Ambraseys et al., 1996, 2005) showing that their medians are more poorly defined. Generally for moderate magnitudes ($5.5 < M_w < 7$) and at moderate distances ($10 \leq d_f \leq 60$ km), the 95%-confidence limits of the median are narrow and are within the bands 10–30% from the median. For smaller and larger earthquakes and particularly at shorter and longer distances the confidence limits become much wider, especially if extrapolation is required, and imply that the estimated median ground motion is only known (to 95% confidence) within a factor of roughly two. Parts of the data-space away from the centroid (e.g., near-source and for large events) where the confidence limits of ground-motion models become much broader are also often where the various models (and also the parts of log-log graphs where differences are most noticeable) diverge. Hence, such divergence between different models should not necessarily be taken as proof of regionally dependent ground motions.

The importance of increasing the quantity of near-source large magnitude data is demonstrated by comparing the confidence limits for the model based on the data of Joyner and Boore (1981) to those based on the data of Boore et al. (1993, 1997), who had new data available from large magnitude events, such as Loma Prieta ($M_w = 6.9$), Cape Mendocino ($M_w = 7.1$) and Landers ($M_w = 7.3$) earthquakes, and consequently the confidence limits are narrower at large magnitudes and at close distances. Similarly, but in a less pronounced manner, the confidence limits of the model derived using the data of Ambraseys et al. (2005) are slightly narrower for large magnitudes and at close distances than those using the data of Ambraseys et al. (1996). This is due to the presence of additional data, such as records from the Kocaeli ($M_w = 7.6$) and Düzce ($M_w = 7.2$) events. On their Figure 4 Sabetta and Pugliese (1987) give distance and magnitude ranges within which their model applies (because of sufficient data): roughly 1.5–30 km for $M = 5$, 4–100 km for $M = 6$, and 10–200 km for $M = 7$. The importance of these recommendations is demonstrated by the large confidence limits of the model derived using these data for distances and magnitudes outside these limits.

As an example of the problem in assessing regional dependence based on published empirical ground-motion models, Figure 4 compares the predicted median PGAs at rock sites for a $M_w = 6.5$ earthquake using the equations derived from the data of Ulusay et al. (2004) (from north-western Turkey) and from the data of Sabetta and Pugliese (1987) (from Italy). This figure shows that if only the predicted median ground motions are considered (the dashed lines) then it appears that there is a difference in shaking between these two areas. However, if the 95% confidence limits are considered, in order to test the significance of this suspected difference, the apparent variation between the two regions is not strong enough to reject the null hypothesis because the confidence limits of the medians of the two curves overlap (except at great distances, where there is very little data).

INVESTIGATION USING OBSERVED GROUND MOTIONS

Luzi et al. (2006) compare predicted ground motions using equations developed by Bindi et al. (2006) from Umbria-Marche data with those they develop using data from the Molise region and find large differences that they propose are due to real differences in ground motions between the two regions. Figure 5 compares the predicted PGAs from the ground-motion model of Luzi et al. (2006) for Molise with those predicted by the models of Bindi et al. (2006) and Zonno and Montaldo (2002) for Umbria-Marche, showing that predicted shaking in Molise is much lower (by about an order of magnitude for $M_L = 4.5$) than that in Umbria-Marche. Molise and Umbria-Marche are geographically close regions within the Italian Apennines, and, therefore, if ground motions in these two areas are truly different it would have serious implications for studies that combine data from various, often widely-separated, parts of the world.

One possible reason why the predicted ground motions from the model of Luzi et al. (2006) do not match those from the model of Bindi et al. (2006) is that Luzi et al. (2006) use data mainly from $2.8 \leq M \leq 5.2$ and $10 \leq d \leq 40$ km whereas the data of Bindi et al. (2006) mainly comes from $4.0 \leq M \leq 5.9$ and $d \leq 40$ km. Pousse et al. (2007) show, using data from the Japanese K-Net and Kik-Net, that ground-motion models developed by regression on data from small earthquakes poorly predict ground motions from large earthquakes and vice versa even for models derived for the same region, due to differences in scaling.

Since the exact datasets used by Bindi et al. (2006) and Luzi et al. (2006) have not been published, the confidence limits of the median predictions, as discussed in the previous section, cannot be assessed here.

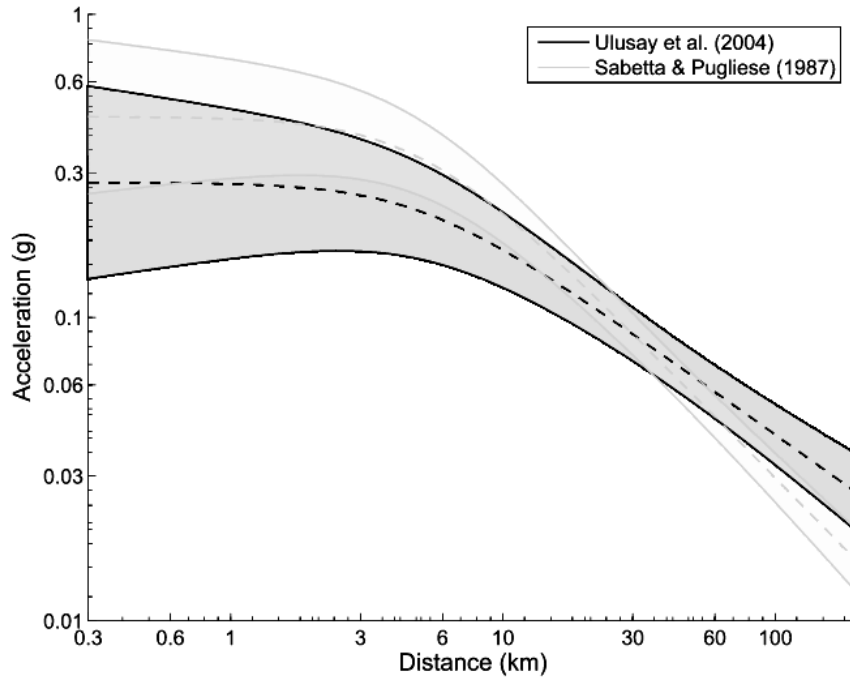


Fig. 4 Predicted median PGAs (dashed lines) and their 95% confidence limits (shaded areas) at rock site for a $M_w = 6.5$ earthquake using the equations derived using the data of Ulusay et al. (2004) (from north-western Turkey) and data of Sabetta and Pugliese (1987) (from Italy)

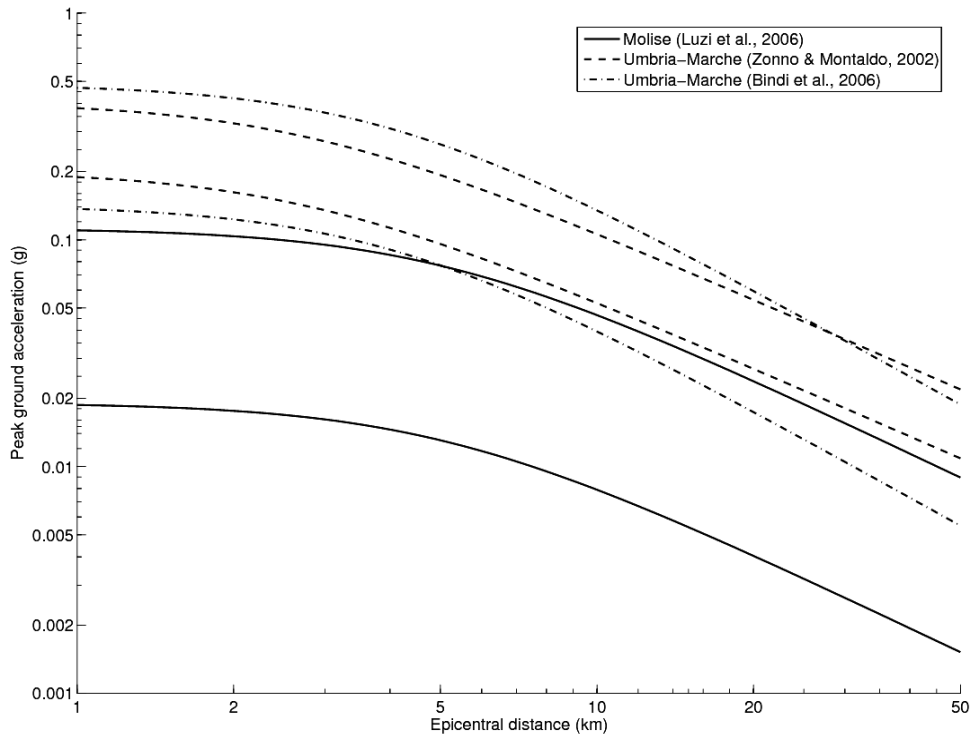


Fig. 5 Comparison of horizontal PGAs predicted by models of Luzi et al. (2006) for Molise (for focal depth of 5 km) and Bindi et al. (2006) and Zonno and Montaldo (2002) for Umbria-Marche at rock sites for earthquakes of $M_L = 4.5$ and 5.5

To investigate further the differences in shaking between these two regions, strong-motion data from the Umbria-Marche 1997–1998 sequence on the CD ROM¹ plus data available on the Internet Site for European Strong-Motion Data (Ambraseys et al., 2004) for a 1979 earthquake in the same region were selected. The same set of records was employed by Douglas et al. (2004) during their validation of the modal summation ground-motion simulation technique, although the sub-crustal 26th March 1998 (focal depth of 48 km) event is excluded here. For the Molise region, the data available on the CD ROM² was analysed. Analysis was confined to ground motions from the larger events ($M > 4$) in both sequences. All available time-histories were examined and those of too poor quality were rejected. Table 2 summarises the data selected. In total, 191 records from 22 earthquakes and 42 stations from the Umbria-Marche region and 70 records from 9 earthquakes and 31 stations in the Molise region were retained. The method of Frohlich and Apperson (1992) has been used here to classify earthquakes by faulting mechanism: earthquakes with plunges of their T -axis greater than 50° are classified as thrust (T), those with plunges of their B -axis or P -axis greater than 60° are classified as strike-slip (S) and normal (N), respectively, and all other earthquakes are classified as odd (O); U stands for unknown faulting mechanism. Table 3 presents the distribution of records with respect to site class and style of faulting for the two regional datasets. Sites have been classified here in terms of the categories proposed by Boore et al. (1993): very soft soil for $V_{s,30} \leq 180$ m/s; soft soil for $180 < V_{s,30} \leq 360$ m/s; stiff soil for $360 < V_{s,30} \leq 750$ m/s; and rock for $V_{s,30} > 750$ m/s.

Table 2: Details of Earthquakes from the Umbria-Marche and Molise Region Analysed in This Study (Y is year; M is month; D is day; T is time; M_w is moment magnitude (those in *italics* have been converted from m_b using the conversion formula of Castellaro et al. (2006)); N is number of records; and d range is the distance range of records selected (epicentral unless in *italics* when it is distance to surface projection))

<i>Y</i>	<i>M</i>	<i>D</i>	<i>T</i>	<i>M_w</i>	Mechanism	<i>N</i>	<i>d</i> range (km)
Umbria-Marche							
1979	09	19	21:35	5.8	N	4	1–37
1997	09	03	22:07	4.5	N	2	4–13
1997	09	26	00:33	5.7	N	15	0–122
1997	09	26	09:40	6.0	N	17	1–128
1997	09	26	13:30	4.5	N	2	3–26
1997	09	27	08:08	4.4	N	4	4–31
1997	10	03	08:55	5.3	N	8	5–37
1997	10	04	16:33	4.7	N	3	11–23
1997	10	06	23:24	5.5	N	17	5–88
1997	10	07	01:24	4.2	N	4	10–16
1997	10	07	05:09	4.5	O	6	3–39
1997	10	12	11:08	5.2	O	12	4–54
1997	10	13	13:09	4.4	N	3	9–25
1997	10	14	15:23	5.6	N	29	9–114
1997	10	16	12:00	4.3	S	6	1–12
1997	10	19	16:00	4.2	N	5	5–17
1997	11	09	19:07	4.9	N	8	7–37
1998	02	07	00:59	4.4	N	7	6–16
1998	03	21	16:45	5.0	O	8	5–19
1998	04	03	07:26	5.1	N	14	6–38
1998	04	03	07:59	4.3	N	6	7–25
1998	04	05	15:52	4.8	N	11	8–39
Molise							
2002	10	31	10:32	5.7	S	11	22–194
2002	11	01	15:08	5.7	S	10	24–187

¹ Windows version of “The Umbria-Marche Strong Motion Data Set (September 1997–June 1998)” published by Servizio Sismico Nazionale—Monitoring System Group in 2002

² Windows version of “The Strong Motion Records of Molise Sequence (October 2002–December 2003)” published by Dipartimento della Protezione Civile, Ufficio Servizio Sismico Nazionale—Monitoring System Group in 2004

2002	11	01	15:20	3.8	U	1	90–90
2002	11	01	17:21	4.5	O	1	94–94
2002	11	04	00:35	4.3	U	9	4–93
2002	11	12	09:27	4.6	S	11	5–91
2002	12	02	20:52	3.8	U	9	4–99
2003	06	01	15:45	4.4	S	6	6–96
2003	12	30	05:31	4.5	S	12	14–160

Table 3: Distribution of Data Used with Respect to Local Site Class and Faulting Mechanism for the Two Regions (left-hand numbers refer to Umbria-Marche and right-hand numbers to Molise)

	Very Soft Soil		Soft Soil		Stiff Soil		Rock		Unknown		Total	
Normal	4	0	32	0	43	0	65	0	15	0	159 (83%)	0 (0%)
Strike-Slip	0	0	1	7	1	22	4	21	0	0	6 (3%)	50 (71%)
Thrust	0	0	0	0	0	0	0	0	0	0	0 (0%)	0 (0%)
Odd	1	0	4	1	7	0	14	0	0	0	26 (14%)	1 (1%)
Unknown	0	0	0	3	0	12	0	4	0	0	0 (0%)	19 (27%)
Total	5	0	37	11	51	34	83	25	15	0	191	70
	(3%)	(0%)	(19%)	(16%)	(27%)	(49%)	(43%)	(36%)	(8%)	(0%)		

Figure 6 displays the normalized residuals, i.e., $\varepsilon_i = (\log y_i - \log y'_i) / \sigma_i$ where y_i is the observed i th ground motion value, y'_i is the predicted i th ground motion and σ_i is the predicted standard deviation of the i th ground motion, of the observed horizontal PGA and SA at 1.0 s for 5% damping with respect to the ground-motion model of Ambraseys et al. (2005) against distance and magnitude, for the two regions. Mean normalized residuals for the two regions are: for Umbria-Marche, -0.06 for PGA and -0.25 for SA at 1.0 s; and for Molise, -1.71 for PGA and -1.60 for SA at 1.0 s. Figure 6 and these mean residuals show that PGA is, on average, well estimated for the Umbria-Marche events and overestimated for the Molise events, and SA at 1.0 s is, on average, overestimated for both sequences, although much less so for the Umbria-Marche events. Note that 88 records from eight Umbria-Marche events were used to derive the equations of Ambraseys et al. (2005) but no records from the Molise sequence were used because they were not available at the time. Figure 6 makes apparent some of the difficulties in assessing regional differences based solely on comparisons with published ground-motion models. The equations of Ambraseys et al. (2005) were derived for the earthquakes with $M_w \geq 5$ and from distances less than or equal to 100 km; therefore, there are possible problems in extrapolating the equations to smaller magnitudes and greater distances but this is required here in order to obtain reasonably large datasets. This extrapolation could be responsible for some of the apparent trends in the residuals for $M_w < 5$ and distances greater than 100 km. In addition, the sets of records from the two regions have different magnitude-distance distributions: for Umbria-Marche most data is from distances less than 30 km and from $M_w \geq 4.5$, whereas for Molise there are many records from greater distances and from smaller magnitudes. Therefore it is difficult to compare the residual plots from the two regions. The following section presents another technique for assessing differences between the two regions without requiring an explicit ground-motion model.

1. Application of Analysis of Variance

In order to investigate further the possible differences in ground motion between these two zones, the technique proposed by Douglas (2004b) based on one-way analysis of variance (e.g., Green and Margerison, 1979) is applied. Douglas (2004b) used the method to investigate variations in ground motions between five regions (south Iceland, Friuli, central Italy, Greece and the Caucasus region) and found little evidence for differences in ground motions in the different regions, although the analysis technique could only be applied to data from small events due to a lack of data. Differences in ground motions in California, Europe and New Zealand were examined by Douglas (2004c), using the same technique, and some evidence for differences in motions between California and Europe was found.

In this technique, two estimates of the variance of the ground motions are calculated. One estimate is the between-region variance (with $n-1$ degrees of freedom, where n is the number of regions), and the other is the within-region variation (with $N-n$ degrees of freedom, where N is the total number of records within the bin). Whether or not the means of the ground motions for the different regions differ, the within-region variation will be an unbiased estimator of the true variance, σ_2 ; the between-region estimator, however, will only be unbiased if the means of the ground motions are equal, otherwise its expectation will be larger than σ_2 . The ratio of the two estimates of the variance of the ground motions is compared to the critical value of F using an F -test. The null hypothesis that the median ground motions are equal is rejected if this ratio is greater than the critical value of F for the significance level used (in this study, 5%) (e.g., Green and Margerison, 1979). The observed data are analysed at four periods: 0.0 (PGA), 0.2, 0.5 and 1.0 s using the larger horizontal component of each record for each intensity measure. The common (base 10) logarithm of the ground motion amplitudes is taken before the analysis of variance is performed since it has been demonstrated (e.g., Douglas and Smit, 2001) that this transformation is justified because the standard deviations of the untransformed ground motions are proportional to the mean of the ground motions. A logarithmic transformation removes this dependence (e.g., Draper and Smith, 1981).

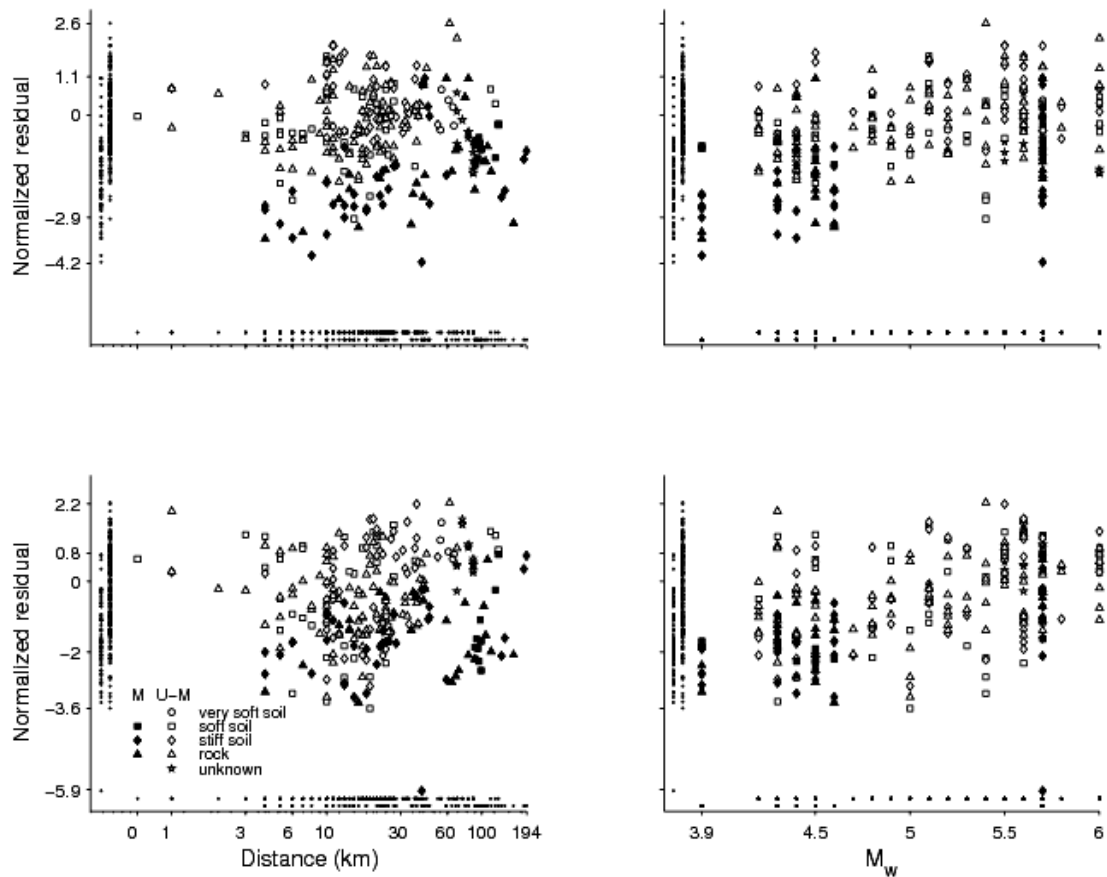


Fig. 6 Normalized residuals for PGA (upper graphs) and SA at 1 for 5% damping (lower graphs) for data from Umbria-Marche (unfilled symbols) and Molise (filled symbols) and the ground-motion model of Ambraseys et al. (2005) with respect to source-to-site distance and M_w (residuals for records with unknown site classes (for Umbria-Marche) have been computed with respect to predicted rock motions; residuals for unknown mechanisms (for Molise) have been computed with respect to predicted strike-slip motions (the predominant mechanism for these events); also shown, as small dots close to the x - and y -axes, are the marginal distributions)

In this study the data-space was divided into small intervals within which an analysis of variance was performed. Intervals of $10 \text{ km} \times 0.25 M_w$ units were used for this analysis so that there were sufficient records within each bin. This is a larger interval size than that used by Douglas (2004b), who used 5 km

$\times 0.25 M_S$ units, because, unfortunately, there are not sufficient records available from Molise to use smaller bins. In each interval a one-way analysis of variance calculation is made to assess whether the means of the transformed ground motion amplitudes from the different regions are significantly different. Only bins with two or more records from each region were considered. A key assumption in analysis of variance is that the variances of each subset are equal. This seems reasonably justified because, for example, Table 1 shows that the developed ground-motion models for Umbria-Marche and Molise have similar standard deviations.

In order to approximately correct for local site response the site coefficients derived by Ambraseys et al. (2005) for the three site classes (soft soil, stiff soil and rock) were used to adjust the observed ground motions at non-rock sites to estimated ground motions on rock. Therefore SAs at non-rock sites were divided by the corrective factors reported in Table 4. There is not enough data available that the analysis could be repeated for an individual site class (e.g., rock). An analysis was conducted without applying corrective site factors and similar results were obtained.

Table 4: Corrective Factors Applied to Adjust Non-rock Accelerations (PGA or SA) to Approximate Rock Accelerations (from Ambraseys et al. (2005); they did not find the factor in *italics* to be statistically significant different than unity, at the 5% level)

Period (s)	Soft Soil	Stiff Soil
0.0	1.37	<i>1.12</i>
0.2	1.33	1.17
0.5	1.95	1.36
1.0	2.28	1.63

Figure 7 displays the means of the four transformed strong-motion intensity measures for each region and for each of the eight bins with sufficient data. On this figure the bins and intensity measures that display a significant difference in the means are indicated by crosses as opposed to dots in case of no significant difference. From this figure it can be seen that for most intervals there are significant differences between the ground motions in Molise and Umbria-Marche, with PGA and SA in Umbria-Marche being significantly higher than in Molise and thus confirming the findings of Luzi et al. (2006) based on regionally specific empirical equations and the analysis of residuals with respect to a common ground-motion model shown above. Interestingly the most distant bin (that at $40\text{--}50$ km for $5.50 \leq M_w \leq 5.75$) shows no significant difference in ground motions between the two regions suggesting that the cause of the variation in shaking between the two regions may be a near-source effect (although two near-source bins: $20\text{--}30$ km for $4.25 \leq M_w \leq 4.50$ and $0\text{--}10$ km for $4.50 \leq M_w \leq 4.75$ also show similar ground motions in the two regions).

2. Possible Reasons for Observed Differences

One possible cause for lower ground motions within the Molise 2002–2003 sequence compared to earthquakes in Umbria-Marche is the difference in average focal depths of the two sequences. Bindi et al. (2006) report the focal depths of the 45 Umbria-Marche events they study; they range between 1 and 9 km (not including the single sub-crustal event of depth 48 km) with most between 3 and 6 km. This contrasts with the deeper focal depths of the Molise events reported by Chiarabba et al. (2005) who find that the events occurred at depths between 8 and 20 km. The effect of these greater focal depths on ground motions could be partly modelled with empirical equations by using a distance measure that accounts for depth of the source but this will not predict large differences in motions especially distant from the source where the effect of depth on source-to-site distances is small. For example, Luzi et al. (2006) find that the Molise ground motions were lower than those predicted by the model of Bindi et al. (2006) even when hypocentral distance was used.

Differences in local site response for stations within the two areas could be responsible for some of the observed differences (e.g., if rock sites in Molise were, on average, much harder than those in Umbria-Marche). An average local site amplification for horizontal PGA for Molise stations on soil is estimated by Luzi et al. (2006) via regression as 1.33. Bindi et al. (2006) also present average local site amplifications for four site classes in Umbria-Marche via regression. They report factors for PGA of between 1.10 (for deep soft soil sites) to 2.75 (for sites with shallow soft soil overlying rock). Due to the

similarity between these estimated site effects in the two regions it is unlikely that regional differences in average site conditions is the main cause of the observed variations.

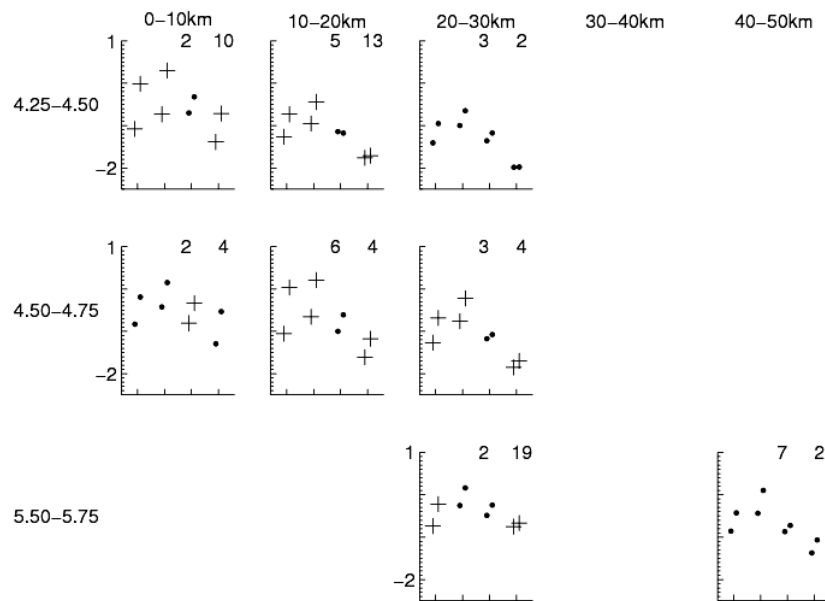


Fig. 7 Graphs for each bin where analysis of variance was performed to compare ground motions in Molise and Umbria-Marche (each small graph displays the means of the transformed ground motions for each of the four strong-motion intensity measures considered (the first two points are PGA, the second two points are SA at 0.2 s, the third two points are SA at 0.5 s and the final two points are SA at 1.0 s); the ordinate of the small graphs is logarithm of acceleration in m/s^2 ; therefore, they can be thought of as response spectra with only four ordinates; the left point in each pair is for Molise and the right point is for Umbria-Marche; if the difference in means was found to be significant at the 5% significance level using the F -test then the marker is a cross rather than a dot; the two numbers in the top right corner are the total number of records in the bin from each region (the left number is for Molise and the right number is for Umbria-Marche); the small graphs are arranged in an overall plot showing the magnitude (on the y -axis) and distance (on the x -axis) ranges of the bins; since no comparisons could be performed due to insufficient data, the magnitude range between 4.75 and 5.50 is not shown)

Different predominant faulting mechanism in the two sequences (mainly normal faulting for the Umbria-Marche sequence and mainly strike-slip for the Molise events) is also unlikely to be responsible for the large differences in observed ground motions since, as noted by Bommer et al. (2003), ground motions are not strongly dependent on style of faulting (average factors between shaking from events with different mechanisms are 10–30%). In fact, spectral ordinates from normal faulting earthquakes are generally similar or slightly lower (about 10%) than those from strike-slip events (Bommer et al., 2003).

Via ground-motion modelling, Di Luccio et al. (2005) and Vallée and Di Luccio (2005) have calculated quite slow rupture velocities for the Molise mainshock of 1.1 km/s and 2.0 km/s, respectively. These relatively low ruptures velocities contrast with more usual rupture velocities reported by, for example, Capuano et al. (2000) for the main Umbria-Marche events of 2.6–3.0 km/s. These differences in velocities should have an important effect on ground motions due to more prominent directivity effects in faster rupturing earthquakes. Also, slow rupture velocities could imply a sparse distribution of asperities and, therefore, a larger fault area for the same magnitude, which could explain differences for intermediate and long periods (M.D. Trifunac, written communication, 2007).

An important question is whether the ground motions observed in the Molise and Umbria-Marche sequences are typical for their regions. If so, then corrective factors to adjust ground-motion models derived for other regions would need to be applied in these parts of Italy in order to avoid general over- or under-estimation of shaking. Chiarabba et al. (2005) note that earthquakes of the Molise 2002 sequence

were deeper than is usual in the southern Apennines normal fault belt; therefore, the data from this sequence may not be sufficient to develop such corrective factors because the ground motions observed may be atypical.

INVESTIGATION USING STOCHASTIC MODELS

The stochastic method (Boore, 2003) has become a widely-used technique for the simulation of ground motions especially for regions lacking observational data from damaging earthquakes, such as eastern North America, because the parameters required can be estimated using data from standard seismological networks. Following Boore (2003), ‘stochastic model’ refers here to the parameters used within the stochastic method for a particular application.

In the stochastic method a Fourier spectrum of ground motion is estimated using a model of the source spectrum that is transferred to the site by considering geometric decay and anelastic attenuation. The parameters that define the source spectrum and the geometric and anelastic attenuation are based on simple physical models of the earthquake process and wave propagation and these parameters are estimated by analysing many seismograms. After the Fourier spectrum at a site is estimated time-histories can be computed by adjusting and enveloping white noise to give the desired spectrum and duration of shaking. The main input parameters in this method that make the stochastic model regionally dependent are (divided into source, path and site factors): the source spectral amplitude and shape, and the source duration; the geometric decay rates with respect to distance, the anelastic attenuation with respect to frequency and the path duration with respect to distance; and the local site amplification and attenuation. Since the method does not account for phase effects due to propagating rupture or wave propagation the results in the near-source region may not be appropriate. In addition, there is much debate over the shape of source spectra for moderate and large events (M_w greater than roughly 6) where the commonly used one-corner frequency spectrum of Brune (1970, 1971) for body waves may not be appropriate (e.g., Gusev, 1983; Joyner, 1984; Atkinson and Silva, 2000). Since only body waves are usually considered, long-period ground motions could be poorly estimated by this method (see Trifunac (1993) on the estimation of long-period spectral ordinates). The reader is referred to the comprehensive review article by Boore (2003) for details of the stochastic method and a discussion of its limitations.

In this article, comparisons are made of the elastic response spectra predicted using stochastic models developed for different regions that are classified into a number of broad seismotectonic categories: stable continental regions (low strain rates) and regions of moderate and high strain rates. If such a classification of regions is justified with respect to the ground motions estimated for the same magnitude and distance, variations between ground motions predicted using models from different tectonic categories should be larger than those predicted from models within the same tectonic class. For example, predictions of ground motions from different models for stable continental regions should be closer together than predictions from various models for high-strain-rate regions, i.e., the intra-region variation should be less than the inter-region variation.

Sokolov (2000) also makes comparisons of ground motions predicted by various stochastic models (for the Racha and Spitak regions of the Caucasus region and Taiwan) and concludes that there are regional variations in ground motions between the three regions compared. However, the models compared by Sokolov (2000) were based on strong-motion datasets of different distributions in terms of magnitude and distance, which could have strongly contributed to the variation in predicted motions. Stochastic models are subjected to large uncertainties due to trade-offs between different parameters (e.g., Bay et al., 2005) and it is important that this epistemic uncertainty is appreciated while making comparisons between models. One difficulty in making comparisons between predicted median ground motions from different stochastic models is that the uncertainties in the median predictions are rarely given. Unlike empirical models that are derived by regression and where the uncertainty can be easily computed using the difference between observed and predicted ground motions, stochastic models are derived through complex analysis and hence it is difficult to estimate uncertainties.

In an earlier study using stochastic models, Chen and Atkinson (2002) compared apparent earthquake source radiations for six different regions: Japan, Mexico, Turkey, California, British Columbia (western Canada) and eastern North America, and they concluded that there is little evidence for inter-regional differences.

1. Stochastic Models Considered

Due to the possible trade-off between parameters (e.g., Bay et al., 2005) within stochastic models, only studies that report all required parameters of the stochastic model are considered here. Therefore studies, such as Castro et al. (2004) who study the attenuation in southern Italy but do not provide estimates of $\Delta\sigma$, are excluded. Also excluded are those models that have adopted all or some of the main parameters of their stochastic models, such as $\Delta\sigma$, from the studies for other regions (e.g., Douglas et al., 2006b). Finally, models developed for use in stochastic methods that include finite fault effects (e.g., Beresnev and Atkinson, 1998) have not been included since their parameters may not be appropriate for use in the standard stochastic approach. The model of Allen et al. (2006) from Western Australia is not included since it is developed from data from earthquakes with $2.2 \leq M_w \leq 4.6$; therefore, its suitability for predictions of ground motions from larger earthquakes is not known. The model of Sokolov et al. (2005) for earthquakes occurring in the Vrancea region of Romania is not considered due to the large depths (60–170 km) of these events.

A quantitative comparison of epistemic and aleatoric variabilities of these stochastic models is not possible since to correctly estimate the aleatoric variabilities within ground motions simulated using the stochastic method one requires that each parameter within the stochastic model has a range of possible values in order that the complete range of ground motions is computed (e.g., Sigbjörnsson and Ambraseys, 2003). In this study, the epistemic uncertainty within the expected ground motions for broad seismogenic domains is approximated by the variation between different models for the regions classified within common domains.

To separate ground-motion models by their seismotectonic regime, the global map of second-invariant strain rates published by Kreemer et al. (2003) has been used. Since within the regions covered by the considered stochastic models the strain rates vary, an average strain rate is given in Table 5. Strain rates for the models given in Table 5 fall into three broad categories: $0 \times 10^{-9} \text{ yr}^{-1}$ (stable continental regions), between 0 and $100 \times 10^{-9} \text{ yr}^{-1}$ and $> 100 \times 10^{-9} \text{ yr}^{-1}$; therefore, these three classes have been used for the analysis. If a fault length of 100 km is assumed, this classification corresponds to the classification of earthquakes proposed by Scholz et al. (1986), namely, ‘intraplate (mid-plate)’, ‘intraplate (plate boundary related)’, and ‘interplate’. The distribution of number of models with respect to the different classes is: six for the high strain rate class, eight for the intermediate class and four for the low class.

As discussed in Bommer et al. (2003) and mentioned above, the faulting mechanism of an earthquake can have a measurable impact on the observed strong ground motions. Since this effect could be important when comparing stochastic models studied here, Table 5 also reports the predominant faulting mechanism of earthquakes within the region for which the model was derived. This information is taken, either from the articles themselves or from the World Stress Map³.

Table 5: Stochastic Models Considered in This Study, Average Strain Rate in the Region from Kreemer et al. (2003), Region Type (S is subduction, SC is shallow crustal, V is volcanic and SCR is stable continental region), and the Region’s Predominant Faulting Mechanism (N is normal, R is reverse and SS is strike-slip)

Study	Region	Strain Rate ($\times 10^{-9} \text{ yr}^{-1}$)	Region Type	Mechanism
Sokolov et al. (2000)	Taiwan (shallow)	500	S/SC	R
Chung (2006)	SW Taiwan	500	S/SC	R
Campbell (2003)	California	200	SC	SS/R
Akinci et al. (2006)	Marmara	200	SC	SS/N
Atkinson (1996)	Cascadia	100	S/SC	R/SS
Akinci et al. (2001)	Erzincan	100	SC	SS
Jeon and Herrmann (2004)	Yellowstone	100	V	N
Margaris and Boore (1998), Margaris and Hatzidimitriou (2002)	Greece	100	SC	N/SS
Malagnini et al. (2002)	North-East Italy	20	SC	R
Sokolov (1998)	Spitak, Caucasus	20	SC	R

³ The 2005 Release of the World Stress Map, at <http://www.world-stress-map.org>

Sokolov (1997)	Racha, Caucasus	20	SC	R
Jeon and Herrmann (2004)	Utah	20	SC	N
Scognamiglio et al. (2005)	Eastern Sicily	20	SC	N/R/SS
Malagnini and Herrmann (2000)	Umbria-Marche	10	SC	N
Malagnini et al. (2000a)	Apennines	10	SC	N
Morasca et al. (2006)	Western Alps	5	SC	R/N/SS
Malagnini et al. (2000b)	Central Europe	0	SCR	SS
Campbell (2003) (modal parameters)	Eastern North America	0	SCR	R
Bay et al. (2005)	Switzerland (Alps/foreland)	0	SCR	SS/N

2. Comparisons between Different Models

The computer program SMSIM (Boore, 2005) was used to compute elastic response spectra on generic rock sites. Simulations were computed for each model for $M_w = 4.5, 5.5$ and 6.5 , and for hypocentral distances of 5, 10, 20 and 50 km. The reliability of some of the stochastic models studied here at larger magnitudes is questionable for two reasons. Firstly, many studies used data from small and moderate earthquakes, so it is not known if the parameters of the models, particularly $\Delta\sigma$, are applicable for larger earthquakes (e.g., Ide and Beroza, 2001). Secondly, for larger earthquakes and especially for short source-to-site distances, finite fault effects, which are not modelled using the standard stochastic method, become important. Therefore, comparisons for $M_w > 6.5$ are not made. Ground motions at distances greater than 50 km are rarely of engineering interest due to their low amplitudes; therefore, no far-source comparisons are made.

Figures 8 to 10 display the predicted median response spectra from the studied stochastic models grouped with respect to the strain rate categories defined above. Within each category there are some models that systemically predict greatly different response spectra than the others for that regime, which probably demonstrates regional dependence for the areas covered by these models. For the models from stable continental regions, the predictions from eastern North America (Campbell, 2003) are much higher than those from the other three regions, especially at short periods, whereas predicted spectra from the other three models are generally similar considering the uncertainties in median predictions. Note, however, that predicted spectra (especially at short periods) are highly sensitive to the choice of parameters in the models (particularly $\Delta\sigma$, near-surface attenuation, e.g., the value of κ , and near-surface shear-wave velocities) as Campbell (2003) shows for predicted spectra from eastern North America. The spectra predicted by the model of Campbell (2003), which is for a very hard rock site with low near-surface attenuation, need modification for other types of sites with lower near-surface shear-wave velocities and greater attenuation. The predictions from the models for moderate strain regions are approximately separated into two groups: higher amplitudes predicted from the models for eastern Sicily (Scognamiglio et al., 2005), the Apennines (Malagnini et al., 2000a) and the western Alps (Morasca et al., 2006), and lower amplitudes predicted for north-east Italy (Malagnini et al., 2002), Spitak (Sokolov, 1998), Racha (Sokolov, 1997), Utah (Jeon and Herrmann, 2004) and Umbria-Marche (Malagnini and Herrmann, 2000). Spectra predicted for the high strain regions show large dispersions of factors of more than 10 times (for example, compare the predicted spectra for Taiwan and Erzincan for $M_w = 6.5$ at 5 km). Such large dispersion is not observable in strong-motion data from these high strain regions, which are often combined when deriving empirical models.

Interestingly, the variation in predicted response spectra between models that could be considered to have been developed for comparable tectonic regions is similar to the variation between models from tectonically different regions. This suggests that the stochastic models are not developed well enough to be able to draw definitive conclusions regarding the regional dependence of ground motions based on stochastic modelling. This does not necessarily mean that ground motions are not regionally dependent but that the stochastic models are not yet sufficiently accurate. Due to the large variation in the predicted spectra for each group it is not currently possible to clearly observe whether variations in faulting mechanism between regions within each tectonic group are responsible for the differences in estimated ground motions. As mentioned above, observations from analyses of recorded strong ground motions show that, although measurable differences in spectra due to differing faulting mechanism exist, the effect of mechanism is relatively small (usually 10–30%) (e.g., Bommer et al., 2003). Therefore, other variations in the stochastic models could be obscuring this effect.

One important parameter within the regional stochastic models that could be obscuring a regional dependence in response spectra due to source or path differences is that the stochastic models have been derived for different average rock conditions. For example, for stable continental regions, Campbell (2003) proposes his model for very hard rock sites (average shear-wave velocities in upper 30 m of 2800 m/s) with high near-surface shear-wave velocities and low attenuation ($\kappa = 0.006$ s) that are common in eastern North America, whereas the model of Bay et al. (2005) is for sites in the Swiss Alpine foreland of softer rock (average shear-wave velocities in upper 30 m of 750–1500 m/s) and higher attenuation ($\kappa = 0.0125$ s).

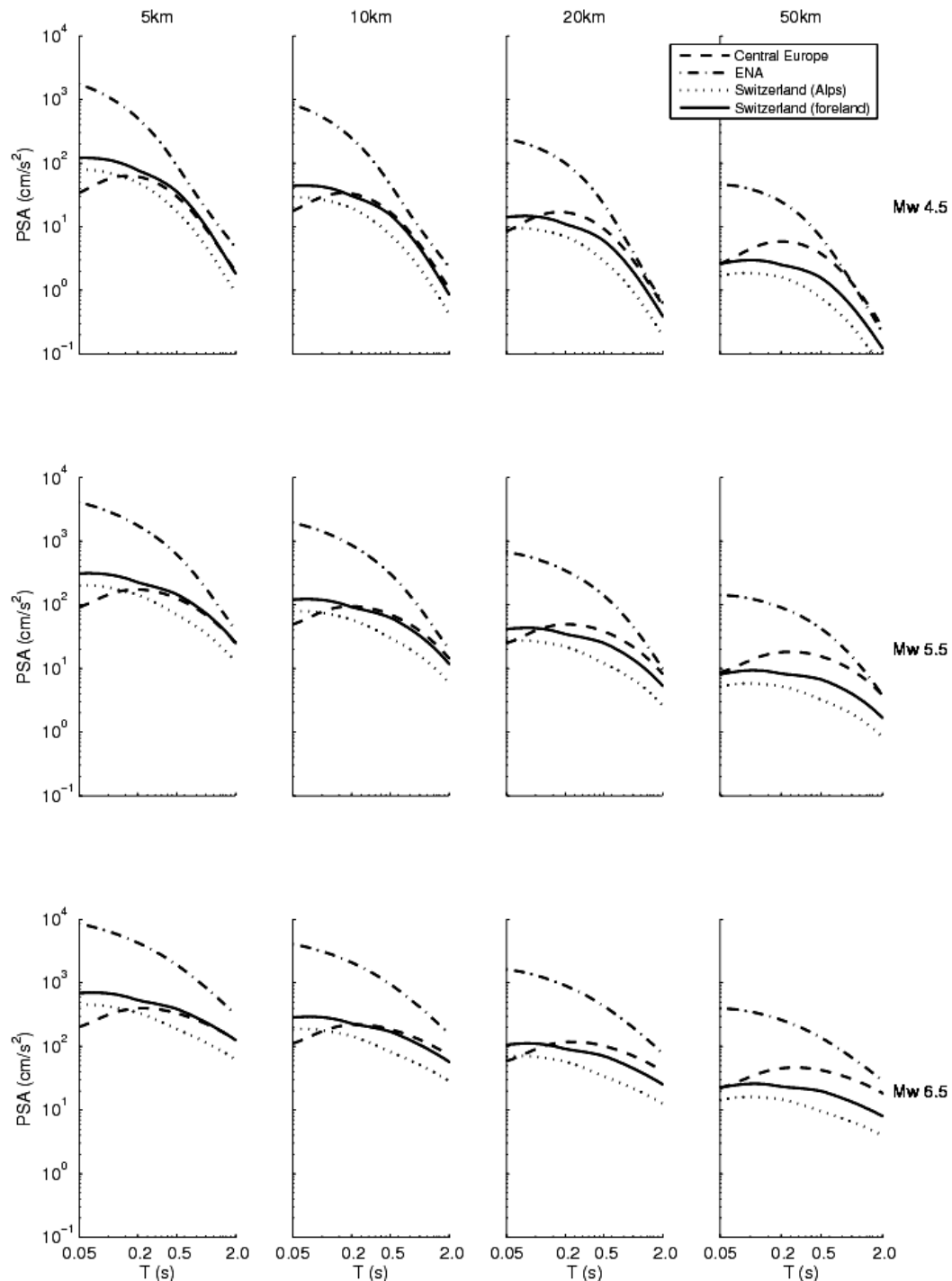


Fig. 8 Comparison of the elastic acceleration response spectra predicted using stochastic models for stable continental regions: central Europe (Malagnini et al., 2000b), eastern North America (Campbell, 2003) and Switzerland (Alps and foreland) (Bay et al., 2005), for different magnitudes (rows) and distances (columns)

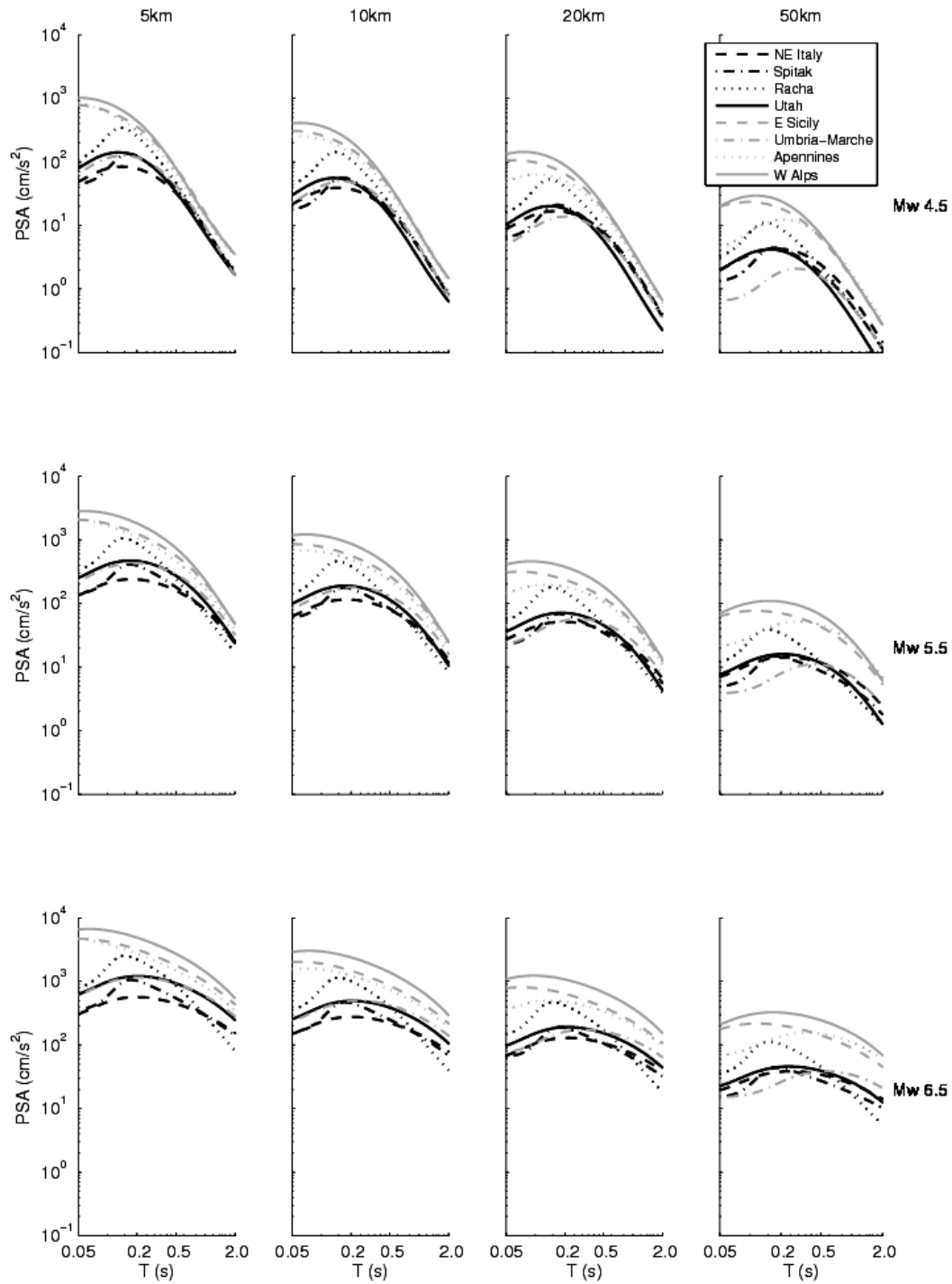


Fig. 9 Comparison of the elastic acceleration response spectra predicted using stochastic models for intermediate strain regions: north-east Italy (Malagnini et al., 2002), Spitak (Sokolov, 1998), Racha (Sokolov, 1997), Utah (Jeon and Herrmann, 2004), eastern Sicily (Scognamiglio et al., 2005), Umbria-Marche (Malagnini and Herrmann, 2000), Apennines (Malagnini et al., 2000a) and western Alps (Morasca et al., 2006), for different magnitudes (rows) and distances (columns)

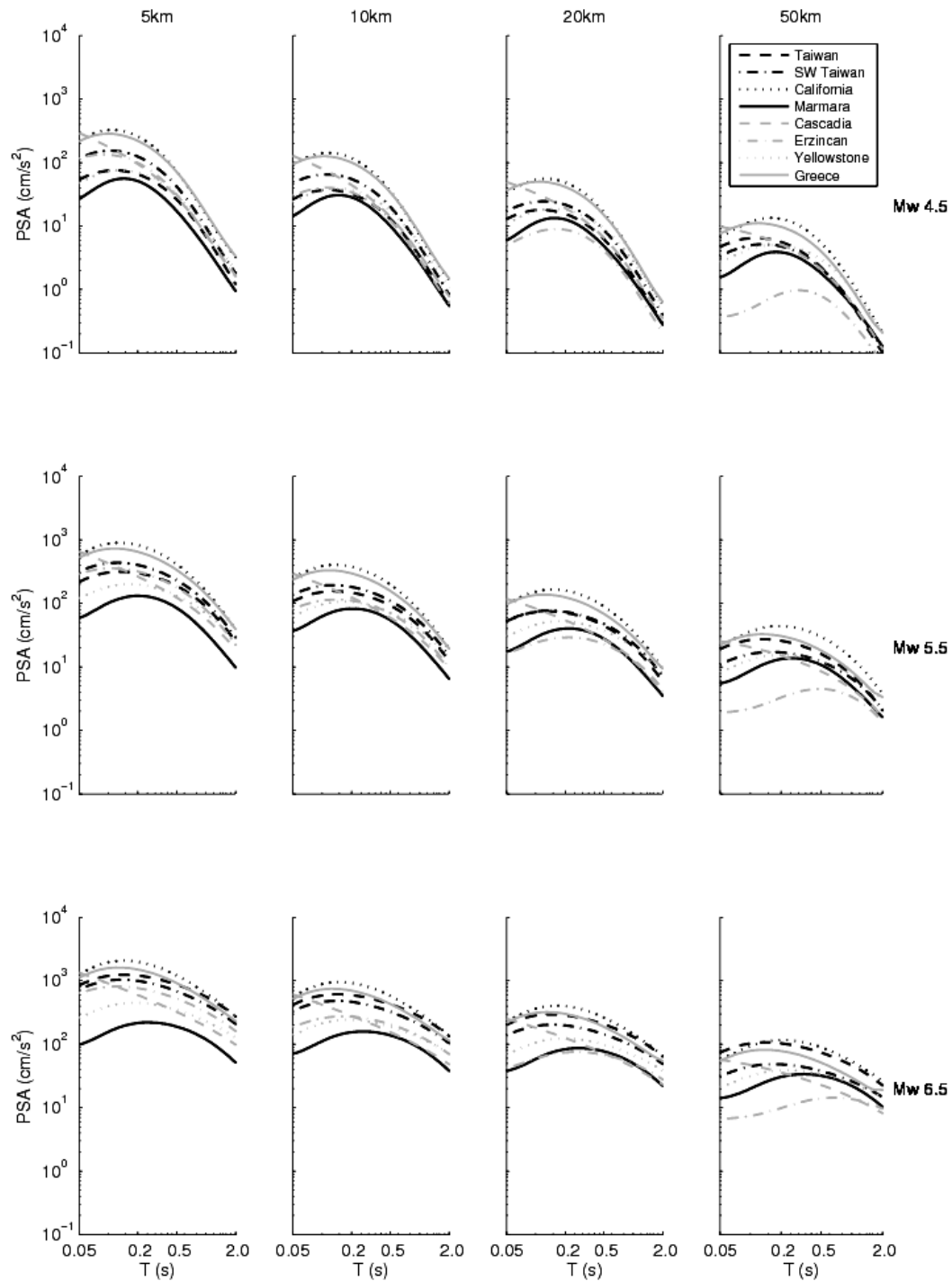


Fig. 10 Comparison of the elastic acceleration response spectra predicted using stochastic models for high strain regions: Taiwan (Sokolov et al., 2000), south-west Taiwan (Chung, 2006), California (Campbell, 2003), Marmara (Akinci et al., 2006), Cascadia (Atkinson, 1995, 1996), Erzincan (Akinci et al., 2001), Yellowstone (Jeon and Herrmann, 2004) and Greece (Margaris and Boore, 1998; Margaris and Hatzidimitriou, 2002), for different magnitudes (rows) and distances (columns)

CONCLUSIONS

This article has investigated the question of whether average ground motions for the same magnitude and source-to-site distance show significant regional variations. A number of different techniques are employed to examine this question: comparison of published empirical and stochastic ground-motion

models, comparison of empirical models considering the confidence limits on the median predictions, residual plots and analysis of variance.

It is shown that predictions from empirical models derived through regression analysis are associated with large epistemic uncertainties due to insufficient data to constrain the median prediction, especially for magnitudes and distances where earthquake ground motions could be of engineering concern. These epistemic uncertainties are shown by large variations in median predictions even when basically the same set of records is used but the functional form and the regression method is varied. This article presents the 95% confidence limits of ground-motion models derived by regression on various sets of records and shows that the predicted median ground motions are not well-constrained away from the centroid of the data, especially for sparse datasets. Therefore conclusions concerning regional dependence based on apparent differences in predicted median ground motions should be made with great caution unless the confidence limits of the models are known. It is suggested that developers of ground-motion models report the confidence limits of their models in order to more reliably make comparisons between predicted median spectra. In the distant future when large well-distributed datasets become available, the medians of predicted earthquake response spectra will become perfectly constrained through the reduction of epistemic uncertainties, and the confidence limits of the medians will be very narrow. These precisely known confidence limits will improve the reliability of conclusions based on comparisons between empirical models.

Residual analysis of spectral ordinates with respect to well-constrained ground-motion models provide an attractive approach for the investigation of regional dependence since it does not rely on the availability of large numbers of records. However, comparing two regions by examining their residuals can be difficult if the distribution of records with respect to their independent variables (e.g., magnitude, distance and site class) is not similar and/or does not match the distribution of records used to derive the ground-motion model.

If data is sufficient, comparisons between earthquake response spectra from different regions should be solely made by comparing observed spectra, in order to reduce uncertainties due to differences in the distributions of datasets from various regions. In this article, an approach based on analysis of variance of observed spectra is applied to two close-together Italian regions (Umbria-Marche and Molise), having been already used in previous studies for various regions in Europe, California and New Zealand. The results confirm the observations made using other techniques.

Finally, numerous stochastic models for the prediction of strong motions were examined. Such models have the advantage of not requiring as much strong-motion data in order to constrain their parameters due to the underlying physical model. Hence, they appear to be an appealing method for comparing ground motions in different regions with insufficient data to apply other methods. By comparing estimated median response spectra for various regions separated into three broad tectonic regimes based on their average strain rates, it is found that some regions seem to display significantly higher or lower spectra than others; however, most models within each type of regime predict similar spectra especially when considering the (unknown) uncertainties of models. There is no strong evidence for large differences between spectra from different tectonic regimes.

From the evidence discussed in this article and other studies, it currently seems to be more defensible for many parts of the world, where observational data is limited, to use well-constrained ground-motion models, possibly developed using data from other regions, than to base design ground-motion estimates on local models, which are often less robust. An important question is whether the ground motions observed during short observational histories (about a decade for many parts of the world) are typical for their regions. It is important to carefully study possible differences in ground motions between regions using, for example, the techniques discussed here; but rather than systemically assuming regional dependence of shaking once a new dataset becomes available, physical reasons for regional dependence should be sought. For example, Dowrick and Rhoades (2004) present an analysis of relations between magnitude and fault rupture dimensions (length, width, area, slip and aspect ratio) and find strong evidence for regional differences within relations between these parameters. The differences were statistically significant between New Zealand and California, New Zealand and Japan, New Zealand and China, and Japan and California. These differences in gross features of earthquakes should translate into differences in strong ground motions since they will affect static stress drops.

If it is found that ground motions vary significantly between regions, the hybrid method introduced and applied by Campbell (2003) for eastern North America and applied by Douglas et al. (2006b) for sites

in southern Spain and southern Norway could be useful for the development of robust predictive models. This technique seeks to combine the benefits of empirical and stochastic modelling. Another method that could model the effect of crustal structure on ground motions, which is a potentially important source of regional dependence, is the use of equivalent hypocentral distance introduced by Douglas et al. (2004).

ACKNOWLEDGEMENTS

Some of the work presented in this article was funded by the Agence Nationale de la Recherche (ANR) for the Quantitative Seismic Hazard Assessment (QSHA) project. The rest was funded by internal BRGM research projects. The writer thanks V.K. Gupta for inviting him to contribute an article to this special issue of the *ISSET Journal of Earthquake Technology*. Also, he thanks those organisations operating the strong-motion networks from which data was used and for disseminating these data. Hideo Aochi helped create Figure 4. Nick Ambraseys has shared with the writer many wise comments on this subject over the years. Roger Musson provided some useful comments on an earlier draft. The books of Edward R. Tufte (e.g., Tufte, 1983) have influenced the design of figures and tables in this and previous articles. K.W. Campbell provided useful comments on his stochastic model for eastern North America. Finally, reviews by Guest Editor M.D. Trifunac, D. Boore, V. Sokolov and two anonymous reviewers were useful and led to significant improvements to the article.

REFERENCES

1. Abrahamson, N.A. and Silva, W.J. (1997). "Empirical Response Spectral Attenuation Relations for Shallow Crustal Earthquakes", *Seismological Research Letters*, Vol. 68, No. 1, pp. 94–127.
2. Akinci, A., Malagnini, L., Herrmann, R.B., Pino, N.A., Scognamiglio, L. and Eyidogan, H. (2001). "High-Frequency Ground Motion in the Erzincan Region, Turkey: Inferences from Small Earthquakes", *Bulletin of the Seismological Society of America*, Vol. 91, No. 6, pp. 1446–1455.
3. Akinci, A., Malagnini, L., Herrmann, R.B., Gok, R. and Sørensen, M.B. (2006). "Ground Motion Scaling in the Marmara Region, Turkey", *Geophysical Journal International*, Vol. 166, No. 2, pp. 635–651.
4. Allen, T.I., Dhu, T., Cummins, P.R. and Schneider, J.F. (2006). "Empirical Attenuation of Ground-Motion Spectral Amplitudes in Southwestern Western Australia", *Bulletin of the Seismological Society of America*, Vol. 96, No. 2, pp. 572–585.
5. Aman, A., Singh, U.K. and Singh, R.P. (1995). "A New Empirical Relation for Strong Seismic Ground Motion for the Himalayan Region", *Current Science*, Vol. 69, No. 9, pp. 772–777.
6. Ambraseys, N.N. and Bommer, J.J. (1991). "The Attenuation of Ground Accelerations in Europe", *Earthquake Engineering & Structural Dynamics*, Vol. 20, No. 12, pp. 1179–1202.
7. Ambraseys, N.N. and Free, M.W. (1997). "Surface-Wave Magnitude Calibration for European Region Earthquakes", *Journal of Earthquake Engineering*, Vol. 1, No. 1, pp. 1–22.
8. Ambraseys, N.N., Simpson, K.A. and Bommer, J.J. (1996). "Prediction of Horizontal Response Spectra in Europe", *Earthquake Engineering & Structural Dynamics*, Vol. 25, No. 4, pp. 371–400.
9. Ambraseys, N.N., Simpson, K.A. and Bommer, J.J. (1997). "Authors' Reply", *Earthquake Engineering & Structural Dynamics*, Vol. 26, No. 2, pp. 295–300.
10. Ambraseys, N.N., Smit, P., Douglas, J., Margaris, B., Sigbjörnsson, R., Ólafsson, S., Suhadolc, P. and Costa, G. (2004). "Internet Site for European Strong-Motion Data", *Bollettino di Geofisica Teorica e Applicata*, Vol. 45, No. 3, pp. 113–129.
11. Ambraseys, N., Douglas, J., Sarma, S.K. and Smit, P. (2005). "Equations for the Estimation of Strong Ground Motions from Shallow Crustal Earthquakes Using Data from Europe and the Middle East: Horizontal Peak Ground Acceleration and Spectral Acceleration", *Bulletin of Earthquake Engineering*, Vol. 3, No. 1, pp. 1–53.
12. Atkinson, G.M. (1995). "Attenuation and Source Parameters of Earthquakes in the Cascadia Region", *Bulletin of the Seismological Society of America*, Vol. 85, No. 5, pp. 1327–1342.

13. Atkinson, G.M. (1996). "The High-Frequency Shape of the Source Spectrum for Earthquakes in Eastern and Western Canada", *Bulletin of the Seismological Society of America*, Vol. 86, No. 1A, pp. 106–112.
14. Atkinson, G.M. and Boore, D.M. (2003). "Empirical Ground-Motion Relations for Subduction-Zone Earthquakes and Their Application to Cascadia and Other Regions", *Bulletin of the Seismological Society of America*, Vol. 93, No. 4, pp. 1703–1729.
15. Atkinson, G.M. and Silva, W. (2000). "Stochastic Modeling of California Ground Motions", *Bulletin of the Seismological Society of America*, Vol. 90, No. 2, pp. 255–274.
16. Bay, F., Wiemer, S., Fäh, D. and Giardini, D. (2005). "Predictive Ground Motion Scaling in Switzerland: Best Estimates and Uncertainties", *Journal of Seismology*, Vol. 9, No. 2, pp. 223–240.
17. Beresnev, I.A. and Atkinson, G.M. (1998). "FINSIM—A FORTRAN Program for Simulating Stochastic Acceleration Time Histories from Finite Faults", *Seismological Research Letters*, Vol. 69, No. 1, pp. 27–32.
18. Berge-Thierry, C., Cotton, F., Scotti, O., Griot-Pommer, D.A. and Fukushima, Y. (2003). "New Empirical Response Spectral Attenuation Laws for Moderate European Earthquakes", *Journal of Earthquake Engineering*, Vol. 7, No. 2, pp. 193–222.
19. Bindi, D., Luzi, L., Pacor, F., Franceschina, G. and Castro, R.R. (2006). "Ground-Motion Predictions from Empirical Attenuation Relationships versus Recorded Data: The Case of the 1997–1998 Umbria-Marche, Central Italy, Strong-Motion Data Set", *Bulletin of the Seismological Society of America*, Vol. 96, No. 3, pp. 984–1002.
20. Bommer, J.J. (2006). "Empirical Estimation of Ground Motion: Advances and Issues", *Proceedings of the Third International Symposium on the Effects of Surface Geology on Seismic Motion*, Grenoble, France, Vol. 1, pp. 115–135.
21. Bommer, J.J., Douglas, J. and Strasser, F.O. (2003). "Style-of-Faulting in Ground-Motion Prediction Equations", *Bulletin of Earthquake Engineering*, Vol. 1, No. 2, pp. 171–203.
22. Boore, D.M. (2001). "Comparisons of Ground Motions from the 1999 Chi-Chi Earthquake with Empirical Predictions Largely Based on Data from California", *Bulletin of the Seismological Society of America*, Vol. 91, No. 5, pp. 1212–1217.
23. Boore, D.M. (2003). "Simulation of Ground Motion Using the Stochastic Method", *Pure and Applied Geophysics*, Vol. 160, No. 3–4, pp. 635–676.
24. Boore, D.M. (2005). "SMSIM—Fortran Programs for Simulating Ground Motions from Earthquakes: Version 2.3—A Revision of OFR 96-80-A", A Modified Version of OFR 00-509, Describing the Program as of 15 August, 2005, http://quake.usgs.gov/~boore/smsim/smsim_manual.pdf.
25. Boore, D.M. and Atkinson, G.M. (2007). "Boore-Atkinson NGA Ground Motion Relations for the Geometric Mean Horizontal Component of Peak and Spectral Ground Motion Parameters", Report PEER 2007/01, University of California, Berkeley, U.S.A.
26. Boore, D.M., Joyner, W.B., Oliver, III, A.A. and Page, R.A. (1980). "Peak Acceleration, Velocity, and Displacement from Strong-Motion Records", *Bulletin of the Seismological Society of America*, Vol. 70, No. 1, pp. 305–321.
27. Boore, D.M., Joyner, W.B. and Fumal, T.E. (1993). "Estimation of Response Spectra and Peak Accelerations from Western North American Earthquakes: An Interim Report", Open-File Report 93-509, United States Geological Survey, Denver, U.S.A.
28. Boore, D.M., Joyner, W.B. and Fumal, T.E. (1997). "Equations for Estimating Horizontal Response Spectra and Peak Acceleration from Western North American Earthquakes: A Summary of Recent Work", *Seismological Research Letters*, Vol. 68, No. 1, pp. 128–153.
29. Bragato, P.L. and Slejko, D. (2005). "Empirical Ground-Motion Attenuation Relations for the Eastern Alps in the Magnitude Range 2.5–6.3", *Bulletin of the Seismological Society of America*, Vol. 95, No. 1, pp. 252–276.
30. Brune, J.N. (1970). "Tectonic Stress and the Spectra of Seismic Shear Waves from Earthquakes", *Journal of Geophysical Research*, Vol. 75, No. 26, pp. 4997–5009.
31. Brune, J.N. (1971). "Correction", *Journal of Geophysical Research*, Vol. 76, No. 20, p. 5002.

32. Campbell, K.W. (1985). "Strong Motion Attenuation Relations: A Ten-Year Perspective", *Earthquake Spectra*, Vol. 1, No. 4, pp. 759–804.
33. Campbell, K.W. (2003). "Prediction of Strong Ground Motion Using the Hybrid Empirical Method and Its Use in the Development of Ground-Motion (Attenuation) Relations in Eastern North America", *Bulletin of the Seismological Society of America*, Vol. 93, No. 3, pp. 1012–1033.
34. Campbell, K.W. and Bozorgnia, Y. (2003). "Updated Near-Source Ground-Motion (Attenuation) Relations for the Horizontal and Vertical Components of Peak Ground Acceleration and Acceleration Response Spectra", *Bulletin of the Seismological Society of America*, Vol. 93, No. 1, pp. 314–331.
35. Campbell, K.W. and Bozorgnia, Y. (2007). "Campbell-Bozorgnia NGA Ground Motion Relations for the Geometric Mean Horizontal Component of Peak and Spectral Ground Motion Parameters", Report PEER 2007/02, University of California, Berkeley, U.S.A.
36. Capuano, P., Zollo, A., Emolo, E., Marcucci, S. and Milana, G. (2000). "Rupture Mechanism and Source Parameters of Umbria-Marche Mainshocks from Strong Motion Data", *Journal of Seismology*, Vol. 4, No. 4, pp. 463–478.
37. Castellaro, S., Mulargia, F. and Kagan, Y.Y. (2006). "Regression Problems for Magnitudes", *Geophysical Journal International*, Vol. 165, No. 3, pp. 913–930.
38. Castro, R.R., Gallipoli, M.R. and Mucciarelli, M. (2004). "An Attenuation Study in Southern Italy Using Local and Regional Earthquakes Recorded by Seismic Network on Basilicata", *Annals of Geophysics*, Vol. 47, No. 5, pp. 1597–1608.
39. CEN (2005). "Eurocode 8: Design of Structures for Earthquake Resistance—Part 1: General Rules, Seismic Actions and Rules for Buildings", EN 1998-1:2004, Comité Européen de Normalisation, Brussels, Belgium.
40. Chen, S.Z. and Atkinson, G.M. (2002). "Global Comparisons of Earthquake Source Spectra", *Bulletin of the Seismological Society of America*, Vol. 92, No. 3, pp. 885–895.
41. Chiarabba, C., De Gori, P., Chiaraluce, L., Bordonì, P., Cattaneo, M., De Martin, M., Frepoli, A., Michelini, A., Monachesi, A., Moretti, M., Augliera, G.P., D'Alema, E., Frapiccini, M., Gassi, A., Marzorati, S., Di Bartolomeo, P., Gentile, S., Govoni, A., Lovisa, L., Romanelli, M., Ferretti, G., Pasta, M., Spallarossa, D. and Zunino, E. (2005). "Mainshocks and Aftershocks of the 2002 Molise Seismic Sequence, Southern Italy", *Journal of Seismology*, Vol. 9, No. 4, pp. 487–494.
42. Chiou, S.-J. and Youngs, R.R. (2006). "Chiou and Youngs PEER-NGA Empirical Ground Motion Model for the Average Horizontal Component of Peak Acceleration and Pseudo-Spectral Acceleration for Spectral Periods of 0.01 to 10 Seconds", Interim Report, Pacific Earthquake Engineering Research Center, University of California, Berkeley, U.S.A.
43. Chung, J.K. (2006). "Prediction of Peak Ground Acceleration in Southwestern Taiwan as Revealed by Analysis of CHY Array Data", *Terrestrial, Atmospheric and Oceanic Sciences*, Vol. 17, No. 1, pp. 139–167.
44. Costa, G., Suhadolc, P., Delise, A., Moratto, L., Furlanetto, E. and Fitzko, F. (2006). "Estimation of Site Effects at Some Stations of the Friuli (NE Italy) Accelerometric Network (RAF)", *Proceedings of the Third International Symposium on the Effects of Surface Geology on Seismic Motion*, Grenoble, France, Vol. 1, pp. 729–739.
45. Cotton, F., Scherbaum, F., Bommer, J.J. and Bungum, H. (2006). "Criteria for Selecting and Adjusting Ground-Motion Models for Specific Target Regions: Application to Central Europe and Rock Sites", *Journal of Seismology*, Vol. 10, No. 2, pp. 137–156.
46. Di Luccio, F., Fukuyama, E. and Pino, N.A. (2005). "The 2002 Molise Earthquake Sequence: What Can We Learn about the Tectonics of Southern Italy?", *Tectonophysics*, Vol. 405, No. 1–4, pp. 141–154.
47. Douglas, J. (2003). "Earthquake Ground Motion Estimation Using Strong-Motion Records: A Review of Equations for the Estimation of Peak Ground Acceleration and Response Spectral Ordinates", *Earth-Science Reviews*, Vol. 61, No. 1, pp. 43–104.
48. Douglas, J. (2004a). "Ground Motion Estimation Equations 1964–2003: Reissue of ESEE Report No. 01-1: 'A Comprehensive Worldwide Summary of Strong-Motion Attenuation Relationships for Peak Ground Acceleration and Spectral Ordinates (1969 to 2000)' with Corrections and Additions", Research Report 04-001-SM, Imperial College of Science, Technology and Medicine, London, U.K.

49. Douglas, J. (2004b). "An Investigation of Analysis of Variance as a Tool for Exploring Regional Differences in Strong Ground Motions", *Journal of Seismology*, Vol. 8, No. 4, pp. 485–496.
50. Douglas, J. (2004c). "Use of Analysis of Variance for the Investigation of Regional Dependence of Strong Ground Motions", *Proceedings of the 13th World Conference on Earthquake Engineering*, Vancouver, Canada, Paper No. 29 (on CD).
51. Douglas, J. (2006). "Errata of and Additions to 'Ground Motion Estimation Equations 1964–2003'. Intermediary Report", Report BRGM/RP-54603-FR, Bureau de Recherches Géologiques et Minières, Orléans, France.
52. Dowrick, D.J. and Rhoades, D.A. (2004). "Relations between Earthquake Magnitude and Fault Rupture Dimensions: How Regionally Variable Are They?", *Bulletin of the Seismological Society of America*, Vol. 94, No. 3, pp. 776–788.
53. Douglas, J. and Smit, P.M. (2001). "How Accurate Can Strong Ground Motion Attenuation Relations Be?", *Bulletin of the Seismological Society of America*, Vol. 91, No. 6, pp. 1917–1923.
54. Douglas, J., Suhadolc, P. and Costa, G. (2004). "On the Incorporation of the Effect of Crustal Structure into Empirical Strong Ground Motion Estimation", *Bulletin of Earthquake Engineering*, Vol. 2, No. 1, pp. 75–99.
55. Douglas, J., Bertil, D., Roullé, A., Dominique, P. and Jousset, P. (2006a). "A Preliminary Investigation of Strong-Motion Data from the French Antilles", *Journal of Seismology*, Vol. 10, No. 3, pp. 271–299.
56. Douglas, J., Bungum, H. and Scherbaum, F. (2006b). "Ground-Motion Prediction Equations for Southern Spain and Southern Norway Obtained Using the Composite Model Perspective", *Journal of Earthquake Engineering*, Vol. 10, No. 1, pp. 33–72.
57. Douglas, J., Aochi, H., Suhadolc, P. and Costa, G. (2007). "The Importance of Crustal Structure in Explaining the Observed Uncertainties in Ground Motion Estimation", *Bulletin of Earthquake Engineering*, Vol. 5, No. 1, pp. 17–26.
58. Draper, N.R. and Smith, H. (1981). "Applied Regression Analysis", John Wiley & Sons, New York, U.S.A.
59. Drouet, S., Scherbaum, F., Cotton, F. and Souriau, A. (2007). "Selection and Ranking of Ground Motion Models for Seismic Hazard Analysis in the Pyrenees", *Journal of Seismology*, Vol. 11, No. 1, pp. 87–100.
60. Frisenda, M., Massa, M., Spallarossa, D., Ferretti, G. and Eva, C. (2005). "Attenuation Relationships for Low Magnitude Earthquakes Using Standard Seismometric Records", *Journal of Earthquake Engineering*, Vol. 9, No. 1, pp. 23–40.
61. Frohlich, C. and Apperson, K.D. (1992). "Earthquake Focal Mechanisms, Moment Tensors, and the Consistency of Seismic Activity near Plate Boundaries", *Tectonics*, Vol. 11, No. 2, pp. 279–296.
62. Green, J.R. and Margerison, D. (1979). "Statistical Treatment of Experimental Data, Physical Sciences Data 2", Elsevier Scientific Publishing Company, Amsterdam, The Netherlands.
63. Gusev, A.A. (1983). "Descriptive Statistical Model of Earthquake Source Radiation and Its Application to an Estimation of Short-Period Strong Motion", *Geophysical Journal of the Royal Astronomical Society*, Vol. 74, No. 3, pp. 787–808.
64. Hintersberger, E., Scherbaum, F. and Hainzl, S. (2007). "Update of Likelihood-Based Ground-Motion Model Selection for Seismic Hazard Analysis in Western Central Europe", *Bulletin of Earthquake Engineering*, Vol. 5, No. 1, pp. 1–16.
65. Ide, S. and Beroza, G.C. (2001). "Does Apparent Stress Vary with Earthquake Size?", *Geophysical Research Letters*, Vol. 28, No. 17, pp. 3349–3352.
66. Jain, S.K., Roshan, A.D., Arlekar, J.N. and Basu, P.C. (2000). "Empirical Attenuation Relationships for the Himalayan Earthquakes Based on Indian Strong Motion Data", *Proceedings of the Sixth International Conference on Seismic Zonation*, Palm Springs, U.S.A. (on CD).
67. Jeon, Y.S. and Herrmann, R.B. (2004). "High-Frequency Earthquake Ground-Motion Scaling in Utah and Yellowstone", *Bulletin of the Seismological Society of America*, Vol. 94, No. 5, pp. 1644–1657.
68. Joyner, W.B. (1984). "A Scaling Law for the Spectra of Large Earthquakes", *Bulletin of the Seismological Society of America*, Vol. 74, No. 4, pp. 1167–1188.

69. Joyner, W.B. and Boore, D.M. (1981). "Peak Horizontal Acceleration and Velocity from Strong-Motion Records Including Records from the 1979 Imperial Valley, California, Earthquake", *Bulletin of the Seismological Society of America*, Vol. 71, No. 6, pp. 2011–2038.
70. Kalkan, E. and Gülkan, P. (2004). "Site-Dependent Spectra Derived from Ground Motion Records in Turkey", *Earthquake Spectra*, Vol. 20, No. 4, pp. 1111–1138.
71. Klügel, J.U. (2005). "Problems in the Application of the SSHAC Probability Method for Assessing Earthquake Hazards at Swiss Nuclear Power Plants", *Engineering Geology*, Vol. 78, No. 3–4, pp. 285–307.
72. Kreemer, C., Holt, W.E. and Haines, A.J. (2003). "An Integrated Global Model of Present-Day Plate Motions and Plate Boundary Deformation", *Geophysical Journal International*, Vol. 154, No. 1, pp. 8–34.
73. Lee, V.W. (1997). "Discussion: Prediction of Horizontal Response Spectra in Europe", *Earthquake Engineering & Structural Dynamics*, Vol. 26, No. 2, pp. 289–293.
74. Lee, V.W. and Trifunac, M.D. (1995). "Pseudo Relative Velocity Spectra of Strong Earthquake Ground Motion in California", Report CE 95-04, University of Southern California, Los Angeles, U.S.A.
75. Lussou, P., Bard, P.-Y., Cotton, F. and Fukushima, Y. (2001). "Seismic Design Regulation Codes: Contribution of K-Net Data to Site Effect Evaluation", *Journal of Earthquake Engineering*, Vol. 5, No. 1, pp. 13–33.
76. Luzi, L., Morasca, P., Zolezzi, F., Bindi, D., Pacor, F., Spallarossa, D. and Franceschina, G. (2006). "Ground Motion Models for Molise Region (Southern Italy)", *Proceedings of the First European Conference on Earthquake Engineering and Seismology*, Geneva, Switzerland, Paper No. 938 (on CD).
77. Malagnini, L. and Herrmann, R.B. (2000). "Ground-Motion Scaling in the Region of the 1997 Umbria-Marche Earthquake (Italy)", *Bulletin of the Seismological Society of America*, Vol. 90, No. 4, pp. 1041–1051.
78. Malagnini, L., Herrmann, R.B. and Di Bona, M. (2000a). "Ground-Motion Scaling in the Apennines (Italy)", *Bulletin of the Seismological Society of America*, Vol. 90, No. 4, pp. 1062–1081.
79. Malagnini, L., Herrmann, R.B. and Koch, K. (2000b). "Regional Ground-Motion Scaling in Central Europe", *Bulletin of the Seismological Society of America*, Vol. 90, No. 4, pp. 1052–1061.
80. Malagnini, L., Akinci, A., Herrmann, R.B., Pino, N.A. and Scognamiglio, L. (2002). "Characteristics of the Ground Motion in Northeastern Italy", *Bulletin of the Seismological Society of America*, Vol. 92, No. 6, pp. 2186–2204.
81. Margaris, B.N. and Boore, D.M. (1998). "Determination of $\Delta\sigma$ and κ_0 from Response Spectra of Large Earthquakes in Greece", *Bulletin of the Seismological Society of America*, Vol. 88, No. 1, pp. 170–182.
82. Margaris, B.N. and Hatzidimitriou, P.M. (2002). "Source Spectral Scaling and Stress Release Estimates Using Strong-Motion Records in Greece", *Bulletin of the Seismological Society of America*, Vol. 92, No. 3, pp. 1040–1059.
83. Marin, S., Avouac, J.P., Nicolas, M. and Schlupp, A. (2004). "A Probabilistic Approach to Seismic Hazard in Metropolitan France", *Bulletin of the Seismological Society of America*, Vol. 94, No. 6, pp. 2137–2163.
84. McCann, Jr., M.W. and Echezwia, H. (1984). "Investigating the Uncertainty in Ground Motion Prediction", *Proceedings of the Eighth World Conference on Earthquake Engineering*, San Francisco, U.S.A., Vol. II, pp. 297–304.
85. McGarr, A. (1984). "Scaling of Ground Motion Parameters, State of Stress, and Focal Depth", *Journal of Geophysical Research*, Vol. 89, No. B8, pp. 6969–6979.
86. McGuire, R.K. (1977). "Seismic Design Spectra and Mapping Procedures Using Hazard Analysis Based Directly on Oscillator Response", *Earthquake Engineering & Structural Dynamics*, Vol. 5, No. 3, pp. 211–234.
87. Morasca, P., Malagnini, L., Akinci, A., Spallarossa, D. and Herrmann, R.B. (2006). "Ground-Motion Scaling in the Western Alps", *Journal of Seismology*, Vol. 10, No. 3, pp. 315–333.

88. Moroney, M.J. (1990). "Facts from Figures", Penguin Books, London, U.K.
89. Musson, R.M.W., Toro, G.R., Coppersmith, K.J., Bommer, J.J., Deichmann, N., Bungum, H., Cotton, F., Scherbaum, F., Slejko, D. and Abrahamson, N.A. (2005). "Evaluating Hazard Results for Switzerland and How Not to Do It: A Discussion of 'Problems in the Application of the SSHAC Probability Method for Assessing Earthquake Hazards at Swiss Nuclear Power Plants' by J.-U. Klügel", *Engineering Geology*, Vol. 82, No. 1, pp. 43–65.
90. Novikova, E.I., Todorovska, M.I. and Trifunac, M.D. (1994). "Frequency Dependent Duration of Strong Earthquake Ground Motion on the Territory of Former Yugoslavia, Part I: Magnitude Models", *European Earthquake Engineering*, Vol. VIII, No. 3, pp. 11–25.
91. Özbey, C., Sari, A., Manuel, L., Erdik, M. and Fahjan, Y. (2004). "An Empirical Attenuation Relationship for Northwestern Turkey Ground Motion Using a Random Effects Approach", *Soil Dynamics and Earthquake Engineering*, Vol. 24, No. 2, pp. 115–125.
92. Pousse, G., Cotton, F., Bonilla, F. and Scherbaum, F. (2007). "On the Discrepancy of Ground Motion Predictions Derived from Weak and Strong Motion Records", *Bulletin of the Seismological Society of America* (under review).
93. Sabetta, F. and Pugliese, A. (1987). "Attenuation of Peak Horizontal Acceleration and Velocity from Italian Strong-Motion Records", *Bulletin of the Seismological Society of America*, Vol. 77, No. 5, pp. 1491–1513.
94. Sadigh, K., Chang, C.Y., Egan, J.A., Makdisi, F. and Youngs, R.R. (1997). "Attenuation Relationships for Shallow Crustal Earthquakes Based on California Strong Motion Data", *Seismological Research Letters*, Vol. 68, No. 1, pp. 180–189.
95. Scherbaum, F., Cotton, F. and Smit, P. (2004). "On the Use of Response Spectral-Reference Data for the Selection and Ranking of Ground-Motion Models for Seismic-Hazard Analysis in Regions of Moderate Seismicity: The Case of Rock Motion", *Bulletin of the Seismological Society of America*, Vol. 94, No. 6, pp. 2164–2185.
96. Scherbaum, F., Bommer, J.J., Bungum, H., Cotton, F. and Abrahamson, N.A. (2005). "Composite Ground-Motion Models and Logic Trees: Methodology, Sensitivities and Uncertainties", *Bulletin of the Seismological Society of America*, Vol. 95, No. 5, pp. 1575–1593.
97. Scholz, C.H., Aviles, C.A. and Wesnousky, S.G. (1986). "Scaling Differences between Large Interplate and Intraplate Earthquakes", *Bulletin of the Seismological Society of America*, Vol. 76, No. 1, pp. 65–70.
98. Scognamiglio, L., Malagnini, L. and Akinci, A. (2005). "Ground-Motion Scaling in Eastern Sicily, Italy", *Bulletin of the Seismological Society of America*, Vol. 95, No. 2, pp. 568–578.
99. Seed, H.B., Ugas, C. and Lysmer, J. (1976). "Site-Dependent Spectra for Earthquake-Resistant Design", *Bulletin of the Seismological Society of America*, Vol. 66, No. 1, pp. 221–243.
100. Sharma, M.L. (1998). "Attenuation Relationship for Estimation of Peak Ground Horizontal Acceleration Using Data from Strong-Motion Arrays in India", *Bulletin of the Seismological Society of America*, Vol. 88, No. 4, pp. 1063–1069.
101. Sharma, M.L. and Bungum, H. (2006). "New Strong Ground-Motion Spectral Acceleration Relations for the Himalayan Region", *Proceedings of the First European Conference on Earthquake Engineering and Seismology*, Geneva, Switzerland, Paper No. 459 (on CD).
102. Sigbjörnsson, R. and Ambraseys, N.N. (2003). "Uncertainty Analysis of Strong-Motion and Seismic Hazard", *Bulletin of Earthquake Engineering*, Vol. 1, No. 3, pp. 321–347.
103. Singh, R.P., Aman, A. and Prasad, Y.J.J. (1996). "Attenuation Relations for Strong Seismic Ground Motion in the Himalayan Region", *Pure and Applied Geophysics*, Vol. 147, No. 1, pp. 161–180.
104. Sokolov, V. (1997). "Empirical Models for Estimating Fourier-Amplitude Spectra of Ground Acceleration in the Northern Caucasus (Racha Seismogenic Zone)", *Bulletin of the Seismological Society of America*, Vol. 87, No. 6, pp. 1401–1412.
105. Sokolov, V. (2000). "Spectral Parameters of Ground Motion in Different Regions: Comparison of Empirical Models", *Soil Dynamics and Earthquake Engineering*, Vol. 19, No. 3, pp. 173–181.

106. Sokolov, V., Loh, C.H. and Wen, K.L. (2000). "Empirical Model for Estimating Fourier Amplitude Spectra of Ground Acceleration in Taiwan Region", *Earthquake Engineering & Structural Dynamics*, Vol. 29, No. 3, pp. 339–357.
107. Sokolov, V., Bonjer, K.P., Oncescu, M. and Rizescu, M. (2005). "Hard Rock Spectral Models for Intermediate-Depth Vrancea, Romania, Earthquakes", *Bulletin of the Seismological Society of America*, Vol. 95, No. 5, pp. 1749–1765.
108. Sokolov, V.Y. (1998). "Spectral Parameters of the Ground Motions in Caucasian Seismogenic Zones", *Bulletin of the Seismological Society of America*, Vol. 88, No. 6, pp. 1438–1444.
109. Souriau, A. (2006). "Quantifying Felt Events: A Joint Analysis of Intensities, Accelerations and Dominant Frequencies", *Journal of Seismology*, Vol. 10, No. 1, pp. 23–38.
110. Spudich, P., Joyner, W.B., Lindh, A.G., Boore, D.M., Margaris, B.M. and Fletcher, J.B. (1999). "SEA99: A Revised Ground Motion Prediction Relation for Use in Extensional Tectonic Regimes", *Bulletin of the Seismological Society of America*, Vol. 89, No. 5, pp. 1156–1170.
111. Trifunac, M.D. (1990). "How to Model Amplification of Strong Earthquake Motions by Local Soil and Geologic Site Conditions", *Earthquake Engineering & Structural Dynamics*, Vol. 19, No. 6, pp. 833–846.
112. Trifunac, M.D. (1993). "Long Period Fourier Amplitude Spectra of Strong Motion Acceleration", *Soil Dynamics and Earthquake Engineering*, Vol. 12, No. 6, pp. 363–382.
113. Trifunac, M.D. and Todorovska, M.I. (2000). "Can Aftershock Studies Predict Site Amplification Factors? Northridge, CA, Earthquake of 17 January 1994", *Soil Dynamics and Earthquake Engineering*, Vol. 19, No. 4, pp. 233–251.
114. Tufte, E.R. (1983). "The Visual Display of Quantitative Information", Graphics Press, Cheshire, U.S.A.
115. Ulusay, R., Tuncay, E., Sonmez, H. and Gokceoglu, C. (2004). "An Attenuation Relationship Based on Turkish Strong Motion Data and Iso-Acceleration Map of Turkey", *Engineering Geology*, Vol. 74, No. 3–4, pp. 265–291.
116. Vallée, M. and Di Luccio, F. (2005). "Source Analysis of the 2002 Molise, Southern Italy, Twin Earthquakes (10/31 and 11/01)", *Geophysical Research Letters*, Vol. 32, No. 12, pp. 38–41.
117. Youngs, R.R., Abrahamson, N., Makdisi, F.I. and Sadigh, K. (1995). "Magnitude-Dependent Variance of Peak Ground Acceleration", *Bulletin of the Seismological Society of America*, Vol. 85, No. 4, pp. 1161–1176.
121. Zonno, G. and Montaldo, V. (2002). "Analysis of Strong Ground Motions to Evaluate Regional Attenuation Relationships", *Annals of Geophysics*, Vol. 45, No. 3–4, pp. 439–454.

A NOTE ON SPATIAL VARIATIONS IN RESPONSE SPECTRA OF EARTHQUAKE GROUND MOTIONS

Hideji Kawakami*, Hidenori Mogi** and Eric Augustus J. Tingatinga***

*Geosphere Research Institute

**Department of Civil and Environmental Engineering

***Graduate School

Saitama University, Saitama, 338-8570, Japan

ABSTRACT

Response spectra of earthquake ground motions are important in the earthquake-resistant design and reliability analysis of structures. The purpose of this paper is to examine the spatial variability of response spectra recorded at the same epicentral distance as a function of frequency and separation distance. To do this, we define response spectrum ratios as spatial intra-event variations of response spectra and examine their statistical characteristics. Then we analyze the probability distribution of the ratios and formulate equations for their probability density functions, mean values, standard deviations, and percentiles. These statistics are estimated using accelerometer arrays of the Chiba and SMART-1 databases, and their relationships with the station separation distance are analyzed. It has been found out that the means and standard deviations have almost linear relationship with the logarithms of the station separation distances ranging from several meters to several kilometers. Finally, based on these findings, the differences between response spectra at two different sites due to future earthquakes are discussed.

KEYWORDS: Spatial Variation, Response Spectrum, Dense Instrument Arrays, Statistical Study

INTRODUCTION

Past significant earthquakes have seriously damaged many engineering structures, and field studies have reported that the degree of damage to each structure varied significantly from one location to another, even if the two structures were similar and the distance between them was small. This variation in structural damage, according to the reliability theory, is due to the differences in structural strength and the ground motion amplitude at these two separate locations.

The variations in structural strength and ground motion amplitude are taken into account in the current building design codes, i.e., today's seismic design of structures is based on the reliability theory. Fragility curves showing the relationship between the probability of structural damage and the amplitude of ground motion are based on the damage statistics obtained from large earthquakes. It is important to note, however, that the amplitudes of ground motion, e.g., the peak ground acceleration and the response spectrum amplitude, are estimated from earthquake records detected using seismometers located nearest to the structure. This estimation of the ground motion amplitude is noticeably affected by the distance between the structure and the seismometer, i.e., the amplitude is expected to have been more precisely estimated if the distance between the structure and the sensor is short; otherwise it is expected to contain error. However, how much error is to be expected quantitatively? If the spatial variance in the ground motion amplitude is examined based on the observed seismic records, whose number has been increasing remarkably in recent years, a more precise ground motion amplitude and a more reliable fragility curve can be obtained.

In light of these considerations, we have conducted statistical analyses of the spatial variations in peak ground accelerations (Kawakami and Mogi, 1999, 2003; Mogi and Kawakami, 2000). These analyses, however, ignored the effect of period or frequency of the seismic motions, which is very important when considering damage to structures with specific natural periods. Therefore, in this paper, we examined the response spectrum amplitude, which is the central scaling tool in earthquake engineering (Biot, 1932, 1933, 1934; Gupta, 2004). Trifunac (1978) and Trifunac and Anderson (1977) proposed differences (residuals) between the estimated and observed response spectrum amplitudes and their probability distribution functions using regression analysis. As several important parameters necessary in building design were taken into account, their results are very significant and useful when designing

earthquake-resistant structures. However, since the regression analysis was made by using data from many earthquakes simultaneously, residuals included intra-event as well as inter-event variability.

In this study, we focused on the intra-event variability in the ground motion amplitude of earthquakes. In other words, we considered the spatial variability in the damage and, more specifically, the spatial variability in the ground motion amplitude of each (one) earthquake. Moreover, it is not the purpose of this paper to discuss the variability in the damage or ground motion due to earthquakes having the same magnitude, focal depth, and epicentral distance at sites classified in the same category. The spatial variability in the ground motion amplitude of an earthquake, i.e., the intra-event variability, can be considered to be due to variations in: (1) the directions of the waves radiating from the epicenter, (2) the physical material encountered along the path, and (3) the surface soil conditions.

This study on the intra-event spatial variability in ground motion amplitude will be useful in generating input ground motions for the design of spatially extended structures, such as pipelines. When designing such structures, spatially distributed seismic motions must be applied to the structure. Hence, taking into account the effects of variation in seismic motion will help improve the design.

Several pioneering studies have investigated the use of the response spectrum in the design of extended structures. Trifunac and Todorovska (1997) and Trifunac and Gicev (2006) extended the common response spectrum method for synchronous ground motion to deal with extended structures experiencing differential ground motion and proposed the relative displacement response spectrum. To generate the spectrum, however, they assumed the propagation of waves and approximated strain as the particle velocity divided by the average shear wave velocity in the top 30 meters of soil.

Although the relative displacement response spectrum is very useful in designing extended structures, we used a different approach by focusing only on the intra-event variability in the ground motion amplitude, i.e., the relative displacement in each earthquake. We did not consider the inter-event variability (differences in the ground motion between two earthquakes having the same magnitude, focal depth, and epicentral distance) because it does not affect the strain or relative displacement in an extended structure.

It should be noted that the ground motion amplitudes in the current research were assumed to be lognormal random variables. Indeed, this assumption may not be accurate, as described elsewhere (Trifunac, 1978; Lee, 2002), and the lognormal distribution may only provide a rough approximation. However, as mentioned above, the safety probability in structural designs based on reliability theory is evaluated by comparing the structural strength and the ground motion amplitude and is ordinarily calculated by using their means and variances. Therefore, the variance in ground motion amplitude is as important in the engineering field as the mean value itself (Schuëller, 1981), and this assumption becomes very useful because the failure probability can be easily obtained analytically if the strength and the load (in this paper, the ground motion amplitude) are described by normal or lognormal distributions.

ANALYTICAL MODEL OF GROUND MOTION AMPLITUDES

1. Definition of Ratios

The ratio of ground motion amplitudes such as peak ground acceleration (PGA) and response spectrum represents a spatial intra-event difference between those amplitudes observed at two sites. These ratios are obtained by dividing the smaller value by the larger one for all possible station pairs for each earthquake (Kawakami and Sharma, 1999; Kawakami and Mogi, 2002; Mogi and Kawakami, 2002). Closer the values of the ratios are to one, higher is the correlation between the ground motion amplitudes in question. Statistical analyses of the ratios are valuable for the following two reasons: (1) they avoid estimating the mean value of the amplitudes at the sites, which depends on individual earthquakes; and (2) they can directly compare the statistical results for the different kinds of amplitudes because the ratios are non-dimensional.

2. Probability Density Function of Ratios

Ground motion amplitudes related to the peak value of a waveform such as PGA and response spectrum can be treated as a lognormal random variable (e.g., Katayama et al., 1978; Boore et al., 1980). In this study, we also assume that ground motion amplitudes, such as PGA and response spectrum

amplitude, are the lognormal random variables and express their joint probability density function (PDF) as

$$f_{Z_1, Z_2}(z_1, z_2) = \frac{1}{2\pi\sigma_Z^2\sqrt{1-\rho^2}} \exp\left[-\frac{1}{2\sigma_Z^2(1-\rho^2)}\{(z_1 - \mu_Z)^2 - 2\rho(z_1 - \mu_Z)(z_2 - \mu_Z) + (z_2 - \mu_Z)^2\}\right] \quad (1)$$

where Z_1 and Z_2 are the logarithms of amplitudes X_1 and X_2 observed at the two sites, σ_Z is the standard deviation, and ρ is the correlation coefficient between Z_1 and Z_2 .

From Equation (1), the PDF of $P = |Z_1 - Z_2|$ can be derived as

$$f_P(p) = \frac{2}{\sqrt{2\pi}\sigma_{P'}} \exp\left(-\frac{p^2}{2\sigma_{P'}^2}\right), \quad p \geq 0 \quad (2)$$

where $\sigma_{P'}$ is the standard deviation of $P' = Z_1 - Z_2$, given by

$$\sigma_{P'} = \sigma_Z \sqrt{2(1-\rho)} \quad (3)$$

Furthermore, by changing the variables from P to R such that $-P = \ln(R)$, the PDF of the ratios, R , becomes

$$f_R(r) = \frac{2}{\sqrt{2\pi}\sigma_{P'}r} \exp\left(-\frac{(\ln r)^2}{2\sigma_{P'}^2}\right), \quad 0 < r \leq 1 \quad (4)$$

Because the difference $P' = Z_1 - Z_2$ is a Gaussian random variable with zero mean and its PDF is not affected by the mean value, μ_Z , as shown in Equation (2), it is neither necessary to estimate earthquake-specific μ_Z nor to normalize by μ_Z . It is also evident that, since the standard deviation $\sigma_{P'}$ is the only parameter of the PDF of the ratios, it can be used to compare the scatter of various intra-event ground motion amplitudes.

3. Mean Value and Percentile

The mean values of the ratios and their logarithms, μ_R and μ_P , can be obtained from Equations (4) and (2), respectively, as

$$\mu_R = \exp\left(\frac{\sigma_{P'}^2}{2}\right) \left\{1 - \operatorname{erf}\left(\frac{\sigma_{P'}}{\sqrt{2}}\right)\right\} \quad (5)$$

$$\mu_P = \sqrt{\frac{2}{\pi}} \sigma_{P'} \quad (6)$$

where $\operatorname{erf}(\cdot)$ is the error function (Abramowitz and Stegun, 1972). We define the γ th percentile of a ratio r_γ , and its logarithm p_γ , as the value for which R and P in the range of

$$r_\gamma \leq R \leq 1, 0 \leq P \leq p_\gamma \quad (7)$$

have the probability of γ percent. In this study, we focused on the 50th and 95th percentiles; the former is used because it is a median value of the ratio, and the latter is used because it is a minimum (R) or maximum (P) expected value (i.e., 5% significance level is assumed). These percentiles were estimated by

$$\begin{aligned} p_{50} &= 0.68\sigma_{P'}, & r_{50} &= \exp(-p_{50}) \\ p_{95} &= 1.96\sigma_{P'}, & r_{95} &= \exp(-p_{95}) \end{aligned} \quad (8)$$

based on the properties of the Gaussian distribution.

ARRAY DATABASES

The dense-array databases of the Chiba array in Japan and SMART-1 array in Lotung, Taiwan, were used to statistically analyze the ratios. The instrument arrangements of the Chiba and SMART-1 arrays are shown in Figures 1 and 2, respectively.

The separation distances are unevenly distributed because of the configuration of seismometers. Taking this distribution into account, the PGA ratios were divided into several groups depending on the distance between two stations. Table 1 lists (a) Chiba array groups and (b) SMART-1 array groups, with the records at a rock site (E02 station in Figure 2) removed, for the PGA and response spectrum ratios. Statistical analyses of the ratios were carried out for each station separation group.

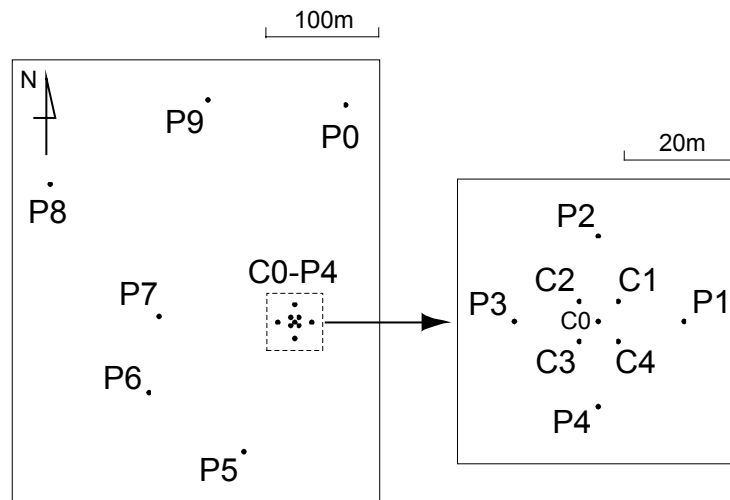


Fig. 1 Instruments in Chiba array (Katayama et al., 1990)

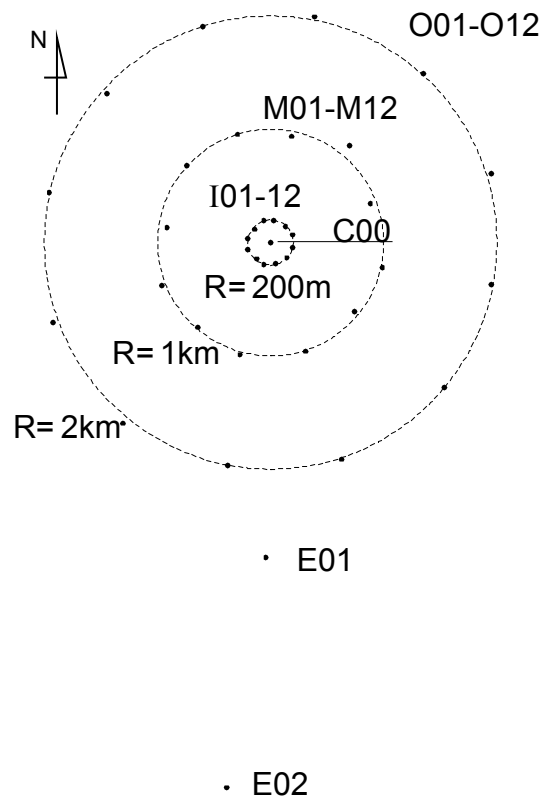


Fig. 2 Instruments in SMART-1 array (Bolt et al., 1982; Figueras et al., 1992)

Table 1: Station Separation Groups and Corresponding Number of Data Per Component

(a) Chiba Array				
Group	Station Separation	Number of Data		
	L (m)	EW	NS	UD
A	$0 < L \leq 40$	1,368	1,368	1,368
B	$40 < L \leq 160$	819	819	819
C	$160 < L$	108	108	108
Total		2,295	2,295	2,295

(b) SMART-1 Array				
Group	Station Separation	Number of Data		
	L (m)	EW	NS	UD
a	$0 < L \leq 650$	1,368	1,389	1,357
b	$650 < L \leq 1,600$	3,628	3,628	3,583
c	$1,600 < L \leq 2,400$	3,803	3,777	3,787
d	$2,400 < L \leq 3,200$	1,315	1,297	1,305
e	$3,200 < L$	571	563	571
Total		10,685	10,654	10,603

STATISTICAL RESULTS

1. Standard Deviations and Percentiles of Ground Motion Amplitudes

The standard deviations of the ratios of the ground motion amplitudes versus the station separations are plotted in Figure 3. The station separation distance is the average value of separation for each station separation group. The left-side ordinate is the standard deviation (sixty-eighth percentile) and its corresponding ratio, while the right-side ordinates are the fiftieth and ninety-fifth percentiles and their corresponding ratios. In this figure, the results for the PGA ratios (EW and NS components) and for the acceleration and velocity response spectrum ratios (EW and NS components) at 2 and 6 Hz are plotted. These frequencies were chosen because standard deviations $\sigma_{p'}$ of acceleration response spectrum ratios are at their minimum and maximum values at 2 and 6 Hz, respectively (see Figure 4).

It should be noted in Figure 3 that the scatters of ground motion amplitudes generally increase as distance between stations increases, though there are discontinuities in the plots between the Chiba and SMART-1 arrays. The response spectrum ratios at 6 Hz show the largest scatter among these results. The response spectrum ratios at 2 Hz show smaller scatter for station separation up to about 300 m, but their scatter increases abruptly for station separation of about 1 km. It can also be observed that the velocity response spectrum ratios have a slightly larger scatter than the acceleration ratios at either frequency. Furthermore, it can be observed that the scatter of the PGA ratios increases linearly with station separation and is generally between the scatter of the response spectrum ratios at 2 and 6 Hz for station separation less than about 1 km.

As shown in Figure 3, the 50th percentiles of the response spectrum ratios, r_{50} , are approximately 0.9–0.95 and 0.83–0.87 at 2 and 6 Hz, respectively, for Group A of the Chiba array and are 0.7–0.72 and 0.65–0.67 at 2 Hz and 6 Hz, respectively, for Group e of the SMART-1 array. The 95th percentiles, r_{95} , are approximately 0.8 and 0.6–0.66 at 2 and 6 Hz, respectively, for Group A of the Chiba array and are 0.33–0.38 and 0.26–0.3 for Group e of the SMART-1 array.

2. Mean and Probability Density Functions of Ground Motion Amplitude Ratios

As pointed out above, standard deviation $\sigma_{p'}$ is a useful index for examining the scatter of the ground motion amplitudes. However, to recognize the scatter of the ground motion amplitudes intuitively, the

mean value of the ratios, μ_R , calculated from Equation (6), is more useful than the standard deviation $\sigma_{P'}$.

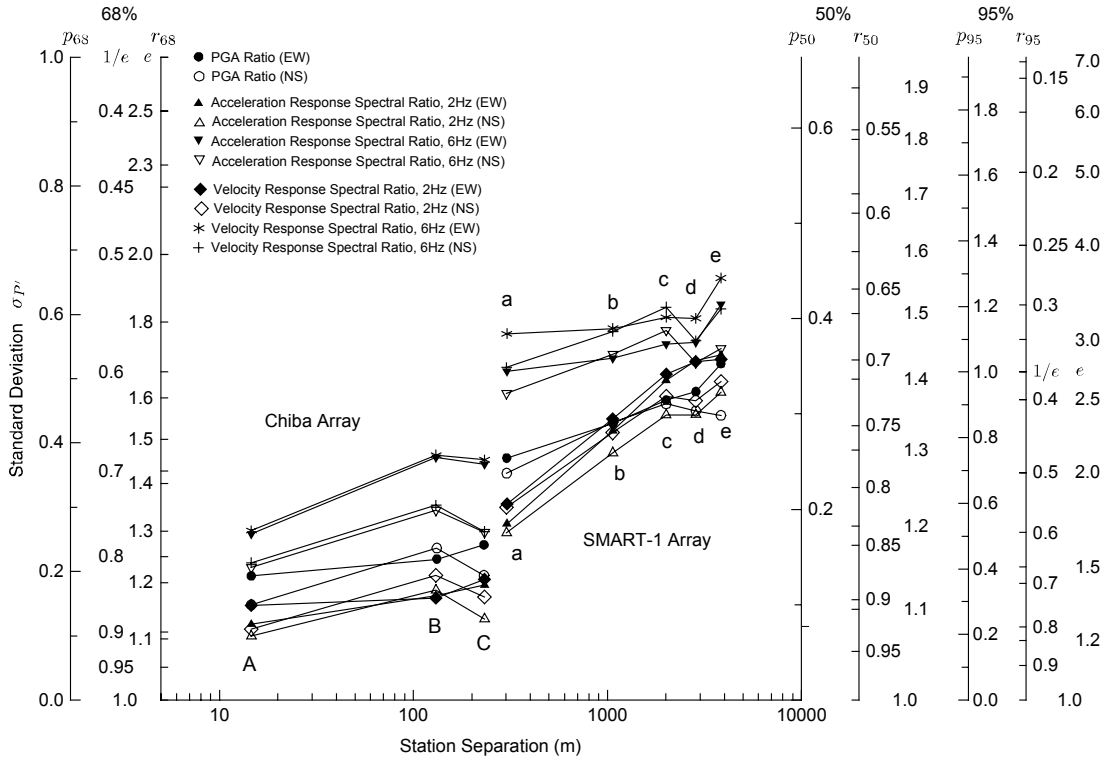


Fig. 3 Standard deviations and 50th and 95th percentiles of ratios R and differences P

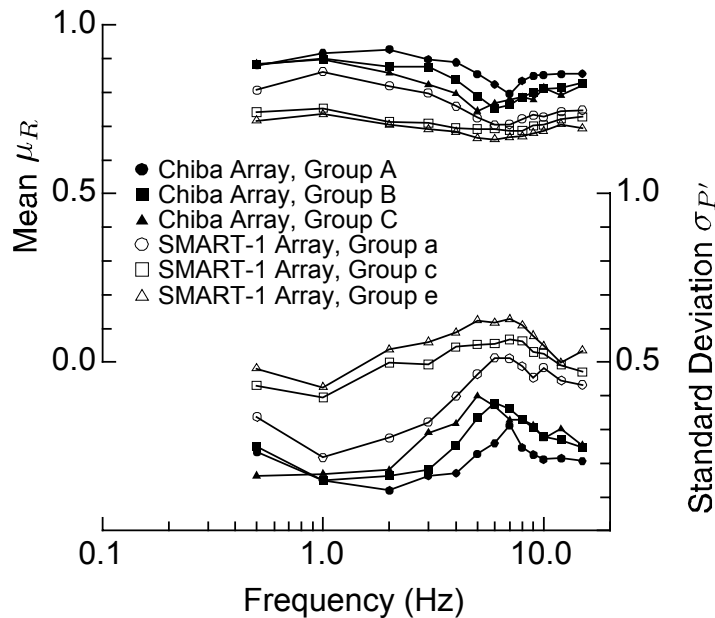


Fig. 4 Mean and standard deviation of acceleration spectrum ratios for EW components with damping ratio $h = 0.05$

The mean value of the ratios is plotted against station separation in Figure 5 for the same sets of ground motion amplitudes as considered in Figure 3. An inverse relation between mean value of ratios and station separation is shown in this figure; e.g., for the station pair with the station separation less than a few tens of meters (Group A in the Chiba array) the mean value of the ratio is 0.8 to 0.95, and for the pair with the station separation of three kilometers (Group d in the SMART-1 array) the mean value is

0.65 to 0.8. This inverse relation between mean value of ratios and station separation implies that ground motion amplitudes with larger standard deviations generally have smaller mean values.

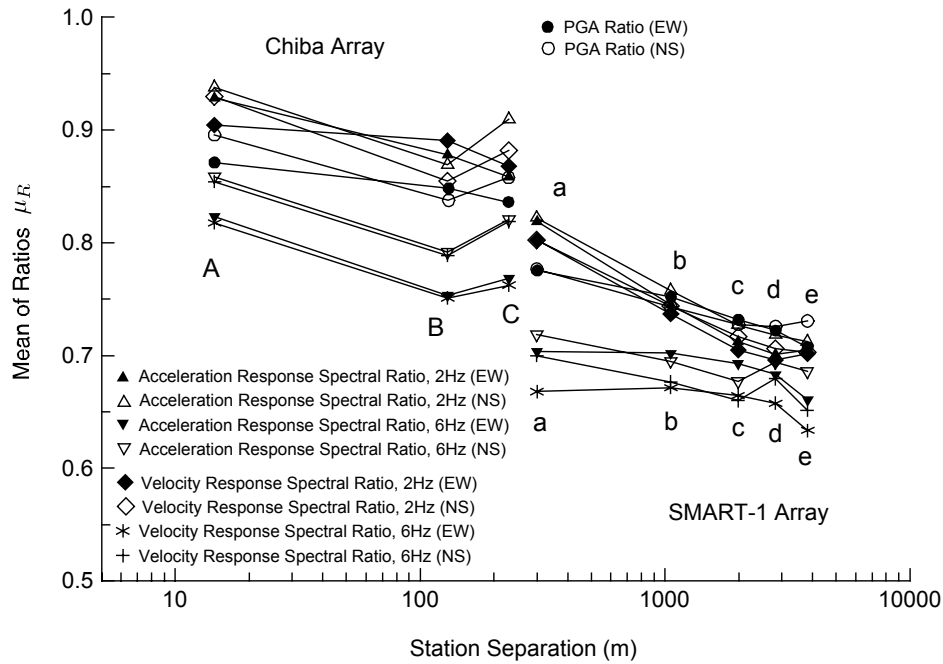


Fig. 5 Mean of ratios R versus station separation

The probability density functions (PDFs) of Group A in the Chiba array and Group d in the SMART-1 array are shown in Figure 6. For both groups in this figure, the PDFs estimated from the frequencies of occurrence are shown by the lines with symbols, and the analytical functions calculated from the observational standard deviations using Equation (4) are shown by the smooth solid lines. Figure 6 shows that the analytical expression of the PDF in Equation (4) is a good approximation of the probability distribution of the ground motion amplitude ratios.

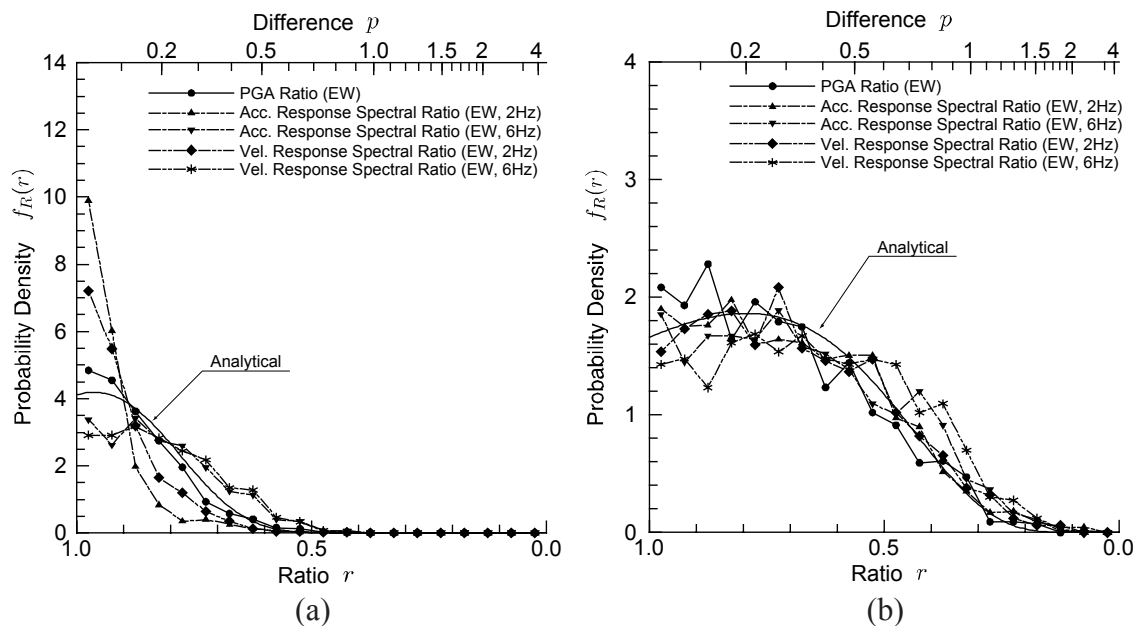


Fig. 6 Probability density functions of ratio R for (a) Group A of Chiba array, and (b) Group d of SMART-1 array

In addition, we can observe in Figure 6 the differences in the scatters of various kinds of amplitudes even for the same station-separation group. For example, in Figure 6(a) the PDFs of the acceleration and

velocity response spectrum ratios at 6 Hz, which have larger standard deviations than the others, are flatter. Similar tendencies can also be observed in Figure 6(b). Thus, when the ratio is small, the probability of ratios with larger scatter is higher.

CONCLUSIONS

In this study, the scatter of ground motion amplitudes (peak ground acceleration (PGA) and response spectrum) was examined using accelerometer arrays of the Chiba and SMART-1 databases, and the scatters of the PGA ratios and response spectrum ratios were compared with each other based on the properties of the Gaussian distribution. Results can be summarized as follows:

1. The standard deviation $\sigma_{p'}$ increases monotonically as distance between stations increases. The standard deviation $\sigma_{p'}$ of the PGA ratios has an almost linear relationship with the logarithm of the station separation distances ranging from several meters to several kilometers.
2. The standard deviation $\sigma_{p'}$ of the response spectrum ratios is strongly influenced by frequency. In the statistical analysis, the response spectrum ratios at 6 Hz showed the largest scatter. Conversely, response spectrum ratios at 2 Hz showed the smallest scatter, but those increased abruptly for station separation greater than 1 km, and were almost equal to those at 6 Hz for distances between stations of about 3 km.

ACKNOWLEDGEMENTS

The authors wish to thank the Association for Earthquake Disaster Prevention of Japan and National Geophysical Data Center in U.S.A. for publishing the strong motion array record database and to the University of Tokyo for providing the strong motion records.

REFERENCES

1. Abramowitz, M. and Stegun, I.A. (editors) (1972). "Handbook of Mathematical Functions with Formulas, Graphs, and Mathematical Tables", Dover Publications, New York, U.S.A.
2. Biot, M.A. (1932). "Transient Oscillations in Elastic Systems", Ph.D. Thesis No. 259, Aeronautics Department, California Institute of Technology, Pasadena, U.S.A.
3. Biot, M.A. (1933). "Theory of Elastic Systems Vibrating under Transient Impulse with an Application to Earthquake-Proof Buildings", Proceedings of the National Academy of Sciences of the United States of America, Vol. 19, No. 2, pp. 262–268.
4. Biot, M.A. (1934). "Theory of Vibration of Buildings during Earthquake", Zeitschrift für Angewandte Mathematik und Mechanik, Vol. 14, No. 4, pp. 213–223.
5. Bolt, B.A., Loh, C.H., Penzien, J., Tsai, Y.B. and Yeh, Y.T. (1982). "Preliminary Report on the SMART 1 Strong Motion Array in Taiwan", Report UCB/EERC-82/13, University of California, Berkeley, U.S.A.
6. Boore, D.M., Joyner, W.B., Oliver, A.A. and Page, R.A. (1980). "Peak Acceleration, Velocity, and Displacement from Strong-Motion Records", Bulletin of the Seismological Society of America, Vol. 70, No. 1, pp. 305–321.
7. Figueras, S., Roca, A., Goula, X. and Bl'azquez, R. (1992). "Larger Soil Amplification for Stronger Ground Motion from SMART-1 Records", Proceedings of the Tenth World Conference on Earthquake Engineering, Madrid, Spain, Vol. 2, pp. 1043–1048.
8. Gupta, V.K. (editor) (2004). "From Seismic Source to Structural Response: Contributions of Professor Mihailo D. Trifunac", Report CE 04-04, University of Southern California, Los Angeles, U.S.A.
9. Katayama, T., Iwasaki, T. and Saeki, M. (1978). "Statistical Analysis of Earthquake Acceleration Response Spectra", Structural Engineering/Earthquake Engineering, JSCE, No. 275, pp. 29–40 (in Japanese).

10. Katayama, T., Yamazaki, F., Nagata, S., Lu, L. and Turker, T. (1990). "A Strong Motion Database for the Chiba Seismometer Array and Its Engineering Analysis", *Earthquake Engineering & Structural Dynamics*, Vol. 19, No. 8, pp. 1089–1106.
11. Kawakami, H. and Mogi, H. (1999). "Probability Distribution of Peak Ground Acceleration Ratios Estimated from Strong Ground Motion Array Database", *Structural Engineering/Earthquake Engineering*, JSCE, No. 626/I-48, pp. 219–230 (in Japanese).
12. Kawakami, H. and Mogi, H. (2002). "Determination of Spatial Distribution of Response Spectral Ratios", *Journal of Structural and Construction Engineering*, Transactions of AIJ, No. 551, pp. 37–44 (in Japanese).
13. Kawakami, H. and Mogi, H. (2003). "Analyzing Spatial Intraevent Variability of Peak Ground Accelerations as a Function of Separation Distance", *Bulletin of the Seismological Society of America*, Vol. 93, No. 3, pp. 1079–1090.
14. Kawakami, H. and Sharma, S. (1999). "Statistical Study of Spatial Variation of Response Spectrum Using Free Field Records of Dense Strong Motion Arrays", *Earthquake Engineering & Structural Dynamics*, Vol. 28, No. 11, pp. 1273–1294.
15. Lee, V.W. (2002). "Empirical Scaling of Strong Earthquake Ground Motion—Part I: Attenuation and Scaling of Response Spectra", *ISET Journal of Earthquake Technology*, Vol. 39, No. 4, pp. 219–254.
16. Mogi, H. and Kawakami, H. (2000). "Spatial Distribution of Peak Ground Accelerations Estimated from 'SIGNAL' Database", *Structural Engineering/Earthquake Engineering*, JSCE, No. 647/I-51, pp. 369–378 (in Japanese).
17. Mogi, H. and Kawakami, H. (2002). "Probability Distribution of JMA Seismic Intensity Differences between Arbitrary Site Pairs on Laterally Homogeneous Ground Estimated from Seismometer Array Database", *Jishin*, Vol. 55, No. 2, pp. 167–180 (in Japanese).
18. Schuëller, G.I. (1981). "Einführung in die Sicherheit und Zuverlässigkeit von Tragwerken", Verlag Wilhelm Ernst & Sohn, Berlin/Munchen, Germany (in German; translated into Japanese by I. Konishi, N. Takaoka and H. Ishikawa).
19. Trifunac, M.D. (1978). "Response Spectra of Earthquake Ground Motion", *Journal of the Engineering Mechanics Division*, Proceedings of ASCE, Vol. 104, No. EM5, pp. 1081–1097.
20. Trifunac, M.D. and Anderson, J.G. (1977). "Preliminary Empirical Models for Scaling Absolute Acceleration Spectra", Report CE 77-03, University of Southern California, Los Angeles, U.S.A.
21. Trifunac, M.D. and Gicev, V. (2006). "Response Spectra for Differential Motion of Columns Paper II: Out-of-Plane Response", *Soil Dynamics and Earthquake Engineering*, Vol. 26, No. 12, pp. 1149–1160.
22. Trifunac, M.D. and Todorovska, M.I. (1997). "Response Spectra for Differential Motion of Columns", *Earthquake Engineering & Structural Dynamics*, Vol. 26, No. 2, pp. 251–268.

EFFECT OF SYSTEM INITIAL CONDITIONS ON SEISMIC DESIGN OF LONG-PERIOD STRUCTURES

Carlos E. Ventura* and Rafael Blázquez**

*Department of Civil Engineering
The University of British Columbia, Vancouver, B.C., Canada

**Department of Civil Engineering
Universidad de Castilla-La Mancha, Ciudad Real, Spain

ABSTRACT

Initial conditions for the computation of response spectra are unknown in the case of analog earthquake records that have lost the initial portion of motion and are assumed to be zero for calculation purposes. This assumption, rigorously speaking, is only valid for high-frequency systems, such as rigid structures. Both rigid and flexible structures are sensitive to the initial conditions of the motion. The spectral values for long-period, elastic or inelastic systems tend to be particularly sensitive to the initial conditions of motion. Unconservative designs of long-period structures may result if the initial condition effects are not properly accounted for. In this paper two practical methods are developed to approximate the true “non-resting” response spectra from the conventional ones for a given set of initial conditions. As expected, these conditions clearly control the free-vibration part of the response of long-period systems, as opposed to short-period systems which are governed by the transient phase of the response.

KEYWORDS: Initial Conditions, Response Spectra, Long-Period Systems, Accelerograms

INTRODUCTION

The response spectrum method of analysis is widely used for evaluating the dynamic response of structural systems subjected to earthquake motions. In this approach, the peak response of a system due to a prescribed earthquake motion is generally computed assuming that the system is initially at rest, that is, assuming zero initial conditions. Although the significant aspects of response spectra computed assuming zero initial conditions have been extensively studied (see, for example, Veletsos and Newmark (1964)), the effects of assuming non-zero initial conditions in the spectral computations are not well understood.

Non-zero initial conditions may arise for systems already undergoing vibrations when a seismic event occurs (Trifunac and Udawadia, 1979) or from evaluation of earthquake records where a segment at the beginning of the record is not available (Pecknold and Riddell, 1978, 1979; Blázquez and Kelly, 1988; Uang and Bertero, 1990). Also, from the seismological point of view, initial conditions are very important in the near field, where the ground motion contains powerful pulses that can have very large initial velocities (M.D. Trifunac, written communication, 2006).

In many practical applications, the initial conditions are not included in the computation of response spectra, and often this can be reasonably justified. There is, however, a paucity of information on the consequences of ignoring these effects when the response spectrum method is used for the dynamic analysis of structures, especially for those with long natural periods. This research responds to this need.

1. Statement of Problem

The dynamic response of base-excited, viscously damped, single-degree-of-freedom (SDOF) system is considered here. It is assumed that the system is already vibrating at the reference time $t = 0$ when a ground acceleration, $\ddot{y}(t)$, is applied. The relative displacement and velocity of each system at $t = 0$ are known and identified as U_o and \dot{U}_o , respectively. A general form of the equation of motion of the SDOF system can be written as

$$m\ddot{u}(t) + c\dot{u}(t) + R(t) = -m\ddot{y}(t) \quad (1)$$

in which m is the mass, c is the coefficient of viscous damping, $R(t)$ is the restoring force (which depends on the displacement amplitude at time t), and $\dot{u}(t)$ and $\ddot{u}(t)$ are the system's relative velocity and acceleration with respect to the base motion.

For the case of elastic systems, the restoring force is expressed as $R(t) = ku(t)$, where k is the stiffness coefficient and $u(t)$ is the relative displacement of the system. In this case, Equation (1) can be expressed as

$$\ddot{u}(t) + 2\xi p\dot{u}(t) + p^2u(t) = -\ddot{y}(t) \quad (2)$$

where $p = \sqrt{k/m} = 2\pi/T$ is the undamped circular natural frequency of the system (T is the undamped natural period), and $\xi = c/2pm = c/2\sqrt{km}$ is the fraction of critical damping.

It is of interest to evaluate the influence of U_o and \dot{U}_o on the absolute value of the numerically largest values of relative displacement, SD, and absolute acceleration, SA, for moving ground-excited systems. To state the problem, the solution of the differential equation of motion of the oscillator (Equation (2)), can be expressed as follows:

$$u(t) = u_i + u_f \quad (3)$$

where u_i and u_f stand, respectively, for the forced- and free-vibration parts of the motion. The latter depends on U_o and \dot{U}_o , which are the system's initial conditions.

The physical existence of initial conditions in recorded earthquake motions can be explained by analyzing the way these instruments function. Unavoidably for levels of signal which fall below a prefixed threshold level (\ddot{y}_0), the recorder of the instrument is not triggered and that portion of the accelerogram (for $t < t_0$) remains unrecorded. This results in unknown values of the ground and the mass motion at time $t = 0$ due to information gap. These values depend on the characteristics of the excitation and the mechanical properties of the system. Modern seismic instruments overcome this problem by incorporating in their design a pre-event buffer memory to record the ground motion for a few seconds before the trigger level is exceeded. However, the database of earthquake motions recorded without the benefit of a pre-event memory is extensive and widely used in earthquake engineering research and practice. It is, therefore, of significant interest to examine in detail the consequences of ignoring the initial state of motion of the system at the instant in which the instrument starts recording the ground motion.

Using a single cycle sinusoidal acceleration wave of period T_0 as excitation of a system of period T , Blázquez and Kelly (1988) have shown that, for short-period systems ($T \leq T_0$), the free-vibration component in Equation (3) can be neglected and the effect of the initial conditions is negligible regardless of the damping level. Thus it can be reasonably assumed that

$$U_o = u(0) \approx 0 ; \dot{U}_o = \dot{u}(0) \approx 0 \quad (4)$$

In contrast, for long-period systems ($T \geq T_0$), the following asymptotic relations can be used to approximate initial conditions:

$$U_o = u(0) \approx -y_o ; \dot{U}_o = \dot{u}(0) \approx -\dot{y}_o \quad (5)$$

where y_o and \dot{y}_o are, respectively, the input displacement and the input velocity at the triggering time (t_0) of the instrument recording the excitation motion.

Since the standard method for calculating response spectra assumes zero initial conditions, it is concluded that, strictly speaking, such a procedure applies only to high-frequency systems (e.g., rigid structures) for non-zero initial conditions. For other types of systems (particularly flexible ones), the effect of initial conditions on the long-period regions of response spectra remains to be clarified.

2. Objectives of This Study

The objectives of this study are: (1) to help understand better the influence of initial conditions on the response spectra for elastic and inelastic viscously damped single-degree-of-freedom (SDOF) systems, (2) to investigate the implications of considering or neglecting the effects of the initial conditions in the response spectrum analysis, and (3) to develop a method to approximate the true response spectrum from the conventional one and a given set of initial conditions.

EVALUATION OF SEISMIC RESPONSE OF SDOF SYSTEMS

The response of a system to a prescribed excitation depends on the characteristics of the excitation, the properties of the system and the initial state of motion. If the system is either originally at rest and subjected to a transient excitation, or is subjected to prescribed initial displacement and velocity and let to vibrate in free-vibration motion only, the combined effect of both actions will represent the response of that system with non-zero initial conditions and subjected to a base excitation. Most algorithms used for evaluating the response to transient excitations can easily account for the effect of non-zero initial conditions, but it is of interest here to evaluate the responses separately.

Accordingly, the transient response, u_t , in Equation (3) can be expressed in terms of the well-known Duhamel's integral (Von Karman and Biot, 1940) as

$$u_t = -\int_0^t \ddot{y}(\mu)h(t-\mu)d\mu \quad (6)$$

and the free-vibration response part is given by (Veletsos and Ventura, 1985)

$$u_f = U_o g(t) + \dot{U}_o h(t) \quad (7)$$

in which $g(t)$ and $h(t)$ are defined as the unit response functions of the system. These functions represent the displacement at time t produced by a unit initial displacement and a unit initial velocity, respectively, and are given by

$$g(t) = \left[\cos \bar{p}t + \left(\frac{\xi}{\sqrt{1-\xi^2}} \right) \sin \bar{p}t \right] \exp(-\xi pt) \quad (8a)$$

and

$$h(t) = (1/\bar{p}) \exp(-\xi pt) \sin \bar{p}t \quad (8b)$$

where $\bar{p} = p\sqrt{1-\xi^2}$ is the damped circular natural frequency of the system.

The relative velocity, $\dot{u}(t)$, can be obtained by differentiation of Equation (3) with respect to time. In a stepwise numerical evaluation of the response of a SDOF system, the transient relative velocity, \dot{u}_t , is normally computed during the process of obtaining u_t . The free-vibration component of the relative velocity, \dot{u}_f , would require the evaluation of the time derivatives of the unit response functions $g(t)$ and $h(t)$, given by Equations (8a) and (8b), respectively. Then, the absolute acceleration, \ddot{x} , can be computed by differentiation of the relative velocity to obtain the relative acceleration, \ddot{u} , and then by adding the base acceleration, \ddot{y} , to the resulting response. Alternatively, from Equation (1) and the relation, $\ddot{x} = \ddot{y} + \ddot{u}$, one obtains (see Equation (2))

$$\ddot{x} = -(2\xi p\dot{u} + p^2u) \quad (9)$$

This expression can be used to evaluate separately the transient and free-vibration components of the absolute acceleration. The shear force at the support of the SDOF system, V , can then be computed as $V = m\ddot{x}$.

Response Spectra for Linear Systems

The response values that are of practical interest are the relative displacement, u , the relative velocity, \dot{u} , and the absolute acceleration, \ddot{x} , of systems with the same level of damping and different values of the natural period, $T = 2\pi/p$. The numerically largest values are used to develop response spectrum plots for each of these quantities. Since the maximum response of the system may be attained after cessation of the excitation during the first half-cycle of free vibration, the analysis should be carried out over a time interval, T_d , which exceeds T_0 (the duration of the excitation) by at least one-half the natural period of the system, T , i.e., $T_d = T_0 + T/2$.

For practical structural engineering applications, true relative velocity and absolute acceleration response spectra (SV and SA, respectively) have been approximated in the past by the corresponding “pseudo” spectra, defined as follows:

$$\text{PSV} = p \cdot \text{SD} = \frac{2\pi}{T} \cdot \text{SD} \quad (10a)$$

$$\text{PSA} = p^2 \cdot \text{SD} = \left(\frac{2\pi}{T}\right)^2 \cdot \text{SD} \quad (10b)$$

where SD stands for the relative displacement response spectrum. As it is well known, PSA is directly related to the maximum force (or base shear), and PSV is related to the maximum stored energy.

For systems, for which the damping ratio is less than 5% and a quasi-linear behaviour of the system can be assumed, it has been customary to assume that the numerical values of SV and SA are about the same as the corresponding PSV and PSA, respectively. The accuracy of this assumption depends on the type of excitation, the damping and natural period of the system.

It is well known that for long-period and short-period systems, SV and PSV are not always exchangeable. Figure 1 proves this assertion for the normalized response spectra of a very simple sinusoidal wave. Two damping values are considered in this case: 0% and 10%. The single sine wave pulse has duration of $T_0 = 1$ sec and amplitude of 1g, and it is assumed that the oscillator starts from “at rest conditions”. As expected, PSA and SA are the same for all periods for the undamped system and are very close to each other for the damped system. In contrast, PSV and SV are different for very short periods and long periods, the difference becoming larger as the damping increases. Beyond a certain critical period (at about $T = 3.3$ sec), the SV curve departs clearly from the PSV curve and approaches its asymptotic value, the maximum velocity of the ground, $|\dot{y}(t)|_{\max}$. For the same conditions, however,

$\text{PSV} = \frac{2\pi}{T} \cdot \text{SD} \rightarrow 0$, since SD approaches its limiting value $|y(t)|_{\max}$ while T increases indefinitely (Hudson, 1979).

EFFECT OF INITIAL CONDITIONS ON SDOF RESPONSE

The state of motion of an elastic SDOF system just before the occurrence of ground motion can be characterized in terms of the initial displacement, U_o , and the initial velocity, \dot{U}_o . The response of the system to these initial conditions depends on its natural frequency and damping. Systems subjected to the same initial displacement and velocity, but with different natural frequency and damping, will respond differently.

The nature of the system is also important, since different responses are expected for elastic systems (such as the viscously damped system described by Equation (2)) and inelastic systems (such as the type described by Equation (1)) to the same set of initial conditions. This is shown next.

1. Elastic Systems

The peak value of the ground motion is the parameter commonly used for describing the level of ground excitation and for comparing it with the maximum response of the system. Therefore, it would be practical to relate the initial conditions of the system to this parameter. To this end, the peak ground

acceleration, \ddot{Y} , the initial conditions, U_o and \dot{U}_o , and the natural frequency of the system, p , can be interrelated by the dimensionless coefficients:

$$\alpha = -p^2 U_o / \ddot{Y} \quad (11a)$$

$$\beta = -p \dot{U}_o / \ddot{Y} \quad (11b)$$

where $\ddot{Y} = |\ddot{y}(t)|_{\max}$.

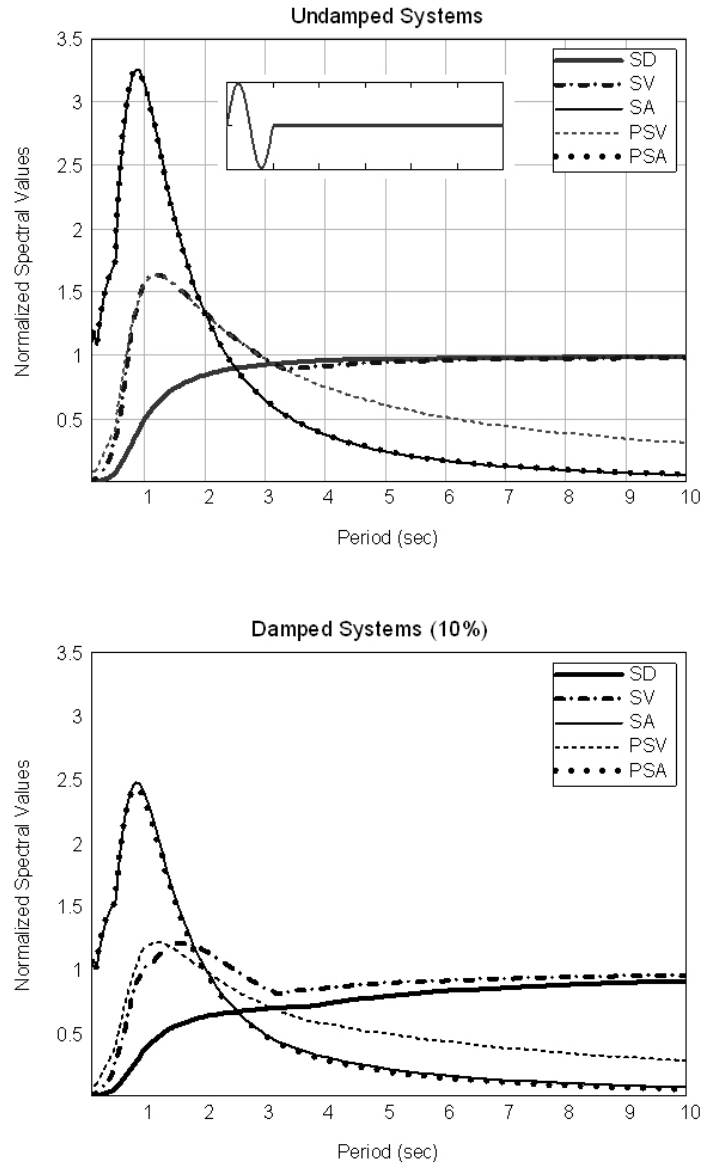


Fig. 1 Comparison of true and pseudo-response spectra for single sine acceleration pulse

The coefficients α and β represent the ratio of equivalent instantaneous accelerations of magnitude $p^2 U_o$ and $p \dot{U}_o$, respectively, to the peak base acceleration, \ddot{Y} . Alternatively, α can be described as the ratio of the base shear kU_o (resulting from inducing into the undamped system a static displacement U_o) to the equivalent static force $m\ddot{Y}$, produced by the peak ground acceleration. Similarly, β can be described as the ratio of the peak base shear $mp\dot{U}_o$ (produced by an impulse $p\dot{U}_o$ applied instantaneously to the undamped system) to the equivalent static force $m\ddot{Y}$, produced by the peak ground acceleration.

The sensitivity of the response to various combinations of α and β can be evaluated for SDOF systems subjected to a single cycle of sinusoidal base excitation of the form $\ddot{y}(t) = \ddot{Y} \sin(2\pi t/T_0)$, in which T_0 is the duration of the cycle.

Veletsos and Newmark (1964) have demonstrated that, for base excitations of the complexity of earthquake records, the response spectra are similar to those for simple excitations, and that their salient features can be reasonably identified from the spectra for single pulses, provided the gross characteristics of the ground acceleration, velocity and displacement are known. To this end, normalized displacement, SD/Y , velocity, SV/\dot{Y} , and absolute acceleration, SA/\ddot{Y} , response spectra of undamped systems were computed for various combinations of α and β (Ventura and Blázquez, 1990, 1992). The results are shown in Figures 2–4, where the spectra are plotted as a function of the ratio T/T_0 , and the spectral amplitudes are normalized with respect to the corresponding peak value of the ground motion. To complete the picture, 5%-damped PSV spectra normalized with respect to the peak base velocity are drawn on log-log scale in Figure 5(a) and are complemented with the corresponding SA values drawn in linear scale and normalized with respect to the peak base acceleration (Figure 5(b)).

It is clear from Figure 3 (relative displacement spectra) that non-zero initial conditions, when expressed in terms of α and β , have a greater effect on the response of very flexible systems, $T \gg T_0$, than on the response of less flexible systems. This effect is not very significant for rigid systems (that are more sensitive to high-frequency inputs) nor is it significant at the resonant period. The response for flexible systems can be reliably predicted via reasoning as follows. It has been demonstrated by Veletsos and Newmark (1964) that for a truly undamped, very flexible system with $\alpha = \beta = 0$, the relative displacement is opposite and nearly equal to the base displacement, i.e., $u \approx -y$. By disregarding the sign of the peak response, this result is shown by the solid line in Figure 2, where the normalized displacement converges to 1 for large values of T/T_0 .

If the values of α and β differ from zero, one can derive from Equations (11a) and (11b) the following expressions:

$$U_o = -\ddot{Y}\alpha / p^2 = -Y\alpha(T/T_0)^2 \quad (12a)$$

and

$$\dot{U}_o = -\dot{Y}\beta / p = -\dot{Y}\beta(T/T_0) \quad (12b)$$

From these expressions it can be seen that, for fixed values of α and β , U_o and \dot{U}_o are proportional to $(T/T_0)^2$ and (T/T_0) , respectively. For very flexible systems the ratio (T/T_0) is large, and U_o and \dot{U}_o are much larger than the peak value of the base displacement, Y , and the peak value of the base velocity, \dot{Y} , respectively. Since the maximum response of the transient part, u_t in Equation (3), approaches Y , it becomes clear that the response is dominated by the free-vibration part, u_f . This is the reason why the broken lines in Figure 2 exhibit a parabolic shape for large values of T/T_0 . This effect is most significant for the systems where α and β are both different from zero.

The behaviour of the relative velocity spectra is quite similar to the displacement spectra. It can be seen from Figure 3 that non-zero initial conditions affect a wide range of systems. Again, the effect is not very significant for rigid systems, but the response at the resonant period is affected in some cases. The response for flexible systems can also be predicted in a manner similar to that discussed above. For the systems initially at rest, the response is essentially equal and opposite to the base velocity, i.e., $\dot{u}_t \approx -\dot{y}$, as shown by the solid lines in Figure 3, where the normalized velocity converges to 1 for large values of T/T_0 . For values of α and β different from zero, Equations (12a) and (12b) apply, and the response for flexible systems is controlled by the derivative of the free-vibration part of Equation (3). In this case the broken lines in Figure 3 show a linear shape for large values of T/T_0 .

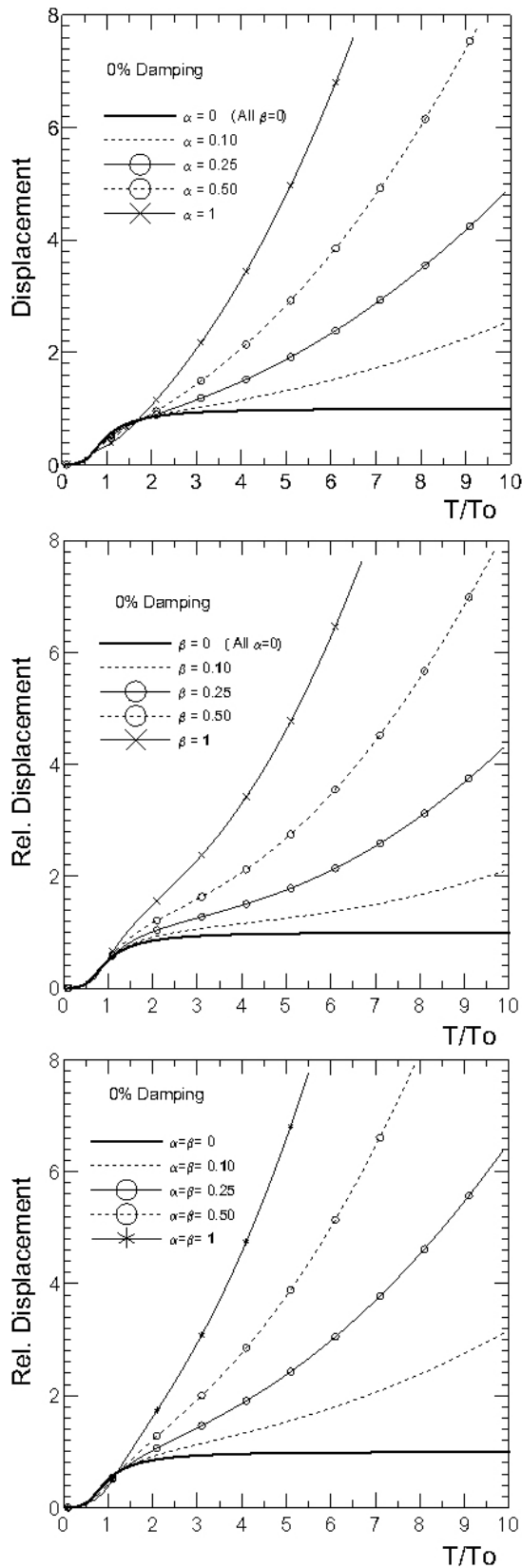


Fig. 2 Effect of initial conditions on the relative displacement spectra of undamped SDOF systems subjected to sinusoidal base acceleration

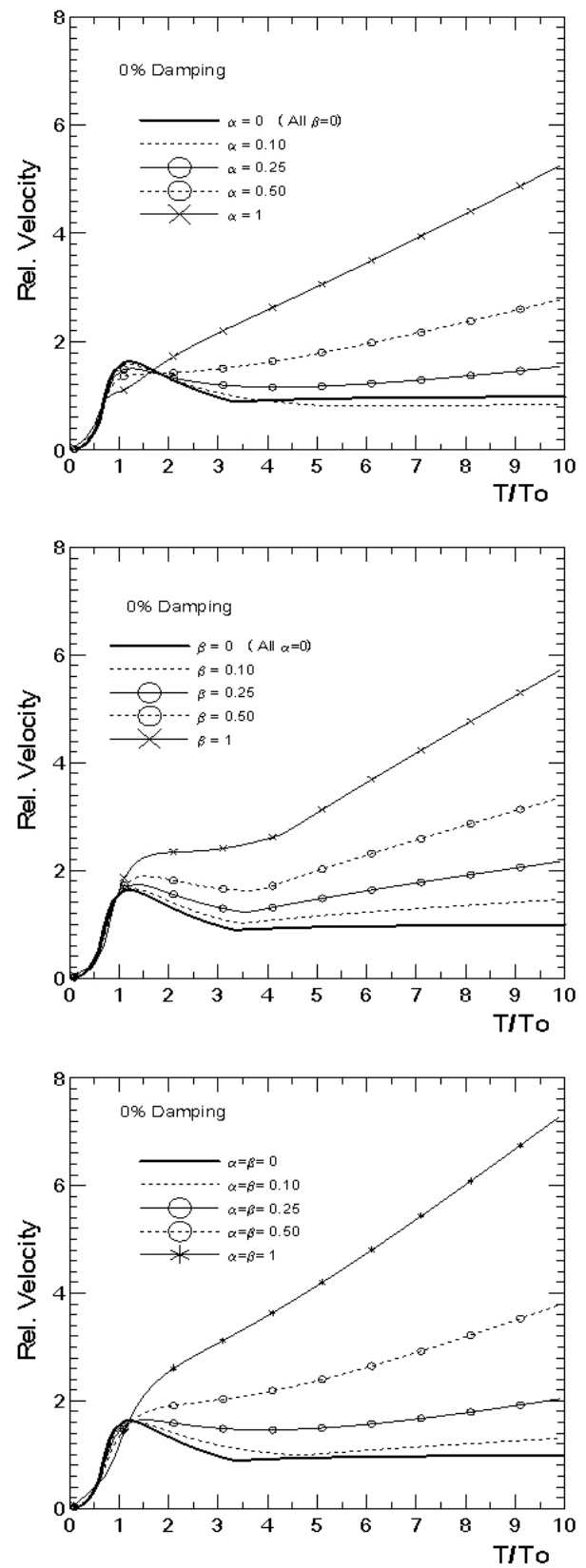


Fig. 3 Effect of initial conditions on the relative velocity spectra of undamped SDOF systems subjected to sinusoidal base acceleration

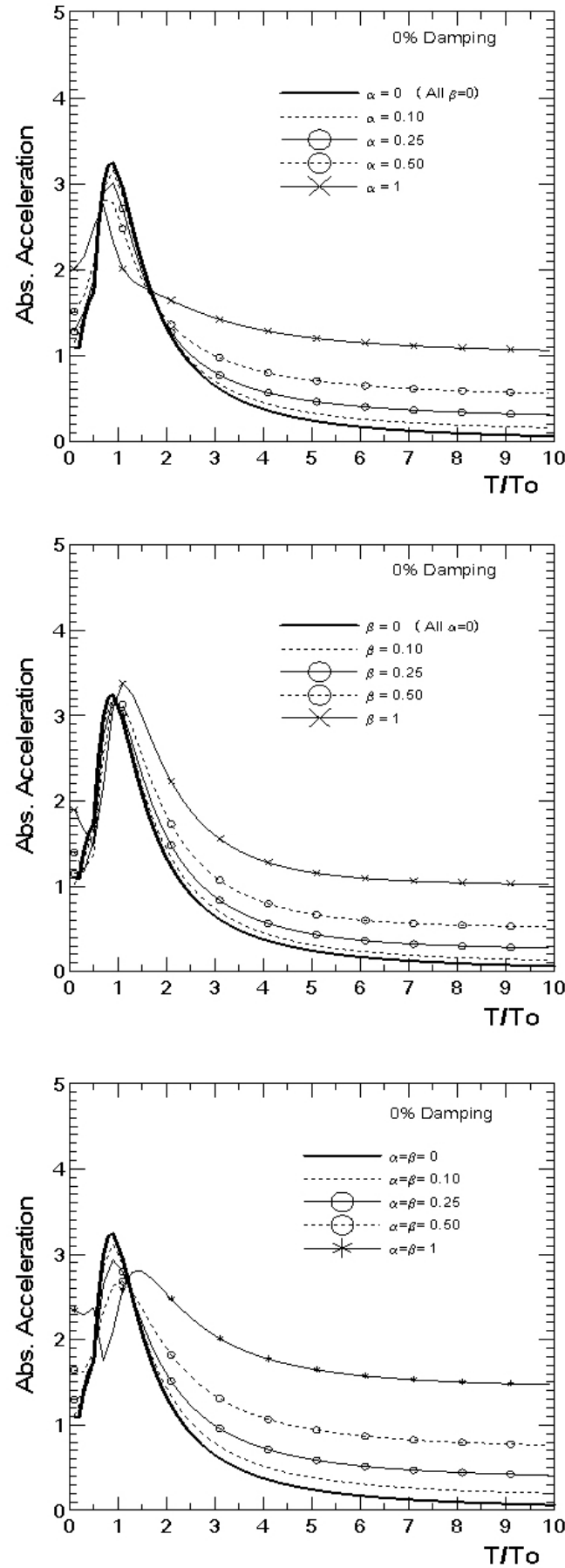


Fig. 4 Effect of initial conditions on the absolute acceleration spectra of undamped SDOF systems subjected to sinusoidal base acceleration

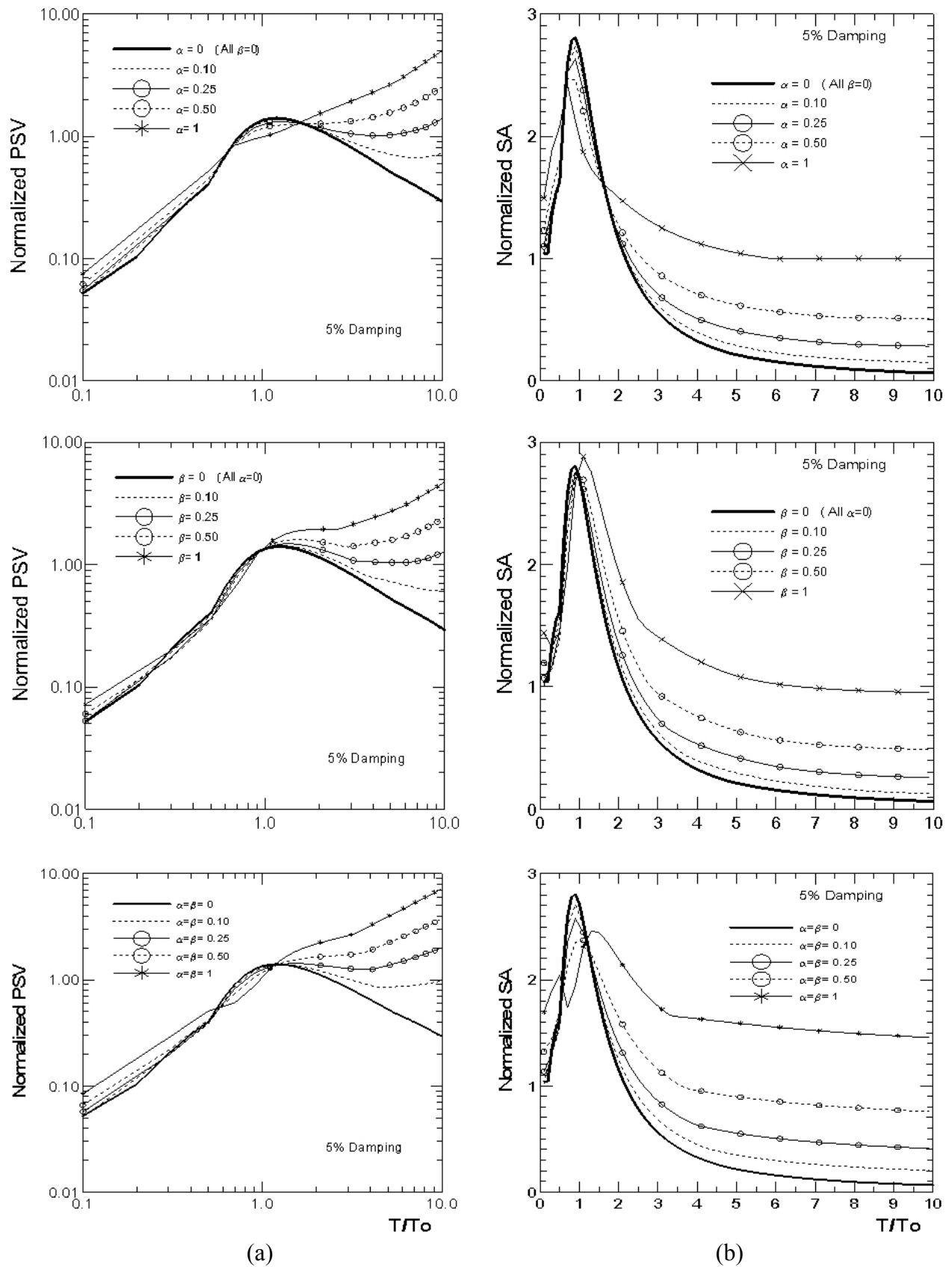


Fig. 5 Influence of initial displacement (α) and initial velocity (β) on pseudo-velocity (PSV) and absolute acceleration (SA) response spectra for elastic systems subjected to sinusoidal base excitation

The effect of initial conditions on the absolute acceleration spectra for undamped and damped systems is visualized in Figures 4 and 5(b), respectively. It can be seen that non-zero initial conditions affect the response of systems over the whole range of values of T/T_0 , but most significantly for systems in the long-period range. This is expected, since \ddot{x} is a function of u and \dot{u} as shown in Equation (9), and for undamped systems, $\ddot{x} = -p^2 u$. As T becomes larger, p decreases, cancelling the multiplying effect of $(T/T_0)^2$ in the displacement, and \ddot{x} becomes proportional to α and β . It follows that the peak value of \ddot{x} of undamped systems is proportional to $\ddot{Y}\sqrt{\alpha^2 + \beta^2}$. For values of α and β different from zero the effects at the resonant period are very significant, since the amplitude of the response is less than that for a system initially at rest. Damping simply reduces the amplitude of motion, as a direct comparison of Figures 4 and 5(b) clearly shows.

Figure 5 evidences that the effect of initial conditions on the response of rigid systems is quite negligible, since they are more sensitive to the high-frequency components of the input motion than to the initial state of the system.

For more complex excitations the same trends on the variation of the response spectra can be expected. The response spectra for the 1940 El Centro earthquake record (north-south component) are shown in Figure 6, and the spectra for the 1985 Mexico earthquake recorded at the SCT station (east-west component) are shown in Figure 7. The El Centro earthquake record was selected for this study because it produces significant responses over a wide band of system periods, while the Mexico earthquake record was selected because it produces significant responses for a narrow range of periods, mostly for periods around 1.5 to 3 sec. Figures 6(a) and 7(a) show the 5%-damped PSV elastic spectra, and Figures 6(b) and 7(b) show the SA elastic spectra, both for different values of α (with $\beta = 0$). These spectra represent the peak values of pseudo-velocity and absolute acceleration during the duration of the excitation only.

As in the case for sinusoidal base motion, the long-period regions of the PSV and SA spectra are more sensitive to the effects of the initial conditions than the other regions of the spectra. The SA spectra also show that the base shear for a long-period system with non-zero initial conditions is larger than that for a system initially at rest. This may lead to unconservative designs of long-period structures if the effects of initial conditions are not properly accounted for.

2. Inelastic Systems

Two important parameters that usually characterize the response of inelastic systems are the yield displacement, U_y , and the associated force level, R_y , that produces this displacement. To obtain the dynamic response of an inelastic system for which its force-deformation characteristics are known, Equation (1) can be solved directly. However, it is more desirable to express this equation in a normalized form such that the specific parameters that influence the response can be more readily identified, as in the case of elastic systems (Mahin and Lin, 1983). A possible normalized version of Equation (1) can be written as

$$\ddot{\mu}(t) + 2\xi p \dot{\mu}(t) + p^2 \rho(t) = -A \ddot{y}(t) \quad (13)$$

in which $\mu(t) = u(t)/U_y$ is defined as the displacement ductility and its peak value, U_y , is referred to as the ductility factor (Clough and Penzien, 2003), $\rho(t) = R(t)/R_y$ and $A = p^2 / \eta \ddot{Y}$. The dimensionless parameter $\eta = R_y / m \ddot{Y}$ represents the yield strength relative to the peak inertia force of the system. Note that for truly undamped elastic systems, the peak inertia force is equal and opposite to the peak value of the base shear. So the strength index is directly related to the peak base shear of the undamped elastic version of the system.

Equation (13) provides an efficient way to evaluate $\mu(t)$ for all systems that have the same elastic natural frequency, the same hysteretic characteristics, the same strength index, and are subjected to ground motions having the same time histories.

For systems with hysteresis diagrams that exhibit an initial elastic behaviour, like the elasto-plastic systems, R_y and U_y can be related by $R_y = kU_y$, and the displacement ductility can be expressed directly in terms of η as

$$\mu(t) = p^2 u(t) / \eta \ddot{Y} \quad (14)$$

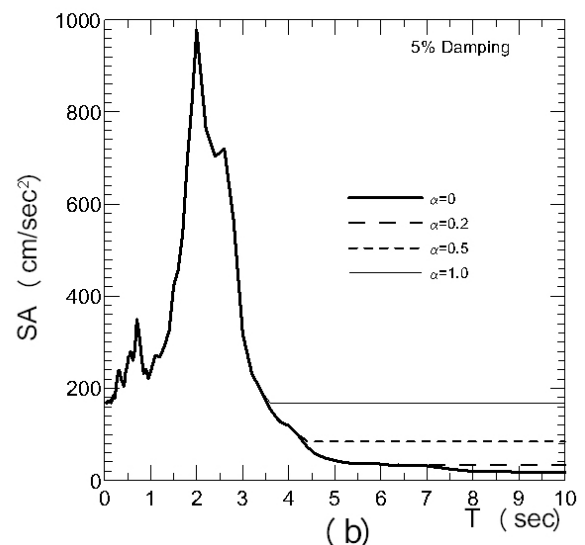
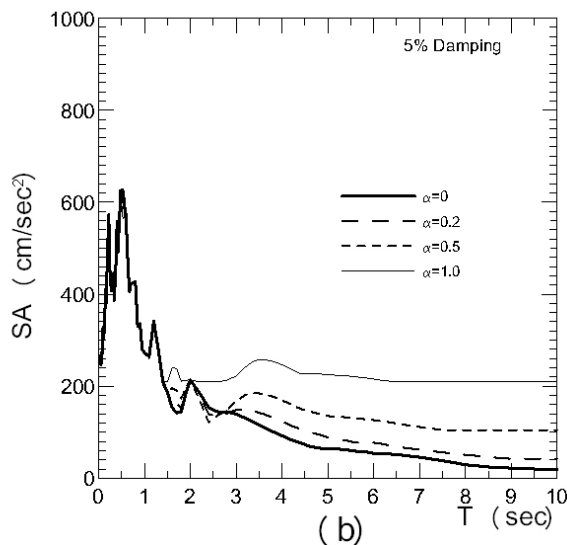
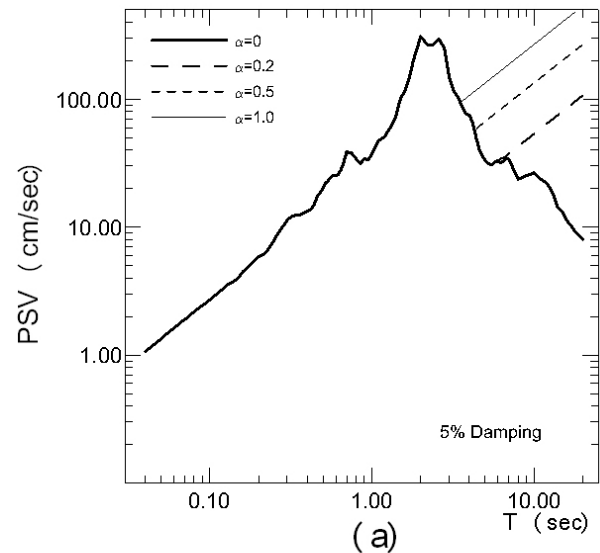
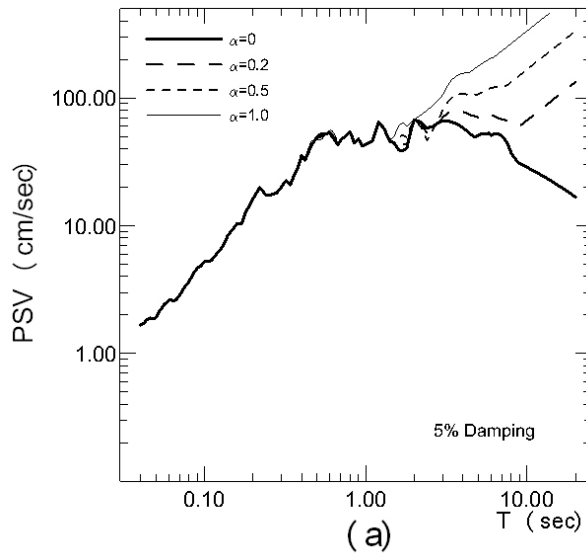


Fig. 6 Influence of initial displacement (α) on pseudo-velocity (PSV) and absolute acceleration (SA) response spectra for elastic systems subjected to El Centro 1940 earthquake, N-S component

Fig. 7 Influence of initial displacement (α) on pseudo-velocity (PSV) and absolute acceleration (SA) response spectra for elastic systems subjected to Mexico 1985 earthquake, E-W component

In a response spectrum analysis, for a given value of η , the peak value of $u(t)$ can be obtained from the corresponding response spectrum and the ductility factor can be readily computed from Equation (14). To illustrate the sensitivity of the response of elasto-plastic systems to variations in η , the maximum responses due to El Centro and Mexico records were computed using a modified version of the computer program as described in Mahin and Lin (1983).

The maximum responses for systems initially at rest ($\alpha = \beta = 0$) are shown in Figures 8(a) and 9(a), where they are presented as pseudo-velocity spectral values using the natural period of the elastic portion of the hysteresis diagram as the reference period. The corresponding absolute acceleration spectra are

shown in Figures 8(b) and 9(b). For reference, the associated elastic spectra are also included in the figures and are used as a basis of comparison between the elastic and inelastic responses.

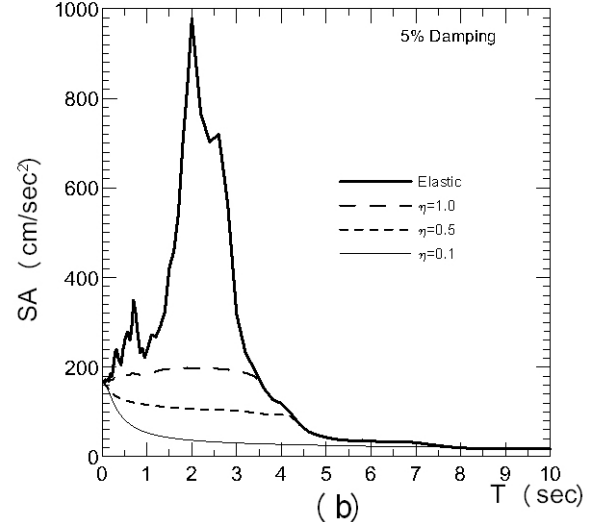
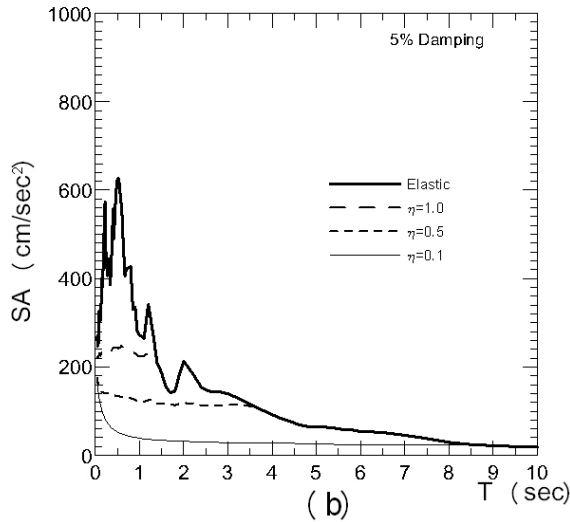
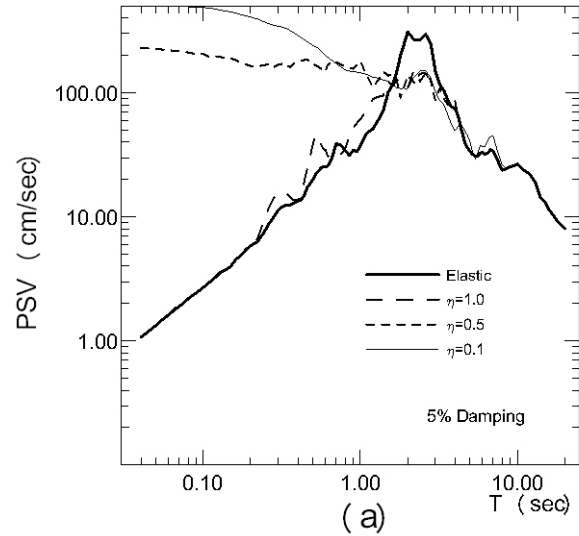
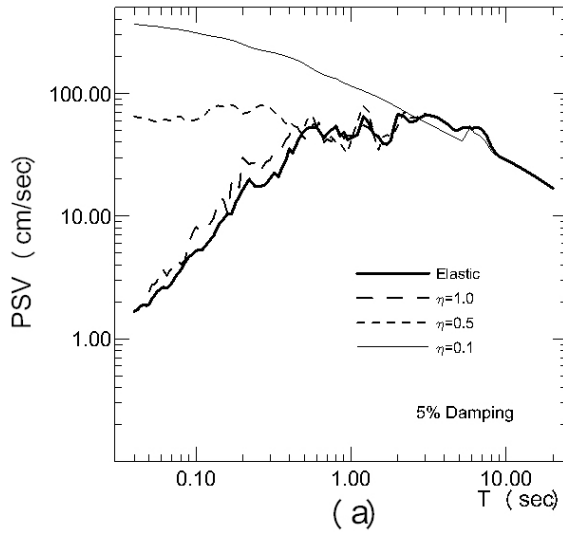


Fig. 8 El Centro 1940 earthquake: pseudo-velocity (PSV) and absolute acceleration (SA) response spectra for elastic and elasto-plastic systems initially at rest

Fig. 9 Mexico 1985 earthquake: pseudo-velocity (PSV) and absolute acceleration (SA) response spectra for elastic and elasto-plastic systems initially at rest

These figures show that, for $\eta > 0.5$, the responses of systems with periods less than 4 sec are generally more sensitive to variations of η than those for very flexible systems. As the value of η increases, the response approaches that of the truly elastic systems, and the results become less sensitive to variations of η . For small values of η ($\eta = 0.1$) a wider range of systems are affected, since low values of η correspond to the systems that have a low equivalent value of the maximum elastic base shear force and, therefore, are expected to undergo large excursions beyond the yield displacement, U_y .

Introducing initial conditions into the computation of the PSV spectra for elasto-plastic systems has the effect shown in Figures 10(a) and 11(a). The effect on the SA spectra is shown in Figures 10(b) and 11(b). In these cases, including only an initial displacement ($\alpha = 0.5$, $\beta = 0$) in the computation of the inelastic response of systems to the El Centro and Mexico records completely alters the shape of the spectrum in the long-period region when compared to that of the inelastic systems with zero initial conditions. Including the initial velocity effects will further alter the shape of the spectrum. The middle-

and low-period regions of the spectrum remain more sensitive to variations of the strength over inertia force index (η) than to variations of the initial conditions (α). For small values of η the SA values are insensitive to the effects of initial conditions.

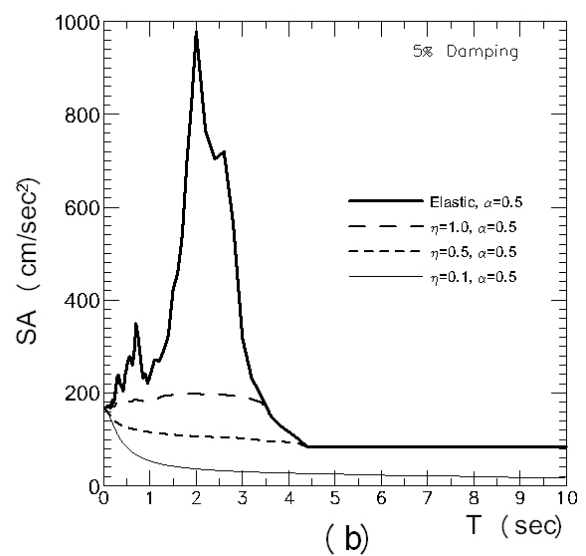
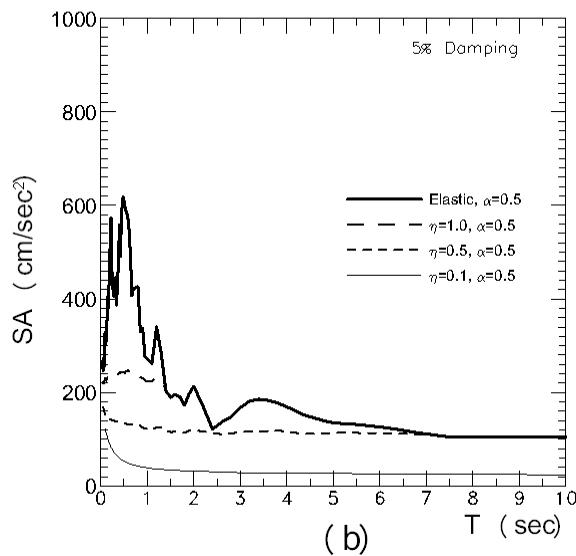
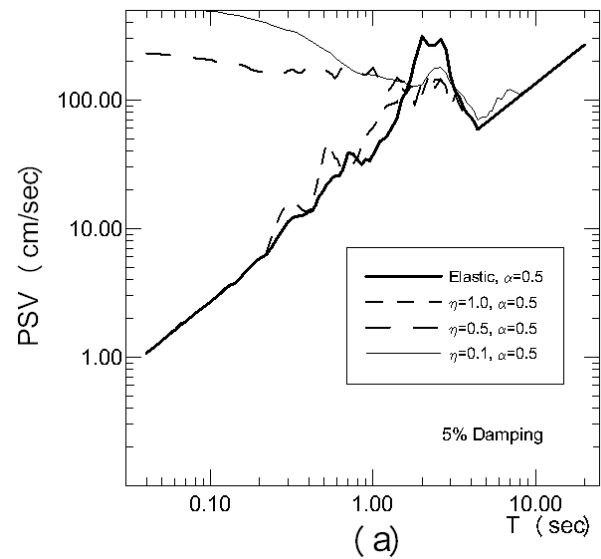
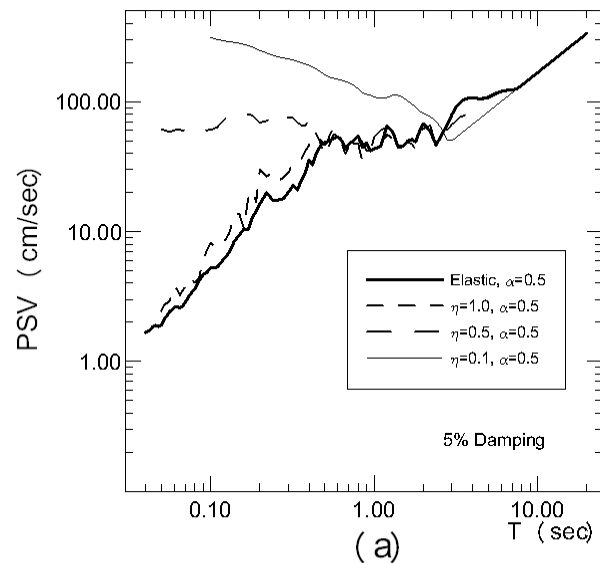


Fig. 10 Influence of initial displacement (α) on pseudo-velocity (PSV) and absolute acceleration (SA) response spectra for elasto-plastic systems subjected to El Centro 1940 earthquake

Fig. 11 Influence of initial displacement (α) on pseudo-velocity (PSV) and absolute acceleration (SA) response spectra for elasto-plastic systems subjected to Mexico 1985 earthquake

APPROXIMATE CORRECTION PROCEDURES TO ACCOUNT FOR INITIAL CONDITIONS (ELASTIC SYSTEMS)

The maximum response of long-period systems is controlled by the free-vibration part of Equation (3) as discussed earlier. The response for other systems is a combination of the transient and free-vibration parts. If the response spectrum for a system initially at rest is readily available, and if one assumes that the initial conditions can be determined or are given, then it is of interest to develop a method to approximate the true response spectrum using the information provided.

Let U_f be the maximum free-vibration response of a system subjected to initial displacement U_0 and initial velocity \dot{U}_0 , and let U_t be the maximum relative displacement of a SDOF system initially at rest. The value of U_t can be obtained from the available response spectrum and U_f can be obtained by maximizing Equation (7). The latter operation leads to a closed-form expression for U_f that can be readily used, instead of performing a time-domain analysis, to find the maximum response value (Veletsos and Ventura, 1984). Two methods are investigated here: (a) the Sum of Absolute Values (SAV) Method (Biot, 1941); and (b) the Square Root of the Sum of the Squares (SRSS) Method (Rosenblueth, 1951). In the SAV method, the true response, U , is approximated by a linear combination of the individual absolute maximum values, i.e.,

$$U \approx |U_t| + |U_f| \quad (15)$$

in which the pairs of vertical bars denote absolute value of the quantity enclosed. For the proposed approximation using the SRSS method, U is computed as

$$U \approx (U_t^2 + U_f^2)^{1/2} \quad (16)$$

Equations (15) and (16) are also applicable for the computation of the relative velocity and absolute acceleration response spectra. The response spectra for systems with 5% damping and approximated by the SAV method are shown in Figure 12 where they are compared with the true spectra. The approximation leads to excellent results for relative displacement, conservative results for relative velocity, and very conservative results for absolute acceleration values of rigid and intermediate systems. However, the results for flexible-period systems are in good agreement. The results using the SRSS method are shown in Figure 13. In this case the relative displacement and velocity values are less than the true values, but the absolute acceleration values for rigid and intermediate systems are closer to the true values than those obtained by the SAV method. For flexible systems, the results underestimate the exact ones. It can be concluded that, for the type of excitation considered, the SAV method leads to better results, in general, except for the computation of maximum absolute acceleration of rigid and intermediate systems where the SRSS method leads to better results.

CONCLUSIONS

- For long-period (flexible) systems, the effect of non-zero initial conditions in the motion is a magnification of the computed spectral responses (displacement, velocity and acceleration), regardless of the damping level of the system.
- For rigid systems the above effect is negligible, since they are more sensitive to the high-frequency components of the input motion than to the initial state of the system.
- The spectral values in the long-period range are dominated by the free-vibration part of the response of the system.
- The base shear for a long-period elastic system with non-zero initial conditions may be significantly larger than that for a system initially at rest, leading to an unconservative design if this effect is not properly accounted for.
- Omitting initial conditions makes the pseudo-velocity spectrum deviate from zero at very long periods and asymptotically approach the initial absolute velocity of the system (equal to the initial excitation velocity).
- For non-resting elastic systems, the SAV method (adding the peak absolute value of free-vibration response to the standard response spectrum) leads to an acceptable degree of approximation of all spectral values in the long-period range.
- Response spectra of inelastic systems are influenced by the initial conditions but are also sensitive to the value of the system's yield strength index (parameter η). For high η values ($\eta > 0.5$), the sensitivity of very flexible systems to variations in η decreases and the response approaches that of the truly elastic systems.

- Although it has been proved that initial conditions of the motion of the system are a crucial factor in the computation of response spectra, these conditions have a lesser influence on modern digital recording systems, since those incorporate a buffer memory that allows convenient retrieval of the initial portion of the acceleration record.

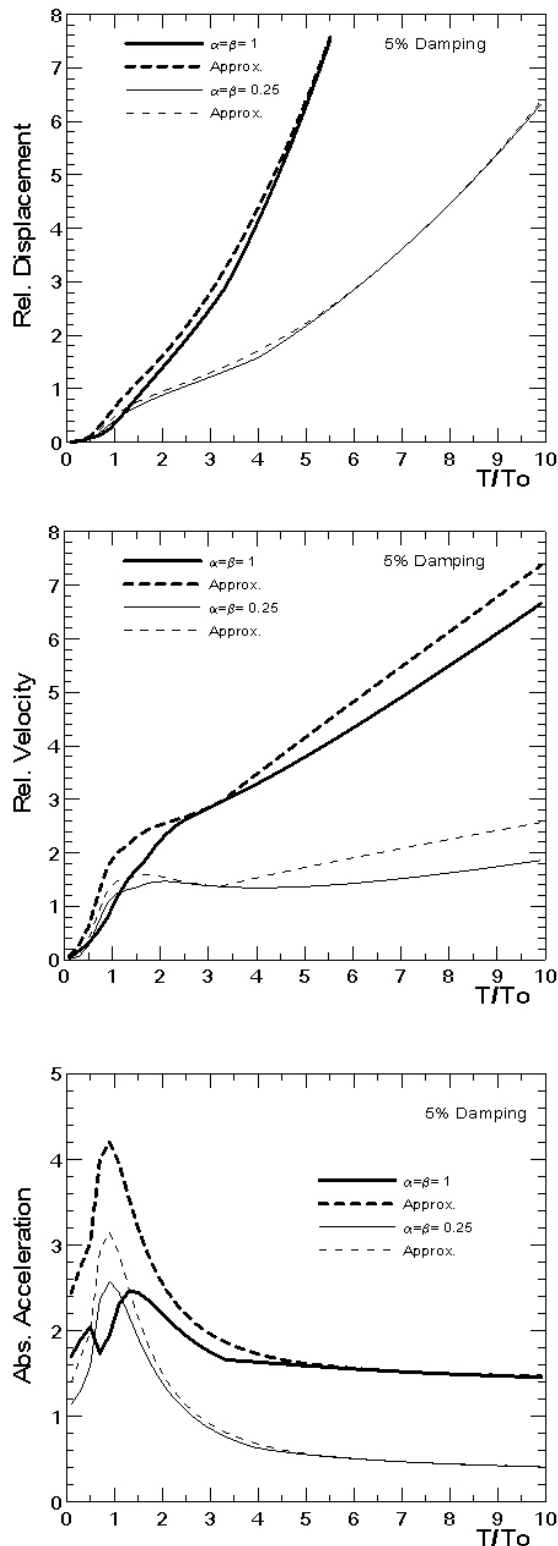


Fig. 12 Comparison of exact and approximate normalized response spectra computed by the proposed SAV method: sinusoidal excitation

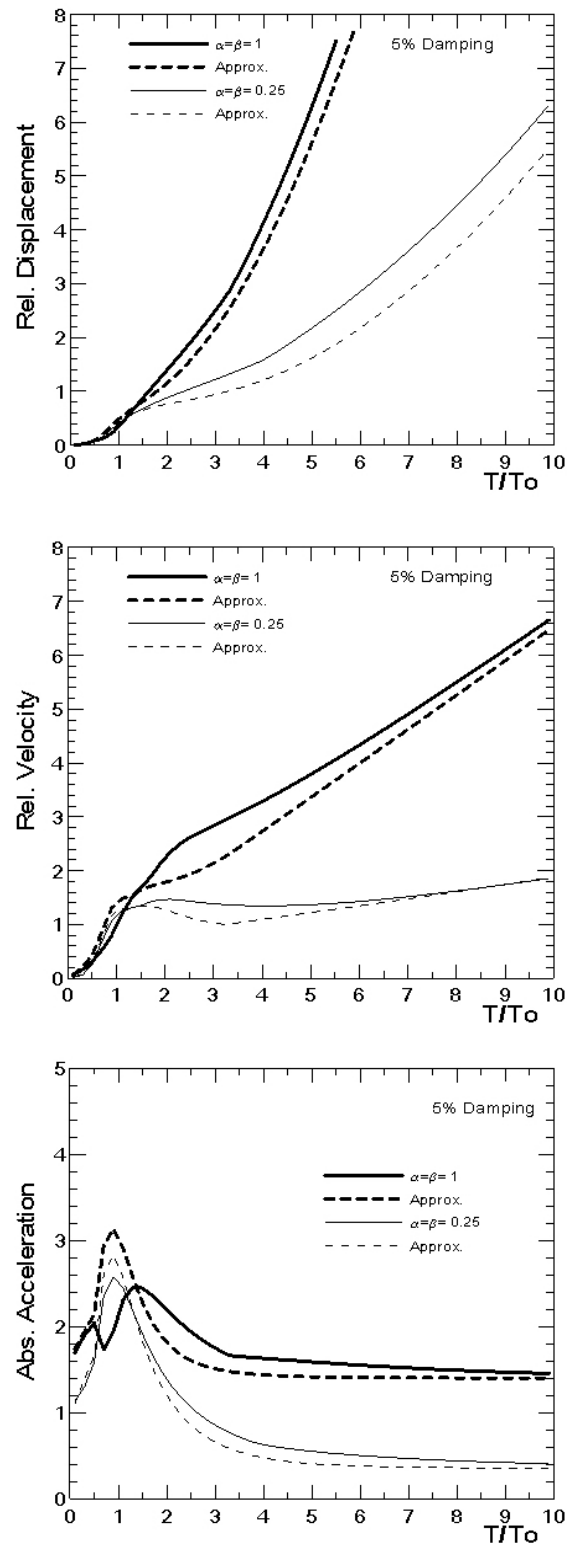


Fig. 13 Comparison of exact and approximate normalized response spectra computed by the proposed SRSS method: sinusoidal excitation

ACKNOWLEDGEMENTS

Partial support for this study was provided by the Natural Sciences and Engineering Research Council of Canada (NSERC) and the Ministry of Education and Science of Spain (MEC). We thank Prof. Mihailo Trifunac of the University of Southern California for reading the first version of this manuscript, and for offering many useful suggestions and bringing to our attention key seminal references that led to a significant improvement of this paper.

REFERENCES

1. Biot, M.A. (1941). "A Mechanical Analyzer for the Prediction of Earthquake Stresses", *Bulletin of the Seismological Society of America*, Vol. 31, No. 2, pp. 151–171.
2. Blázquez, R. and Kelly, J.M. (1988). "Effect of Initial Conditions and Computational Algorithm on Long Period Response Spectra", *Proceedings of the Ninth World Conference on Earthquake Engineering*, Tokyo-Kyoto, Japan, Vol. V, pp. 1051–1056.
3. Clough, R.W. and Penzien, J. (2003). "Dynamics of Structures", Computers and Structures, Inc., Berkeley, U.S.A.
4. Hudson, D.E. (1979). "Reading and Interpreting Strong Motion Accelerograms", Monograph MNO-1, Earthquake Engineering Research Institute, Berkeley, U.S.A.
5. Mahin, S.A. and Lin, J. (1983). "Construction of Inelastic Response Spectra for Single-Degree-of-Freedom Systems: Computer Program and Applications", Report UCB/EERC-83/17, University of California, Berkeley, U.S.A.
6. Pecknold, D.A. and Riddell, R. (1978). "Effect of Initial Base Motion on Response Spectra", *Journal of the Engineering Mechanics Division*, *Proceedings of ASCE*, Vol. 104, No. EM2, pp. 485–491.
7. Pecknold, D.A. and Riddell, R. (1979). "Closure of 'Effect of Initial Base Motion on Response Spectra'", *Journal of the Engineering Mechanics Division*, *Proceedings of ASCE*, Vol. 105, No. EM6, pp. 1057–1060.
8. Rosenblueth, E. (1951). "A Basis for a Seismic Design", Ph.D. Thesis, University of Illinois, Urbana, U.S.A.
9. Trifunac, M.D. and Udawadia, F.E. (1979). "Discussion of 'Effect of Initial Base Motion on Response Spectra'", *Journal of the Engineering Mechanics Division*, *Proceedings of ASCE*, Vol. 105, No. EM1, pp. 204–206.
10. Uang, C.M. and Bertero, V.V. (1990). "Evaluation of Seismic Energy in Structures", *Earthquake Engineering & Structural Dynamics*, Vol. 19, No. 1, pp. 77–90.
11. Veletsos, A.S. and Newmark, N.M. (1964). "Design Procedures for Shock Isolation Systems of Underground Protective Structures. Volume III. Response Spectra of Single-Degree-of-Freedom Elastic and Inelastic Systems", Report RTD TDR 63-3096 (prepared for Air Force Weapons Laboratory, Kirtland Air Force Base, Albuquerque, New Mexico), Newmark Hansen and Associates, Urbana, U.S.A.
12. Veletsos, A.S. and Ventura, C.E. (1984). "Efficient Analysis of Dynamic Response to Linear Systems", *Earthquake Engineering & Structural Dynamics*, Vol. 12, No. 4, pp. 521–536.
13. Veletsos, A.S. and Ventura, C.E. (1985). "Dynamic Analysis of Structures by the DFT Method", *Journal of Structural Engineering*, ASCE, Vol. 111, No. 12, pp. 2625–2642.
14. Ventura, C.E. and Blázquez, R. (1990). "Sensitivity Analysis of Response Spectra to System Initial Conditions", *Proceedings of the Ninth European Conference on Earthquake Engineering*, Moscow, U.S.S.R., Vol. 10-B, pp. 100–110.
15. Ventura, C.E. and Blázquez, R. (1992). "Influence of System Initial Conditions on Elastic and Inelastic Response Spectra", *Proceedings of the Tenth World Conference on Earthquake Engineering*, Madrid, Spain, Vol. 1, pp. 195–200.
16. Von Karman, T. and Biot, M.A. (1940). "Mathematical Methods in Engineering", McGraw-Hill, New York, U.S.A.

PROBABILISTIC SEISMIC HAZARD ANALYSIS METHOD FOR MAPPING OF SPECTRAL AMPLITUDES AND OTHER DESIGN-SPECIFIC QUANTITIES TO ESTIMATE THE EARTHQUAKE EFFECTS ON MAN-MADE STRUCTURES

I.D. Gupta

Central Water and Power Research Station
Khadakwasla, Pune-411024

ABSTRACT

Along with the commonly used parameters like peak acceleration and response spectral amplitudes, knowledge of many other parameters like strong-motion duration, peak strains, likelihood for initiation of liquefaction, and permanent dislocations across faults is necessary to have a more comprehensive estimate of the earthquake effects on a variety of man-made structures. The present paper provides a concise but complete description of the probabilistic seismic hazard analysis (PSHA) method to map any of these quantities with a uniform probability of not being exceeded due to the total expected seismicity during a specified life period. Example results are presented to illustrate the application of the PSHA method in preparing the microzonation maps for several different hazard parameters. The paper also proposes simple practical solutions for some of the difficulties faced in implementing the existing PSHA method in real applications.

KEYWORDS: Probabilistic Seismic Hazard, Uncertainties, Hazard Parameters, Microzonation Maps

INTRODUCTION

The seismic hazard analysis is concerned with the evaluation of the levels of various natural effects of earthquakes, which may be of consequence for the safety of an existing or a proposed man-made structure at a site. Some important parameters used for characterization of seismic hazard can be listed as the peak ground acceleration (Cornell, 1968), Fourier and response spectrum amplitudes (McGuire, 1977; Anderson and Trifunac, 1977, 1978; Lee and Trifunac, 1985), strong motion duration (Papazachos et al., 1992), peak strains (Todorovska and Trifunac, 1996), surface faulting (Todorovska et al., 2005; Stepp et al., 2001), soil liquefaction (Todorovska and Trifunac, 1999), and landslides (Del Gaudio and Wasowski, 2004), out of which the response spectrum is the most widely used and extensively studied strong-motion functional. The concept of response spectrum method was introduced in early 1930s (Biot, 1932, 1933, 1934); and since 1970, it has become the principal tool in the design of earthquake-resistant structures (Trifunac, 2003), because of the simplicity and directness with which it relates the strong motion with the response of a structure.

The deterministic and the probabilistic are the two commonly used approaches for the seismic hazard analysis. In the deterministic approach, the value of a hazard parameter of interest is estimated for a specified earthquake magnitude assumed to occur at a fixed source-to-site distance (e.g., Reiter, 1990; Anderson, 1997; Krinitzsky, 2002). However, a single scenario earthquake is not able to provide a true picture of the seismic hazard at a site because different combinations of magnitude and distance contribute more significantly in different frequency bands. On the other hand, the probabilistic seismic hazard analysis (PSHA) approach takes into account the effects of all the earthquakes by considering the inherent random nature of earthquake magnitude, recurrence time, and epicentral location as well as that of the amplitude of the hazard parameter of interest (e.g., Cornell, 1968; McGuire, 1977; Anderson and Trifunac, 1978). The estimate of a hazard parameter by PSHA approach is thus not expected to be exceeded with a desired confidence level due to any of the earthquakes expected to occur during a given exposure period.

The PSHA formulation was first presented by Cornell (1968) for the peak ground acceleration. He modeled the randomness in magnitude by the Gutenberg-Richter's frequency-magnitude relationship (Gutenberg and Richter, 1944), that in recurrence time by Poisson probability distribution, and that in

location by considering the epicenters to be confined to a point source, or distributed uniformly over a straight line fault or an annular area around the site. But the formulation of Cornell (1968) did not consider the random scattering in the amplitudes of the hazard parameter around the median attenuation relationship. Many other early studies (e.g., Milne and Davenport, 1969; Douglas and Ryall, 1975) as well as some later studies also (e.g., Kijko and Graham, 1999) have not considered the randomness in hazard parameter. Der Kiureghian (1977) showed that this randomness may be a significant source of uncertainty in the results of the hazard analysis. To have a uniformly conservative estimate of the hazard at all the frequencies, McGuire (1974, 1977) performed the PSHA for response spectrum amplitudes at several different frequencies, with the randomness in spectral amplitudes considered by a lognormal distribution. Anderson and Trifunac (1977, 1978) generalized the PSHA formulation by modeling the seismicity in a more realistic way and applied that to compute the Fourier amplitude spectra. They employed five different types of source: (a) a point source, (b) a line source (not necessarily straight), (c) an areal source with arbitrary boundary, (d) an arbitrarily dipping fault surface, and (e) a volume of arbitrary shape, to define the seismicity. Their formulation also included the effect of fault rupture dimensions, which may have significant effect on the hazard estimation (e.g., Ang, 1973; Der Kiureghian and Ang, 1975; Anderson and Trifunac, 1977).

Most of the recent developments in the PSHA approach have been primarily concerned with introducing different probabilistic models to describe the randomness in earthquake magnitude, recurrence time, and epicentral location to get more realistic descriptions for specific practical applications. However, due to inadequacy or lack of available data and incomplete understanding of the earthquake and ground-motion generating processes, it is generally difficult to specify the various input models and their parameters without any uncertainty. The current PSHA approach utilizes the logic-tree methodology (Kulkarni et al., 1984) to quantify the effect of these additional uncertainties, termed commonly as “epistemic” uncertainties. On the other hand, the basic PSHA approach considers only the inherent random uncertainties, which are termed as “aleatory” uncertainties. The logic-tree methodology provides a systematic graphical procedure for identifying all possible sets of input models and their parameters. An appropriate weight is assigned to each set of these inputs to the PSHA by assigning suitable weights to the various logic-tree branches for each input element. The basic PSHA is then performed for each set of inputs to get a complete picture of the effect of the epistemic uncertainties on the hazard estimation. However, there is no consensus on the way the uncertainties are to be assigned and on how to take the final decision with epistemic uncertainties (e.g., Klügel, 2005a, 2005b, 2005c; Musson et al., 2005; Budnitz et al., 2005).

If applied properly, the PSHA approach may prove a powerful method for estimation of site-specific design ground motions for practical applications (e.g., EPRI, 1986; Bernreuter et al., 1987; Todorovska et al., 1995; Senior Seismic Hazard Analysis Committee, 1997; USACE, 1999; Gupta, 2002a; McGuire, 2004). The results of PSHA may form a basis for earthquake-resistant design using both the simplified elastic analysis (e.g., BSSC, 1997) as well as more rigorous performance-based analysis (e.g., FEMA, 2000; Ellingwood, 2001; Bertero and Bertero, 2004). Another practical application of PSHA approach is in preparation of seismic zoning maps. Zoning may be done on a macro scale, such as those under GSHAP (1999) and several other studies (e.g., Frankel et al., 2002; Adams and Atkinson, 2003; Das et al., 2006), or on a micro scale including the regional and local site effects in a more detailed way (e.g., Lee and Trifunac, 1987; Trifunac, 1990a). The microzoning maps need not be limited only to the peak acceleration and the spectral amplitudes at selected frequencies. The recent developments have enabled to prepare the microzonation maps in terms of normalized peak strains (Todorovska and Trifunac, 1996), surface faulting (Todorovska et al., 2005), and liquefaction potential (Todorovska and Trifunac, 1999). The present paper provides an overview of the various aspects of the currently used PSHA approach with a number of illustrative example results. Many studies have proposed the deaggregation of probabilistic seismic hazard to represent the hazard equivalently by a single pair of earthquake magnitude and distance, which is considered necessary and useful in making certain engineering decisions (e.g., Chapman, 1995; Ishikawa and Kameda, 1988; Bazzurro and Cornell, 1999; McGuire, 1995). However, the use of PSHA to arrive at a single scenario earthquake by deaggregation has not been described in any detail.

THE PSHA FORMULATION

The PSHA formulation is fundamentally concerned with estimating the expected occurrence rate, $\nu(Z > z)$, of exceeding a specified value, z , of a random parameter, Z , used for characterization of hazard at a site. For this purpose, the original formulation due to Cornell (1968) uses only those combinations of earthquake magnitude and distance, which may cause a specified mean or median estimate of Z to be exceeded. However, by considering the random scattering of the amplitudes of hazard parameter around the mean or median estimate, the occurrence rate can be defined using total probability theorem by the following generalized form of expression.

$$\nu(Z > z) = \sum_{n=1}^N N_n(M_{\min}) \iiint \delta(Z > z | M, R, \varepsilon) f_n(M) g_n(R) h(\varepsilon) dM dR d\varepsilon \quad (1)$$

In this expression, $N_n(M_{\min})$ represents the occurrence rate of earthquakes above a selected threshold magnitude M_{\min} in the n th source zone, and the summation is taken over all the N number of source zones. Functions $f_n(M)$ and $g_n(R)$ are the probability density functions of magnitude and distance for this source. Further, the expression of Equation (1) is based on the assumption that the logarithm of the values of the hazard parameter for magnitude M and distance R follows a Gaussian distribution with mean value $\mu(M, R)$ and standard deviation $\sigma(M, R)$. The quantity $\delta(Z > z | M, R, \varepsilon)$ is taken as 1.0 for $\ln z$ equal to $\mu(M, R)$ plus ε times $\sigma(M, R)$ and zero otherwise, with $h(\varepsilon)$ as the standard Gaussian distribution with zero mean and unit standard deviation. In practical applications, the probability distribution of the amplitudes of hazard parameter is usually truncated arbitrarily at two to three standard deviations, which cannot be considered appropriate. If at all, any upper limit on the hazard parameter has to be based on the physical grounds. However, it seems unlikely that this problem may be solved in the near future (Bommer et al., 2004).

Contrary to that assumed in Equation (1), the residuals of the hazard parameter need not necessarily be defined by a Gaussian density function (Trifunac and Lee, 1979). It will therefore be more generalized to replace the integral of the product of $\delta(Z > z | M, R, \varepsilon)$ and $h(\varepsilon)$ over ε by the probability of exceeding level z due to magnitude M at distance R . Representing this probability by $q(Z > z | M, R)$, the expression for the occurrence rate becomes

$$\nu(Z > z) = \sum_{n=1}^N N_n(M_{\min}) \iint q(Z > z | M, R) f_n(M) g_n(R) dM dR \quad (2)$$

By discretizing the magnitude and distance for the n th source zone into small intervals like $(M_j - \delta M_j, M_j + \delta M_j)$ and $(R_i - \delta R_i, R_i + \delta R_i)$ with central values M_j and R_i , the occurrence rate of earthquakes in the j th magnitude and the i th distance interval can be defined as

$$\lambda_n(M_j, R_i) = N_n(M_{\min}) \int_{M_j - \delta M_j}^{M_j + \delta M_j} \int_{R_i - \delta R_i}^{R_i + \delta R_i} f_n(M) g_n(R) dM dR \quad (3)$$

The expression of Equation (2) can thus be written in the following discrete form:

$$\nu(Z > z) = \sum_{n=1}^N \sum_{j=1}^J \sum_{i=1}^I q(Z > z | M_j, R_i) \lambda_n(M_j, R_i) \quad (4)$$

A total of J magnitude ranges and I distance ranges are considered for the summations in Equation (4). Further, if the same attenuation relation is applicable to all the seismic source zones, it is possible to use directly the total annual number, $n(M_j, R_i)$, of earthquakes obtained by adding the numbers for all the source zones. The expression of Equation (4) thus becomes (Anderson and Trifunac, 1977, 1978)

$$\nu(Z > z) = \sum_{j=1}^J \sum_{i=1}^I q(Z > z | M_j, R_i) n(M_j, R_i) \quad (5)$$

In practical applications, the probabilistic hazard computation is commonly based on the expressions of Equations (4) and (5). By using the numbers, $\lambda_n(I_{0j}, R_i)$ or $n(I_{0j}, R_i)$, of earthquakes with epicentral intensity I_{0j} at distance R_i , the probabilistic hazard can also be performed using the intensity data (Gupta, 1991). For this purpose, the probability, $q(Z > z | I_{0j}, R_i)$, of $Z > z$ is obtained by summing over all the site intensities the product of the probability of exceeding value z due to a specified site intensity multiplied by the probability of occurrence of that site intensity due to the combination of I_{0j} and R_i .

The reciprocal of $v(Z > z)$ gives the return period for the occurrence of an amplitude z or above of the hazard parameter. Assuming the occurrence rate $\lambda_n(M_j, R_i)$ to follow a Poisson probability distribution, the occurrence rate $v(Z > z)$, which is a linear combination of $\lambda_n(M_j, R_i)$, can also be described by a Poisson probability distribution. Thus, the probability of $Z > z$ due to all the earthquakes in all the sources during an exposure period of Y years can be written as

$$P(Z > z | Y) = 1 - \exp\{-Yv(Z > z)\} \quad (6)$$

From this, the return period for the occurrence of $Z > z$ can be defined in terms of $P(Z > z | Y)$ as

$$T(Z > z) = \frac{1}{\ln(1 - P(Z > z | Y))} \quad (7)$$

The plot of the probability $P(Z > z | Y)$ versus z is commonly known as the “hazard curve”. The most widely adopted practice is to plot the hazard curve in terms of the annual ($Y = 1$) probability of exceedance. Assuming $v(Z > z)$ to be very small, the annual probability of exceedance is generally approximated by $v(Z > z)$. The hazard curves are sometimes also plotted as $T(Z > z)$ versus z . The various representations of the hazard curve are shown schematically in Figure 1. It may be noted that though the PSHA can equivalently be described by any of the quantities $v(Z > z)$, $T(Z > z)$, $P(Z > z | Y = 1)$ or $P(Z > z | Y)$, which are interrelated by simple relations, the use of $P(Z > z | Y)$ provides a direct physical interpretation of the results of PSHA. If Z represents the Fourier or response spectral amplitudes at different periods, the hazard curves in terms of $P(Z > z | Y)$ can be used to obtain the complete spectrum with a constant probability of exceedance. A spectrum thus obtained is commonly termed as “uniform hazard spectrum”.

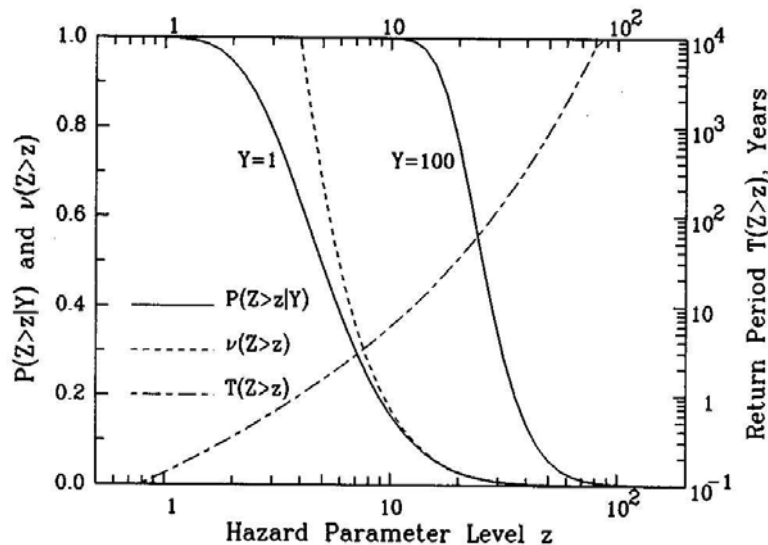


Fig. 1 The various commonly used representations of the seismic hazard curves

An alternative to the above analytical formulation for PSHA is the use of Monte Carlo simulation, in which a very long duration of earthquake catalog is generated from the probability density functions of magnitude, epicentral location, and the inter-event time for each source zone (e.g., Musson, 1999a; Smith, 2003). The amplitudes of the hazard parameter are then computed for all the earthquakes in the simulated catalog using a suitable probability density function for the residuals of the hazard parameter. The annual rate, $v(Z > z)$, is finally obtained by counting the number of years in which the maximum value of Z exceeds a specified value z , and by dividing it by the total duration (in years) of the catalog. This procedure generally takes much more computational time without any apparent advantage for the case of Poisson occurrences of earthquakes. However, it may sometimes be more convenient to use the simulation to account for the epistemic type of uncertainties (e.g., Musson, 1999b; Smith, 2003).

1. PSHA with Non-Poisson Earthquake Occurrences

The foregoing hazard formulation is based on the Poisson assumption for the occurrences of earthquakes in a region, which may be violated in that the earthquakes may be characterized by long as well as short-term temporal correlations. Under the Poisson assumption, the inter-event times follow an exponential distribution with a constant rate of occurrence. However, very large magnitude events in seismically active areas may follow a long-term cyclic behavior with time-varying rate of occurrence. Such events are required to be described by a real-time renewal model, wherein the occurrence rate is small soon after a large earthquake and increases with the lapse of time since the last such event (e.g., Rikitake, 1976; Vere-Jones and Ozaki, 1982; Sykes and Nishenko, 1984; Thacher, 1984; Nishenko and Buland, 1987; Jara and Rosenblueth, 1988). Several studies have implemented the time-dependent renewal models in the PSHA approach (e.g., Kameda and Takagi, 1981; Kiremidjian and Suzuki, 1987; Cornell and Winterstein, 1988; Lee, 1992; Todorovska, 1994). A renewal process that satisfies all the Poisson assumptions except the constant occurrence rate is called as a “non-homogeneous Poisson process”. It is required to be defined by a time-dependent occurrence rate, which can be obtained from the hazard function based on the probability distribution of inter-event times. The PSHA formulation of Equation (6) for the stationary Poisson processes is applicable to such events also if their average occurrence rate is obtained using a time-dependent hazard function (Lee, 1992).

The expression of Equation (6) is, however, not applicable to the events like aftershocks and sequential earthquakes, which are characterized by strong spatio-temporal correlation among themselves as well as with the main shock. To include the effect of the aftershocks it is necessary to decluster the available earthquake catalog using a suitable algorithm (e.g., Keilis-Borok et al., 1972; Reasenber, 1985; Maeda, 1996). Only the background seismicity is then described by the Poisson model, and the aftershocks by some other suitable model (e.g., Hagiwara, 1974; Utsu, 1984; Hong and Guo, 1995; Corral, 2004; Molchan, 2005). The aftershocks can also be described by a Poisson model with time-dependent occurrence rate defined by the modified Omori's law (Utsu et al., 1995). If no standard distribution is found suitable, an actual probability density function can be obtained by summation of a suitable kernel function with the observed interevent times (Silverman, 1986). A large number of earthquake catalogs of Y years duration are then simulated using Poisson distribution with constant occurrence rate for the mainshocks, and some of the above mentioned distributions for the aftershocks. Beauval et al. (2006) have proposed to simulate the combined seismicity using epidemic type aftershock sequence (Ogata, 1988). Next, the amplitudes of hazard parameters are simulated for all the earthquakes in these catalogs, from which the probability $P(Z > z|Y)$ is defined as the fraction of the total number of catalogs with the maximum value of the hazard parameter exceeding the value z .

A more efficient method to account for the effect of the aftershocks may perhaps be to generate only a single catalog of Y years duration for the aftershocks, and assume them to occur in a literal way. If $\eta(M_l, R_k|Y)$ is the total number of aftershocks in Y years in a small magnitude interval around central magnitude M_l and in a small distance interval around central distance R_k , the probability of $Z > z$ due to these events to occur in a deterministic way can be defined as (Anderson and Trifunac, 1977)

$$P^*(Z > z|Y) = 1 - \exp \left\{ - \sum_{k=1}^K \sum_{l=1}^L \ln(1 - q(Z > z|M_l, R_k)) \eta(M_l, R_k|Y) \right\} \quad (8)$$

By carrying out the hazard analysis for the declustered catalog of the main shocks using the expression of Equation (6), the combined probability of $Z > z$ from both the main earthquakes and the aftershocks can be defined as

$$P^+(Z > z|Y) = 1 - \exp\{-Y\nu(Z > z)\} \{1 - P^*(Z > z|Y)\} \quad (9)$$

This expression is expected to provide adequately conservative estimate of the hazard for practical applications. Further, the effect of any other type of events occurring in a literal way (e.g., earthquake prediction) can also be included in $P^*(Z > z|Y)$ by including their numbers in $\eta(M_i, R_k|Y)$.

2. Steps Involved in PSHA Approach

The four basic steps involved in the implementation of the foregoing PSHA formulation are depicted schematically in Figure 2. The first step is to identify and demarcate the boundaries of the various seismic sources. Normally, the sources within about 300 to 400 km (depending on the tectonic region) of the site are sufficient for this purpose. Each of the sources is divided into a large number of small-size elements, and the expected seismicity in a source is distributed suitably among all the elements. The epicenters of all the earthquakes in an element are assumed to occur at the geometric center of the element. The probability distribution function $G(R)$ of the source-to-site distance R is then defined using the distances to all the elements as illustrated in the top left panel in Figure 2.

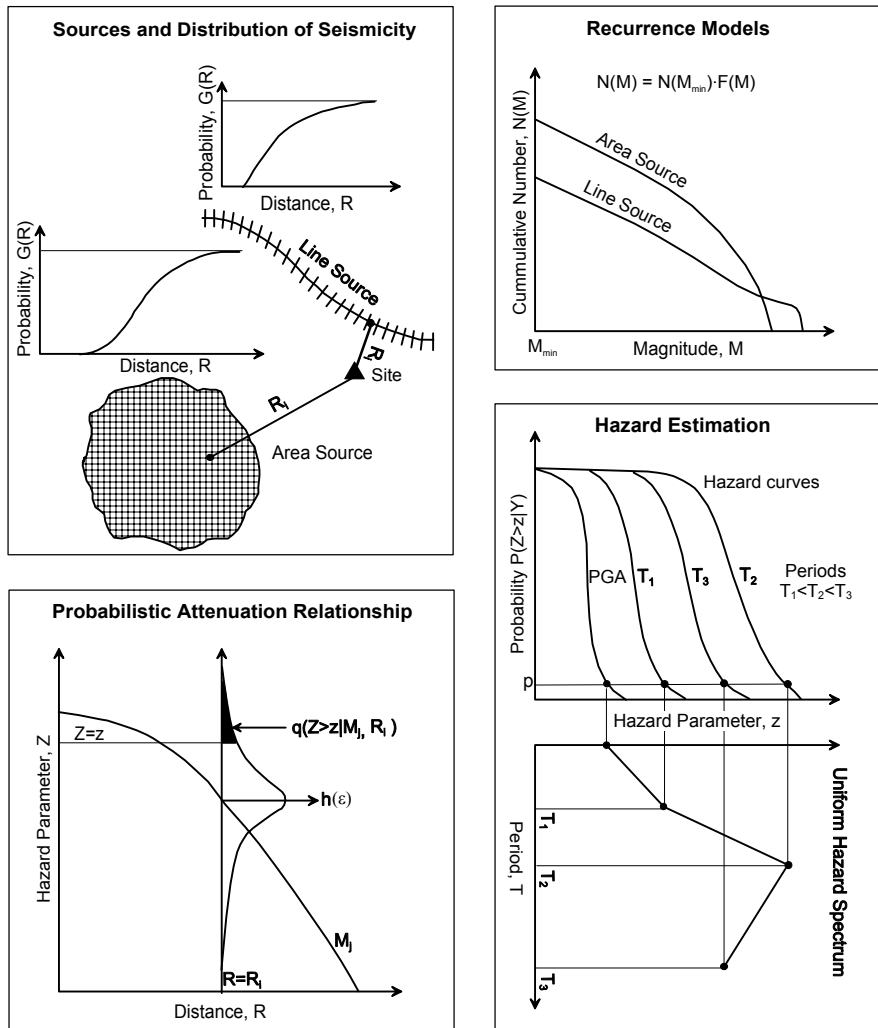


Fig. 2 Illustration of the basic elements of the PSHA formulation

To estimate the total number, $N_n(M_{min})$, of earthquakes with magnitude above M_{min} in a source zone, the frequency-magnitude relationship due to Gutenberg and Richter (1944) is defined for each

source zone in Step 2. A magnitude distribution function, $F(M)$, is also defined for each source to distribute these numbers among different magnitude intervals between a minimum magnitude, M_{\min} , and a maximum magnitude, M_{\max} . The exponentially decaying magnitude distribution is generally found suitable for area sources, whereas a characteristic earthquake model (Youngs and Coppersmith, 1985) is commonly used for individual faults. Alternatively, one may generate the synthetic catalogs for each source zone by estimating the parameters of the probability density functions for magnitude, occurrence time, and distance, defined from the available earthquake catalog.

A suitable attenuation relationship providing a probabilistic description of the amplitudes of the hazard parameter is required to be selected in Step 3. This should provide the mean or median estimate and the corresponding probability distribution of the residuals for specified earthquake magnitude, source-to-site distance, and site geologic and soil conditions. This is used to estimate the probability $q(Z > z|M, R)$ as illustrated in bottom left panel in Figure 2. A single attenuation relation may normally be applicable to all the source zones, but different relations may also be used, if necessary. For example, as in the northeast India, if a site is affected simultaneously by shallow crustal and deep subduction zone earthquakes, those are required to be described by different attenuation relations.

The fourth and the final step in the basic PSHA is to compute the hazard curves by integrating over all the magnitudes and distances in all the source zones. Several hazard curves are required to compute the uniform hazard spectra as shown in the bottom right panel in Figure 2 (Anderson and Trifunac, 1977). It may be noted that due to lack of exact scientific knowledge and inadequacy of available data, it may not be possible to establish the first three steps of PSHA in a unique way (Gupta, 2005). For example, there could be several possible choices for the definition of seismic source zones and distribution of distance, type of earthquake recurrence model and the maximum magnitude for each source, as well as for the attenuation relationship for the hazard parameter of interest. Due to these epistemic uncertainties, a large number of different sets of input with different weights may be possible in the PSHA, which can be identified by the logic-tree method (Kulkarni et al., 1984). A typical logic tree depicting the possible uncertainties in the various elements of the basic PSHA is shown in Figure 3. The basic principle to be followed in setting up a logic tree is that the branches emanating from a single node should cover only the physically realizable distinct possibilities, which may lead to significantly different estimate of the hazard.

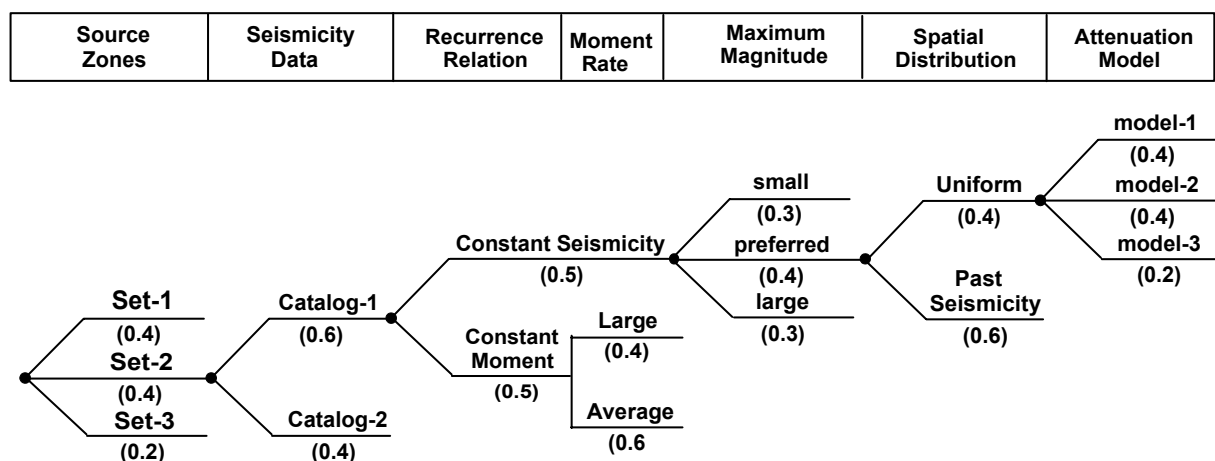


Fig. 3 A typical logic tree to account for the epistemic type of uncertainties in the PSHA formulation

In the logic tree of Figure 3, three sets of source zones with different weights may result from different interpretations and subjective judgments for a given database on seismotectonics and geological features in the region of interest. Two different sets with weights of 0.6 and 0.4 for the past earthquake catalog form the second element of the logic tree, which may result from the availability of several catalogs prepared by different organizations or from the use of different methods for homogenization of magnitudes in a given catalog. Two options with equal weights are shown for the two different types of recurrence relationships (to be explained in more detail later). Further, two different moment release rates

are considered in the recurrence relationship with constant moment rate. The next element in the logic tree is the maximum magnitude, for which three options as small, large and preferred with weights of 0.3, 0.3 and 0.4 are considered for each source zone. The spatial distribution of seismicity in a source zone is considered in two different ways as (a) uniform distribution, and (b) that based on spatially smoothed past seismicity. Finally, there are three different options for the ground motion attenuation model, with weights equal to 0.4, 0.3 and 0.3.

The example logic tree in Figure 3 has a total of 324 end branches, which are given by the product of the number of different options for each input element. The weight for an end branch is given by the product of the weights of all the intermediate branches leading to that branch. To account for the effect of the epistemic uncertainties, the basic PSHA is performed for all the combinations of the input leading to various end branches, and the resulting hazard curves are assigned the corresponding weights. These can be used to define the mean or the median hazard curve, as well as the hazard curves with desired confidence levels. However, at present, there is no widely accepted practice for the choice of the hazard curve for use in practical applications. The subsequent sections in the paper describe the first three steps providing the input for the fourth step in PSHA, and the possible epistemic uncertainties involved in each step. Illustrative example results are then presented for the uniform hazard Fourier and response spectra, and some other parameters of importance for characterizing the hazard.

SEISMIC SOURCES AND DISTANCE DISTRIBUTION

In an ideal situation, each source zone has to be an individual fault or fault segment. However, due to lack of knowledge about all the faults and wide dispersion of the epicenters of past earthquakes in relation to the known faults, broad area sources encompassing several faults are commonly used in real practice. Such seismic sources may be associated with the geological structures like uplifts, rifts, folds and volcanoes, which release the tectonic stresses and localize the seismic activity. Another type of seismic source used in practical applications is the “tectonic province”, which generally covers a large geographic area of diffused seismicity with no identifiable active faults or geological structures. The observed seismicity is sometimes seen to be highly concentrated in a very small area. This can be defined by a point source, if located far away from the site of interest. The source zones in a region are identified on the basis of some sort of geological, geophysical, geodetic and seismotectonic uniformity. The seismic potential of a source zone has to be distinctly different from the other adjacent sources. As the available data in most cases are not adequate, expert knowledge, detailed familiarity with the geology in the area, interpretation and judgment play important role in defining the seismic sources. The following four types of source zones can be considered sufficient for most of the practical PSHA applications.

Point Source: The seismicity in a point source is concentrated in a small area at very long distance from the site, and the fault with which it can be associated generally does not have to be identifiable. The geometric center of this small area is assumed to be the epicentral location for all the earthquakes expected to occur in the point source. Thus, the epicentral distance has a single fixed value in this case. However, the probability distribution of the closest distance to fault rupture can be defined assuming fault rupture to be a straight line and equally likely in all azimuthal directions (Anderson and Trifunac, 1977).

Line Source: In this type of source, the seismicity is related to a long fault and is usually, but not necessarily, assumed to be distributed uniformly over its entire length. Cornell (1968) considered a straight-line fault and provided an expression for the distance to a site from any point on the fault. Anderson and Trifunac (1977) included consideration of curved faults also. They divided the fault length L into N small elements of length ΔL each, and assumed the midpoint of each element to be the location of the epicenters. Each fault element is normally assigned the same weight, but non-uniform weights may also be assigned if different segments of the fault are known to be characterized by different levels of seismicity. The distances to all the fault elements with corresponding weights can be used to find the probability distribution of the epicentral distance from the site selected for the estimation of hazard. Anderson and Trifunac (1977) also proposed to consider the effect of fault rupture. For this purpose, if l is the fault rupture length for a given earthquake magnitude, the epicenters are assumed to be located sequentially in any continuous fault segment of length $(L-l)$. This obviates the need to account for the “unilateral” or “bilateral” nature of rupture propagation. The closest distance to the fault rupture is then estimated for each epicentral location for a given magnitude, and it is assigned a weight equal to that for

the corresponding epicentral location. All the closest distances with weights can be used to find the probability distribution of the closest distance.

Dipping Plane Source: Anderson and Trifunac (1977) introduced this type of source zone to describe the seismicity associated with a dipping fault plane. To find the probability distribution of the closest distance to fault rupture, let L be the total length and W the total width of the fault plane, and let l and w be the rupture length and width for a given earthquake magnitude. Then, similar to the line source, assuming the hypocenters to lie in any continuous area of length $(L-l)$ and width $(W-w)$ of the fault plane, one can find the closest distance to the fault rupture for each hypocentral location considered sequentially by dividing this area of the fault plane into small-size elements of length ΔL and width ΔW . The probability distribution of the closest distance to fault rupture can be obtained by assigning suitable weights to each hypocentral location, which may be uniform or non-uniform.

Area Source: This is the most widely used type of source zone in the PSHA studies. One has to use gross area sources when the observed seismicity is associated with a localizing geologic structure or a tectonic province. Cornell (1968) considered the area type of source defined by an annular area around the site of interest, which was generalized by Anderson and Trifunac (1977) to be of any arbitrary shape and located anywhere with respect to the site. One may refer to Gupta (2006a) for a very comprehensive description and examples on defining the area type of source zones for India and surrounding areas. The probability density of epicentral distances for an area source can be obtained easily by dividing the source zone into small-size elements and by assuming the epicenters to lie at the geometric center of each element. For uniform distribution of seismicity, each epicentral location is assigned a weight in proportion to the area of the corresponding element. One can also consider non-uniform distribution on the basis of the past seismicity with proper spatial smoothing (e.g., Frankel, 1995; Woo, 1996; Kagan and Jackson, 2000). Similar to the point source, the effect of fault rupture length may be accounted by assuming the rupture to be straight and equally likely in all the directions for each epicentral location (Anderson and Trifunac, 1977). If aftershocks are included separately in the analysis, those can be distributed around the main shocks according to an isotropic probability density function (e.g., Helmstetter et al., 2003; Zhuang et al., 2004).

To illustrate the application of the foregoing procedure for arriving at the probability distribution of the source-to-site distance, Figure 4 shows the hypothetical examples of two area sources A1 and A2 of diffused seismicity and two line sources L1 and L2 represented by vertical faults. To consider the effect of fault rupture, the rupture length and width are estimated using the empirical correlations due to Wells and Coppersmith (1994) for all fault types. Assuming the two faults to be characterized by the same seismic potential, the combined probability distribution function $G(R)$ of the distances for them has been obtained as shown in Figure 5. In general, one can combine any number of faults in this way. The results in Figure 5 represent the probability distributions without the fault rupture as well as with the fault rupture for magnitudes equal to 5.5, 6.5 and 7.5. Similar results for the area source A1 with uniform spatial distribution of seismicity are shown in Figure 6, whereas Figure 7 shows the results with spatial distribution based on the spatially averaged past seismicity. Compared to the distances without fault rupture considered, the closest distances to fault rupture are seen to have increasingly smaller values with increase in the magnitude for both the line and the area sources. Further, the probability distributions based on the spatial distribution of past seismicity for the area source have shifted towards longer distances compared to those for the uniformly distributed seismicity. The probability density function, $g(R)$, of source-to-site distance can be obtained by differentiating the distribution function $G(R)$. Thus the value of the integral over distance in Equation (3) can directly be written as $(G(R_i + \delta R_i) - G(R_i - \delta R_i))$.

As mentioned before, in practical applications, the seismic sources cannot be defined in a unique way (Bender, 1986). Some subjectivity is inevitable due to inadequacy or non-availability of the required data, and also due to possible alternative interpretations of the available data. Borders between source regions are usually not sharp with respect to seismic activity. Furthermore, the complete understanding of the long-term tectonic processes is generally lacking in many cases. To account for the uncertainties in defining the source zones, more than one set of source zones are required to be used as indicated in the logic tree diagram of Figure 3. If considerable seismicity is known to have occurred in the region of interest, the spatial distribution can also be based purely on the past seismicity with a zoneless approach (e.g., Frankel, 1995; Woo, 1996; Das et al., 2006). However, ignoring the distinct geological and seismological knowledge may not always be appropriate.

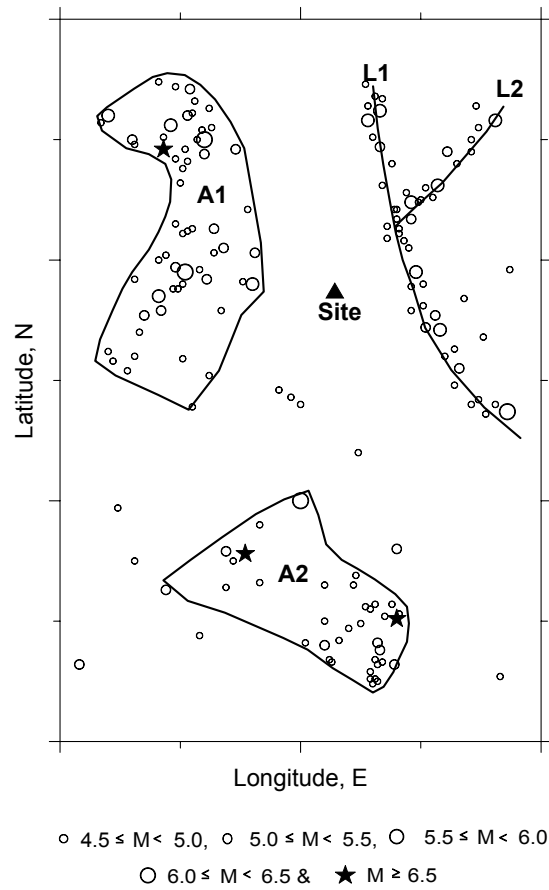


Fig. 4 Typical examples of the area and line types of seismic sources

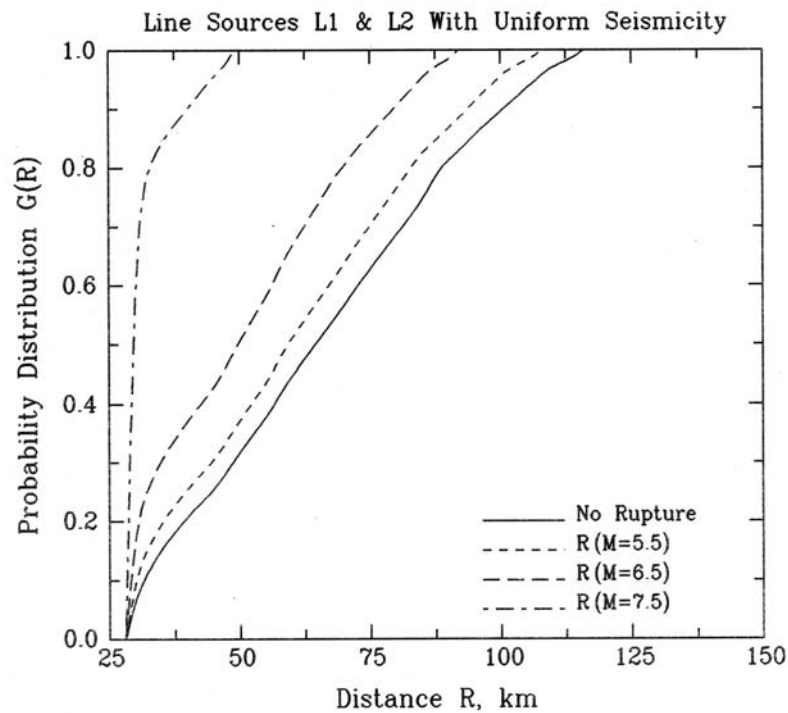


Fig. 5 Probability distribution of the source-to-site distance for the line sources in Figure 4 with uniform distribution of seismicity (the solid curve corresponds to the epicentral distance and the dashed curves to the closest distance to the fault rupture for different earthquake magnitudes)

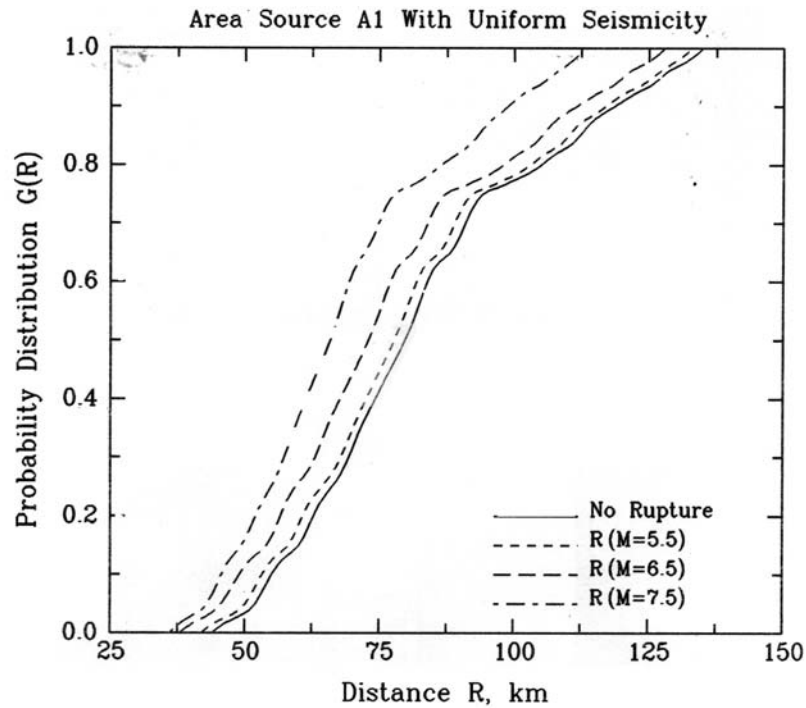


Fig. 6 Probability distribution of the source-to-site distance for the area source A1 in Figure 4 with uniform distribution of seismicity (the solid curve corresponds to the epicentral distance and the dashed curves to the closest distance to the fault rupture for different earthquake magnitudes)

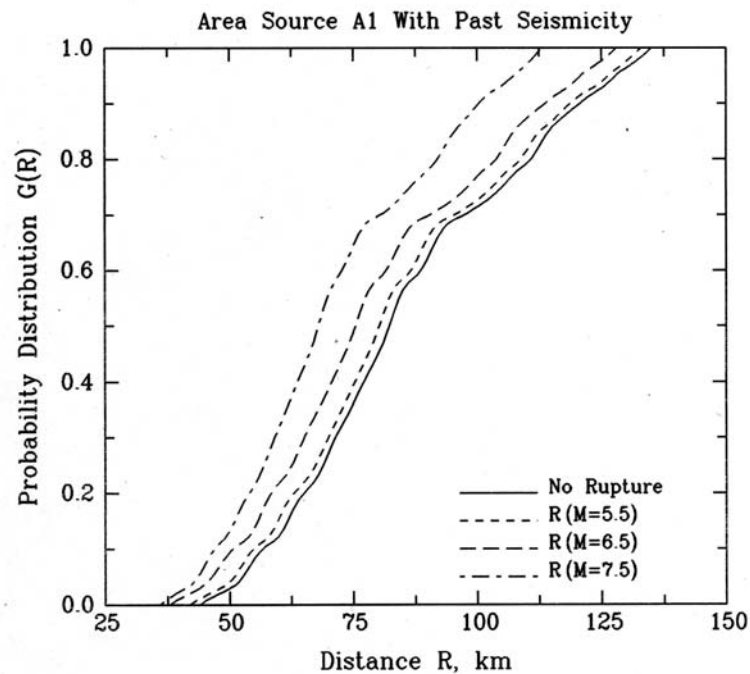


Fig. 7 Probability distribution of the source-to-site distance for the area source A1 in Figure 4 with non-uniform distribution of seismicity based on spatially averaged past seismicity with a correlation distance of 20 km

RECURRENCE RELATIONSHIP AND MAGNITUDE DISTRIBUTION

An earthquake recurrence relationship defines the annual occurrence rate, $N(M)$, of earthquakes with magnitude greater than or equal to M . Anagnos and Kiremidjian (1988) have reviewed the earthquake recurrence models for seismic hazard analysis. If $N(M_{\min})$ is the total number of earthquakes above a selected threshold magnitude M_{\min} , the number $N(M)$ can be written as a product of $N(M_{\min})$ and the probability distribution function, $F(M)$, of the earthquake magnitude. The negative of the derivative of $F(M)$ gives the density function, $f(M)$, of the magnitude. Thus, the recurrence relationship can be used to obtain directly the value of the $N_n(M_{\min})$ times the integral of $f(M)$ over the magnitude in Equation (3) as $(N_n(M_j - \delta M_j) - N_n(M_j + \delta M_j))$. Thus, along with the probability distribution of source-to-site distance, the occurrence rate, $\lambda_n(M_j, R_i)$, in Equation (3) can be obtained as

$$\lambda_n(M_j, R_i) = [N_n(M_j - \delta M_j) - N_n(M_j + \delta M_j)] [G(R_i + \delta R_i) - G(R_i - \delta R_i)] \quad (10)$$

Gutenberg and Richter (1944) have defined a form of the earthquake recurrence relationship as

$$\log N(M) = a - bM \quad (11)$$

In this relation, a and b are the constants specific to a seismic source, which are commonly estimated using available data on past earthquakes. To evaluate a and b , it is necessary to convert the available data into a common magnitude scale using suitable empirical conversion relations (e.g., Chung and Bernreuter, 1981; Utsu, 1982) and to remove the dependent events using an appropriate algorithm (e.g., Reasenbereg, 1985; Maeda, 1996; Hainzl et al., 2006). It is also necessary to account for the incompleteness of lower magnitude earthquakes, for which several methods have been proposed by different investigators (e.g., Stepp, 1972; Lee and Brillinger, 1979; Tinti and Mulargia, 1985; Rydelek and Sacks, 1989; Weimer and Wyss, 2000; Albarello et al., 2001). However, the procedure due to Stepp (1972) can be considered quite suitable and convenient for the practical hazard analysis applications. Then, the parameters a and b in Equation (11) can be evaluated by least squares, maximum likelihood (e.g., Weicher, 1980; Bender, 1983), or the maximum entropy (Dong et al., 1984) method, but the maximum likelihood method is, in general, considered quite appropriate.

By defining $\beta = b \ln 10$, the relationship of Equation (11) can be expressed in terms of the total number, $N(M_{\min})$, of earthquakes above a threshold magnitude M_{\min} and the probability distribution $F(M)$ as

$$N(M) = N(M_{\min}) \exp(-\beta(M - M_{\min})) \quad (12)$$

This relation does not impose an upper limit on the magnitude, whereas it is necessary to consider an upper bound magnitude, M_{\max} , in the practical applications. An abrupt truncation of the relation of Equation (12) at magnitude M_{\max} is not considered appropriate, as it will result in an infinitely large value of the density function at magnitude M_{\max} . This problem could be avoided if $N(M)$ tends asymptotically to zero as M reaches M_{\max} . For this purpose, the recurrence relationship has to be defined as (Page, 1968; Cornell and Vanmarcke, 1969)

$$N(M) = N(M_{\min}) \frac{\exp(-\beta(M - M_{\min})) - \exp(-\beta(M_{\max} - M_{\min}))}{1 - \exp(-\beta(M_{\max} - M_{\min}))} \quad (13)$$

Many investigators have suggested other alternative models with faster decay for larger magnitudes to avoid the estimation of the maximum magnitude, which generally suffers from large uncertainties (Bollinger et al., 1992; Kijko and Graham, 1998; Kijko, 2004). For example, Merz and Cornell (1973) used a quadratic model, and Lomnitz-Adler and Lomnitz (1979) suggested a double exponential model. Some more sophisticated models have been proposed by the later studies (e.g., Main and Burton, 1984; Main, 1996; Kagan, 1991, 1997; Burroughs and Tebbens, 2002).

The relation of Equation (13) is known as constant seismicity model, because it approaches zero asymptotically as M approaches M_{\max} , without altering the number of lower magnitude earthquakes. Thus, lowering of M_{\max} will result in lower moment release rate, if it is not compensated by increasing the total number of earthquakes, $N(M_{\min})$. By relating the seismic moment, M_0 , to the earthquake magnitude, M , with an empirical relation of the form, $\log M_0(M) = c + dM$ (Hanks and Kanamori, 1979), the relationship of Equation (13) can be used to obtain the following relationship for the moment release rate:

$$\dot{M}_0 = N(M_{\min}) \frac{\exp(-\beta(M_{\max} - M_{\min}))}{1 - \exp(-\beta(M_{\max} - M_{\min}))} M_0(M_{\max}) \frac{b}{d - b} \quad (14)$$

For a given value of \dot{M}_0 , the use of numbers $N(M_{\min})$ obtained from this expression in the recurrence relation of Equation (13) will ensure the conservation of moment release for varying M_{\max} . The moment rate \dot{M}_0 can be obtained from $\dot{M}_0 = \mu A \dot{u}$ (Brune, 1968), where \dot{u} is the geologically estimated long-term slip rate, A is the total fault rupture area, and μ is the shear modulus of the rock mass at the fault. The constraint imposed by fault slip rate allows the development of fault-specific recurrence relationship in regions where the historical seismicity data are only sufficient to establish the regional recurrence rate for small-to-moderate size earthquakes. The expression of Equation (14) can also be used to determine the upper bound magnitude from knowledge of the fault slip rate for given values of $N(M_{\min})$ and b from historical seismicity.

The exponentially decaying recurrence model of Equation (13) is able to describe the observed seismicity in non-fault-specific area type of sources. For many of the individual faults, the characteristic magnitude recurrence model due to Youngs and Coppersmith (1985) can describe better the behaviour of the observed seismicity. Certain faults are seen to generate repeatedly the maximum earthquakes in a narrow magnitude range with a much higher occurrence rate than that predicted by the recurrence relationship for smaller magnitudes on the same fault. This has given rise to the concept of characteristic earthquakes (Wesnousky et al., 1983; Schwartz and Coppersmith, 1984). The characteristic model assumes that more of the seismic energy is released by large magnitude events than that in the exponential model. The magnitude distribution for characteristic earthquakes is assumed to be uniform over the range $M_c = (M_{\max} - \Delta M_c)$ to M_{\max} . This is taken equal to the probability density at magnitude $M' = (M_c - \Delta M')$, as defined by the exponential distribution of Equation (13) fitted to the earthquake data up to the magnitude M_c . The characteristic recurrence model with $N(M_{\min})$ as the rate of non-characteristic earthquakes, that is the total number of earthquakes in the magnitude range, M_{\min} to M_c , can thus be written as (Youngs and Coppersmith, 1985)

$$N(M) = \begin{cases} N(M_{\min}) \frac{\exp(-\beta(M - M_{\min})) - \exp(-\beta(M_c - M_{\min}))}{1 - \exp(-\beta(M_c - M_{\min}))} + \dot{n}(M_c) \Delta M_c; & M_{\min} \leq M < M_c \\ \dot{n}(M_c)(M_{\max} - M); & M_c \leq M < M_{\max} \end{cases} \quad (15)$$

In this expression, $\dot{n}(M)$ is the probability density for the occurrence rate of the characteristic earthquakes, which is taken equal to the rate density at magnitude M' , as given by the exponential distribution for magnitudes up to M_c :

$$\dot{n}(M_c) = N(M_{\min}) \frac{\beta \exp(-\beta(M' - M_{\min}))}{1 - \exp(-\beta(M_c - M_{\min}))} \quad (16)$$

Similar to that for Equation (14), the moment release rate for the recurrence relationship of Equation (15) can be obtained as

$$\dot{M}_0 = N(M_{\min}) \frac{\exp(-\beta(M_c - M_{\min}))}{1 - \exp(-\beta(M_c - M_{\min}))} M_0(M_{\max}) \left[\frac{b}{d-b} 10^{-d\Delta M_c} + \frac{b \exp(\beta)(1 - 10^{-d\Delta M_c})}{d} \right] \quad (17)$$

The use of $N(M_{\min})$ obtained from this expression for a given \dot{M}_0 into Equation (15) provides the characteristic recurrence model with constant moment release rate.

For the purpose of illustration, Figure 8 shows the abruptly truncated exponential model, asymptotically decaying exponential model, and the characteristic earthquake recurrence model for a moment release rate of $\dot{M}_0 = 1.0 \times 10^{25}$ dyne-cm/year, $M_{\min} = 3.8$, and $M_{\max} = 8.0$. For the characteristic model, ΔM_c and $\Delta M'$ are both taken as 0.8. As mentioned before, for a fixed \dot{M}_0 , a change in M_{\max} causes a change in the number of all the lower magnitude earthquakes in all the recurrence models. On the other hand, for a fixed total number $N(M_{\min})$ in the constant seismicity models, the change in M_{\max} causes a change in the recurrence curves in the vicinity of magnitude M_{\max} only. These characteristics are illustrated for the asymptotically decaying recurrence model in Figure 9, which shows the results for $M_{\max} = 6.0, 7.0$ and 8.0 . For the constant seismicity case, the number $N(M_{\min})$ is kept fixed and equal to the number for $M_{\max} = 7.0$ in the constant moment case. The truncated exponential and the characteristic models will also show similar behaviour.

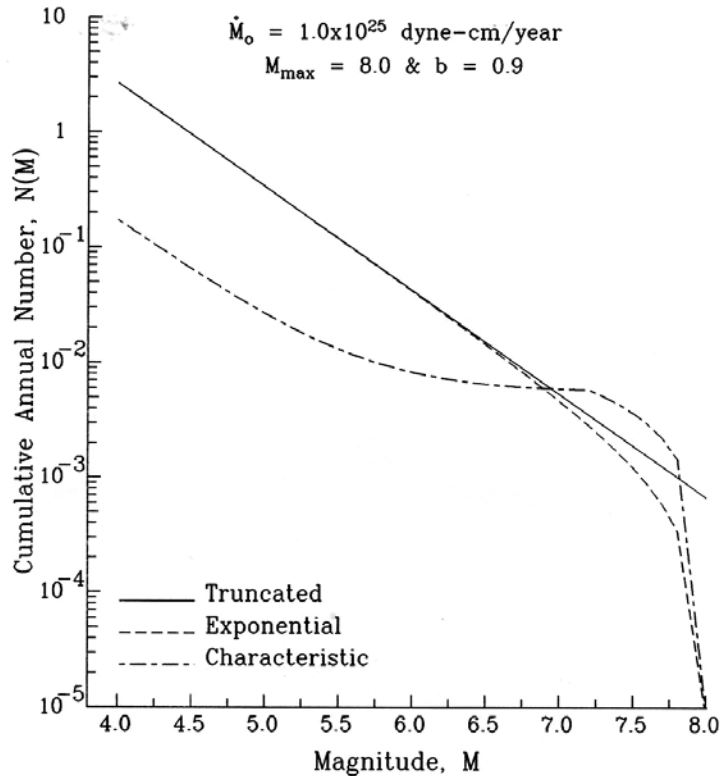


Fig. 8 Comparison of three commonly used models of the recurrence relationship with the constant-moment-release constraint

From the above description it is apparent that the specification of the magnitude-recurrence relation for a source zone may be associated with considerable epistemic uncertainties. There may be uncertainties in use of the exponential, characteristic, or some other model, and also as to the use of the constant-seismicity- or the constant-moment-release-rate model. The choice of the lower threshold and the maximum magnitudes, as well as the estimation of the moment release rate, may also be associated with some uncertainties. Further, depending on the empirical conversion relations used for homogenization of magnitude, criteria adopted for removal of dependent events, and the method used for identification of the

periods of completeness for different magnitude ranges, the recurrence parameters a and b may vary substantially. Lastly, all the other things being the same, the values of a and b may also vary with the method of estimation (e.g., least squares, maximum likelihood, or maximum entropy method). To account for the epistemic uncertainties in the recurrence relationship by the logic-tree approach, one may have to deal with several recurrence models with parameters varying over wide ranges as shown in Figure 3. However, rather than considering a large number of separate options, Lee and Trifunac (1985) have proposed to account for the random uncertainties in parameters a and b and that in M_{\max} by using a Bayesian estimate $N(M)$, obtained by multiplying the expected value of $N(M)$ with the probability of $M \leq M_{\max}$.

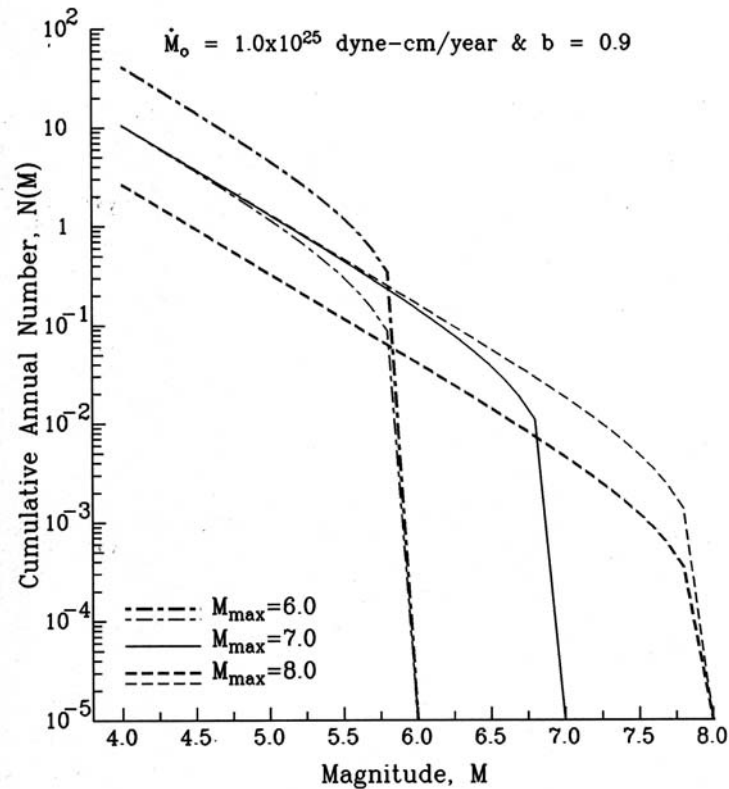


Fig. 9 Comparison of the exponential recurrence model with constant-seismicity-rate (thin curves) and constant-moment-release-rate (thick curves) constraints

ATTENUATION AND SCALING RELATIONSHIPS

An attenuation or scaling relationship is required to obtain the probability, $q(Z > z | M, R)$, of exceeding a specified value, z , of a hazard parameter, Z , due to an earthquake of magnitude M at a source-to-site distance R . A median attenuation or scaling relationship is commonly developed by fitting a simple equation in terms of a limited number of earthquake and site parameters to the z -values observed during past earthquakes. For areas deficient in recorded data, simulated data using seismological source model approach have been also used to develop the attenuation relations for some of the hazard parameters (e.g., Huang and Huo, 1997; Gregor et al., 2002). A median attenuation relation is seen to be associated with large random uncertainties in that the observed or simulated z values are generally scattered widely. This scattering can mainly be attributed to not considering the dependence on several parameters (e.g., stress-drop, radiation pattern), possible random errors in the values of the governing parameters (e.g., magnitude, distance, and site condition), and to the use of a simplified and idealized form for the attenuation equation. To quantify the random scattering in the data, the residuals between the observed values and the corresponding model predictions are defined by suitable probability distributions, due to which the attenuation relations become probabilistic in nature.

The random (aleatory) uncertainties in the attenuation and scaling relations can, in principle, be reduced to some extent by incorporating additional governing parameters in the model and by using more complicated functional forms for the attenuation equation. But in reality, it may not be possible to define accurately the values of the additional parameters and to get stable estimates of the added regression coefficients involved. Thus, the reduction in the aleatory uncertainties may be offset by an increase in the epistemic type of uncertainties in specifying the values of the input governing parameters and by inaccuracies in estimating the regression coefficients. Thus, unlike other input quantities to the PSHA, the classification of uncertainties as aleatory and epistemic in case of attenuation relationships is somewhat dubious (Atkinson and Boore, 1997; Toro et al., 1997). Therefore, only simple attenuation models with a limited number of parameters are used in practical applications. However, due to a limited database available in most real situations, the estimated mean or median relationship as well as the distribution of the residuals is generally associated with significant epistemic uncertainties. As these uncertainties cannot be defined directly from the database, several different attenuation relations with appropriate weights are used to account for their effects in practical applications (e.g., Sabetta et al., 2005; Bommer et al., 2005). This section presents a brief description of the attenuation and scaling relationships for several hazard parameters of importance to the safety of man-made structures.

1. Ground Motion Amplitudes

A complete description of the ground motion for earthquake engineering applications is provided by the acceleration time-histories for three orthogonal components of motion. However, it is not feasible to develop the attenuation relations directly for the acceleration time-histories. Therefore, the commonly used engineering practice is to synthesize the acceleration time-histories compatible to the response spectra (e.g., Tsai, 1972; Gasparini and Vanmarcke, 1976; Silva and Lee, 1987; Lee and Trifunac, 1989; Gupta and Joshi, 1993; Abrahamson, 1998). In this sense, the response spectrum is commonly considered to represent the intensity of ground motion, though in reality it represents the maximum response of a single-degree-of-freedom oscillator. An early approach to obtain the response spectra was to scale a normalized spectral shape (e.g., Seed et al., 1976; Mohraz, 1976; Newmark and Hall, 1982) by the peak ground acceleration (PGA), which is equivalent to the zero-period amplitude of the absolute acceleration spectrum. Most of the attenuation relations in the past were therefore developed for the PGA only. However, it is now well recognized that a normalized spectral shape is unable to represent the dependence on earthquake magnitude, distance, and site condition in a realistic way (Trifunac, 1992; Gupta, 2002b). A more appropriate method to estimate the response spectrum ordinates at different natural periods is to use the empirical attenuation relationships directly for the spectral amplitudes at each natural period (Trifunac, 1976b, 1978). Most of the recent attenuation relations have been, therefore, developed for both the peak acceleration and the response spectrum amplitudes at different natural periods or frequencies (Douglas, 2003). Alternatively, the acceleration time-histories can also be synthesized from the Fourier amplitude spectrum (Trifunac, 1971; Wong and Trifunac, 1979). Though some empirical attenuation relations are available for the Fourier spectrum amplitudes at different wave-periods or frequencies (e.g., Trifunac, 1976b, 1987, 1989; McGuire, 1978), the prediction of the Fourier amplitude spectra is more commonly based on the source-model approach (e.g., Petukhin et al., 1999; Sokolov et al., 2000).

The available studies on frequency-dependent attenuation relations have used widely differing functional forms, different types of earthquake magnitude (moment, surface-wave, or body-wave), and different measures of the source-to-site distance (epicentral, hypocentral, closest distance to the rupture surface, or closest distance to the surface projection of the rupture plane). Also, the site condition in different relations has been defined in widely varying ways, ranging from qualitative descriptions of the near-surface material to quantitative definitions based on shear-wave velocity. Nonlinear soil behaviour has been also accounted in some of the relations (Tsai, 2000; Atkinson and Boore, 2003). Following the work of Trifunac (1987) for the Fourier amplitude spectrum, Lee (1987) developed the attenuation relations for response spectrum amplitudes considering the effects of both local geological condition up to depths of a few kilometers and site soil condition up to 200 m depth. These relations have also accounted at each frequency the magnitude and distance saturation effects as well as the variation of geometrical spreading with distance, and they are thus considered to possess the properties desired on physical grounds. Many of the available relations lack in some or the other of these fundamental requirements, and hence the future developments are required to take these into account.

A site-specific estimation of design ground motion needs the attenuation relations based on the strong-motion data recorded in the target area of interest. However, the required data is either lacking or

inadequate for many parts of the world. It thus becomes necessary to use the relations based on the global data or those developed for some other regions. Due to strong regional dependence, the selection of suitable attenuation relations from the available relations for other host regions is not a straightforward task. Several different relations are thus required to be used with appropriate weights as indicated in the logic-tree diagram of Figure 3. The uncertainties arising due to the inability of defining the ground motion attenuation model for an area in a unique way is found to be a major source of uncertainty in the seismic hazard assessment (Stepp et al., 2001, Sabetta et al., 2005).

The initial selection of the ground motion relations is normally based on the geo-scientific criteria like similarities in the tectonic setting (e.g., compressional or extensional regime), source characteristics (e.g., stress drop), and the anelastic attenuation modeled by the Q -factor. As this selection may suffer from considerable personal judgment and biases, many investigators have proposed simple numerical criteria for updating and ranking the initial choice. The simplest update may be to adjust a selected attenuation relation by a constant scale factor to have closer fitting to the strong-motion data for the target region, if available. The hybrid empirical approach due to Campbell (2003, 2004) may provide a more comprehensive way for the purpose. Scherbaum et al. (2004) have proposed simple numerical criteria using available limited data to rank the selected and updated attenuation relations for their appropriateness for the target region, the application of which has been illustrated in some other studies (Cotton et al., 2006; Douglas et al., 2006). The ranking methodology has been also used to assign branch weights in the logic-tree for the ground attenuation model (Scherbaum et al., 2005; Bommer et al., 2005). However, the updating and ranking is generally based on very limited data from one or two earthquakes, which may sometimes lead to highly unrealistic results. Instead, one may impose higher confidence in a relation based on a very large worldwide database and accounting for the various dependencies in a physically realistic way.

In addition to updating for the fundamental differences between the target and the host regions, to combine several attenuation relations in a logic-tree, it is also necessary to make them uniform with respect to the definitions of the various governing parameters (Bommer et al., 2005). The effect of such conversions for the type of horizontal component of ground motion, magnitude scale, source-to-site distance, site condition, and the type of faulting, on the response spectral amplitudes computed from five typical attenuation relations (Abrahamson and Silva, 1997; Boore et al., 1997; Sabetta and Pugliese, 1996; Lussou et al., 2001; Berge-Thierry et al., 2003) is illustrated in Figure 10. The upper left panel in this figure shows the median spectra on the rock type of site condition as obtained by taking the distance as 5 km and magnitude as 5.0 in the original attenuation relations, with no regard to their compatibility. The lower left panel shows the corresponding spectra after converting all the relations into moment magnitude, shortest distance to the surface projection of fault rupture, and the geometric mean of the two horizontal components. For the relations that include the style of faulting as a predictor variable, the effect has been removed by assuming a reverse faulting with dip angle of 50° . The results in Figure 10 indicate that the homogenization of the attenuation equations may help in reducing the epistemic uncertainty to some extent. However, the reliability and applicability of such conversions to a target area of interest cannot generally be established. Further, Bommer et al. (2005) have proposed to carry across the random variability associated with the empirical conversion relations used for homogenization by enhancing the aleatory uncertainties in the original ground-motion relations, which cannot be considered appropriate on physical grounds. The upper and lower right panels in Figure 10 show the comparison between the original and the enhanced standard deviations for the adjusted attenuation equations.

On physical grounds, the conversion of the type of governing parameters in an attenuation equation should sometimes also help in reducing the errors. For example, the attenuation relationships in terms of the closest distance to fault rupture, R_{rup} , are expected to be characterized by smaller dispersion than those in terms of the epicentral distance, R_{epic} . Thus, enhancing the standard deviation for an equation adjusted from R_{epic} to R_{rup} is not appropriate. Similarly, an attenuation relationship for the random horizontal component is expected to show larger scattering than that in terms of the geometric mean of the two horizontal components, and enhancing the variability for such a conversion is also not reasonable. In addition, the transfer of aleatory component of the epistemic type of uncertainties into the aleatory type of uncertainties in the basic PSHA is not in order, because the effects of the epistemic and the aleatory uncertainties are accounted differently. Thus, it is proposed that the aleatory uncertainties in the conversion relations for various parameters in the attenuation relations be accounted by using the

expected estimate of the converted attenuation relationship without any change in the original aleatory uncertainties. However, if several different conversion relations are the likely candidates, one may consider additional branches in the logic tree for each set of conversion relations.

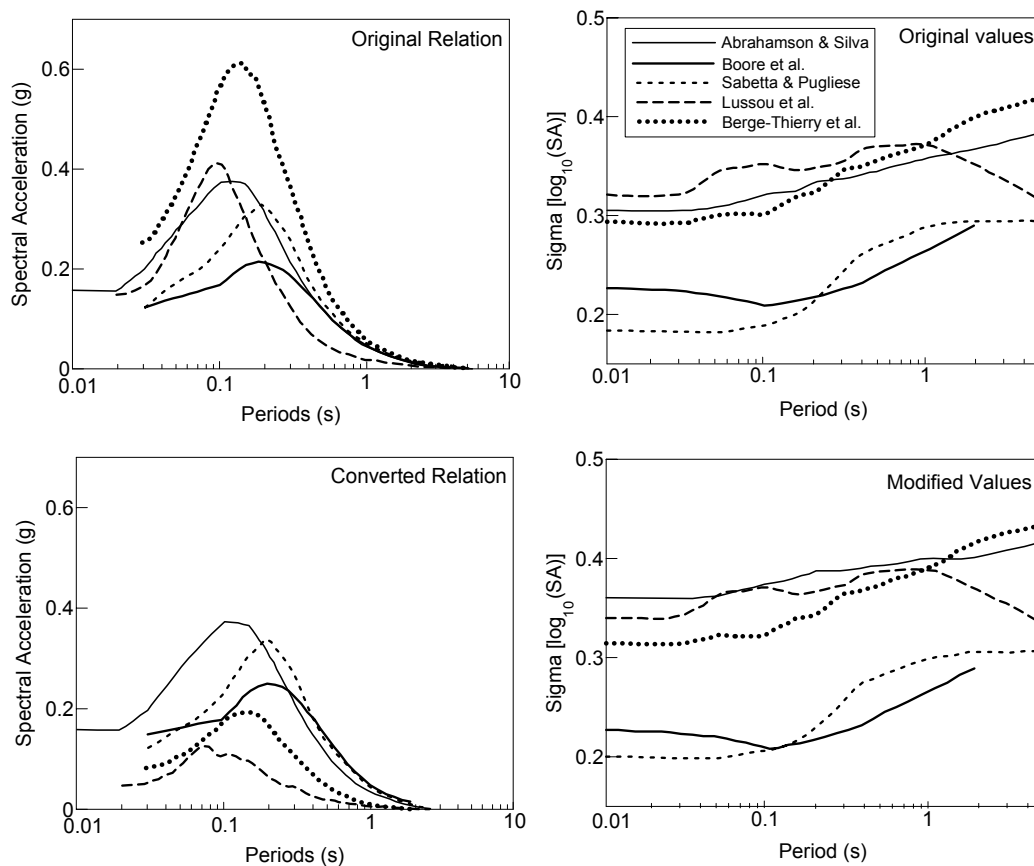


Fig. 10 Comparison of the original median acceleration response spectra and associated standard deviations obtained from five selected attenuation relations (upper panels) with those obtained after modifying the relations for the compatibility of various governing parameters (lower panels) (the results correspond to a magnitude 5.0 earthquake at a distance of 5 km and rock type of site condition; after Bommer et al., 2005)

2. Strong-Motion Duration

In addition to the amplitudes, it is also necessary to define the duration of strong motion to estimate the potential of an earthquake to cause damage to the structure at a site (Jeong and Iwan, 1988; Anderson and Bertero, 1991) and ground failure by liquefaction (Todorovska and Trifunac, 1999). However, for use in different applications, the strong-motion duration is defined in several different ways (Theofanopoulos and Watabe, 1989; Kawashima and Aizawa, 1989; Bommer and Martinez-Pereira, 1999). Also, duration depends on frequency (Bolt, 1973), and frequency-dependent duration is required for assigning the duration to generate the synthetic accelerograms (Wong and Trifunac, 1979; Gupta and Joshi, 1993). Some studies (Mohraz and Peng, 1989; Gupta and Trifunac, 1998) have also introduced the role of structural frequency and damping into the definition of duration. Most of the available studies are however concerned only with proposing new definitions of the duration, rather than developing prediction models needed for the PSHA studies.

The early studies on developing the prediction models for frequency-dependent duration are due to Trifunac and Westermo (1976, 1977, 1982). They defined the duration in several frequency bands as the sum of the separate strong-motion portions during which the Husid plot has the steepest slope and gains 90% of its final value. Novikova and Trifunac (1993, 1994a, 1994b, 1995) updated the early studies by using a much bigger database of uniformly processed accelerograms for the California region. They presented a family of prediction models, which can be used straightaway in seismic hazard analysis. Their

fundamental model for the durations of horizontal and vertical components is defined in terms of magnitude M and epicentral distance Δ , for a frequency band with central frequency f as

$$dur^{(h)/(v)}(f) = a_1^{(h)/(v)}(f) + a_2(f)M + a_3(f)M^2 + a_4(f)\Delta \quad (18)$$

In this expression, if M is less than $M_{\min}(f) = -a_2(f)/(2a_3(f))$, it is replaced by $M_{\min}(f)$. To consider the effects of depth of sediments at the site, characteristic horizontal distance, R , to the nearest rock outcrop capable of producing reflections, and the angle, ϕ , subtended at the site by the surface of the reflecting rock, Novikova and Trifunac (1993) obtained some more comprehensive models by incorporating additional terms in the basic relationship of Equation (18).

Two relatively simple models also have been presented by considering the effect of only the depth of sediments at the site in one model, and that of only R and ϕ in the other model. Another simplified model, which may find wider practical applications, has been defined by adding the following two terms to characterize the site geology in a qualitative way:

$$a_{13}(f)S^{(1)} + a_{14}(f)S^{(0)} \quad (19)$$

where $S^{(1)}$ and $S^{(0)}$ are the index variables for the site geological condition defined as

$$S^{(1)} = \begin{cases} 1; & \text{Intermediate or undefinable} \\ & \text{type of site geology} \\ 0; & \text{Otherwise} \end{cases} \quad \text{and} \quad S^{(0)} = \begin{cases} 1; & \text{Sites over deep} \\ & \text{sediments} \\ 0; & \text{Otherwise} \end{cases} \quad (20)$$

Another useful model considering the effects of both the local geological and site soil conditions is obtained by adding the following terms to the fundamental model of Equation (18):

$$a_{15}(f)(2-s) + a_{11}(f)S_L^{(1)} + a_{12}(f)S_L^{(2)} \quad (21)$$

In this expression, parameter s defines the site geological condition ($s = 2$ for basement rock, 0 for deep sediments, and 1 for intermediate or indefinable type of sites), and $S_L^{(1)}$ and $S_L^{(2)}$ are the index variables for the local soil condition defined as

$$S_L^{(1)} = \begin{cases} 1; & \text{Stiff soil sites} \\ 0; & \text{Otherwise} \end{cases} \quad \text{and} \quad S_L^{(2)} = \begin{cases} 1; & \text{Deep soil sites} \\ 0; & \text{Otherwise} \end{cases} \quad (22)$$

The values of the coefficients $a_1^{(h)}(f)$, $a_1^{(v)}(h)$, $a_2(f)$, $a_3(f)$, and $a_4(f)$ in Equation (18), as well as the other coefficients in Equations (19)–(22), have been estimated by Novikova and Trifunac (1993) for 12-frequency bands with central frequencies ranging from 0.075 to 21.0 Hz. To define the probability of exceeding a specified value, $dur(f)$, of the strong motion duration in a particular frequency band, Novikova and Trifunac (1993) have also presented probability density function for the relative residuals, $\varepsilon = dur(f)/dur^{\text{model}}(f)$, where $dur^{\text{model}}(f)$ is the duration estimated from a predictive model for specified M , Δ , and site condition. This density function is given by

$$p(\varepsilon) = \frac{1}{\eta} \frac{\varepsilon^b}{a + \varepsilon^c}; \quad \eta = a^{\frac{b+1}{c}-1} \frac{\pi}{c} \left[\sin \frac{(b+1)\pi}{c} \right]^{-1} \quad (23)$$

The coefficients a , b and c in this relationship are also estimated by Novikova and Trifunac (1993) for the various predictive models by using the observed values of ε for each of the 12 frequency bands. The probability, $q(dur(f)|M, \Delta)$, of exceeding a specified duration, $dur(f)$, due to magnitude M at distance Δ can thus be obtained using the density function of Equation (23) as

$$q(dur(f)|M, \Delta) = 1 - \int_0^{\varepsilon} p(x) dx \quad (24)$$

This can be used to carry out the PSHA studies for the strong motion duration in different frequency-bands for the same description of the seismicity as that used for the ground motion evaluation.

3. Critical SPT Value for Initiation of Liquefaction

Initiation of liquefaction in water-saturated cohesionless sands occurs when the effective stress in the ground is reduced to zero. The methodology of probabilistic seismic hazard analysis can also be used to estimate the likelihood of liquefaction at a site during specified exposure time. The basis for this is provided by the study of Trifunac (1995) on the occurrence or nonoccurrence of liquefaction due to specified earthquake magnitude and distance. Using 90 worldwide observations, Trifunac (1995) has proposed five different empirical models to obtain the standard penetration test (SPT) value, \bar{N} , corrected for the overburden pressure σ_0 , that separates on average the observed cases of liquefaction from those of no liquefaction. These models are based on the seismic energy and are functions of σ_0 and the earthquake magnitude, distance and site geological condition. The model prediction can be viewed as a critical value, \bar{N}_{crit} , of \bar{N} for liquefaction to occur under specified conditions. Liquefaction will occur at a site if the actual \bar{N} value is smaller than the estimated \bar{N}_{crit} value.

As the ground motion and the site characterization are associated with many inherent uncertainties, the observed data points are found scattered randomly around the model predictions. To consider the points in the database that violated the prediction, Trifunac (1995) defined the probability of liquefaction using a Gaussian probability distribution as the probability of \bar{N}_{crit} being greater than the actual \bar{N} value:

$$\text{Prob}\{\bar{N}_{crit} > \bar{N}\} = \frac{1}{\sqrt{2\pi}\sigma_{\bar{N}}} \int_{\bar{N}}^{\infty} \exp\left\{-\frac{1}{2}\left(\frac{x - \mu_{\bar{N}}}{\sigma_{\bar{N}}}\right)^2\right\} dx \quad (25)$$

In this equation, $\mu_{\bar{N}}$ is the mean value and $\sigma_{\bar{N}}$ the standard deviation of the corrected SPT value from the model. From the “ $v^2 \cdot dur$ ” model of Trifunac (1995), $\mu_{\bar{N}}$ can be obtained as

$$\mu_{\bar{N}} = 87.3 \left(\frac{v_{max}^2 \cdot dur}{\sigma_0^{3/2}} \right)^{1/3.4} + 0.95 \quad (26)$$

In this expression, v_{max} is the peak ground velocity in cm/sec, which can be obtained from the following empirical relationship (Trifunac, 1976a):

$$\log_{10} v_{max} = \log_{10} A_0(R) + 3.059M - 0.201M^2 - 0.134s - 9.8135 \quad (27)$$

Here, $\log_{10} A_0(R)$ is the Richter's attenuation factor, and s takes values of 0, 1 and 2 to define the local geological condition as explained earlier. Also, from the relationships due to Novikova and Trifunac (1993), the strong-motion duration dur in Equation (27) can be defined as

$$dur = 7.8 - 3.86M + 0.57M^2 + 0.07R + 1.14(-s/2) \quad (28)$$

For the model of Equation (26), the value of $\sigma_{\bar{N}}$ is specified to be 5.5 (Trifunac, 1995). Thus, the probability of Equation (25) is equivalent to the conditional probability that liquefaction will occur at a site due to earthquake magnitude M at distance R . This provides a basis to carry out the PSHA to evaluate the average return period of occurrence of liquefaction at a site with given \bar{N} and σ_0 values. Equivalently, one can estimate the probability that liquefaction will occur during a specified exposure period. For a given value of σ_0 at the site, it is also possible to estimate with a specified confidence level the value of \bar{N} for which liquefaction may occur during a given exposure period.

4. Permanent Fault Displacement

In addition to the ground motion amplitudes and the strong-motion duration, the estimation of hazard in terms of the permanent dislocations across faults may be required for situations like bridges, tunnels, aqueducts, and water and gas lines crossing over faults. For this purpose, it is necessary to predict the probability of exceeding a specified value of displacement due to a given magnitude of earthquake at a

given location on a fault plane. Unlike for other hazard parameters, the earthquakes on the fault of interest only are to be considered for assessing the hazard of permanent displacement. Further, one has to consider only those earthquakes on the fault, which will be able to cause fault rupture reaching the ground surface as well as the site on the fault. Thus, the conditional probability that the displacement at a site on the fault will exceed a specified value, d , due to an earthquake of magnitude M_j at distance R_i on the fault can be defined as

$$q(D > d | M_j, R_i) = \text{Prob}\{D > d | M_j, R_i\} \times \text{Prob}(\text{Rupture breaks the ground surface}) \times \text{Prob}(\text{Rupture extends horizontally to the site}) \quad (29)$$

Depending on the assumptions regarding the distribution of earthquake locations on the fault plane and the direction of rupture (unilateral or bilateral), there may be several different ways to define the second and third probabilities on the right hand side of the above expression. For a fault plane with given length and width, Todorovska et al. (2007) have proposed a simple way to define these probabilities using the mean values and the standard deviations of rupture width and rupture length defined by empirical equations in terms of earthquake magnitude.

The mean value μ and the standard deviation σ of the logarithm of the displacement d are defined by Todorovska et al. (2007) by the following empirical relationship:

$$\mu = M - 2.2470 \log_{10}(\Delta | L_R) + 0.6489M + 0.0518 \times 2 - 0.3407\nu - 2.9850 - 0.1369M^2 - 0.0306 + \log_{10} 2 - 0.0090; \quad \sigma = 0.3975 \quad (30)$$

where M is the earthquake magnitude, Δ is the representative source-to-station distance, L_R is the rupture length, and ν represents the direction of motion ($\nu = 0$ for horizontal and 1 for vertical component). The distance Δ depends on both the physical distance and the size of the rupture as

$$\Delta = S \left(\ln \frac{R^2 + H_R^2 + S^2}{R^2 + H_R^2 + S_0^2} \right)^{-1/2} \quad (31)$$

where H_R is the focal depth, S is the source dimension, and S_0 is the source coherence radius. To estimate μ from Equation (30), R is taken as zero, and H_R is taken as the depth to the center of the fault width. The source dimension, S , has been defined by Todorovska et al. (2007) as

$$S = \begin{cases} 0.0729(5.5 - M) \times 10^{0.5M}; & M < 4.5 \\ -25.34 + 8.51M; & 4.5 \leq M \leq 7.25 \end{cases} \quad (32)$$

S_0 is proposed to be taken as half of the smaller of S and S_f , with S_f defined as

$$S_f = \begin{cases} L_R(M); & M < 3.5 \\ L_R(M) / 2.2 + W_R(M) / 6; & 3.5 \leq M \leq 7.0 \\ L_R(M_{\max}) / 2.2 + W_R(M_{\max}) / 6; & M > M_{\max} = 7.0 \end{cases} \quad (33)$$

where $L_R(M)$ and $W_R(M)$ are the median values of the fault rupture length and width for magnitude M . Using the μ and σ values obtained as above, Todorovska et al. (2007) have approximated the probability, $\text{Prob}\{D > d | M_j, R_i\}$, by a lognormal distribution as

$$\text{Prob}\{D > d | M_j, R_i\} = \frac{1}{\sqrt{2\pi}\sigma} \int_{\log d}^{\infty} \exp\left\{-\frac{1}{2}\left(\frac{\log x - \mu}{\sigma}\right)^2\right\} dx \quad (34)$$

It is thus possible to compute the probabilistic hazard of permanent dislocation at a site on a fault for a given description of the expected seismicity.

SENSITIVITY ANALYSIS OF PSHA

To illustrate the sensitivity of the PSHA results to the possible aleatory uncertainties in the various input models and their parameters, example results are computed for a hypothetical seismic source, i.e., a 200 km long straight line vertical fault, with the site located at a closest distance of 10 km from the mid-point of the fault trace. To define the seismicity of this fault, the preferred value of the moment release rate \dot{M}_0 is assumed to be 1.0×10^{25} dyne-cm/year, that of the b value as 0.9, and that of the maximum magnitude M_{\max} as 8.0. To study the sensitivity of the hazard estimation, the values of the source parameters are varied around the preferred values as assumed. The hazard is evaluated in the form of uniform hazard Fourier spectra (UHFS) for an exposure period of 100 years, using the residual two-step mag-site-soil model due to Trifunac (1987). In this model, the Fourier amplitude spectrum, $FS(T)$, at each of several wave-periods, T , is defined by an empirical scaling relationship in terms of earthquake magnitude M , the representative source-to-site distance Δ , site geologic condition defined by the parameter s ($= 0$ for deep sediments, 2 for basement rock, and 1 for difficult-to-classify or intermediate type of sites), and site soil condition defined by the parameter S_L ($= 0$ for rock, 1 for stiff, and 2 for deep soil sites). All the results are computed for a focal depth of 10 km. It may be mentioned that the generality of the results will not be affected due to these assumptions regarding the seismic source and its seismicity. Further, only the median estimates of UHFS are presented for the purpose of illustration, because the results for other confidence levels will qualitatively show similar behaviour.

First of all, Figure 11 presents the UHFS for the preferred values of all the source parameters and the seismicity corresponding to three different types of recurrence models, viz., the truncated, exponential, and characteristic models. For each of the models, the estimated seismicity is distributed uniformly over the complete fault length without considering the effect of fault rupture length for different magnitudes. The spectra for the truncated and the exponential models are seen to be quite close, and both are substantially higher than that for the characteristic model. Thus, the spectral amplitudes are seen to be dominated by the larger number of smaller magnitude earthquakes in the truncated and exponential models, and not by the higher moment release rate in the larger magnitude range in the characteristic model. This is further confirmed by the results in Figure 12, which shows the UHFS for the case of exponential recurrence model with three different values of M_{\max} . In the low-period range, the spectrum for the lowest M_{\max} of 6.0 is seen to be the highest. Also, the spectrum for the M_{\max} value of 7.0 is throughout higher than that for M_{\max} of 8.0. The increase in the spectral amplitudes for lower values of M_{\max} is also due to the increase in the number of all the earthquakes up to the magnitude M_{\max} . However, the increase in the spectral amplitudes is comparatively smaller in the longer period range, because larger magnitudes contribute more in the longer period range. The effect of the larger number of smaller magnitude earthquakes is further illustrated by the results in Figure 13 for varying value of b . The spectra for higher values of b are seen to be higher, because the relative number of smaller magnitude earthquakes increases with increase in the value of b .

Further, the results in Figure 14 show the variation in the uniform hazard Fourier spectra with change in the moment release rate for a fixed M_{\max} of 8.0. Though a change in \dot{M}_0 changes the number of earthquakes of all the magnitudes by a constant factor, the spectral amplitudes are not seen to change uniformly at all the wave periods. The middle curve in Figure 14 corresponds to the preferred value of \dot{M}_0 , whereas the upper and lower curves correspond respectively to twice and half of the preferred value. An increase in \dot{M}_0 is seen to cause comparatively more increase in the longer period amplitudes. This is because larger magnitudes are characterized by higher contents of longer period waves, and also because the ground motion due to smaller magnitudes is not perceptible at larger distances.

The sensitivity of the uniform hazard Fourier spectra to the local soil and the site-geologic conditions has been studied the next. To illustrate only the effect of the local soil condition, Figure 15 presents the UHFS for various types of soil conditions overlying the basement rock. The spectral amplitudes on stiff and deep soil sites are seen to be amplified compared to those on rock sites for periods greater than about 0.34 s, whereas they are deamplified for the smaller periods. Compared to the spectrum for stiff soil site, the spectrum for deep soil condition is seen to have further amplification for the periods greater than

about 1.6 s. The amplification of the longer period waves is due to the resonance of the soil layer, whereas the attenuation of low period waves is due to lower Q -value for the soil layer.

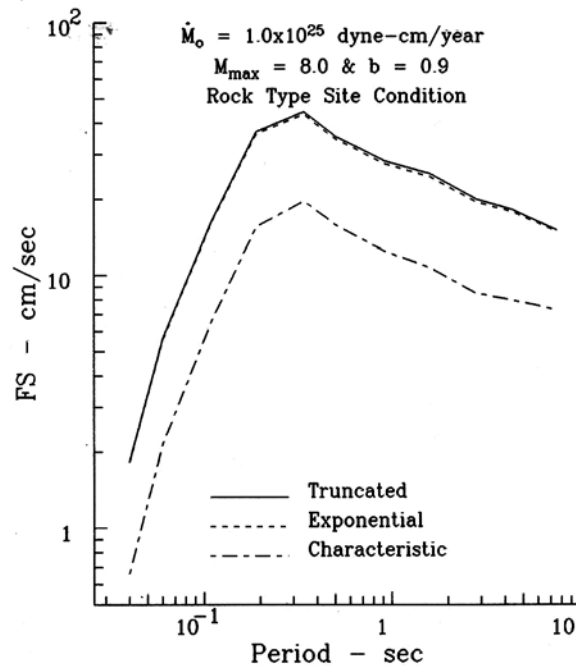


Fig. 11 Sensitivity of the UHFS to three different recurrence models with the same moment release rate

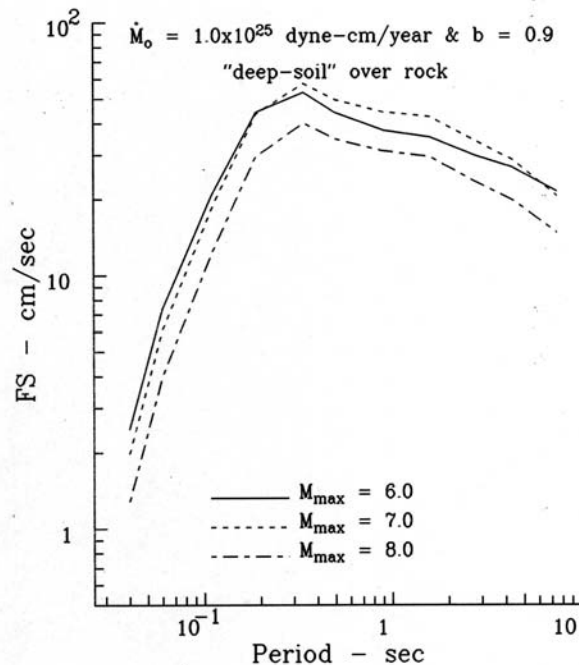


Fig. 12 Sensitivity of the UHFS to the maximum magnitude in the exponential recurrence model with a constant moment release rate

To illustrate the effect of the site geologic condition, Figure 16 presents the UHFS for a deep soil site lying over three different types of geologic site conditions. Compared to the deep soil site on basement rock, the spectrum for the deep soil site on deep sediments is seen to have significant amplification for the periods greater than about 0.11 s, and slight deamplification for the lower periods. The deamplification can be attributed to lower Q -value for sediments, whereas amplification is due to the resonance effect. On

the other hand, due to higher Q -value, there is slight amplification in the low-period range also; for the intermediate type of site geologic condition, due to smaller impedance contrast, the amplification in the longer period range is smaller than that for the deep sediments. All these observations can be explained on the basis of physical considerations that the amplification effect predominates the anelastic attenuation of the soil layer, and that the anelastic attenuation in the sediments is much less than that in the soil layer (Trifunac, 1990a; Gupta and Joshi, 1996). Thus the uniform hazard spectra are able to account for the dependence on the various governing parameters in a very realistic way.

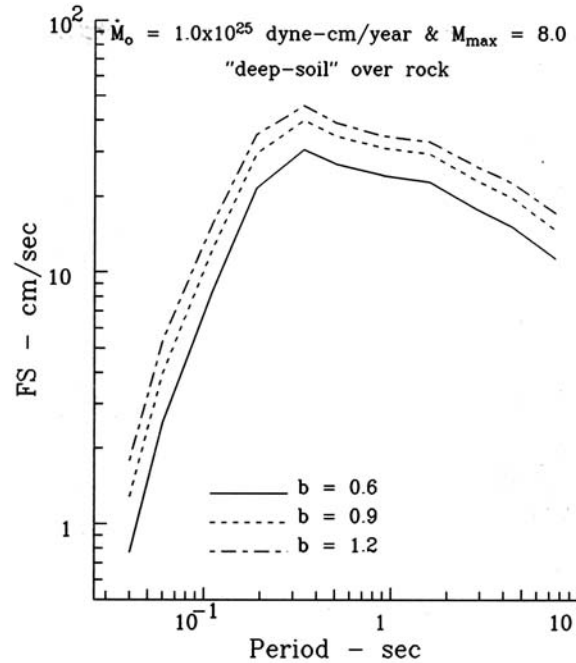


Fig. 13 Sensitivity of the UHFS to the b -values in the exponential recurrence model with a constant moment release rate

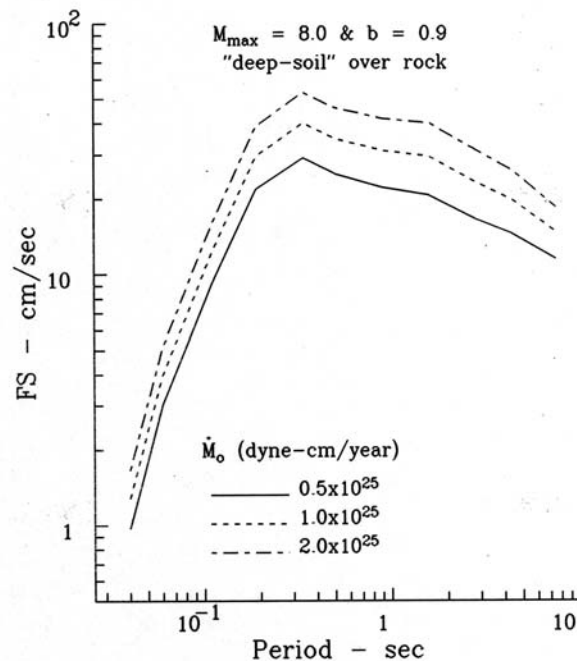


Fig. 14 Sensitivity of the UHFS to moment release rate in the exponential recurrence model with a constant maximum magnitude

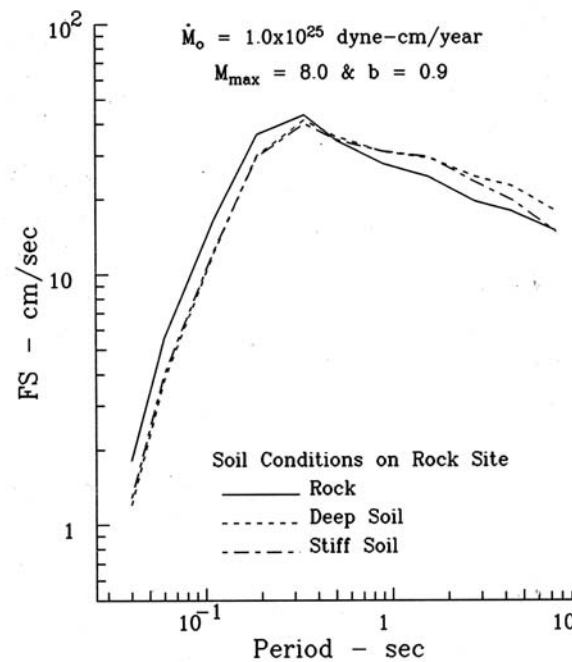


Fig. 15 Typical variations in the UHFS with the site soil condition for the rock type of site geological condition

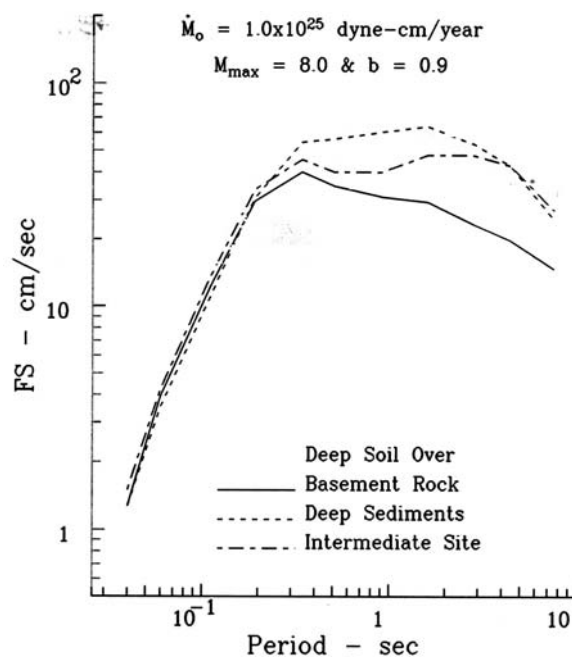


Fig. 16 Typical variations in the UHFS with the local geological condition for the deep soil type of site soil condition

EXAMPLES OF PROBABILISTIC HAZARD MAPPING

The PSHA method can be used to prepare a microzonation map by estimating the values of a hazard parameter at a closely spaced grid of sites in the area of interest. Similar to that for a single site such maps are able to account, in a realistic way, for the effects of the level and distribution of seismicity in various earthquake sources as well as those of the soil and geological features in the area. Several typical examples of the microzonation maps for the Los Angeles metropolitan area, prepared by Lee and Trifunac (1987), Todorovska and Trifunac (1996, 1999), and Trifunac (1990b), are described in this section for the

purpose of illustration. These studies for the Los Angeles area have considered 29 fault segments and a rectangular area of diffused seismicity as the seismic source zones, which are shown in Figure 17. Each fault segment in this figure is labeled by a serial number followed by two values within parentheses. The first value in the parentheses is the estimate of the moment release rate \dot{M}_0 in dyne-cm/year, and the second value is the activity rate a for an exposure period of 50 years. The value of b for all the faults is taken as 0.86, and the values of M_{\min} and M_{\max} as 2.75 and 7.0, respectively. The expected number of earthquakes in 50 years for different values of central magnitude in the diffused rectangular source, as indicated in Figure 17, is assumed to occur uniformly over the entire source area. The major faults in the Los Angeles metropolitan area and the local geological condition in terms of the depth of sediments in kilometers at 5'×5' grid points are shown in Figure 18, with grey areas indicating the rock outcrops (Lee and Trifunac, 1987; Todorovska and Trifunac, 1999).

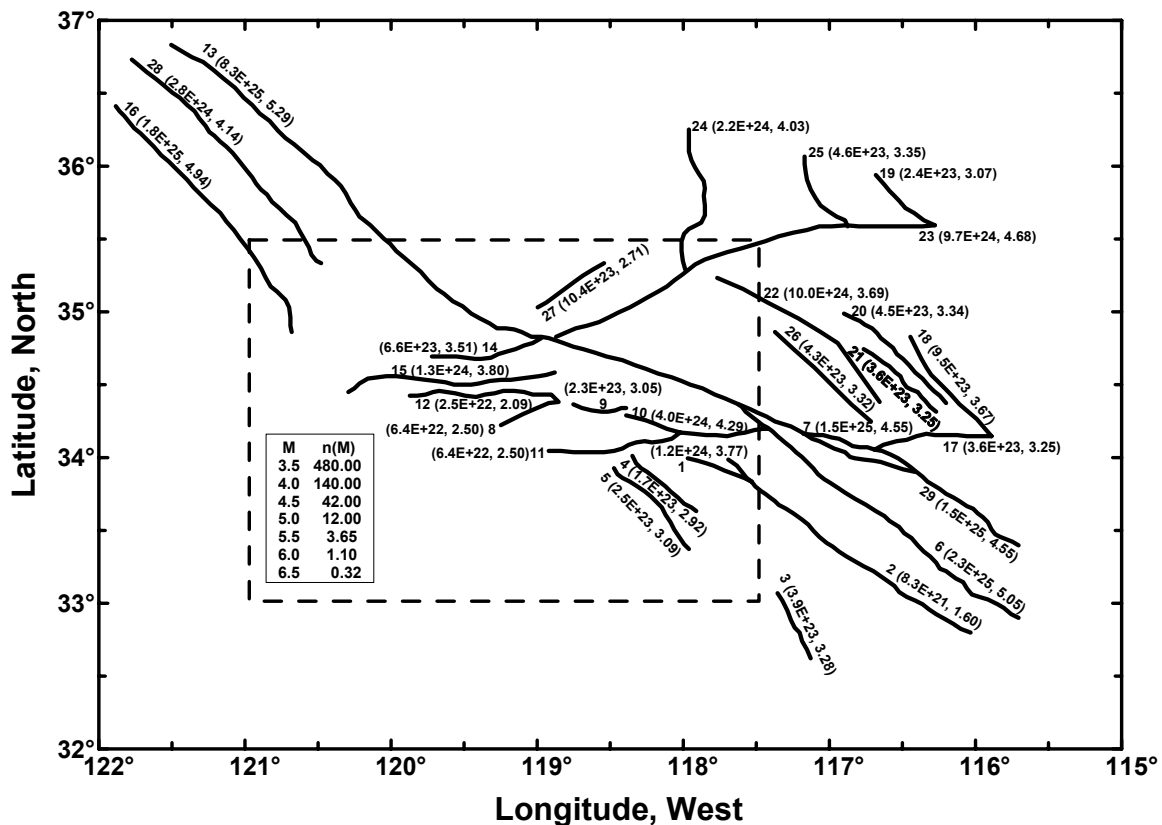


Fig. 17 Various faults and a rectangular area type of source in the California region (the seismic potential of each fault is specified by \dot{M}_0 and activity rate a in the parentheses, and that of the area source by the expected number of earthquakes in different magnitude intervals during a period of 50 years)

1. Microzoning in Terms of PSV Amplitudes

Lee and Trifunac (1987) and Trifunac (1990b) have prepared microzonation maps for the Los Angeles metropolitan area in terms of the pseudo relative velocity (PSV) spectrum amplitudes at different natural periods, using the empirical scaling relations due to Trifunac and Lee (1985). These relations define the spectral amplitude, $PSV(T)$, at period T , in terms of the earthquake magnitude, source-to-site distance, and the site geological condition defined by the depth of sediments in kilometers. Using the probability distribution of the residuals, these scaling relations can be used to obtain the conditional probability, $q(PSV(T)|M_j, R_i)$, that a spectral amplitude $PSV(T)$ will be exceeded at a site due to the earthquake magnitude M_j at the distance R_i from the site. Using these probabilities and the seismicity associated with the 29 fault segments and the diffused rectangular area source, PSHA has been carried out

to compute the $PSV(T)$ amplitudes with different confidence levels at each of the $1' \times 1'$ grid points. Some typical microzonation maps thus obtained for a confidence level of 0.50 and natural periods equal to 0.04, 0.34, 0.90 and 2.8 s are shown in Figure 19. The microzonation maps for many other natural periods and confidence levels are available in Lee and Trifunac (1987).

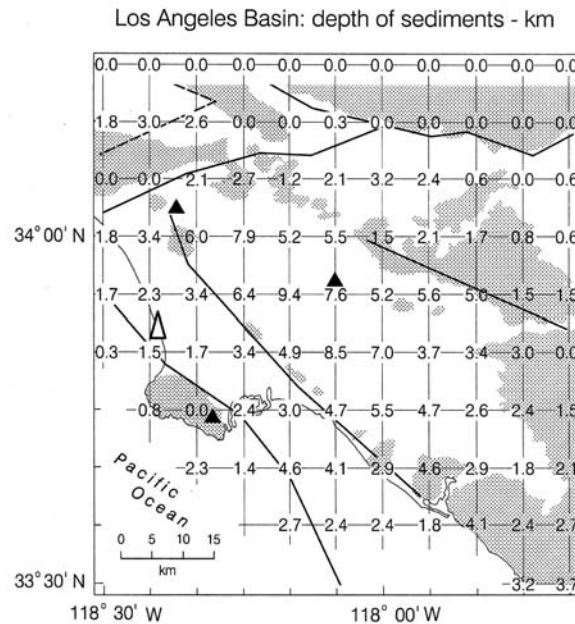


Fig. 18 Thickness of sedimentary deposits in the Los Angeles Metropolitan area at a 5' grid of points, with the grey areas indicating the rock outcrops

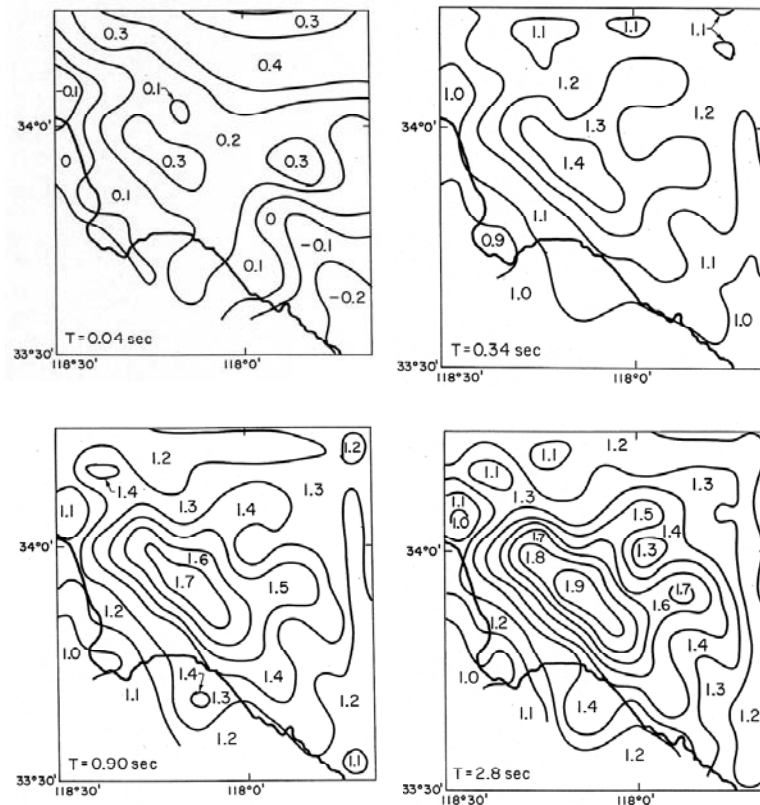


Fig. 19 Typical microzonation maps for the Los Angeles metropolitan area in terms of 5%-damped PSV spectrum amplitude for a confidence level of 0.50 and exposure period of 50 years for $T = 0.04, 0.34, 0.90$ and 2.8 s (after Lee and Trifunac, 1987)

The maps in Figure 19 correspond to the horizontal-component PSV spectrum with 5% damping. By reading the spectral amplitudes from such maps for a series of natural periods and for a particular set of confidence level and damping value, one can readily construct the uniform hazard response spectrum for any site in the area. Examples of such spectra for two typical sites, one at 33°45'N and 118°20'W on rock and the other at 33°45'N and 118°05'W on about 7.5 km thick sediments, are presented in Figure 20. It is seen that the difference between the two spectra is drastic, although both the sites are in the same metropolitan area. Similar situation may exist in the Delhi metropolitan area in India, where the seismicity can be associated with several fault segments and the site soil and geological conditions vary widely.

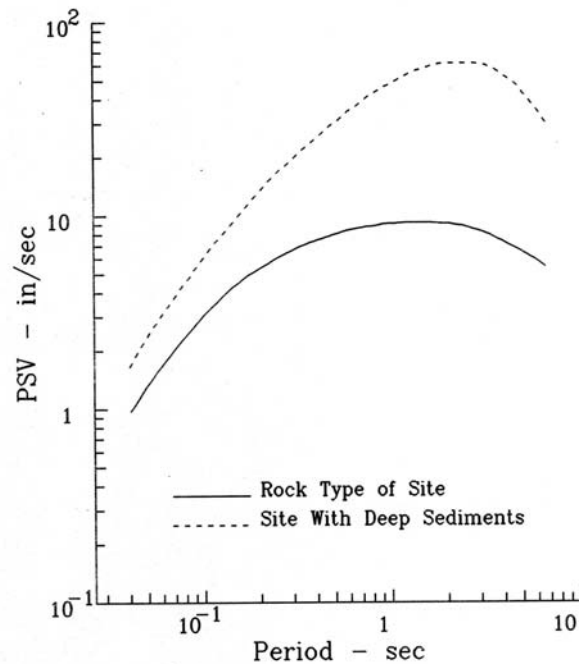


Fig. 20 Uniform risk spectra for two typical sites in the Los Angeles metropolitan area as obtained from the microzonation maps like those given in Figure 19

2. Microzonation for the Occurrence of Liquefaction

Using the formulation described earlier to evaluate the probability of occurrence of liquefaction at a site with a specified SPT value, \bar{N} , and the overburden pressure σ_0 , due to an earthquake magnitude M_j at distance R_i , Todorovska and Trifunac (1999) have prepared microzonation maps for the occurrence of liquefaction in the Los Angeles metropolitan area. Two typical maps showing the average return periods for the occurrence of liquefaction are shown in Figure 21 for two different \bar{N} values and σ_0 taken as 40 kPa. If a site is characterized by the \bar{N} and σ_0 values as specified in such a map, the corresponding return period gives the period for the liquefaction to occur at that site. By preparing such maps for a large number of \bar{N} and σ_0 values, it is possible to identify the average recurrence period for the liquefaction to occur at any site in the area.

For a given value of the overburden pressure, the microzonation maps for the occurrence of liquefaction can also be prepared in terms of the distribution of the critical SPT values for which liquefaction may initiate at a site with a specified probability during a specified exposure period. A typical microzonation map of this type for the Los Angeles metropolitan area is shown in Figure 22. By preparing such maps for several different values of σ_0 , the occurrence of liquefaction with desired probability and exposure period can be found readily at a site with the known \bar{N} and σ_0 values. Such maps can therefore be considered more useful for practical engineering applications.

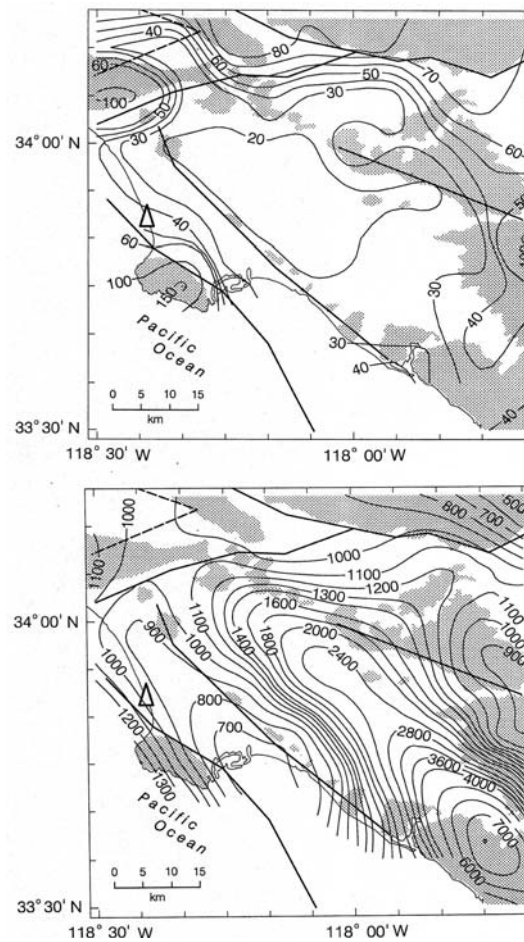


Fig. 21 Typical microzonation maps for the Los Angeles metropolitan area showing the average return period for initiation of liquefaction with overburden pressure of 40 kPa and the corrected SPT values of 10 (top) and 20 (bottom) (after Todorovska and Trifunac, 1999)

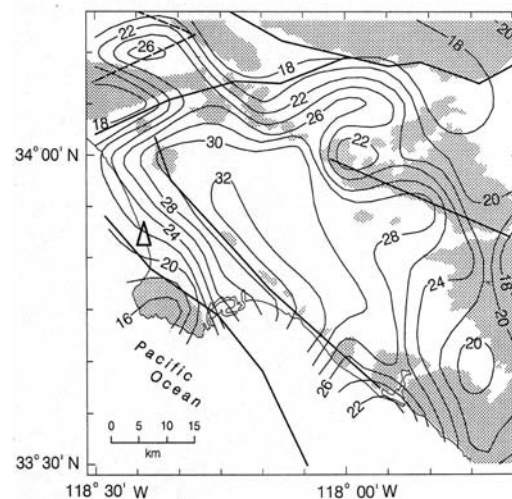


Fig. 22 Typical microzonation map for the Los Angeles metropolitan area showing the critical SPT values for the overburden pressure of 40 kPa, and probability to liquefy equal to 0.1 during the exposure of 50 years (the liquefaction may initiate at a site if the actual SPT value with the specified overburden pressure is less than that in the map; triangles in this and in the previous figures show the location of the King Harbor site, for which Todorovska and Trifunac (1999) showed the average return period, and liquefaction occurrence hazard versus \bar{N})

SUMMARY AND CONCLUSIONS

The paper has presented a critical overview on the various aspects of the currently used probabilistic seismic hazard analysis (PSHA) formulation to compute the probability of exceeding a specified level of a hazard parameter at a site due to any of the earthquakes expected to occur during a given life-period. The PSHA formulation is fundamentally based on evaluating the annual frequency of occurrence for different levels of the hazard parameter due to the total expected seismicity. The probability of exceedance or the occurrence rate, plotted as a function of the level of hazard parameter, is known as the hazard curve. The inherent random uncertainties in the location, magnitude and inter-event times of an earthquake, and that in the observed amplitudes of the hazard parameter, are taken into account in defining the hazard curves. A hazard curve forms the basis for estimating the level of hazard with a desired confidence level or the annual frequency of occurrence.

To consider the randomness in earthquake location by defining the probability distribution of the source-to-site distance, the paper has described four different types of sources, covering the most practical conditions. These include a point source represented by highly concentrated seismicity at a long distance from the site, a line source corresponding to a vertical fault, a dipping fault plane source with specified location and orientation, and an arbitrarily shaped area source of diffused seismicity. For an assumed spatial distribution of the seismicity, it is straightforward to estimate any desired measure of the source-to-site distance and its probability distribution for a line or a dipping fault plane source (Gupta, 2006b). The point source is characterized by only a single fixed value of the distance, which can be defined easily when the fault rupture is not considered. However, for a point source with unknown fault, a fault rupture distance is proposed to be obtained by averaging over the distances corresponding to uniformly distributed fault length in all the directions. Similarly, the probability distribution of a measure of distance for the area source can be obtained by dividing the entire source area into a large number of small-size elements, and by assuming the geometric center of each element to be a point source with suitable weight. Recommendations have been made for using both uniform as well as non-uniform weights for this purpose.

The randomness in earthquake magnitude is considered by defining an appropriate recurrence relationship for each source. Though the exponential model with a lower and an upper bound magnitude is found to be suitable in most cases, the characteristic model may provide better description in the case of some fault-specific sources. Both these models can be defined with a constant seismicity or a constant-moment-release-rate constraint. If the available data on past earthquakes in a source does not fit any of the standard recurrence relationships well, it has been proposed to use the observed probability distribution obtained by summation of a suitable kernel function.

The randomness in the times of earthquake occurrence in a source is considered by defining a probability distribution function for the inter-event times. The PSHA formulation is most commonly based on the Poisson assumption, under which the inter-event times are described by an exponential distribution with a constant occurrence rate. This formulation is also applicable to a non-homogeneous Poisson process characterized by a time-dependent occurrence rate, such as large subduction zone earthquakes. However, the aftershocks and sequential events, which are characterized by strong spatio-temporal correlations, cannot be included in this category. The Monte-Carlo simulation method is commonly used to incorporate the effect of such dependent events into the PSHA formulation. To account for the effect of the dependent events in a more efficient and practically simple way with adequate conservatism, it has been proposed to model their occurrences in a literal way.

To consider the effect of the random scattering in the observed values of a parameter used to characterize the hazard, the PSHA formulation needs the probability distribution of the residuals between the observed and the mean or median estimates of the hazard parameter obtained by fitting an empirical attenuation relationship to the available data. Such probabilistic attenuation or scaling relations have to be specific to the region of an area selected for the mapping of hazard. In the absence of the region-specific relationships, suitably selected and updated relations from other regions are used commonly in practical applications. A larger number of such relations are known widely for the peak ground acceleration and the response spectrum amplitudes. The paper has also described the relations for many other parameters like the Fourier amplitude spectrum, frequency-dependent strong-motion duration, permanent displacement across a fault, and the critical SPT value for the initiation of liquefaction with a specified

overburden pressure at a site, which are not that well known. The mapping of these additional parameters is necessary to have a more realistic assessment of the seismic risk in an area.

Due to limited amount of the available data and incomplete scientific knowledge of the various physical phenomena involved in the generation of earthquakes and their various natural effects, it is generally difficult to define in a unique way the models and the parameters of a model used to describe the inherent randomness in the basic PSHA formulation. Based on subjective decisions by different experts or different interpretations by a single expert, in practical applications, several different alternatives are generally possible even with the same database and the state of knowledge. The inherent randomness and the inability to define this randomness in a unique way are commonly termed as aleatory and epistemic types of uncertainties, respectively. The paper gives a brief description of the logic-tree approach to consider the effects of the possible epistemic uncertainties in the various steps of the basic PSHA formulation. By assigning suitable weights that represent relative levels of confidence imposed in the various options for each of the input elements to the PSHA, the logic-tree approach is used to define all the different combinations of the input elements and the corresponding hazard curves with weights. It generally becomes very difficult to arrive at the final decision due to a wide dispersion in the hazard curves. By computing the example results for the Fourier amplitude spectra for a site, it has been illustrated that large epistemic uncertainties in some of the input model parameters may result in very large uncertainties in the hazard estimate. The effect of the epistemic uncertainties is, therefore, accounted commonly by using a higher level of hazard curve, leading to unduly large conservatism.

To rationalize the use of epistemic uncertainties, the paper has first proposed to reduce the number of hazard curves by treating the aleatory component of the epistemic uncertainty in defining the model parameters by using the Bayesian estimate of the parameters. Then, to the extent possible, a single consensus or a limited number of most appropriate models have been proposed to be used for each of the input elements. A model based purely on speculation and not supported by the available data or not having a plausible physical basis should not be included in the analysis. Finally, to avoid unreasonable conservatism, it has been recommended to use the hazard curve with the maximum weight to represent the decision with the highest level of confidence for the currently available data and knowledge. The use of this hazard curve with a suitably chosen confidence level is considered more rational in practical engineering applications, even if it differs from the reality to be known in future.

The PSHA formulation can thus be used to account for the effects of the random (aleatory) as well as the epistemic uncertainties in a reasonable way. However, perhaps with an intention to get an upper bound value of the hazard, the PSHA is sometimes used with extremely low annual frequencies of the order of 10^{-7} to 10^{-8} (Abrahamson et al., 2002; Stepp et al., 2001). If applied without imposing a truncation on the distribution of the residuals of the hazard parameter, this may result in unrealistically high estimate of the hazard, whereas truncation cannot be considered to provide a reliable estimate of the hazard for such small values of the annual frequency. It has been thus recommended that the PSHA be used without any truncation for only those applications where the safety requirements are within the practically realizable limits.

To illustrate the application of the PSHA method for hazard mapping, the paper has finally presented typical examples of microzonation maps for several parameters representing different natural effects of the earthquakes. These maps are able to exhibit in a balanced and physically realistic way the effects of the spatial distribution of the seismicity and the site condition in the area of interest. The implementation of the various proposals made in the paper is expected to make the PSHA method more amenable to practical applications for the hazard mapping to estimate the earthquake effects on man-made structures.

ACKNOWLEDGEMENTS

The author is very thankful to Mrs. V.M. Bendre, Director, CWPRS, for taking keen interest in the present study and for permitting to publish this paper.

REFERENCES

1. Abrahamson, N.A. (1998). "Non-stationary Spectral Matching Program RSPMATCH", Internal Report, Pacific Gas and Electric Company, U.S.A.

2. Abrahamson, N.A. and Silva, W.J. (1997). "Empirical Response Spectral Attenuation Relations for Shallow Crustal Earthquakes", *Seismological Research Letters*, Vol. 68, No. 1, pp. 94–127.
3. Abrahamson, N.A., Birkhauser, P., Koller, M., Mayer-Rosa, D., Smit, P., Sprecher, C., Tinic, S. and Graf, R. (2002). "PEGASOS—A Comprehensive Probabilistic Seismic Hazard Assessment for Nuclear Power Plants in Switzerland", *Proceedings of the 12th European Conference on Earthquake Engineering*, London, U.K., Paper No. 633 (on CD).
4. Adams, J. and Atkinson, G. (2003). "Development of Seismic Hazard Maps for the Proposed 2005 Edition of the National Building Code of Canada", *Canadian Journal of Civil Engineering*, Vol. 30, No. 2, pp. 255–271.
5. Albarello, D., Camassi, R. and Rebez, A. (2001). "Detection of Space and Time Heterogeneity in the Completeness of a Seismic Catalog by a Statistical Approach: An Application to the Italian Area", *Bulletin of the Seismological Society of America*, Vol. 91, No. 6, pp. 1694–1703.
6. Anagnos, T. and Kiremidjian, A.S. (1988). "A Review of Earthquake Occurrence Models for Seismic Hazard Analysis", *Probabilistic Engineering Mechanics*, Vol. 3, No. 1, pp. 3–11.
7. Anderson, J.G. (1997). "Benefits of Scenario Ground Motion Maps", *Engineering Geology*, Vol. 48, No. 1, pp. 43–57.
8. Anderson, J.C. and Bertero, V.V. (1991). "Seismic Performance of an Instrumented Six-Story Steel Building", Report UCB/EERC-91/11, University of California, Berkeley, U.S.A.
9. Anderson, J.G. and Trifunac, M.D. (1977). "On Uniform Risk Functionals Which Describe Strong Earthquake Ground Motion: Definition, Numerical Estimation, and an Application to the Fourier Amplitude Spectrum of Acceleration", Report CE 77-02, University of Southern California, Los Angeles, U.S.A.
10. Anderson, J.G. and Trifunac, M.D. (1978). "Uniform Risk Functionals for Characterization of Strong Earthquake Ground Motion", *Bulletin of the Seismological Society of America*, Vol. 68, No. 1, pp. 205–218.
11. Ang, A.H.-S. (1973). "Structural Risk Analysis and Reliability-Based Design", *Journal of the Structural Division*, *Proceedings of ASCE*, Vol. 99, No. ST9, pp. 1891–1910.
12. Atkinson, G.M. and Boore, D.M. (1997). "Some Comparisons between Recent Ground-Motion Relations", *Seismological Research Letters*, Vol. 68, No. 1, pp. 24–40.
13. Atkinson, G.M. and Boore, D.M. (2003). "Empirical Ground-Motion Relations for Subduction-Zone Earthquakes and Their Applications to Cascadia and Other Regions", *Bulletin of the Seismological Society of America*, Vol. 93, No. 4, pp. 1703–1729.
14. Bazzurro, P. and Cornell, C.A. (1999). "Disaggregation of Seismic Hazard", *Bulletin of the Seismological Society of America*, Vol. 89, No. 2, pp. 501–520.
15. Beauval, C., Hainzl, S. and Scherbaum, F. (2006). "Probabilistic Seismic Hazard Estimation in Low-Seismicity Regions Considering Non-Poissonian Seismic Occurrence", *Geophysical Journal International*, Vol. 164, No. 3, pp. 543–550.
16. Bender, B. (1983). "Maximum Likelihood Estimation of b Value for Magnitude Grouped Data", *Bulletin of the Seismological Society of America*, Vol. 73, No. 3, pp. 831–851.
17. Bender, B. (1986). "Modelling Source Zone Boundary Uncertainty in Seismic Hazard Analysis", *Bulletin of the Seismological Society of America*, Vol. 76, No. 2, pp. 329–341.
18. Berge-Thierry, C., Cotton, F., Scotti, O., Griot-Pommeroy, D.A. and Fukushima, Y. (2003). "New Empirical Response Spectral Attenuation Laws for Moderate European Earthquakes", *Journal of Earthquake Engineering*, Vol. 7, No. 2, pp. 193–222.
19. Bernreuter, D.L., Chen, J.C. and Savy, J.B. (1987). "Development of Site Specific Response Spectra", Report NUREG/CR-4861, United States Nuclear Regulatory Commission, Washington, DC, U.S.A.
20. Bertero, R.D. and Bertero, V.V. (2004). "Performance-Based Seismic Engineering: Development and Application of a Comprehensive Conceptual Approach to the Design of Buildings" in "Earthquake Engineering: From Engineering Seismology to Performance-Based Engineering (edited by Y. Bozorgnia and V.V. Bertero)", CRC Press, Boca Raton, U.S.A.

21. Biot, M.A. (1932). "Transient Oscillations in Elastic Systems", Ph.D. Thesis No. 259, Aeronautics Department, California Institute of Technology, Pasadena, U.S.A.
22. Biot, M.A. (1933). "Theory of Elastic Systems Vibrating under Transient Impulse with an Application to Earthquake-Proof Buildings", *Proceedings of the National Academy of Sciences of the United States of America*, Vol. 19, No. 2, pp. 262–268.
23. Biot, M.A. (1934). "Theory of Vibration of Buildings during Earthquake", *Zeitschrift für Angewandte Mathematik und Mechanik*, Vol. 14, No. 4, pp. 213–223.
24. Bollinger, G.A., Sibol, M.S. and Chapman, M.C. (1992). "Maximum Magnitude Estimation for an Intraplate Setting—Example: The Giles County, Virginia, Seismic Zone", *Seismological Research Letters*, Vol. 63, No. 2, pp. 139–152.
25. Bolt, B.A. (1973). "Duration of Strong Ground Motion", *Proceedings of the Fifth World Conference on Earthquake Engineering*, Rome, Italy, Vol. 1, pp. 1304–1313.
26. Bommer, J.J. and Martinez-Pereira, A. (1999). "The Effective Duration of Earthquake Strong Motion", *Journal of Earthquake Engineering*, Vol. 3, No. 2, pp. 127–172.
27. Bommer, J.J., Abrahamson, N.A., Strasser, F.O., Pecker, A., Bard, P.Y., Bungum, H., Cotton, F., Fah, D., Sabetta, F., Scherbaum, F. and Studer, J. (2004). "The Challenge of Defining Upper Bounds on Earthquake Ground Motions", *Seismological Research Letters*, Vol. 75, No. 1, pp. 82–95.
28. Bommer, J.J., Scherbaum, F., Bungum, H., Cotton, F., Sabetta, F. and Abrahamson, N.A. (2005). "On the Use of Logic Trees for Ground-Motion Prediction Equations in Seismic-Hazard Analysis", *Bulletin of the Seismological Society of America*, Vol. 95, No. 2, pp. 377–389.
29. Boore, D.M., Joyner, W.B. and Fumal, T.E. (1997). "Equations for Estimating Horizontal Response Spectra and Peak Acceleration from Western North American Earthquakes: A Summary of Recent Work", *Seismological Research Letters*, Vol. 68, No. 1, pp. 128–153.
30. Brune, J.N. (1968). "Seismic Moment, Seismicity, and Rate of Slip along Major Fault Zones", *Journal of Geophysical Research*, Vol. 73, No. 2, pp. 777–784.
31. BSSC (1997). "NEHRP Recommended Provisions for Seismic Regulations for New Buildings and Other Structures. 1997 Edition. Part 1: Provisions (FEMA 302)", Report Prepared for the Federal Emergency Management Agency, Building Seismic Safety Council, National Institute of Building Sciences, Washington, DC, U.S.A.
32. Budnitz, R.J., Cornell, C.A. and Morris, P.A. (2005). "Discussion: Comment on J.U. Klügel's 'Problems in the Application of the SSHAC Probability Method for Assessing Earthquake Hazards at Swiss Nuclear Power Plants,' in *Engineering Geology*, Vol. 78, pp. 285–307", *Engineering Geology*, Vol. 82, No. 1, pp. 76–78.
33. Burroughs, S.M. and Tebbens, S.F. (2002). "The Upper-Truncated Power Law Applied to Earthquake Cumulative Frequency-Magnitude Distributions: Evidence for a Time-Independent Scaling Parameter", *Bulletin of the Seismological Society of America*, Vol. 92, No. 8, pp. 2983–2993.
34. Campbell, K.W. (2003). "Prediction of Strong Ground Motion Using the Hybrid Empirical Method and Its Use in the Development of Ground-Motion (Attenuation) Relations in Eastern North America", *Bulletin of the Seismological Society of America*, Vol. 93, No. 3, pp. 1012–1033.
35. Campbell, K.W. (2004). "Erratum to Prediction of Strong Ground Motion Using the Hybrid Empirical Method and Its Use in the Development of Ground-Motion (Attenuation) Relations in Eastern North America", *Bulletin of the Seismological Society of America*, Vol. 94, No. 6, p. 2418.
36. Chapman, M.C. (1995). "A Probabilistic Approach to Ground-Motion Selection for Engineering Design", *Bulletin of the Seismological Society of America*, Vol. 85, No. 3, pp. 937–942.
37. Chung, D.H. and Bernreuter, D.L. (1981). "Regional Relationships among Earthquake Magnitude Scales", *Reviews of Geophysics and Space Physics*, Vol. 19, No. 4, pp. 649–663.
38. Cornell, C.A. (1968). "Engineering Seismic Risk Analysis", *Bulletin of the Seismological Society of America*, Vol. 58, No. 5, pp. 1583–1606.
39. Cornell, C.A. and Vanmarcke, E.H. (1969). "The Major Influences on Seismic Risk", *Proceedings of the Fourth World Conference on Earthquake Engineering*, Santiago, Chile, Vol. A-1, pp. 69–93.

40. Cornell, C.A. and Winterstein, S.R. (1988). "Temporal and Magnitude Dependence in Earthquake Recurrence Models", *Bulletin of the Seismological Society of America*, Vol. 78, No. 4, pp. 1522–1537.
41. Corral, A. (2004). "Long-Term Clustering, Scaling, and Universality in the Temporal Occurrence of Earthquakes", *Physical Review Letters*, Vol. 92, No. 10, pp. 108501.1–108501.4.
42. Cotton, F., Scherbaum, F., Bommer, J.J. and Bungum, H. (2006). "Criteria for Selecting and Adjusting Ground-Motion Models for Specific Target Regions: Application to Central Europe and Rock Sites", *Journal of Seismology*, Vol. 10, No. 2, pp. 137–156.
43. Das, S., Gupta, I.D. and Gupta, V.K. (2006). "A Probabilistic Seismic Hazard Analysis of Northeast India", *Earthquake Spectra*, Vol. 22, No. 1, pp. 1–27.
44. Del Gaudio, V. and Wasowski, J. (2004). "Time Probabilistic Evaluation of Seismically Induced Landslide Hazard in Irpinia (Southern Italy)", *Soil Dynamics and Earthquake Engineering*, Vol. 24, No. 12, pp. 915–928.
45. Der Kiureghian, A. (1977). "Uncertainty Analysis in Seismic Risk Evaluation", *Proceedings of the Second Annual Engineering Mechanics Division Specialty Conference*, Raleigh, U.S.A., pp. 320–323.
46. Der Kiureghian, A. and Ang, A.H.S. (1975). "A Line Source Model for Seismic Risk Analysis", *Structural Research Series 419*, Department of Civil Engineering, University of Illinois at Urbana-Champaign, Urbana, U.S.A.
47. Dong, W.M., Bao, A.B. and Shah, H.C. (1984). "Use of Maximum Entropy Principle in Earthquake Recurrence Relationships", *Bulletin of the Seismological Society of America*, Vol. 74, No. 2, pp. 725–737.
48. Douglas, J. (2003). "Earthquake Ground Motion Estimation Using Strong-Motion Records: A Review of Equations for the Estimation of Peak Ground Acceleration and Response Spectral Ordinates", *Earth-Science Reviews*, Vol. 61, No. 1, pp. 43–104.
49. Douglas, B.M. and Ryall, A. (1975). "Return Periods for Rock Acceleration in Western Nevada", *Bulletin of the Seismological Society of America*, Vol. 65, No. 6, pp. 1599–1611.
50. Douglas, J., Bungum, H. and Scherbaum, F. (2006). "Ground-Motion Prediction Equations for Southern Spain and Southern Norway Obtained Using the Composite Model Perspective", *Journal of Earthquake Engineering*, Vol. 10, No. 1, pp. 33–72.
51. Ellingwood, B.R. (2001). "Earthquake Risk Assessment of Building Structures", *Reliability Engineering & System Safety*, Vol. 74, No. 3, pp. 251–262.
52. EPRI (1986). "Seismic Hazard Methodology for the Central and Eastern United States", Report NP-4726, Electric Power Research Institute, Palo Alto, U.S.A.
53. FEMA (2000). "Recommended Seismic Design Criteria for New Steel Moment-Frame Buildings", Report FEMA-350, Federal Emergency Management Agency, Washington, DC, U.S.A.
54. Frankel, A. (1995). "Mapping Seismic Hazard in the Central and Eastern United States", *Seismological Research Letters*, Vol. 66, No. 4, pp. 4–8.
55. Frankel, A.D., Petersen, M.D., Mueller, C.S., Haller, K.M., Wheeler, R.L., Leyendecker, E.V., Wesson, R.L., Harmsen, S.C., Cramer, C.H., Perkins, D.M. and Rukstales, K.S. (2002). "Documentation for the 2002 Update of the National Seismic Hazard Maps", Open-File Report 02-420, United States Geological Survey, Denver, U.S.A.
56. Gasparini, D.A. and Vanmarcke, E.H. (1976). "SIMQKE: A Program for Artificial Motion Generation. User's Manual and Documentation", Technical Report, Department of Civil Engineering, Massachusetts Institute of Technology, Cambridge, U.S.A.
57. Gregor, N.J., Silva, W.J., Wong, I.G. and Youngs, R.R. (2002). "Ground-Motion Attenuation Relationships for Cascadia Subduction Zone Megathrust Earthquakes Based on a Stochastic Finite-Fault Model", *Bulletin of the Seismological Society of America*, Vol. 92, No. 5, pp. 1923–1932.
58. GSHAP (1999). "The Global Seismic Hazard Assessment Program (GSHAP)-1992/1999", *Annali di Geofisica*, Vol. 42, No. 6, pp. 957–1229.
59. Gupta, I.D. (1991). "A Note on Computing Uniform Risk Spectra from Intensity Data on Earthquake Occurrence", *Soil Dynamics and Earthquake Engineering*, Vol. 10, No. 8, pp. 407–413.

60. Gupta, I.D. (2002a). "The State of the Art in Seismic Hazard Analysis", *ISET Journal of Earthquake Technology*, Vol. 39, No. 4, pp. 311–346.
61. Gupta, I.D. (2002b). "Should Normalized Spectral Shapes be Used for Estimating Site-Specific Design Ground Motion?", *Proceedings of the 12th Symposium on Earthquake Engineering*, Roorkee, Vol. 1, pp. 168–175.
62. Gupta, I.D. (2005). "Probabilistic Seismic Hazard Analysis with Uncertainties", *Proceedings of the Symposium on Seismic Hazard Analysis and Microzonation*, Roorkee, Vol. I, pp. 97–117.
63. Gupta, I.D. (2006a). "Delineation of Probable Seismic Sources in India and Neighbourhood by a Comprehensive Analysis of Seismotectonic Characteristics of the Region", *Soil Dynamics and Earthquake Engineering*, Vol. 26, No. 8, pp. 766–790.
64. Gupta, I.D. (2006b). "Defining Source-to-Site Distances for Evaluation of Design Earthquake Ground Motion", *Proceedings of the 13th Symposium on Earthquake Engineering*, Roorkee, Vol. I, pp. 295–306.
65. Gupta, I.D. and Joshi, R.G. (1993). "On Synthesizing Response Spectrum Compatible Accelerograms", *European Earthquake Engineering*, Vol. VII, No. 2, pp. 25–33.
66. Gupta, I.D. and Joshi, R.G. (1996). "Evaluation of Design Earthquake Ground Motion for Soil and Rock Sites", *Proceedings of the Workshop on Design Practices in Earthquake Geotechnical Engineering*, Roorkee, pp. 58–87.
67. Gupta, I.D. and Trifunac, M.D. (1998). "Defining Equivalent Stationary PSDF to Account for Nonstationarity of Earthquake Ground Motion", *Soil Dynamics and Earthquake Engineering*, Vol. 17, No. 2, pp. 89–99.
68. Gutenberg, B. and Richter, C.F. (1944). "Frequency of Earthquakes in California", *Bulletin of the Seismological Society of America*, Vol. 34, No. 4, pp. 185–188.
69. Hagiwara, Y. (1974). "Probability of Earthquake Occurrence as Obtained from a Weibull Distribution Analysis of Crustal Strain", *Tectonophysics*, Vol. 23, No. 3, pp. 313–318.
70. Hainzl, S., Scherbaum, F. and Beauval, C. (2006). "Estimating Background Activity Based on Interevent-Time Distribution", *Bulletin of the Seismological Society of America*, Vol. 96, No. 1, pp. 313–320.
71. Hanks, T.C. and Kanamori, H. (1979). "A Moment Magnitude Scale", *Journal of Geophysical Research*, Vol. 84, No. B5, pp. 2348–2350.
72. Helmstetter, A., Ouillon, G. and Sornetter, D. (2003). "Are Aftershocks of Large California Earthquakes Diffusing?", *Journal of Geophysical Research*, Vol. 108, No. B10, p. 2483.
73. Hong, L.L. and Guo, S.W. (1995). "Nonstationary Poisson Model for Earthquake Occurrences", *Bulletin of the Seismological Society of America*, Vol. 85, No. 3, pp. 814–824.
74. Hwang, H. and Huo, J.R. (1997). "Attenuation Relations of Ground Motion for Rock and Soil Sites in Eastern United States", *Soil Dynamics and Earthquake Engineering*, Vol. 16, No. 6, pp. 363–372.
75. Ishikawa, Y. and Kameda, H. (1988). "Hazard-Consistent Magnitude and Distance for Extended Seismic Risk Analysis", *Proceedings of the Ninth World Conference on Earthquake Engineering*, Tokyo-Kyoto, Japan, Vol. II, pp. 89–94.
76. Jara, J.M. and Rosenblueth, E. (1988). "The Mexico Earthquake of September 19, 1985—Probability Distribution of Times between Characteristic Subduction Earthquakes", *Earthquake Spectra*, Vol. 4, No. 3, pp. 449–529.
77. Jeong, G.D. and Iwan, W.D. (1988). "The Effect of Earthquake Duration on the Damage of Structures", *Earthquake Engineering & Structural Dynamics*, Vol. 16, No. 8, pp. 1201–1211.
78. Kagan, Y.Y. (1991). "Seismic Moment Distribution", *Geophysical Journal International*, Vol. 106, No. 1, pp. 123–134.
79. Kagan, Y.Y. (1997). "Seismic Moment-Frequency Relation for Shallow Earthquakes: Regional Comparison", *Journal of Geophysical Research*, Vol. 102, No. B2, pp. 2835–2852.
80. Kagan, Y.Y. and Jackson, D.D. (2000). "Probabilistic Forecasting of Earthquakes", *Geophysical Journal International*, Vol. 143, No. 2, pp. 438–453.

81. Kameda, H. and Takagi, H. (1981). "Seismic Hazard Estimation Based on Non-Poisson Earthquake Occurrences", *Memoirs of the Faculty of Engineering, Kyoto University, Japan*, Vol. XLIII, Part 3, pp. 397–433.
82. Kawashima, K. and Aizawa, K. (1989). "Bracketed and Normalized Durations of Earthquake Ground Acceleration", *Earthquake Engineering & Structural Dynamics*, Vol. 18, No. 7, pp. 1041–1051.
83. Keilis-Borok, V.I., Podgaetskaya, V.M. and Prozorov, A.G. (1972). "Local Statistics of Earthquake Catalogs" in "Computational Seismology (edited by V.I. Keilis-Borok)", Consultants Bureau, New York, U.S.A.
84. Kijko, A. (2004). "Estimation of the Maximum Earthquake Magnitude, m_{\max} ", *Pure and Applied Geophysics*, Vol. 161, No. 8, pp. 1655–1681.
85. Kijko, A. and Graham, G. (1998). "Parametric-Historic Procedure for Probabilistic Seismic Hazard Analysis. Part I: Estimation of Maximum Regional Magnitude m_{\max} ", *Pure and Applied Geophysics*, Vol. 152, No. 3, pp. 413–442.
86. Kijko, A. and Graham, G. (1999). "'Parametric-Historic' Procedure for Probabilistic Seismic Hazard Analysis. Part II: Assessment of Seismic Hazard at Specified Site", *Pure and Applied Geophysics*, Vol. 154, No. 1, pp. 1–22.
87. Kiremidjian, A.S. and Suzuki, S. (1987). "A Stochastic Model for Site Ground Motions from Temporally Dependent Earthquakes", *Bulletin of the Seismological Society of America*, Vol. 77, No. 4, pp. 1110–1126.
88. Klügel, J.-U. (2005a). "Problems in the Application of the SSHAC Probability Method for Assessing Earthquake Hazards at Swiss Nuclear Power Plants", *Engineering Geology*, Vol. 78, No. 3-4, pp. 285–307.
89. Klügel, J.-U. (2005b). "Discussion: Reply to the Comment on J.U. Klügel's: 'Problems in the Application of the SSHAC Probability Method for Assessing Earthquake Hazards at Swiss Nuclear Power Plants,' Eng. Geol. Vol. 78, pp. 285–307, by Musson et al.", *Engineering Geology*, Vol. 82, No. 1, pp. 56–65.
90. Klügel, J.-U. (2005c). Discussion: Reply to the Comment on J.U. Klügel's: 'Problems in the Application of the SSHAC Probability Method for Assessing Earthquake Hazards at Swiss Nuclear Power Plants', in *Engineering Geology*, Vol. 78, pp. 285–307, by Budnitz, by J.U. Klügel", *Engineering Geology*, Vol. 82, No. 1, pp. 79–85.
91. Krinitzsky, E.L. (2002). "How to Obtain Earthquake Ground Motions for Engineering Design", *Engineering Geology*, Vol. 65, No. 1, pp. 1–16.
92. Kulkarni, R.B., Youngs, R.R. and Coppersmith, K.J. (1984). "Assessment of Confidence Intervals for Results of Seismic Hazard Analysis", *Proceedings of the Eighth World Conference on Earthquake Engineering*, San Francisco, U.S.A., Vol. 1, pp. 263–270.
93. Lee, V.W. (1987). "Influence of Local Soil and Geologic Site Conditions on Pseudo Relative Velocity Response Spectrum Amplitudes of Recorded Strong Motion Accelerations", Report CE 87-06, University of Southern California, Los Angeles, U.S.A.
94. Lee, V.W. (1992). "On Strong-Motion Uniform Risk Functionals Computed From General Probability Distributions of Earthquake Recurrences", *Soil Dynamics and Earthquake Engineering*, Vol. 11, No. 6, pp. 357–367.
95. Lee, W.H.K. and Brillinger, D.R. (1979). "On Chinese Earthquake History—An Attempt to Model an Incomplete Data Set by Point Process Analysis", *Pure and Applied Geophysics*, Vol. 117, No. 6, pp. 1229–1257.
96. Lee, V.W. and Trifunac, M.D. (1985). "Uniform Risk Spectra of Strong Earthquake Ground Motion: NEQRISK", Report CE 85-05, University of Southern California, Los Angeles, U.S.A.
97. Lee, V.W. and Trifunac, M.D. (1987). "Microzonation of a Metropolitan Area", Report CE 87-02, University of Southern California, Los Angeles, U.S.A.
98. Lee, V.W. and Trifunac, M.D. (1989). "A Note on Filtering Strong Motion Accelerograms to Produce Response Spectra of Specified Shape and Amplitude", *European Earthquake Engineering*, Vol. III, No. 2, pp. 38–45.

99. Lomnitz-Adler, J. and Lomnitz, C. (1979). "A Modified Form of the Gutenberg-Richter Magnitude-Frequency Relation", *Bulletin of the Seismological Society of America*, Vol. 69, No. 4, pp. 1209–1214.
100. Lussou, P., Bard, P.Y., Cotton, F. and Fukushima, Y. (2001). "Seismic Design Regulation Codes: Contribution of K-Net Data to Site Effect Evaluation", *Journal of Earthquake Engineering*, Vol. 5, No. 1, pp. 13–33.
101. Maeda, K. (1996). "The Use of Foreshocks in Probabilistic Prediction along the Japan and Kuril Trenches", *Bulletin of the Seismological Society of America*, Vol. 86, No. 1A, pp. 242–254.
102. Main, I. (1996). "Statistical Physics, Seismogenesis, and Seismic Hazard", *Reviews of Geophysics*, Vol. 34, No. 4, pp. 433–462.
103. Main, I.G. and Burton, P.W. (1984). "Information Theory and the Earthquake Frequency-Magnitude Distribution", *Bulletin of the Seismological Society of America*, Vol. 74, No. 4, pp. 1409–1426.
104. McGuire, R.K. (1974). "Seismic Structural Response Risk Analysis, Incorporating Peak Response Regressions on Earthquake Magnitude and Distance", Report R74-51, Department of Civil Engineering, Massachusetts Institute of Technology, Cambridge, U.S.A.
105. McGuire, R.K. (1977). "Seismic Design Spectra and Mapping Procedures Using Hazard Analysis Based Directly on Oscillator Response", *Earthquake Engineering & Structural Dynamics*, Vol. 5, No. 3, pp. 211–234.
106. McGuire, R.K. (1978). "A Simple Model for Estimating Fourier Amplitude of Horizontal Ground Acceleration", *Bulletin of the Seismological Society of America*, Vol. 68, No. 3, pp. 803–822.
107. McGuire, R.K. (1995). "Probabilistic Seismic Hazard Analysis and Design Earthquakes: Closing the Loop", *Bulletin of the Seismological Society of America*, Vol. 85, No. 5, pp. 1275–1284.
108. McGuire, R.K. (2004). "Seismic Hazard and Risk Analysis", Monograph MNO-10, Earthquake Engineering Research Institute, Oakland, U.S.A.
109. Merz, H.A. and Cornell, C.A. (1973). "Seismic Risk Analysis Based on a Quadratic Magnitude-Frequency Law", *Bulletin of the Seismological Society of America*, Vol. 63, No. 6-1, pp. 1999–2006.
110. Milne, W.G. and Davenport, A.G. (1969). "Distribution of Earthquake Risk in Canada", *Bulletin of the Seismological Society of America*, Vol. 59, No. 2, pp. 729–754.
111. Mohraz, B. (1976). "A Study of Earthquake Response Spectra for Different Geological Conditions", *Bulletin of the Seismological Society of America*, Vol. 66, No. 3, pp. 915–935.
112. Mohraz, B. and Peng, M.-H. (1989). "Use of a Low-Pass Filter in Determining the Duration of Strong Ground Motion" in "1989 Proceedings of the ASME Pressure Vessels and Piping Division", Publication PVP-182, American Society of Mechanical Engineers, New York, U.S.A.
113. Molchan, G. (2005). "Interevent Time Distribution in Seismicity: A Theoretical Approach", *Pure and Applied Geophysics*, Vol. 162, No. 6-7, pp. 1135–1150.
114. Musson, R.M.W. (1999a). "Determination of Design Earthquakes in Seismic Hazard Analysis through Monte Carlo Simulation", *Journal of Earthquake Engineering*, Vol. 3, No. 4, pp. 463–474.
115. Musson, R.M.W. (1999b). "Probabilistic Seismic Hazard Maps for the North Balkan Region", *Annali di Geofisica*, Vol. 42, No. 6, pp. 1109–1124.
116. Musson, R.M.W., Toro, G.R., Coppersmith, K.J., Bommer, J.J., Deichmann, N., Bungum, H., Cotton, F., Scherbaum, F., Slejko, D. and Abrahamson, N.A. (2005). "Discussion—Evaluating Hazard Results for Switzerland and How Not to Do It: A Discussion of 'Problems in the Application of the SSHAC Probability Method for Assessing Earthquake Hazards at Swiss Nuclear Power Plants' by J-U Klügel", *Engineering Geology*, Vol. 82, No. 1, pp. 43–55.
117. Newmark, N.M. and Hall, W.J. (1982). "Earthquake Spectra and Design", Monograph MNO-3, Earthquake Engineering Research Institute, Berkeley, U.S.A.
118. Nishenko, S.P. and Buland, R. (1987). "A Generic Recurrence Interval Distribution for Earthquake Forecasting", *Bulletin of the Seismological Society of America*, Vol. 77, No. 4, pp. 1382–1399.
119. Novikova, E.I. and Trifunac, M.D. (1993). "Duration of Strong Earthquake Ground Motion: Physical Basis and Empirical Equations", Report CE 93-02, University of Southern California, Los Angeles, U.S.A.

120. Novikova, E.I. and Trifunac, M.D. (1994a). "Duration of Strong Ground Motion: Scaling in Terms of Earthquake Magnitude, Epicentral Distance and Geological and Local Soil Conditions", *Earthquake Engineering & Structural Dynamics*, Vol. 23, No. 6, pp. 1023–1043.
121. Novikova, E.I. and Trifunac, M.D. (1994b). "State of the Art Review on Strong Motion Duration", *Proceedings of the Tenth European Conference on Earthquake Engineering*, Vienna, Austria, Vol. 1, pp. 131–140.
122. Novikova, E.I. and Trifunac, M.D. (1995). "Frequency Dependent Duration of Strong Earthquake Ground Motion: Updated Empirical Equations", Report CE 95-01, University of Southern California, Los Angeles, U.S.A.
123. Ogata, Y. (1988). "Statistical Models for Earthquake Occurrences and Residual Analysis for Point Processes", *Journal of the American Statistical Association*, Vol. 83, No. 401, pp. 9–27.
124. Page, R. (1968). "Aftershocks and Microaftershocks of the Great Alaska Earthquake of 1964", *Bulletin of the Seismological Society of America*, Vol. 58, No. 3, pp. 1131–1168.
125. Papazachos, B.C., Papaioannou, Ch.A., Margaris, V.N. and Theodulidis, N.P. (1992). "Seismic Hazard Assessment in Greece Based on Strong Motion Duration", *Proceedings of the Tenth World Conference on Earthquake Engineering*, Madrid, Spain, Vol. 2, pp. 425–430.
126. Petukhin, A.G., Gusev, A.A., Guseva, E.M., Gordeev, E.L. and Chebrov, V.N. (1999). "Preliminary Model for Scaling of Fourier Spectra of Strong Ground Motion Recorded on Kamchatka", *Pure and Applied Geophysics*, Vol. 156, No. 3, pp. 445–468.
127. Reasenber, P. (1985). "Second-Order Moment of Central California Seismicity, 1969–1982", *Journal of Geophysical Research*, Vol. 90, No. B7, pp. 5479–5495.
128. Reiter, L. (1990). "Earthquake Hazard Analysis: Issues and Insights", Columbia University Press, New York, U.S.A.
129. Rikitake, T. (1976). "Recurrence of Great Earthquakes at Subduction Zones", *Tectonophysics*, Vol. 35, No. 4, pp. 335–362.
130. Rydelek, P.A. and Sacks, I.S. (1989). "Testing the Completeness of Earthquake Catalogues and the Hypothesis of Self-Similarity", *Nature*, Vol. 337, No. 6204, pp. 249–251.
131. Sabetta, F. and Pugliese, A. (1996). "Estimation of Response Spectra and Simulation of Nonstationary Earthquake Ground Motions", *Bulletin of the Seismological Society of America*, Vol. 86, No. 2, pp. 337–352.
132. Sabetta, F., Lucantoni, A., Bungum, H. and Bommer, J.J. (2005). "Sensitivity of PSHA Results to Ground Motion Prediction Relations and Logic-Tree Weights", *Soil Dynamics and Earthquake Engineering*, Vol. 25, No. 4, pp. 317–329.
133. Scherbaum, F., Cotton, F. and Smit, P. (2004). "On the Use of Response Spectral-Reference Data for the Selection and Ranking of Ground-Motion Models for Seismic-Hazard Analysis in Regions of Moderate Seismicity: The Case of Rock Motion", *Bulletin of the Seismological Society of America*, Vol. 94, No. 6, pp. 2164–2185.
134. Scherbaum, F., Bommer, J.J., Bungum, H., Cotton, F. and Abrahamson, N.A. (2005). "Composite Ground-Motion Models and Logic Trees: Methodology, Sensitivities, and Uncertainties", *Bulletin of the Seismological Society of America*, Vol. 95, No. 5, pp. 1575–1593.
135. Schwartz, D.P. and Coppersmith, K.J. (1984). "Fault Behavior and Characteristic Earthquakes: Examples from the Wasatch and San Andreas Fault Zones", *Journal of Geophysical Research*, Vol. 89, No. B7, pp. 5681–5698.
136. Seed, H.B., Ugas, C. and Lysmer, J. (1976). "Site-Dependent Spectra for Earthquake-Resistant Design", *Bulletin of the Seismological Society of America*, Vol. 66, No. 1, pp. 221–243.
137. Silva, W.J. and Lee, K. (1987). "State-of-the-Art for Assessing Earthquake Hazards in the United States. Report 24. WES RASCAL Code for Synthesizing Earthquake Ground Motions", *Miscellaneous Paper S-73-1*, Waterways Experiment Station, U.S. Army Corps of Engineers, Vicksburg, U.S.A.
138. Silverman, B.W. (1986). "Density Estimation for Statistics and Data Analysis", Chapman & Hall, London, U.K.

139. Smith, W.D. (2003). "Earthquake Hazard and Risk Assessment in New Zealand by Monte Carlo Methods", *Seismological Research Letters*, Vol. 74, No. 3, pp. 298–304.
140. Sokolov, V., Loh, C.H. and Wen, K.L. (2000). "Empirical Model for Estimating Fourier Amplitude Spectra of Ground Acceleration in Taiwan Region", *Earthquake Engineering & Structural Dynamics*, Vol. 29, No. 3, pp. 339–357.
141. Senior Seismic Hazard Analysis Committee (1997). "Recommendations for Probabilistic Seismic Hazard Analysis: Guidance on Uncertainty and Use of Experts", Report NUREG/CR-372, United States Nuclear Regulatory Commission, Washington, DC, U.S.A.
142. Stepp, J.C. (1972). "Analysis of Completeness of the Earthquake Sample in the Puget Sound Area and Its Effect on Statistical Estimates of Earthquake Hazard", *Proceedings of the International Conference on Microzonation*, Seattle, U.S.A., Vol. 2, pp. 897–910.
143. Stepp, J.C., Wong, I., Whitney, J., Quittmeyer, R., Abrahamson, N., Toro, G., Youngs, R., Coppersmith, K., Savy, J. and Sullivan, T. (2001). "Probabilistic Seismic Hazard Analyses for Ground Motions and Fault Displacement at Yucca Mountain, Nevada", *Earthquake Spectra*, Vol. 17, No. 1, pp. 113–151.
144. Sykes, L.R. and Nishenko, S.P. (1984). "Probabilities of Occurrence of Large Plate Rupturing Earthquakes for the San Andreas, San Jacinto and Imperial Faults, California, 1983–2003", *Journal of Geophysical Research*, Vol. 89, No. B7, pp. 5905–5928.
145. Thacher, W. (1984). "The Earthquake Deformation Cycle, Recurrence, and the Time-Predictable Model", *Journal of Geophysical Research*, Vol. 89, No. B7, pp. 5674–5680.
146. Theofanopoulos, N.A. and Watabe, M. (1989). "A New Definition of Strong Motion Duration and Comparison with Other Definitions", *Structural Engineering/Earthquake Engineering*, JSCE, Vol. 6, No. 1, pp. 111s–122s.
147. Tinti, S. and Mulargia, F. (1985). "Completeness Analysis of a Seismic Catalog", *Annales Geophysicae*, Vol. 3, No. 3, pp. 407–414.
148. Todorovska, M.I. (1994). "Comparison of Response Spectrum Amplitudes from Earthquakes with Lognormally and Exponentially Distributed Return Period", *Soil Dynamics and Earthquake Engineering*, Vol. 13, No. 2, pp. 97–116.
149. Todorovska, M.I. and Trifunac, M.D. (1996). "Hazard Mapping of Normalized Peak Strain in Soils during Earthquakes: Microzonation of a Metropolitan Area", *Soil Dynamics and Earthquake Engineering*, Vol. 15, No. 5, pp. 321–329.
150. Todorovska, M.I. and Trifunac, M.D. (1999). "Liquefaction Opportunity Mapping via Seismic Wave Energy", *Journal of Geotechnical and Geoenvironmental Engineering*, ASCE, Vol. 125, No. 12, pp. 1032–1042.
151. Todorovska, M.I., Gupta, I.D., Gupta, V.K., Lee, V.W. and Trifunac, M.D. (1995). "Selected Topics in Probabilistic Seismic Hazard Analysis", Report CE 95-08, University of Southern California, Los Angeles, U.S.A.
152. Todorovska, M.I., Trifunac, M.D. and Lee, V.W. (2005). "Probabilistic Assessment of Permanent Ground Displacement across Earthquake Faults", *Proceedings of the International Conference on Earthquake Engineering "Earthquake Engineering in the 21st Century—IZIIS 40 EE-21C"*, Skopje/Ohrid, Macedonia (on CD).
153. Todorovska, M.I., Trifunac, M.D. and Lee, V.W. (2007). "Shaking Hazard Compatible Methodology for Probabilistic Assessment of Permanent Ground Displacement across Earthquake Faults", *Soil Dynamics and Earthquake Engineering*, Vol. 27, No. 6, pp. 586–597.
154. Toro, G.R., Abrahamson, N.A. and Schneider, J.F. (1997). "Model of Strong Ground Motions from Earthquakes in Central and Eastern North America: Best Estimates and Uncertainties", *Seismological Research Letters*, Vol. 68, No. 1, pp. 41–57.
155. Trifunac, M.D. (1971). "A Method for Synthesizing Realistic Strong Ground Motion", *Bulletin of the Seismological Society of America*, Vol. 61, No. 6, pp. 1739–1753.
156. Trifunac, M.D. (1976a). "Preliminary Analysis of the Peaks of Strong Earthquake Ground Motion-Dependence of Peaks on Earthquake Magnitude, Epicentral Distance, and Recording Site Conditions", *Bulletin of the Seismological Society of America*, Vol. 66, No. 1, pp. 189–219.

157. Trifunac, M.D. (1976b). "Preliminary Empirical Model for Scaling Fourier Amplitude Spectra of Strong Ground Acceleration in Terms of Earthquake Magnitude, Source-to-Station Distance, and Recording Site Conditions", *Bulletin of the Seismological Society of America*, Vol. 66, No. 4, pp. 1343–1373.
158. Trifunac, M.D. (1978). "Response Spectra of Earthquake Ground Motion", *Journal of the Engineering Mechanics Division, Proceedings of ASCE*, Vol. 104, No. EM5, pp. 1081–1097.
159. Trifunac, M.D. (1987). "Influence of Local Soil and Geologic Site Conditions on Fourier Spectrum Amplitudes of Recorded Strong Motion Accelerations", Report CE 87-04, University of Southern California, Los Angeles, U.S.A.
160. Trifunac, M.D. (1989). "Dependence of Fourier Spectrum Amplitudes of Recorded Earthquake Accelerations on Magnitude, Local Soil Conditions and on Depth of Sediments", *Earthquake Engineering & Structural Dynamics*, Vol. 18, No. 7, pp. 999–1016.
161. Trifunac, M.D. (1990a). "How to Model Amplification of Strong Earthquake Motions by Local Soil and Geologic Site Conditions", *Earthquake Engineering & Structural Dynamics*, Vol. 19, No. 6, pp. 833–846.
162. Trifunac, M.D. (1990b). "A Microzonation Method Based on Uniform Risk Spectra", *Soil Dynamics and Earthquake Engineering*, Vol. 9, No. 1, pp. 34–43.
163. Trifunac, M.D. (1992). "Should Peak Acceleration be Used to Scale Design Spectrum Amplitudes", *Proceedings of the Tenth World Conference on Earthquake Engineering*, Madrid, Spain, Vol. 10, pp. 5817–5822.
164. Trifunac, M.D. (1995). "Empirical Criteria for Liquefaction in Sands via Standard Penetration Tests and Seismic Wave Energy", *Soil Dynamics and Earthquake Engineering*, Vol. 14, No. 6, pp. 419–426.
165. Trifunac, M.D. (2003). "23rd ISET Annual Lecture: 70-th Anniversary of Biot Spectrum", *ISET Journal of Earthquake Technology*, Vol. 40, No. 1, pp. 19–50.
166. Trifunac, M.D. and Lee, V.W. (1979). "Dependence of Pseudo Relative Velocity Spectra of Strong Motion Acceleration on the Depth of Sedimentary Deposits", Report CE 79-02, University of Southern California, Los Angeles, U.S.A.
167. Trifunac, M.D. and Lee, V.W. (1985). "Preliminary Empirical Models for Scaling Pseudo Relative Velocity Spectra of Strong Earthquake Accelerations in Terms of Magnitude, Distance, Site Intensity and Recording Site Conditions", Report CE 85-04, University of Southern California, Los Angeles, U.S.A.
168. Trifunac, M.D. and Westermo, B. (1976). "Dependence of the Duration of Strong Earthquake Ground Motion on Magnitude, Epicentral Distance, Geological Conditions at the Recording Stations and Frequency of Motion", Report CE 76-02, University of Southern California, Los Angeles, U.S.A.
169. Trifunac, M.D. and Westermo, B.D. (1977). "Recent Developments in the Analysis of the Duration of Strong Earthquake Ground Motion", *Proceedings of the Sixth World Conference on Earthquake Engineering*, New Delhi, Vol. I, pp. 365–371.
170. Trifunac, M.D. and Westermo, B.D. (1982). "Duration of Strong Earthquake Shaking", *International Journal of Soil Dynamics and Earthquake Engineering*, Vol. 1, No. 3, pp. 117–121.
171. Tsai, N.C. (1972). "Spectrum-Compatible Motions for Design Purposes", *Journal of the Engineering Mechanics Division, Proceedings of ASCE*, Vol. 98, No. EM2, pp. 345–356.
172. Tsai, C.-C.P. (2000). "Probabilistic Seismic Hazard Analysis Considering Nonlinear Site Effect", *Bulletin of the Seismological Society of America*, Vol. 90, No. 1, pp. 66–72.
173. USACE (1999). "Engineering and Design: Response Spectra and Seismic Analysis for Concrete Hydraulic Structures", Engineer Manual EM 1110-2-6050, U.S. Army Corps of Engineers, Washington, DC, U.S.A.
174. Utsu, T. (1982). "Relationships between Earthquake Magnitude Scales", *Bulletin of the Earthquake Research Institute, University of Tokyo*, Vol. 57, No. 3, pp. 465–497.
175. Utsu, T. (1984). "Estimation of Parameters for Recurrence Models of Earthquakes", *Bulletin of the Earthquake Research Institute, University of Tokyo*, Vol. 59, No. 1, pp. 53–66.

176. Utsu, T., Ogata, Y. and Matsu'ura, R.S. (1995). "The Centenary of the Omori Formula for a Decay Law of Aftershock Activity", *Journal of Physics of the Earth*, Vol. 43, No. 1, pp. 1–33.
177. Vere-Jones, D. and Ozaki, T. (1982). "Some Examples of Statistical Estimation Applied to Earthquake Data: I. Cyclic Poisson and Self-Exciting Models", *Annals of the Institute of Statistical Mathematics*, Vol. 34, No. 1, pp. 189–207.
178. Weichert, D.H. (1980). "Estimation of the Earthquake Recurrence Parameters for Unequal Observation Periods for Different Magnitudes", *Bulletin of the Seismological Society of America*, Vol. 70, No. 4, pp. 1337–1346.
179. Weimer, S. and Wyss, M. (2000). "Minimum Magnitude of Completeness in Earthquake Catalogs: Examples from Alaska, the Western United States, and Japan", *Bulletin of the Seismological Society of America*, Vol. 90, No. 4, pp. 859–869.
180. Wells, D.L. and Coppersmith, K.J. (1994). "New Empirical Relationships among Magnitude, Rupture Length, Rupture Width, Rupture Area and Surface Displacement", *Bulletin of the Seismological Society of America*, Vol. 84, No. 4, pp. 974–1002.
181. Wesnousky, S.G., Scholz, C.H., Shimazaki, K. and Matsuda, T. (1983). "Earthquake Frequency Distribution and the Mechanics of Faulting", *Journal of Geophysical Research*, Vol. 88, No. B11, pp. 9331–9340.
182. Wong, H.L. and Trifunac, M.D. (1979). "Generation of Artificial Strong Motion Accelerograms", *Earthquake Engineering & Structural Dynamics*, Vol. 7, No. 6, pp. 509–527.
183. Woo, G. (1996). "Kernel Estimation Methods for Seismic Hazard Area Source Modelling", *Bulletin of the Seismological Society of America*, Vol. 86, No. 2, pp. 353–362.
184. Youngs, R.R. and Coppersmith, K.J. (1985). "Implications of Fault Slip Rates and Earthquake Recurrence Models to Probabilistic Seismic Hazard Estimates", *Bulletin of the Seismological Society of America*, Vol. 75, No. 4, pp. 939–964.
185. Zhuang, J., Ogata, Y. and Vere-Jones, D. (2004). "Analyzing Earthquake Clustering Features by Using Stochastic Reconstruction", *Journal of Geophysical Research*, Vol. 109, No. B5, pp. 1–17.

A RESPONSE SPECTRUM-BASED NONLINEAR ASSESSMENT TOOL FOR PRACTICE: INCREMENTAL RESPONSE SPECTRUM ANALYSIS (IRSA)

M. Nuray Aydınoğlu

Department of Earthquake Engineering
Kandilli Observatory and Earthquake Research Institute (KOERI)
Boğaziçi University, Istanbul, Turkey

ABSTRACT

Response Spectrum Analysis (RSA) procedure has become a standard analysis tool in traditional strength-based design of buildings and bridges under reduced seismic loads. RSA has been recently extended to estimate nonlinear seismic demands. The Incremental Response Spectrum Analysis (IRSA) procedure is based on a straightforward implementation of RSA at each piecewise linear incremental step in between the formation of consecutive plastic hinges. The practical version of IRSA works directly with smoothed elastic response spectrum and makes use of the well-known “equal displacement rule” to scale modal displacement increments at each piecewise linear step. IRSA can be characterized as an adaptive multi-mode pushover procedure, in which modal pushover analyses are simultaneously performed for each mode at each incremental step under appropriately scaled modal displacements followed by an application of a modal combination rule. Examples are given to demonstrate the practical implementation of IRSA.

KEYWORDS: Incremental Response Spectrum Analysis, Multi-mode Pushover Analysis, Performance-Based Assessment and Design, Inelastic Spectral Displacement, Equal Displacement Rule

INTRODUCTION

The “Response Spectrum Analysis” (RSA) procedure has become a standard design tool in analysis of buildings and bridges under reduced seismic loads. In spite of the approximate nature of modal combination rules involved, multi-mode RSA has proven to be a powerful and easy-to-use method with a rational representation of modal dynamic properties as well as the direct definition of the seismic input through design response spectrum. Today RSA has been incorporated in a standard fashion in almost all modern seismic design codes as part of the “strength-based seismic design” process and it provides a reasonably accurate estimation of the peak seismic demand quantities in the linear range.

On the other hand, during the course of progress of earthquake engineering in the last few decades researchers and engineers have become well aware that structural behavior and eventual damageability of structures during strong earthquakes were essentially controlled by the inelastic deformation capacities of the ductile structural elements. Accordingly, it has been concluded that the seismic evaluation and design of structures should be based on nonlinear deformation demands, not on linear stresses induced by reduced seismic forces that crudely correlated with an “assumed” overall ductility capacity of a given type of a structure. Consequently, the last decade has witnessed the advent of the “performance-based design” concept, in which significant progress has been achieved with the development of “practice-oriented nonlinear analysis procedures” based on the so-called “pushover analysis”.

All pushover analysis procedures can be considered as approximate extensions of the response spectrum method to the nonlinear response analysis with varying degrees of sophistication. For example, “Nonlinear Static Procedure—NSP” (ATC, 1996; FEMA, 2000) may be looked upon as a “single-mode inelastic response spectrum analysis” procedure where the peak response is obtained through a nonlinear analysis of a modal single-degree-of-freedom (SDOF) system. In practical applications, modal peak response can be appropriately estimated through “inelastic displacement spectrum” (FEMA, 2000; CEN, 2003).

Note that single-mode pushover analysis can be reliably applied to only two-dimensional response of low-rise building structures regular in plan or simple regular bridges, where the seismic response is essentially governed by the fundamental mode. There is no doubt that application of single-mode pushover to high-rise buildings or any building irregular in plan as well as to irregular bridges involving three-dimensional response would lead to incorrect, unreliable results. Therefore, a number of improved pushover analysis procedures have been offered in recent years in an attempt to take higher mode effects into account (Gupta and Kunnath, 2000; Elnashai, 2002; Antoniou et al., 2002; Chopra and Goel, 2002; Kalkan and Kunnath, 2004; Antoniou and Pinho, 2004a, 2004b). In this context, “Incremental Response Spectrum Analysis (IRSA)” procedure has been introduced as a direct extension of the traditional RSA procedure (Aydinoğlu, 2003, 2004).

Despite the fact that pushover analysis has become extremely popular in recent years, there is still a lack of agreement on a universally accepted definition of the procedure. From a historical perspective, pushover analysis has always been understood as a nonlinear “capacity estimation tool” and generally called as “capacity analysis”. The nonlinear structure is monotonically pushed by a set of forces with an invariant distribution until a predefined displacement limit at a given location (say, lateral displacement limit at the roof level of a building) is attained. Such predefined displacement limit is generally termed “target displacement”. The structure may be further pushed up to the collapse condition in order to estimate its “ultimate” deformation and load carrying capacities. It is for this reason that pushover analysis has been also called as “collapse analysis”.

However, in view of performance-based seismic assessment and design requirements, the above definition is not sufficient. According to the new concept introduced by Freeman et al. (1975) and Fajfar and Fischinger (1988), which was subsequently adopted in ATC 40 (ATC, 1996) and FEMA 273 (BSSC, 1997; FEMA, 2000), pushover analysis with its above-given historical definition represents only the first stage of a two-stage nonlinear static procedure, where it simply provides the nonlinear capacity curve of an equivalent single-degree-of-freedom (SDOF) system. The peak response, i.e., seismic demand, is then estimated through nonlinear analysis of this equivalent SDOF system under a given earthquake or through an inelastic displacement spectrum. In this sense the term “pushover analysis” now includes as well the estimation of the so-called “target displacement”. Eventually, controlling seismic demand parameters, such as plastic hinge rotations, are obtained and compared with the specified limits (acceptance criteria) to verify the performance of the structure according to a given performance objective under a given earthquake. Thus according to this broader definition, pushover analysis is not only a capacity estimation tool, but at the same time it is a “demand estimation tool”.

It is rather surprising that among the various multi-mode methods that appeared in the literature during the last decade, only two procedures, i.e., “Modal Pushover Analysis (MPA)” introduced by Chopra and Goel (2002) and “Incremental Response Spectrum Analysis (IRSA)” developed by Aydinoglu (2003, 2004) conform to the above-given contemporary definition (for refined versions of MPA, see Hernandez-Montes et al. (2004), and Kalkan and Kunnath (2006)). Others have actually dealt with “structural capacity estimation” only, although this important limitation has been generally overlooked. It means that none of them aimed at estimating the nonlinear deformation demands (such as plastic hinge rotations or story drifts) under a given earthquake. Although elastic response spectrum of a specified earthquake was utilized, it was not for demand estimation, but only for scaling the relative contributions of vibration modes to obtain seismic load vectors (Antoniou et al., 2002; Elnashai, 2002; Gupta and Kunnath, 2000; Kalkan and Kunnath, 2004; Antoniou and Pinho, 2004a) or to obtain displacement vectors (Antoniou and Pinho, 2004b). Generally, building is pushed to a selected target displacement that is actually obtained from a nonlinear response history analysis (Gupta and Kunnath, 2000; Kalkan and Kunnath, 2004). Alternatively a pushover analysis is performed for a target building drift and the earthquake ground motion is scaled to match that drift (Antoniou and Pinho, 2004a, 2004b). Therefore the results are always presented in a relative manner, generally in the form of story displacement or story drift profiles where pushover and nonlinear response history analysis results are superimposed for a matching target displacement or building drift. Thus, such pushover procedures are able to estimate only the relative distribution of deformation demand quantities, not their magnitudes, and hence their role in a contemporary deformation-based seismic evaluation/design scheme is questionable.

In view of the above assessment, the main objective of this paper is to present the salient features of IRSA procedure (Aydinoğlu, 2003, 2004), which has been recently included in the Turkish Seismic Code (Ministry of Public Works and Settlement, 2006; Aydinoglu, 2006) as a practical tool for performance-

based seismic assessment of existing buildings. But in a broader framework, the paper aims as well to provide a clear insight to the theoretical and practical aspects of the pushover analysis methods, in general. Towards this end, it will start with exploring the theoretical roots of the pushover methods, and will continue with the basic development and implementation of adaptive and invariant single-mode and multi-mode pushover procedures, including IRSA.

EXPLORING THE THEORETICAL ROOTS OF PUSHOVER ANALYSIS

As it is stated above, all pushover methods can be looked upon as nonlinear extensions of the Response Spectrum Analysis (RSA). In this direction, nonlinear response history analysis of a MDOF system will be treated in the following through a “piecewise linear process” where the nonlinear behavior is modeled by simple “plastic hinges”.

1. Piecewise Linear Modeling of Nonlinear Response

Plastic hinges are zero-length elements through which the nonlinear behavior is assumed to be “concentrated” or “lumped” at predetermined sections. A typical plastic hinge is ideally located at the centre of a plastified zone called “plastic hinge length” to be defined at the each end of a clear length of a beam or column. A one-component plastic hinge model with or without strain hardening can be appropriately used to characterize a bi-linear moment-curvature relationship. The so-called “normality condition” can be used to account for the interaction between plastic axial and bending deformation components (McGuire et al., 2000).

Plastic hinge concept is ideally suited to the piecewise linear representation of concentrated nonlinear response. Linear behavior is assumed in between predetermined plastic hinge sections as well as temporally in between the formation of two consecutive plastic hinges. As part of a piecewise linearization process, yield surfaces of plastic hinge sections may be appropriately linearized, i.e., they may be represented by finite number of lines or planes in two- and three-dimensional response models, respectively. As an example, two-dimensional yield surfaces (lines) of reinforced concrete and wide flanged steel sections are shown in Figure 1. Note that number of linear segments may be increased in reinforced concrete section for an enhanced accuracy.

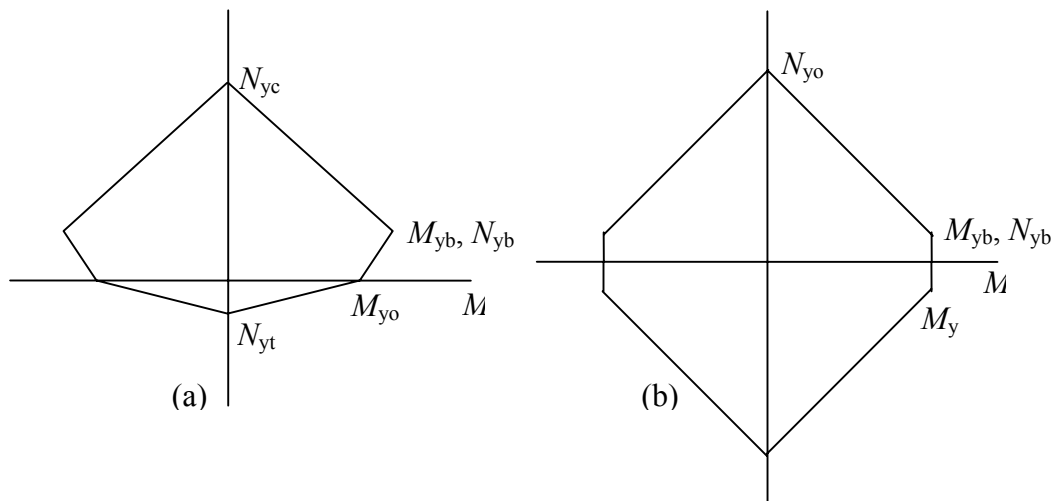


Fig. 1 Piecewise linearised yield surfaces (lines) of typical (a) reinforced concrete section, (b) wide flanged steel section

2. Piecewise Linear Equations of Motion of Nonlinear System

In a plastic hinge model with multi-linear hysteretic behavior, the dynamic response would be essentially linear during an incremental step (i) between a time t and a previous time station t_{i-1} at which the response is already determined. Thus, “piecewise linear” incremental equations of motion of a nonlinear multi-degree-of-freedom (MDOF) structure subjected to a uni-directional ground motion can be written for $t > t_{i-1}$ as

$$\mathbf{M}[\ddot{\mathbf{u}}(t) - \ddot{\mathbf{u}}(t_{i-1})] + \mathbf{C}^{(i)}[\dot{\mathbf{u}}(t) - \dot{\mathbf{u}}(t_{i-1})] + (\mathbf{K}^{(i)} - \mathbf{K}_G^{(i)})[\mathbf{u}(t) - \mathbf{u}(t_{i-1})] = -\mathbf{M}\mathbf{I}_x^g[\ddot{u}_x^g(t) - \ddot{u}_x^g(t_{i-1})] \quad (1)$$

where $\mathbf{u}(t)$ represents the relative displacement vector and $\ddot{u}_x^g(t)$ refers to the ground acceleration of a given earthquake in x -direction. \mathbf{I}_x^g is a kinematic vector representing the pseudo-static transmission of the ground acceleration to the structure, whose components associated with the degrees of freedom in x earthquake direction are unity and others are zero. In Equation (1), \mathbf{M} denotes the mass matrix, $\mathbf{K}^{(i)}$ represents the instantaneous (tangent) stiffness matrix in incremental step (i) and $\mathbf{K}_G^{(i)}$ refers to geometric stiffness matrix accounting for second-order (P-delta) effects. The instantaneous damping matrix $\mathbf{C}^{(i)}$ is assumed to be Rayleigh type, i.e., it is formed as a linear combination of mass and stiffness matrices.

3. Piecewise Linear Mode-Superposition

The instantaneous displacement response during a piecewise linear incremental step (i) can be expanded to the modal coordinates as

$$\mathbf{u}(t) = \sum_{n=1}^{N_m} \mathbf{u}_n(t); \quad \mathbf{u}_n(t) = \Phi_n^{(i)} \Gamma_{xn}^{(i)} d_n(t) \quad (2)$$

in which N_m refers to the number of modes to be considered in the modal expansion, $d_n(t)$ is the modal displacement, and $\Phi_n^{(i)}$ is the instantaneous n th mode shape vector to be obtained from a free-vibration analysis:

$$(\mathbf{K}^{(i)} - \mathbf{K}_G^{(i)}) \Phi_n^{(i)} = (\omega_n^{(i)})^2 \mathbf{M} \Phi_n^{(i)} \quad (3)$$

where $\omega_n^{(i)}$ represents the instantaneous natural frequency. $\Gamma_{xn}^{(i)}$ in Equation (2) denotes the instantaneous participation factor for an earthquake in x -direction, which is defined as

$$\Gamma_{xn}^{(i)} = \frac{L_{xn}^{(i)}}{M_n^{(i)}} = \frac{\Phi_n^{(i)T} \mathbf{M} \mathbf{I}_x^g}{\Phi_n^{(i)T} \mathbf{M} \Phi_n^{(i)}} \quad (4)$$

Substituting Equation (2) and time derivatives into Equation (1) and pre-multiplying with $\Phi_n^{(i)}$ followed by applying modal orthogonality conditions and considering Equation (4) result in an uncoupled instantaneous modal equation of motion in the n th mode:

$$\ddot{d}_n(t) + 2\xi_n^{(i)}\omega_n^{(i)}\dot{d}_n(t) + (\omega_n^{(i)})^2 d_n(t) = -[\ddot{u}_x^g(t) - \ddot{u}_x^g(t_{i-1})] + \ddot{d}_n^*(t_{i-1}) + 2\xi_n^{(i)}\omega_n^{(i)}\dot{d}_n^*(t_{i-1}) + (\omega_n^{(i)})^2 d_n^*(t_{i-1}) \quad (5)$$

Here, $\xi_n^{(i)}$ represents modal damping ratio, and $d_n^*(t_{i-1})$ is expressed as

$$d_n^*(t_{i-1}) = \frac{\Phi_n^{(i)T} \mathbf{M} \mathbf{u}(t_{i-1})}{L_{xn}^{(i)}} \quad (6)$$

where $L_{xn}^{(i)}$ is as defined in Equation (4). Equations (5) and (6) reveal that each modal equation is dependent upon the past response history of the MDOF structural system in terms of displacement vector and its time derivatives developed at the previous time instant. Applying modal expansion to $\mathbf{u}(t_{i-1})$ as in Equation (2), $d_n^*(t_{i-1})$ given in Equation (6) can be expressed as

$$d_n^*(t_{i-1}) = \frac{\Phi_n^{(i)T} \mathbf{M} \sum_{m=1}^{N_m} \Phi_m^{(i-1)} \Gamma_{xm}^{(i-1)} d_m(t_{i-1})}{L_{xn}^{(i)}} \quad (7)$$

from which it can be observed that if $\Phi_n^{(i-1)}$ were close enough to $\Phi_n^{(i)}$, the above-mentioned coupling would cease to exist. Indeed, if it is assumed that $\Phi_n^{(i)} \cong \Phi_n^{(i-1)}$ for all modes, which is expected to hold

in relatively “redundant” systems, then modal orthogonality conditions would result in the following simplification:

$$d_n^*(t_{i-1}) \cong d_n(t_{i-1}) \quad (8)$$

For the sake of simplicity, the following modified notation is used in all expressions to follow:

$$d_n(t_i) \rightarrow d_n^{(i)}; \quad d_n(t_{i-1}) \rightarrow d_n^{(i-1)} \quad (9)$$

Thus from Equations (5), (8) and (9), typical n th modal equation can be expressed approximately in an incremental form as

$$\Delta \ddot{d}_n^{(i)} + 2\xi_n^{(i)} \omega_n^{(i)} \Delta \dot{d}_n^{(i)} + (\omega_n^{(i)})^2 \Delta d_n^{(i)} = -\Delta \ddot{u}_x^{g(i)} \quad (10)$$

where $\Delta \ddot{u}_x^{g(i)} = \ddot{u}_x^{g(i)} - \ddot{u}_x^{g(i-1)}$ is the ground acceleration increment and $\Delta d_n^{(i)}$ represents the modal displacement increment, the latter of which can be expressed as

$$d_n^{(i)} = d_n^{(i-1)} + \Delta d_n^{(i)} \quad (11)$$

Note that the third term at the left-hand side of Equation (10) is called “modal pseudo-acceleration increment”, which is defined as

$$\Delta a_n^{(i)} = (\omega_n^{(i)})^2 \Delta d_n^{(i)} \quad (12)$$

where its cumulative value at the (i) th step can be written as similar to the cumulative modal displacement given in Equation (11):

$$a_n^{(i)} = a_n^{(i-1)} + \Delta a_n^{(i)} \quad (13)$$

Thus Equation (10) can be rewritten as

$$\Delta \ddot{d}_n^{(i)} + 2\xi_n^{(i)} \omega_n^{(i)} \Delta \dot{d}_n^{(i)} + \Delta a_n^{(i)} = -\Delta \ddot{u}_x^{g(i)} \quad (14)$$

With respect to the exact incremental equations of motion given in Equation (1), approximate modal incremental equations given in Equation (10) or (14) are expected to provide better results in relatively “redundant systems” due to the assumptions indicated in Equation (8). Such systems have the potential of developing large number of plastic hinges and therefore the formation of a new hinge would only marginally (or even negligibly) modify the mode shapes of the structural system. On the contrary, in structural systems where only a small number of hinges can potentially develop, such as bridges with few isolated single-column piers, the use of incremental equations of motion (see Equation (10) or (14)) could lead to erroneous results, because significant changes could occur in mode shapes in successive incremental steps. Note that these observations apply as well to those systems whose response is practically governed by a single mode only.

4. Modal Hysteresis Loops and Modal Capacity Diagrams

It is shown above that incremental solution of Equation (1) can be approximately reduced to the incremental solution of Equation (10) or (14), through which “modal displacement versus modal pseudo-acceleration diagrams” can be constructed. Those hypothetical diagrams represent the “modal hysteresis loops”, which are schematically depicted in Figure 2(a). The outer hysteresis loops should be the fattest in the first mode and get thinner and steeper as the mode number increases. According to Equation (12), the instantaneous slope of a given diagram is equal to the eigenvalue (natural frequency squared) of the corresponding mode at the piecewise linear increment concerned. The backbone curves of the hypothetical modal hysteresis loops in the first quadrant may be appropriately called the “modal capacity diagrams”, which are indicated by solid curves in Figure 2(a). In the special case where the first mode alone is assumed to represent the dynamic response, the modal capacity diagram is, by definition, identical to the so-called “capacity spectrum” defined in the Capacity Spectrum Method (ATC, 1996). The term “modal capacity diagram” is introduced by Aydinoglu (2003) by adding the word “modal” to the terminology proposed by Chopra and Goel (1999). Note that in linearly elastic response, modal hysteresis curves and modal capacity diagrams degenerate into straight lines as shown in Figure 2(b).

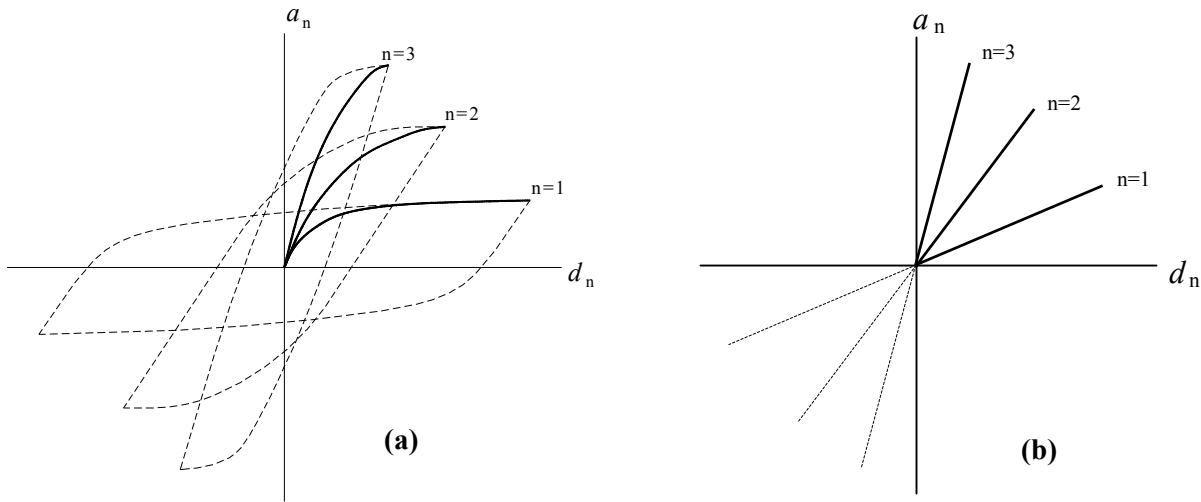


Fig. 2 (a) Schematic representation of hypothetical modal hysteresis loops and their backbone curves (modal capacity diagrams—solid curves); (b) Corresponding curves and diagrams in linear response

5. A Generic Definition of Pushover Analysis

Within the framework of the theoretical basis explained above, pushover analysis can be defined as a “monotonic nonlinear analysis” of progressively yielding MDOF system with a simultaneous “monotonic” construction of the modal capacity diagram(s) until the peak response is obtained for a given earthquake ground motion, so that the analysis procedure can be used as an essential tool in performance assessment process. Thus, according to the classification given in the introductory section of this paper, pushover analysis is ultimately defined as a “seismic demand estimation tool”. More specifically, the analysis should be able to produce ductile deformation demands, such as plastic hinge rotations or corresponding strains, as well as brittle force demands, e.g., shears in reinforced concrete elements.

With respect to the above presented analytical formulation, now the analysis process is changed from a “dynamic response history analysis” of MDOF system to a “monotonic pushover history analysis”, while the “incremental time step” (i) transforms to a monotonic “pushover step” (i), which is defined as the “analysis step in between the formation of two consecutive plastic hinges”. Since modal capacity diagrams are defined as the backbone curves of the modal hysteresis loops, their peak values, i.e., modal seismic demand, can be obtained from the nonlinear solution of Equation (10) under a given earthquake ground motion. Alternatively, “inelastic response spectrum” can be utilized for the same purpose, which is the preferred option for routine engineering applications.

The “pushover history analysis” can be performed either in the form of a static analysis under the specified equivalent seismic loads with adaptive or invariant distributions, or it may be formulated as a piecewise linear response spectrum analysis by considering the continuously changing properties of the structure. The latter may be interpreted as performing pushover analyses in various modes simultaneously.

As a general background to pushover history analyses, relationships between the coordinates of modal capacity diagrams, i.e., modal displacement and modal pseudo-acceleration of modal SDOF systems versus the corresponding response quantities of the MDOF system, can be expressed as in the following:

- (a) Piecewise linear relationship between the n th modal displacement increment and the corresponding displacement increment of MDOF system at the (i)th pushover step is

$$\Delta \mathbf{u}_n^{(i)} = \Phi_n^{(i)} \Gamma_{xn}^{(i)} \Delta d_n^{(i)} \quad (15)$$

- (b) Piecewise linear relationship between the n th modal pseudo-acceleration increment and the corresponding equivalent seismic load increment of MDOF system at the (i)th pushover step is

$$\Delta \mathbf{f}_n^{(i)} = \mathbf{M} \Phi_n^{(i)} \Gamma_{xn}^{(i)} \Delta a_n^{(i)} \quad (16)$$

Note that the above expression is adopted from the monotonic counterpart of the third term on the left-hand side of Equation (1), which can be expressed as

$$\Delta \mathbf{f}_n^{(i)} = (\mathbf{K}^{(i)} - \mathbf{K}_G^{(i)}) \Delta \mathbf{u}_n^{(i)} \quad (17)$$

In fact, substituting Equation (15) into Equation (17) and utilizing Equations (3) and (12) results in Equation (16).

SINGLE-MODE PUSHOVER ANALYSIS: PIECEWISE LINEAR IMPLEMENTATION WITH ADAPTIVE AND INVARIANT LOAD PATTERNS

Single-mode piecewise linear pushover procedure is applicable to low-to-medium rise regular buildings whose response is effectively controlled by the first (predominant) mode. Slight torsional irregularities may be allowed provided that a 3-D structural model is employed.

Regarding the adaptive pattern, the first-mode counterpart of equivalent seismic load increment given in Equation (16) can be written for the (i) th pushover step as

$$\Delta \mathbf{f}_1^{(i)} = \bar{\mathbf{m}}_1^{(i)} \Delta a_1^{(i)}; \quad \bar{\mathbf{m}}_1^{(i)} = \mathbf{M} \Phi_1^{(i)} \Gamma_{x1}^{(i)} \quad (18)$$

where $\bar{\mathbf{m}}_1^{(i)}$ represents the vector of “participating modal masses” effective in the first mode. Superscript (i) on the participating modal mass and mode shape vectors as well as on the modal participation factor indicates that instantaneous first-mode shape corresponding to the current configuration of the structural system is considered following the formation of the last plastic hinge at the end of the previous pushover step. In adaptive case, a fully compatible modal expression can be written from Equation (15) for the increment of displacement vector as well:

$$\Delta \mathbf{u}_1^{(i)} = \bar{\mathbf{u}}_1^{(i)} \Delta d_1^{(i)}; \quad \bar{\mathbf{u}}_1^{(i)} = \Phi_1^{(i)} \Gamma_{x1}^{(i)} \quad (19)$$

Since both $\Delta \mathbf{u}_1^{(i)}$ and $\Delta \mathbf{f}_1^{(i)}$ are based on the same instantaneous modal quantities, there is a one-to-one correspondence between them. Thus, adaptive implementation of the single-mode pushover analysis can be based on either a monotonic increase of displacements or equivalent seismic loads. However, this is not the case when the load pattern is kept invariant during pushover history, i.e., a compatible modal displacement expression cannot be provided. In the following paragraph, pushover analysis will be treated on the basis of monotonic increase in the equivalent seismic loads where both adaptive and invariant patterns will be considered in a common framework.

In the case of invariant load pattern, Equation (18) is modified as

$$\Delta \mathbf{f}_1^{(i)} = \bar{\mathbf{m}}_1^{(1)} \Delta a_1^{(i)}; \quad \bar{\mathbf{m}}_1^{(1)} = \mathbf{M} \Phi_1^{(1)} \Gamma_{x1}^{(1)} \quad (20)$$

where the vector of first-mode participating modal masses, $\bar{\mathbf{m}}_1^{(1)}$, is defined at the first pushover step ($i = 1$) and retained “invariant” during the entire course of pushover history. Note that inverted triangular or even height-wise constant amplitude mode shapes are being used in practice (FEMA, 2000) in place of $\Phi_1^{(1)}$.

1. Pushover History Analysis

In piecewise linear pushover history analysis equivalent seismic load vector of the MDOF system, which could have either adaptive or invariant pattern, is increased monotonically in the increments of $\Delta \mathbf{f}_1^{(i)}$ where modal pseudo-acceleration increment, $\Delta a_1^{(i)}$, is simultaneously calculated as the single unknown quantity at each (i) th pushover step leading to the formation of a new hinge. In this respect any response quantity of interest, such as the increment of an internal force, a displacement component, a story drift, or a plastic hinge rotation of a previously formed hinge, to be developed at the end of the (i) th pushover step may be written in a generic form as

$$q^{(i)} = q^{(i-1)} + \Delta q^{(i)} = q^{(i-1)} + \bar{q}^{(i)} \Delta a_1^{(i)} \quad (21)$$

Here, $q^{(i)}$ and $q^{(i-1)}$ are the “generic response quantities” to develop at the end of current and previous pushover steps, $\Delta q^{(i)}$ is the respective increment, and $\bar{q}^{(i)}$ represents a generic response quantity to be obtained for $\Delta a_1^{(i)} = 1$, i.e., from the application of $\bar{\mathbf{m}}_1^{(i)}$ or $\bar{\mathbf{m}}_1^{(1)}$ as equivalent seismic loads, representing the adaptive or invariant pattern, respectively. Now, the above generic expression is specialized for the response quantities that define the coordinates of the “yield surfaces” of all potential plastic hinges, e.g., biaxial bending moments and axial forces in a general, three-dimensional response of a framed structure. In the first pushover step ($i = 1$), response quantities due to gravity loading are considered as $q^{(0)}$ in Equation (21). As part of the piecewise linearization process of pushover analysis as well as to avoid iterative operations in the hinge identification process, yield surfaces are appropriately linearized in a piecewise fashion as mentioned above (Figure 1), i.e., they are represented by finite number of lines or planes in two- and three-dimensional response models, respectively. As an example, planar yield surfaces (lines) of a reinforced concrete or steel section (j) as shown in Figure 1 where a typical line (s) can be expressed as

$$\alpha_{j,s} M_{jp} + \beta_{j,s} N_{jp} = 1 \quad (22)$$

Here, M_{jp} and N_{jp} represent the yield bending moment and corresponding axial force, respectively, at the section j while $\alpha_{j,s}$ and $\beta_{j,s}$ refer to the coefficients defining the yield line (s). For the (i)th pushover step, Equation (21) is specialized for bending moment and axial force as

$$M_{j,l}^{(i)} = M_{j,l}^{(i-1)} + \bar{M}_{j,l}^{(i)} \Delta a_1^{(i)}; \quad N_{j,l}^{(i)} = N_{j,l}^{(i-1)} + \bar{N}_{j,l}^{(i)} \Delta a_1^{(i)} \quad (23)$$

which are then substituted into Equation (22), and $\Delta a_1^{(i)}$ is extracted as

$$(\Delta a_1^{(i)})_{j,s} = \frac{1 - \alpha_{j,s} M_{j,l}^{(i-1)} - \beta_{j,s} N_{j,l}^{(i-1)}}{\alpha_{j,s} \bar{M}_{j,l}^{(i)} + \beta_{j,s} \bar{N}_{j,l}^{(i)}} \quad (24)$$

The yield line (s) at the section (j) that intersected with a minimum positive $(\Delta a_1^{(i)})_{j,s}$ among all yield lines of all potential plastic hinges identifies the new hinge formed at the end of the (i)th pushover step. Once $\Delta a_1^{(i)}$ is determined, any response quantity of interest developed at the end of that step can be obtained from the generic expression of Equation (21).

As the formation of the new hinge is identified, the current global stiffness matrix of the structure is locally modified such that only the element stiffness matrix affected by the new hinge is replaced with a new one for the next pushover step. Normality criterion is enforced in columns and walls for the coupling of internal forces as well as plastic deformation components of the newly formed plastic hinge.

Provided that the load pattern is adaptive and therefore resulting displacement increments are always compatible with the equivalent seismic load increments, modal displacement increment, $\Delta d_1^{(i)}$, is related through Equation (12) to the corresponding modal pseudo-acceleration increment, $\Delta a_1^{(i)}$, obtained at each pushover step:

$$\Delta d_1^{(i)} = \frac{\Delta a_1^{(i)}}{(\omega_1^{(i)})^2} \quad (25)$$

Here, $\omega_1^{(i)}$ represents the instantaneous natural circular frequency calculated at the (i)th pushover step. In the case of an invariant pattern, however, since modal equivalent loads and resulting displacement increments are not compatible, two procedures can be suggested to estimate the modal displacement increments.

- (a) The first procedure involves the approximate calculation of the instantaneous eigenvalue, $(\omega_1^{(i)})^2$, as a Rayleigh quotient (Aydinoğlu, 2005):

$$(\omega_1^{(i)})^2 \cong \frac{\sum_k \bar{m}_{k,1}^{(1)} \bar{u}_{k,1}^{(i)}}{\sum_k m_k \bar{u}_{k,1}^{(i)2}} \quad (26)$$

in which $\bar{u}_{k,1}^{(i)}$ represents the displacement component at the k th DOF under the equivalent seismic loads $\bar{m}_{k,1}^{(1)}$ with invariant pattern that are defined through Equation (20) for $\Delta a_1^{(i)} = 1$. Thus, the modal displacement increment, $\Delta d_1^{(i)}$, is obtained by substituting Equation (26) into Equation (25).

- (b) The second procedure is the one already applied in practice (ATC, 1996; FEMA, 2000), where modal displacement increment is calculated through Equation (19), i.e., by specializing it for the roof displacement increment with the corresponding first-mode shape amplitude of the first pushover step:

$$\Delta d_1^{(i)} = \frac{\Delta u_{N,1}^{(i)}}{\Phi_{N,1}^{(1)} \Gamma_{x1}^{(1)}} \quad (27)$$

It is worth noting that in the single-mode pushover procedure presented herein, there is no need to plot the conventional pushover curve, with vertical axis representing the sum of equivalent seismic loads, i.e., base shear. Accordingly, conversion of the base shear increments to pseudo-acceleration increments is not required, because those are obtained directly by Equation (24) at each pushover step. In fact, it can be shown that even if the conventional approach had been applied the same results would be obtained, i.e., the base shear in x earthquake direction is obtained by summing up the equivalent seismic loads given by Equation (20) in that direction:

$$\Delta V_{x1}^{(i)} = \mathbf{I}_x^g T \Delta \mathbf{f}_1^{(i)} = \mathbf{I}_x^g T \bar{\mathbf{m}}_1^{(1)} \Delta a_1^{(i)} \quad (28)$$

On the other hand, total participating modal mass of the MDOF system in the x -direction is obtained by summing up the elements of the vector of participating masses given in Equation (20), i.e.,

$$\bar{M}_{x1}^{(1)} = \mathbf{I}_x^g T \bar{\mathbf{m}}_1^{(1)} = \frac{L_{x1}^{(1)2}}{M_1^{(1)}} \quad (29)$$

Thus modal pseudo-acceleration increment at the (i) th pushover step is obtained from Equations (28) and (29) as

$$\Delta a_1^{(i)} = \frac{\Delta V_{x1}^{(i)}}{\bar{M}_{x1}^{(1)}} \quad (30)$$

which is nothing but the conversion relationship used in the traditional pushover procedure (ATC, 1996; FEMA, 2000).

With $\Delta d_1^{(i)}$ and $\Delta a_1^{(i)}$ determined as above, adding to those obtained at the end of the previous pushover step, modal displacement and modal pseudo-acceleration are calculated from Equations (11) and (13) at the end of the (i) th step as

$$d_1^{(i)} = d_1^{(i-1)} + \Delta d_1^{(i)}; \quad a_1^{(i)} = a_1^{(i-1)} + \Delta a_1^{(i)} \quad (31)$$

It is noted that essentially $\Delta d_1^{(i)}$ and $\Delta a_1^{(i)}$ are the elements of an incremental modal equation of motion of the first-mode equivalent SDOF system:

$$\Delta \ddot{d}_1^{(i)} + 2\xi_1^{(i)} \omega_1^{(i)} \Delta \dot{d}_1^{(i)} + \Delta a_1^{(i)} = -\Delta \ddot{u}_x^{g(i)} \quad (32)$$

Thus modal capacity diagram of the fundamental mode is obtained directly as shown schematically in Figure 3, which is nothing but the so-called “capacity spectrum” (ATC, 1996) obtained from the traditional pushover curve through a modal coordinate transformation. According to Equation (25), instantaneous slope of the linear segment of the modal capacity diagram at the pushover step (i) in between the plastic hinge points $(i-1)$ and (i) is equal to the fundamental “eigenvalue” of the structural system at that step as shown in Figure 3.

Note that instantaneous slope of the capacity diagram could turn out to be negative due to the P-delta effects, as indicated in Figure 3, when accumulated plastic deformations result in a negative-definite

second-order stiffness matrix. In the case of invariant load pattern, at such a critical pushover step, the monotonic load increase process is terminated. From such a step onwards, analysis is generally continued with a monotonic displacement increment process, while retaining a constant displacement pattern obtained at the critical step. The accuracy of this approach is doubtful.

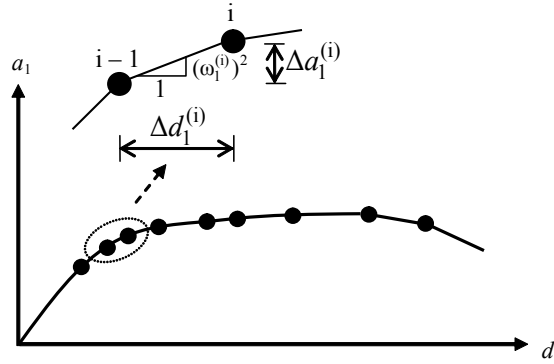


Fig. 3 Modal capacity diagram of the fundamental mode

In the case of adaptive solution, the analysis process is not influenced by a negative instantaneous slope of the capacity diagram. A negative slope means a negative eigenvalue and thus an imaginary natural frequency, which leads to a modal response that resembles the non-vibratory response of an over-damped system (Aydinoğlu and Fahjan, 2003). The corresponding mode shape has a remarkable physical significance, representing the post-buckling deformation state of the structure. Although structural engineers are not familiar with the negative (or zero) eigenvalues due to negative-definite (or singular) stiffness matrices, such eigenvalues and corresponding eigenvectors do exist, which can be routinely calculated by “matrix transformation methods” of eigenvalue analysis, such as the well-known “Jacobi Method” (Bathe, 1996).

As mentioned above, a remarkable aspect of the above-presented adaptive procedure is that it does not necessitate the plotting of conventional pushover curve in terms of base shear versus roof displacement. Instead, modal capacity diagram, which itself is the essential tool for the estimation of modal displacement demand, is obtained directly on including direct consideration of the P-delta effects.

2. Estimation of Modal Displacement Demand: Inelastic Spectral Displacement

The above-described process of pushover history analysis is continued until cumulative modal displacement calculated by Equation (31) exceeds the first-mode “inelastic spectral displacement”. It means that the last pushover step has been reached, and, therefore, the modal displacement to develop at the end of this step, $d_1^{(p)}$ (superscript p stands for “peak”), is made equal to the inelastic spectral displacement, $S_{di,1}$:

$$d_1^{(p)} = S_{di,1} \quad (33)$$

This is followed by the calculation of the modal displacement increment in the last step (p):

$$\Delta d_1^{(p)} = S_{di,1} - d_1^{(p-1)} \quad (34)$$

The inelastic first-mode spectral displacement, $S_{di,1}$, can be calculated for a given ground motion record through nonlinear analysis of the modal SDOF system according to Equation (32) by considering hysteresis loops defined by the bi-linearized modal capacity diagram as the backbone curve (see Figure 4(b)). However for practical purposes, inelastic first-mode spectral displacement, $S_{di,1}$, can be appropriately defined through a simple procedure based on the “equal displacement rule” (FEMA, 2000):

$$S_{di,1} = C_{R,1} S_{de,1} \quad (35)$$

in which $S_{de,1}$ represents the elastic spectral displacement of the corresponding linear SDOF system with the same period (stiffness) as the initial period of the bilinear inelastic system. Note that in practice

cracked section stiffnesses are used in reinforced concrete systems throughout the pushover analysis and therefore the fundamental period of the system calculated at the first “linear” pushover step ($i = 1$) is taken as the initial period of the bilinear inelastic system. This is contrary to the traditional approach where the fundamental period is further lengthened excessively due to the bi-linearization of modal capacity diagram. In Figure 4, modal capacity diagram and the elastic response spectrum are combined in a “displacement—pseudo-acceleration” format. In the case where $T_1^{(1)} > T_S$ (with T_S being the characteristic spectrum period at the intersection of constant velocity and constant acceleration regions), bi-linearization of the modal capacity diagram is even unnecessary as indicated in Figure 4(a), because “spectral displacement amplification factor” $C_{R,1}$ is always equal to unity:

$$C_{R,1} = 1 \quad (T_1^{(1)} > T_S) \quad (36)$$

In the case where $T_1^{(1)} \leq T_S$, initial period is still defined as above; however, an iteration is necessary to calculate the spectral displacement amplification factor by using the following familiar relationship (FEMA, 2000; MPWS, 2006):

$$C_{R,1} = \frac{1 + (R_{y,1} - 1)T_S / T_1^{(1)}}{R_{y,1}} \geq 1 \quad (T_1^{(1)} \leq T_S) \quad (37)$$

in which $R_{y,1}$ refers to the yield reduction factor (Figure 4(b)):

$$R_{y,1} = \frac{S_{ae,1}}{a_{y,1}} \quad (38)$$

Note that alternative relationships are available for the displacement amplification factor that can be used in practical applications in lieu of those given by Equations (36) and (37). For those reference may be given to Aydınoğlu and Kaçmaz (2002), and to FEMA 440 (FEMA, 2005).

Once modal displacement increment in the last step, $\Delta d_1^{(p)}$, is estimated, the corresponding $\Delta a_1^{(p)}$ is determined, and in turn, any response quantity of interest developed at the end of that step can be obtained from the generic expression of Equation (21).

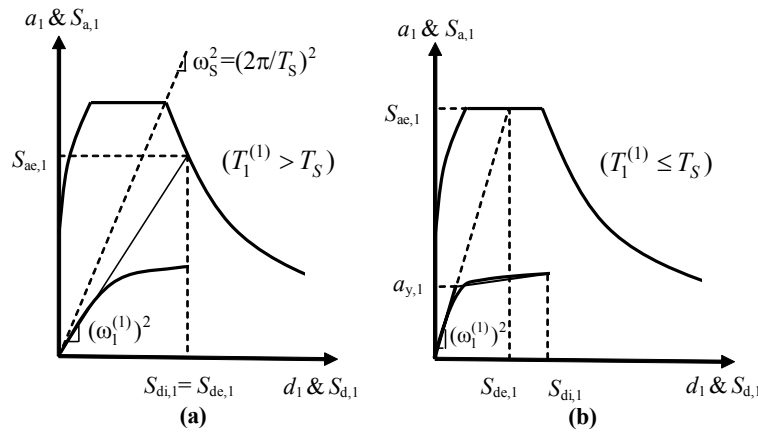


Fig. 4 Estimating modal displacement demand

MULTI-MODE ADAPTIVE PUSHOVER ANALYSIS: INCREMENTAL RESPONSE SPECTRUM ANALYSIS (IRSA) PROCEDURE

Multi-mode pushover procedure is intended for application on high-rise and/or irregular buildings and bridges where the seismic response cannot be effectively represented by the first mode only. These include torsionally sensitive buildings with 3-D response characteristics.

In line with the theoretical background provided above, in the multi-mode case monotonic pushover history analyses have to be performed “simultaneously” in all the modes considered. As with the single-mode pushover, in the adaptive case both MDOF system displacement increments and equivalent seismic load increments are based on the same instantaneous modal quantities. Thus the implementation of multi-mode pushover analysis can be based on either a monotonic increase of displacements or equivalent seismic loads. These may be called “displacement-controlled” and “force-controlled” pushovers, respectively. To start with, using Equation (15), modal displacement increments of MDOF system can be expressed as

$$\Delta \mathbf{u}_n^{(i)} = \bar{\mathbf{u}}_n^{(i)} \Delta d_n^{(i)} ; \quad \bar{\mathbf{u}}_n^{(i)} = \Phi_n^{(i)} \Gamma_{xn}^{(i)} \quad (39)$$

and corresponding expressions for the compatible seismic load increments can be written as multi-mode counterparts of those given in Equation (18) as

$$\Delta \mathbf{f}_n^{(i)} = \bar{\mathbf{m}}_n^{(i)} \Delta a_n^{(i)} ; \quad \bar{\mathbf{m}}_n^{(i)} = \mathbf{M} \Phi_n^{(i)} \Gamma_{xn}^{(i)} \quad (40)$$

1. Modal Scaling

In order to define modal MDOF response, modal displacement increments $\Delta d_n^{(i)}$ or modal pseudo-acceleration increments $\Delta a_n^{(i)}$ have to be determined in all modes at each pushover step, depending on whether displacement- or force-controlled pushover is applied. Since just a single plastic hinge forms and therefore only one yield condition is applicable at the end of each piecewise linear step, a reasonable assumption needs to be made for the relative values of modal displacement or modal pseudo-acceleration increments, so that the number of unknowns are reduced to one. This is called “modal scaling”, which is the most critical assumption to be made in all multi-mode pushover procedures, including IRSA. In this respect the only exception is the Modal Pushover Analysis—MPA (Chopra and Goel, 2002) where modal coupling is completely disregarded in the formation of plastic hinges and therefore modal scaling is omitted.

1.1 Modal Scaling Based on Instantaneous Elastic Spectral Quantities

Modal scaling is probably the most critical and, at the same time, one of the most controversial issues of multi-mode pushover analysis. In a number of studies, such as Gupta and Kunnath (2000), Elnashai (2002), Antoniou et al. (2002), Antoniou and Pinho (2004a), force-controlled pushover is implemented where modal scaling is performed on “instantaneous” modal pseudo-accelerations. Using the terminology and notation of the present paper such a modal scaling can be expressed as

$$\Delta a_n^{(i)} = \Delta F^{(i)} S_{aen}^{(i)} \quad (41)$$

where $S_{aen}^{(i)}$ represents the instantaneous n th mode “elastic” spectral pseudo-acceleration at the (i) th pushover step, and $\Delta F^{(i)}$ refers to an incremental scale factor, which is independent of the mode number. Thus Equation (41) means that modal pseudo-acceleration increments are scaled in proportion to the respective elastic spectral accelerations. Note that the above-defined modal scaling is essentially identical to the scaling of modal displacement increments in proportion to respective elastic spectral displacements, which may be expressed as

$$\Delta d_n^{(i)} = \Delta F^{(i)} S_{den}^{(i)} \quad (42)$$

where $S_{den}^{(i)}$ represents the instantaneous n th mode “elastic” spectral displacement corresponding to the above-given $S_{aen}^{(i)}$, i.e., $S_{den}^{(i)} = (\omega_n^{(i)})^2 S_{aen}^{(i)}$. Such a scaling has been used recently in a displacement-controlled pushover procedure (Antoniou and Pinho, 2004b).

Naturally this type of modal scaling is exact for a single-step linear analysis with $\Delta F^{(1)} = 1$; however it is doubtful whether it should be implemented in a nonlinear case. In fact, instantaneous elastic spectral parameters have no relation at all with the instantaneous nonlinear modal response increments. When the structure softens due to accumulated plastic deformations, the instantaneous “elastic” spectral displacement of the first mode increases disproportionately with respect to those of the higher modes,

leading to an exaggeration of the effect of the first mode in the hinge formation process prior to reaching the peak response.

1.2 Modal Scaling Based on Instantaneous Inelastic Spectral Displacements

Displacement-controlled pushover is the preferred approach in the Incremental Response Spectrum Analysis—IRSA (Aydinoğlu, 2003, 2004), and modal pushovers are implemented simultaneously by imposing instantaneous displacement increments of the MDOF system at each pushover step according to Equation (39). In principle, modal displacements are scaled in IRSA with respect to the “inelastic spectral displacements”, $S_{din}^{(i)}$, associated with the “instantaneous” configuration of the structure (Aydinoğlu, 2003). This is the main difference between IRSA and other studies referred to above where modal scaling is based on “instantaneous elastic” spectral pseudo-accelerations or displacements. IRSA’s adoption of “inelastic spectral displacements” for modal scaling may be considered as a “rational choice”, because those spectral displacements are nothing but the “peak” values of the modal displacements to be reached, as will be shown in the following.

In practice, modal scaling based on “inelastic spectral displacements” can be easily achieved by taking advantage of the “equal displacement rule”. Assuming that seismic input is defined via “smoothed elastic response spectrum”, according to this simple and well-known rule (which is already utilized above for the estimation of modal displacement demand in single-mode pushover), “peak displacement” of an inelastic SDOF system and that of the corresponding elastic system are assumed practically equal to each other, provided that the effective initial period is longer than the “characteristic period” of the elastic response spectrum. The characteristic period is approximately defined as the transition period from the constant acceleration segment to the constant velocity segment of the spectrum. For periods shorter than the characteristic period, elastic spectral displacement is amplified using a displacement modification factor, i.e., C_1 coefficient given in FEMA 356 (FEMA, 2000). However, such a situation is seldom encountered in mid- to high-rise buildings and long bridges involving multi-mode response. In such structures, effective initial periods of the first few modes are likely to be longer than the characteristic period and therefore those modes automatically qualify for the equal displacement rule. On the other hand, effective post-yield slopes of the modal capacity diagrams get steeper and steeper in higher modes with gradually diminishing inelastic behavior (Figure 5). Thus, it can be comfortably assumed that inelastic spectral displacement response in higher modes would not be different from the corresponding spectral elastic response. Hence, smoothed elastic response spectrum may be used in its entirety for scaling modal displacements without any modification. As in the single-mode analysis, in reinforced concrete buildings elastic periods calculated at the first pushover step may be considered in lieu of the initial periods obtained from the bi-linearization of modal capacity diagrams (see Figure 4(b)).

In line with the “equal displacement rule”, scaling procedure applicable to the n th mode increment of modal displacement at the (i) th pushover step is simply expressed as

$$\Delta d_n^{(i)} = \Delta \tilde{F}^{(i)} S_{den}^{(1)} \quad (43)$$

where $\Delta \tilde{F}^{(i)}$ is an “incremental scale factor”, which is applicable to all modes at the (i) th pushover step. $S_{den}^{(1)}$ represents the “initial elastic spectral displacement” defined at the first step (Figure 5), which is taken equal to the “inelastic spectral displacement” associated with the “instantaneous” configuration of the structure at any pushover step. Cumulative modal displacement at the end of the same pushover step can then be written as

$$d_n^{(i)} = \tilde{F}^{(i)} S_{den}^{(1)} \quad (44)$$

in which $\tilde{F}^{(i)}$ represents the “cumulative scale factor” with a maximum value of unity:

$$\tilde{F}^{(i)} = \tilde{F}^{(i-1)} + \Delta \tilde{F}^{(i)} \leq 1 \quad (45)$$

Note that the modal scaling expressions given above correspond to a monotonic increase of the elastic response spectrum progressively at each step with a cumulative scale factor increasing from zero until unity. Physically speaking, the structure is being pushed such that at every pushover step modal displacements of all modes are increased by increasing elastic spectral displacements, defined at the first step ($i = 1$) in the same proportion (according to the “equal displacement rule”), until they simultaneously reach the target “spectral displacements” on the response spectrum. Shown in Figure 5 are the scaled

spectra corresponding to the first yield, to an intermediate pushover step ($\tilde{F}^{(i)} < 1$), and to the final step ($\tilde{F}^{(i)} = 1$), which are plotted in the ADRS (Acceleration-Displacement Response Spectrum) format and superimposed onto the modal capacity diagrams.

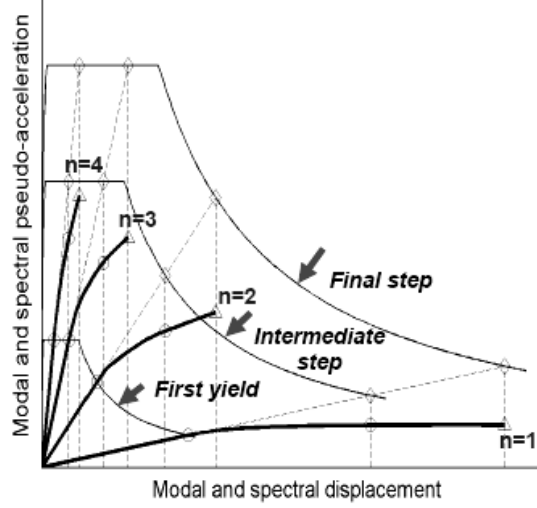


Fig. 5 Scaling of modal displacements through monotonic scaling of response spectrum

It is worth warning that the equal displacement rule may not be valid at near-fault situations with forward directivity effect.

Again, it needs to be stressed that IRSA is a “displacement-controlled” procedure and, therefore, the above-mentioned monotonic spectrum scaling applies to spectral displacements only, not to the elastic spectral pseudo-accelerations. For the sake of completeness, however, a “compatible” modal pseudo-acceleration increment, $\Delta a_n^{(i)}$, corresponding to the increment of “scaled” modal displacement may be defined from Equations (12) and (43) as

$$\Delta a_n^{(i)} = \tilde{F}^{(i)} S_{ain}^{(i)}; \quad S_{ain}^{(i)} = \frac{(\omega_n^{(i)})^2}{(\omega_n^{(1)})^2} S_{aen}^{(1)} \quad (46)$$

where $S_{ain}^{(i)}$ represents “compatible inelastic spectral pseudo-acceleration”, and $S_{aen}^{(1)}$ refers to “initial elastic spectral pseudo-acceleration” corresponding to the elastic spectral displacement, $S_{den}^{(1)}$, defined at the first pushover step.

2. Multi-mode Pushover History Analysis: Simultaneous Pushovers in All Modes and Modal Combination

Substituting Equation (43) into Equation (15) leads to the following expression for the displacement vector increment in the n th mode at the (i) th pushover step:

$$\Delta \mathbf{u}_n^{(i)} = \tilde{\mathbf{u}}_n^{(i)} \Delta \tilde{F}^{(i)}; \quad \tilde{\mathbf{u}}_n^{(i)} = \Phi_n^{(i)} \Gamma_{xn}^{(i)} S_{den}^{(1)} \quad (47)$$

Utilizing Equations (16) and (46), equivalent seismic load vector increment corresponding to the displacement vector increment given above in Equation (47) may be written for an alternative load-controlled process:

$$\Delta \mathbf{f}_n^{(i)} = \tilde{\mathbf{f}}_n^{(i)} \Delta \tilde{F}^{(i)}; \quad \tilde{\mathbf{f}}_n^{(i)} = \mathbf{M} \Phi_n^{(i)} \Gamma_{xn}^{(i)} S_{ain}^{(i)} \quad (48)$$

in which $S_{ain}^{(i)}$ is the compatible inelastic spectral pseudo-acceleration defined by Equation (46).

Now, piecewise linear multi-mode pushover history analysis can be performed at a given pushover step (i) , by monotonically imposing displacement increments $\Delta \mathbf{u}_n^{(i)}$ of the MDOF system, as defined in Equation (47), or alternatively, by applying equivalent seismic load increments $\Delta \mathbf{f}_n^{(i)}$ given by

Equation (48) “simultaneously in all modes” considered. In this process, the increment of a “generic response quantity” of interest, such as the increment of an internal force, a displacement component, a story drift or the plastic rotation of a previously developed plastic hinge, may be calculated in each mode as

$$\Delta r_n^{(i)} = \tilde{r}_n^{(i)} \Delta \tilde{F}^{(i)} \quad (49)$$

where $\tilde{r}_n^{(i)}$ represents the generic response quantity to be obtained in each mode for $\Delta \tilde{F}^{(i)} = 1$, i.e., by imposing the displacement vector $\tilde{\mathbf{u}}_n^{(i)}$ given in Equation (47), or alternatively, by applying the load vector $\tilde{\mathbf{f}}_n^{(i)}$ given in Equation (48). Incremental scale factor $\Delta \tilde{F}^{(i)}$ is the single unknown at each pushover step leading to the formation of a new plastic hinge.

In the next stage, modal generic response quantity increments are combined by an appropriate modal combination rule, such as the Complete Quadratic Combination (CQC) rule as

$$\tilde{r}^{(i)} = \sqrt{\sum_{m=1}^{N_m} \sum_{n=1}^{N_m} (\tilde{r}_m^{(i)} \rho_{mn}^{(i)} \tilde{r}_n^{(i)})} \quad (50)$$

where $\rho_{mn}^{(i)}$ is the cross-correlation coefficient of the CQC rule. Thus, generic response quantity at the end of the (i) th pushover step can be estimated as

$$r^{(i)} = r^{(i-1)} + \Delta r^{(i)} = r^{(i-1)} + \tilde{r}^{(i)} \Delta \tilde{F}^{(i)} \quad (51)$$

in which $r^{(i)}$ and $r^{(i-1)}$ are the “generic response quantities” to develop at the end of current and previous pushover steps, respectively. In the first pushover step ($i = 1$), response quantities due to gravity loading are considered as $r^{(0)}$.

The next stage of multi-mode pushover history analysis is similar to the single-mode analysis where the above-given generic expression is specialized for the response quantities that define the coordinates of the “yield surfaces” of all potential plastic hinges, e.g., biaxial bending moments and axial forces in a general, three-dimensional response of a framed structure. As part of the piecewise linearization process of pushover analysis as well as to avoid iterative operations in the hinge identification process, yield surfaces are appropriately linearized in a piecewise fashion as mentioned above (Figure 1), i.e., they are represented by finite number of lines or planes in two- and three-dimensional response models, respectively. As an example, planar yield surfaces (lines) of a reinforced concrete or steel section (j) are shown in Figure 1 where a typical line (s) can be expressed as

$$\alpha_{j,s} M_{jp} + \beta_{j,s} N_{jp} = 1 \quad (52)$$

in which M_{jp} and N_{jp} represent the yield bending moment and corresponding axial force, respectively, at section j while $\alpha_{j,s}$ and $\beta_{j,s}$ refer to the coefficients defining the yield line (s). For the (i) th pushover step, Equation (51) is specialized for bending moment and axial force as

$$M_{j,1}^{(i)} = M_{j,1}^{(i-1)} + \tilde{M}_{j,1}^{(i)} \Delta \tilde{F}^{(i)}; \quad N_{j,1}^{(i)} = N_{j,1}^{(i-1)} + \tilde{N}_{j,1}^{(i)} \Delta \tilde{F}^{(i)} \quad (53)$$

which are then substituted into Equation (52) and $\Delta \tilde{F}^{(i)}$ is extracted as

$$(\Delta \tilde{F}^{(i)})_{j,s} = \frac{1 - \alpha_{j,s} M_{j,1}^{(i-1)} - \beta_{j,s} N_{j,1}^{(i-1)}}{\alpha_{j,s} \tilde{M}_{j,1}^{(i)} + \beta_{j,s} \tilde{N}_{j,1}^{(i)}} \quad (54)$$

The yield line (s) at section (j) that intersected with a minimum positive $(\Delta \tilde{F}^{(i)})_{j,s}$ among all yield lines of all potential plastic hinges identifies the new hinge formed at the end of the (i) th pushover step.

Once $\Delta \tilde{F}^{(i)}$ is determined, any response quantity of interest developed at the end of that step can be obtained from the generic expression of Equation (51). Modal displacement increment $\Delta d_n^{(i)}$ in any mode can be obtained from Equation (43), and in turn, modal pseudo-acceleration increment from Equation (12), leading to the simultaneous estimation of respective cumulative quantities, i.e., the new coordinates of all modes, which can be obtained through Equations (11) and (13).

As mentioned in the case of single-mode pushover, when the formation of the new hinge is identified, the current global stiffness matrix of the structure is locally modified such that only the element stiffness matrix affected by the new hinge is replaced with a new one for the next pushover step. The normality criterion is enforced in columns and walls for the coupling of internal forces as well as plastic deformation components of the newly formed plastic hinge.

Thus it is seen that multi-mode pushover history analysis with IRSA is the extension of single-mode pushover history analysis described earlier. Indeed, instead of running a static analysis under equivalent seismic loads at each step, a response spectrum analysis is performed in IRSA at each step where seismic input data is specified either in the form of initial spectral displacement in each mode, $S_{den}^{(1)}$ (which is calculated in the first pushover step and remains unchanged at all pushover steps), or seismic input is given in terms of “compatible inelastic spectral pseudo-acceleration” $S_{ain}^{(i)}$ defined by Equation (46).

3. Estimation of Peak Quantities: Inelastic Seismic Demand

The above-described “pushover-history” process is repeated for all pushover steps until cumulative spectrum scale factor defined by Equation (45) exceeds unity at the end of a given pushover step. When such a step is detected, which is indicated by superscript (p), incremental scale factor corresponding to this final pushover step is re-calculated from Equation (45) as

$$\Delta \tilde{F}^{(p)} = 1 - \tilde{F}^{(p-1)} \quad (55)$$

In the last pushover step, modal displacement increment is redefined as

$$\Delta d_n^{(p)} = C_{Rn} S_{den}^{(1)} \Delta \tilde{F}^{(p)} \quad (56)$$

where C_{Rn} represents “spectral displacement amplification factor” in the n th mode. If $C_{Rn} > 1$, then seismic input for the n th mode is modified from $S_{den}^{(1)}$ to $C_{Rn} S_{den}^{(1)}$, and the generic response quantity $\tilde{r}_j^{(p)}$ is recalculated at the last step by repeating the elastic response spectrum analysis. Finally peak value of any response quantity of interest is obtained from the generic expression of Equation (51) for $i = p$:

$$r^{(p)} = r^{(p-1)} + \Delta r^{(p)} = r^{(p-1)} + \tilde{r}^{(p)} \Delta \tilde{F}^{(p)} \quad (57)$$

Spectral displacement amplification factor C_{Rn} is calculated as shown below.

If $T_n^{(1)} > T_B$, i.e., $(\omega_n^{(1)})^2 < \omega_B^2$, then $C_{Rn} = 1$. If $T_n^{(1)} < T_B$, i.e., $(\omega_n^{(1)})^2 > \omega_B^2$, then C_{Rn} is determined approximately as (MPWS, 2006)

$$\begin{aligned} C_{Rn} &= \frac{1 + (R_{yn} - 1)T_B / T_n^{(1)}}{R_{yn}} \geq 1 & (\lambda_n^{(p)} \leq 0.10) \\ C_{Rn} &= \frac{1 + (R_{yn} - 1)T_B / T_n^{(1)}}{10\lambda_n^{(p)} R_{yn}} \geq 1 & (\lambda_n^{(p)} > 0.10) \end{aligned} \quad (58)$$

where R_{yn} is the n th mode yield reduction factor as defined below, i.e., the n th mode counterpart of the first mode yield reduction factor defined in Equation (38) (Figure 4(b)). Post-yield slope $\lambda_n^{(p)}$ is also defined below:

$$R_{yn} = \frac{S_{aen}^{(1)}}{a_{yn}}; \lambda_n^{(p)} = \frac{(\omega_n^{(p)})^2}{(\omega_n^{(1)})^2} \quad (59)$$

Note that the second spectral displacement amplification factor given in Equation (58) is intended for higher modes with shorter natural periods where inelastic spectral displacements would be reduced due to steeper post-yield slopes of higher-mode capacity diagrams (Önem, 2006).

4. Treatment of P-Delta Effects in IRSA

P-delta effects are rigorously considered in IRSA through straightforward consideration of geometric stiffness matrix in each increment of the response spectrum analysis performed. Along the pushover-

history process, accumulated plastic deformations result in negative-definite second-order stiffness matrices, which in turn yield negative eigenvalues, and hence, negative post-yield slopes in the modal capacity diagrams of the lower modes. The corresponding mode shapes are representative of the post-buckling deformation state of the structure, which may significantly affect the distribution of internal forces and inelastic deformations of the structure.

Analysis of inelastic SDOF systems based on bilinear backbone curves with negative post-yield slopes indicate that such systems are susceptible to “dynamic instability” rather than having amplified displacements due to the P-delta effects. Therefore, the use of P-delta amplification coefficient (C_3) defined in FEMA 356 (FEMA, 2000) is no longer recommended (FEMA, 2005). The dynamic instability is known to depend on the yield strength, initial stiffness, negative post-yield stiffness, and the hysteretic model of SDOF oscillator as well as on the characteristics of the earthquake ground motion. Accordingly, practical guidelines have been proposed for the minimum strength limits in terms of other parameters to avoid instability (Miranda and Akkar, 2003; FEMA, 2005). Further research is needed for the realistic cases of backbone curves resulting from modal capacity diagrams, which exhibit multiple post-yield slopes with both ascending and descending branches. For the time being, equal displacement rule is used in IRSA, even when P-delta effects are present, as long as an imminent danger of dynamic instability is not expected according to the above-mentioned practical guidelines.

5. Summary of IRSA

The analysis stages to be applied at each piecewise linear pushover step (i) of IRSA are summarized below:

- (1) Run a linear response spectrum analysis (RSA) with a sufficient number of modes by considering instantaneous second-order stiffness matrix corresponding to the current plastic hinge configuration. RSA at each step actually corresponds to performing simultaneous pushover analyses in all modes for a unit value of incremental scale factor $\Delta\tilde{F}^{(i)}$. In running RSA, the seismic input is specified in terms of initial spectral displacements $S_{den}^{(1)}$, which would be the same at all pushover steps according to the “equal displacement rule”. They are calculated only once at the first pushover step as elastic spectral displacements. Alternatively, compatible spectral pseudo-accelerations $S_{ain}^{(i)}$ defined at each step by Equation (46) may be specified as seismic input. All response quantities of interest, $r^{(i)}$, are obtained by applying an appropriate modal combination rule (e.g., CQC rule in Equation (50)).
- (2) Specialize the generic expression of Equation (51) for the response quantities that define the coordinates of the yield surfaces of all potential plastic hinges, i.e., biaxial bending moments and axial forces in a general, three-dimensional response of a framed structure. Response quantities due to the gravity loading are considered as $r^{(0)}$ at the first pushover step. Calculate the incremental scale factor $\Delta\tilde{F}^{(i)}$ according to the yield conditions of all potential plastic hinges and identify the new yielded hinge.
- (3) Calculate cumulative scale factor $\tilde{F}^{(i)}$ from Equation (45) and check if it exceeded unity. If exceeded, calculate the incremental scale factor $\Delta\tilde{F}^{(p)}$ from Equation (55) for the final pushover step and carry on according to Equations (56)–(59). If not, continue with the next stage.
- (4) Calculate all response quantities of interest developed at the end of the pushover step from the generic expression of Equation (51). If the final pushover step has been reached, terminate the analysis. If not, continue with the next stage.
- (5) Modify the current second-order stiffness matrix by considering the last yielded hinge identified at Stage (2) and return to Stage (1) for the next pushover step.

6. Special Cases

Single-mode adaptive pushover analysis presented earlier in this paper is a special case of IRSA with $n = 1$. Since no modal scaling is involved in the single-mode analysis, the incremental scale factor $\Delta\tilde{F}^{(i)}$ becomes directly proportional to the modal displacement increment $\Delta d_1^{(i)}$ as follows (see Equation (43)):

$$\Delta \tilde{F}^{(i)} = \frac{\Delta d_1^{(i)}}{S_{del}^{(1)}} \quad (60)$$

On the other hand, when large values are assigned for yield moments such that no plastic hinging occurs, IRSA automatically degenerates to the linear response spectrum analysis (RSA) (see Figure 2(b)). These two special cases confirm the generality of the IRSA procedure.

FURTHER OBSERVATIONS ON OTHER PUSHOVER PROCEDURES

For the sake of completeness in covering the multi-mode pushover procedures, two classes of methods are briefly highlighted.

1. Multi-mode Pushover Analysis with Combined Seismic Loads or Displacements

It is interesting to note that in a number of multi-mode pushover procedures, e.g., Elnashai (2002), Antoniou et al. (2002), Antoniou and Pinho (2004a, 2004b), which employ modal scaling based on “instantaneous” elastic spectral quantities (see the discussion on “modal scaling” above), scaled seismic loads or displacements are combined with a modal combination rule, normalized, and then are applied to the structure at each step to obtain the increments of “combined” pushover curve coordinates. Note that a pitfall is inherent in these procedures regarding the application of the modal combination in defining applied loads or displacements instead of combining the individual response quantities induced by those loads or displacements in each mode (see Chopra, 2001). Thus, individual modal capacity diagrams cannot be defined, and consequently, modal peaks and hence seismic demand quantities cannot be obtained for a given earthquake, as discussed earlier.

2. Multi-mode Pushover Analysis without Modal Scaling: Modal Pushover Analysis (MPA)

It is worth noting that one of the methods for multi-mode pushover analysis, namely Modal Pushover Analysis (MPA), which was developed by Chopra and Goel (2002) based upon earlier studies (Paret et al., 1996; Sasaki et al., 1998), completely ignores the modal contributions to the section forces in the formation of plastic hinges. Nonlinear response is estimated independently for each mode with a single-mode pushover analysis based on an invariant load pattern proportional to the initial linear elastic mode shape of a given mode. Since modal coupling is ignored, modal scaling is not required. Peak response quantities, i.e., modal demands, are obtained for each mode from a SDOF system analysis independently, and are then combined (exactly as in the linear response spectrum analysis) with an appropriate modal combination rule. It is reported that the above-described MPA procedure is able to estimate story drifts with a reasonable accuracy (Chopra and Goel, 2002). However it fails to estimate the locations of plastic hinges as well as the plastic hinge rotations and section forces, the essential demand quantities for performance assessment in ductile and brittle behaviour modes, for which supplementary analyses are needed (Goel and Chopra, 2004, 2005). Recently certain refinements have been made on MPA through energy-based development of modal capacity diagrams (Hernandez-Montes et al., 2004; Kalkan and Kunnath, 2006).

EXAMPLES

Several examples have already been presented on IRSA applications in previously published material (see Aydinoglu, 2003, 2004). In this paper, some of the results of an ongoing parametric study (Önem and Aydinoglu, 2006) are presented. The 8-, 12-, 16- and 20-storey reinforced concrete frames shown in Figure 6 were designed to Turkish Seismic Code (MPWS, 2006) provisions with the characteristics given in Table 1. For nonlinear response history analysis, 20 real records with earthquake magnitude between 6.0 and 7.5 were employed (Table 2). The records were appropriately scaled to match a smoothed elastic response spectrum that was also used in the multi-mode pushover analysis by IRSA (Figure 7). Results of the nonlinear response history analysis (NRHA), 4-mode IRSA, and single-mode IRSA are presented in terms of mean values of story displacements, inter-story drift ratios, and plastic hinge rotations of central span beams, as shown in Figures 8, 9, and 10, respectively. The differences between the multi-mode and single-mode pushover analyses are clearly visible, especially in story drift ratios and plastic hinge

rotations. It is observed that IRSA is able to predict all nonlinear response quantities with a reasonable accuracy.

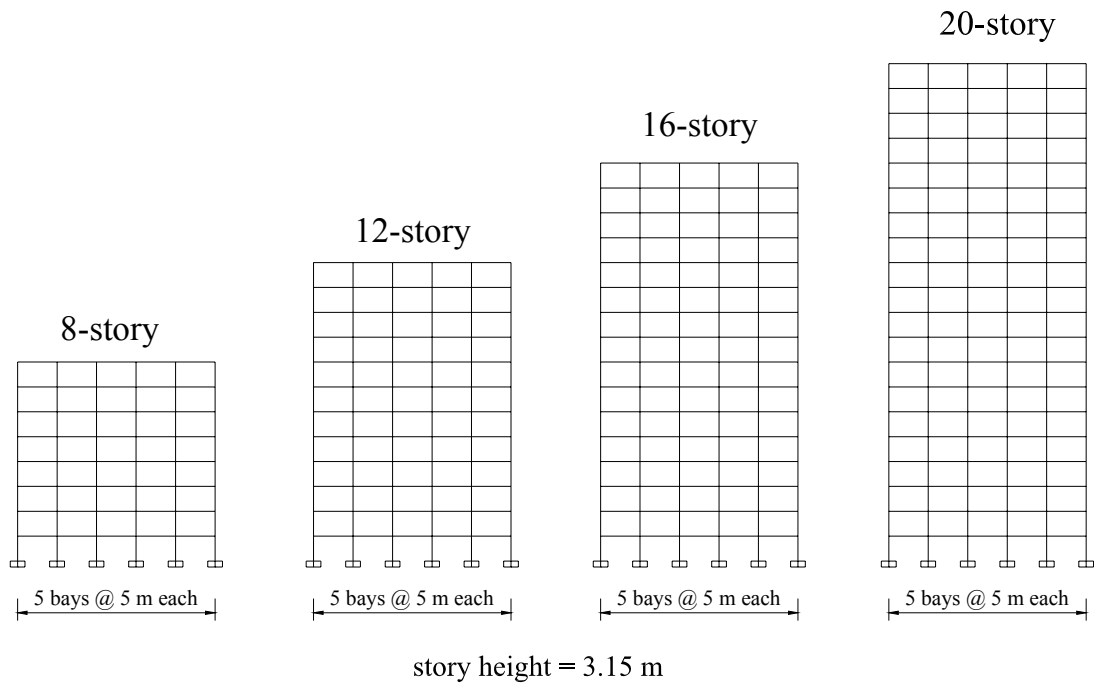


Fig. 6 Reinforced concrete frames considered in the parametric study

Table 1: Characteristics of Reinforced Concrete Frames

Number of Stories	Story	Side Columns (cm)	Internal Columns (cm)	Beam (cm)
8	1–5	45×45	50×50	30×60
	6–8	45×45	45×45	30×60
12	1–3	55×55	60×60	30×60
	4–12	55×55	55×55	30×60
16	1–3	60×70	60×70	30×60
	4–6	60×60	60×60	30×60
	7–9	60×50	60×50	30×60
	10–16	60×40	60×40	30×60
20	1–3	70×70	70×70	30×60
	4–6	60×70	60×70	30×60
	7–9	60×60	60×60	30×60
	10–12	60×50	60×50	30×60
	13–20	60×40	60×40	30×60

Table 2: Characteristics of Earthquake Records

No.	Earthquake	Mag.	Station	Dist. (km)	Site Cond.	PGA (g)	PGV (cm/s)	PGD (cm)
1	Chalfant Valley	6.2	54428 Zack Brothers Ranch	18.7	D	0.447	36.9	7.01
2	Chalfant Valley	6.2	54429 Zack Brothers Ranch	18.7	D	0.4	44.5	8.56
3	Loma Prieta, 1989	6.9	APEEL 2, Redwood City	47.9	D	0.22	34.3	6.87

4	Loma Prieta, 1989	6.9	1686 Fremont, Emerson Court	43.4	B	0.192	12.7	5.5
5	Mammoth Lakes, 1980	6	54214 Long Valley Dam	19.7	A	0.484	14.2	1.77
6	Mammoth Lakes, 1980	5.7	54214 Long Valley Dam	14.4	A	0.245	18.5	1.56
7	Mammoth Lakes, 1980	6	54301 Mammoth Lakes H.S.	14.2	D	0.39	23.9	2.72
8	Morgan Hill, 1984	6.2	47380 Gilroy Array #2	15.1	C	0.212	12.6	2.1
9	Morgan Hill, 1984	6.2	57382 Gilroy Array #4	12.8	C	0.348	17.4	3.11
10	Northridge, 1994	6.7	90074 La Habra, Briarcliff	61.6	C	0.206	12.3	1.23
11	Northridge, 1994	6.7	24575 Elizabeth Lake	37.2	C	0.155	7.3	2.7
12	Northridge, 1994	6.7	24611 LA—Temple	32.3	B	0.184	20	2.74
13	Northridge, 1994	6.7	90061 Big Tujunga, Los Angeles	24	B	0.245	12.7	1.12
14	Northridge, 1994	6.7	90021 LA—North Westmoreland	29	B	0.401	20.9	2.29
15	Whittier Narrows, 1987	6	Brea Dam (Downstream)	23.3	D	0.313	14.5	0.77
16	Whittier Narrows, 1987	6	108 Carbon Canyon Dam	26.8	A	0.221	8.7	0.64
17	Whittier Narrows, 1987	6	90034 LA—Fletcher Drive	14.4	C	0.213	12.6	1.45
18	Whittier Narrows, 1987	6	90063 Glendale—Las Palmas	19	C	0.296	17.1	1.82
19	Whittier Narrows, 1987	6	90021 LA—North Westmoreland	16.6	B	0.214	9.7	0.98
20	Whittier Narrows, 1987	6	24461 Alhambra, Fremont School	13.2	B	0.333	22	2.42

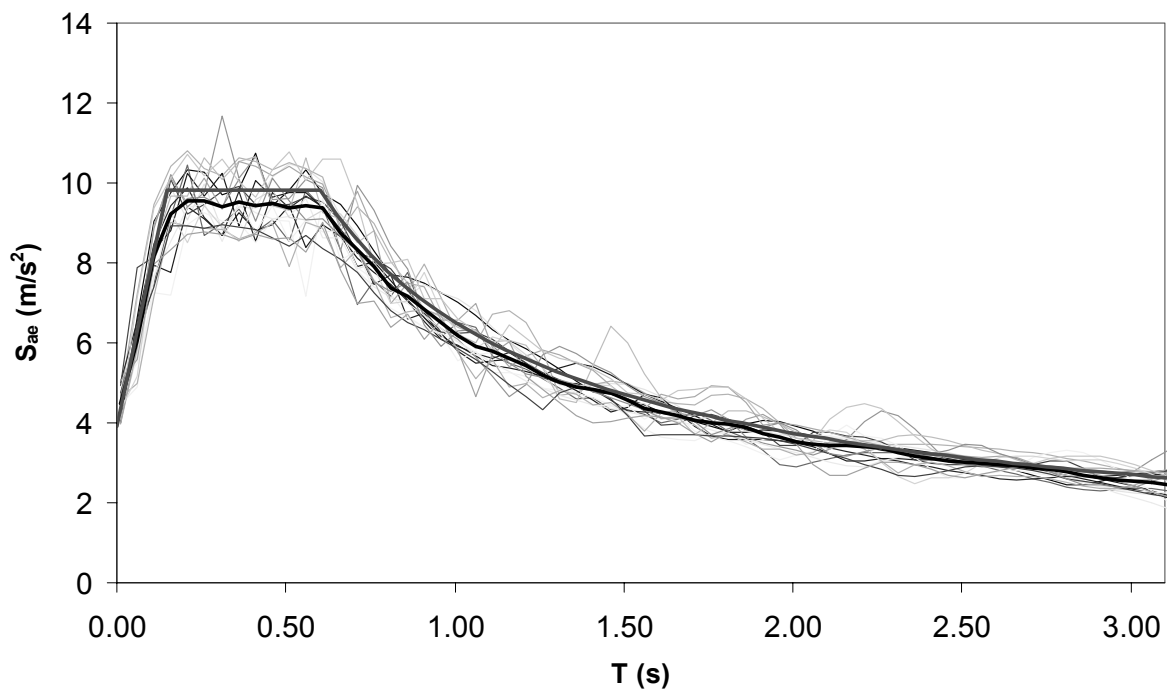


Fig. 7 Acceleration response spectra of the normalized records, and their mean superimposed on the code spectrum

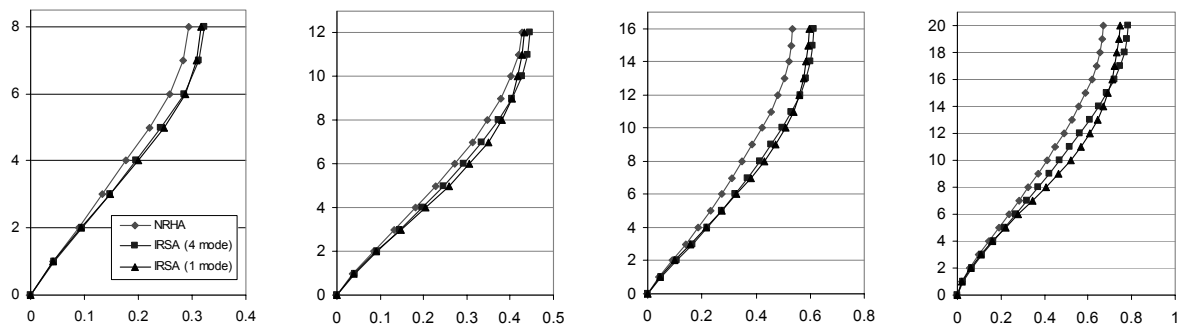


Fig. 8 Mean story displacements estimated by the nonlinear response history analysis (NRHA), four-mode IRSA, and single-mode IRSA for the 8-, 12-, 16- and 20-story frames

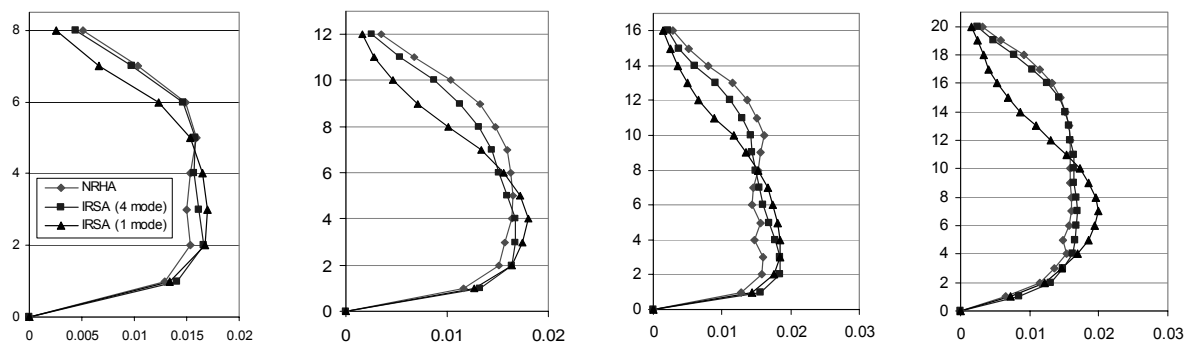


Fig. 9 Mean story drift ratios estimated by the nonlinear response history analysis (NRHA), four-mode IRSA, and single-mode IRSA for the 8-, 12-, 16- and 20-story frames

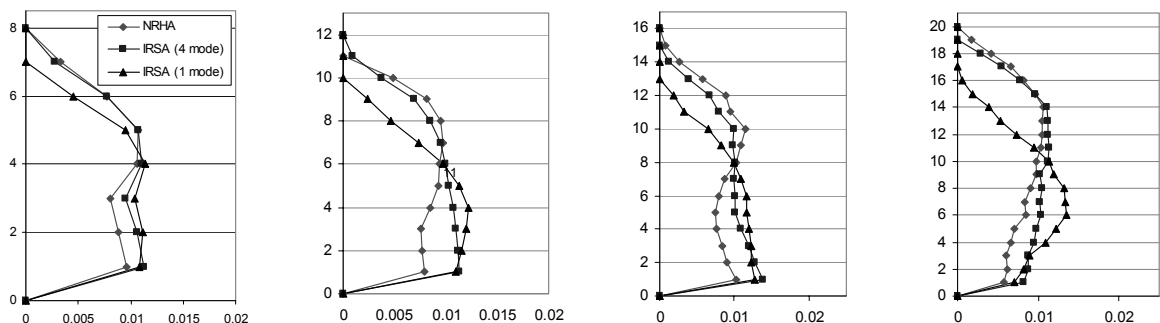


Fig. 10 Mean plastic rotations of central beams estimated by the nonlinear response history analysis (NRHA), four-mode IRSA, and single-mode IRSA for the 8-, 12-, 16- and 20-story frames

CONCLUSIONS

Incremental Response Spectrum Analysis (IRSA) procedure is presented as a direct extension of the linear Response Spectrum Analysis (RSA), which represents an improved multi-mode pushover analysis for performance-based nonlinear seismic assessment of existing buildings. The method is based on a piecewise linear approach, in which all linear operations are applicable in a piecewise linear pushover step in between the formation of consecutive plastic hinges. IRSA can be readily applied to any structure in practice where the earthquake input can be specified in the form of a smoothed response spectrum. To provide a clear and broader picture to the interested reader, in addition to the multi-mode analysis, single-mode pushover analyses with adaptive and invariant load patterns are also presented in detail.

As discussed in the introductory section of the paper, a clear distinction needs to be made between two types of pushover analysis, i.e., whether the analysis is performed for “capacity estimation” only or

whether it can be used as well for a “demand estimation” under a given earthquake ground motion. In this respect, attention was drawn to the fact that surprisingly a very small number of multi-mode pushover methods are available in the literature, which are capable of estimating the seismic demand.

Probably one of the most critical issues of almost all multi-mode pushover procedures is the “modal scaling”, i.e., the assumption that has to be made for estimating the relative values of the modal displacement or modal pseudo-acceleration increments among various modes. In this respect, IRSA utilizes a novel approach based on scaling the modal displacements through instantaneous “inelastic spectral displacements”. For practical applications this allows the direct use of linear response spectrum, thanks to the well-known “equal displacement rule”. It was shown through a parametric study that IRSA is able to provide a reasonable accuracy for all nonlinear response quantities, including story drifts and plastic hinge rotations.

It should be stressed that all pushover procedures are approximate by nature and that none of them, including IRSA, can replace the rigorous nonlinear response history analysis, which is believed to prevail in the long run as a preferred engineering tool for seismic demand estimation. In the interim, pushover methods are expected to serve as practical nonlinear procedures, through which engineers will become acquainted with a realistic nonlinear seismic behavior of structures and which quantify the extent of structural damage, alas approximately, induced by a design earthquake. In this respect, it is believed that a practical pushover procedure must comply with the code practice, especially in specifying the seismic input in the form of a standard elastic response spectrum. This requirement is fully satisfied by IRSA. However it must be admitted that the application of IRSA is limited to the far-field earthquakes, as its fundamental assumption, i.e., equal displacement rule, is not applicable to the near-field earthquakes.

REFERENCES

1. Antoniou, S. and Pinho, R. (2004a). “Advantages and Limitations of Adaptive and Non-adaptive Force-Based Pushover Procedures”, *Journal of Earthquake Engineering*, Vol. 8, No. 4, pp. 497–552.
2. Antoniou, S. and Pinho, R. (2004b). “Development and Verification of a Displacement-Based Adaptive Pushover Procedure”, *Journal of Earthquake Engineering*, Vol. 8, No. 5, pp. 643–661.
3. Antoniou, S., Rovithakis, A. and Pinho, R. (2002). “Development and Verification of a Fully Adaptive Pushover Procedure”, *Proceedings of the 12th European Conference on Earthquake Engineering*, London, U.K., Paper No. 822 (on CD).
4. ATC (1996). “Seismic Evaluation and Retrofit of Concrete Buildings: Volume 1”, Report ATC-40, Applied Technology Council, Redwood City, California, U.S.A.
5. Aydınoğlu, M.N. (2003). “An Incremental Response Spectrum Analysis Based on Inelastic Spectral Displacements for Multi-Mode Seismic Performance Evaluation”, *Bulletin of Earthquake Engineering*, Vol. 1, No. 1, pp. 3–36.
6. Aydınoğlu, M.N. (2004). “An Improved Pushover Procedure for Engineering Practice: Incremental Response Spectrum Analysis (IRSA)” in “Performance-Based Seismic Design Concepts and Implementation: Proceedings of an International Workshop, Bled, Slovenia, June 28–July 1, 2004 (edited by P. Fajfar and H. Krawinkler)”, Report PEER 2004/05, University of California, Berkeley, U.S.A.
7. Aydınoğlu, M.N. (2005). “A Code Approach for Deformation-Based Seismic Performance Assessment of Reinforced Concrete Buildings”, *Proceedings of the International Workshop on Seismic Performance Assessment and Rehabilitation of Existing Buildings (SPEAR)*, Ispira, Italy, pp. 65–74.
8. Aydınoğlu, M.N. (2006). “Nonlinear Procedures in Revised Turkish Code for Seismic Performance Assessment and Retrofit Design”, *Proceedings of the First European Conference on Earthquake Engineering and Seismology*, Geneva, Switzerland, Paper No. 450 (on CD).
9. Aydınoğlu, M.N. and Fahjan, Y.M. (2003). “A Unified Formulation of the Piecewise Exact Method for Inelastic Seismic Demand Analysis Including the P-Delta Effect”, *Earthquake Engineering & Structural Dynamics*, Vol. 32, No. 6, pp. 871–890.
10. Aydınoğlu, M.N. and Kaçmaz, Ü. (2002). “Strength-Based Displacement Amplification Spectra for Inelastic Seismic Performance Evaluation”, Report 2002/2, Kandilli Observatory and Earthquake Research Institute, Bogazici University, Istanbul, Turkey.

11. Bathe, K.J. (1996). "Finite Element Procedures", Prentice Hall, Upper Saddle River, U.S.A.
12. BSSC (1997). "NEHRP Guidelines for the Seismic Rehabilitation of Buildings (FEMA 273)", Report Prepared for the Federal Emergency Management Agency, Building Seismic Safety Council, National Institute of Building Sciences, Washington, DC, U.S.A.
13. CEN (2003). "Eurocode 8: Design of Structures for Earthquake Resistance—Part 1: General Rules, Seismic Actions and Rules for Buildings", prEN 1998-1 (Final Draft), Comité Européen de Normalisation, Brussels, Belgium.
14. Chopra, A.K. (2001). "Dynamics of Structures: Theory and Applications to Earthquake Engineering", Prentice Hall, Upper Saddle River, U.S.A.
15. Chopra, A.K. and Goel, R.K. (1999). "Capacity-Demand-Diagram Methods Based on Inelastic Design Spectrum", *Earthquake Spectra*, Vol. 15, No. 4, pp. 637–656.
16. Chopra, A.K. and Goel, R.K. (2002). "A Modal Pushover Analysis Procedure for Estimating Seismic Demands for Buildings", *Earthquake Engineering & Structural Dynamics*, Vol. 31, No. 3, pp. 561–582.
17. Elnashai, A.S. (2002). "Do We Really Need Inelastic Dynamic Analysis?", *Journal of Earthquake Engineering*, Vol. 6, No. 1 spec, pp. 123–130.
18. Fajfar, P. and Fischinger, M. (1988). "N-2-A Method for Nonlinear Seismic Analysis of Regular Structures", *Proceedings of the Ninth World Conference on Earthquake Engineering*, Tokyo-Kyoto, Japan, Vol. 5, pp. 111–116.
19. FEMA (2000). "Prestandard and Commentary for the Seismic Rehabilitation of Buildings", Report FEMA 356, Federal Emergency Management Agency, Washington, DC, U.S.A.
20. FEMA (2005). "Improvement of Nonlinear Static Seismic Analysis Procedures", Report FEMA 440, Federal Emergency Management Agency, Washington, DC, U.S.A.
21. Freeman, S.A., Nicoletti, J.P. and Tyrell, J.V. (1975). "Evaluations of Existing Buildings for Seismic Risk—A Case Study of Puget Sound Naval Shipyard, Bremerton, Washington", *Proceedings of U.S. National Conference on Earthquake Engineering*, Seattle, U.S.A., pp. 113–122.
22. Goel, R.K. and Chopra, A.K. (2004). "Evaluation of Modal and FEMA Pushover Analyses: SAC Buildings", *Earthquake Spectra*, Vol. 20, No. 1, pp. 225–254.
23. Goel, R.K. and Chopra, A.K. (2005). "Extension of Modal Pushover Analysis to Compute Member Forces", *Earthquake Spectra*, Vol. 21, No. 1, pp. 125–139.
24. Gupta, B. and Kunnath, S.K. (2000). "Adaptive Spectra-Based Pushover Procedure for Seismic Evaluation of Structures", *Earthquake Spectra*, Vol. 16, No. 2, pp. 367–391.
25. Hernandez-Montes, E., Kwon, O.-S. and Aschheim, M.A. (2004). "An Energy-Based Formulation for First- and Multiple-Mode Nonlinear Static (Pushover) Analyses", *Journal of Earthquake Engineering*, Vol. 8, No. 1, pp. 69–88.
26. Kalkan, E. and Kunnath, S.K. (2004). "Method of Modal Combinations for Pushover Analysis of Buildings", *Proceedings of the 13th World Conference on Earthquake Engineering*, Vancouver, Canada, Paper No. 2713 (on CD).
27. Kalkan, E. and Kunnath, S.K. (2006). "Adaptive Modal Combination Procedure for Nonlinear Static Analysis of Building Structures", *Journal of Structural Engineering*, ASCE, Vol. 132, No. 11, pp. 1721–1731.
28. McGuire, W., Gallagher, R.H. and Ziemian, R.D. (2000). "Matrix Structural Analysis", John Wiley & Sons, New York, U.S.A.
29. Miranda, E. and Akkar, S.D. (2003). "Dynamic Instability of Simple Structural Systems", *Journal of Structural Engineering*, ASCE, Vol. 129, No. 12, pp. 1722–1726.
30. MPWS (2006). "Specification for Buildings to be Built in Earthquake Zones", Ministry of Public Works and Settlement, Turkish Government, Ankara, Turkey (in Turkish).
31. Önem, G. (2006). "Spectral Displacement Amplification Factors for Higher Mode Capacity Diagrams with Steeper Post-Yield Slopes", Unpublished Report, Kandilli Observatory and Earthquake Research Institute, Bogazici University, Istanbul, Turkey.

32. Önem, G. and Aydinoglu, M. (2006). "Verification of Improved Pushover Procedure IRSA (Incremental Response Spectrum Analysis)", Proceedings of the First European Conference on Earthquake Engineering and Seismology, Geneva, Switzerland, Paper No. 452 (on CD).
33. Paret, T.F., Sasaki, K.K., Eilbeck, D.H. and Freeman, S.A. (1996). "Approximate Inelastic Procedures to Identify Failure Mechanisms from Higher Mode Effects", Proceedings of the 11th World Conference on Earthquake Engineering, Acapulco, Mexico, Paper No. 966 (on CD).
34. Sasaki, K.K., Freeman, S.A. and Paret, T.F. (1998). "Multi-Mode Pushover Procedure (MMP)—A Method to Identify the Effects of Higher Modes in a Pushover Analysis", Proceedings of the Sixth U.S. National Conference on Earthquake Engineering, Seattle, U.S.A., Paper No. 271 (on CD).

AN EARTHQUAKE RESPONSE SPECTRUM METHOD FOR LINEAR LIGHT SECONDARY SUBSTRUCTURES

Giuseppe Muscolino and Alessandro Palmeri

Department of Civil Engineering
University of Messina
Vill. S. Agata, 98166, Messina, Italy

ABSTRACT

Earthquake response spectrum is the most popular tool in the seismic analysis and design of structures. In the case of combined primary-secondary (P-S) systems, the response of the supporting P substructure is generally evaluated without considering the S substructure, which in turn is only required to bear displacements and/or forces imposed by the P substructure (“cascade” approach). In doing so, however, dynamic interaction between the P and S components is neglected, and the seismic-induced response of the S substructure may be heavily underestimated or overestimated. In this paper, a novel CQC (Complete Quadratic Combination) rule is proposed for the seismic response of linear light S substructures attached to linear P substructures. The proposed technique overcomes the drawbacks of the cascade approach by including the effects of dynamic interaction and different damping in the substructures directly in the cross-correlation coefficients. The computational effort is reduced by using the eigenproperties of the decoupled substructures and only one earthquake response spectrum for a reference value of the damping ratio.

KEYWORDS: CQC (Complete Quadratic Combination) Rule, Earthquake Response Spectrum, Light Secondary Substructures, Non-classically Damped Structures, Non-structural Components

INTRODUCTION

Although light secondary (S) attachments to buildings or industrial facilities are not part of the primary (P) load-bearing structural system, their seismic analysis and design is a topic of broad engineering interest (among others, Chen and Soong, 1988; Singh, 1988; Villaverde, 2004; Singh et al., 2006a, 2006b; and references provided therein). Past experiences, in fact, prove that S substructures such as suspended ceilings and non-structural walls, piping systems and antennas, storage tanks and electrical transformers must survive earthquakes in order to facilitate emergency and recovery services in the aftermath and avoid direct and/or indirect human and/or economical losses. On the other hand, some special dynamic properties make S substructures particularly vulnerable to earthquakes. First of all, S substructures are usually much lighter than the P substructure to which they are attached, and the stiffness of S components, including anchors, is much smaller than the stiffness of P components: as a result, in most of the real cases the modal frequencies of S substructures are close to, and sometimes tuned to, those of the P substructure. Moreover, the vibration of the P substructure tends to amplify the effects of the ground motion on the S substructures, principally on those attached at the top (e.g., antennas). In addition, the damping capabilities of S attachments are generally much smaller than those of the P supporting system, and so the resonance phenomenon may occur.

The above considerations would suggest the use of rigorous approaches, in which the dynamic interaction among P and S substructures is fully accounted for. In practical applications, however, combined P-S systems have an excessive number of degrees of freedom and show large differences in the mass, stiffness and damping coefficients. Therefore, conventional methods, such as modal analysis with the earthquake response spectrum and time-history analysis with recorded and/or generated accelerograms, may become too expensive and inaccurate. Conversely, the so-called “cascade” approximation, in which feedback of the S substructures on the P substructure is neglected, may be too simplistic even though it is very popular. In this approach, P and S substructures are decoupled and analysed in sequence (e.g., Falsone et al., 1991; Lavelle et al., 1991): in the first stage, the seismic response of the P substructure is evaluated neglecting the presence of any S substructure; in the second

stage, the dynamic response of each S substructure is evaluated considering the motion of the P substructure at the anchor points, other than the ground motion. Unfortunately, in a number of real cases this approach may lead to inaccurate predictions, e.g., when the effect of spatial coupling is significant.

In this paper, the concept of “Light Secondary Substructure” (LSS) approximation is stressed, and the limits of validity are investigated with reference to a simple 2-DOF combined P-S system. This approximation is used in deriving a novel CQC (Complete Quadratic Combination) rule, which can be viewed as a special variant of the method recently formulated by Falsone and Muscolino (1999, 2004) for the seismic analysis of non-classically damped structures. For the validation purposes, numerical results are presented in the simplest case where the new combination coefficients are consistent with the assumption of white noise excitation, while the formulation can be easily extended to any power spectral density (PSD) function of the seismic input. Advantages of the proposed approach are: (i) the eigenproperties involved in the computations (modal frequencies and modal shapes) are those of the decoupled substructures, assumed to be fixed to their own bases; (ii) the cross-correlation coefficients incorporate the effects of frequency tuning and different damping in the substructures; and (iii) just a single earthquake response spectrum, for a reference value of the viscous damping ratio, is required. The latter feature of the proposed approach is probably the most important one. Methods based on the direct characterization of the seismic hazard by the PSD of the ground acceleration, in fact, enable to account for the dynamic interaction among P and S substructures through the appropriate definition of the frequency response function (FRF) of the combined P-S system, for which the individual fixed-base modal properties can be used (Dey and Gupta, 1999). However, to date, the PSD function is considered almost exclusively in the academic community and for studying structures of exceptional importance. Seventy-five years after the pioneering work by Professor Maurice Biot (Biot, 1932, 1933, 1934), the earthquake response spectrum is still the most popular tool for the analysis and design of conventional earthquake-resistant structures. Moreover, given its extreme simplicity, a number of deterministic and stochastic extensions have been proposed in the literature. Among others, Amini and Trifunac (1985) developed a stochastic method for estimating not just the largest, but all the ordered peaks of the seismic response of linear structures; this method has been refined by Gupta and Trifunac (1988), and can be useful in order to better understand the progressive damage under successive excursions of the seismic response beyond a certain design level; Gupta and Trifunac (1989) formulated a probabilistic extension, which takes into account the rotational components of the ground motion along with the translational components; the effects of wave passage, loss of coherency with distance and variation of local soil conditions are included in the method proposed by Der Kiureghian and Neuenhofer (1992) for the seismic analysis of multiply-supported structures subjected to spatially-varying ground motions; Iwan (1997) proposed a new earthquake drift spectrum based on a continuous shear-beam model rather than a single-degree-of-freedom oscillator, which provides important information for near-source pulse-like ground shakings. From this point of view, then, the main intent of the CQC rule proposed in this paper could be claimed to be the attempt of extending to light secondary attachments the original statement by Professor Maurice Biot: “the maximum effect of earthquakes on buildings will be easily evaluated...” (Biot, 1933).

EQUATIONS OF MOTION

In this section, the equations of motion of a primary (P) structural system with n_p DOFs (degrees of freedom), connected to a lighter secondary (S) attachment with n_s DOFs, are established in the linear range. In the following, the damping of both P and S substructures is assumed to be linear hysteretic (among others, Nashif et al., 1985; Inaudi and Kelly, 1995; Muscolino et al., 2005; and references provided therein). Experimental analyses, in fact, demonstrate that in most of the cases the dissipation of engineering materials is nearly frequency-independent. This means that, ideally, the damping forces are proportional to the strains, but in phase with the strain rates. This behaviour can be easily introduced in the frequency domain, while much more complicated is the application in the time domain (Makris, 1997; Makris and Zhang, 2000; Muscolino et al., 2005), and for this reason the linear viscous damping is usually preferred in structural dynamics. However, when combined P-S systems are dealt with, the formation of the viscous damping matrix is not straightforward (e.g., Gupta and Jaw, 1986; Muscolino, 1990; Feriani and Perotti, 1996), and the use of the linear hysteretic damping is preferable.

1. Combined P-S System

In the mixed time-frequency domain, the seismic motion of the combined P-S system shown in Figure 1 is governed by

$$\mathbf{M}\ddot{\mathbf{u}}(t) + \mathbf{K}(\omega)\mathbf{u}(t) = -\mathbf{M}\boldsymbol{\tau}\ddot{u}_g(t) \quad (1)$$

Here $\mathbf{u}(t) = [\mathbf{u}_s^T(t) \ \vdots \ \mathbf{u}_p^T(t)]^T$ is the $n \times 1$ array ($n = n_s + n_p$) of the DOFs (total displacements), in which those of the P substructure, as listed in the array $\mathbf{u}_p(t)$, are appended to the DOFs of the S substructure, as listed in the array $\mathbf{u}_s(t)$; $\ddot{u}_g(t)$ is the time history of the ground acceleration; $\boldsymbol{\tau}$ is its influence vector whose elements can be partitioned as $\boldsymbol{\tau} = [\boldsymbol{\tau}_s^T \ \vdots \ \boldsymbol{\tau}_p^T]^T$; \mathbf{M} and $\mathbf{K}(\omega)$ are the inertia matrix and the complex-valued dynamic stiffness matrix, respectively; and, as usual, the over-dot means time derivative. The matrices \mathbf{M} and $\mathbf{K}(\omega)$ can be partitioned as

$$\mathbf{M} = \begin{bmatrix} \mathbf{M}_s & \mathbf{0} \\ \mathbf{0} & \mathbf{M}_p \end{bmatrix} \quad (2)$$

$$\mathbf{K}(\omega) = \begin{bmatrix} \mathbf{K}_s \times [1 + j\eta_s \text{sign}(\omega)] & \mathbf{0} \\ \mathbf{0} & \mathbf{K}_p \times [1 + j\eta_p \text{sign}(\omega)] \end{bmatrix} + \begin{bmatrix} \mathbf{0} & \mathbf{K}_{sp} \\ \mathbf{K}_{sp}^T & \Delta\mathbf{K}_p \end{bmatrix} \times [1 + j\eta_s \text{sign}(\omega)]$$

Here the real-valued mass and stiffness matrices of the S substructure, \mathbf{M}_s and \mathbf{K}_s , and of the P substructure, \mathbf{M}_p and \mathbf{K}_p , refer to the substructures assembled under the assumption of being fixed to their respective bases, i.e., the P substructure is fixed to the ground (Figure 2(a)), while the S substructure is fixed to the support points on the P substructure as well as to the ground (Figure 2(b)); \mathbf{K}_{sp} is the stiffness matrix coupling the P and S substructures; $\Delta\mathbf{K}_p$ is the increment in the stiffness matrix of the P substructure due to the presence of the S substructure; η_s and η_p are the loss factors of the S and P substructures, respectively; $j = \sqrt{-1}$ is the imaginary unit; and ω is the vibration frequency.

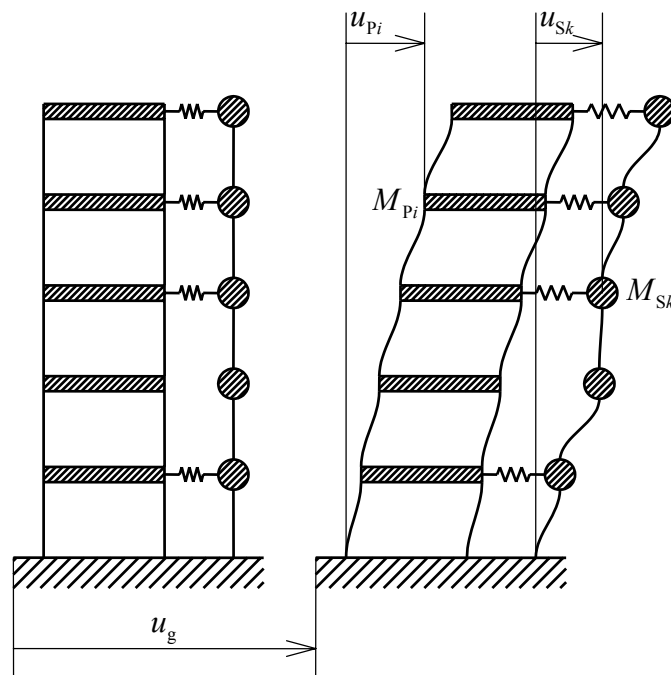


Fig. 1 Sketch of the combined primary-secondary (P-S) system

The seismic response of the coupled P-S system is given in the frequency domain by

$$\mathbf{F}\langle \mathbf{u}(t) \rangle = \mathbf{H}(\omega) \mathbf{F}\langle \ddot{\mathbf{u}}_g(t) \rangle \quad (3)$$

where the symbol $\mathbf{F}\langle \cdot \rangle$ stands for the Fourier transform operator, and $\mathbf{H}(\omega)$ is the $n \times 1$ array listing the frequency response functions (FRFs) of various DOFs:

$$\mathbf{H}(\omega) = -[\mathbf{M}^{-1}\mathbf{K}(\omega) - \omega^2\mathbf{I}_n]^{-1} \boldsymbol{\tau} \quad (4)$$

with \mathbf{I}_n being the $n \times n$ identity matrix.

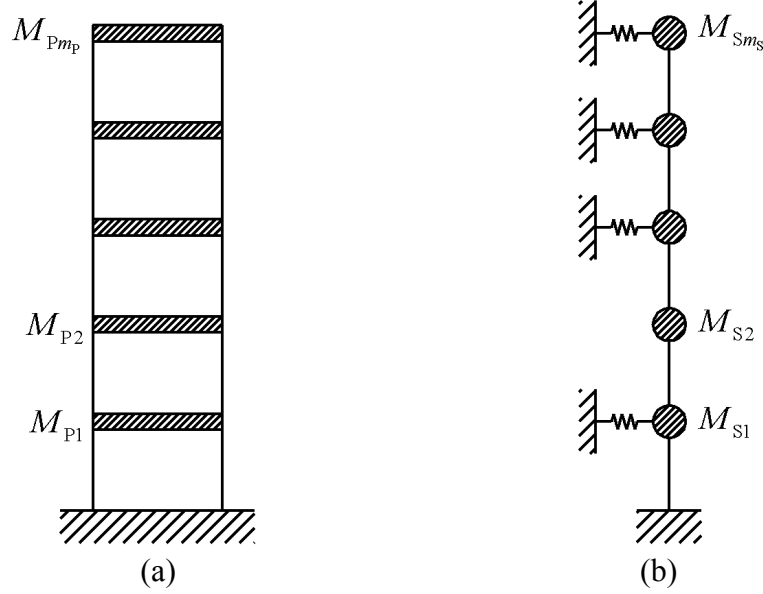


Fig. 2 Fixed-base substructures: (a) P structural system; (b) S attachment

2. Modal Transformations

The dynamic response of the combined P-S system can be conveniently represented in the reduced modal space by means of the so-called “admissible coordinate transformation” (Muscolino, 1990), given by

$$\mathbf{u}(t) = \mathbf{\Gamma} \mathbf{q}(t) \quad (5)$$

Here $\mathbf{q}(t) = [\mathbf{q}_s^T(t) \ \mathbf{q}_p^T(t)]^T$ is the $m \times 1$ array ($m = m_s + m_p \leq n$) listing the modal coordinates of the combined P-S system, in which the array of the $m_p \leq n_p$ modal coordinates of the P substructure, $\mathbf{q}_p(t)$, is appended to the array of the $m_s \leq n_s$ modal coordinates of the S substructure, $\mathbf{q}_s(t)$; and $\mathbf{\Gamma}$ is the transformation matrix, which is partitioned as

$$\mathbf{\Gamma} = \begin{bmatrix} \mathbf{\Phi}_S & \mathbf{\Psi}_{SP} \\ \mathbf{0} & \mathbf{\Phi}_P \end{bmatrix} \quad (6)$$

with $\mathbf{\Phi}_S = [\phi_{S1} \ \cdots \ \phi_{Sm_s}]$ and $\mathbf{\Phi}_P = [\phi_{P1} \ \cdots \ \phi_{Pm_p}]$ being the modal matrices of the S and P substructures, of dimensions $n_s \times m_s$ and $n_p \times m_p$, respectively. The columns of these matrices are the modal shapes of the two fixed-base substructures (Figures 3(a) and 3(b)). In Equation (6), $\mathbf{\Psi}_{SP} = [\psi_{SP1} \ \cdots \ \psi_{SPm_s}]$ is the modal coupling matrix, of dimensions $n_s \times m_p$, whose columns are the deformed shapes of the S substructure due to the displacements at the support points for the modal shapes of the P substructure (Figure 3(c)). The modal matrices $\mathbf{\Phi}_S$ and $\mathbf{\Phi}_P$ can be evaluated by solving the following classical eigenproblems:

$$\mathbf{M}_S \Phi_S \Omega_S^2 = \mathbf{K}_S \Phi_S; \quad \mathbf{M}_P \Phi_P \Omega_P^2 = \mathbf{K}_P \Phi_P \quad (7)$$

$\Omega_S = \text{diag}\{\omega_{S1}, \dots, \omega_{Sm_S}\}$ and $\Omega_P = \text{diag}\{\omega_{P1}, \dots, \omega_{Pm_P}\}$ being the spectral matrices of the S and P substructures, respectively. The elements of these matrices are the undamped modal circular frequencies of the two fixed-base substructures. Further, the modal coupling matrix Ψ_{SP} is given by

$$\Psi_{SP} = \mathbf{N}_{SP} \Phi_P; \quad \mathbf{N}_{SP} = -\mathbf{K}_S^{-1} \mathbf{K}_{SP} \quad (8)$$

with \mathbf{N}_{SP} being the so-called pseudo-static influence matrix of the P substructure on the S substructure.

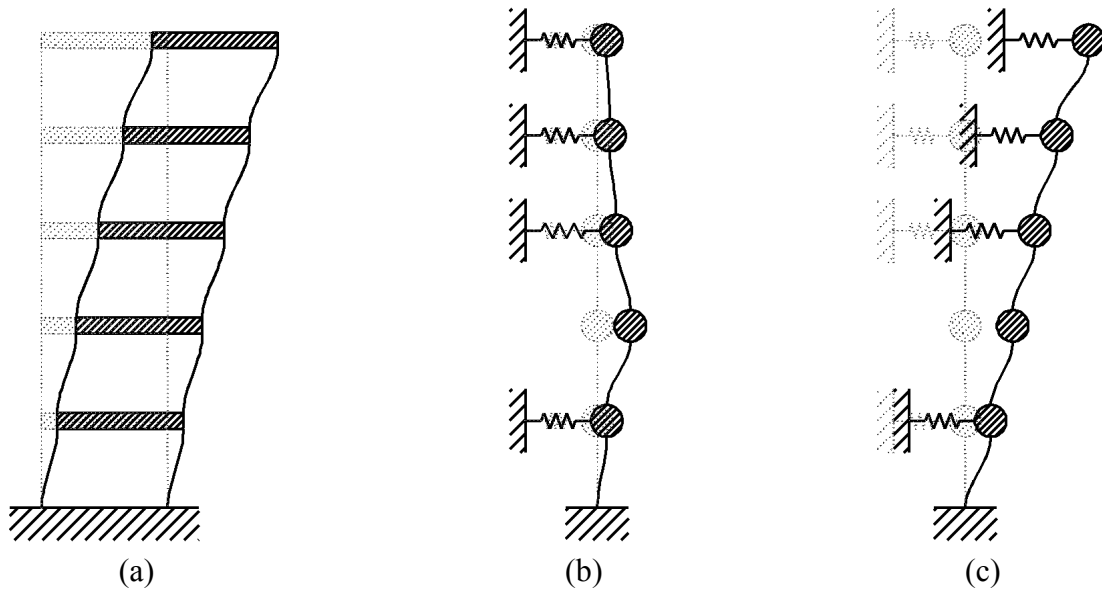


Fig. 3 (a) Modal shape of the P structural system; (b) Modal shape of the fixed-base S attachment; (c) Deformed shape of the S attachment induced by the modal shape of the P structural system

Upon substitution of Equation (5) into Equation (1), one obtains

$$\mathbf{m} \ddot{\mathbf{q}}(t) + \mathbf{k}(\omega) \mathbf{q}(t) = \mathbf{g} \ddot{u}_g(t) \quad (9)$$

where the symmetric matrices \mathbf{m} and $\mathbf{k}(\omega)$ are the inertia matrix and the complex-valued dynamic stiffness matrix in the reduced modal space, respectively, while \mathbf{g} is the modal influence vector of the seismic input. These quantities are expressed as

$$\mathbf{m} = \Gamma^T \mathbf{M} \Gamma = \begin{bmatrix} \mathbf{I}_{m_S} & \mathbf{m}_{SP} \\ \mathbf{m}_{SP}^T & \mathbf{I}_{m_P} + \Delta \mathbf{m}_P \end{bmatrix}$$

$$\mathbf{k}(\omega) = \Gamma^T \mathbf{K}(\omega) \Gamma = \begin{bmatrix} \Omega_S^2 \gamma(\omega) & \mathbf{0} \\ \mathbf{0} & \Omega_P^2 + \Delta \mathbf{k}_P \gamma(\omega) \end{bmatrix} \times [1 + j \eta_P \text{sign}(\omega)] \quad (10)$$

$$\mathbf{g} = -\Gamma^T \mathbf{M} \boldsymbol{\tau} = -\begin{bmatrix} \mathbf{p}_S \\ \mathbf{p}_P + \Delta \mathbf{p}_P \end{bmatrix}$$

where the off-diagonal term \mathbf{m}_{SP} in the inertia matrix is defined by

$$\mathbf{m}_{SP} = \Phi_S^T \mathbf{M}_S \Psi_{SP} \quad (11)$$

and \mathbf{p}_S and \mathbf{p}_P are the arrays listing the usual modal participation factors of the P and S substructures, respectively:

$$\mathbf{p}_s = \Phi_s^T \mathbf{M}_s \boldsymbol{\tau}_s; \quad \mathbf{p}_p = \Phi_p^T \mathbf{M}_p \boldsymbol{\tau}_p \quad (12)$$

Further, the increments $\Delta \mathbf{m}_p$, $\Delta \mathbf{k}_p$ and $\Delta \mathbf{p}_p$ are given by

$$\begin{aligned} \Delta \mathbf{m}_p &= \Psi_{sp}^T \mathbf{M}_s \Psi_{sp}; \quad \Delta \mathbf{k}_p = \Phi_p^T \left(\Delta \mathbf{K}_p + \mathbf{K}_{sp}^T \mathbf{N}_{sp} \right) \Phi_p \\ \Delta \mathbf{p}_p &= \Phi_p^T \mathbf{N}_{sp}^T \mathbf{M}_s \boldsymbol{\tau}_s \end{aligned} \quad (13)$$

and $\gamma(\omega)$ is a complex-valued function that accounts for the different damping in the substructures:

$$\gamma(\omega) = \frac{1 + j\eta_s \operatorname{sign}(\omega)}{1 + j\eta_p \operatorname{sign}(\omega)} = \frac{(1 + \eta_s \eta_p) + j(\eta_s - \eta_p) \operatorname{sign}(\omega)}{1 + \eta_p^2} \quad (14)$$

According to Equations (5) and (10), the seismic response of the coupled P-S system can be evaluated in the frequency domain as

$$\mathbf{F}\langle \mathbf{u}(t) \rangle = \mathbf{\Gamma} \mathbf{h}(\omega) \mathbf{F}\langle \ddot{\mathbf{u}}_g(t) \rangle \quad (15)$$

where $\mathbf{h}(\omega)$ is the $m \times 1$ array listing the modal FRFs:

$$\mathbf{h}(\omega) = [\mathbf{k}(\omega) - \omega^2 \mathbf{m}]^{-1} \mathbf{g} = [\mathbf{A}(\omega) - \omega^2 \mathbf{I}_m]^{-1} \mathbf{b} \quad (16)$$

with

$$\mathbf{A}(\omega) = \mathbf{m}^{-1} \mathbf{k}(\omega); \quad \mathbf{b} = \mathbf{m}^{-1} \mathbf{g} \quad (17)$$

APPROXIMATE RESPONSE OF A SIMPLE 2-DOF COMBINED P-S SYSTEM

In this section, the simplest case in which both P and S substructures are single-DOF oscillators is considered, with the aim of investigating the effects that two different approximations, namely the “Light Secondary Substructure” (LSS) approximation and the “cascade” approximation, may have on the seismic response of the combined P-S system. This analysis reveals which terms are negligible when the S substructure is much lighter than the P substructure, and these results are extended in the next section to the general case in which both P and S substructures are multi-DOF systems.

With reference to the combined P-S system depicted in Figure 4(a), the matrices \mathbf{M} and $\mathbf{K}(\omega)$ in Equation (2) are simplified as

$$\begin{aligned} \mathbf{M} &= \begin{bmatrix} M_s & 0 \\ 0 & M_p \end{bmatrix} \\ \mathbf{K}(\omega) &= \begin{bmatrix} K_s \gamma(\omega) & -\frac{K_s}{2} \gamma(\omega) \\ -\frac{K_s}{2} \gamma(\omega) & K_p + \frac{K_s}{2} \gamma(\omega) \end{bmatrix} \times [1 + j\eta_p \operatorname{sign}(\omega)] \end{aligned} \quad (18)$$

while $\mathbf{u}(t) = [u_s(t) \mid u_p(t)]^T$ and $\boldsymbol{\tau} = [1 \mid 1]^T$. After some algebra, one can prove that the transformation matrix $\mathbf{\Gamma}$ consistent with Equation (6) is

$$\mathbf{\Gamma} = \begin{bmatrix} M_s^{-1/2} & \frac{1}{2} M_p^{-1/2} \\ 0 & M_p^{-1/2} \end{bmatrix} \quad (19)$$

The modal quantities in Equation (10) are then expressed as

$$\mathbf{m} = \begin{bmatrix} 1 & \frac{\sqrt{\alpha}}{2} \\ \frac{\sqrt{\alpha}}{2} & 1 + \frac{\alpha}{4} \end{bmatrix}; \quad \mathbf{k}(\omega) = \omega_p^2 \times \begin{bmatrix} \beta^2 \gamma(\omega) & 0 \\ 0 & 1 + \frac{\alpha \beta^2 \gamma(\omega)}{4} \end{bmatrix} \times [1 + j \eta_p \text{sign}(\omega)] \quad (20)$$

$$\mathbf{g} = - \begin{bmatrix} \frac{\sqrt{\alpha}}{2} \\ 1 + \frac{\alpha}{4} \end{bmatrix}$$

where α is the mass ratio and β is a tuning parameter:

$$\alpha = \frac{M_s}{M_p}; \quad \beta = \frac{\omega_s}{\omega_p} \quad (21)$$

ω_p and ω_s being the undamped natural circular frequencies of the P (Figure 4(b)) and S (Figure 4(c)) oscillators:

$$\omega_p = \sqrt{\frac{K_p}{M_p}}; \quad \omega_s = \sqrt{\frac{K_s}{M_s}} \quad (22)$$

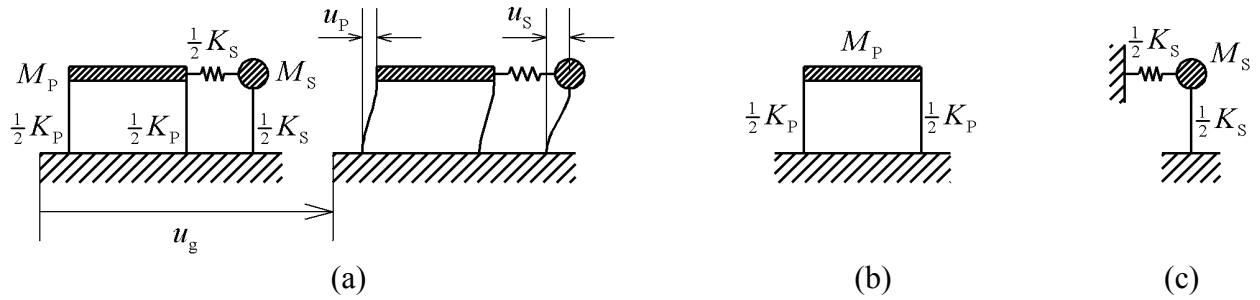


Fig. 4 (a) 2-DOF combined P-S system; (b) P oscillator; (c) S oscillator

1. LSS Approximation

When the S substructure is light with respect to the P substructure, i.e., $M_s \ll M_p$, the mass ratio (first of Equations (21)) is much less than one, i.e., $\alpha \ll 1$. Accordingly, this term can be neglected in the dynamic stiffness matrix and in the influence vector given in Equations (20):

$$\hat{\mathbf{k}}(\omega) = \omega_p^2 \times \begin{bmatrix} \beta^2 \gamma(\omega) & 0 \\ 0 & 1 \end{bmatrix} \times [1 + j \eta_p \text{sign}(\omega)]; \quad \hat{\mathbf{g}} = - \begin{bmatrix} \frac{\sqrt{\alpha}}{2} \\ 1 \end{bmatrix} \quad (23)$$

Additionally, in the complex-valued modal stiffness matrix $\hat{\mathbf{k}}(\omega)$ (first of Equations (23)) it is assumed that $|\alpha \beta^2 \gamma(\omega)| \ll 1$. In practical applications, in fact, $|\gamma(\omega)| \cong 1$, while from Equations (21) and (22) it follows that the stiffness ratio K_s/K_p is given by $\alpha \beta^2$. This ratio needs to be much less than one in order for the “secondary” stiffness K_s to be negligible with respect to the “primary” stiffness K_p .

Upon substitution of Equation (23) into Equation (17), one obtains for the proposed LSS approximation

$$\hat{\mathbf{A}}(\omega) = \mathbf{m}^{-1} \hat{\mathbf{k}}(\omega) = \omega_p^2 \times \left[\begin{array}{c|c} \left(1 + \frac{\alpha}{4}\right) \beta^2 \gamma(\omega) & -\frac{\sqrt{\alpha}}{2} \\ \hline -\frac{\sqrt{\alpha}}{2} \beta^2 \gamma(\omega) & 1 \end{array} \right] \times [1 + j \eta_p \text{sign}(\omega)] \quad (24)$$

$$\hat{\mathbf{b}} = \mathbf{m}^{-1} \hat{\mathbf{g}} = - \left[\begin{array}{c|c} \frac{\sqrt{\alpha}}{2} + \frac{\alpha \sqrt{\alpha}}{4} & \\ \hline 1 - \frac{\alpha}{2} & \end{array} \right] \cong - \left[\begin{array}{c|c} \frac{\sqrt{\alpha}}{2} & \\ \hline 1 & \end{array} \right]$$

with

$$\mathbf{m}^{-1} = \left[\begin{array}{c|c} 1 + \frac{\alpha}{4} & -\frac{\sqrt{\alpha}}{2} \\ \hline -\frac{\sqrt{\alpha}}{2} & 1 \end{array} \right] \quad (25)$$

The approximate array of the modal FRFs, then, can be evaluated as

$$\hat{\mathbf{h}}(\omega) = [\hat{\mathbf{A}}(\omega) - \omega^2 \mathbf{I}_2]^{-1} \hat{\mathbf{b}} = \begin{bmatrix} \hat{h}_s(\omega) \\ \hat{h}_p(\omega) \end{bmatrix} \quad (26)$$

where $\hat{h}_s(\omega)$ and $\hat{h}_p(\omega)$ are the approximate FRFs of the modal coordinates of the S oscillator, $q_s(t) = \sqrt{M_s} [u_s(t) - u_p(t)/2]$, and of the P oscillator, $q_p(t) = \sqrt{M_p} u_p(t)$, respectively. The comparison between Equations (3) and (15), finally, gives the array of the corresponding FRFs of the DOFs, $u_s(t)$ and $u_p(t)$, in that order:

$$\hat{\mathbf{H}}(\omega) = \mathbf{\Gamma} \hat{\mathbf{h}}(\omega) = \left[\begin{array}{c} M_s^{-1/2} \hat{h}_s(\omega) + \frac{1}{2} M_p^{-1/2} \hat{h}_p(\omega) \\ \hline M_p^{-1/2} \hat{h}_p(\omega) \end{array} \right] \quad (27)$$

2. Cascade Approximation

When the S substructure is much lighter than the P substructure, i.e., $\alpha \ll 1$, the dynamic interaction in the coupled P-S system is often ignored, and the seismic responses of the P and S substructures are evaluated in cascade. Accordingly, in the first stage the response of the P substructure to the ground motion is computed by neglecting the feedback of the S substructure, while in the second stage the response of the S substructure is computed by taking into account both the response of the P substructure and the seismic input. As a result, the dynamic stiffness matrix $\mathbf{K}(\omega)$ in the second of Equations (18) becomes asymmetric, since the lower off-diagonal term becomes zero:

$$\bar{\mathbf{K}}(\omega) = \left[\begin{array}{c|c} K_s [1 + j \eta_s \text{sign}(\omega)] & -\frac{K_s}{2} [1 + j \eta_s \text{sign}(\omega)] \\ \hline 0 & K_p [1 + j \eta_p \text{sign}(\omega)] \end{array} \right] \quad (28)$$

The approximate array of the FRFs of the DOFs then takes the form

$$\begin{aligned}\bar{\mathbf{H}}(\omega) &= -[\mathbf{M}^{-1}\bar{\mathbf{K}}(\omega) - \omega^2\mathbf{I}_n]^{-1}\boldsymbol{\tau} \\ &= \begin{bmatrix} \frac{\omega^2 - \left[1 + \frac{\beta^2\gamma(\omega)}{2}\right]\omega_p^2[1 + j\eta_p \text{sign}(\omega)]}{\frac{\{\omega^2 - \beta^2\omega_s^2[1 + j\eta_s \text{sign}(\omega)]\}\{\omega^2 - \omega_p^2[1 + j\eta_p \text{sign}(\omega)]\}}{1}} \\ \frac{1}{\omega^2 - \omega_p^2[1 + j\eta_p \text{sign}(\omega)]} \end{bmatrix}\end{aligned}\quad (29)$$

3. Numerical Examples

The accuracy of the approximations summarized in the previous subsections has been investigated in the frequency domain. In Figure 5 the absolute values of the exact FRFs of both P and S substructures (shown by solid lines) are compared with those given by the LSS approximation (as in Equation (27); shown by circles) and cascade approximation (as in Equation (29); shown by dashed lines). The mass ratio and the tuning parameter are $\alpha = 0.02$ and $\beta = 1.0$, respectively, while the loss factors for the P and S substructures are $\eta_s = 0.04$ and $\eta_p = 0.10$. These comparisons demonstrate that the proposed LSS approximation is in good agreement with the exact solution even when the P and S oscillators are perfectly tuned, i.e., $\beta = 1.0$. On the contrary, the cascade approximation is unable to recover the bimodal FRF of the P oscillator (Figure 5, left), and overestimates the peak for the S oscillator (Figure 5, right). The semi-logarithmic plots in Figure 6 confirm the higher accuracy of the proposed LSS approximation (shown by circles) with respect to the classical cascade approximation (shown by dashed line) for a larger mass ratio ($\alpha = 0.10$) and different values of the tuning parameter ($\beta = 0.50, 1.0$ and 1.5). However, only when $\beta = 1.0$, the inaccuracy of the cascade approximation drastically affects the results.

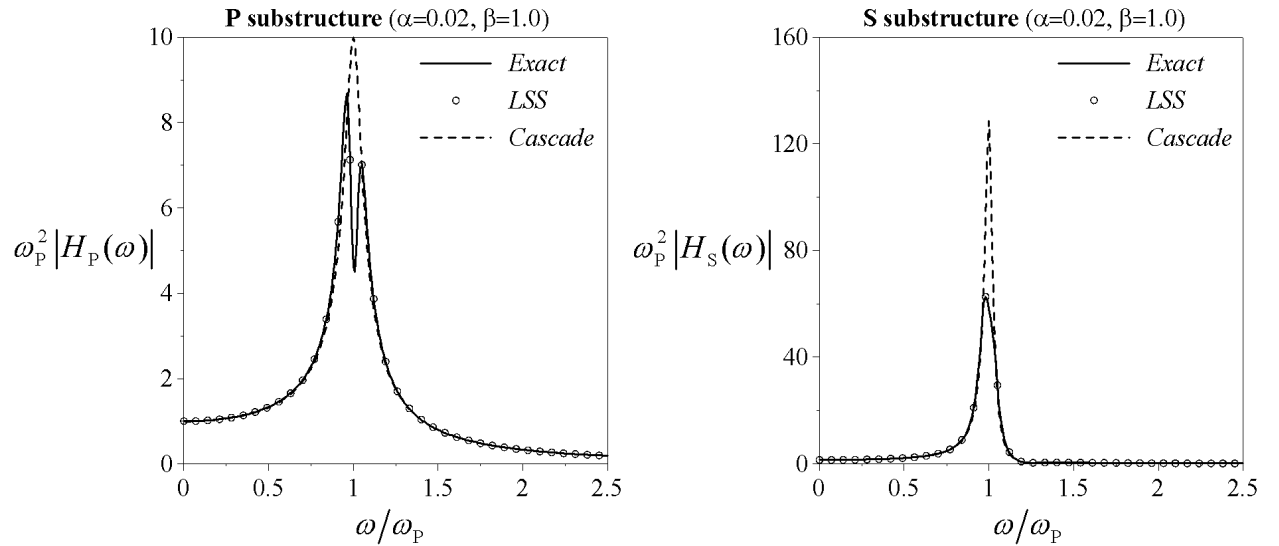


Fig. 5 Dimensionless absolute values of the frequency response functions of the 2-DOF combined P-S system with mass ratio $\alpha = 0.02$ and tuning parameter $\beta = 1.0$: P oscillator (left); S oscillator (right)

APPROXIMATE RESPONSE OF MULTI-DOF COMBINED P-S SYSTEMS

Let us go back to the modal equations of motion of multi-DOF P and S substructures (Equations (9) and (10)). The comparison with the first of Equations (20) suggests that in the first of Equations (10) the off-diagonal term \mathbf{m}_{sp} in the modal inertia matrix, \mathbf{m} , is proportional to the square root of the mass

ratio, $\sqrt{\alpha}$ (which is not negligible), while the increment $\Delta \mathbf{m}_p$ is proportional to the mass ratio, α (which is negligible). Accordingly, the inverse of the matrix \mathbf{m} for the multi-DOF P and S substructures can be approximated in a form similar to the one presented in Equation (25) for single-DOF P and S oscillators:

$$\hat{\mathbf{m}}^{-1} \cong \begin{bmatrix} \mathbf{I}_{m_s} + \mathbf{m}_{SP} \mathbf{m}_{SP}^T & -\mathbf{m}_{SP} \\ -\mathbf{m}_{SP}^T & \mathbf{I}_{m_p} \end{bmatrix} \quad (30)$$

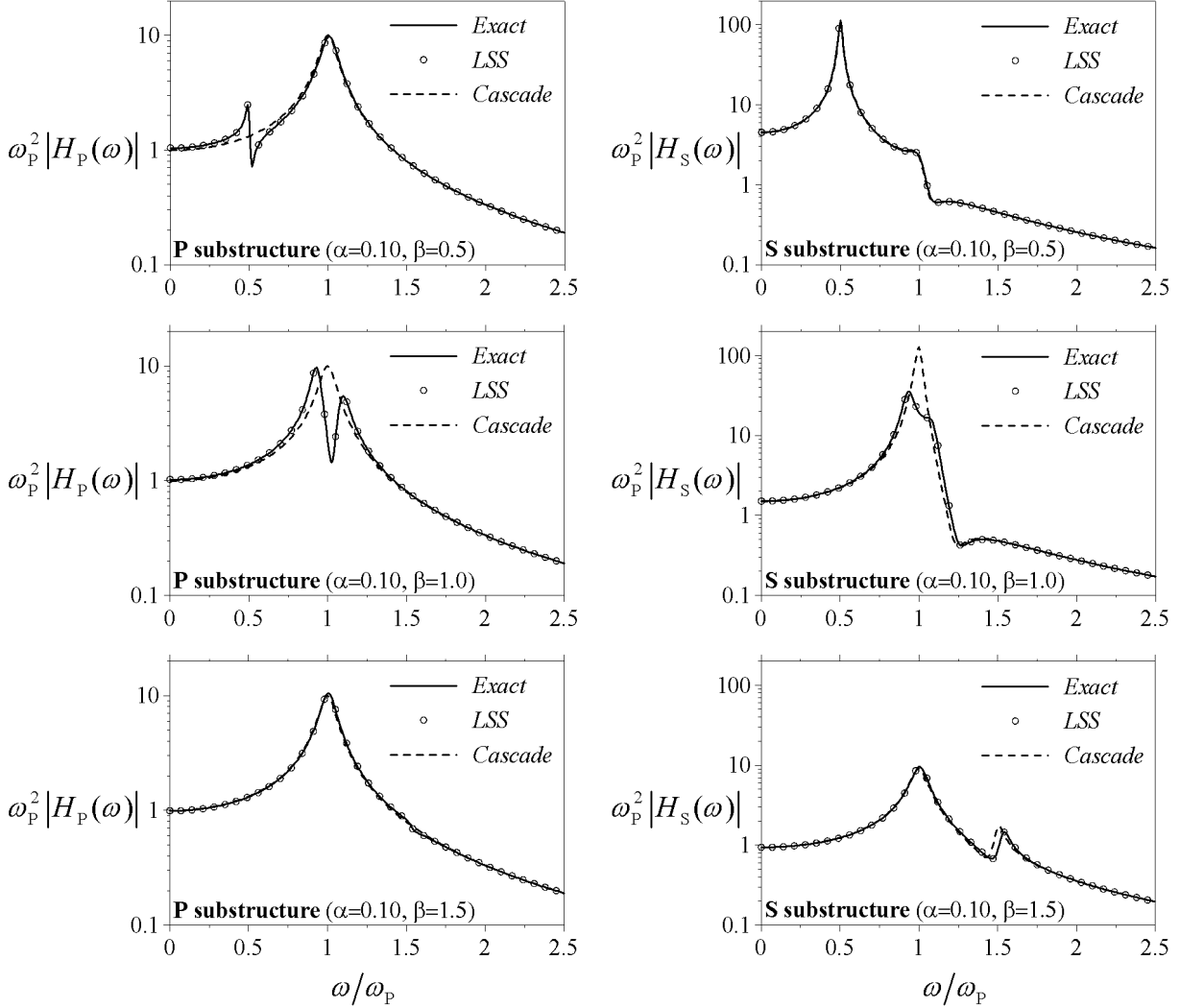


Fig. 6 Dimensionless absolute values of the frequency response functions of the 2-DOF combined P-S system with mass ratio $\alpha = 0.10$ and tuning parameter $\beta = 0.5, 1.0$ and 1.5 : P oscillator (left); S oscillator (right)

Following the above approach, the dynamic stiffness matrix and the influence vector also take approximate forms similar to those derived in the case of single-DOF P and S oscillators (Equation (23)):

$$\hat{\mathbf{k}}(\omega) = \begin{bmatrix} \mathbf{\Omega}_s^2 \gamma(\omega) & \mathbf{0} \\ \mathbf{0} & \mathbf{\Omega}_p^2 \end{bmatrix} \times [1 + j \eta_p \text{sign}(\omega)]; \quad \hat{\mathbf{g}} = - \begin{bmatrix} \mathbf{p}_s \\ \mathbf{p}_p \end{bmatrix} \quad (31)$$

Then, substitution of Equations (30) and (31) into Equation (17) gives expressions similar to those of Equation (24):

$$\hat{\mathbf{A}}(\omega) = \hat{\mathbf{m}}^{-1} \hat{\mathbf{k}}(\omega) = \left[\begin{array}{c|c} (\mathbf{I}_{m_s} + \mathbf{m}_{sp} \mathbf{m}_{sp}^T) \boldsymbol{\Omega}_s^2 \gamma(\omega) & -\mathbf{m}_{sp} \boldsymbol{\Omega}_p^2 \\ \hline -\mathbf{m}_{sp}^T \boldsymbol{\Omega}_s^2 \gamma(\omega) & \boldsymbol{\Omega}_p^2 \end{array} \right] \times [1 + j \eta_p \text{sign}(\omega)] \quad (32)$$

$$\hat{\mathbf{b}} = \hat{\mathbf{m}}^{-1} \hat{\mathbf{g}} = - \left[\frac{\mathbf{p}_s - \mathbf{m}_{sp} \mathbf{p}_p}{\mathbf{p}_p} \right]$$

Moreover, substitution of Equation (32) into Equation (26) gives the array of the modal FRFs in the form,

$$\hat{\mathbf{h}}(\omega) = - \left\{ \left[\begin{array}{c|c} \hat{\mathbf{A}}_s \gamma(\omega) & \hat{\mathbf{A}}_{sp} \\ \hline \hat{\mathbf{A}}_{ps} \gamma(\omega) & \boldsymbol{\Omega}_p^2 \end{array} \right] \times [1 + j \eta_p \text{sign}(\omega)] - \omega^2 \left[\begin{array}{c|c} \mathbf{I}_{m_s} & \mathbf{0} \\ \hline \mathbf{0} & \mathbf{I}_{m_p} \end{array} \right] \right\}^{-1} \left[\begin{array}{c} \hat{\mathbf{b}}_s \\ \hline \mathbf{p}_p \end{array} \right] \quad (33)$$

with $\hat{\mathbf{A}}_s = (\mathbf{I}_{m_s} + \mathbf{m}_{sp} \mathbf{m}_{sp}^T) \boldsymbol{\Omega}_s^2$, $\hat{\mathbf{A}}_{sp} = -\mathbf{m}_{sp} \boldsymbol{\Omega}_p^2$, $\hat{\mathbf{A}}_{ps} = -\mathbf{m}_{sp}^T \boldsymbol{\Omega}_s^2$, and $\hat{\mathbf{b}}_s = \mathbf{p}_s - \mathbf{m}_{sp} \mathbf{p}_p$. Interestingly, in Equation (33) only the direct terms of the P substructure, namely the squared spectral matrix, $\boldsymbol{\Omega}_p^2$, and the array of the modal participation factors, \mathbf{p}_p , are unmodified by the coupling matrix \mathbf{m}_{sp} . Finally, once the array of Equation (33) is partitioned as $\hat{\mathbf{h}}(\omega) = [\hat{\mathbf{h}}_s^T(\omega) \mid \hat{\mathbf{h}}_p^T(\omega)]^T$, the FRFs of various DOFs can be written similar to Equation (27):

$$\hat{\mathbf{H}}(\omega) = \Gamma \hat{\mathbf{h}}(\omega) = \left[\frac{\boldsymbol{\Phi}_s \hat{\mathbf{h}}_s(\omega) + \boldsymbol{\Psi}_{sp} \hat{\mathbf{h}}_p(\omega)}{\boldsymbol{\Phi}_p \hat{\mathbf{h}}_p(\omega)} \right] \quad (34)$$

MAXIMUM SECONDARY RESPONSE BY EARTHQUAKE RESPONSE SPECTRUM

The aim of this section is to derive a novel definition of the cross-correlation coefficients $\rho(i, k)$ that would enable the Complete Quadratic Combination (CQC) rule (Wilson et al., 1981) to be extended to the seismic analysis and design of multi-DOF secondary (S) substructures attached to a multi-DOF primary (P) load-bearing substructure. It is worth noting that, in order to be attractive for practical applications, (i) the proposed combination rule takes advantage of the LSS (light secondary substructure) approximation presented in the previous sections, and operates without evaluating the eigenproperties of the combined P-S system, while (ii) the seismic input is represented through a conventional earthquake response spectrum. Following the idea of Falsone and Muscolino (1999, 2004), the proposed cross-correlation coefficients would incorporate the dynamic effects which complicate the seismic response of S substructures with respect to the conventional fixed-base structures with equal viscous damping ratio in all the modes of vibration.

1. Preliminary Expressions

Let $y_s(t)$ be a generic response of interest (e.g., an internal force or a deformation measure) for the S attachment as well as for the P-S anchors. Owing to the linearity of both P and S substructures, $y_s(t)$ can be expressed as linear combination of the modal coordinates of the coupled P-S system:

$$\begin{aligned} y_s(t) &= \mathbf{E}_{ss}^T \mathbf{u}_s(t) + \mathbf{E}_{sp}^T \mathbf{u}_p(t) = \mathbf{E}_{ss}^T \boldsymbol{\Phi}_s \mathbf{q}_s(t) + (\mathbf{E}_{ss}^T \boldsymbol{\Psi}_{sp} + \mathbf{E}_{sp}^T \boldsymbol{\Phi}_p) \mathbf{q}_p(t) \\ &= \mathbf{e}_{ss}^T \mathbf{q}_s(t) + \mathbf{e}_{sp}^T \mathbf{q}_p(t) = \sum_{i=1}^{m_s} e_{ssi} q_{si}(t) + \sum_{i=1}^{m_p} e_{spi} q_{pi}(t) \end{aligned} \quad (35)$$

where \mathbf{E}_{ss} (of dimensions $n_s \times 1$) and \mathbf{E}_{sp} (of dimensions $n_p \times 1$) are the arrays listing the contributing coefficients for the DOFs, while the corresponding ones for the modal coordinates are given by $\mathbf{e}_{ss} = \boldsymbol{\Phi}_s^T \mathbf{E}_s$ (of dimensions $m_s \times 1$) and $\mathbf{e}_{sp} = \boldsymbol{\Phi}_p^T \mathbf{E}_{sp} + \boldsymbol{\Psi}_{sp}^T \mathbf{E}_{ss}$ (of dimensions $m_p \times 1$). According to the CQC rule (Wilson et al., 1981), the maximum seismic response can be computed as

$$\begin{aligned} \max |y_S(t)| = & \left[\sum_{i=1}^{m_S} \sum_{k=1}^{m_S} \rho_{SS}(i, k) e_{SSi} e_{SSk} \max |q_{Si}(t)| \max |q_{Sk}(t)| \right. \\ & + \sum_{i=1}^{m_P} \sum_{k=1}^{m_P} \rho_{PP}(i, k) e_{SPi} e_{SPk} \max |q_{Pi}(t)| \max |q_{Pk}(t)| \\ & \left. + 2 \sum_{i=1}^{m_S} \sum_{k=1}^{m_P} \rho_{SP}(i, k) e_{SSi} e_{SPk} \max |q_{Si}(t)| \max |q_{Pk}(t)| \right]^{1/2} \end{aligned} \quad (36)$$

Here $\rho_{AB}(i, k)$ stands for the cross-correlation coefficient among the i th modal coordinate of the A substructure, $q_{Ai}(t)$, and the k th modal coordinate of the B substructure, $q_{Bk}(t)$, with $A = P, S$, $B = P, S$, $i = 1, \dots, m_A$ and $k = 1, \dots, m_B$:

$$\rho_{AB}(i, k) = \frac{E \langle q_{Ai}(t) q_{Bk}(t) \rangle}{\sqrt{E \langle q_{Ai}^2(t) \rangle} \sqrt{E \langle q_{Bk}^2(t) \rangle}} \quad (37)$$

In Equation (37), $E \langle \cdot \rangle$ denotes the expectation operator. The cross-correlation coefficients are usually evaluated under the assumption that the seismic acceleration is a zero-mean, stationary, Gaussian process, which can be modelled as white noise (Der Kiureghian, 1981), filtered white noise (Der Kiureghian and Nakamura, 1993), or spectrum-compatible coloured process (Cacciola et al., 2004). Moreover, it should be emphasized that the CQC rule has been originally derived under the assumption that the peak factor, PF , of the structural response of interest, $y(t)$, is approximately equal to the peak factors of the contributing modal coordinates, $q_i(t)$, i.e.,

$$PF = \frac{\max |y(t)|}{\sqrt{E \langle y^2(t) \rangle}} = \frac{\max |q_i(t)|}{\sqrt{E \langle q_i^2(t) \rangle}} \quad (38)$$

2. Proposed Cross-Correlation Coefficients

Let us now rewrite Equation (37) in the equivalent form:

$$\rho_{AB}(i, k) = r_{AB}(i, k) \frac{\hat{b}_{Ai} \hat{b}_{Bk} \sigma_{Ai} \sigma_{Bk}}{\sqrt{E \langle q_{Ai}^2(t) \rangle} \sqrt{E \langle q_{Bk}^2(t) \rangle}} \quad (39)$$

where

$$r_{AB}(i, k) = \frac{E \langle q_{Ai}(t) q_{Bk}(t) \rangle}{(\hat{b}_{Ai} \sigma_{Ai})(\hat{b}_{Bk} \sigma_{Bk})} \quad (40)$$

Here, σ_{Ai} and σ_{Bk} are the standard deviations of the stationary seismic response of auxiliary single-DOF oscillators having unit mass, a reference value of the viscous damping ratio, ζ_{ref} , for which the earthquake response spectrum is known (usually, $\zeta_{\text{ref}} = 0.05$), and undamped natural periods of the decoupled A and B substructures, respectively. For instance, the undamped natural period of the A ith auxiliary oscillator is

$$T_{Ai} = \frac{2\pi}{\omega_{Ai}} \quad (A = P, S; i = 1, \dots, m_A) \quad (41)$$

Further, according to the second of Equations (32), the coefficient \hat{b}_{Ai} in Equations (39) and (40) plays the role of modal participation factors, and is expressed for the P and S substructures as

$$\hat{b}_{Ai} = \begin{cases} -p_{Pi}; & A = P \\ -p_{Si} + \Phi_{Si}^T \sum_{k=1}^{m_P} p_{Pk} \mathbf{M}_S \Psi_{SPk}; & A = S \end{cases} \quad (42)$$

In other words, for the P substructure the coefficients \hat{b}_{p_i} are the modal participation factors p_{p_i} , evaluated without considering the presence of attachments (as in second of Equations (12)), while for the S substructure the coefficients \hat{b}_{s_i} are given by the modal participation factors p_{s_i} of the fixed-base attachment (as in first of Equation (12)), appropriately modified by the interaction with the P structural system.

As a result of the above definitions, the product $(\hat{b}_{A_i}\sigma_{A_i})$ in Equation (40) is the standard deviation of the steady-state response of a classical single-DOF oscillator governed by

$$\ddot{q}_{A_i}^{(0)}(t) + 2\zeta_{\text{ref}}\omega_{A_i}\dot{q}_{A_i}^{(0)}(t) + \omega_{A_i}^2 q_{A_i}^{(0)}(t) = \hat{b}_{A_i}\ddot{u}_g(t) \quad (43)$$

Under the assumption that the ground acceleration is a white noise of unit one-sided power spectral density, this quantity is expressed in closed-form as

$$(\hat{b}_{A_i}\sigma_{A_i}) = \sqrt{E\left[\left(q_{A_i}^{(0)}(t)\right)^2\right]} = \frac{1}{2}\sqrt{\frac{\pi}{\zeta_{\text{ref}}\omega_{A_i}^3}} \quad (44)$$

On the other hand, the expectation in the numerator of Equation (40) can be evaluated in the frequency domain through the numerical integral:

$$E\langle q_{A_i}(t)q_{B_k}(t) \rangle = \int_0^{\omega_c} \hat{h}_{A_i}(\omega)\hat{h}_{B_k}^*(\omega)d\omega \quad (45)$$

where ω_c is the cut-off circular frequency, and the superscripted asterisk means complex conjugate. Further, $\hat{h}_{A_i}(\omega)$ and $\hat{h}_{B_k}(\omega)$ are the approximate complex-valued FRFs of the modal coordinates $q_{A_i}(t)$ and $q_{B_k}(t)$, given by the i th element of $\hat{\mathbf{h}}_A(\omega)$ and the k th element of $\hat{\mathbf{h}}_B(\omega)$, respectively. It is worth noting that the assumption of white noise input, although effective in a number of real circumstances, should be carefully checked in the cases of soft soil and/or stiff structural system (Der Kiureghian and Nakamura, 1993; Cacciola et al., 2004; Palmeri, 2006). Since the proposed cross-correlation coefficients are evaluated in the frequency domain, the effects of a non-white input can be easily included.

The new coefficients $r_{AB}(i, k)$ defined in Equation (40) can be evaluated by using Equations (44) and (45), and thus, each term in the double summations of Equation (36) can be written as

$$\rho_{AB}(i, k) \max|q_{A_i}(t)| \max|q_{B_k}(t)| = r_{AB}(i, k) \left[\frac{\hat{b}_{A_i}\sigma_{A_i} \max|q_{A_i}(t)|}{\sqrt{E\langle q_{A_i}^2(t) \rangle}} \right] \left[\frac{\hat{b}_{B_k}\sigma_{B_k} \max|q_{B_k}(t)|}{\sqrt{E\langle q_{B_k}^2(t) \rangle}} \right] \quad (46)$$

Taking into account Equation (38), this expression can be approximated as

$$\rho_{AB}(i, k) \max|q_{A_i}(t)| \max|q_{B_k}(t)| = r_{AB}(i, k) \hat{b}_{A_i} \hat{b}_{B_k} [\sigma_{A_i} PF][\sigma_{B_k} PF] \quad (47)$$

Further, the terms $[\sigma_{A_i} PF]$ and $[\sigma_{B_k} PF]$ can be viewed as the maximum seismic responses of the auxiliary single-DOF oscillators with undamped natural periods T_{A_i} and T_{B_k} , respectively, and therefore, the previous expression can be rewritten as

$$\rho_{AB}(i, k) \max|q_{A_i}(t)| \max|q_{B_k}(t)| = r_{AB}(i, k) \hat{b}_{A_i} \hat{b}_{B_k} \frac{S_a(T_{A_i}, \zeta_{\text{ref}})}{(2\pi/T_{A_i})^2} \frac{S_a(T_{B_k}, \zeta_{\text{ref}})}{(2\pi/T_{B_k})^2} \quad (48)$$

Here $S_a(T, \zeta)$ denotes the earthquake response spectrum in terms of pseudo-acceleration for undamped natural period T and viscous damping ratio ζ , and the coefficients $r_{AB}(i, k)$ are obtained by substituting Equation (44) into Equation (40):

$$r_{AB}(i, k) = \frac{4\zeta_{\text{ref}}}{\pi} \omega_{A_i} \omega_{B_k} \sqrt{\omega_{A_i} \omega_{B_k}} E\langle q_{A_i}(t)q_{B_k}(t) \rangle \quad (49)$$

In Equation (49) only the expectation of Equation (45) has to be computed. Finally, upon substitution of Equation (48) into Equation (36), one obtains the CQC rule for the response of interest:

$$\begin{aligned} \max |y_s(t)| = & \frac{1}{4\pi^2} \left[\sum_{i=1}^{m_s} \sum_{k=1}^{m_s} r_{ss}(i, k) e_{ss_i} e_{ss_k} \hat{b}_{s_i} \hat{b}_{s_k} T_{s_i}^2 T_{s_k}^2 S_a(T_{s_i}, \zeta_{\text{ref}}) S_a(T_{s_k}, \zeta_{\text{ref}}) \right. \\ & + \sum_{i=1}^{m_p} \sum_{k=1}^{m_p} r_{pp}(i, k) e_{sp_i} e_{sp_k} \hat{b}_{p_i} \hat{b}_{p_k} T_{p_i}^2 T_{p_k}^2 S_a(T_{p_i}, \zeta_{\text{ref}}) S_a(T_{p_k}, \zeta_{\text{ref}}) \\ & \left. + 2 \sum_{i=1}^{m_s} \sum_{k=1}^{m_p} r_{sp}(i, k) e_{ss_i} e_{sp_k} \hat{b}_{s_i} \hat{b}_{p_k} T_{s_i}^2 T_{p_k}^2 S_a(T_{s_i}, \zeta_{\text{ref}}) S_a(T_{p_k}, \zeta_{\text{ref}}) \right]^{1/2} \end{aligned} \quad (50)$$

NUMERICAL APPLICATION

The CQC rule proposed in the previous section has been applied to the 6-DOF P-S system shown in Figure 7. The P substructure is a planar shear-type 3-DOF frame, with storey mass $M_p = 3,000$ kg and storey stiffness $K_p = 3,000$ kN/m, while the loss coefficient is $\eta_p = 0.10$ (the equivalent viscous damping ratio is $\zeta_p = \eta_p/2 = 0.05$). The S substructure is a 3-DOF attachment, with lumped mass $M_s = \alpha M_p$, lumped stiffness $K_s = 889 \alpha \beta^2$ kN/m, and anchor stiffness $K_{sp} = 1,207 \alpha \beta^2$ kN/m (the dimensionless variables α and β being the mass ratio and tuning parameter, respectively), while the loss coefficient is $\eta_s = 0.04$ (equivalent viscous damping ratio $\zeta_s = 0.02$). The undamped modal circular frequencies of the fixed-base substructures, i.e., solutions of the eigenproblems given in Equation (7), are $\omega_{p1} = 16.4$, $\omega_{p2} = 44.7$ and $\omega_{p3} = 61.1$ rad/s for the P frame, and $\omega_{s1} = 16.4\beta$, $\omega_{s2} = 28.6\beta$ and $\omega_{s3} = 34.6\beta$ rad/s for the S attachment.

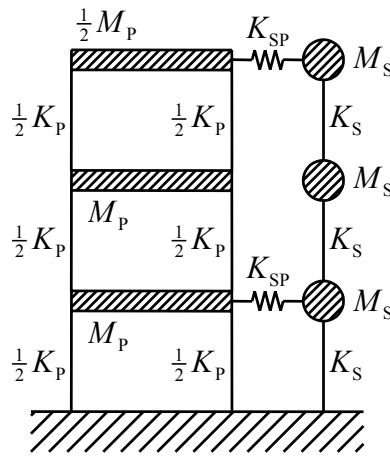


Fig. 7 Combined P frame-S attachment under investigation

When the coupled P-S system is considered, the undamped modal circular frequencies, ω_i , and the corresponding viscous damping ratios, ζ_i (with $i = 1, \dots, 6$), strongly depend on mass ratio and tuning parameter. For comparison, the values of ω_i (in rad/s) and of ζ_i , given by the modal strain energy (Johnson and Kienholz, 1982), are listed in Table 1 for $\alpha = 0.05$ and $\beta = 0.50, 1.00$, and 1.50 . Interestingly, all the computed viscous damping ratios are in the range $0.02 \leq \zeta_i \leq 0.05$, and those take values close to $\zeta_p = 0.05$ or to $\zeta_s = 0.02$ when the corresponding modal shapes resemble those of the P frame or of the S attachment, respectively. On the contrary, intermediate values of the viscous damping ratio indicate coupling between the fixed-base modal shapes of P and S substructures (e.g., ω_1 and ω_2 for $\beta = 1.00$; ω_3 and ω_4 for $\beta = 1.50$).

The reference earthquake response spectrum for the viscous damping ratio $\zeta_{\text{ref}} = 0.05$ (Figure 8, thick line) has been defined by averaging the spectra of eight recorded accelerograms (Figure 8, thin lines) normalized with respect to the peak ground acceleration, PGA . These accelerograms, depicted in Figure 9, are the orthogonal components of the four strong ground motions chronologically listed in Table 2 (PEER Strong Motion Database¹).

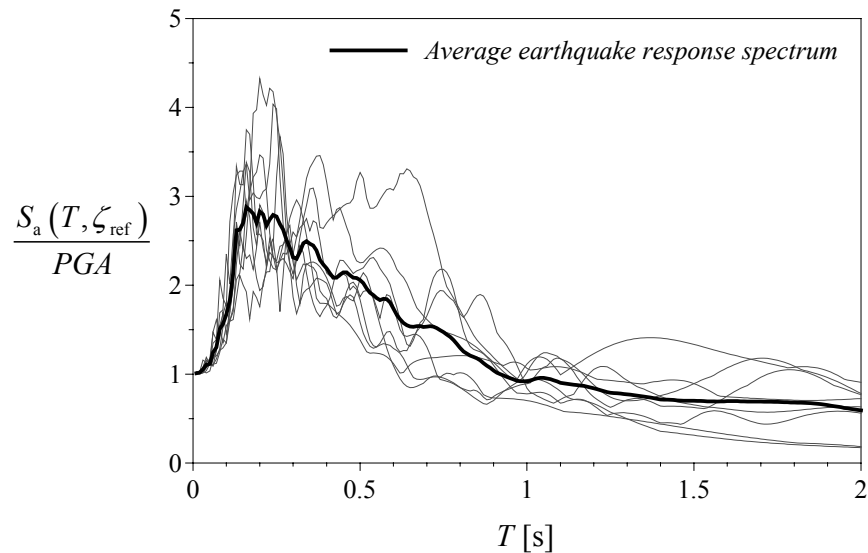


Fig. 8 Normalized response spectra for the recorded accelerograms listed in Table 2 (thin lines) and average earthquake response spectrum (thick line)

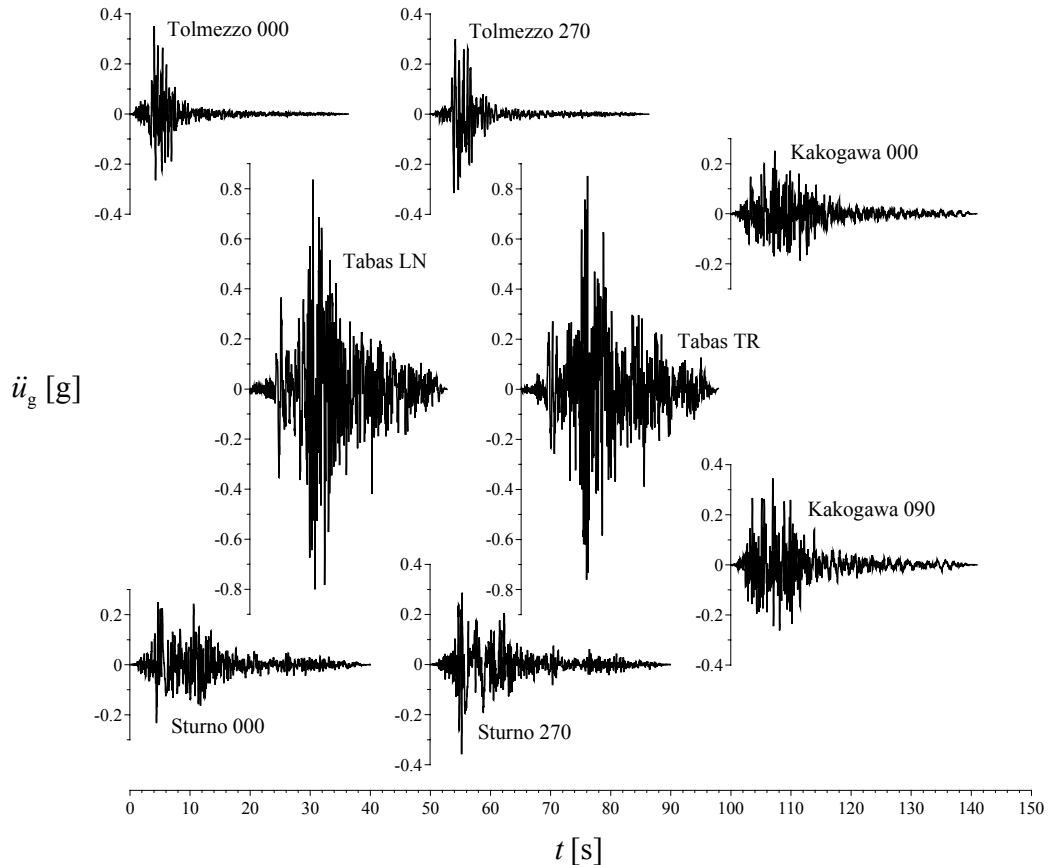


Fig. 9 Recorded accelerograms listed in Table 2

¹ Website of PEER Strong Motion Database, <http://peer.berkeley.edu/smcat/>

Table 1: Undamped Natural Frequencies (in rad/s) and Viscous Damping Ratios of the Combined P-S System Depicted in Figure 7 for Mass Ratio $\alpha = 0.05$ and Tuning Parameter $\beta = 0.50, 1.00$ and 1.50

$\alpha = 0.05, \beta = 0.50$		$\alpha = 0.05, \beta = 1.00$		$\alpha = 0.05, \beta = 1.50$	
$\omega_1 = 8.13$	$\zeta_1 = 0.0205$	$\omega_1 = 14.9$	$\zeta_1 = 0.0359$	$\omega_1 = 16.0$	$\zeta_1 = 0.0480$
$\omega_2 = 14.3$	$\zeta_2 = 0.0208$	$\omega_2 = 18.0$	$\zeta_2 = 0.0338$	$\omega_2 = 25.2$	$\zeta_2 = 0.0216$
$\omega_3 = 16.4$	$\zeta_3 = 0.0449$	$\omega_3 = 28.5$	$\zeta_3 = 0.0205$	$\omega_3 = 41.3$	$\zeta_3 = 0.0300$
$\omega_4 = 17.5$	$\zeta_4 = 0.0239$	$\omega_4 = 34.6$	$\zeta_4 = 0.0201$	$\omega_4 = 46.8$	$\zeta_4 = 0.0393$
$\omega_5 = 44.8$	$\zeta_5 = 0.0499$	$\omega_5 = 45.1$	$\zeta_5 = 0.0492$	$\omega_5 = 52.0$	$\zeta_5 = 0.0208$
$\omega_6 = 61.1$	$\zeta_6 = 0.0500$	$\omega_6 = 61.2$	$\zeta_6 = 0.0498$	$\omega_6 = 61.6$	$\zeta_6 = 0.0491$

Table 2: Information Pertinent to the Strong Motions Selected in This Study

Earthquake, Date	M, MI	Station	Component	PGA (g)	PGV (cm/s)	PGD (cm)
Friuli, Italy, May 6, 1976	6.5, 6.2	Tolmezzo	000	0.351	22.0	4.1
			270	0.315	30.8	5.1
Tabas, Iran, September 16, 1978	7.4, 7.7	Tabas	LN	0.836	97.8	36.92
			TR	0.852	121.4	94.58
Irpinia, Italy, November 23, 1980	-, 6.5	Sturno	000	0.251	37.0	11.77
			270	0.358	52.7	33.08
Kobe, Japan, January 16, 1995	6.9, -	Kakogawa	000	0.251	18.7	5.83
			090	0.345	27.6	9.6

The average drifts in the S attachment, i.e., the mean value of the strains in the secondary springs k_s (as in Figure 7), and the average deformations in the P-S anchors, i.e., the mean value of the strains in the primary-secondary springs k_{sp} (as in Figure 7), have been selected as seismic responses of interest. Two values of the mass ratio, $\alpha = 0.01$ and 0.05 , have been considered. Only the first mode has been retained for the P frame ($m_p = 1$, modal participating mass = 92.3%) in the proposed CQC rule (as in Equation (50)), while two modes have been retained for the S attachment ($m_s = 2$, modal participating mass = 89.5%). Figure 10 shows the percentage error ε as function of the tuning parameter in the range $0.5 \leq \beta \leq 2.0$, assuming that the “exact” values are the respective average maxima given by the eight time-history analyses. The accuracy of the proposed approach (shown by the solid line) proves to be very good from an engineering point of view. More precisely, in the case of “soft” attachments ($0.5 \leq \beta \leq 1.2$) the results are slightly conservative ($0 < \varepsilon < 25\%$), while for the “stiff” attachments ($1.2 \leq \beta \leq 2.0$) the seismic demand is slightly underestimated ($-25 < \varepsilon < 0\%$). A couple of considerations would confirm the effectiveness of the proposed method: (i) the numerical test is extremely severe, since the analyses are carried out not with stochastically generated accelerograms, but with recorded accelerograms, having quite different time-frequency characteristics; and (ii) the level of confidence is similar to that of the original CQC rule for the classically damped structures. On the contrary, a conventional analysis with the earthquake response spectrum based on the cascade approximation (shown by the dashed lines) proves to be absolutely inadequate: the seismic response of soft attachments, in fact, is heavily underestimated, since the percentage error may be as low as -100% ; conversely, the results for the anchors of stiff attachment are excessively conservative, since the percentage error may be larger than 100% . It is worth noting that according to the current Italian seismic code (PCM, 2003), the conventional response of the S attachment is evaluated as the quasi-static response to the seismic motion of the P frame. More precisely, in this (cascade) approximation, the maximum seismic response, $\max |y_s(t)|$, is still given by Equation (36) in which the coefficients $\rho_{ss}(i, k)$ and

$\rho_{SP}(i,k)$ go to zero and in which $\rho_{PP}(i,k)$ is the cross-correlation coefficient proposed by Der Kiureghian (1981).

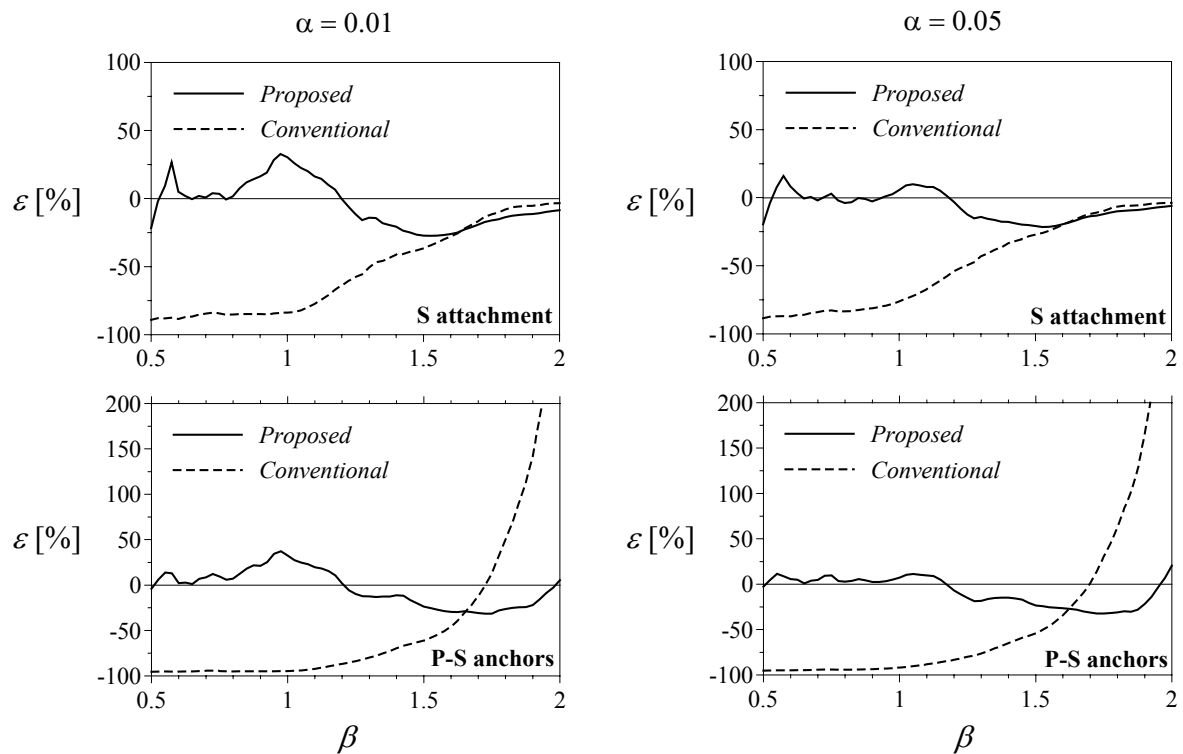


Fig. 10 Comparison between the proposed (solid lines) and conventional (dashed lines) CQC rules for the S attachment (top) and the P-S anchors (bottom); tuning parameter in the range $0.5 \leq \beta \leq 2.0$; mass ratios $\alpha = 0.01$ (left) and 0.05 (right)

CONCLUSIONS

In this paper, a novel Complete Quadratic Combination (CQC) rule for the seismic analysis and design of multi-DOF secondary (S) attachments to multi-DOF primary (P) structural systems has been proposed and numerically validated. In the first stage, in contrast with the classical “cascade” approximation, which neglects the feedback of the S substructure to the P substructure, the accuracy of the “Light Secondary Substructure” (LSS) approximation has been proved. In the second stage, the latter approximation has been used in evaluating the cross-correlation coefficients in the CQC rule. These coefficients are quite different from those available in the literature, since they would directly include, in the combination rule, the effects of frequency tuning among P and S frequencies and different damping ratios in the components. For the purpose of validation, the results of a severe numerical investigation, with eight recorded accelerograms, have been presented and discussed.

Two main features make the proposed method particularly attractive for practical analyses: (i) modal frequencies and modal shapes used in the combination rule are those of the decoupled substructures, assumed to be fixed to their own bases, i.e., the eigenproperties of the combined P-S system are not required; and (ii) the earthquake response spectrum for only a single value of the viscous damping ratio is used, and this reference value can be different from the viscous damping ratios of the components.

Finally, it is worth noting that the cross-correlation coefficients have been derived in this paper under the restrictive assumptions that (i) the ground acceleration is a stationary white noise, and that (ii) the peak factors of the structural response of interest are equal to those of the contributing modal coordinates. More accurate results, therefore, can be obtained by removing these assumptions, even if at the same time the procedure would become cumbersome; these possible improvements will be the subject of future work.

REFERENCES

1. Amini, A. and Trifunac, M.D. (1985). "Statistical Extension of Response Spectrum Superposition", *International Journal of Soil Dynamics and Earthquake Engineering*, Vol. 4, No. 2, pp. 54–63.
2. Biot, M.A. (1932). "Transient Oscillations in Elastic Systems", Ph.D. Thesis No. 259, Aeronautics Department, California Institute of Technology, Pasadena, U.S.A.
3. Biot, M.A. (1933). "Theory of Elastic Systems Vibrating under Transient Impulse with an Application to Earthquake-Proof Buildings", *Proceedings of the National Academy of Sciences of the United States of America*, Vol. 19, No. 2, pp. 262–268.
4. Biot, M.A. (1934). "Theory of Vibration of Buildings during Earthquake", *Zeitschrift für Angewandte Mathematik und Mechanik*, Vol. 14, No. 4, pp. 213–223.
5. Cacciola, P., Colajanni, P. and Muscolino, G. (2004). "Combination of Modal Responses Consistent with Seismic Input Representation", *Journal of Structural Engineering, ASCE*, Vol. 130, No. 1, pp. 47–55.
6. Chen, Y. and Soong, T.T. (1988). "State-of-the-Art Review: Seismic Response of Secondary Systems", *Engineering Structures*, Vol. 10, No. 4, pp. 218–228.
7. Der Kiureghian, A. (1981). "A Response Spectrum Method for Random Vibration Analysis of MDF systems", *Earthquake Engineering & Structural Dynamics*, Vol. 9, No. 5, pp. 419–435.
8. Der Kiureghian, A. and Nakamura, Y. (1993). "CQC Modal Combination Rule for High-Frequency Modes", *Earthquake Engineering & Structural Dynamics*, Vol. 22, No. 11, pp. 943–956.
9. Der Kiureghian, A. and Neuenhofer, A. (1992). "Response Spectrum Method for Multi-Support Seismic Excitations", *Earthquake Engineering & Structural Dynamics*, Vol. 21, No. 8, pp. 713–740.
10. Dey, A. and Gupta, V.K. (1999). "Stochastic Seismic Response of Multiply-Supported Secondary Systems in Flexible-Base Structures", *Earthquake Engineering & Structural Dynamics*, Vol. 28, No. 4, pp. 351–369.
11. Falsone, G. and Muscolino, G. (1999). "Cross-Correlation Coefficients and Modal Combination Rules for Non-classically Damped Systems", *Earthquake Engineering & Structural Dynamics*, Vol. 28, No. 12, pp. 1669–1684.
12. Falsone, G. and Muscolino, G. (2004). "New Real-Value Modal Combination Rules for Non-classically Damped Structures", *Earthquake Engineering & Structural Dynamics*, Vol. 33, No. 12, pp. 1187–1209.
13. Falsone, G., Muscolino, G. and Ricciardi, G. (1991). "Combined Dynamic Response of Primary and Multiply Connected Cascaded Secondary Subsystems", *Earthquake Engineering & Structural Dynamics*, Vol. 20, No. 8, pp. 749–767.
14. Feriani, A. and Perotti, F. (1996). "The Formation of Viscous Damping Matrices for the Dynamic Analysis of MDOF Systems", *Earthquake Engineering & Structural Dynamics*, Vol. 25, No. 7, pp. 689–709.
15. Gupta, A.K. and Jaw, J.W. (1986). "Seismic Response of Nonclassically Damped Systems", *Nuclear Engineering and Design*, Vol. 91, No. 2, pp. 153–159.
16. Gupta, I.D. and Trifunac, M.D. (1988). "Order Statistics of Peaks in Earthquake Response", *Journal of Engineering Mechanics, ASCE*, Vol. 114, No. 10, pp. 1605–1627.
17. Gupta, V.K. and Trifunac, M.D. (1989). "Investigation of Building Response to Translational and Rotational Earthquake Excitations", Report CE 89-02, University of Southern California, Los Angeles, U.S.A.
18. Inaudi, J.A. and Kelly, J.M. (1995). "Linear Hysteretic Damping and the Hilbert Transform", *Journal of Engineering Mechanics, ASCE*, Vol. 121, No. 5, pp. 626–632.
19. Iwan, W.D. (1997). "Drift Spectrum: Measure of Demand for Earthquake Ground Motions", *Journal of Structural Engineering, ASCE*, Vol. 123, No. 4, pp. 397–404.
20. Johnson, C.D. and Kienholz, D.A. (1982). "Finite Element Prediction of Damping in Structures with Constrained Viscoelastic Layers", *AIAA Journal*, Vol. 20, No. 9, pp. 1284–1290.

21. Lavelle, F.M., Bergman, L.A. and Spanos, P.D. (1991). "Seismic Response Spectra of a Combined System by Green's Functions", *Soil Dynamics and Earthquake Engineering*, Vol. 10, No. 2, pp. 93–100.
22. Makris, N. (1997). "Causal Hysteretic Element", *Journal of Engineering Mechanics*, ASCE, Vol. 123, No. 11, pp. 1209–1214.
23. Makris, N. and Zhang, J. (2000). "Time-Domain Viscoelastic Analysis of Earth Structures", *Earthquake Engineering & Structural Dynamics*, Vol. 29, No. 6, pp. 745–768.
24. Muscolino, G. (1990). "Dynamic Response of Multiply Connected Primary-Secondary Systems", *Earthquake Engineering & Structural Dynamics*, Vol. 19, No. 2, pp. 205–216.
25. Muscolino, G., Palmeri, A. and Ricciardelli, F. (2005). "Time-Domain Response of Linear Hysteretic Systems to Deterministic and Random Excitations", *Earthquake Engineering & Structural Dynamics*, Vol. 34, No. 9, pp. 1129–1147.
26. Nashif, A.D., Jones, D.I. and Henderson, J.P. (1985). "Vibration Damping", John Wiley & Sons, New York, U.S.A.
27. Palmeri, A. (2006). "Correlation Coefficients for Structures with Viscoelastic Dampers", *Engineering Structures*, Vol. 28, No. 8, pp. 1197–1208.
28. PCM (2003). "Ordinanza 3274: Primi Elementi in Materia di Criteri Generali per la Classificazione Sismica del Territorio Nazionale e di Normative Tecniche per le Costruzioni in Zona Sismica", Presidenza del Consiglio dei Ministri, Rome, Italy (in Italian).
29. Singh, M.P. (1988). "Seismic Design of Secondary Systems", *Probabilistic Engineering Mechanics*, Vol. 3, No. 3, pp. 151–158.
30. Singh, M.P., Moreschi, L.M., Suárez, L.E. and Matheu, E.E. (2006a). "Seismic Design Forces. I: Rigid Nonstructural Components", *Journal of Structural Engineering*, ASCE, Vol. 132, No. 10, pp. 1524–1532.
31. Singh, M.P., Moreschi, L.M., Suárez, L.E. and Matheu, E.E. (2006b). "Seismic Design Forces. II: Flexible Nonstructural Components", *Journal of Structural Engineering*, ASCE, Vol. 132, No. 10, pp. 1533–1542.
32. Villaverde, R. (2004). "Seismic Analysis and Design of Nonstructural Elements" in "Earthquake Engineering: From Engineering Seismology to Performance-Based Engineering (edited by Y. Bozorgnia and V.V. Bertero)", CRC Press, Boca Raton, U.S.A.
33. Wilson, E.L., Der Kiureghian, A. and Bayo, E.P. (1981). "A Replacement for the SRSS Method in Seismic Analysis", *Earthquake Engineering & Structural Dynamics*, Vol. 9, No. 2, pp. 187–192.

A MODAL COMBINATION RULE FOR PEAK FLOOR ACCELERATIONS IN MULTISTORIED BUILDINGS

Rashmi Kumari and Vinay K. Gupta

Department of Civil Engineering
Indian Institute of Technology Kanpur
Kanpur-208016

ABSTRACT

It is useful to estimate peak floor accelerations consistent with the specified seismic hazard for ensuring the safety of rigid nonstructural components in structural systems. A modal combination rule is formulated here to estimate peak floor accelerations in a multistoried building directly in terms of the dynamic properties of the building and pseudo spectral acceleration ordinates of the base excitation. The formulation is developed under the framework of stationary random vibration theory for a linear, lumped-mass, classically damped, multi-degree-of-freedom system with the help of some approximations. A numerical study shows that the proposed rule performs well with the maximum average absolute error in any combination of building and excitation being less than 20% in case of 5% damping. Two simpler SRSS-type variants of the proposed rule, one considering modal cross-correlation and another ignoring this, are also shown to perform reasonably well, particularly when the building is not flexible to the ground motion.

KEYWORDS: Rigid Nonstructural Components, Peak Floor Accelerations, Modal Combination Rule, Pseudo Spectral Acceleration Spectrum, SRSS Method

INTRODUCTION

Safety of a structural system against seismic hazard is ensured in practice by designing it as per the codal provisions in force at its location. This process usually ensures that the main skeleton of the system that consists of beams, columns, shear walls, floor diaphragms, structural connections, etc. remains intact without collapse during the extreme event expected during the life of the structure. Much of the attention paid in the past 30–40 years to the improvement of aseismic design procedures has been devoted to ensuring better and economical performance of such structural components as those provide stability and strength to the structure to survive during the earthquake ground motion. There are, however, nonstructural components also in a building that are attached to the main skeleton at different locations. Those may include masonry panels, parapets, chimneys, ceilings, water heaters, pressure vessels, generators, piping, storage tanks, escalators, equipments, and lighting fixtures, among various possibilities depending on the functional requirements expected of the building. Scant attention has been paid to the task of ensuring the safety of such components, except in critical installations like nuclear power plants, and as a result, there have been numerous cases of large damage, and thus heavy financial losses, in the last 10–15 years even when the damage to the main skeletons was not significant. In some cases, this has even led to undesirable consequences, like hospitals being closed down during the 1994 Northridge earthquake (Hall, 1994). Damage to nonstructural components also poses threat to the lives of the building occupants in the near vicinity.

Nonstructural components respond primarily to the accelerations of the floors on which those are supported. The peak values of these floor accelerations may often be greater than the peak ground acceleration (PGA), depending on the building characteristics and the location of the floor, and thus, the nonstructural components may be effectively subjected to amplified ground motions. There may be a further amplification if the fundamental periods of these components are close to the natural periods of the structural system, resulting in severe damage to the components and to their attachments to the structural system. It is also important that the nonstructural components are not usually as ductile as the supporting structure and, therefore, those may fail even during small-to-moderate magnitude ground motions. It may not always be sufficient to simply anchor these components to the supporting system and, therefore, one may have to properly design these components and their attachments.

Some efforts have been made in the past 10 years to improve the codal provisions to avoid damage to the nonstructural components (see Singh et al. (2006) for an up-to-date review), but much still remains to be done in this direction. The present codal provisions (see, for example, ASCE (2003)) are still oversimplified and do not adequately account for the role of all the governing parameters. As shown by Taghavi and Miranda (2005) and Singh et al. (2006), these provisions may in fact lead to too conservative estimates. Despite the significant research efforts, like those by Singh et al. (1998, 2006), Villaverde (1997), Soong et al. (1998), the present codal provisions for nonstructural components have yet to strike the right balance between simplicity and rigour. It is nevertheless clear that the future provisions in various codes will continue to depend on the use of pseudo-spectral acceleration (PSA) spectrum for the characterization of the input excitation. It is also clear that the future provisions will depend on the estimation of linear response of nonstructural components and the supporting structure, and that the nonlinear behaviour of these components and/or supporting structure will be accounted for via the use of some kind of response modification factor (Rodriguez et al., 2002).

The nonstructural components may be considered as rigid if those are sufficiently stiff to vibrate in phase with their attachment points. For such components it is desirable to properly estimate the absolute floor accelerations consistent with the specified seismic hazard. Restricting discussion just to the use of response-spectrum based techniques, there is no modal combination rule derived till date to predict the peak floor accelerations in a structural system by directly using the response spectrum ordinates. This is despite the fact that several researchers like Goodman et al. (1955), Rosenblueth and Elorduy (1969), Wilson et al. (1981), Singh and Mehta (1983) have proposed schemes to estimate the largest peak in the response of a base-excited linear system by combining the response maxima in different modes, after Biot (1934, 1942) outlined the basic superposition of modal responses in earthquake engineering. Nevertheless, there have been several efforts to estimate the PSA ordinates corresponding to the floor motions, known popularly as floor response spectrum, and since peak floor accelerations are zero-period ordinates of floor response spectra, those response spectrum-based formulations can be theoretically used to estimate the peak floor accelerations as well. For example, the papers by Singh and co-workers (Singh, 1980; Singh and Sharma, 1985; Suarez and Singh, 1987) and Der Kiureghian and co-workers (Der Kiureghian et al., 1983; Igusa and Der Kiureghian, 1985) give elegant formulations to estimate floor response spectra for classically-damped structural systems and directly in terms of ground spectrum input by making varying sets of assumptions. The simplest of these, e.g., that by Singh (1980), is based on ignoring the interaction between the support and supported systems and may thus be used by lumping the mass of the nonstructural component with the supporting mass and by estimating the zero-period ordinate of the floor response spectrum. The formulations including the interaction, e.g., those by Suarez and Singh (1987) and Der Kiureghian et al. (1983), can be used by lumping the mass of the nonstructural component and by estimating the zero-period ordinate of the floor response spectrum for zero value of the supported mass. It is also possible to use a generalized response spectrum formulation (Singh et al., 2006), but clearly there remains a need to develop a closed-form expression or a modal combination rule that can be used to estimate the peak floor accelerations directly in terms of the PSA ordinates and modal properties of a linear structural system.

This study considers the development of a modal combination rule from the power spectral density function (PSDF) of the floor acceleration response of a linear, lumped-mass, multistoried shear building. For this purpose, both excitation and response processes are assumed to be stationary, and the effects of nonstationarity are included in peak floor acceleration via the use of response spectrum ordinates and nonstationarity factors as in Gupta (2002). The modal combination rule and its two simpler variants on the lines of SRSS (square-root-of-sum-of-squares) rule (Goodman et al., 1955) are obtained by making suitable assumptions regarding nonstationarity factors and peak factors. Performance of the proposed rule and its variants is investigated through consideration of three example buildings and six example ground motions.

FORMULATION OF THE PROPOSED RULE

1. PSDF of the Absolute Acceleration Response

Let us consider a symmetric shear building as shown in Figure 1 where the lumped floor masses m_i , $i = 1, 2, \dots, n$ are interconnected through massless column springs of stiffnesses k_i , $i = 1, 2, \dots, n$, and the

viscous dampers representing the interstory dampings of magnitudes c_i , $i = 1, 2, \dots, n$. The building is subjected to the ground acceleration $\ddot{z}(t)$ at its base. The n -coupled equations of motion for this system can be written as

$$[m]\{\ddot{x}\} + [c]\{\dot{x}\} + [k]\{x\} = -\ddot{z}[m]\{\Gamma\} \quad (1)$$

where $[m]$, $[c]$ and $[k]$ respectively are the $n \times n$ mass, damping and stiffness matrices in terms of m_i , c_i and k_i , $i = 1, 2, \dots, n$; $\{\Gamma\}$ is the $n \times 1$ ground displacement influence vector; $\{x\}$ is the $n \times 1$ vector comprising of the relative displacements $x_i(t)$, $i = 1, 2, \dots, n$ of the floor masses; and $\{\dot{x}\}$ ($= \frac{d}{dt}\{x\}$), $\{\ddot{x}\}$ ($= \frac{d^2}{dt^2}\{x\}$) are the time derivatives of $\{x\}$. It is assumed that the building is classically damped and therefore the viscous damping matrix $[c]$ can be diagonalized by the transformation $[\Phi]^T[c][\Phi]$ where $[\Phi]$ ($= [\{\phi^{(1)}\} \{\phi^{(2)}\} \dots \{\phi^{(n)}\}]$) is the $n \times n$ modal matrix of the eigenvectors $\{\phi^{(j)}\}$, $j = 1, 2, \dots, n$ obtained by solving the eigenvalue problem, $\omega^2[m]\{\phi\} = [k]\{\phi\}$. The j th element of this diagonal form is denoted as $2\zeta_j\omega_j M_j$ where ω_j and ζ_j respectively are the natural frequency and damping ratio in the j th mode and $M_j = \{\phi^{(j)}\}^T [m] \{\phi^{(j)}\}$ is the j th modal mass.

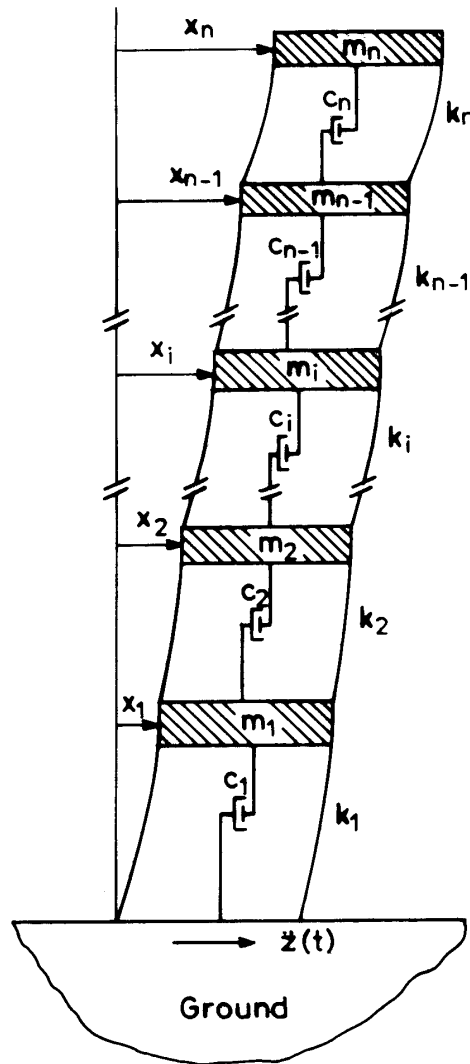


Fig. 1 Shear building model of n -storied building

On using normal mode decomposition of the relative displacement of the i th floor, the transfer function relating the absolute acceleration response of the i th floor to the input ground acceleration may be expressed as

$$H_{a_i}(\omega) = 1 - \omega^2 \sum_{j=1}^n \phi_i^{(j)} \alpha_j H_j(\omega) \quad (2)$$

where $\phi_i^{(j)}$ is the i th element of the j th mode shape vector, $\alpha_j = \{\phi^{(j)}\}^T [m] \{\Gamma\} / M_j$ is the modal participation factor in the j th mode, and

$$H_j(\omega) = \frac{-1}{\omega_j^2 - \omega^2 + 2i\zeta_j \omega \omega_j} \quad (3)$$

(with $i = \sqrt{-1}$) is the transfer function relating the relative displacement of the equivalent SDOF oscillator in the j th mode to the input base excitation. On assuming stationarity in the excitation and the response, the PSDF of a response may be obtained by multiplying the PSDF of the excitation with the squared modulus of the corresponding transfer function. The PSDF of the absolute acceleration response of the i th floor may thus be expressed as

$$S_{a_i}(\omega) = S_z(\omega) \left[1 + \sum_{j=1}^n \left\{ 2\phi_i^{(j)} \alpha_j \operatorname{Re}(\bar{H}_j(\omega)) + (\phi_i^{(j)})^2 \alpha_j^2 |\bar{H}_j(\omega)|^2 + \sum_{k=1, k \neq j}^n \phi_i^{(j)} \phi_i^{(k)} \alpha_j \alpha_k \operatorname{Re}(\bar{H}_j(\omega) \bar{H}_k^*(\omega)) \right\} \right] \quad (4)$$

where $S_z(\omega)$ is the PSDF of the input base excitation $\ddot{z}(t)$, $\bar{H}_j(\omega) (= -\omega^2 H_j(\omega))$ is the transfer function relating the relative acceleration of the equivalent SDOF oscillator in the j th mode to the input base excitation, and $\bar{H}_k^*(\omega)$ is the complex conjugate of $\bar{H}_k(\omega)$. On the right hand side of Equation (4), the second term represents the cross-correlation of the ground acceleration with the relative acceleration response of the i th floor, and the third and fourth terms together represent the PSDF of the relative acceleration response of the i th floor. In the latter, the term involving the summation over k represents the cross-correlation of the j th mode with the remaining $n-1$ modes. On expanding this term by using the partials for $\operatorname{Re}(\bar{H}_j(\omega) \bar{H}_k^*(\omega))$ (Vanmarcke, 1972) and on rearranging terms, Equation (4) becomes

$$S_{a_i}(\omega) = S_z(\omega) \left[1 + \sum_{j=1}^n \left\{ \left(2 + \sum_{k=1, k \neq j}^n \phi_i^{(k)} \alpha_k D_{jk} \right) \phi_i^{(j)} \alpha_j \omega_j^2 |\omega H_j(\omega)|^2 + \left(\phi_i^{(j)} \alpha_j - 2 + \sum_{k=1, k \neq j}^n \phi_i^{(k)} \alpha_k (C_{jk} - D_{jk}) \right) \phi_i^{(j)} \alpha_j |\bar{H}_j(\omega)|^2 \right\} \right] \quad (5)$$

where C_{jk} and D_{jk} are the coefficients given in terms of ζ_j , ζ_k and $\varrho = \omega_k / \omega_j$ as

$$C_{jk} = \frac{1}{B_{jk}} \left[8\varrho \zeta_j (\zeta_k + \zeta_j \varrho) \left\{ (1 - \varrho^2)^2 - 4\varrho (\zeta_j - \zeta_k \varrho) (\zeta_k - \zeta_j \varrho) \right\} \right] \quad (6)$$

$$D_{jk} = \frac{1}{B_{jk}} \left[2(1 - \varrho^2) \left\{ 4\varrho (\zeta_j - \zeta_k \varrho) (\zeta_k - \zeta_j \varrho) - (1 - \varrho^2)^2 \right\} \right] \quad (7)$$

with

$$B_{jk} = 8\varrho^2 \left[(\zeta_j^2 + \zeta_k^2) (1 - \varrho^2)^2 - 2(\zeta_k^2 - \zeta_j^2 \varrho^2) (\zeta_j^2 - \zeta_k^2 \varrho^2) \right] + (1 - \varrho^2)^4 \quad (8)$$

2. Largest Peak of the Absolute Acceleration Response

Ordered peaks (largest, second largest, third largest, ...) of a response process are estimated in stationary random vibration theory by (i) computing moments of the PSDF of the process, (ii) computing

root-mean-square (r.m.s.) value of the process and peak factors for the ordered peaks from the moments, and (iii) by multiplying the r.m.s. value with the peak factors (Gupta and Trifunac, 1988; Gupta, 2002). This procedure is followed in this section to formulate the expression for the largest peak of the absolute acceleration response at the i th floor.

Taking p th moment of $S_{a_i}(\omega)$ about the origin leads to

$$\lambda_p^{a_i} = \lambda_p^G + \sum_{j=1}^n \left[\left\{ 2 + \sum_{k=1, k \neq j}^n \phi_i^{(k)} \alpha_k D_{jk} \right\} \phi_i^{(j)} \alpha_j \omega_j^2 \lambda_{p,j}^V + \left\{ \phi_i^{(j)} \alpha_j - 2 + \sum_{k=1, k \neq j}^n \phi_i^{(k)} \alpha_k (C_{jk} - D_{jk}) \right\} \phi_i^{(j)} \alpha_j \lambda_{p,j}^A \right]; \quad p = 0, 1, 2, \dots \quad (9)$$

In this equation,

$$\lambda_p^G = \int_0^\infty \omega^p S_z(\omega) d\omega \quad (10)$$

is the p th moment of the PSDF of the ground acceleration process, $\ddot{z}(t)$;

$$\lambda_{p,j}^V = \int_0^\infty \omega^p S_z(\omega) \left| \omega H_j(\omega) \right|^2 d\omega \quad (11)$$

is the p th moment of the PSDF of the relative velocity response of a SDOF oscillator with ω_j frequency and ζ_j damping ratio and subjected to the base acceleration $\ddot{z}(t)$; and

$$\lambda_{p,j}^A = \int_0^\infty \omega^p S_z(\omega) \left| \bar{H}_j(\omega) \right|^2 d\omega \quad (12)$$

is the p th moment of the PSDF of the relative acceleration response of this oscillator.

By calculating the moments from Equation (9) for $p = 0, 2$ and 4 and then multiplying the r.m.s. value ($= \sqrt{\lambda_0^{a_i}}$) with a suitable peak factor, the largest peak amplitude of the desired absolute acceleration response can be determined at a given level of confidence. The peak factor depends on $\lambda_0^{a_i}$, $\lambda_2^{a_i}$, $\lambda_4^{a_i}$, strong motion duration of the excitation, and the level of confidence at which the response amplitude is to be obtained (see Gupta (2002) for details). The largest peak amplitude so obtained has to be multiplied with a suitable nonstationarity factor in order to account for the fact that the response process is not a stationary process. Such a factor may be close to unity if $S_z(\omega)$ is a spectrum-compatible PSDF (see, for example, Kaul (1978), Unruh and Kana (1981), Christian (1989)). Thus, the largest peak amplitude of the absolute acceleration of the i th floor becomes

$$a_{i,\max} = \eta^{a_i} \beta^{a_i} \left[\lambda_0^G + \sum_{j=1}^n \left\{ \left(2 + \sum_{k=1, k \neq j}^n \phi_i^{(k)} \alpha_k D_{jk} \right) \phi_i^{(j)} \alpha_j \omega_j^2 \lambda_{0,j}^V + \left(\phi_i^{(j)} \alpha_j - 2 + \sum_{k=1, k \neq j}^n \phi_i^{(k)} \alpha_k (C_{jk} - D_{jk}) \right) \phi_i^{(j)} \alpha_j \lambda_{0,j}^A \right\} \right]^{\frac{1}{2}} \quad (13)$$

where η^{a_i} is the corresponding peak factor and β^{a_i} is the nonstationarity factor, for this response process.

In continuation with the above logic, λ_0^G in Equation (13) may be expressed as $(PGA/\eta^G \beta^G)^2$, where PGA is the largest peak amplitude of the ground acceleration process $\ddot{z}(t)$ for the same level of confidence to which η^{a_i} corresponds, η^G is the corresponding peak factor, and β^G is the nonstationarity factor for the acceleration process. In the same way, $\lambda_{0,j}^V$ may be expressed as $(SV_j/\eta_j^V \beta_j^V)^2$, where SV_j is the largest peak amplitude of the relative velocity response of the SDOF oscillator with ω_j frequency

and ζ_j damping ratio in response to the excitation process $\ddot{z}(t)$, η_j^V is the corresponding peak factor, and β_j^V is the nonstationarity factor associated with the relative velocity response process. Further, $\lambda_{0,j}^A$ may be expressed as $(RSA_j/\eta_j^A\beta_j^A)^2$, where RSA_j is the largest peak amplitude of the relative acceleration response of the SDOF oscillator (with ω_j frequency and ζ_j damping ratio) in response to the excitation process $\ddot{z}(t)$, η_j^A is the corresponding peak factor, and β_j^A is the nonstationarity factor associated with the relative acceleration response process. Thus, $a_{i,\max}$ may be expressed as

$$a_{i,\max} = \left[\left(\frac{\eta^{a_i}}{\eta^G} \right)^2 \left(\frac{\beta^{a_i}}{\beta^G} \right)^2 PGA^2 + \sum_{j=1}^n \left\{ \left(2 + \sum_{k=1, k \neq j}^n \phi_i^{(k)} \alpha_k D_{jk} \right) \phi_i^{(j)} \alpha_j \omega_j^2 \left(\frac{\eta^{a_i}}{\eta_j^V} \right)^2 \left(\frac{\beta^{a_i}}{\beta_j^V} \right)^2 SV_j^2 \right. \right. \\ \left. \left. + \left(\phi_i^{(j)} \alpha_j - 2 + \sum_{k=1, k \neq j}^n \phi_i^{(k)} \alpha_k (C_{jk} - D_{jk}) \right) \phi_i^{(j)} \alpha_j \left(\frac{\eta^{a_i}}{\eta_j^A} \right)^2 \left(\frac{\beta^{a_i}}{\beta_j^A} \right)^2 RSA_j^2 \right\} \right]^{\frac{1}{2}} \quad (14)$$

In the next section, suitable approximations will be made to develop a modal combination rule from this equation.

3. Approximations for the Proposed Rule

One can use Equation (14) to estimate the largest peak amplitude of the absolute acceleration at the i th floor for the same level of confidence for which PGA , SV_j and RSA_j have been estimated. Hence, if the seismic design levels at a site are characterized by certain PGA , and spectral velocity (SV) and relative spectral acceleration (RSA) curves, this equation can be used to estimate the largest floor acceleration at the i th floor consistent with these design levels. For this, however, one needs to have reasonable estimates of η ratios (i.e., η^{a_i}/η^G , η^{a_i}/η_j^V and η^{a_i}/η_j^A) and β ratios (i.e., β^{a_i}/β^G , β^{a_i}/β_j^V and β^{a_i}/β_j^A). Further, it is unusual to have the SV and RSA curves available in a design situation. Suitable approximations, therefore, need to be made in order to obtain a useful expression for the peak floor accelerations from Equation (14).

It is proposed to first assume that various η and β ratios are unity. It will be shown in the next section through numerical examples that these ratios are usually not unity. While the η ratios are not very far from unity, the β ratios show considerable scatter around their mean values, depending on the characteristics of the structural system and excitation. However, since the mean beta ratios for the first few modes stay close to unity, this assumption is deemed to be appropriate.

Secondly, pseudo-spectral velocity (PSV) curves may be used in place of the SV curves as per the existing engineering practice. The RSA values may also be estimated approximately from the knowledge of PGA , pseudo-spectral acceleration (PSA), and energy distribution in the ground motion. As shown by Trifunac and Gupta (1991), this approximation of RSA, known as PRSA (pseudo-relative spectral acceleration), may be expressed as

$$PRSA(T) = \sqrt{\{PSA(T)\}^2 - PGA^2}; \quad T \leq T_c \\ PRSA(T) = \sqrt{\{PSA(T)\}^2 + PGA^2}; \quad T > T_c \quad (15)$$

where $PRSA(T)$ and $PSA(T)$, respectively, are the PRSA and PSA values for the SDOF oscillator of period T , and T_c is the period corresponding to the centre of gravity of the Fourier spectrum $|\ddot{Z}(\omega)|$ of ground motion. T_c will be referred to in this study as the mean period of ground motion.

Incorporating the above approximations, Equation (14) leads to the proposed modal combination rule as

$$a_{i,\max} = \left[PGA^2 + \sum_{j=1}^n \left\{ \left(2 + \sum_{k=1, k \neq j}^n \phi_i^{(k)} \alpha_k D_{jk} \right) \phi_i^{(j)} \alpha_j PSA_j^2 + \left(\phi_i^{(j)} \alpha_j - 2 + \sum_{k=1, k \neq j}^n \phi_i^{(k)} \alpha_k (C_{jk} - D_{jk}) \right) \phi_i^{(j)} \alpha_j PRSA_j^2 \right\} \right]^{\frac{1}{2}} \quad (16)$$

Since the PSDF of the relative acceleration response at the i th floor cannot be negative, it is necessary to apply the following check in the above rule:

$$\sum_{j=1}^n \left[\sum_{k=1, k \neq j}^n \phi_i^{(j)} \phi_i^{(k)} \alpha_j \alpha_k D_{jk} PSA_j^2 + \left(\phi_i^{(j)} \alpha_j + \sum_{k=1, k \neq j}^n \phi_i^{(k)} \alpha_k (C_{jk} - D_{jk}) \right) \phi_i^{(j)} \alpha_j PRSA_j^2 \right] \geq 0 \quad (17)$$

If this check fails (due to the various approximations that have been made), the summation of terms on the left-hand side of (17) should be taken as zero. In view of this, the proposed rule may be expressed as

$$a_{i,\max} = \left[PGA^2 + \sum_{j=1}^n 2\phi_i^{(j)} \alpha_j \{ PSA_j^2 - PRSA_j^2 \} + ra_{i,\max}^2 \right]^{\frac{1}{2}} \quad (18)$$

or, depending on how the mean period of ground motion compares with the natural periods of the system, $T_j (= 2\pi/\omega_j)$, $j = 1, 2, \dots, n$,

$$\begin{aligned} a_{i,\max} &= \left[PGA^2 \left(1 + \sum_{j=1}^n 2\phi_i^{(j)} \alpha_j \right) + ra_{i,\max}^2 \right]^{\frac{1}{2}} ; T_1 < T_c \\ &= \left[PGA^2 \left(1 - \sum_{j=1}^n 2\phi_i^{(j)} \alpha_j \right) + ra_{i,\max}^2 \right]^{\frac{1}{2}} ; T_n > T_c \\ &= \left[PGA^2 \left(1 - \sum_{j=1}^{\hat{n}} 2\phi_i^{(j)} \alpha_j + \sum_{j=\hat{n}+1}^n 2\phi_i^{(j)} \alpha_j \right) + ra_{i,\max}^2 \right]^{\frac{1}{2}} ; T_{\hat{n}+1} < T_c < T_{\hat{n}} \end{aligned} \quad (19)$$

where

$$ra_{i,\max}^2 = \sum_{j=1}^n \left[\sum_{k=1, k \neq j}^n \phi_i^{(j)} \phi_i^{(k)} \alpha_j \alpha_k D_{jk} PSA_j^2 + \left(\phi_i^{(j)} \alpha_j + \sum_{k=1, k \neq j}^n \phi_i^{(k)} \alpha_k (C_{jk} - D_{jk}) \right) \phi_i^{(j)} \alpha_j PRSA_j^2 \right] \quad (20)$$

or 0, whichever is greater

A simpler variant of the proposed rule may be obtained by ignoring the cross-correlation between the ground acceleration and the relative floor acceleration. In that case, we obtain

$$a_{i,\max} = \left[PGA^2 + ra_{i,\max}^2 \right]^{\frac{1}{2}} \quad (21)$$

with restriction as in Equation (20) remaining applicable. Further, on ignoring the cross-correlation of the j th mode with the remaining $n-1$ modes (in the relative acceleration response), a further simpler variant of the proposed rule is obtained as

$$a_{i,\max} = \left[PGA^2 + \sum_{j=1}^n \left(\phi_i^{(j)} \right)^2 \alpha_j^2 PRSA_j^2 \right]^{\frac{1}{2}} \quad (22)$$

Since this form of the modal combination rule does not consider any cross-correlation, it will be referred to in this study as the SRSS rule for the peak floor acceleration response. Further, since Equation (21) ignores only the cross-correlation between the ground and relative floor accelerations, it will be referred to as the quasi-SRSS rule for the peak floor acceleration response.

It may be noted that both variants of the proposed rule lead to peak floor accelerations greater than or equal to PGA. Peak floor accelerations may however be less than PGA, when $\sum_{j=1}^{\hat{n}} \phi_i^{(j)} \alpha_j >$

$\sum_{j=\hat{n}+1}^n \phi_i^{(j)} \alpha_j$ and the peak relative acceleration $ra_{i,\max}$ is not large enough in comparison with PGA.

Such a situation may arise when the structural system is flexible with respect to the ground motion. If the system is only moderately flexible and just a few of its significant modes have periods greater than the mean period of the ground motion, lower floors may experience “less than PGA” peak accelerations. This may however be true for upper floors also when the system is very flexible and the periods of several significant modes exceed the mean period. It is shown in the next section that both variants usually lead to conservative to overconservative estimates of peak floor accelerations and are more suitable for use when the structural system is not flexible with respect to the ground motion.

NUMERICAL ILLUSTRATION OF THE PROPOSED RULE

1. Example Buildings and Excitations

In order to illustrate the proposed rule, six earthquake ground motions with the details as in Table 1 are considered. Five of these motions (Nos. 1–3 and 5–6) are recorded motions while one motion (No. 4) has been synthetically generated for a Mexico City site during the 1985 Michoacan earthquake (see Gupta and Trifunac (1990) for details). The Fourier spectra of these motions (as normalized to the unit maximum value) are shown in Figures 2(a)–2(f) (solid lines without dots). Also shown are the 5%-damping PSA spectra after normalization with respect to their respective maxima (solid lines with dots). It may be observed that all six motions cover a wide range of energy distributions. The dominant period in these motions varies from about 0.48 s in the Parkfield motion (see Figure 2(e)) to about 5.5 s in the Borrego Mountain and San Fernando motions (see Figures 2(a) and 2(f)). The Michoacan motion (see Figure 2(d)) is also a long-period motion with the dominant period of about 2.6 s. The Imperial Valley motion (see Figure 2(b)) and the Kern County motion (see Figure 2(c)) are medium-period motions with dominant periods as 0.85 and 0.65 s, respectively. In terms of the band of significant energy, the Michoacan motion is on one extreme with significant energy over a narrow band of 1.8–3 s. The Kern County motion is on another extreme with significant energy over a large band of 0.2–5 s. In the San Fernando motion also, the energy is concentrated in a narrow band of periods, while in the Imperial Valley motion, the band of energy is fairly wide. The remaining two motions (Borrego Mountain and Parkfield) fall in between with the band of energy not being narrow or wide.

Table 1: Details of the Example Ground Motions

Record No.	Earthquake	Site	Component
1	Borrego Mountain Earthquake, 1968	Engineering Building, Santa Ana, Orange County, California	S04E
2	Imperial Valley Earthquake, 1940	El Centro Site, Imperial Valley Irrigation District, California	S00E
3	Kern County Earthquake, 1952	Taft Lincoln School Tunnel, California	N21E
4	Michoacan Earthquake, 1985	Mexico City	Synthetic
5	Parkfield Earthquake, 1966	Array No. 5, Cholame, Shandon, California	N05W
6	San Fernando Earthquake, 1971	Utilities Building, 215 West Broadway, Long Beach, California	N90E

Three example buildings are considered such that the range of fundamental periods typically found in multistoried buildings is covered to a large extent. The first example building, henceforth denoted as Building-1 (or BD1), is a 24-story symmetric building with 2 s as its fundamental period. This building is same as that considered by Singh et al. (2003). The second example building (Building-2 or BD2) is a 15-story symmetric building with 1.2 s as its fundamental period. This building is similar to that considered by Ray Chaudhuri and Gupta (2003). Building-3 (or BD3) is the third example (symmetric) building with 5 stories and 0.514 s fundamental period. This example building is similar to that considered by Hu et al. (2007). The values of floor masses and story stiffnesses for the three example buildings are given in Table 2, and natural frequencies in various modes of vibration are given in Table 3. The fundamental

periods of the example buildings are also indicated in Figures 2(a)–2(f) (dashed lines) in order to clearly show the relative stiffnesses of the example buildings with respect to the example ground motions. On assuming that the effects of soil-structure interaction are negligibly small, it may be observed that BD1 is very stiff to the San Fernando motion, stiff to the Michoacan and Borrego Mountain motions, flexible to the Imperial Valley and Kern County motions, and very flexible to the Parkfield motion. On the other hand, BD3 is very stiff to the Borrego Mountain, Michoacan and San Fernando motions, little stiff to Imperial Valley and Kern County motions, and is in near resonance with the Parkfield motion. The example buildings are assumed to be classically damped with damping ratio of 0.05 in all modes.

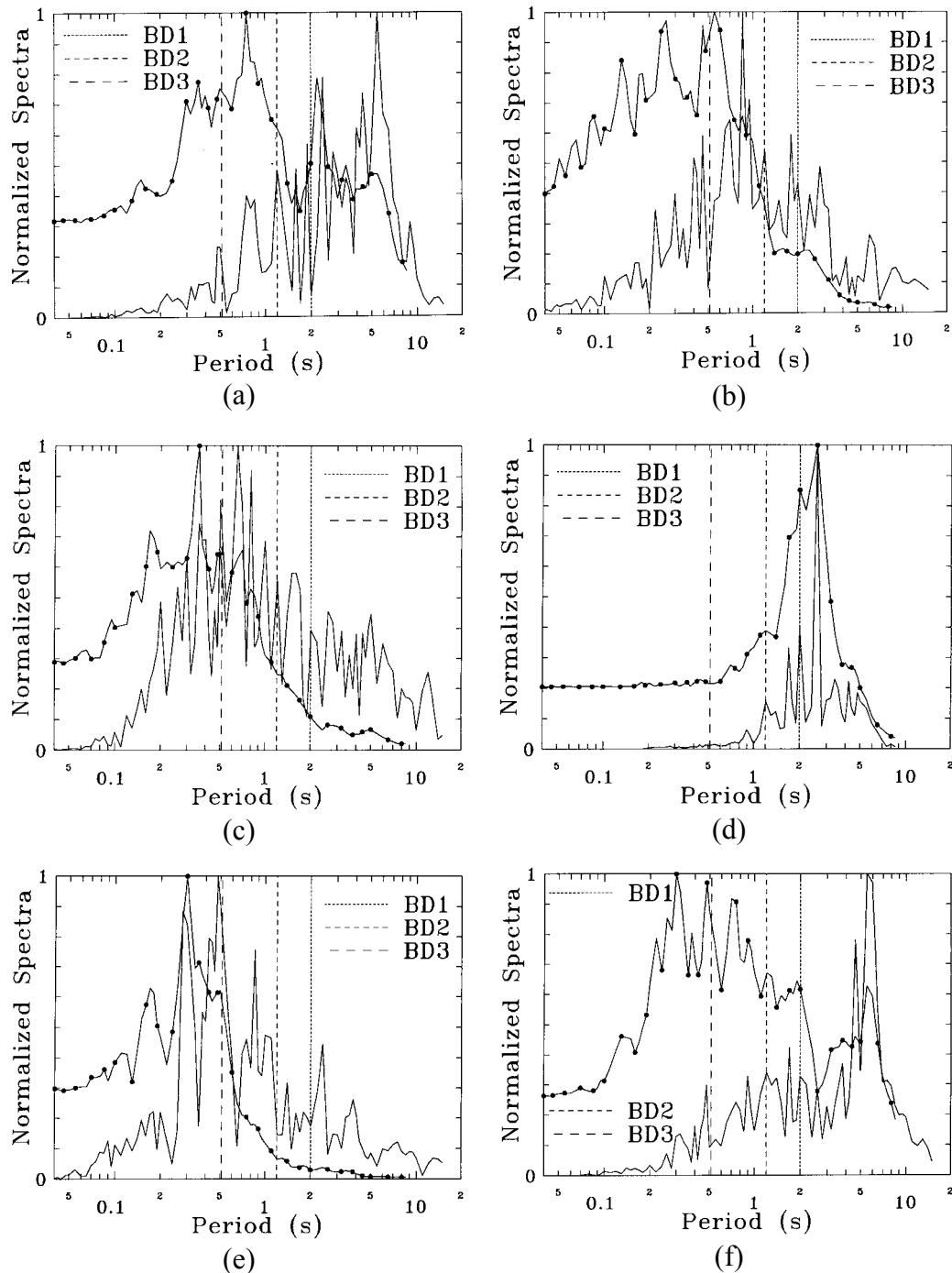


Fig. 2 Normalized Fourier amplitude spectrum (solid line without dots) and PSA spectrum (solid line with dots) for (a) Borrego Mountain, (b) Imperial Valley, (c) Kern County, (d) Michoacan, (e) Parkfield, and (f) San Fernando earthquake motions (dashed lines indicate the fundamental periods for BD1, BD2 and BD3)

Table 2: Mass and Stiffness Properties of the Example Buildings

i	Floor Mass m_i (t)			Story Stiffness k_i (kN/mm)		
	BD1	BD2	BD3	BD1	BD2	BD3
1	7,426	280	166	6650	525	290
2	7,426	200	166	6260	536	290
3	6,918	200	166	5880	536	290
4	6,970	200	166	5880	536	290
5	5,849	200	141	5510	536	290
6	5,587	200		5480	536	
7	5,569	200		5480	536	
8	4,063	200		5100	536	
9	3,678	200		5010	536	
10	3,678	200		5010	536	
11	3,678	200		4960	536	
12	3,415	200		4920	536	
13	3,415	200		4920	536	
14	2,855	200		4720	536	
15	2,469	200		4670	536	
16	2,469			4670		
17	2,329			4610		
18	1,769			4220		
19	1,769			4220		
20	1,524			4260		
21	1,278			4240		
22	1,261			4260		
23	928			4250		
24	771			4420		

Table 3: Natural Frequencies of the Example Buildings

Mode No.	Frequencies (Hz)		
	BD1	BD2	BD3
1	0.50	0.83	1.94
2	1.24	2.49	5.65
3	2.00	4.10	8.86
4	2.78	5.64	11.29
5	3.51	7.11	12.78
6	4.30	8.50	
7	4.97	9.83	

8	5.70	11.09
9	6.34	12.26
10	6.98	13.32
11	7.58	14.25
12	8.09	15.03
13	8.61	15.65
14	8.96	16.11
15	9.37	16.38
16	9.80	
17	10.51	
18	11.10	
19	11.59	
20	12.39	
21	13.24	
22	14.49	
23	16.42	
24	19.33	

2. Results and Discussion: η and β Ratios

The proposed rule is based on assuming η and β ratios uniformly as unity. It will, therefore, be first seen via a numerical study how good this assumption is. For this purpose, it is assumed that the response spectra associated with the example ground motions represent expected levels of the largest peak responses to the ground motion processes to which these example motions correspond. The peak floor acceleration responses of the example buildings, as computed from the time-history analyses for the example motions, also thus correspond to the expected levels of the responses to these processes. The PSDF of the base excitation process, $S_z(\omega)$, is obtained in case of each example motion by dividing the squared Fourier spectrum of the record by πT_s where T_s is the strong motion duration of the record given by Trifunac and Brady (1975). The values of T_s are obtained as 54.74, 24.44, 30.54, 47.28, 7.52, 44.34 s respectively for the Borrego Mountain, Imperial Valley, Kern County, Michoacan, Parkfield and San Fernando motions. Further, for the calculation of PRSA curves, the mean period T_c is obtained as 0.38, 0.17, 0.25, 0.96, 0.19, 0.39 s respectively for these motions.

The calculations of η^{a_i} and β^{a_i} are based on the expression of PSDF $S_{a_i}(\omega)$, as given in Equation (5), and on the maximum values of the absolute acceleration $a_i(t)$, as obtained via time-history analyses. The calculations of η^G and β^G are based on the $S_z(\omega)$ and PGA values. Further, η_j^V and β_j^V are computed from the use of PSDF, $|\omega H_j(\omega)|^2 S_z(\omega)$, and SV curve, and η_j^A and β_j^A from the use of PSDF, $|\bar{H}_j(\omega)|^2 S_z(\omega)$, and RSA curve.

The results for the η and β ratios are shown in Figures 3(a)–3(c) and 4(a)–4(d), respectively. Figures 3(a) and 4(a) show the results for η^{a_i}/η^G and β^{a_i}/β^G , respectively, in the case of the three example buildings (Building Nos. 1–3 referring to BD1, BD2 and BD3, respectively). Each of these figures shows the scatter of $6n$ values (for six ground motions and n floors) of the η or β ratio for each example building. The solid lines depict the respective average values while the dashed line shows the

value assumed for developing the proposed rule. Figures 3(b) and 3(c) show the plots for η^{a_i}/η_j^V and η^{a_i}/η_j^A , respectively, in the case of BD1. Figures 4(b) and 4(c) show the plots for β^{a_i}/η_j^V in the case of BD1 and BD2, respectively. Further, Figure 4(d) shows the plot for β^{a_i}/η_j^A in the case of BD1. Each of these figures (i.e., 3(b)–3(c) and 4(b)–4(d)) shows the scatter of $6n$ values (of η or β ratio) for each of the n modes. The solid curve depicts the variation of average ratio with the mode number, while the dashed line shows the assumed value.

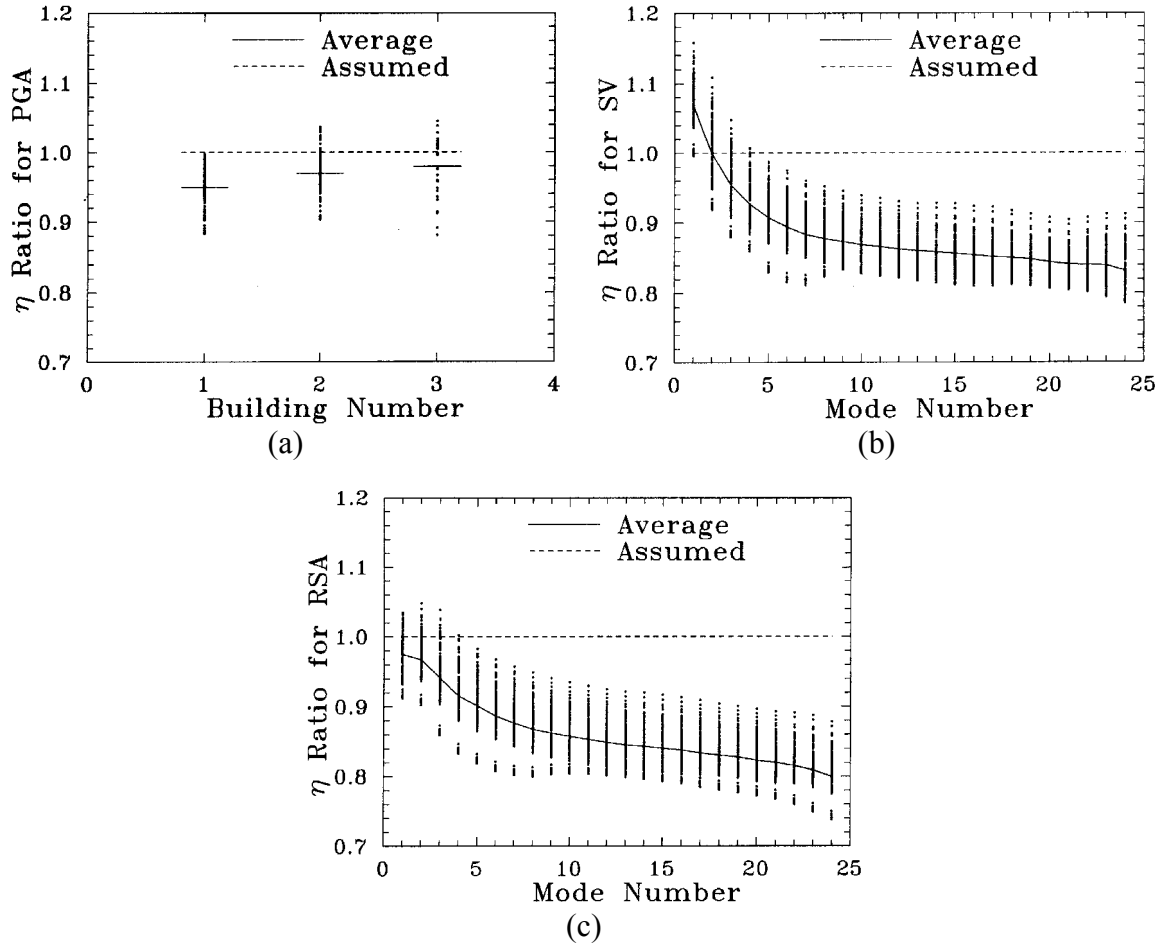


Fig. 3 (a) η^{a_i}/η_j^G ratio values for Building-1 (BD1), Building-2 (BD2) and Building-3 (BD3); (b) η^{a_i}/η_j^V ratio values for BD1; (c) η^{a_i}/η_j^A ratio values for BD1

It may be observed from Figures 3(a)–3(c) (and more such figures in Kumari (2007)) that all cases are associated with small scatters (within a range of about 0.15) in η ratios. Further, the average η ratio appears to depend on the mode number (in the cases of η^{a_i}/η_j^V and η^{a_i}/η_j^A), decreasing approximately in an exponential manner with an increase in the mode number; in the case of BD1 (see Figure 3(b)), it decreases from 1.07 to 0.83. This is expected as higher modes are associated with greater number of peaks and thus with higher peak factors (Gupta (1994)). In the case of η^{a_i}/η_j^V (see Figure 3(b)), it appears reasonable to assume the ratio as unity because the first mode that contributes maximum to the total response is associated with a ratio greater than or equal to unity. In the case of η ratios for PGA and RSA spectra, a value slightly less than unity could be assumed. However, for simplicity in the proposed rule, it has been preferred to continue with the value of unity.

In comparison with the η ratios, the β ratios are associated with much larger scatters as shown by Figures 4(a)–4(d). The range of scatter can be as large as 1.8 (see the 1st mode in Figure 4(c), and 20th mode in Figure 4(d)) and the use of mean value in such a case may not be justified. The observed large

scatter is due to the results for different ground motions taken together, as the characteristics of ground motions seem to affect the β ratios significantly. To illustrate, if the results for each ground motion are considered separately in the case of the β^{a_i}/β_j^V ratio for BD1, the coefficient of variation (COV) in any mode can vary from 0.034 in the Michoacan motion to 0.125 in the Parkfield motion. This is much less than the minimum COV value of 0.236 (the maximum value is 0.516), obtained for all six ground motions taken together (as in Figure 4(b)). It is, therefore, clear that each of the β ratios should be correlated with the ground motion characteristics. Further, if we ignore scatter in the β ratios and look at their average values, it is observed that these ratios can be as large as 1.02 and as small as 0.79 in the case of PGA, as large as 1.18 and as small as 0.57 in the case of SV, and as large as 1.00 and as small as 0.48 in the case of RSA. Therefore, the β ratios should also be correlated with (i) the fundamental period of the building, and (ii) the mode number in the case of the β^{a_i}/β_j^V and β^{a_i}/β_j^A ratios (these ratios appear to decrease with increase in the mode number, though in an irregular fashion). However, considering that the average β^{a_i}/β^G ratio is close to unity and that β^{a_i}/β_j^V and β^{a_i}/β_j^A ratios are close to unity for the fundamental mode in each case, it has been decided to assume all β ratios to be uniformly equal to unity. These ratios could perhaps be assumed as 0.9 in the cases of β^{a_i}/β^G and η^{a_i}/η_j^A . However, this value is not very different from 1.0, and therefore, a uniform value of 1.0 has been assumed for the sake of simplicity.

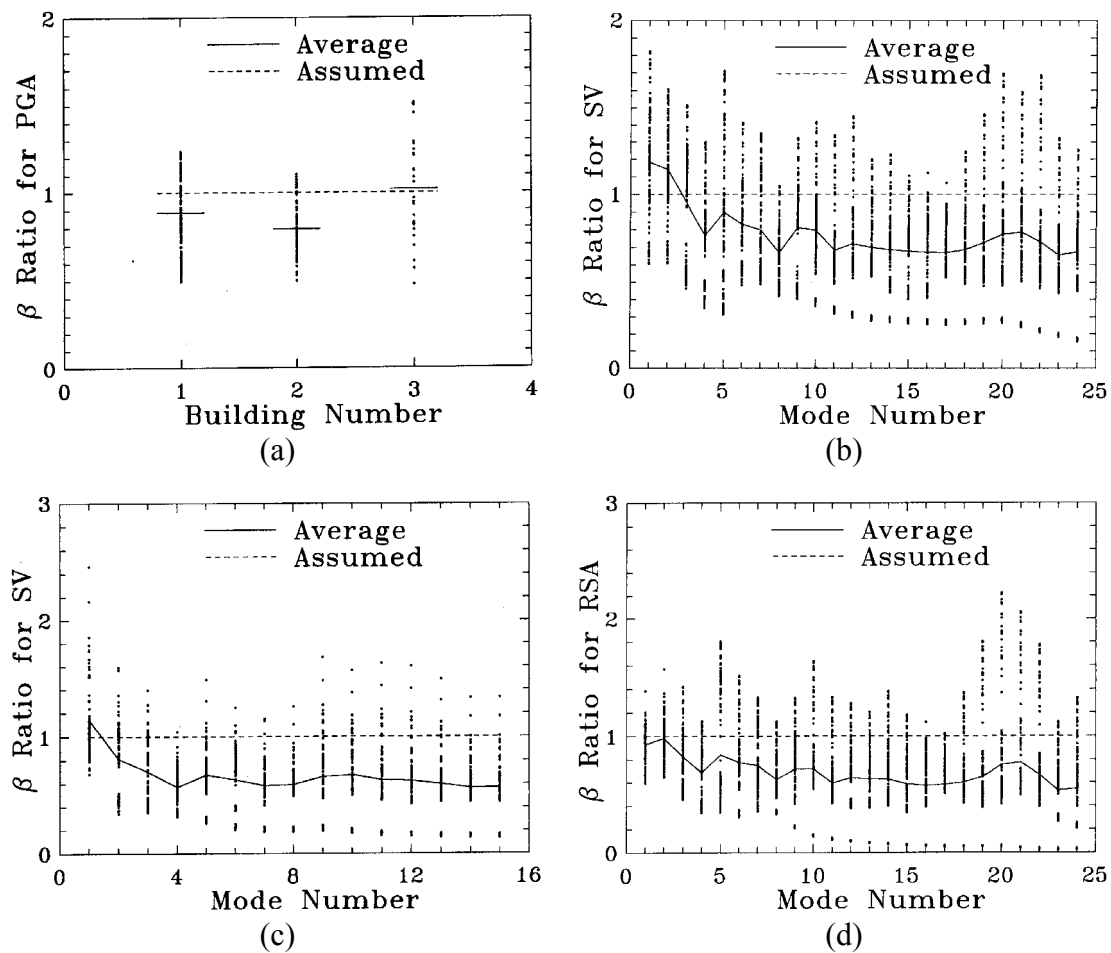


Fig. 4 (a) β^{a_i}/β^G ratio values for Building-1 (BD1), Building-2 (BD2) and Building-3 (BD3); (b) β^{a_i}/β_j^V ratio values for BD1; (c) β^{a_i}/β_j^V ratio values for BD2; (d) β^{a_i}/β_j^A ratio values for BD1

3. Results and Discussion: Proposed Rule and Its Variants

To illustrate and compare performances of the proposed rule and its variants (SRSS and quasi-SRSS), the three example buildings have been subjected to the six example ground motions and the estimates of peak floor accelerations obtained from (i) the (exact) time-history analysis, (ii) the proposed rule (see Equations (18) and (20)), (iii) the SRSS variant (see Equation (22)), and (iv) the quasi-SRSS variant (see Equations (20) and (21)). Absolute error averaged over all floors has been calculated for all 18 combinations of example buildings and ground motions for the ‘proposed’, ‘SRSS’ and ‘quasi-SRSS’ rules and shown in Table 4. It is clear from this table that the performance of the proposed rule is quite good with the average error being less than 10% in most cases. The maximum average error of 19.9% is observed in the case of BD1 subjected to the Parkfield motion, and the minimum average error of 2.26% is observed in the case of BD1 subjected to the Michoacan motion. Since BD1 is very flexible with respect to the Parkfield motion, it appears that the approximations made in developing the proposed rule are most inappropriate when the structural system is very flexible to the ground motion. Further, since BD1 is stiff with respect to the Michoacan motion, these approximations may be most appropriate when the system is relatively very stiff.

Table 4: Comparison of the Averaged Percentage Absolute Error (over Floors) in Peak Floor Acceleration for 5% Damping Ratio

Record No.	1	2	3	4	5	6
Example Building	BD1					
Proposed*	12.67	8.18	11.73	2.26	<u>19.88</u>	<u>6.07</u>
SRSS**	28.50	58.73	39.78	5.20	56.56	24.37
Quasi-SRSS***	27.50	52.19	33.92	8.35	47.58	24.02
Singh et al. (2006)	16.23	15.82	17.91	23.35	16.62	21.94
Example Building	BD2					
Proposed*	<u>15.75</u>	7.03	<u>11.81</u>	2.56	12.31	4.09
SRSS**	25.25	46.93	29.87	19.60	83.93	13.45
Quasi-SRSS***	28.97	49.42	30.91	20.85	84.00	14.29
Singh et al. (2006)	38.58	30.07	18.06	40.87	37.70	30.34
Example Building	BD3					
Proposed*	4.17	<u>9.29</u>	4.62	<u>3.56</u>	4.07	5.68
SRSS**	12.93	7.20	16.91	0.65	20.44	11.01
Quasi-SRSS***	15.44	10.51	12.98	9.05	15.73	7.63
Singh et al. (2006)	106.73	85.31	101.71	122.84	109.94	120.26
*Equations (18) and (20); **Equation (22); ***Equations (20) and (21)						

The envelopes of floor accelerations for the worst case for each ground motion (see the error figures underlined in Table 4) are compared in Figures 5(a)–5(f). Figures 5(e) and 5(f) show the comparisons for BD1 in the cases of Parkfield and San Fernando motions, respectively. Figures 5(a) and 5(c) show the comparisons for BD2 in the cases of Borrego Mountain and Kern County motions, respectively. Figures 5(b) and 5(d) show the comparisons for BD2 in the cases of Imperial Valley and Michoacan motions, respectively. Comparisons for the remaining cases may be seen in Kumari (2007). In each of Figures 5(a)–5(f), ‘S’ refers to the results from the SRSS variant of the proposed rule, ‘E’ refers to the exact results, ‘P’ refers to the results from the proposed rule, and ‘Q’ refers to the quasi-SRSS variant of the proposed rule. It is seen from these figures that the results of the proposed rule follow the exact results well despite these being the worst cases for each ground motion. The results of the SRSS and quasi-SRSS variants follow the exact results on the conservative side. The results in Figures 5(c)–5(f) do not also

support the assumptions of ASCE (2003) regarding the (i) linear variation of peak floor acceleration with height, and (ii) peak roof accelerations as much as three times the peak ground accelerations. As shown by Figure 5(f), peak roof acceleration may even be greater than three times the peak ground acceleration.

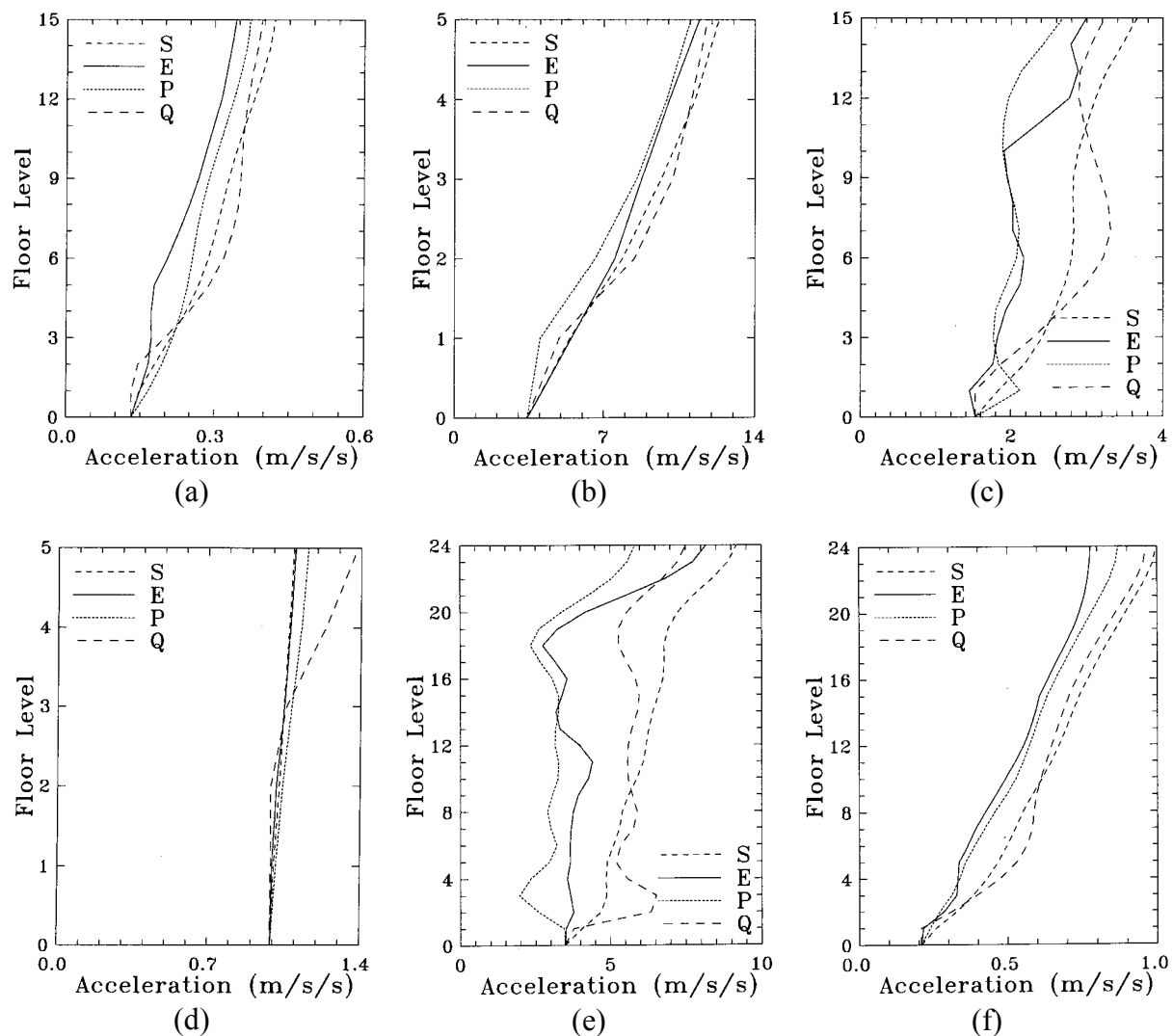


Fig. 5 Comparison of the floor acceleration envelopes for SRSS (S), exact (E), proposed (P) and quasi-SRSS (Q) estimates in the case of (a) BD2 and Borrego Mountain motion, (b) BD3 and Imperial Valley motion, (c) BD2 and Kern County motion, (d) BD3 and Michoacan motion, (e) BD1 and Parkfield motion, and (f) BD1 and San Fernando motion (see Equations (18) and (20) for the proposed estimates, Equation (22) for the SRSS estimates, and Equations (20) and (21) for the quasi-SRSS estimates)

On comparing the errors associated with the SRSS and quasi-SRSS variants of the proposed rule in Table 4, it is seen that both rules give comparable errors. This is expected since both rules differ from each other only in terms of the cross-modal correlation terms and since these terms do not play a significant role (the modes in all three example buildings are well-separated). Both SRSS and quasi-SRSS variants ignore correlation between the ground acceleration and relative floor acceleration, and this appears to lead to relatively larger errors in the cases like BD2 subjected to the Parkfield motion and BD1 and BD2 subjected to the Imperial Valley motion. This may be due to the building being very flexible with respect to the ground motion (fundamental period of the building becoming as large as 10 times the mean period of the ground motion) and periods of several significant modes exceeding the mean period. Both SRSS and quasi-SRSS variants of the proposed rule are thus likely to work well as long as the structural system is not flexible with respect to the ground motion. Based on the example buildings and motions considered in this study, it appears that a range of 0.5–3 times the mean period (of ground

In order to see how the simple SRSS variant compares with the recent recommendation of Singh et al. (2006), absolute error (averaged over all floors) in the case of Singh et al. (2006) has also been shown in Table 4 for the 18 example cases. It may be observed from this table that the maximum average absolute error in the case of the SRSS variant of the proposed rule is 83.93%, while it is 122.84% in the case of Singh et al. (2006). Further, out of the 18 cases considered, there are 8 cases in which the recommendation of Singh et al. (2006) gives lesser errors. Based on this limited study, therefore, SRSS variant of the proposed rule may be expected to perform better than the recommendation of Singh et al. (2006), particularly when the structural system is not flexible with respect to the ground motion.

Table 5: Comparison of the Averaged Percentage Absolute Error (over Floors) in Peak Floor Acceleration for 2% Damping Ratio

Record No.	1	2	3	4	5	6
Example Building	BD1					
Proposed*	7.84	14.09	16.37	3.02	25.31	3.38
SRSS**	16.16	31.72	10.32	3.57	29.35	13.06
Quasi-SRSS***	15.28	28.14	9.84	5.90	27.36	12.64
Example Building	BD2					
Proposed*	9.73	10.25	14.26	4.54	14.11	5.16
SRSS**	13.08	22.35	8.60	12.82	56.86	9.43
Quasi-SRSS***	15.19	24.31	14.85	15.74	57.02	8.50
Example Building	BD3					
Proposed*	1.98	8.94	6.47	6.22	8.46	3.70
SRSS**	10.83	2.72	14.10	2.14	10.42	10.11
Quasi-SRSS***	12.40	5.97	11.66	10.60	7.25	7.58
*Equations (18) and (20); **Equation (22); ***Equations (20) and (21)						

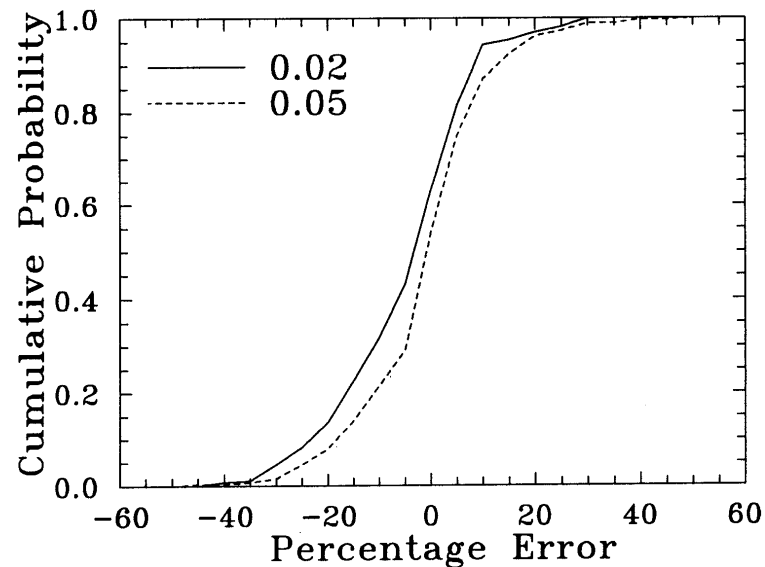


Fig. 6 Comparison of cumulative probability density functions for percentage error in the peak floor acceleration estimate from the proposed rule for 2% and 5% damping ratios

Though the cases considered in this study are not necessarily exhaustive or consider various possibilities in a balanced way, we can make following preliminary conclusions regarding the proposed rule. First, the absolute error in estimating absolute acceleration at the floor of a building does not exceed 50%. Second, the probability of a negative error in this estimation is about 55%. Third, the probability of an absolute error within 10% is about 65%. The proposed rule can be improved further by considering more realistic β ratios. This, however, requires an in-depth study on the correlations of these ratios with the ground motion characteristics and building periods.

CONCLUSIONS

A modal combination rule has been formulated to estimate maximum values of the absolute accelerations of floors in a multistoried shear building. The building is assumed to be a linear, lumped mass, classically damped, fixed-base system, which is excited at its base by the ground motion described by a given PSA spectrum. The proposed rule is based on assuming the excitation and responses processes to be stationary and on the use of nonstationarity and peak factors to relate the (stationary) r.m.s. response with the (nonstationary) largest peak response. It is further assumed for simplicity that the peak factors for the modal responses and the total responses are equal and that the nonstationarity factors for these responses are also equal. The spectral velocity and relative spectral acceleration spectra are assumed to be approximated by PSV and PRSA spectra, respectively. The proposed rule includes (i) correlations between the ground acceleration and the relative acceleration in each mode, and (ii) the correlations between the relative accelerations in various modes. This rule requires just the knowledge of the dynamic properties of the building (mode shapes, modal frequencies and modal participation factors), the PSA ordinates, and the mean period of the ground motion.

A numerical study carried out with the help of three example buildings and six example ground motions with widely different characteristics shows that the peak floor acceleration estimates of the proposed rule follow the (exact) time-history estimates reasonably well through the building height and that the maximum average absolute error in any combination of building and excitation is less than 20% in the case of 5% damping. It is also seen that the probability of absolute error at any floor of being less than 10% is about 65%. In any case, this error does not exceed 50%. The performance of the proposed rule is excellent particularly when the building is stiff or very stiff relative to the excitation. It is also observed that two simpler variants of the proposed rule: (i) SRSS, ignoring all cross-correlations, and (ii) quasi-SRSS, ignoring the correlation between the ground and relative accelerations, give comparable errors for the example buildings with well-separated modes. Both ignore correlation between the ground acceleration and relative floor acceleration, and give estimates greater than or equal to PGA. In comparison with the proposed rule, the estimates from these variants are associated with greater errors

and those errors are usually on the conservative side. However, both variants are likely to work reasonably well provided the building is not flexible with respect to the ground motion.

The proposed rule is very convenient to apply as it uses the easily available PSA ordinates (including that at the zero period). For calculation of the mean period of the ground motion, it may be more convenient to use the PSV spectrum in place of the Fourier spectrum. The proposed rule can be made even more accurate by using more appropriate nonstationarity factor ratios. This however requires an in-depth study on how to account for the effects of building and modal periods and ground motion characteristics on these ratios.

REFERENCES

1. ASCE (2003). "SEI/ASCE 7-02: Minimum Design Loads for Buildings and Other Structures", ASCE Standard No. 7-02, American Society of Civil Engineers, Reston, U.S.A.
2. Biot, M.A. (1934). "Theory of Vibration of Buildings during Earthquake", *Zeitschrift für Angewandte Mathematik und Mechanik*, Vol. 14, No. 4, pp. 213–223.
3. Biot, M.A. (1942). "Analytical and Experimental Methods in Engineering Seismology", *ASCE Transactions*, Vol. 108, pp. 365–408.
4. Christian, J.T. (1989). "Generating Seismic Design Power Spectral Density Functions", *Earthquake Spectra*, Vol. 5, No. 2, pp. 351–368.
5. Der Kiureghian, A., Sackman, J.L. and Nour-Omid, B. (1983). "Dynamic Analysis of Light Equipment in Structures: Response to Stochastic Input", *Journal of Engineering Mechanics*, ASCE, Vol. 109, No. 1, pp. 90–110.
6. Goodman, L.E., Rosenblueth, E. and Newmark, N.M. (1955). "Aseismic Design of Firmly Founded Elastic Structures", *ASCE Transactions*, Vol. 120, pp. 782–802.
7. Gupta, V.K. (1994). "Higher Order Peaks in the Seismic Response of Multistoried Buildings", Report 94-03, Department of Civil Engineering, Indian Institute of Technology Kanpur, Kanpur.
8. Gupta, V.K. (2002). "Developments in Response Spectrum-Based Stochastic Response of Structural Systems", *ISET Journal of Earthquake Technology*, Vol. 39, No. 4, pp. 347–365.
9. Gupta, I.D. and Trifunac, M.D. (1988). "Order Statistics of Peaks in Earthquake Response", *Journal of Engineering Mechanics*, ASCE, Vol. 114, No. 10, pp. 1605–1627.
10. Gupta, V.K. and Trifunac, M.D. (1990). "Response of Multistoried Buildings to Ground Translation and Rocking during Earthquakes", *Probabilistic Engineering Mechanics*, Vol. 5, No. 3, pp. 138–145.
11. Hall, J.F. (editor) (1994). "Northridge Earthquake January 17, 1994: Preliminary Reconnaissance Report", Report 94-01, Earthquake Engineering Research Institute, El Cerrito, U.S.A.
12. Hu, S.L.J., Li, H. and Wang, S. (2007). "Cross-Model Cross-Mode Method for Model Updating", *Mechanical Systems and Signal Processing*, Vol. 21, No. 4, pp. 1690–1703.
13. Igusa, T. and Der Kiureghian, A. (1985). "Generation of Floor Response Spectra Including Oscillator-Structure Interaction", *Earthquake Engineering & Structural Dynamics*, Vol. 13, No. 5, pp. 661–676.
14. Kaul, M.K. (1978). "Stochastic Characterization of Earthquakes through Their Response Spectrum", *Earthquake Engineering & Structural Dynamics*, Vol. 6, No. 5, pp. 497–509.
15. Kumari, R. (2007). "A Response Spectrum Method for Peak Floor Accelerations in Multistoried Buildings", M.Tech. Thesis, Department of Civil Engineering, Indian Institute of Technology Kanpur, Kanpur.
16. Ray Chaudhuri, S. and Gupta, V.K. (2003). "Mode Acceleration Approach for Generation of Floor Spectra Including Soil-Structure Interaction", *ISET Journal of Earthquake Technology*, Vol. 40, No. 2-4, pp. 99–115.
17. Rodriguez, M.E., Restrepo, J.I. and Carr, A.J. (2002). "Earthquake-Induced Floor Horizontal Accelerations in Buildings", *Earthquake Engineering & Structural Dynamics*, Vol. 31, No. 3, pp. 693–718.

18. Rosenblueth, E. and Elorduy, J. (1969). "Response of Linear Systems to Certain Transient Disturbances", *Proceedings of the Fourth World Conference on Earthquake Engineering*, Santiago, Chile, Vol. 1, pp. 185–196.
19. Singh, M.P. (1980). "Seismic Design Input for Secondary Systems", *Journal of the Structural Division*, *Proceedings of ASCE*, Vol. 106, No. ST2, pp. 505–517.
20. Singh, M.P. and Mehta, K.B. (1983). "Seismic Design Response by an Alternative SRSS Rule", *Earthquake Engineering & Structural Dynamics*, Vol. 11, No. 6, pp. 771–783.
21. Singh, M.P. and Sharma, A.M. (1985). "Seismic Floor Spectra by Mode Acceleration Approach", *Journal of Engineering Mechanics*, Vol. 111, No. 11, pp. 1402–1419.
22. Singh, M.P., Suárez, L.E. and Moreschi, L.M. (1998). "Simplified Methods for Calculating Seismic Forces for Nonstructural Components", *Proceedings of the ATC-29-1 Seminar on Seismic Design, Retrofit, and Performance of Nonstructural Components*, San Francisco, U.S.A., pp. 43–56.
23. Singh, M.P., Verma, N.P. and Moreschi, L.M. (2003). "Seismic Analysis and Design with Maxwell Dampers", *Journal of Engineering Mechanics*, *ASCE*, Vol. 129, No. 3, pp. 273–282.
24. Singh, M.P., Moreschi, L.M., Suárez, L.E. and Matheu, E.E. (2006). "Seismic Design Forces. I: Rigid Nonstructural Components", *Journal of Structural Engineering*, *ASCE*, Vol. 132, No. 10, pp. 1524–1532.
25. Soong, T.T., Bachman, R.E. and Drake, R.M. (1998). "Implications of 1994 Northridge Earthquake on Design Guidelines for Nonstructural Components", *Proceedings of the NEHRP Conference and Workshop on Research on the Northridge, California Earthquake of January 17, 1994*, Consortium of Universities for Research in Earthquake Engineering, Richmond, U.S.A., Vol. III, pp. 441–448.
26. Suarez, L.E. and Singh, M.P. (1987). "Floor Response Spectra with Structure-Equipment Interaction Effects by a Mode Synthesis Approach", *Earthquake Engineering & Structural Dynamics*, Vol. 15, No. 2, pp. 141–158.
27. Taghavi, S. and Miranda, E. (2005). "Approximate Floor Acceleration Demands in Multistory Buildings. II: Applications", *Journal of Structural Engineering*, *ASCE*, Vol. 131, No. 2, pp. 212–220.
28. Trifunac, M.D. and Brady, A.G. (1975). "A Study on the Duration of Strong Earthquake Ground Motion", *Bulletin of the Seismological Society of America*, Vol. 65, No. 3, pp. 581–626.
29. Trifunac, M.D. and Gupta, V.K. (1991). "Pseudo Relative Acceleration Spectrum", *Journal of Engineering Mechanics*, *ASCE*, Vol. 117, No. 4, pp. 924–927.
30. Unruh, J.F. and Kana, D.D. (1981). "An Iterative Procedure for the Generation of Consistent Power/Response Spectrum", *Nuclear Engineering and Design*, Vol. 66, No. 3, pp. 427–435.
31. Vanmarcke, E.H. (1972). "Properties of Spectral Moments with Applications to Random Vibration", *Journal of the Engineering Mechanics Division*, *Proceedings of ASCE*, Vol. 98, No. EM2, pp. 425–446.
32. Villaverde, R. (1997). "Method to Improve Seismic Provisions for Nonstructural Components in Buildings", *Journal of Structural Engineering*, *ASCE*, Vol. 123, No. 4, pp. 432–439.
33. Wilson, E.L., Der Kiureghian, A. and Bayo, E.P. (1981). "A Replacement for the SRSS Method in Seismic Analysis", *Earthquake Engineering & Structural Dynamics*, Vol. 9, No. 2, pp. 187–194.

SPATIAL SEISMIC EXCITATIONS AND RESPONSE SPECTRA

Zbigniew Zembaty

Opole University of Technology
45-271 Opole ul. Mikolajczyka 5
Poland

ABSTRACT

Formal extensions of the response spectrum method to include spatial seismic effects are reviewed. Two approaches are described in detail: the first based on random vibrations of a simple oscillator under two-component excitations, and the second analyzing multi-column building seismic response. The subjective choice of these two complementing approaches aims at analyzing the phenomenon of spatial seismic vibrations of structures from a broader physical perspective of various wave types propagating among structural supports, with detailed random vibration sensitivity analysis of a simple structural system still included.

KEYWORDS: Response Spectrum, Spatial Seismic Effects, Differential Ground Motion, Wave Propagation, Site Amplification

INTRODUCTION

The question of why, after 75 years, the response spectrum method (Biot, 1932) still captures our attention and ignites our imagination is quite a pertinent one. Two different answers to this question come to mind. On one hand, the response spectrum method in its full form, generalized to multi-degree-of-freedom (MDOF) systems, is quite effective and very early it became a standard tool for engineers designing structures to withstand seismic loads. On the other hand, even for single-degree-of-freedom (SDOF) systems, the conceptual clarity of a simple “mechanical analyzer for the prediction of earthquake stresses” (Biot, 1941) made it a very convenient vehicle for analyzing new structural models for various types of ground motions.

Indeed, in spite of the fact that advanced finite element method (FEM) softwares applying dedicated finite element models and nonlinear procedures can solve many sophisticated structural seismic problems using hundreds of thousands degrees of freedom, our ability to understand and predict structural response under seismic excitations still remains substantially limited. This is partly because the more advanced and extended such modeling becomes, and the greater are the dimensions of the analyzed structural system, the more case-dependent our analysis becomes, and the less general conclusions we can draw. Paradoxically, it seems that the larger we make our model the more we are losing the “big picture” of our problem. So, after all the expensive FEM efforts, we are often left powerless like Pooh Bear from the childish book (*...but to his surprise, the more Pooh Bear, looked inside the house, the more Piglet wasn't there; A.A. Milne: “The House at Pooh Corner”*).

The purpose of this paper is to review one particular aspect of the response spectrum method, namely, its formal extension to include the effects of seismic signal variations along or across the structural dimensions. In this case, the advantage of clear physical interpretation of the response spectrum concept is particularly appealing. It is obvious that the modeling simplifications can lead only to approximate results; yet by reducing the number of parameters to a very few—the most necessary ones—a clearer view of the physics of the analyzed problem may be possible. For many practical engineering situations, these approximations are quite adequate.

SPATIAL SEISMIC EFFECTS ON STRUCTURES

The origin of spatial seismic effects can be attributed to following three main sources:

- complexity of seismic focus,
- finite velocity of wave propagation, and
- geological and geometrical heterogeneities of the ground.

The first source of spatial variability can be particularly important for near-field strong motion, and its effects are still difficult to quantify. The second source depends directly upon the ratio of the longest structural dimension to the shortest significant wavelength. The third source of spatial seismic variability leads on one hand to complicated problems of wave diffraction and interference (see, e.g., Aki and Richards, 1980), and on the other hand to local soil amplification (e.g., Trifunac, 1990; Safak, 1995).

Consider a general multi-support structure (as in Figure 1). The seismic waves propagating along this structure excite the motion of structural foundations with a phase shift depending upon the wavelength and the apparent propagation velocities. It can be seen that in addition to the familiar dynamic response the presence of pseudo-static motion will cause substantial strains in the structure. In a situation in which the excitations act slowly, say with vibration periods $\gg T_1$ ($=$ fundamental period of the structure), the strains in the structure will be caused 'solely' by the asynchronous support movements. Thus, it is the combination of the dynamic vibrations and pseudo-static motions, depending upon the spectral content of excitations and the apparent wave propagation velocities, that will determine the overall structural performance under spatial seismic excitations. One should also note that the differential effects among columns of the structure will always be somewhat reduced by the soil compliance, or more generally, by the soil-structure-interaction (SSI) effects (see the zoomed area of Figure 1).

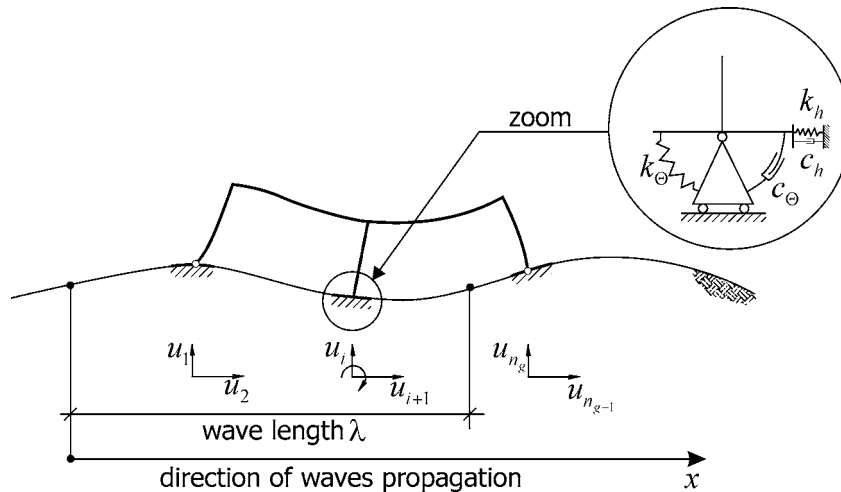


Fig. 1 A structure subjected to multi-support, kinematic wave excitations

The significance and recognition of spatial seismic effects grew following the arrival of experimental evidence since late 1980s, when the records from extended seismic arrays like SMART-1 became available (Abrahamson et al., 1987). From that time the number of journal papers on this subject has increased significantly.

The spatial seismic effects on structures can be analyzed with varying degrees of sophistication. The simplest way to include the effect of spatial seismic effects on a multi-support structure is to simply carry out a time-history analysis with certain seismic record applied to structural supports with some time delay. The time shift among structural supports can be selected so that it reflects the apparent wave velocity in the ground motion. Such an analysis for a typical reinforced concrete bridge structure on multiple supports was described by Leger et al. (1990). Modern computer codes (e.g., ABAQUS) even make it possible to observe the time dependence of a map of particular stresses in the structure as the excitation propagates along the structural supports (Dulinska and Zieba, 2007). Such a simple deterministic analysis can be conceptually clear, but the following aspects of the spatial seismic effects may still not be properly addressed.

The Arbitrary Choice of the Single Apparent Wave Velocity: Theoreticians will note that this approach ignores the fact that there exist multiple apparent wave velocities that also depend upon the frequencies of motion being analyzed and that result from the dispersion in strong-motion waves (Trifunac, 1971).

The Assumption of Uniformity of the Ground Properties along the Structure: In many cases, the ground properties differ among different structural supports. This may be particularly true for the bridges

crossing alluvial valleys with rock outcrops. In such situations, ground motions at different supports of a structure may be very different.

Loss of Coherence among the Motions at the Supports of the Structure: Simultaneous measurements of seismic signals at two distinct points on the ground surface display differences that result from substantial randomness in the medium through which the seismic signal is transmitted. This effect, called loss of coherency, should be taken into account.

Many spatial seismic ground motion models based on the SMART-1 measurements were formulated and analyzed through correlation/coherence functions describing the surface wave field in terms of the random field theory (e.g., Abrahamson and Bolt, 1985; Abrahamson et al., 1991; Harichandran and Vanmarcke, 1986; Shinozuka and Deodatis, 1991; Vanmarcke and Fenton, 1991), and became popular in the analyses of the multi-support structural response based on the random vibration approach. In the papers by Harichandran and Wang (1988, 1990), Zerva (1991), and Hao (1989, 1991), specific multi-support structures were analyzed, taking into account one- or two-dimensional random field models and the orientation of the structure with respect to the source direction (Zembaty, 1997) or local site effects (Zembaty and Rutenberg, 1998). Most of these analyses (except for very few, e.g., Perotti (1990)) assume stationarity of random vibrations. However, such an assumption may be disputable for some important multi-support structures like large bridges with fundamental periods of several seconds or more. On the other hand, there are methods available now (e.g., Gupta and Trifunac, 1998) that properly account for the nonstationarity of seismic excitation and response within the framework of stationary random vibrations.

The random vibration-based approach utilizing SMART-1 data provided good and general results on the spatial seismic effects on structures. However, in the inevitable temporal averaging of the multiple records from dense arrays of instruments, some important pieces of information can be lost, particularly those regarding the phasing and contributions of the specific wave types in the ground motion. Thus, an alternative approach to investigating the effects of the spatial nature of strong ground motion is deterministic and includes analyses of particular wave types arriving at the structures (Trifunac, 1997; Trifunac and Todorovska, 1997; Trifunac and Gicev, 2006) and their propagation inside the structures (Todorovska and Lee, 1989; Todorovska and Trifunac, 1989, 1990a).

The spatial seismic effects were also analyzed for extended structures like dams (Kojic and Trifunac, 1991a, 1991b), dikes (Todorovska et al., 2001a, 2001b), and selected lifeline structures (e.g., buried pipelines (Hindy and Novak, 1980; Datta, 1999)). In this case, instead of differential motion among structural supports, continuous changes of the ground motion occur along the structure. Review of these problems is beyond the scope of this paper, but readers interested in this subject can find further examples in the papers by Novak (1990), Todorovska and Trifunac (1990b), Zerva and Shinozuka (1991), and Datta (1999), among others.

Since most of the analyses of spatial seismic effects on structures are strongly case-dependent, the generalizations of the response spectra to include the spatial effects were searched for, starting from the early proposals of Loh et al. (1982) and Abrahamson and Bolt (1985). Later, the concept of spatial response spectrum was further advanced to include its stochastic description (Zembaty and Krenk, 1993; Zembaty, 1996; Zembaty and Rutenberg, 2002). In a separate development, Der Kiureghian and Neuenhofer (1992) also proposed a concept of random vibration-based response spectrum method for MDOF systems under multi-support excitations, generalized from the earlier concepts of the response spectrum method for stationary random vibrations (Der Kiureghian, 1980, 1981).

In what follows, selected results from the analyses of the simplest SDOF stochastic spatial response spectra from Zembaty and Krenk (1993), Zembaty (1996), and Zembaty and Rutenberg (2002) will be reviewed. Some results of the column response spectra concept of Trifunac and Todorovska (1997), and Trifunac and Gicev (2006) will also be considered. These two approaches were chosen for this review because they cover, in the simplest possible way, most of the physically important aspects of structural response under spatial seismic excitations, and because, in a sense, they complement one another. Our review starts with the presentation of a stochastic model of spatial seismic excitations.

A COMPOSITE COHERENCY MODEL OF SPATIAL SEISMIC EFFECTS

Consider two points A and B on the ground surface. A convenient stochastic measure of the difference between the seismic signals at these two points is its complex coherency $\gamma_{AB}(\omega)$:

$$\gamma_{AB}(\omega) = |\gamma_{AB}| \exp[i\Theta_{AB}] = \frac{S_{AB}(\omega)}{\sqrt{S_A(\omega)S_B(\omega)}} \quad (1)$$

in which $S_A(\omega)$ and $S_B(\omega)$ stand for power spectral densities of accelerations measured along the same direction (x , y , or z) at points A and B , respectively; $|\gamma_{AB}|$ stands for the modulus of the coherence function; Θ_{AB} is the phase of the coherence function; and $S_{AB}(\omega)$ represents the co-spectrum of the two signals. The modulus of coherency $|\gamma_{AB}(\omega)|$ is called loss of coherency or lagged coherency. It is a measure of the similarity of signals at point A and B , excluding the effect of traveling waves, which is included in the phase Θ_{AB} . Sometimes the real value of coherency, $\text{Re}(\gamma_{AB}(\omega))$, called the unlagged coherency, is analyzed. Equation (1) can be rewritten as

$$S_{AB}(\omega) = \gamma_{AB}(\omega) \sqrt{S_A(\omega)S_B(\omega)} \quad (2)$$

to display the dependence between the input spectral densities, S_A and S_B , their coherence γ_{AB} , and the output cross-spectral density function S_{AB} .

Der Kiureghian (1996) proposed a composite model of spatial seismic effects in which the cross-spectral density of accelerations was

$$\gamma_{AB}(\omega) = \gamma_{AB}^{(i)}(\omega) \gamma_{AB}^{(w)}(\omega) \gamma_{AB}^{(s)}(\omega) = \gamma_{AB}^{(i)}(\omega) \exp \left[i \left(\Theta_{AB}^{(w)}(\omega) + \Theta_{AB}^{(s)}(\omega) \right) \right] \quad (3)$$

This is composed of three principal factors, each representing a contribution from a different spatial seismic influence: $\gamma_{AB}^{(i)}$ is a measure of the loss of coherency between A and B ; $\gamma_{AB}^{(w)}$ stands for complex coherency resulting from phase delay due to the wave propagation; and $\gamma_{AB}^{(s)}$ represents local site effects, where $i = \sqrt{-1}$. It should be pointed out that the loss of coherency is represented by a real function, whereas wave-passage and site effects result in the phase changes $\Theta_{AB}^{(w)}$ and $\Theta_{AB}^{(s)}$ of the complex coherency.

The complex coherency contains the key information on spatial distribution of seismic ground motions and constitutes the main input function for random vibration analyses of structural systems. Usually, its parameters are retrieved from the synchronized records of a particular seismic event (see, e.g., SMART-1 data processed by Hao (1989)). Two problems will be noted when analyzing physical interpretations of complex coherency:

- The modulus of coherency appears to be very sensitive to spatial separation, even for relatively low frequencies (Der Kiureghian and Neuenhofer, 1992). On the other hand, there is experimental evidence that during strong earthquakes the peak values of ground motion do not change substantially over rather long distances (Todorovska and Trifunac, 1997). Thus, direct observations of the moduli of coherency can be misleading about important peak response measures of the seismic ground motion.
- The second problem regarding the complex coherency concerns its phase. Usually, a single apparent wave velocity is assumed to describe the spatial phase changes of the coherency function, which is in direct violation of the observations of the records of real earthquakes.

Thus, deeper research regarding rational stochastic models of spatial seismic ground motion seems necessary and inevitable.

SPATIAL RESPONSE SPECTRUM FOR SDOF SYSTEM UNDER TWO-COMPONENT, RANDOM SEISMIC EXCITATIONS

Consider a simple oscillator under two different support excitations (Figure 2). Such a system, though very simple, can represent several important structural response cases, e.g., a symmetric beam vibrating in one dynamic mode (transverse, vertical, or axial; see Figure 3). Its equation of motion takes the form

$$\begin{bmatrix} m & 0 & 0 \\ 0 & 0 & 0 \\ 0 & 0 & 0 \end{bmatrix} \begin{bmatrix} \ddot{q}^t \\ \ddot{u}_A \\ \ddot{u}_B \end{bmatrix} + \begin{bmatrix} c & -c/2 & -c/2 \\ -c/2 & c/2 & 0 \\ -c/2 & 0 & c/2 \end{bmatrix} \begin{bmatrix} \dot{q}^t \\ \dot{u}_A \\ \dot{u}_B \end{bmatrix} + \begin{bmatrix} k & -k/2 & -k/2 \\ -k/2 & k/2 & 0 \\ -k/2 & 0 & k/2 \end{bmatrix} \begin{bmatrix} q^t \\ u_A \\ u_B \end{bmatrix} = \begin{bmatrix} 0 \\ 0 \\ 0 \end{bmatrix} \quad (4)$$

where q^t and q represent total and relative oscillator displacements, respectively (Figure 2). Introducing natural frequency $\omega_0 = \sqrt{(k/m)}$ and damping ratio $\xi = c/(2m\omega_0)$, after some algebra, the above equation can be reduced to that for a SDOF system:

$$\ddot{q} + 2\xi\omega_0\dot{q} + \omega_0^2q = -\frac{1}{2}(\ddot{u}_A + \ddot{u}_B) \quad (5)$$

The column shear forces $f_A(t)$ and $f_B(t)$ are

$$f_A(t) = \frac{k}{2}(q^t - u_A) = \frac{k}{2}\left(\frac{u_B(t) - u_A(t)}{2} + q(t)\right) \quad (6a)$$

$$f_B(t) = \frac{k}{2}(q^t - u_B) = \frac{k}{2}\left(\frac{u_A(t) - u_B(t)}{2} + q(t)\right) \quad (6b)$$

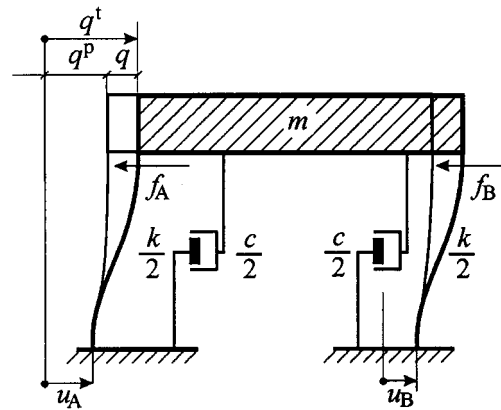


Fig. 2 A single-degree-of-freedom system excited by two different motions

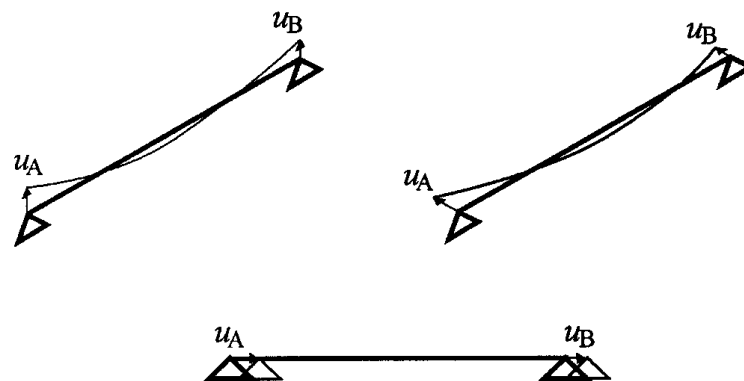


Fig. 3 Examples of simple structures that can be modeled by the SDOF system shown in Figure 2 (after Zembaty and Rutenberg, 2002)

Equation (5) expresses the simple fact that the dynamic response of the analyzed SDOF system represents an oscillator response to the average of support excitations u_A and u_B . Unlike the relative displacements $q(t)$, the force responses (Equations (6a) and (6b)) combine both the dynamic response

and pseudo-static vibrations. Therefore, they are more influenced by the asynchronous support motions than by the displacements of the oscillator.

We assume next that the excitations $u_A(t)$ and $u_B(t)$ can be presented by spectral Stieltjes-Fourier decomposition of stationary random processes:

$$u_A(t) = \int_{-\infty}^{\infty} e^{i\omega t} d\hat{u}_A(\omega) \quad (7a)$$

$$u_B(t) = \int_{-\infty}^{\infty} e^{i\omega t} d\hat{u}_B(\omega) \quad (7b)$$

in which $\hat{u}_A(\omega)$ and $\hat{u}_B(\omega)$ stand for random processes in the frequency domain with orthogonal increments:

$$\langle d\hat{u}_A(\omega_1) d\hat{u}_B^*(\omega_2) \rangle = \begin{cases} S_{u_A u_B}(\omega) d\omega & \text{for } \omega_1 = \omega_2 = \omega \\ 0 & \text{for } \omega_1 \neq \omega_2 \end{cases} \quad (8)$$

Here the symbol $\langle \rangle$ denotes the mathematical expectation, asterisk stands for complex conjugate, and $S_{u_A u_B}(\omega)$ is the cross power spectral density of random processes $u_A(t)$ and $u_B(t)$. It should be noted that for stationary processes, $S_{u_A u_B}(\omega) = S_{\ddot{u}_A \ddot{u}_B}(\omega) / \omega^4$, and for brevity, the acceleration cross spectrum will be denoted by $S_{AB}(\omega)$ and the displacement cross spectra will be denoted by $S_{u_A u_B}(\omega)$. When the processes $u_A(t)$ and $u_B(t)$ are identical, the cross-spectral density in Equation (8) reduces to the respective auto-spectra $S_{u_A}(\omega) = S_{u_B}(\omega) = S_u(\omega)$. The solution of Equation (5) can be given in the form of Duhamel integral:

$$q(t) = -\frac{1}{2} \int_0^t h(\tau) \ddot{u}_A(t-\tau) d\tau - \frac{1}{2} \int_0^t h(\tau) \ddot{u}_B(t-\tau) d\tau \quad (9)$$

Transforming the above equation into the frequency domain, assuming stationarity, and substituting respective spectral representations (as in Equations (7a) and (7b)) for both displacements and accelerations leads to the following solution of Equation (5):

$$q(t) = -\frac{1}{2} \int_{-\infty}^{\infty} H(\omega) e^{i\omega t} d\hat{u}_A(\omega) - \frac{1}{2} \int_{-\infty}^{\infty} H(\omega) e^{i\omega t} d\hat{u}_B(\omega) \quad (10)$$

where $H(\omega) = (\omega_0^2 - \omega^2 + 2i\xi\omega_0\omega)^{-1}$ is the frequency response function of the oscillator. Analogous solutions for the forces f_A and f_B are

$$f_A(t) = \frac{k}{4} \left(\int_{-\infty}^{\infty} e^{i\omega t} d\hat{u}_B(\omega) - \int_{-\infty}^{\infty} e^{i\omega t} d\hat{u}_A(\omega) - \int_{-\infty}^{\infty} H(\omega) e^{i\omega t} d\hat{u}_A(\omega) - \int_{-\infty}^{\infty} H(\omega) e^{i\omega t} d\hat{u}_B(\omega) \right) \quad (11a)$$

$$f_B(t) = \frac{k}{4} \left(\int_{-\infty}^{\infty} e^{i\omega t} d\hat{u}_A(\omega) - \int_{-\infty}^{\infty} e^{i\omega t} d\hat{u}_B(\omega) - \int_{-\infty}^{\infty} H(\omega) e^{i\omega t} d\hat{u}_A(\omega) - \int_{-\infty}^{\infty} H(\omega) e^{i\omega t} d\hat{u}_B(\omega) \right) \quad (11b)$$

Taking into account that $S_{\ddot{u}}(\omega) = \omega^2 S_u(\omega) = \omega^4 S_{uu}(\omega)$, and introducing the complex coherency $\gamma_{AB}(\omega)$ for signals $\ddot{u}_A(t)$ and $\ddot{u}_B(t)$ (in the format of Equation (1)), we can formulate the following spectral matrix for the vector, $[u_A(t) \ u_B(t) \ \ddot{u}_A(t) \ \ddot{u}_B(t)]^T$, which will be useful in deriving formulas for the spectral densities of displacements and forces in the next two points,

$$\begin{bmatrix} \frac{1}{\omega^4} S_A & \frac{1}{\omega^4} \gamma_{AB} \sqrt{S_A S_B} & -\frac{1}{\omega^2} S_A & -\frac{1}{\omega^2} \gamma_{AB} \sqrt{S_A S_B} \\ \frac{1}{\omega^4} \gamma_{AB}^* \sqrt{S_A S_B} & \frac{1}{\omega^4} S_B & -\frac{1}{\omega^2} \gamma_{AB}^* \sqrt{S_A S_B} & -\frac{1}{\omega^2} S_B \\ -\frac{1}{\omega^2} S_A & -\frac{1}{\omega^2} \gamma_{AB} \sqrt{S_A S_B} & S_A & \gamma_{AB} \sqrt{S_A S_B} \\ -\frac{1}{\omega^2} \gamma_{AB}^* \sqrt{S_A S_B} & -\frac{1}{\omega^2} S_B & \gamma_{AB}^* \sqrt{S_A S_B} & S_B \end{bmatrix} \quad (12)$$

The symbols $S_A \equiv S_A(\omega)$, $S_B \equiv S_B(\omega)$ denote (real) point spectral densities of the accelerations $\ddot{u}_A(t)$ and $\ddot{u}_B(t)$. Further analysis depends upon the type of spatial seismic effects to be analyzed (see Equation (3)).

1. The Effect of Wave Passage and Loss of Coherency on Response Spectra

We first assume that both supports A and B have exactly the same site conditions and are separated by the distance $d = |AB|$. In this case, both input spectral densities of accelerations are identical, $S_{\ddot{u}_A}(\omega) = S_{\ddot{u}_B}(\omega)$, and are denoted here for brevity by $S(\omega)$. Following Equation (2), their cross-spectral density equals

$$S_{AB}(\omega) = \gamma_{AB}(\omega) S(\omega) \quad (13)$$

The matrix in (12) can then be simplified to

$$\begin{bmatrix} \frac{1}{\omega^4} & \frac{1}{\omega^4} \gamma_{AB}(\omega) & -\frac{1}{\omega^2} & -\frac{1}{\omega^2} \gamma_{AB}(\omega) \\ \frac{1}{\omega^4} \gamma_{AB}^*(\omega) & \frac{1}{\omega^4} & -\frac{1}{\omega^2} \gamma_{AB}^*(\omega) & -\frac{1}{\omega^2} \\ -\frac{1}{\omega^2} & -\frac{1}{\omega^2} \gamma_{AB}(\omega) & 1 & \gamma_{AB}(\omega) \\ -\frac{1}{\omega^2} \gamma_{AB}^*(\omega) & -\frac{1}{\omega^2} & \gamma_{AB}^*(\omega) & 1 \end{bmatrix} S(\omega) \quad (14)$$

Since only the loss of coherence and wave passage effects are analyzed, following Equation (3), it follows that

$$S_{AB}(\omega) = |\gamma_{AB}^{(i)}(\omega)| \exp[i\Theta_{AB}^{(w)}(\omega)] S(\omega) \quad (15)$$

The loss of coherency denoted here as $|\gamma_{AB}^{(i)}|$ is a real function of frequency ω and distance d , decreasing from 1 at $d = 0$ to 0 for $d \rightarrow \infty$. A simple form of the loss of coherency was proposed by Luco and Wong (1986):

$$|\gamma_{AB}^{(i)}(\omega)| = \exp[-(\kappa d \omega)^2] \quad (16)$$

where κ is a real parameter that controls the dependence of the loss of coherency to remain between 0 and 1.

The auto-spectrum of accelerations $S(\omega)$ often applied in engineering random vibration analyses consists of the familiar Kanai-Tajimi spectral density (Kanai, 1957; Tajimi, 1960) with a filter proposed later by Ruiz and Penzien (1969). Its detailed form is given in Appendix A.

Assuming the plane waves to be propagating with the same apparent velocity, v_g , for all frequencies, the phase term in Equation (15) becomes

$$\Theta_{AB}^{(w)}(\omega) = \frac{\omega d}{v_g} \quad (17)$$

Taking into account Equations (10)–(11) and 14, we can write the equations for spectral densities of relative displacements:

$$S_q(\omega, \omega_0) = \frac{1}{2} |H(\omega, \omega_0)|^2 [1 + \text{Re}(\gamma_{AB}(\omega))] S(\omega) \quad (18)$$

and for column shear forces:

$$S_{f_A}(\omega, \omega_0) = \frac{k^2}{8} \left(\frac{1}{\omega^4} [1 - \text{Re}(\gamma_{AB}(\omega))] - \frac{1}{\omega^2} \text{Im}(H(\omega, \omega_0)) \text{Im}(\gamma_{AB}(\omega)) \right. \\ \left. + |H(\omega, \omega_0)|^2 [1 + \text{Re}(\gamma_{AB}(\omega))] \right) S(\omega) \quad (19a)$$

$$S_{f_B}(\omega, \omega_0) = \frac{k^2}{8} \left(\frac{1}{\omega^4} [1 - \text{Re}(\gamma_{AB}(\omega))] + \frac{1}{\omega^2} \text{Im}(H(\omega, \omega_0)) \text{Im}(\gamma_{AB}(\omega)) \right. \\ \left. + |H(\omega, \omega_0)|^2 [1 + \text{Re}(\gamma_{AB}(\omega))] \right) S(\omega) \quad (19b)$$

The above force spectral densities consist of three terms reflecting (a) the pseudo-static dynamic contribution, (b) cross pseudo-static-dynamic contribution, and (c) the dynamic contribution, respectively. It is noted that the sign of the second term depends upon the wave direction (from *A* to *B* or vice-versa). However, as shown by Zembaty (1996), the contribution of the second term does not exceed a few percent for the realistic values of excitation parameters. Thus, the force spectrum can be approximated by a formula that does not depend upon the direction of wave propagation:

$$S_f(\omega, \omega_0) \cong \frac{k^2}{8} \left(\frac{1}{\omega^4} [1 - \text{Re}(\gamma_{AB}(\omega))] + |H(\omega, \omega_0)|^2 [1 + \text{Re}(\gamma_{AB}(\omega))] \right) S(\omega) \quad (20)$$

In Figure 4, this force spectral density is shown as a function of separation distance *d* for structural damping ratio $\xi = 0.05$ and $\nu = 1000$ m/s. It can be seen from this figure how the pseudo-static contribution in the response (the second “hill” close to the resonance peak) increases with the increasing separation distance.

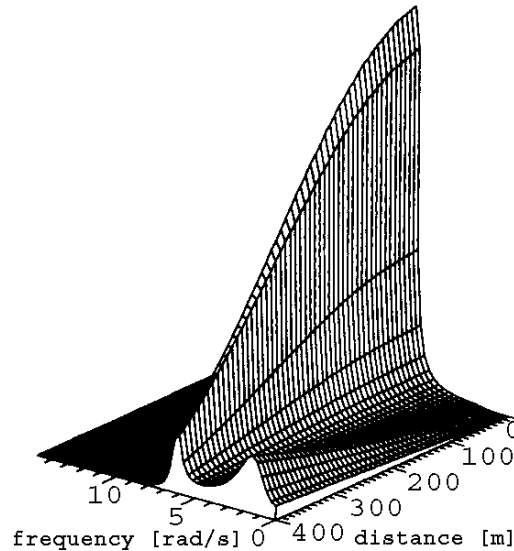


Fig. 4 Spectral density of force response versus frequency and separation distance $d = |AB|$ for $\omega_0 = 2\pi$ rad/s, structural damping ratio $\xi = 0.05$, and apparent wave velocity $\nu = 1000$ m/s (after Zembaty and Krenk, 1993)

Integrating the preceding spectral densities with respect to ω for various values of natural frequency ω_0 , we obtain the displacement mean-square response spectrum:

$$\sigma_q^2(\omega_0) = \int_{-\infty}^{\infty} S_q(\omega, \omega_0) d\omega \quad (21)$$

and the force mean-square response spectrum:

$$\sigma_f^2(\omega_0) = \int_{-\infty}^{\infty} S_f(\omega, \omega_0) d\omega \quad (22)$$

In Figure 5, the force root-mean-square (RMS) response spectrum is shown for $v_g = 1000$ m/s and five values of separation distance d from zero to 400 m. When $d = 0$ (see the dashed line), the force response spectrum goes to zero with decreasing natural period, as it does for a typical displacement response spectrum. This is so because, for the uniform excitations, the force response is a direct function of relative displacement q . It is interesting to note how, for spatial excitations, the force response spectrum goes to a finite, constant value reflecting the purely pseudo-static oscillator response for longer support distances.

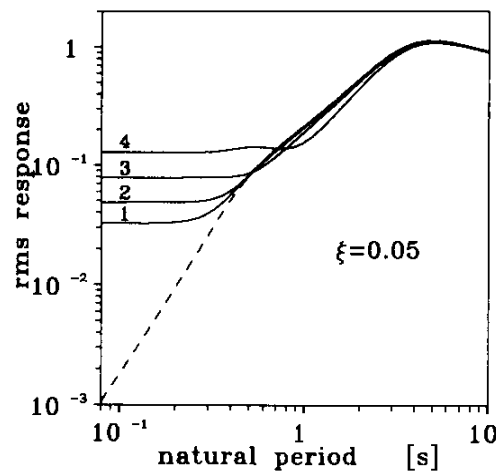


Fig. 5 RMS response spectrum for separation distance $d = 0$ (dashed line) and $d = 50, 100, 200, 400$ m (solid lines, '1', '2', '3' and '4', respectively) (after Zembaty and Krenk, 1993)

The RMS response spectra can be normalized with respect to coherent excitations ($d = 0$). This leads to the following displacement and force response ratios:

$$\Phi_q(\omega_0) = \frac{\sigma_q(\omega_0)}{\sigma_q^{\text{coher}}(\omega_0)} \quad (23)$$

$$\Phi_f(\omega_0) = \frac{\sigma_f(\omega_0)}{\sigma_f^{\text{coher}}(\omega_0)} \quad (24)$$

It can be seen that the response spectra are controlled by three parameters: loss of coherency $|\gamma_{AB}(\omega)|$ measured by the parameter κ , support distance d , and the velocity of wave propagation v_g . To make the analysis more clear, a reduced velocity, $v_r = v_g / d$, and a parameter of reduced loss of coherency, $\kappa_r = \kappa d$, are introduced now. The reduced velocity measures the apparent wave velocity in terms of support distance d , while κ_r is a measure of the actual loss of coherency. With these changes, the equation for complex coherency takes the following form:

$$\gamma_{AB}(\omega, \kappa_r, v_r) = \exp\left[-(\kappa_r \omega)^2\right] \exp[i\omega / v_r] \quad (25)$$

Substituting for the complex coherency in Equations (18) and (20), its exponential form (Equation (25)), and applying Euler's formula gives the following results for displacement and force spectral densities:

$$S_q(\omega, \omega_0, \kappa_r, \nu_r) = \frac{1}{2} |H(\omega, \omega_0)|^2 [1 + |\gamma_{AB}(\omega, \kappa_r)| \cos(\omega / \nu_r)] S(\omega) \quad (26)$$

$$S_f(\omega, \omega_0, \kappa_r, \nu_r) = \frac{k^2}{8} \left(\frac{1}{\omega^4} [1 - |\gamma_{AB}(\omega, \kappa_r)| \cos(\omega / \nu_r)] + |H(\omega, \omega_0)|^2 [1 + |\gamma_{AB}(\omega)| \cos(\omega / \nu_r)] \right) S(\omega) \quad (27)$$

We illustrate the effects of κ_r and ν_r on the displacement (see Figure 6) and force response ratio (see Figure 7) for natural period $T_0 = 1$ s ($\omega_0 = 2\pi$ rad/s). The displacement spectrum always stays below 1, expressing the fact that the combined displacements represent the averaging effect of both support excitations. On the other hand, the force ratio stays either below 1 or above 1, mostly when the velocity is low or κ_r is high (i.e., faster loss of coherency). The values of Φ_f greater than 1 indicate a non-conservative result of spatial seismic effects, occurring mostly in situations when the pseudo-static effects dominate the structural vibrations. It can be seen from Figure 7 that the effect of parameter κ_r on the force response ratio is more important for higher velocities than for the lower ones.

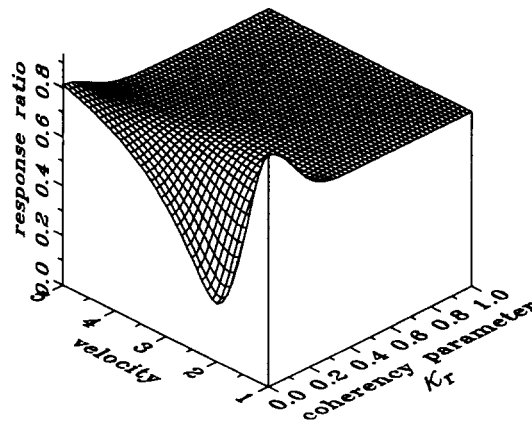


Fig. 6 Effect of loss of coherency κ_r and reduced velocity ν_r on the displacement response ratio for $\omega_0 = 2\pi$ rad/s and $\xi = 0.05$ (after Zembaty, 1996)

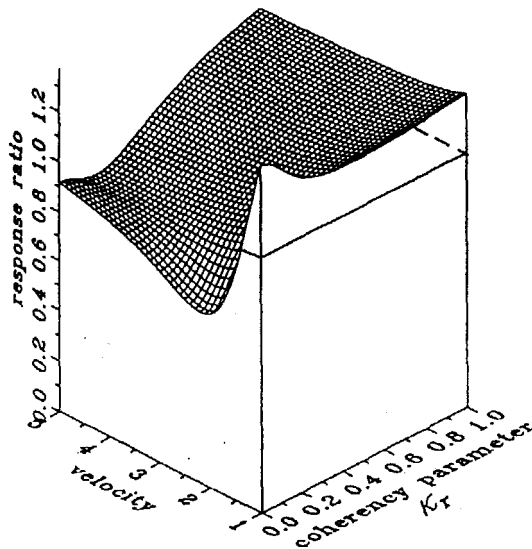


Fig. 7 Effect of loss of coherency κ_r and reduced velocity ν_r on the force response ratio for $\omega_0 = 2\pi$ rad/s and $\xi = 0.05$ (after Zembaty, 1996)

Next, consider various limits of coefficients Φ_q and Φ_f (see Equations (23) and (24)). When $|\gamma_{AB}|$ goes to 1 (or κ_r goes to 0), there is no loss of coherency for the excitations at points *A* and *B* (e.g., for short support distance or no wave attenuation), and only the wave passage contributes to the spatial effects. Equations (26) and (27) then simplify to

$$S_q(\omega, \omega_0, \kappa_r, v_r) = \frac{1}{2} |H(\omega, \omega_0)|^2 [1 + \cos(\omega / v_r)] S(\omega) \quad (28)$$

$$S_f(\omega, \omega_0, \kappa_r, v_r) = \frac{k^2}{8} \left(\frac{1}{\omega^4} [1 - \cos(\omega / v_r)] + |H(\omega, \omega_0)|^2 [1 + \cos(\omega / v_r)] \right) S(\omega) \quad (29)$$

The displacement response ratio (see Equations (23) and (28)) and the force response ratio (see Equations (24) and (29)) are shown in Figures 8 and 9, respectively, as the functions of natural frequency and velocity for v_r varying from 1 to 5. The displacement ratio is always less than 1 and oscillates rapidly with both natural frequency and velocity. On the other hand, the force ratio can be either less or greater than 1, depending upon the natural frequency and velocity. For a low natural frequency, the force ratio increases with increasing velocity and approaches 1. For a higher natural frequency the force ratio decreases with increasing velocity. This difference is based on the fact that for a higher natural frequency and lower velocity the pseudo-static motion dominates in the force response.

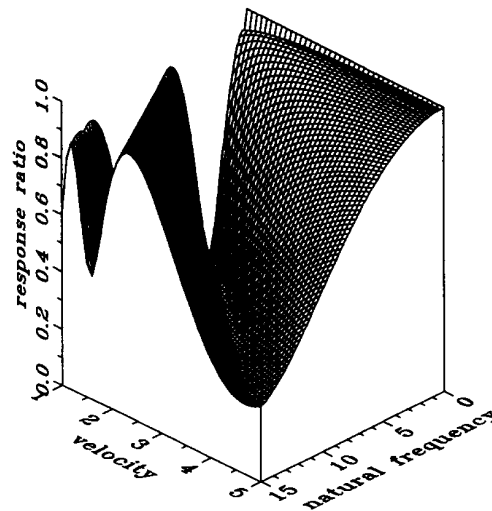


Fig. 8 Displacement response ratio (Equations (15) and (23)) versus reduced velocity v_r and natural frequency ω_0 (after Zembaty, 1996)

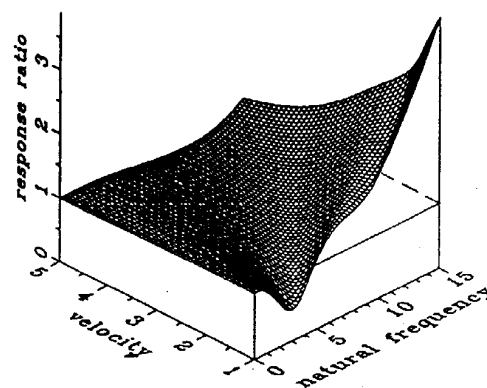


Fig. 9 Force response ratio (Equations (20) and (24)) versus reduced velocity v_r and natural frequency ω_0 (after Zembaty, 1996)

Consider now a situation in which $|\gamma_{AB}|$ goes to 0 (or κ_r goes to infinity):

$$S_q(\omega, \omega_0, \kappa_r, \nu_r) = \frac{1}{2} |H(\omega, \omega_0)|^2 S(\omega) \quad (30)$$

$$S_f(\omega, \omega_0, \kappa_r, \nu_r) = \frac{k^2}{8} \left(\frac{1}{\omega^4} + |H(\omega, \omega_0)|^2 \right) S(\omega) \quad (31)$$

In this case there is a total loss of coherency between support points, regardless of the distance or wave velocity. The oscillating cosine terms (from wave propagation) vanish. The displacement spectral density equals just half of the solution for uniform excitations. The force spectral density displays two terms contributing to both the pseudo-static and dynamic motions.

Next, we consider the limits of Equations (26) and (27) when the reduced velocity ν_r goes to infinity. The spectral densities depend now only upon the loss of coherency, and again the oscillating terms vanish:

$$S_q(\omega, \omega_0, \kappa_r, \nu_r) = \frac{1}{2} |H(\omega, \omega_0)|^2 [1 + |\gamma_{AB}(\omega, \kappa_r)|] S(\omega) \quad (32)$$

$$S_f(\omega, \omega_0, \kappa_r, \nu_r) = \frac{k^2}{8} \left(\frac{1}{\omega^4} [1 - |\gamma_{AB}(\omega, \kappa_r)|] + |H(\omega, \omega_0)|^2 [1 + |\gamma_{AB}(\omega)|] \right) S(\omega) \quad (33)$$

If ν_r goes to 0, formulas as in Equations (26) and (27) diverge and the outcome cannot be predicted.

2. Spatial Response Spectra and Local Site Effects

We consider next a situation depicted schematically in Figure 10. The simple two-support oscillator shown in Figure 2 is now supported with its left column (*A*) on a rock outcrop, while its right column (*B*) is on a soil layer overlaying the bedrock. Such a situation may easily happen for folded sedimentary rocks exposed at the surface or in the basins generated by the folding of sedimentary rocks in alluvial river valleys. In such cases, the significant lateral heterogeneity may be observed even for the adjacent sites, for which the wave passage effects and loss of coherency effects may be less important. For this reason, and to make further analysis more clear, it is assumed now that only site effects are considered and that there is “neither loss of coherency nor wave passage between the sites *A* and *B*” (the “bedrock” motion $x(t)$ in Figure 10 is assumed to be identical for the two sites). The site effects are modeled by the local soil frequency response functions $H_A(\omega)$ and $H_B(\omega)$ at the two stations. This leads to the following relation between the bedrock acceleration cross-spectral density $S_{AB}^{(b)}(\omega)$ and the surface acceleration cross-spectral density $S_{AB}^{(r)}(\omega)$:

$$S_{AB}^{(r)}(\omega) = H_A(\omega) H_B^* S_{AB}^{(b)}(\omega) \quad (34)$$

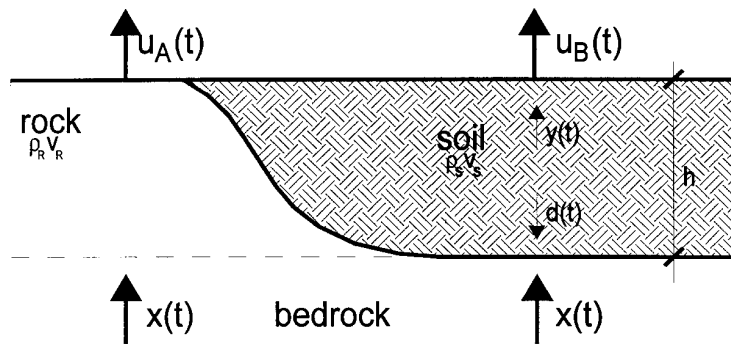


Fig. 10 Ground motion from bedrock to the surface for rock outcrop (left) and for a soil layer (right) (after Zembaty and Rutenberg, 2002)

When the two sites *A* and *B* coincide, these cross-spectra reduce to the respective auto-spectra, and instead of Equation (34) we can write two equations for the sites *A* and *B*:

$$S_{AA}^{(r)}(\omega) = |H_A(\omega)|^2 S_{AA}^{(b)}(\omega) \quad (35a)$$

$$S_{BB}^{(r)}(\omega) = |H_B(\omega)|^2 S_{BB}^{(b)}(\omega) \quad (35b)$$

When only the site effects are considered, as is the case for this point, the complex coherency γ_{AB} includes only the third term of Equation (3):

$$\gamma_{AB}(\omega) = \gamma_{AB}^{(s)}(\omega) = \exp[i\Theta_{AB}^{(s)}(\omega)] \quad (36)$$

with the phase difference $\Theta_{AB}^{(s)}(\omega)$ given by

$$\Theta_{AB}^{(s)}(\omega) = \arctan \frac{\text{Im}[H_A(\omega)H_B^*(\omega)]}{\text{Re}[H_A(\omega)H_B^*(\omega)]} \quad (37)$$

Using Equations (10) and (11) and applying the orthogonality property (Equation (8)) together with the co-spectral matrix (Equation (12)), we can obtain the mean square displacements from

$$S_q(\omega, \omega_0) = \frac{1}{2} |H|^2 \left(\frac{|H_A|^2 + |H_B|^2}{2} + |H_A| |H_B| \text{Re}(\gamma_{AB}) \right) S \quad (38)$$

and forces from

$$S_{f_A}(\omega, \omega_0) = \frac{k^2}{8} \left\{ \frac{1}{\omega^4} \left[\frac{|H_A|^2 + |H_B|^2}{2} - |H_A| |H_B| \text{Re}(\gamma_{AB}) \right] - \frac{2}{\omega^2} \left(\frac{|H_A|^2 - |H_B|^2}{2} \text{Re} H + |H_A| |H_B| \text{Im} H \text{Im}(\gamma_{AB}) \right) + |H|^2 \left[\frac{|H_A|^2 + |H_B|^2}{2} + |H_A| |H_B| \text{Re}(\gamma_{AB}) \right] \right\} S \quad (39a)$$

$$S_{f_B}(\omega, \omega_0) = \frac{k^2}{8} \left\{ \frac{1}{\omega^4} \left[\frac{|H_A|^2 + |H_B|^2}{2} - |H_A| |H_B| \text{Re}(\gamma_{AB}) \right] - \frac{2}{\omega^2} \left(\frac{|H_A|^2 - |H_B|^2}{2} \text{Re} H + |H_A| |H_B| \text{Im} H \text{Im}(\gamma_{AB}) \right) + |H|^2 \left[\frac{|H_A|^2 + |H_B|^2}{2} + |H_A| |H_B| \text{Re}(\gamma_{AB}) \right] \right\} S \quad (39b)$$

in which the dependence on ω for the parameters on the right side of these equations is dropped for brevity. As before, the difference between forces f_A and f_B depends upon the sign of the second, cross-acceleration-displacement component. As will be shown later, the difference between these two forces may be substantial, particularly when the properties of the sites are drastically different. Integrating the spectral densities (Equations (38), (39a), and (39b)) with respect to ω leads to the RMS response

$$\sigma_{\text{resp}}^2(\omega_0) = \int_{-\infty}^{\infty} S_{\text{resp}}(\omega, \omega_0) d\omega \quad (40)$$

where subscript 'resp' represents either displacement q or force f_A or f_B . Normalization of the resulting RMS response may be done with respect to the RMS response at the soil site at one of the two points A or B or with respect to the rock properties at both sites. The latter normalization seems more appropriate in this case:

$$\Phi(\omega_0) = \frac{\sigma_{\text{resp}}(\omega_0)}{\sigma_{\text{resp}}^{\text{rock}}(\omega_0)} \quad (41)$$

Next, we present selected examples of the sensitivity analysis of the above spatial seismic coefficient for the SDOF system shown in Figure 2, when it is resting on a rock-soil system (see Figure 10). Adopting the soil model of Safak (1995), after some algebra (Zembaty and Rutenberg, 2002), transfer function of the soil layer is obtained as

$$H_s(\omega) = \frac{\left(1 + r - \frac{i}{4Q}\right) \exp[-i\omega\tau_s(1 - i/2Q)]}{1 + \left(r - \frac{i}{4Q}\right) \exp[-2i\omega\tau_s(1 - i/2Q)]} \quad (42)$$

in which τ_s is the S-wave propagation time in soil ($\tau_s = h/\nu_s$; see Figure 10), and Q is the quality factor measuring the ability of the medium to attenuate seismic waves. This can be related to the soil damping ratio as $\xi_{\text{soil}} = 1/(2Q)$. Finally, r is the wave-reflection coefficient:

$$r = \frac{\rho_R \nu_R - \rho_S \nu_S}{\rho_R \nu_R + \rho_S \nu_S} \quad (43)$$

for two media with mass densities, ρ_R and ρ_S , and S-wave velocities, ν_R and ν_S (here, these media are rock and soil, respectively). An analogous measure of the two media interfaces can be given by the rock/soil impedance ratio (e.g., Roesset, 1977):

$$I_{R/S} = \frac{\rho_R \nu_R}{\rho_S \nu_S} \quad (44)$$

In contrast to the soil transfer function $H_s(\omega)$, the transfer function of the rock outcrop represents only the propagation time in rock $\tau_R = h/\nu_R$ and equals

$$H_R(\omega) = \exp(-i\omega\tau_R) \quad (45)$$

Consider now the rock and soil parameters as follows: $\rho_R = 3 \text{ g/cm}^3$, $\nu_R = 1500 \text{ m/s}$, $\rho_S = 2 \text{ g/cm}^3$, $\nu_S = 750 \text{ m/s}$, $h = 150 \text{ m}$, $Q = 30$. For these data, the reflection coefficient $r = 0.5$; propagation times in soil and rock are, respectively, $\tau_s = 0.2 \text{ s}$, $\tau_R = 0.1 \text{ s}$; and the first three soil “resonant” frequencies are 7.85, 23.6, and 39.3 rad/s (i.e., the peaks of transfer functions from Equations (39a) and (39b)). In Figure 11, the spectral density of displacements (as in Equation (38); see upper part of the figure) and forces f_A and f_B (as in Equations (39a) and (39b); see lower part of the figure) are plotted for the oscillator with $\omega_0 = 2 \text{ rad/s}$ ($T_0 = 1 \text{ s}$). The displacement spectral density is that of a typical oscillator response to wide-band excitations, with most of the spectrum concentrated about the resonant frequency $\omega_0 = 2\pi$. On the other hand, in addition to the resonance peak, the force spectral densities display a low frequency “peak” resulting from the pseudo-static component of motion. The difference between the spectral densities of the forces f_A and f_B is very small for the above values of soil and oscillator parameters, and the presence of soil resonance cannot be seen in the displacement spectral density plots. Also, the second resonance of the forces at $\omega = 23.6 \text{ rad/s}$ can hardly be detected (see the lower part of Figure 11).

Next, consider the mean-square response. The RMS displacement response spectrum is shown in Figure 12(a) for the soil parameters, $\rho_S = 2 \text{ g/cm}^3$, $\nu_S = 750 \text{ m/s}$, $Q = 30$, and soil depth $h = 150 \text{ m}$. The same displacement response spectrum is shown again in Figure 12(b), after normalization with respect to Equation (41). The two plots in Figures 12(a) and 12(b) differ substantially. As would be expected, the RMS displacement response spectrum decreases steadily as T_0 goes to zero. In contrast, the normalized plot stays well below 1 for T_0 less than about 0.1 s, showing some excursions above 1 for $0.1 < T_0 < 1$, and it decays to 1 for $T_0 > 1$. The peaks of the plot in Figure 12(b) reflect the oscillator-soil resonance. As the natural period decreases, the peaks also decrease.

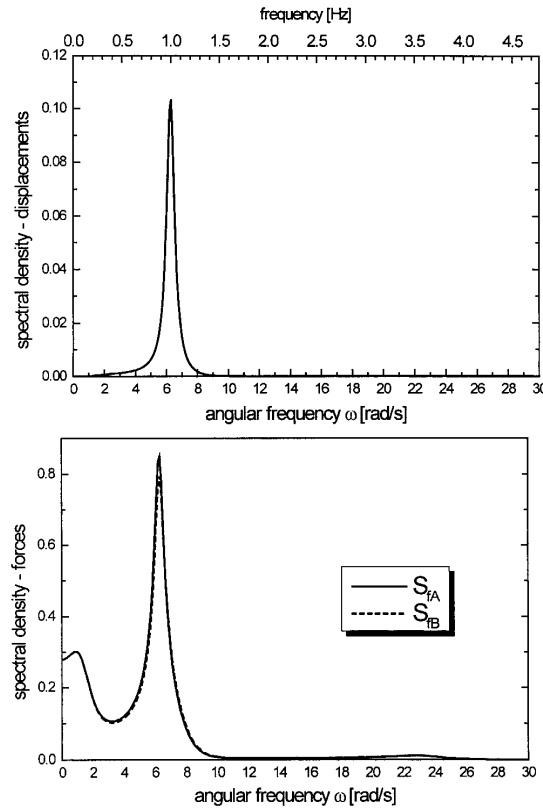


Fig. 11 SDOF system spectral densities (for $\omega_0 = 2\pi$ rad/s, $\xi = 0.05$, $\rho_R = 3$ g/cm³, $\nu_R = 1500$ m/s, $\rho_S = 2$ g/cm³, $\nu_S = 750$ m/s, $h = 150$ m, $Q = 30$, $r = 0.5$): displacements (upper) and forces f_A and f_B (lower) (after Zembaty and Rutenberg, 2002)

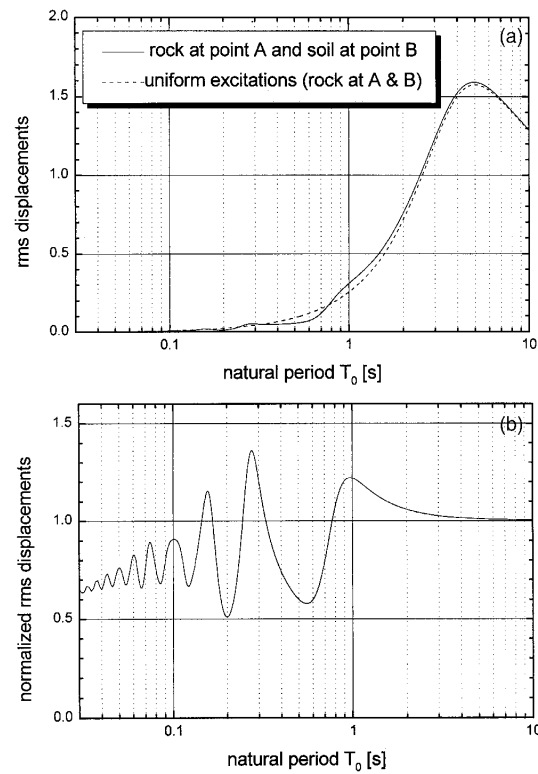


Fig. 12 RMS response spectra for (a) displacements, and (b) displacements normalized with respect to uniform excitations at A and B (rock at both sites) (after Zembaty and Rutenberg, 2002)

The plots of force response spectra (for forces f_A and f_B) are shown for the same set of parameters ($\rho_s = 2 \text{ g/cm}^3$, $v_s = 750 \text{ m/s}$, $Q = 30$) in Figure 13. Unlike the displacements, the force response spectra in Figure 13(a) do not vanish with falling T_0 . This is due to the fact that as the inertial effects are reduced, the pseudo-static effects remain, and the response spectra stabilize at some level. In contrast, the force response spectra calculated for uniform excitations go down to zero (similarly as the displacements do) because in this case the pseudo-static effects do not induce forces, i.e., there is no differential motion between the two supports. Thus, the normalized RMS forces increase to infinity with vanishing natural period. Similar effects can be observed when considering the wave-passage effects for multi-support structures on uniform soil (Trifunac and Todorovska, 1997; Zembaty and Krenk, 1993; Zembaty, 1996). Obviously, the large values of the normalized response at very low natural periods shown in Figure 13(b) represent in some cases an “artificial” effect, as soil compliance can reduce it substantially.

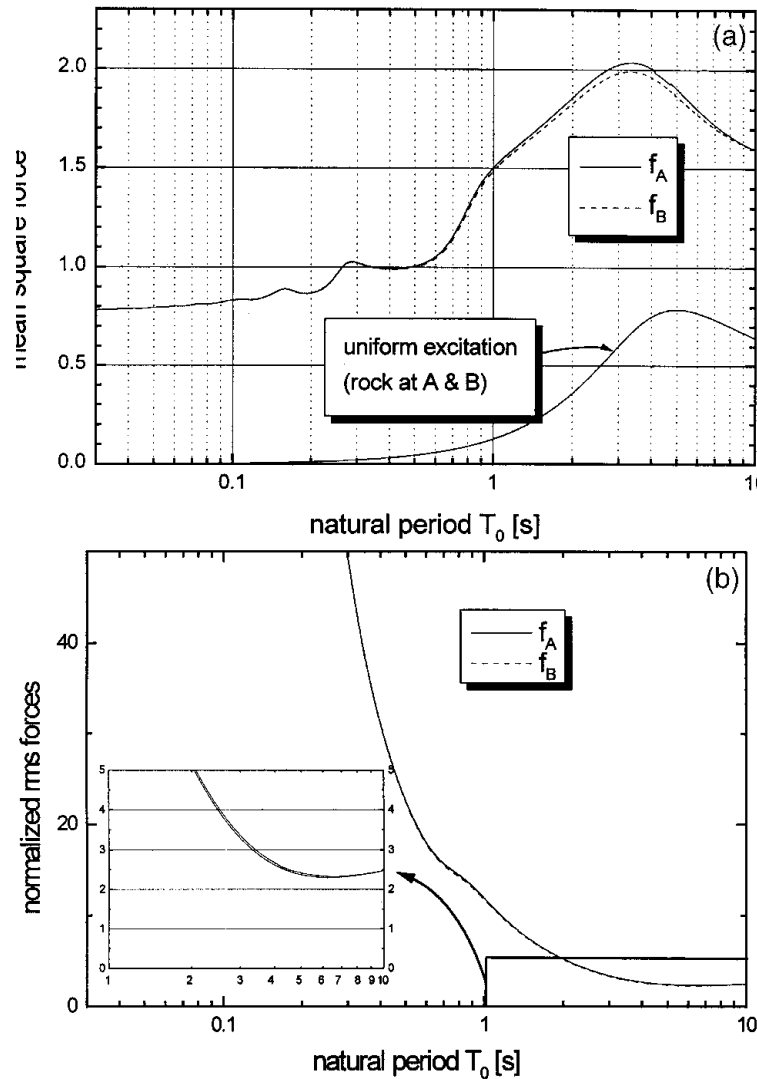


Fig. 13 (a) Spectra for forces f_A and f_B ; (b) Force spectra normalized with respect to uniform excitations (rock at A and B) (after Zembaty and Rutenberg, 2002)

Finally, the ranges of the analyzed response spectra are illustrated in Figure 14 for $v_s = 750 \text{ m/s}$ and ρ_s varying from 2 to 3 g/cm^3 (see Figures 14(a) and 14(c)), as well as for $v_s = 200 \text{ m/s}$ and $\rho_s = 1.5$ –2.5 g/cm^3 (see Figures 14(b) and 14(d)). These two values of v_s represent firm (soft) rock and very soft soils, respectively. The range of ρ_s represents variations in soil properties that are likely to be found in practice. The corresponding variations of the rock/soil impedance ratio range from 2 to 3 for $v_s =$

750 m/s, and from 9 to 15 for $\nu_s = 200$ m/s. As can be seen from the plots in Figures 14(a)–14(d), these variations of soil properties do not substantially affect the results for firm soil ($\nu_s = 750$ m/s). They do affect the displacements and force response spectra for soft soils ($\nu_s = 200$ m/s), but only for the first resonance peak at $T_0 \approx 3$ s. For the force response spectra and $\nu_s = 200$ m/s, a shift in the first resonance peaks of forces f_A and f_B can be observed. It can also be seen that the differences among shear forces f_A and f_B can be more pronounced even for quite realistic values of soil parameters.

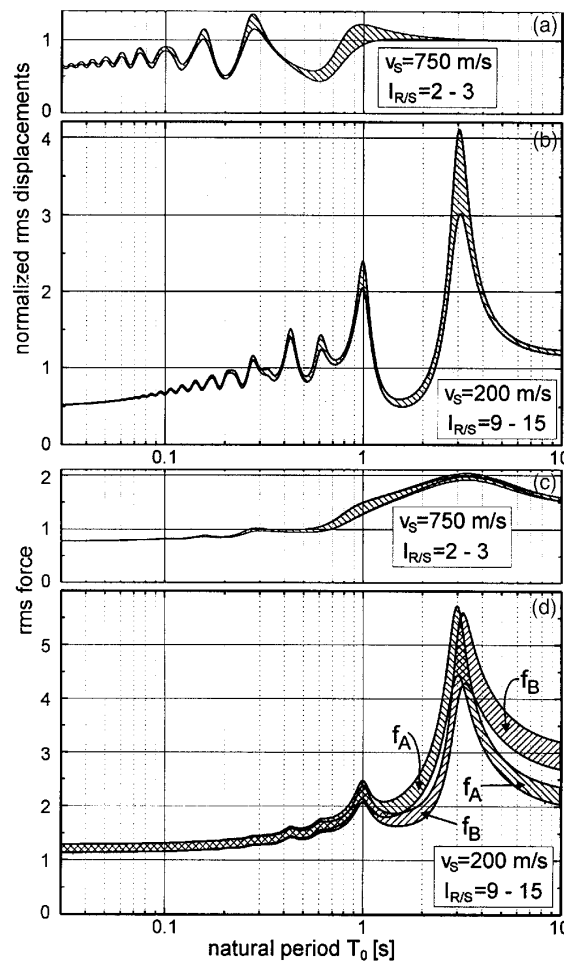


Fig. 14 Range of normalized displacement response spectra ((a), (b)) and force response spectra ((c), (d)) reflecting the range of soil densities $\rho_s = 1.5\text{--}2.0$ g/cm³ for $\nu_s = 750$ m/s ($r = 0.333\text{--}0.500$, shear moduli $G_s = 1125\text{--}1687$ MPa, $I_{R/S} = 2\text{--}3$), and densities $\rho_s = 1.5\text{--}2.0$ g/cm³ for $\nu_s = 200$ m/s ($r = 0.800\text{--}0.875$, $I_{R/S} = 9\text{--}15$) (after Zembaty and Rutenberg, 2002)

RESPONSE SPECTRA FOR COLUMN VIBRATIONS UNDER KINEMATIC WAVE EXCITATIONS

1. Response Spectra for In-plane Differential Motion of Columns of a Building Structure

Trifunac and Todorovska (1997) explored another approach to the problem of spatial seismic response spectra. They analyzed a multi-support, multi-column structure with a stiff first floor (see Figure 15). This structure is excited by the horizontal ground motions $u_1(t), u_2(t), \dots, u_n(t)$ and is situated along the radial direction of the wave propagation from the earthquake source (it is the most

conservative assumption in this case). Two types of waves may take part in these excitations: body waves incident with some angle γ , and surface (Rayleigh) waves. To simplify the analysis, the equivalent phase velocity c_{eq} was introduced, which is constant in time and frequency domain and represents all of the surface wave modes and the body waves propagating among the supports of the structure (Trifunac and Lee, 1996; Trifunac et al., 1996). Based on the detailed experimental data (Trifunac, 1971; Bycroft, 1983), it was possible to assume $c_{eq} \approx \beta_{av}$, where β_{av} is the average shear-wave velocity in the top 30 m below the ground surface. Next, a special reference point R on the ground surface was defined (see Figure 15), to which the individual support motion $u_i(t)$ was related. The point R was defined in such a way that its displacement $u_0(t)$ was a weighted average of the motions at the base of the columns:

$$u_0(t) = \frac{\sum_{i=1}^n k_i u_i(t)}{\sum_{i=1}^n k_i} \quad (46)$$

By considering the strain field in the ground, together with limits for the possible wavelengths along the structure, and by making further detailed assumptions based on earlier experimental studies (Trifunac and Lee, 1996; Trifunac et al., 1996), Trifunac and Todorovska (1997) proposed quite a simple formulation of the response spectrum for differential motion of columns defined for the one-storey structure of Figure 15:

$$SDC(T, \xi, \tau) = \max_t \left[u^r(t) + v(t)\tau - \frac{1}{2}a(t)\tau^2 \right] \quad (47)$$

Here, T stands for the natural period of the structure, ξ is the damping ratio, u^r denotes the relative displacements of the mass (with respect to the reference point R), $v(t)$ and $a(t)$ stand for the velocity and acceleration of the point R , and finally τ is the time required for a wave to propagate from the point R to the i th analyzed column. Assuming reasonable building dimensions and taking into account realistic, experimentally verified wavelengths the values of τ were suggested to stay between 0.001 and 0.1 s.

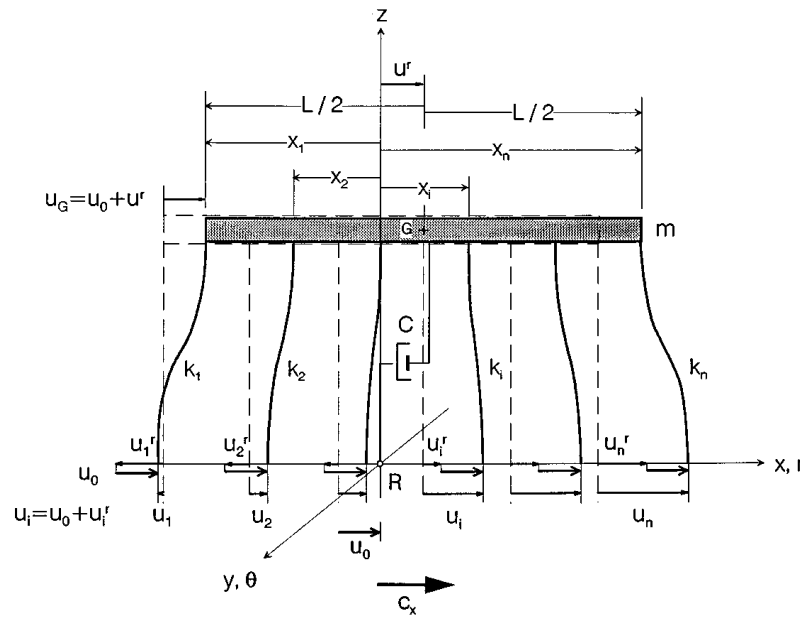


Fig. 15 Model of the one-storey structure excited by horizontal components of Rayleigh and/or SV waves (the columns have stiffness k_i ; absolute displacement at the base of the i th column is u_i ; the point R and the z axis move with displacement u_0 ; the displacement of the mass relative to the point R is u^r) (after Trifunac and Todorovska, 1997)

To include in the analysis the multi-storey buildings vibrating in their first natural mode, an equivalent SDOF system was analyzed (see Figure 16). After a detailed modal analysis, which took into account characteristic simplifications relevant to the multi-storey buildings, an additional parameter δ was added to the whole analysis. This parameter equals 1 for the one-storey structural model of Figure 15, while for a multi-storey building it depends on the number of its storeys as well as on the assumed shape of the 1st mode (sinusoidal or straight line). For example, δ is 0.15 for a 10-storey building with the first natural period $T_1 = 1$ s. Again, the respective response spectrum definition has a very simple form:

$$SDC(T_1, \delta, \xi, \tau) = \max_t \left[u^r(t) \delta + v(t) \tau - \frac{1}{2} a(t) \tau^2 \right] \quad (48)$$

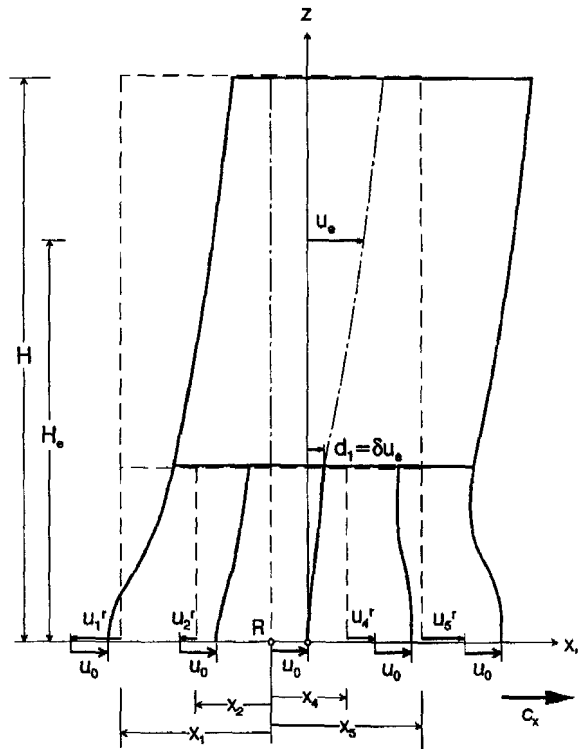


Fig. 16 A multi-storey building excited by asynchronous motion at the base of the first-storey columns (point R and the z axis move with the displacement u_0 ; u_c is the relative displacement of the equivalent SDOF oscillator excited by the acceleration $\ddot{u}_0(t)$, and d_1 is the relative displacement of the first storey) (after Trifunac and Todorovska, 1997)

The SDC spectra can be easily calculated from the existing earthquake records for specific values of δ characteristic of certain building types, with values of τ specified according to column configurations and wave patterns specific for particular ground conditions. Furthermore, as shown by Trifunac and Todorovska (1997), the SDC response spectrum (see Equation (48)) can effectively be approximated by the “square-root-of-sum-of-squares” rule as follows:

$$SDC(T_1, \delta, \xi, \tau) \approx \left[\delta^2 SD^2(T, \xi) + (v_{\max} \tau)^2 - \left(\frac{1}{2} a_{\max} \tau^2 \right)^2 \right]^{1/2} \quad (49)$$

where $SD(T, \xi)$ is the familiar displacement response spectrum while v_{\max} and a_{\max} denote the respective maxima of $v(t)$ and $a(t)$.

In Figure 17, the plots of the column differential response spectra for a one-storey structure ($\delta = 1$) and damping ratio $\xi = 0.05$ are illustrated for various values of τ , with solid lines denoting the application of Equation (48) and dashed lines denoting the approximation (as in Equation (49)). It is interesting to note the flat zones on the left side of Figure 17, in which the SDC response spectrum diverges from the classic displacement response spectrum. It shows the domination of the pseudo-static

component in the structural response for short-natural-period (stiff) buildings. This result can also be observed in the independently obtained plot of force spatial response spectrum as shown in Figure 5.

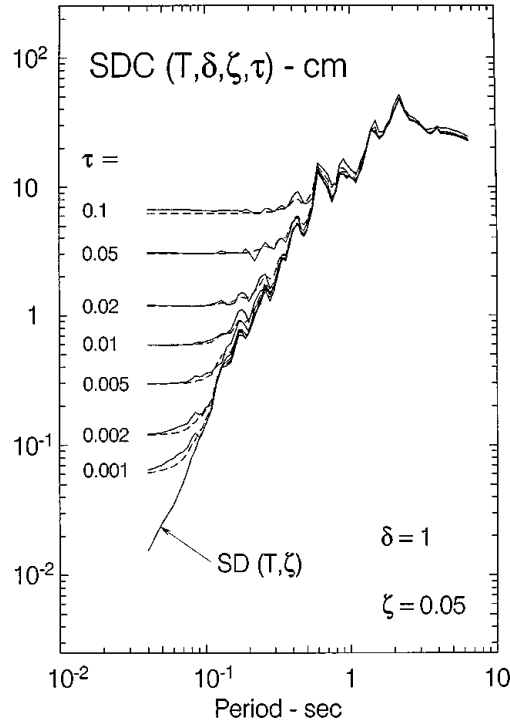


Fig. 17 In-plane building column response spectrum for the S16W component of the acceleration recorded at Station # 53 of the Los Angeles Strong Motion Network during the Northridge, CA, earthquake of 17 January 1994 ($M = 6.7$), at the epicentral distance of 6 km with $\xi = 0.05$ and $\delta = 1$ (one-storey building) (solid line is for Equation (48), and dashed-line approximation for Equation (49)) (after Trifunac and Todorovska, 1997)

2. Response Spectra for Differential, Out-of-plane Motion of Columns of a Building Structure

Figure 18 illustrates the model analyzed by Trifunac and Gicev (2006). In this case, the out-of-plane differential motion of columns, omitted in the analysis of the previous example, is analyzed. Such a motion can be caused by the passage of SH or Love waves among the columns of the structure. The analyzed two-degrees-of-freedom structural model is depicted in Figure 19. As for the in-plane motions, a reference point R is adopted. Its motion $u_0(t)$ (see Equation (46)) represents the ground motion averaged over the length of the structure L . In contrast to the previous example, this time the stiffness k_i works with the out-of-plane component of the motion (see Figure 19). The primary difference between the present and the previous example is the fact that this structural model has following two degrees of freedom:

- transversal motion of the rigid floor with mass m , and
- torsional motion of this floor about the vertical axis through R .

In the analysis presented by Trifunac and Gicev (2006), analogous assumptions are made, as in the paper of Trifunac and Todorovska (1997). In particular, an equivalent phase velocity c_{eq} is defined to represent both body and surface wave effects. Under conditions described by Trifunac and Gicev (2006), the two dynamic degrees of freedom are uncoupled, and the out-of-plane differential response spectra for the columns in the one-storey model of Figure 18 can be described by

$$SDC(T, T_T, \xi, \xi_T, \tau) = \max_i \left[u_r(t) + \Theta(t)x_i v(t)\tau - \frac{1}{2}a(t)\tau^2 \right] \quad (50)$$

where $u_r(t)$ and $\Theta(t)$ are the displacement and torsion of the rigid mass, respectively (see Figure 19), while $v(t)$ and $a(t)$ are the velocity and acceleration of the reference point R . The maxima of the above

four components of the SDC response spectrum occur generally at different time instants, which complicates the analysis. However, assuming that $\Theta_{\max} x_i \approx v_{\max} \tau_i$, neglecting the contribution of $a(t)$ (i.e., the term of Equation (42) with the multiplier, τ^2), and using, as previously, the “root-of-sum-of-squares” approximation, further simplifications can be made and the SDC spectrum can be approximated as

$$SDC(T, T_T, \xi, \xi_T, \tau) \approx \left[u_{r\max}^2 + 2(v_{\max} \tau)^2 \right]^{1/2} \quad (51)$$

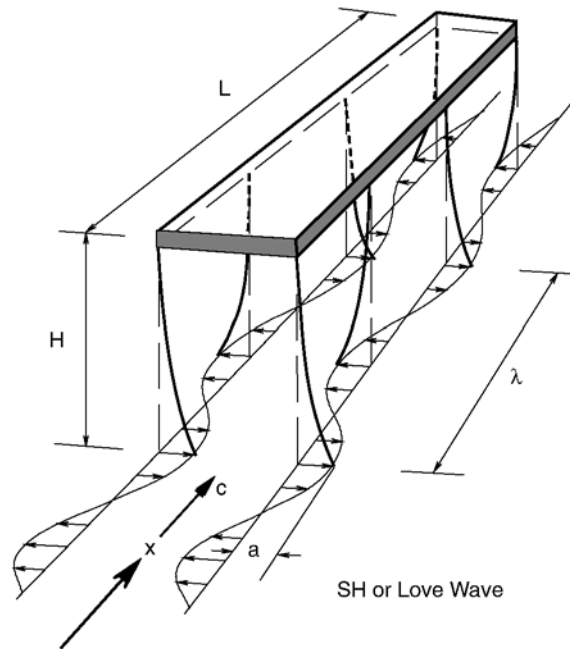


Fig. 18 One-storey structure excited by Love and/or SH waves propagating along its long dimension (after Trifunac and Gicev, 2006)

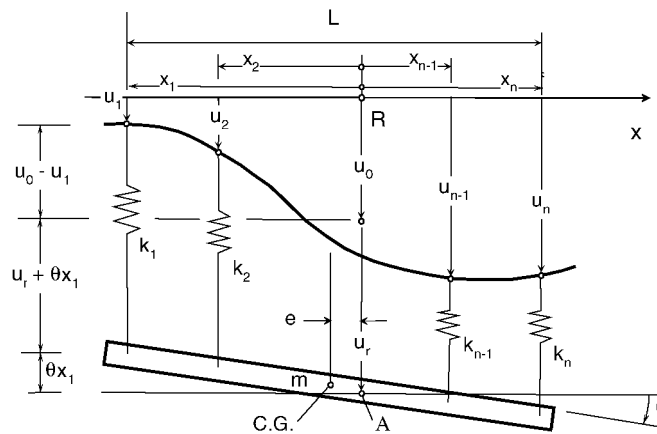


Fig. 19 Simplified 2-DOF model of the structure shown in Figure 18 (after Trifunac and Gicev, 2006)

The out-of-plane SDC spectrum can be generalized further to include, as in the previous example, the effects of differential ground motions on the first-storey columns of a multi-storey building responding in the first vibration mode. In this case, the torsional mode can be approximated by a straight line, and the SDC spectrum for the i th column becomes

$$SDC(T, T_T, \xi, \xi_T, \tau, \delta) = \max_t \left[\delta u_r(t) + \delta \Theta(t) x_i + v(t) \tau_i - \frac{1}{2} a(t) \tau_i^2 \right] \quad (52)$$

With further simplifications (Trifunac and Gicev, 2006), this response spectrum can be approximated by

$$SDC(T, T_T, \xi, \xi_T, \tau) \approx \left[\delta^2 SD^2(T, \xi) + (1 + \delta)(v_{\max} \tau_i)^2 \right]^{1/2} \quad (53)$$

To plot any of the above response spectra, a particular ratio between the transversal natural period T and the torsional period T_T should be established (for a typical building, T/T_T can be, for example, equal to $\sqrt{3} \approx 1.73$).

In Figure 20, the SDC spectrum calculated for a single-storey structural model ($\delta = 1$) is illustrated for various values of τ and compared with the ordinary displacement response spectrum. The solid lines in this figure represent the application of Equation (52), while the dashed lines denote the approximation as in Equation (53). On comparing the plots of Figure 20 with those of Figure 17 (longitudinal vibrations) it can be noted that they are quite similar but due to the additional contributions from torsional vibrations, the spectra in Figure 20 are larger than those in Figure 17.

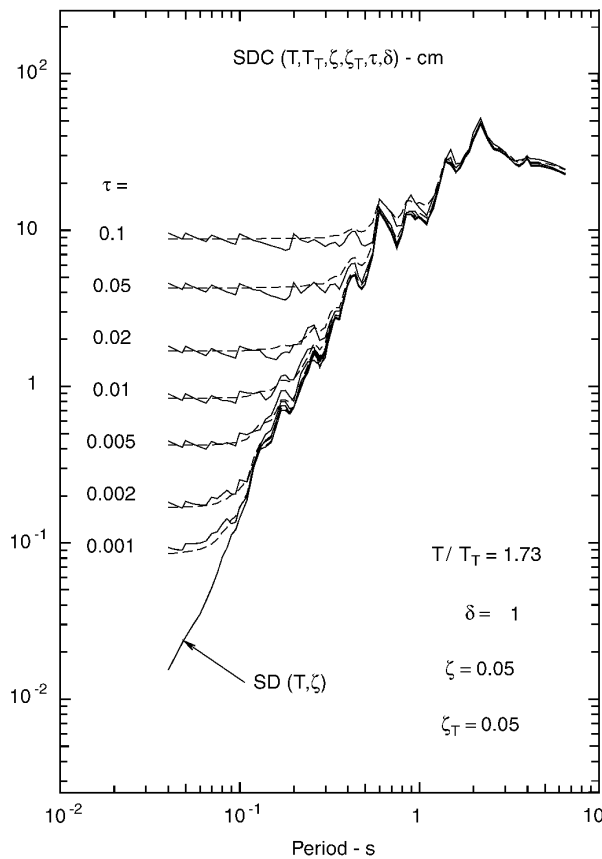


Fig. 20 Out-of-plane SDC response spectrum for the S16W component of the acceleration recorded at Station # 53 of the Los Angeles Strong Motion Network during the Northridge, CA, earthquake of 17 January 1994 ($M = 6.7$), at the epicentral distance of 6 km with $\xi = 0.05$ and $\delta = 1$ (one-storey building) (solid line is for Equation (52), and dashed-line approximation for Equation (53)) (after Trifunac and Gicev, 2006)

SUMMARY AND CONCLUSIONS

Examples of different extensions of the response spectrum method to include the consequences of spatial variations and of propagation of seismic waves were briefly reviewed. Two approaches were described in some detail: random vibrations of a simple SDOF system with two-component seismic excitations, and a multi-component column response spectrum for the multi-storey buildings.

While the random vibration approach is based on rational analyses of the seismic data from dense arrays of synchronized accelerometers (e.g., SMART-1), it actually does not allow in-depth analyses of the specific wave-passage effects due to temporal averaging included in the stochastic processing of the data. That is why the alternative approach using the waves propagating along the columns of a building sheds new light on the problem of spatial seismic effects on structures. It still requires approximations, but their validity can be carefully verified by analyzing a number of recent records of strong ground motion. In particular, it is interesting that such an intuitive, engineering notion as “apparent wave velocity” could also be derived from experimental wave-passage analyses as “equivalent phase velocity”. Both approaches indicate the importance of the spatial seismic effects for the short-period stiff structures (see Figures 5, 17, and 20), but the differences in the local site effects can also be important (as shown in Figures 12–14), thus contributing further to the complexity of the problem.

The need for future research in this area should be apparent. Detailed analyses of wave passages, the role of group velocities of strong motion waves, and of the rotational components of seismic ground motion, will lead to the development of more detailed models of spatial seismic effects on structures. Modern suspension bridges may have their supports as far as 2 km apart (e.g., Akashi bridge in Japan), with the existing designs approaching a 3.3-km span (Messina bridge in Italy). In such cases, the effects of nonstationarity of spatial seismic random fields cannot be neglected. This and further refinements involving soil-structure interaction effects among the multi-support foundations will be the challenging new areas of research for future investigations.

ACKNOWLEDGEMENTS

The author is grateful to Prof. M.D. Trifunac for his valuable suggestions, advice and correction of the manuscript.

APPENDIX I: POWER SPECTRAL DENSITY OF SEISMIC GROUND MOTION

The popular engineering model of power spectral density of the seismic accelerations was proposed by Kanai (1957) and Tajimi (1960):

$$S(\omega) = \frac{\omega_g^4 + (2\xi_g \omega_g \omega)^2}{(\omega_g^2 - \omega^2)^2 + (2\xi_g \omega_g \omega)^2} S_0 \quad (\text{A.1})$$

The advantageous feature of the Kanai-Tajimi ground motion model is its ability to model local site effects by the frequency ω_g and damping ratio ξ_g , which can then be treated as the local soil parameters, while S_0 denotes the seismic intensity factor. Typical ranges for these parameters are: 2π to 6π rad/s for ω_g , and 0.2 to 0.6 for ξ_g . The Kanai-Tajimi spectrum takes an unrealistic non-zero value for $\omega = 0$. This undesirable effect has been corrected by introducing a high-pass filter, as proposed by Ruiz and Penzien (1969), leading to the following spectral density function:

$$S(\omega) = \frac{\omega_g^4 + (2\xi_g \omega_g \omega)^2}{(\omega_g^2 - \omega^2)^2 + (2\xi_g \omega_g \omega)^2} \frac{\omega^4}{(\omega_h^2 - \omega^2)^2 + (2\xi_h \omega_h \omega)^2} S_0 \quad (\text{A.2})$$

in which $\omega_h = 1.636$ and $\xi_h = 0.619$ are the constants proposed by Ruiz and Penzien (1969).

REFERENCES

1. Abrahamson, N.A. and Bolt, B.A. (1985). “The Spatial Variation of the Phasing of Seismic Strong Ground Motion”, *Bulletin of the Seismological Society of America*, Vol. 75, No. 5, pp. 1247–1264.
2. Abrahamson, N.A., Bolt, B.A., Darragh, R.B., Penzien, J. and Tsai, Y.B. (1987). “The SMART 1 Accelerograph Array (1980–1987): A Review”, *Earthquake Spectra*, Vol. 3, No. 2, pp. 263–287.
3. Abrahamson, N.A., Schneider, J.F. and Stepp, J.C. (1991). “Empirical Spatial Coherency Functions for Application to Soil-Structure Interaction Analyses”, *Earthquake Spectra*, Vol. 7, No. 1, pp. 1–27.

4. Aki, K. and Richards, P.G. (1980). "Quantitative Seismology: Theory and Methods", W.H. Freeman & Company, San Francisco, U.S.A.
5. Biot, M.A. (1932). "Transient Oscillations in Elastic Systems", Ph.D. Thesis No. 259, Aeronautics Department, California Institute of Technology, Pasadena, U.S.A.
6. Biot, M.A. (1941). "A Mechanical Analyzer for the Prediction of Earthquake Stresses", Bulletin of the Seismological Society of America, Vol. 31, No. 2, pp. 151–171.
7. Bycroft, G.N. (1983). "Differential-Ground-Motion Array at Hollister Municipal Airport, California", Open-File Report 83-327, United States Geological Survey, Denver, U.S.A.
8. Datta, T.K. (1999). "Seismic Response of Buried Pipelines: A State-of-the-Art Review", Nuclear Engineering and Design, Vol. 192, No. 2-3, pp. 271–284.
9. Der Kiureghian, A. (1980). "Structural Response to Stationary Excitation", Journal of the Engineering Mechanics Division, Proceedings of ASCE, Vol. 106, No. EM6, pp. 1195–1213.
10. Der Kiureghian, A. (1981). "A Response Spectrum Method for Random Vibration Analysis of MDF Systems", Earthquake Engineering & Structural Dynamics, Vol. 9, No. 5, pp. 419–435.
11. Der Kiureghian, A. (1996). "A Coherency Model for Spatially Varying Ground Motions", Earthquake Engineering & Structural Dynamics, Vol. 25, No. 1, pp. 99–111.
12. Der Kiureghian, A. and Neuenhofer, A. (1992). "Response Spectrum Method for Multi-Support Seismic Excitations", Earthquake Engineering & Structural Dynamics, Vol. 21, No. 8, pp. 713–740.
13. Dulinska, J. and Zieba, A. (2007). "The Effect of Mine Shocks and Quarry Blasts on Dynamic Response of a Gas Pipeline", Czasopismo Techniczne, Cracow University of Technology, Vol. 104, No. 2-B/6, pp. 19–27 (in Polish).
14. Gupta, I.D. and Trifunac, M.D. (1998). "Defining Equivalent Stationary PSDF to Account for Nonstationarity of Earthquake Ground Motion", Soil Dynamics and Earthquake Engineering, Vol. 17, No. 2, pp. 89–99.
15. Hao, H. (1989). "Effects of Spatial Variation of Ground Motions on Large Multiply-Supported Structures", Report UCB/EERC-89/06, University of California, Berkeley, U.S.A.
16. Hao, H. (1991). "Response of Multiply Supported Rigid Plate to Spatially Correlated Seismic Excitations", Earthquake Engineering & Structural Dynamics, Vol. 20, No. 9, pp. 821–838.
17. Harichandran, R.S. and Vanmarcke, E.H. (1986). "Stochastic Variation of Earthquake Ground Motion in Space and Time", Journal of Engineering Mechanics, ASCE, Vol. 112, No. 2, pp. 154–174.
18. Harichandran, R.S. and Wang, W. (1988). "Response of Simple Beam to Spatially Varying Earthquake Excitation", Journal of Engineering Mechanics, ASCE, Vol. 114, No. 9, pp. 1526–1541.
19. Harichandran, R.S. and Wang, W. (1990). "Response of Indeterminate Two-Span Beam to Spatially Varying Seismic Excitation", Earthquake Engineering & Structural Dynamics, Vol. 19, No. 2, pp. 173–187.
20. Hindy, A. and Novak, M. (1980). "Pipeline Response to Random Ground Motion", Journal of the Engineering Mechanics Division, Proceedings of ASCE, Vol. 106, No. EM2, pp. 339–360.
21. Kanai, K. (1957). "Semi-Empirical Formula for the Seismic Characteristics of the Ground", Bulletin of the Earthquake Research Institute, University of Tokyo, Vol. 35, pp. 309–325.
22. Kojic, S. and Trifunac, M.D. (1991a). "Earthquake Stresses in Arch Dams. I: Theory and Antiplane Excitation", Journal of Engineering Mechanics, ASCE, Vol. 117, No. 3, pp. 532–552.
23. Kojic, S. and Trifunac, M.D. (1991b). "Earthquake Stresses in Arch Dams. II: Excitation by SV, P and Rayleigh Waves", Journal of Engineering Mechanics, ASCE, Vol. 117, No. 3, pp. 553–574.
24. Leger, P., Ide, M.I. and Paultre, P. (1990). "Multiple-Support Seismic Analysis of Large Structures", Computers & Structures, Vol. 36, No. 6, pp. 1153–1158.
25. Loh, C.H., Penzien, J. and Tsai, Y.B. (1982). "Engineering Analyses of SMART 1 Array Accelerograms", Earthquake Engineering & Structural Dynamics, Vol. 10, No. 4, pp. 575–591.
26. Luco, J.E. and Wong, H.L. (1986). "Response of a Rigid Foundation to a Spatially Random Ground Motion", Earthquake Engineering & Structural Dynamics, Vol. 14, No. 6, pp. 891–908.

27. Novak, M. (1990). "Spatial Correlation Effects in Random Vibration of Structures", Proceedings of the European Conference on Structural Dynamics, EURODYN'90, Bochum, F.R.G., Vol. 2, pp. 631–636.
28. Perotti, F. (1990). "Structural Response to Non-stationary Multiple-Support Random Excitation", Earthquake Engineering & Structural Dynamics, Vol. 19, No. 4, pp. 513–527.
29. Roesset, J.M. (1977). "Soil Amplification of Earthquakes" in "Numerical Methods in Geotechnical Engineering (edited by C.S. Desai and J.T. Christian)", McGraw-Hill, New York, U.S.A.
30. Ruiz, P.T. and Penzien, J. (1969). "Probabilistic Study of the Behavior of Structures during Earthquakes", Report UCB/EERC-69/03, University of California, Berkeley, U.S.A.
31. Safak, E. (1995). "Discrete-Time Analysis of Seismic Site Amplification", Journal of Engineering Mechanics, ASCE, Vol. 121, No. 7, pp. 801–809.
32. Shinozuka, M. and Deodatis, G. (1991). "Stochastic Wave Models for Stationary and Homogeneous Seismic Ground Motion", Structural Safety, Vol. 10, No. 1-3, pp. 235–246.
33. Tajimi, H. (1960). "A Statistical Method of Determining the Maximum Response of a Building Structure during an Earthquake", Proceedings of the Second World Conference on Earthquake Engineering, Tokyo, Japan, Vol. 2, pp. 781–798.
34. Todorovska, M.I. and Lee, V.W. (1989). "Seismic Waves in Buildings with Shear Walls or Central Core", Journal of Engineering Mechanics, ASCE, Vol. 115, No. 2, pp. 2669–2686.
35. Todorovska, M.I. and Trifunac, M.D. (1989). "Antiplane Earthquake Waves in Long Structures", Journal of Engineering Mechanics, ASCE, Vol. 115, No. 12, pp. 2687–2708.
36. Todorovska, M.I. and Trifunac, M.D. (1990a). "A Note on the Propagation of Earthquake Waves in Buildings with Soft First Floor", Journal of Engineering Mechanics, ASCE, Vol. 116, No. 4, pp. 892–900.
37. Todorovska, M.I. and Trifunac, M.D. (1990b). "Note on Excitation of Long Structures by Ground Waves", Journal of Engineering Mechanics, ASCE, Vol. 116, No. 4, pp. 952–964.
38. Todorovska, M.I. and Trifunac, M.D. (1997). "Amplitudes, Polarity and Time of Peaks of Strong Ground Motion during the 1994 Northridge, California, Earthquake", Soil Dynamics and Earthquake Engineering, Vol. 16, No. 4, pp. 235–258.
39. Todorovska, M.I., Hayir, A. and Trifunac, M.D. (2001a). "Antiplane Response of a Dike with Flexible Structure-Soil Interface to Incident SH-Waves", Soil Dynamics and Earthquake Engineering, Vol. 21, No. 7, pp. 603–613.
40. Todorovska, M.I., Hayir, A. and Trifunac, M.D. (2001b). "Antiplane Response of a Dike on a Flexible Embedded Foundation to Incident SH-Waves", Soil Dynamics and Earthquake Engineering, Vol. 21, No. 7, pp. 593–601.
41. Trifunac, M.D. (1971). "Response Envelope Spectrum and Interpretation of Strong Earthquake Ground Motion", Bulletin of the Seismological Society of America, Vol. 61, No. 2, pp. 343–356.
42. Trifunac, M.D. (1990). "How to Model Amplification of Strong Earthquake Motions by Local Soil and Geologic Site Conditions", Earthquake Engineering & Structural Dynamics, Vol. 19, No. 6, pp. 833–846.
43. Trifunac, M.D. (1997). "Relative Earthquake Motion of Building Foundations", Journal of Structural Engineering, ASCE, Vol. 123, No. 4, pp. 414–422.
44. Trifunac, M.D. and Gicev, V. (2006). "Response Spectra for Differential Motion of Columns. Paper II: Out-of-Plane Response", Soil Dynamics and Earthquake Engineering, Vol. 26, No. 12, pp. 1149–1160.
45. Trifunac, M.D. and Lee, V.W. (1996). "Peak Surface Strains during Strong Earthquake Motion", Soil Dynamics and Earthquake Engineering, Vol. 15, No. 5, pp. 311–319.
46. Trifunac, M.D. and Todorovska, M.I. (1997). "Response Spectra for Differential Motion of Columns", Earthquake Engineering & Structural Dynamics, Vol. 26, No. 2, pp. 251–268.
47. Trifunac, M.D., Todorovska, M.I. and Ivanovic, S.S. (1996). "Peak Velocities and Peak Surface Strains during Northridge, California, Earthquake of 17 January 1994", Soil Dynamics and Earthquake Engineering, Vol. 15, No. 5, pp. 301–310.

48. Vanmarcke, E.H. and Fenton, G.A. (1991). "Conditioned Simulation of Local Fields of Earthquake Ground Motion", *Structural Safety*, Vol. 10, No. 1-3, pp. 247–264.
49. Zembaty, Z. (1996). "Spatial Seismic Coefficients, Some Sensitivity Results", *Journal of Engineering Mechanics*, ASCE, Vol. 122, No. 4, pp. 379–382.
50. Zembaty, Z. (1997). "Vibrations of Bridge Structure under Kinematic Wave Excitations", *Journal of Structural Engineering*, ASCE, Vol. 123, No. 4, pp. 479–488.
51. Zembaty, Z. and Krenk, S. (1993). "Spatial Seismic Excitations and Response Spectra", *Journal of Engineering Mechanics*, ASCE, Vol. 119, No. 12, pp. 2449–2460.
52. Zembaty, Z. and Rutenberg, A. (1998). "On the Sensitivity of Bridge Seismic Response with Local Soil Amplification", *Earthquake Engineering & Structural Dynamics*, Vol. 27, No. 10, pp. 1095–1099.
53. Zembaty, Z. and Rutenberg, A. (2002). "Spatial Response Spectra and Site Amplification Effects", *Engineering Structures*, Vol. 24, No. 11, pp. 1485–1496.
54. Zerva, A. (1991). "Effect of Spatial Variability and Propagation of Seismic Ground Motions on the Response of Multiply Supported Structures", *Probabilistic Engineering Mechanics*, Vol. 6, No. 3-4, pp. 212–221.
55. Zerva, A. and Shinozuka, M. (1991). "Stochastic Differential Ground Motion", *Structural Safety*, Vol. 10, No. 1-3, pp. 129–143.

MULTI-COMPONENT GROUND MOTION RESPONSE SPECTRA FOR COUPLED HORIZONTAL, VERTICAL, ANGULAR ACCELERATIONS, AND TILT

Erol Kalkan and Vladimir Graizer

California Geological Survey
Sacramento, CA 95814-3500, U.S.A.

ABSTRACT

Rotational and vertical components of ground motion are almost always ignored in design or in the assessment of structures despite the fact that vertical motion can be twice as much as the horizontal motion and may exceed $2g$ level, and rotational excitation may reach few degrees in the proximity of fault rupture. Coupling of different components of ground excitation may significantly amplify the seismic demand by introducing additional lateral forces and enhanced P- Δ effects. In this paper, a governing equation of motion is postulated to compute the response of a SDOF oscillator under a multi-component excitation. The expanded equation includes secondary P- Δ components associated with the combined impacts of tilt and vertical excitations in addition to the inertial forcing terms due to the angular and translational accelerations. The elastic and inelastic spectral ordinates traditionally generated considering the uniaxial input motion are compared at the end with the multi-component response spectra of coupled horizontal, vertical and tilting motions. The proposed multi-component response spectrum reflects kinematic characteristics of the ground motion that are not identifiable by the conventional spectrum itself, at least for the near-fault region where high intensity vertical shaking and rotational excitation are likely to occur.

KEYWORDS: Rotational Motion, Tilt, Vertical Acceleration, Response Spectrum, P- Δ Effects

BACKGROUND

Ground motion response spectrum is defined as a graphical relationship of the peak response of a single-degree-of-freedom (SDOF) oscillator having certain damping to dynamic motion or forces. Since it was first introduced by Biot (1932, 1933, 1934, 1941, 1942), and later introduced to engineering applications by Housner (1959) and Newmark et al. (1973), it has often been utilized for the purposes of recognizing the significant characteristics of accelerograms and evaluating the response of structures to strong ground shaking in a simple fashion. Due to inherent theoretical simplicity and ease in computer applications, the response spectrum concept quickly became the standard tool of structural design and performance assessment.

Earthquake recordings generally produce jagged spectral response shapes manifesting large record-to-record variability. Due to abrupt changes from maxima to minima over a narrow band of spectral periods, use of a single-record response spectrum in generalizing the seismic demand is generally avoided. Instead, spectra from a suite of ground motions are smoothed, scaled and averaged; thereby inherent variability in ground motion process is statistically accounted for. To be used directly in design, Biot (1941, 1942) and then Housner (1959) were the first to propose a smooth-response spectrum. Later, Newmark and Hall (1969, 1982) followed the same idea. Newmark-Hall's smooth spectrum constituted three regions along the spectral periods: (i) acceleration (short-period range), (ii) velocity (intermediate-period range), and (iii) displacement (long-period range). Each of these regions is constructed by applying dynamic amplifications to the design values of peak ground acceleration (PGA), velocity (PGV) and displacement (PGD). Following Newmark and Hall (1969, 1982), many researchers contributed to the development of the smooth spectrum, e.g., Hall et al. (1975), Mohraz (1976), Seed et al. (1976), Lam et al. (2000), Kalkan and Gülkan (2004a), and Malhotra (2006). A common feature of these studies is that the proposed smooth spectra were developed utilizing a uniaxially excited SDOF oscillator, while contributions of the other ground motion components on translational response were not included.

In reality, earthquakes create movements in three-translational and three-rotational directions; hence the exact response at a point on the ground surface during an earthquake can only be obtained by recording the motions of all six degrees of freedom (DOF). Except for some attempts in recent years towards measuring rotational components, it is routine in seismology to record only translational components in three orthogonal directions. Among these three, only two horizontal components have been almost always involved in spectral response computations. This routine is mainly driven by the common perception, which has been long established considering far-fault earthquake recordings, that rotational components of motion are small so as not to add significantly to the seismic loads, and that structures have sufficient overstrength against the vertical component since they have already been designed for the gravitational acceleration. In fact, the importance of vertical component of ground motion in design and performance assessment was addressed long ago (e.g., Chopra, 1966; Lee, 1979). Yet, it received more attention just after the earthquakes in the last 15 years, which provided plethora of data in the near field of earthquake source having significantly higher vertical acceleration than its horizontal counterparts (Niazi and Bozorgnia, 1991; Bozorgnia et al., 1995; Silva, 1997; Kalkan and Gülkan, 2004b). Such near-fault data has eventually changed the misleading assumption that the vertical ground motion can be taken to be two-thirds of the horizontal motion, as postulated earlier by Newmark et al. (1973), and Newmark and Hall (1982). At short periods and near-source distances, vertical component of the ground motion may be noticeably more severe than the horizontal component. A remarkable field evidence of this fact was found in the recent past, during the 1995 Kobe earthquake, when ground vertical acceleration experienced little attenuation from rock-outcrop to the ground surface, as opposed to the horizontal ones, even in potentially liquefiable soils. As a consequence, high vertical seismic inputs to structures were observed, and unusual failures of vertical structural members occurred (JSCE, 1995; Papazoglou and Elnashai, 1996; Uenishi and Sakurai, 2000). Another example of intense vertical acceleration was observed during the aftershock of 1985 Nahanni earthquake in Canada. The aftershock ($M_s = 6.9$) created a peak horizontal acceleration of 1.25g at a station located 8–10 km of the rupture. The peak vertical acceleration (recorded by an analog type accelerograph, SMA-1) got off-scale and exceeded 2g (Weichert et al., 1986).

In recognition of high-intensity vertical shaking in the vicinity of active faults, many studies have been devoted to investigate the detrimental impacts of vertical ground motion on structural systems. Elnashai and Papazoglou (1997) and Ranzo et al. (1999) demonstrated that shear resistance of the vertical members is more sensitive to the vertical excitation, and that shear failure is anticipated when a reduction in the axial contribution to the section shear capacity occurs. In parallel, Salazar and Halder (2000) emphasized the increased level of axial load and its damaging effects on the performance of columns designed by the beam-column methodology. Similar findings on the eroded shear capacity of columns due to vertical excitation influences were also highlighted by Abdelkareem and Machida (2000), and Diotallevi and Landi (2000). As recently shown by Kunnath et al. (2005), vertical motion may magnify and potentially create reversal of bending moment in longitudinal bridge girders. Widespread phenomenon of bearing failure and deck unseating, as observed during the recent earthquakes, was partially attributed to the destructive impact of vertical motions (Pamuk et al., 2005). Based on a large body of available studies, it is possible to conclude that vertical shaking may escalate the axial column force, cause an increase in the moment and shear demand, and amplify plastic deformation, extend plastic hinge formation and finally diminish the ductility capacity of structural component. In order to include the vertical motion effects in design, recent efforts have considered the development of vertical ground motion spectra by focusing mostly on near-fault accelerograms (e.g., Ambraseys and Simpson, 1996; Elnashai and Papazoglou, 1997; Bozorgnia and Campbell, 2004; Kalkan and Gülkan, 2004b; Malhotra, 2006). These studies have developed vertical ground motion spectra (for the vertical response computed under unidirectional excitation only) and concentrated on its parallel use with the horizontal ground motion spectra.

In addition to translational ground movement in orthogonal directions and relevant studies quantifying its destructive impacts, studies by Bouchon and Aki (1982), Lee and Trifunac (1985), and Castellani and Boffi (1986) indicated that rotational ground motion could also be important in the near-field zone. Stratta and Griswold (1976), Ghafory-Ashtiany and Singh (1986), and Gupta and Trifunac (1990, 1991) emphasized possible effects of a rotational component on building response. Recently, Graizer (2006a) demonstrated that static tilting of the ground surface could reach a few degrees while dynamic tilting becomes even higher in the proximity of earthquake faults. Such high-intensity ground

tilting becomes detrimental for structures by compelling them to high ductility demand levels (Kalkan and Graizer, 2007).

RESEARCH SIGNIFICANCE

In majority of the past studies, SDOF oscillators were used to compute the response spectra for horizontal and vertical motions separately, assuming that the response to multi-component excitations is uncoupled. However, coupling of different components of ground motion (i.e., concurrent application of different components in computing the SDOF oscillator's response) may significantly amplify the level of seismic demand by producing additional lateral forces and enhanced P- Δ effects without violating the SDOF assumption (i.e., unidirectional response is still valid, while the input is multi-directional). In order to quantify the level of increase in seismic demand, a complete equation of motion for the translational response of a SDOF oscillator is postulated here. The new formulation includes the combined effects of tilt and vertical excitations as the secondary P- Δ components, in addition to the inertial force effects due to the angular and translational accelerations. The inelastic response of a SDOF oscillator to uniaxial input motion and also its response to a three-degree-of-freedom (i.e., horizontal, vertical and rotation) motion are systematically compared and contrasted to isolate the relative contribution of each input motion. The results of this study confirm that higher ductility demand (or dynamic collapse) may ensue due to the effects of vertical and rotational motions when they are coupled with the horizontal excitation. Unlike the conventional spectrum, the proposed multi-component response spectrum (elastic or inelastic) is capable of capturing the enhanced seismic demands associated with multi-component coupling effects.

VERTICAL AND ROTATIONAL GROUND MOTIONS

Prior to investigating the impacts of vertical and rotational (i.e., tilt) components of ground motion on the SDOF oscillator's response, it is instructive first to highlight the fundamental characteristics of the ground motion components. In reviewing the following sections, it should be kept in mind that pendulums (which represent a typical SDOF system) used in strong motion recording instruments are sensitive not only to the horizontal ground shaking, but also to the tilt (i.e., rotational component).

1. Vertical Component of Ground Motion and V/H Ratio

Vertical component of the strong ground motion is mainly associated with body waves: vertically propagating compressional waves (i.e., P-waves) and horizontally propagating dilatational waves (i.e., S-waves). Compared to the horizontal component, vertical motion may be richer in high-frequency content in the near field of an earthquake fault. As the distance from the source increases, difference in the frequency content between horizontal and vertical components becomes much smaller as a result of faster attenuation of high frequencies with distance, and mixing of horizontal and vertical motions due to nonhomogeneities along the wave path.

A common perception in engineering practice is that intensity of vertical ground motion is lower than that of the horizontal; thereby V/H ratio (i.e., the ratio of vertical to horizontal peak ground acceleration) is assumed to remain less than unity. In order to study the variations of V/H ratio, we performed an analysis on 820 three-component strong ground motion records of significant earthquakes in California. This analysis was later extended to cover more than 1400 records. At first, strong motion data from 18 earthquakes of magnitude higher than 5.0 were studied and it was shown that the distribution of V/H ratio could be best presented on the logarithmic scale with the median ratio of 0.47 (Graizer, 2006b). The median ratio of the V/H ratio varied from 0.29 to 0.69 for different events (see Figure 1, where “++” indicates the median V/H ratio for each specific event). To study the distribution of the V/H ratio, the entire data was split into equal bins having $\log(V/H)$ range of 0.05. It was observed that the largest number of V/H ratios lies within the 0.45–0.50 range having 363 data points. As shown in Figure 2 (which includes 1492 data points), in most cases, amplitude of the vertical component is about twice lower than that of the horizontal component. Data points in Figure 2 are from a mixed dataset of far-field and near-field recordings and yield an average V/H ratio of 0.48.

In order to isolate the possible farther distance effects on the resultant V/H ratio, Figure 3 concentrates on recordings measured within 30 km of the closest fault. This subset includes 240 components of ground motions recorded at 80 stations from worldwide earthquakes, and this data was

extracted from the Next Generation Attenuation (NGA) models database (Power et al., 2006). More details of ground motions in this subset are provided in Table 1.

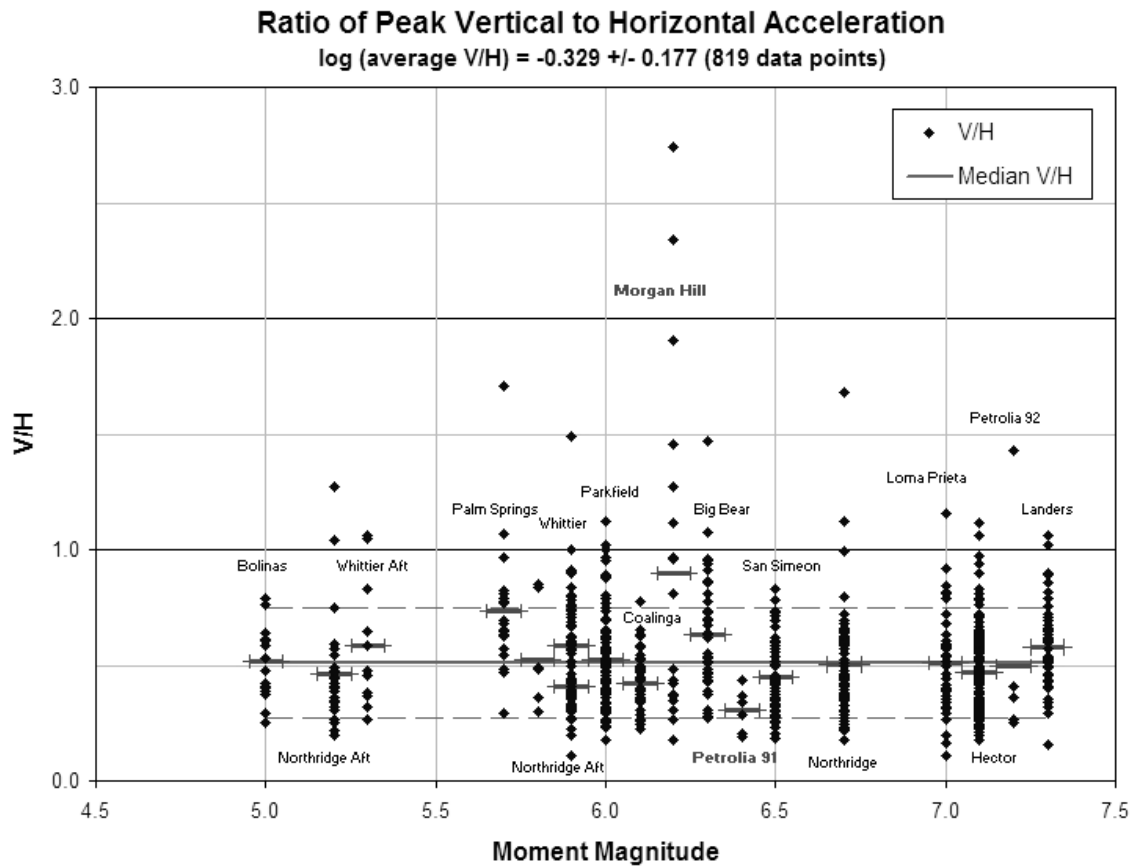


Fig. 1 Ratios of peak vertical to horizontal acceleration (V/H) from 18 Californian earthquakes (dashed lines indicate median \pm standard deviation and “++” marks median V/H ratio for each specific event)

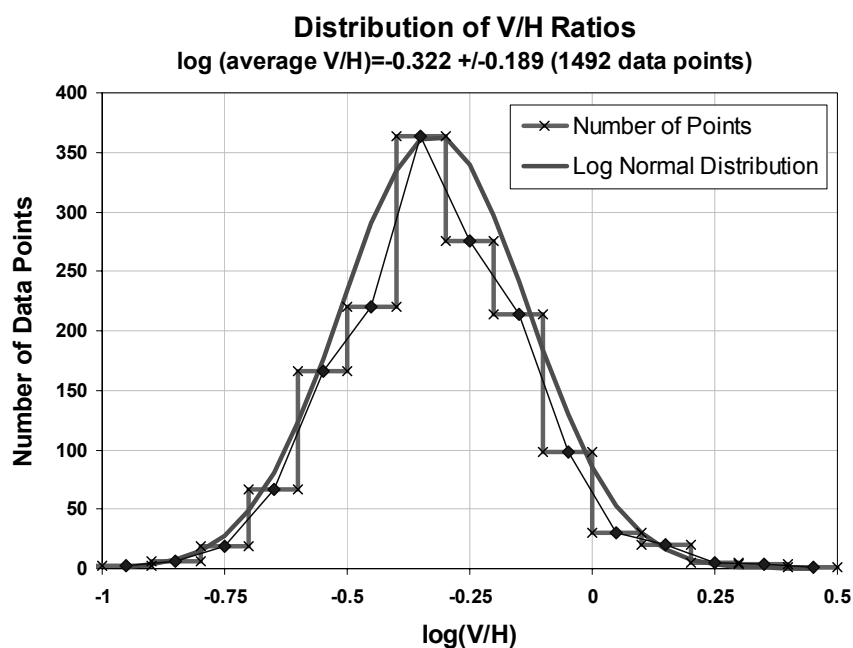


Fig. 2 Log-normal fit to V/H ratio

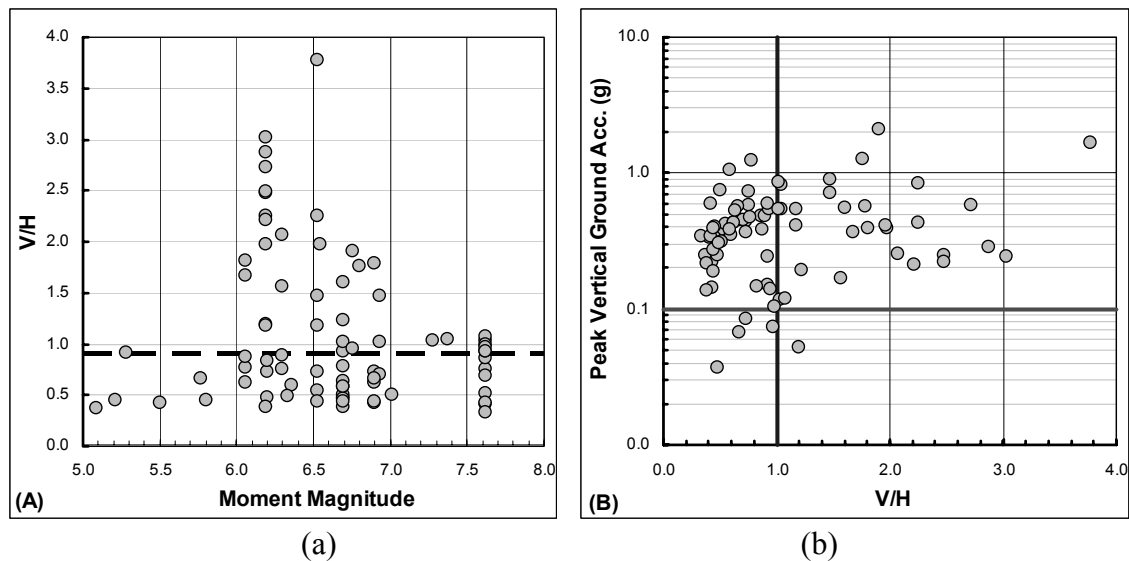


Fig. 3 Ratios of peak vertical to horizontal acceleration (V/H) plotted against (a) moment magnitude, and (b) peak vertical acceleration (dashed lines indicate the sample median)

Figure 3(a) shows the plot of the V/H ratio against the magnitude of the events. It may be seen that the median V/H ratio is equal to 0.9, being much higher than the commonly accepted value of 0.67 or the median of the mixed dataset (i.e., 0.47). The maximum V/H ratio in the subset is close to 4.0. This data point corresponds to the 1979 Imperial Valley earthquake ($M_w = 6.5$) and to the El Centro Array # 6 station, which recorded peak vertical ground acceleration of more than 1.6g. As mentioned earlier, the maximum vertical acceleration exceeding 2g was recorded during the Nahanni earthquake of 1985. This motion produced the vertical-to-horizontal peak ground acceleration ratio (V/H) of at least 2.0. The near-fault dataset used here implies that higher vertical acceleration tends to create larger V/H ratio as shown in Figure 3(b). Similar correlation, however, does not exist between the V/H ratio and peak horizontal acceleration.

The same trends that appeared in Figure 3 were not observed for the 2004 Parkfield event of magnitude 6.0. This relatively large strong-motion dataset (of 94 records) was studied separately by splitting it into two parts: near-fault data (41 data points recorded at distances less than 10 km from the fault) and other data (at more than 10 km from the fault). Interestingly, variations of V/H ratios with distance were found to be insignificant with the median of 0.49 being close to the median of the complete dataset (of 1400 records). The exercises conducted on different ground motion databases collectively confirm that V/H ratio may show significant variations, which depend on source and site characteristics and on seismic radiation pattern. Though not all earthquakes and their corresponding data from the near-fault region substantiate that V/H ratio is larger than unity, many data points confirm the opposite; hence influences of vertical component should not be ignored when seismic demands on structural components are assessed.

2. Rotational Component

Rotational components of ground motion (i.e., rocking and torsion) that are caused due to the incidence of SV-waves and surface waves have long been assumed to have low intensity compared to their horizontal and vertical counterparts; thus their impact on structural response is often overlooked. However, many structural failures and damage caused by the earthquakes can be linked not only to the translational but also to the rotational ground motions. For instance, torsional response of tall buildings in Los Angeles during the 1971 San Fernando, California earthquake could be attributed to the torsional excitation (Hart et al., 1975), while rotational and longitudinal differential motions may have caused the collapse of bridges during the San Fernando 1971 and Miyagi-ken-Oki 1978 earthquakes (Bycroft, 1980), and during the Northridge 1994 earthquake (Trifunac et al., 1996). Earthquake damage to pipelines, which is not associated with faulting or landslides and is due to large differential motions and strains in the soil, reflects the consequences of the propagating seismic waves and of the associated large rotations and twisting of soil blocks that are caused by lateral spreads and early stages of liquefaction (Ariman and Muleski, 1981; Trifunac and Todorovska, 1998).

Table 1: Near-Fault Ground Motion Subset

No.	Year	Event	Mw	Station Name	Peak Ground Acceleration (g)			V/H	Distance* (km)	VS30** (m/s)
					Hor.1	Hor.2	Ver.			
1	1987	Baja California	5.5	Cerro Prieto	1.39	0.89	0.59	0.42	-	660
2	1992	Cape Mendocino	7.0	Cape Mendocino	1.50	1.04	0.75	0.50	7.0	514
4	1999	Chi-Chi, Taiwan	7.6	CHY028	0.65	0.82	0.34	0.41	3.1	543
5	1999	Chi-Chi, Taiwan	7.6	CHY080	0.97	0.97	0.72	0.75	2.7	553
7	1999	Chi-Chi, Taiwan	7.6	TCU068	0.57	0.46	0.49	0.86	0.3	487
8	1999	Chi-Chi, Taiwan	7.6	TCU071	0.57	0.65	0.45	0.69	5.3	625
9	1999	Chi-Chi, Taiwan	7.6	TCU079	0.74	0.39	0.39	0.52	11.0	364
11	1999	Chi-Chi, Taiwan	7.6	TCU088	0.51	0.52	0.22	0.43	18.2	553
12	1999	Chi-Chi, Taiwan	7.6	TCU129	1.01	0.63	0.34	0.34	1.8	664
15	1999	Chi-Chi, Taiwan-06	6.3	TCU079	0.77	0.62	0.58	0.75	10.1	364
16	1999	Chi-Chi, Taiwan-06	6.3	TCU080	0.47	0.54	0.48	0.89	10.2	375
17	1983	Coalinga-02	5.1	Anticline Ridge Free-Field	0.58	0.67	0.25	0.37	-	376
18	1983	Coalinga-05	5.8	Oil City	0.87	0.45	0.57	0.66	-	376
19	1983	Coalinga-07	5.2	Coalinga-14th & Elm (Old CHP)	0.43	0.73	0.33	0.45	-	339
20	1983	Coalinga-01	6.4	Pleasant Valley P.P. - yard	0.59	0.55	0.35	0.60	8.4	257
21	1992	Erzincan, Turkey	6.7	Erzincan	0.50	0.52	0.25	0.48	4.4	275
22	1995	Kobe, Japan	6.9	KJMA	0.82	0.60	0.34	0.42	1.0	312
23	1995	Kobe, Japan	6.9	Takatori	0.61	0.62	0.27	0.44	1.5	256
24	1976	Gazli, USSR	6.8	Karakyr	0.61	0.72	1.26	1.76	5.5	660
25	1979	Imperial Valley-06	6.5	Bonds Corner	0.59	0.77	0.42	0.55	2.7	223
26	1979	Imperial Valley-06	6.5	El Centro Array #8	0.60	0.45	0.44	0.73	3.9	206
27	1995	Kobe, Japan	6.9	Nishi-Akashi	0.51	0.50	0.37	0.73	7.1	609
28	1995	Kobe, Japan	6.9	Takarazuka	0.69	0.69	0.43	0.62	0.3	312
29	1992	Landers	7.3	Lucerne	0.73	0.79	0.82	1.04	2.2	685
30	1989	Loma Prieta	6.9	Corralitos	0.64	0.48	0.46	0.71	3.9	462
31	1989	Loma Prieta	6.9	LGPC	0.56	0.61	0.89	1.47	3.9	478
33	1990	Manjil, Iran	7.4	Abbar	0.51	0.50	0.54	1.05	12.6	724
35	1986	N. Palm Springs	6.1	North Palm Springs	0.59	0.69	0.43	0.63	4.0	345
36	1986	N. Palm Springs	6.1	Whitewater Trout Farm	0.49	0.61	0.47	0.77	6.0	345
37	1985	Nahanni, Canada	6.8	Site 1	0.98	1.10	2.09	1.90	9.6	660
38	1994	Northridge-01	6.7	Beverly Hills - 12520 Mulhol	0.62	0.44	0.31	0.51	18.4	546
39	1994	Northridge-01	6.7	Castaic - Old Ridge Route	0.57	0.51	0.22	0.38	20.7	450
40	1994	Northridge-01	6.7	Newhall - Fire Sta	0.58	0.59	0.55	0.93	5.9	269
41	1994	Northridge-01	6.7	Pacoima Dam (upper left)	1.58	1.29	1.23	0.78	7.0	2016
42	1994	Northridge-01	6.7	Pardee - SCE	0.66	0.41	0.38	0.58	7.5	345
43	1994	Northridge-01	6.7	Rinaldi Receiving Sta	0.84	0.47	0.85	1.02	6.5	282
45	1994	Northridge-01	6.7	Simi Valley - Katherine Rd	0.88	0.64	0.40	0.46	13.4	557
46	1994	Northridge-01	6.7	Sylmar - Olive View Med FF	0.60	0.84	0.54	0.63	5.3	441
47	1994	Northridge-01	6.7	Tarzana - Cedar Hill A	1.78	0.99	1.05	0.59	15.6	257
48	1994	Northridge-06	5.3	Rinaldi Receiving Sta	0.65	0.43	0.60	0.92	-	282
49	1986	San Salvador	5.8	Geotech Investig Center	0.87	0.48	0.39	0.45	6.3	545
50	1980	Victoria, Mexico	6.3	Cerro Prieto	0.62	0.59	0.30	0.49	14.4	660
51	1999	Chi-Chi, Taiwan	7.6	TCU103	0.13	0.16	0.15	0.92	6.1	494
52	1999	Chi-Chi, Taiwan	7.6	TCU118	0.11	0.09	0.12	1.03	26.8	215
53	1999	Chi-Chi, Taiwan	7.6	CHY092	0.08	0.11	0.12	1.07	22.7	254
54	1999	Chi-Chi, Taiwan	7.6	TCU141	0.08	0.11	0.10	0.99	24.2	215
55	1999	Chi-Chi, Taiwan	7.6	CHY026	0.08	0.07	0.07	0.97	29.5	226
56	1999	Chi-Chi, Taiwan	7.6	TCU122	0.22	0.26	0.24	0.92	9.4	475
58	1999	Chi-Chi, Taiwan-03	6.2	TCU116	0.12	0.11	0.08	0.73	22.1	493
59	1999	Chi-Chi, Taiwan-06	6.3	TCU075	0.06	0.11	0.17	1.56	26.3	573
60	1999	Chi-Chi, Taiwan-06	6.3	TCU076	0.11	0.12	0.26	2.07	25.9	615
61	1979	Imperial Valley-06	6.5	El Centro Array #6	0.41	0.44	1.66	3.77	1.4	203
62	1979	Imperial Valley-06	6.5	Agrarias	0.37	0.22	0.83	2.25	0.7	275
63	1979	Imperial Valley-06	6.5	El Centro Array #7	0.34	0.46	0.54	1.18	0.6	211
64	1979	Imperial Valley-06	6.5	El Centro Differential Array	0.35	0.48	0.71	1.47	5.1	202
65	1980	Irpina, Italy-01	6.9	Bisaccia	0.10	0.08	0.07	0.67	21.3	1000
66	1980	Irpina, Italy-02	6.2	Calitri	0.18	0.16	0.15	0.83	8.8	600
67	1995	Kobe, Japan	6.9	Port Island (0 m)	0.31	0.28	0.56	1.79	3.3	198
68	1989	Loma Prieta	6.9	Capitola	0.53	0.44	0.54	1.02	15.2	289
69	1980	Mammoth Lakes-01	6.1	Convict Creek	0.42	0.44	0.39	0.88	6.6	339
70	1984	Morgan Hill	6.2	Gilroy Array #2	0.16	0.21	0.58	2.72	13.7	271
71	1984	Morgan Hill	6.2	Hollister Diff Array #4	0.10	0.09	0.28	2.87	26.4	216
72	1984	Morgan Hill	6.2	Hollister Diff Array #5	0.10	0.10	0.25	2.47	26.4	216
73	1984	Morgan Hill	6.2	Hollister Diff Array #3	0.08	0.08	0.24	3.02	26.4	216
74	1984	Morgan Hill	6.2	Gilroy Array #7	0.19	0.11	0.43	2.25	12.1	334
75	1984	Morgan Hill	6.2	Hollister Diff. Array	0.09	0.09	0.22	2.48	26.4	216
76	1984	Morgan Hill	6.2	Hollister Diff Array #1	0.10	0.09	0.21	2.22	26.4	216
77	1984	Morgan Hill	6.2	Gilroy Array #3	0.19	0.20	0.40	1.97	13.0	350
78	1984	Morgan Hill	6.2	San Juan Bautista, 24 Polk St	0.04	0.04	0.05	1.19	27.2	371
79	1984	Morgan Hill	6.2	Gilroy Array #4	0.22	0.35	0.41	1.17	11.5	222
80	1986	N. Palm Springs	6.1	Morongo Valley	0.22	0.20	0.40	1.81	12.1	345
81	1986	N. Palm Springs	6.1	Cabazon	0.22	0.21	0.36	1.67	7.8	345
82	1985	Nahanni, Canada	6.8	Site 3	0.15	0.14	0.14	0.95	5.3	660
83	1994	Northridge-01	6.7	Arieta - Nordhoff Fire Sta	0.34	0.31	0.55	1.61	8.7	298
84	1994	Northridge-01	6.7	Sunland - Mt Gleason Ave	0.13	0.16	0.19	1.23	13.4	446
85	1987	Superstition Hills-02	6.5	Wildlife Liquef. Array	0.18	0.21	0.41	1.97	23.9	207
91	1979	Imperial Valley-06	6.5	Aeropuerto Mexicali	0.33	0.26	0.14	0.44	0.3	275
94	1980	Irpina, Italy-02	6.2	Sturmo	0.07	0.08	0.04	0.47	20.4	1000
97	1994	Northridge-01	6.7	Pacoima Dam (downstr)	0.42	0.43	0.19	0.44	7.0	2016
98	1966	Parkfield	6.2	Temblor pre-1969	0.36	0.27	0.14	0.38	16.0	528

* Closest distance to fault; ** Average shear-wave velocity for the first 30m

Most instruments used in the seismological practice to record ground motions are pendulum seismographs, velocigraphs or accelerographs. Such instruments are accurately sensitive to the translational motion of their base provided that there is no tilting. Translational components during a seismic event are however accompanied by rotational components because of the traveling wave effects. Studies have showed that tilting of the recorder's base can severely contaminate its response; thereby, the recorded data may become the mixture of translational and rotational motions, and may be far from representing the true acceleration, velocity and displacement in the direction of recording. A number of attempts to measure rotational motion resulted in measurements from explosions, but not from earthquakes (e.g., Kharin and Simonov, 1969; Graizer, 1989; Nigbor, 1994). In the absence of having records of rotational motion, the attempts have been made to define them in terms of the recorded translational components (Trifunac and Hudson, 1971; Lee and Trifunac, 1985; Niazi, 1986; Lee and Trifunac, 1987; Graizer, 1987, 1989, 1991; Oliveira and Bolt, 1989; Takeo and Ito, 1997; Huang, 2003). An effective method of tilt evaluation using uncorrected strong-motion accelerograms was first suggested by Graizer (1989). It was later tested in a number of laboratory experiments at the USGS, Menlo Park, with different strong-motion instruments. Graizer's method is based on the difference in the tilt sensitivity of the horizontal and vertical pendulums. This method was successfully applied to a number of strong ground motion records of the 1994 Northridge earthquake ($M_w = 6.7$) to extract the rotational motions. Among many records from the stations that recorded the Northridge earthquake, a dramatic case was observed at the Pacoima dam—upper left abutment where the residual tilt reached 3.1° in the N45°E direction. It was a result of local earthquake-induced tilting due to the high-amplitude ground shaking (Graizer, 2006a; Kalkan and Graizer, 2007). The computed value of residual tilt was in good agreement with the tilt measured using electronic level a few days after the earthquake (Shakal et al., 1994). Figure 4 depicts the 210°-component horizontal and vertical motions recorded at the Pacoima dam along with the computed rotational component for a cross-comparison. Details of extracting rotational component for this specific station can be found in Graizer (2006a).

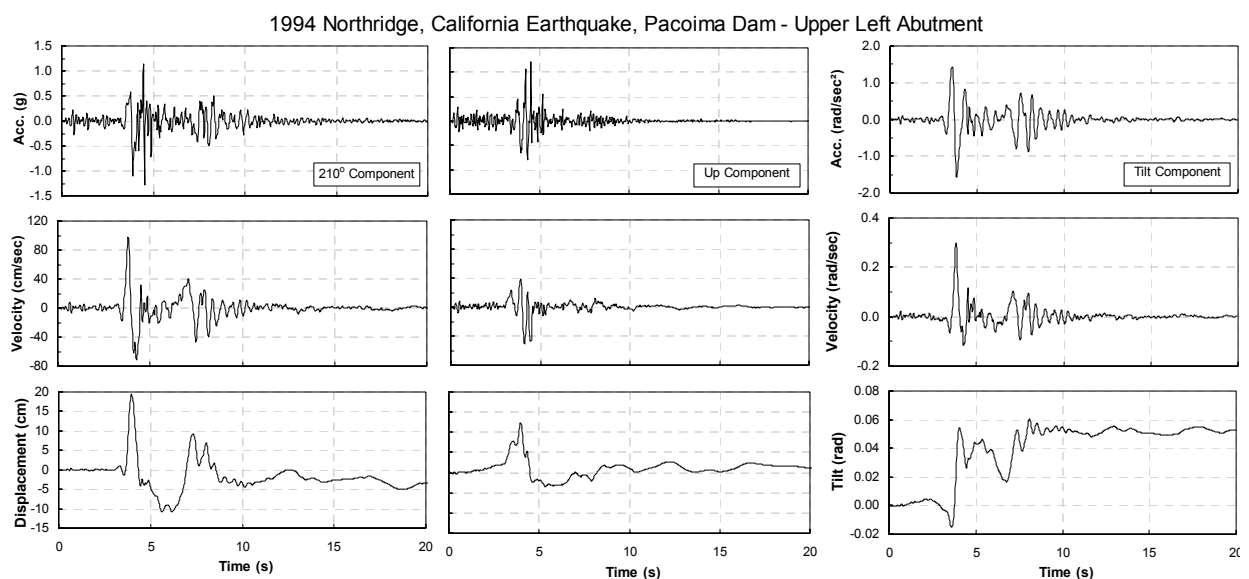


Fig. 4 Horizontal, vertical and tilt components of the Pacoima dam upper left abutment record during the 1994 Northridge earthquake (panels show only the first 20 s of motions)

The tilt motion function obtained from the acceleration record demonstrates the tilt rising from zero to the level of about 3.1° in a period of 3.5 to 8.0 s from the beginning of recording. The main tilt increase (which is a step-type function) is found to correlate well with the highest level of recorded acceleration that occurred with the arrival of strong phase of the S-wave. The estimated velocity of tilting results in a maximum amplitude of about 15° per second (0.26 rad/sec). The residual tilt of about 3.1° (0.054 rad) produces the same result in the accelerometer response as an acceleration of about 0.05g. The two components of translational motion and tilt at Pacoima dam, as shown in Figure 4, are used as the input data (without scaling) for the transient analyses, results of which are presented in the later sections.

UNCOUPLED AND COUPLED GOVERNING EQUATIONS OF MOTION

In the following, uncoupled response of a SDOF oscillator is first revisited to establish a theoretical basis for the derivation of governing equation of motion of a SDOF oscillator when it is subjected to translational, vertical and/or tilting excitations in tandem. It should be noted that all equations derived and the results, which follow, are valid provided that relative displacement of oscillator satisfies the condition, $\sin \phi \cong \phi$, where ϕ is the chord rotation.

1. Uniaxial Translational Excitation

Dynamic equilibrium of the mass m of the inverted pendulum (i.e., a SDOF oscillator) with stiffness k and damping c shown in Figure 5(a) yields

$$m\ddot{u} + c\dot{u} + ku = -m\ddot{u}_g \quad (1)$$

where u is the relative displacement of the oscillator with respect to the ground, and \ddot{u}_g is the ground-induced translational acceleration. For the sake of simplicity, the SDOF oscillator is represented by a rigid bar, and system flexibility is lumped in a rotational spring at the base. The initial stiffness of the system is denoted as k_0 , and a stable bilinear material model with the post-yield stiffness ratio of κ is assumed. The resistance force V is a function of the relative displacement u . The force-deformation plot shown in Figure 5(a) indicates the response of a SDOF oscillator to the translational motion only, whereby the destabilizing effect of the axial load (i.e., P- Δ effect) in the deformed position is ignored. As shown, u can be computed as ϕl for small angles ($\sin \phi \cong \phi$). The P- Δ effects on the response is considered next in Figure 5(b) in which the secondary moment, created by the axial load times the relative displacement u , is represented by the equivalent force-couple $mg\phi$ acting on the mass of the system. Since ϕ is a function of the response parameter u , it is convenient for numerical computations to cast this additional forcing function in a geometric-stiffness term, k_G ($=mg/l$), on the left side of Equation (1). The ratio of the geometric-stiffness term to the initial stiffness yields the well-known stability coefficient, θ :

$$\theta = k_G / k_0 \quad (2)$$

The stiffness apparent in the second-order analysis is called as “effective stiffness”. In the pre-yield condition, it is equal to $k = k_0(1 - \theta)$, while in the post-yield condition it can be expressed as $k = k_0(k - \theta)$. Thus, effective period of the structure, T , accounting for the P- Δ effects, is expressed as

$$T = T_0 / \sqrt{1 - \theta} \quad (3)$$

where T_0 is based on the initial stiffness of the first-order analysis. The dynamic equilibrium equation nesting P- Δ effects in the geometric-stiffness term can be expressed as

$$m\ddot{u} + c\dot{u} + (k_0 - k_G)u = -m\ddot{u}_g \quad (4)$$

For nonlinear response, Equation (4) can be solved incrementally in the time domain by replacing k_0 by instantaneous tangent stiffness that varies according to the hysteretic behavior of the system. Unlike tangent stiffness, the geometric-stiffness term remains unchanged in the inelastic range (provided that there is no vertical excitation). It is also instructive to note that initial period and effective stiffness change by including the P- Δ effects. On the other hand, yield displacement (u_y) remains unchanged, since u_y is directly related to the moment-curvature behavior at the section level, while the P- Δ phenomenon becomes effective at the global system level.

2. Coupled Translational and Tilt Excitations

To fully understand the response of a SDOF oscillator to the tilt motion, it is convenient to examine the P- Δ effects separately. First let us think of a SDOF oscillator with a concentrated mass and height (l) as illustrated in Figure 6(a). When it is subjected to base rotation only, the oscillator mass is influenced by the inertial force (F_α) due to the angular acceleration ($\ddot{\alpha}$). This inertia force is expressed as

$$F_\alpha = m\ddot{\alpha}l \quad (5)$$

It is possible to represent the rotating-base oscillator in Figure 6(a) by an equivalent fixed-base oscillator as illustrated in Figure 6(b). This representation has some computational advantages, especially for the inelastic systems. It directly provides the relative drift associated with the exact deformation. The response of an equivalent fixed-base oscillator therefore does not include the rigid body rotation (α), yet it includes the forcing effects of this rotation. It means that the relative rotations (ϕ) of the rotating-base and fixed-base oscillators become identical, while the total rotation of the fixed-base oscillator can be obtained explicitly by summing up α (i.e., base tilting) and ϕ .

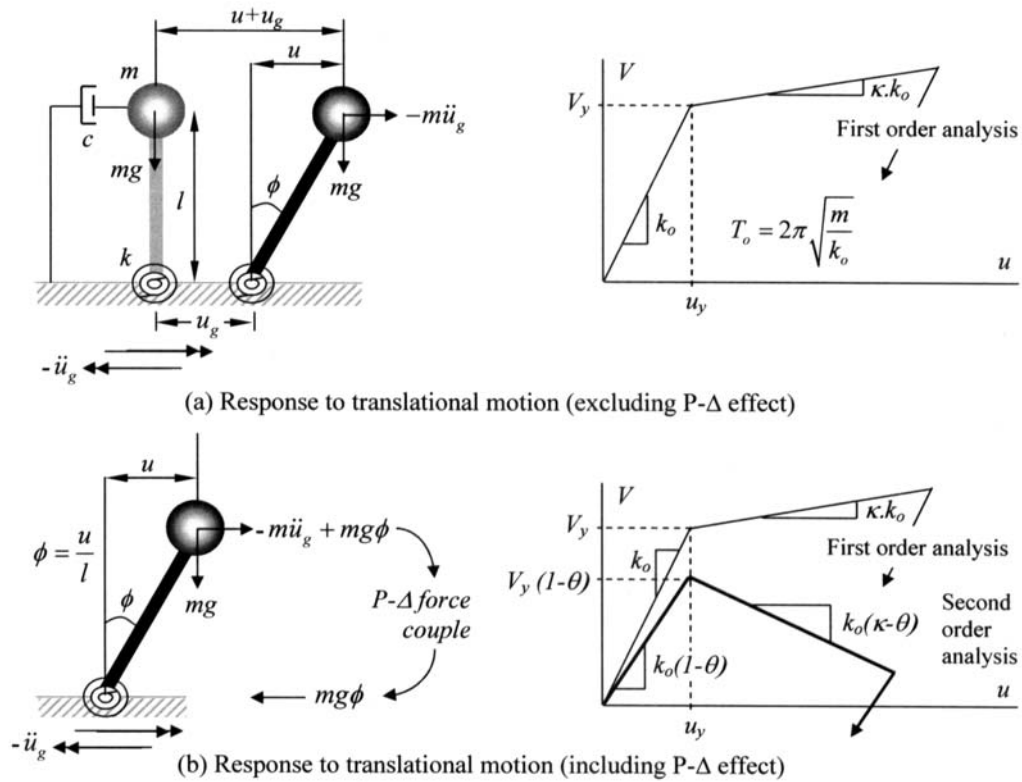


Fig. 5 Fixed-base SDOF oscillator subjected to translational ground motion

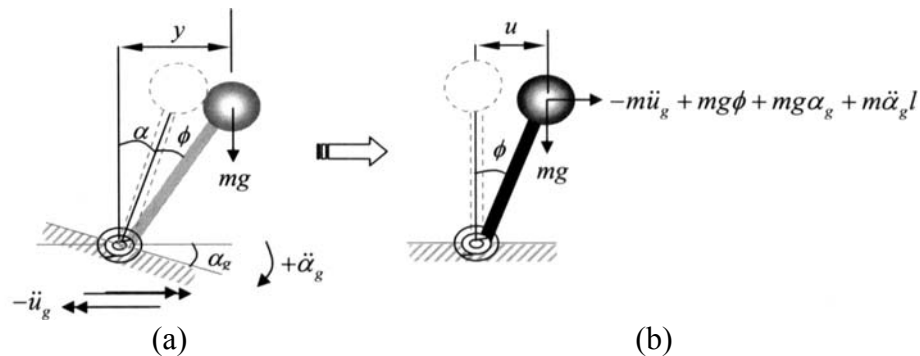


Fig. 6 (a) SDOF oscillator subjected to the coupled tilt and translational ground motion; (b) Equivalent fixed-base system

When the rotating-base oscillator is subjected to the coupled tilt and translational components of ground motion, the resultant force on the corresponding equivalent fixed-base oscillator can be represented by superposing the two inertia forces caused by the translational and angular accelerations (i.e., $-m\ddot{u}_g + m\ddot{\alpha}l$). As evident in Figure 6(a), the additional rigid-body rotation due to the base tilting amplifies the P-Δ effects by increasing the moment arm. In this case, it is convenient to decompose the

total P- Δ contribution into two components. The first component originates due to the base tilting (α) and can be represented as an additional forcing function since it is independent of the oscillator response. The second P- Δ component is a direct consequence of the relative oscillator response (ϕ), and therefore, it can be treated within the geometric-stiffness term (k_G). Again, the total rotation of a fixed-base oscillator can be obtained by adding the base rotation (α) to the system relative rotation (ϕ). Figure 6(b) illustrates the complete forcing function acting on the mass of the equivalent fixed-base oscillator when it is subjected to the coupled tilt and translational motion. The corresponding dynamic equilibrium equation of this physical system can be written as

$$m\ddot{u} + c\dot{u} + ku = -m\ddot{u}_g + mg\phi + mg\alpha_g + m\ddot{\alpha}_g l \quad (6)$$

Equation (6) can also be derived using the Lagrange formulation based on equilibrium of potential and kinetic energies. By representing the P- Δ component due to ϕ as $k_G u$, Equation (6) can be alternatively expressed in the following form:

$$m\ddot{u} + c\dot{u} + (k_0 - k_G)u = -m\ddot{u}_g + mg\alpha_g + m\ddot{\alpha}_g l \quad (7)$$

Equation (7) is theoretically complete to solve the translational response of a SDOF oscillator when it is concurrently subjected to translational and tilting excitations. In the derivation of Equations (6) and (7), positive angular acceleration and corresponding ground tilting are assumed to be in the clockwise direction.

3. Coupled Horizontal, Vertical, Angular Accelerations, and Tilt

In the preceding sections, the effects of vertical ground motion on the translational response of an oscillator are ignored, and the geometric stiffness term of a unit mass system, being a function of the gravitational acceleration and the length of an oscillator, is defined as $k_G = g/l$. In such a case, k_G denotes the characteristics of the SDOF system only: it retains a constant value throughout the elastic or inelastic oscillations while being unaffected by the input motion. Conversely, coupling of vertical excitation with the translational component of motion carries the geometric-stiffness term from static to the dynamic state. Thus, instead of having a constant value, geometric-stiffness term becomes a function of vertical acceleration, and takes the following form:

$$k'_G = \frac{g - \ddot{z}_g}{l} \quad (8)$$

Equation (8) is derived considering a unit-mass system, and upward direction in vertical accelerograms is assumed to be positive. The following discussion is also based on these conditions. Recall that tilt excitation has no influence on geometric stiffness, yet it creates additional P- Δ forces as demonstrated in Figure 6(b). On the other hand, geometric-stiffness term given in Equation (8) becomes time-dependent, and such dynamism creates several complications. As such, k'_G fluctuates, during the transient analysis, around the static geometric-stiffness term (g/l), while its deviation from k_G depends on the relative amplitude of the vertical excitation (\ddot{z}_g) with respect to the gravitational constant. It may show significant differences from its static constant value, which is less than k_G , if the peaks of vertical component are in the upward direction and their amplitudes are closer to or larger than the gravitational acceleration. As a consequence of this, the overall stiffness of an elastic SDOF oscillator (i.e., $k_0 - k'_G$) becomes time-variant. It is, therefore, not possible to have a constant-period oscillator in the elastic domain when the effects of vertical excitation are included. Coupling of high-intensity vertical excitation with the translational motion may initiate a nonlinear elastic system where the oscillation period varies in time, and returns to its initial value at the termination of the ground motion.

Another important complication associated with considering the vertical motion is the eroded overall stiffness of the oscillator due to possible adverse impacts from the geometric-stiffness term. Such effects are even more severe for the inelastic systems where the vertical component may constantly change not only the pre-yield but also the post-yield force-deformation slope (it creates wave-effect on the hysteretic loops as will be shown later). If the vertical component of motion has enough intensity and its peaks are in-phase with the gravity (i.e., it is downward), the associated value of enhanced geometric-stiffness term

leads to ratcheting of the displacement response, which may eventually ensue dynamic instability in the system. It is also noteworthy that the geometric-stiffness term yields larger values as the length of the oscillator decreases. Under the coupled vertical and translational motion, the equation of motion of a SDOF oscillator yields the following form:

$$m\ddot{u} + c\dot{u} + (k_0 - k'_G)u = -m\ddot{u}_g \quad (9)$$

Equation (9) is complete for the SDOF oscillator response in translational direction considering the coupling of vertical excitation only. Incorporating the tilting component does not create any change on the left side of Equation (9); it introduces additional forcing functions on the right side of the equation, as in the case of coupling of horizontal and tilting excitations (see Equation (7)). The first additional forcing term is the inertial force $(= m\ddot{\alpha}_g l)$ due to the angular acceleration. Its amplitude escalates as the length of the oscillator increases. The second forcing term $(= m(g - \ddot{z})\alpha)$ is a supplemental P- Δ force pair due to the coupling of tilting and vertical components. The inclusion of these two forcing functions in Equation (9) yields the theoretically inclusive governing equation of motion for a SDOF oscillator under the influence of multi-component excitations, including horizontal, vertical, and angular accelerations, and ground tilting. This equation is expressed as follows:

$$m\ddot{u} + c\dot{u} + (k_0 - k'_G)u = -m\ddot{u}_g + m(g - \ddot{z})\alpha_g + m\ddot{\alpha}_g l \quad (10)$$

Equation (10) is derived for the SDOF oscillator illustrated in Figure 7(a) where three components of ground shaking are acting on the base of the oscillator. The corresponding forcing functions acting on the mass of the equivalent fixed-base oscillator are illustrated in Figure 7(b). It is worth mentioning that depending on the sign-convention for the angular, vertical and translational accelerations, signs of the forcing functions in Equations (6) and (10) may change (see Figures 6 and 7 for the compatible sign-convention used in the derivation of these equations). As mentioned earlier, the equivalent fixed-base model is easy to implement in a computational framework, particularly for the inelastic systems, since it directly provides the relative drift associated with the exact deformation in the horizontal plane. Once again, the response of an equivalent fixed-base oscillator does not include the rigid body rotation (α) , yet it includes the forcing effects of this rotation. It means that the relative rotations (ϕ) of the rotating-base and fixed-base oscillators become identical while the total rotation of the fixed-base oscillator can be obtained explicitly by summing α (i.e., base tilting) and ϕ .

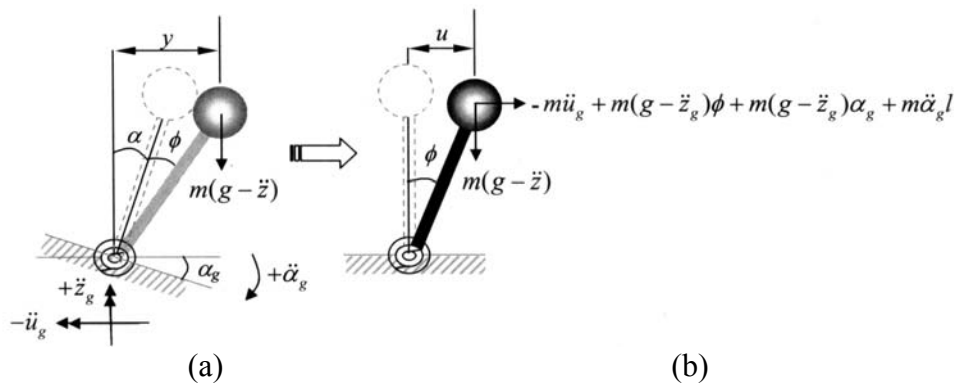


Fig. 7 (a) SDOF oscillator subjected to the coupled tilt, translational and vertical components of ground motion; (b) Equivalent fixed-base system

Based on a new geometric-stiffness formulation given in Equation (8), the stability coefficient can be rewritten as $\theta' = k'_G / k_0$, where θ' now is a function of the vertical excitation. It is obvious that θ' should remain less than unity to maintain stability. Figure 8 compares the plots of the force-deformation relation for the first- and second-order analyses of a SDOF oscillator. Notably, effective yield force $(= V_y (1 - \theta'))$ also becomes time-variant while the yield displacement (u_y) remains unchanged.

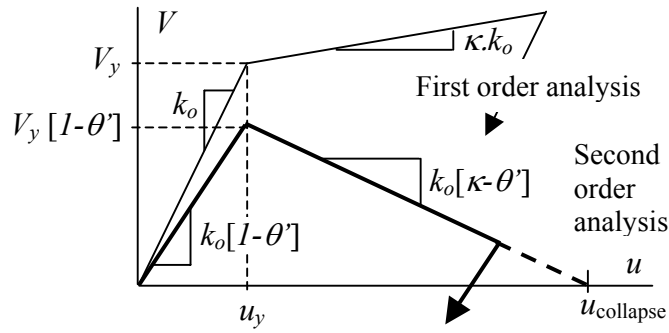


Fig. 8 Force-deformation relation under the coupled tilt, translational and vertical components of ground motion (in second-order analysis, for both pre-yield and post-yield slopes, $V-u$ diagram is conditionally drawn as straight line; in reality, the vertical component may progressively change the slope and create a wave-effect)

It may be noted that θ varies with a change in system stiffness, as implied by Equation (2), meaning that it is a function of the spectral period. Therefore, θ cannot serve as a convenient parameter for direct use in a spectral format unless l (i.e., height or length of the oscillator) is varied at each spectral period to keep θ constant. In lieu of θ , Kalkan and Graizer (2007) proposed a new descriptor, called “geometric oscillation period”, for use as a spectral-period-independent P- Δ parameter. It was originally developed from the P- Δ force pair (i.e., $F_{P-\Delta} = (mg/l)u = k_G u$) for a unit-mass system by neglecting the vertical excitation effects, and it is expressed as

$$T_G = 2\pi\sqrt{l/g} \quad (11)$$

It may be recalled that vertical excitation transforms T_G into a dynamic form:

$$T'_G = 2\pi\sqrt{l/(g - \ddot{z}_g)} \quad (12)$$

T'_G is still independent of the oscillator stiffness but it becomes a function of the vertical excitation; therefore, it is not an invariant parameter, whereas T_G is. It is important to realize that, if the value of $(g - \ddot{z}_g)$ becomes zero (i.e., if $\ddot{z}_g(t) = g$ at a certain time-instant, t), the geometric-stiffness term becomes zero and P- Δ effects are instantaneously deactivated. In parallel, if $(g - \ddot{z}_g)$ yields negative sign, P- Δ effects tend to stabilize the system by changing the direction of P- Δ force towards the opposite direction of inertia force (in the loading cycle). If the system is in the unloading cycle, it can be in the same direction as the inertia force. Vertical excitation is a dynamic parameter, and depending on its intensity in time, it may help to stabilize the system by acting against gravity or destabilize the system by being in phase with the gravity. In parallel, T_G is aimed to serve as a controlling parameter for instability similar to θ . It is independent of the system period (i.e., stiffness), yet it is a function of the vertical acceleration. In this respect, T'_G can be either real-valued, infinite (if $\ddot{z}_g(t) = g$), or complex-valued. Complex value of T'_G implies that the P- Δ force is in the stabilizing mode; on the other hand, its real value indicates that the P- Δ force is in the destabilizing mode. From the structural design and performance assessment point of view, real value of T'_G is a meaningful parameter since it reflects the combined adverse impact of gravity and vertical excitation towards destabilizing the system. For this reason, the following formulations (Equations (13) and (14)) are conditioned on the real-valued T'_G .

The squared ratio of the elastic vibration period (T_0) to the geometric oscillation period (T'_G) defines the time-variant stability coefficient alternatively as

$$\theta' = k'_G / k_0 = (T_0 / T'_G)^2 \quad (13)$$

It is also possible to derive relation between the instantaneous pre-yield effective period ($T_{\text{eff}}(t)$) of the system and the geometric oscillation period (T'_G) as

$$T_{\text{eff}}(t) = T_0 T'_G / \sqrt{T_G'^2 - T_0^2}; \quad t \leq t_{\text{yield}} \quad (14)$$

where t is the time-instant before yielding. Note that the pre-yield effective period is no longer a constant value due to the vertical excitation; it may change at every time-instant. More importantly, Equation (14) indicates that if the geometric oscillation period of the system (T'_G) becomes equal to or smaller than the initial elastic period (T_0), the instability (i.e., $\theta' \geq 1.0$) in the system is initiated. For a stable system, geometric oscillation period should be greater than the initial elastic period. Therefore, T'_G can serve as a valuable tool in seismic design to prevent geometric instability by quantifying lower bound for the lateral stiffness, while considering possible effects of vertical shaking in advance (to be on the conservative side, peak intensity of the vertical motion should be assumed to be in phase with the gravity).

HYSTERETIC BEHAVIOR AND DYNAMIC INSTABILITY

More insight into the progression of dynamic collapse associated with the negative post-yield stiffness due to the presence of enhanced P- Δ effects is conceptually illustrated on a bilinear hysteretic behavior shown in Figure 9. For the sake of simplicity, this figure focuses on the first few (imaginary) inelastic cycles and ignores the vertical excitation effects on the geometric stiffness.

It is apparent that second-order analysis reduces the yield strength by $(1 - \theta)$; therefore, first yielding of the system takes place at point A instead of A' while the yield displacement (u_y) remains unchanged. Following the yielding, velocity of the oscillator becomes zero when the oscillator hits the point B . It means that the kinetic energy of the system becomes zero and the oscillator reaches its positive peak displacement within the first inelastic cycle. Upon unloading, the oscillator moves to the other direction (towards O_1) with increasing negative velocity. Maximum velocity of the system occurs when the inertia force equals zero (i.e., at the points O_1 , O_2). Between O_1 and C , the oscillator slows down. If the ground motion pulse has enough energy to overcome the effective yield strength (if f_c reaches f_c'), the oscillator may advance to left (i.e., in the negative displacement direction) and create an additional plastic half-cycle. Note that the stored strain energy in the system is not sufficient to push the oscillator beyond the point C on the way to the yield line (C'); hence the oscillator does not yield again and comes to rest at the point C . With the incoming of additional pulses, it returns towards B' . Due to the initiation of negative post-yield stiffness, the effective yield strength in the positive displacement direction becomes smaller than that in the negative displacement direction. Therefore, in the next cycle if the incoming pulses are sufficiently strong, the system may tend to move towards right where the yield strength is much less than that for the opposite direction ($f_D < f_E$). In other words, much larger impulses would be needed to overcome the effective yield strength, for instance f_E , in order to cause the system to advance inelastically to the left. For that reason, intensity level of the pulses needed to yield the system in one direction becomes progressively smaller, and inelastic deformation accumulates inherently in one direction and advances the system towards dynamic instability. In this perspective, $(\kappa - \theta)$ becomes an important parameter controlling the cumulative unidirectional deformation.

As Figure 9 indicates, instability in the system occurs when the unidirectional deformation accumulation reaches u_{collapse} ; beyond that, the inertia force would be negative while the system would advance in the positive displacement direction due to the axial load (Jennings and Husid, 1968; Sun et al., 1973; Akiyama, 1985; Ishida and Morisako, 1985). Therefore, u_{collapse} is the limiting point at which collapse in the system gets initiated. The effect of negative post-yield stiffness on the system stability is, in fact, not restricted to the bilinear material model referenced; its severity depends on the unloading and reloading rules of the material model used.

Based on the geometry shown in Figure 9 and on using negative post-yield slope, it is possible to approximate the onset of dynamic collapse as

$$u_{\text{collapse}} = u_y \frac{\kappa - 1}{\kappa - \theta} \quad (15)$$

Vertical component effects on the P- Δ effects are not included in the derivation of Equation (15); therefore, approximation of the collapse displacement (u_{collapse}) requires knowledge only on the yield displacement (u_y), stability coefficient (θ), and on the post-yield stiffness ratio (κ). All of these parameters are known in advance; hence, collapse displacement and associated collapse ductility demand can be estimated via Equation (15) before commencing the transient analysis. It should be noted that Equation (15) can be effectively used to provide a limiting criteria for assessing the tendency for the dynamic collapse of elasto-plastic structural systems. Its formulation is still valid for a simple stiffness-degrading model; yet it may need to be reformulated when different material models are utilized. Inclusion of vertical motion effects in Equation (15) again requires its reformulation since θ now becomes a function of the vertical acceleration pulses (see Equation (13)).

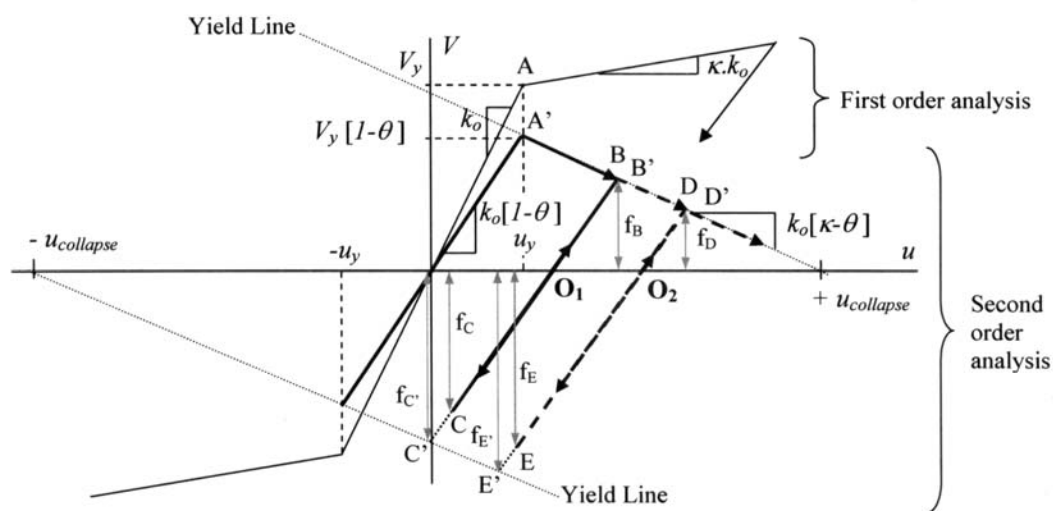


Fig. 9 Progression of dynamic collapse due to the P- Δ effects

RESULTS FROM INELASTIC SDOF ANALYSES

In the previous sections, a set of governing equations of motions for a SDOF oscillator is developed considering different combinations of input motion components. Based on this, an inelastic SDOF oscillator is next subjected to uncoupled and coupled combinations of the three components (i.e., horizontal, vertical and tilting). Results from the inelastic transient analyses are presented in a comparative way to distinguish the relative impacts produced by each component. It should be noted that the horizontal component is applied in each case, while its coupling combinations with the other components are systematically varied. Sign of the vertical motion is also changed to gauge the effects of phase difference.

In order to obtain a realistic set of results, a single-column bent of a highway viaduct (which is a part of a freeway) is used as the reference structure (see Figure 10(a)). This configuration of the bridge bent was previously utilized as a design model by Chopra and Goel (2001). The superstructure has a total weight of 190 kN/m, and is supported on identical bents uniformly spaced at 39.6 m. For the purpose of response evaluation in the transverse direction, the viaduct can be idealized as a SDOF oscillator (see Figure 10(c)). The properties of SDOF oscillator were carefully tuned so as to represent the design dynamic characteristics of the bridge bent in terms of mass, stiffness, damping, height and force-deformation relation. Some of the relevant design parameters are provided in Figure 10(b). Inelastic material behavior is characterized by the rate-independent elasto-plastic model of Ozdemir (1976) with 2 percent kinematic strain hardening (κ). The system under consideration was initially designed by Chopra and Goel (2001) for a ductility (u_d) of 3.25 while ensuring that the plastic rotation at the base of the

column was limited to 0.02 rad. Foundation flexibility and associated rocking response as well as P- Δ effects were not considered in the design process.

The idealized SDOF system shown in Figure 10(c) is taken as a proxy and is subjected to a series of nonlinear transient analyses. First, the translational component of Pacoima Dam record (see Figure 4) is set as an input without paying attention to the P- Δ effects (to be referred to as Case-1). Figure 11 portrays the inelastic results from Case-1 in which the peak relative displacement reaches 26.5 cm (~ 3 percent drift) and produces a ductility demand of 3.24. In the left panel of this figure, y-axis indicates the normalized base shear. Note that the displacement values ($u = \phi l$) plotted are relative values computed from the relative rotation of the oscillator's mass with respect to its base. The computed ductility demand is almost equal to the design ductility level ($\mu_d = 3.25$), implying that the horizontal component of the Pacoima Dam record satisfies the design requirement at a minimum level with no reservations; thereby it can serve as a benchmark against which relative impacts of multi-component excitations on seismic response can ideally be compared and contrasted. Figure 11 also shows the input force time-history normalized by mass, which is same as the ground acceleration (\ddot{u}_g) for this particular case. From the time-response plot, it is possible to observe that the overall deformation demand in the system is produced by a few plastic cycles initiated by the first major acceleration pulse arrival between 3 and 5 s and followed by the second acceleration pulse arrival between 7 and 8 s (see the two right panels in Figure 11).

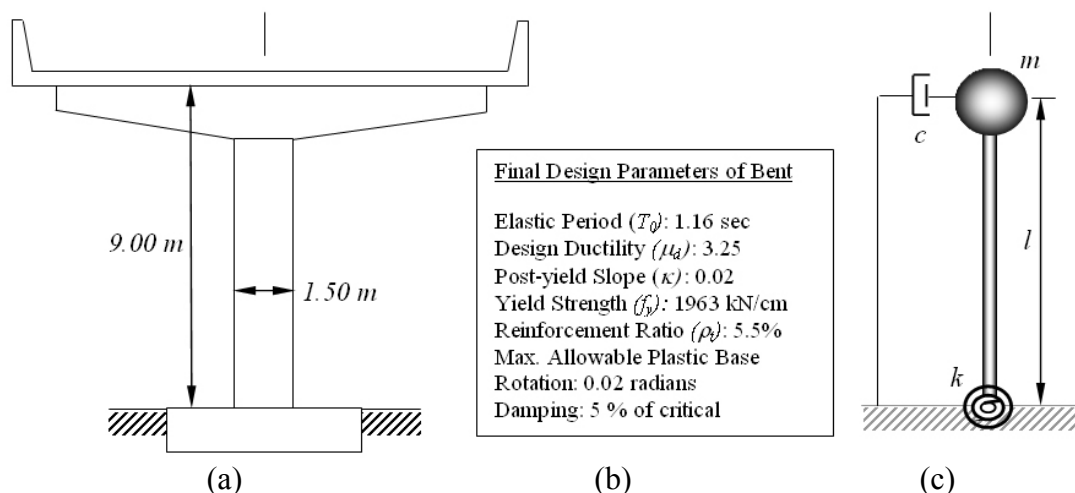


Fig. 10 (a) Single column of a bridge bent; (b) Design parameters; (c) Idealized SDOF system

Repeating the analysis by including the P- Δ effects (to be referred to as Case-2) escalates the ductility demand from 3.24 to 3.32. The difference is only 2.5 percent of the demand for Case-1. Thus, inclusion of the P- Δ effects for a long-length system excited by the translational motion only has limited impact on the peak displacement demand (although the system got pushed to almost 3 percent additional relative drift). The geometric-stiffness term contributes more to the overall stiffness, as the height of the system decreases, as opposed to an increase in the axial load. As compared to Case-2, when the horizontal component is coupled with the vertical component, the P- Δ effects gain more significance since vertical component starts playing role in the geometric-stiffness formulation (see Equation (8)). Figure 12 compares the results for the coupled horizontal and vertical components motion (to be referred to as Case-3) with those of the horizontal excitation with and without the P- Δ effects (i.e., Case-2 and Case-1, respectively). Coupling of the vertical component with the horizontal one essentially has no influence on the inertia force (see Equation (9)), and the normalized input force remains unchanged (see the right top panel in Figures 11 and 12); however influence of the vertical excitation on the geometric-stiffness term and consequently on the SDOF response is evident from the force-deformation relation and displacement time-history plots. Coupling of the horizontal and vertical components in this example raises the ductility demand to 3.63, which is 12 percent larger than the design level (i.e., Case-1). More importantly, the P- Δ effects enhanced by the vertical motion create negative tangent stiffness in the post-yield deformation range by offsetting the effects of kinematic strain hardening. As mentioned earlier this, in turn, can distort

the expected performance of the structure by causing the inelastic deformation accumulation in one direction.

In general, systematic differences between Case-1 and Case-3 show that the structure designed for horizontal component only, without accounting for the influence of vertical component coupling, may lead to non-conservatism. It should be also reminded that the inclusion of vertical component does not necessarily worsen the seismic demand. Depending on the phase difference between the major vertical acceleration pulses and the gravitational acceleration, the vertical component may act conversely and minimize the P- Δ effects.

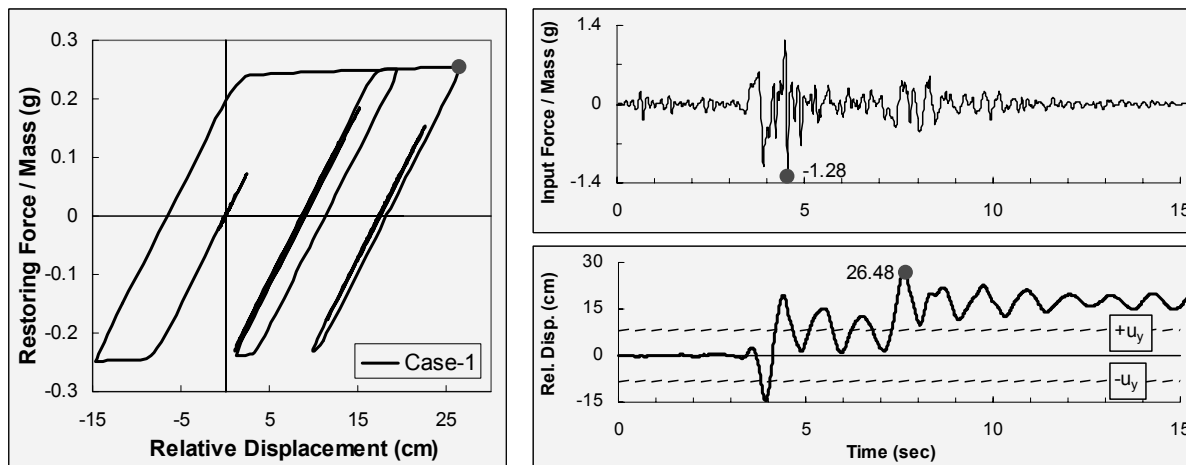


Fig. 11 Inelastic response of the idealized single bridge bent under the translation component of the Pacoima dam upper left abutment record (Case-1) (P- Δ effects are not included; filled circles (●) denote the peak values; dashed lines in the displacement time-history indicate the negative and positive yield-displacement demands)

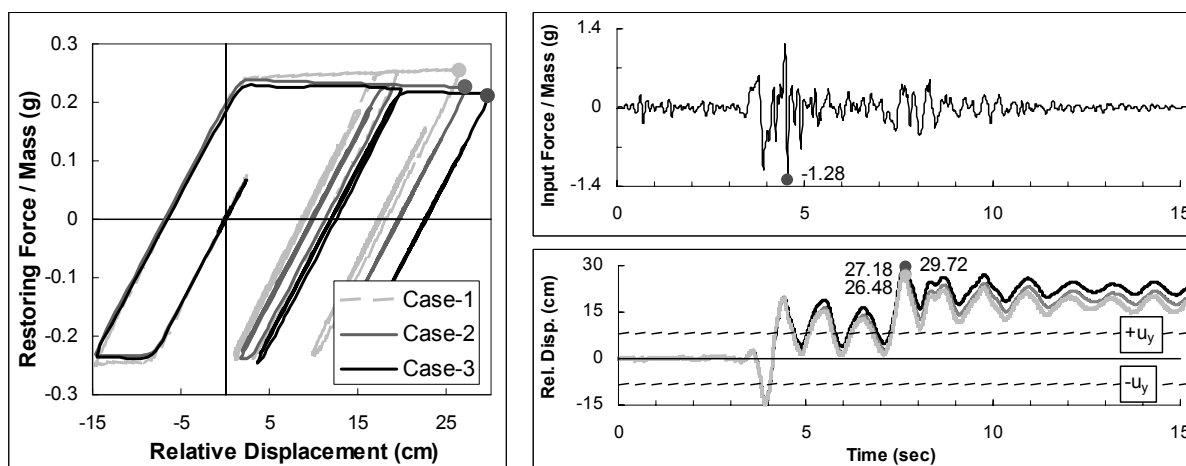


Fig. 12 Comparison of the force-deformation relations for various combinations of the horizontal and vertical components of ground motion and the P- Δ effects (Case-1: horizontal excitation without the P- Δ effects; Case-2: horizontal excitation with the P- Δ effects; Case-3: coupled horizontal and vertical excitations with the P- Δ effects)

In the example shown in Figure 12 (see Case-3), vertical pulses are seen to be in phase with the gravity; therefore, they tend to reduce the overall system stiffness by magnifying the geometric-stiffness term. The vertical component is next applied with opposite sign (to be referred to as Case-4), and corresponding response of the SDOF oscillator is compared in Figure 13(a) with that of Case-1, Case-2 and Case-3. Maximum ductility of the SDOF oscillator in Case-4 is limited to 3.0. Therefore, compared to Case-1 (i.e., the design case), the coupling of horizontal and vertical components either causes 8

percent reduction or 12 percent increase in the ductility demand, depending on the direction of the acceleration pulses contained in the vertical component of the motion. It is also important to observe that the vertical component progressively influences the overall stiffness of the system. Such behaviour manifests itself as distortions (due to the wave-effect) on the slope of the force-deformation relation, which is initially set as a smooth transition in the nonlinear material model (see the small window in Figure 13(b); these distortions become more obvious as the ductility demand increases).

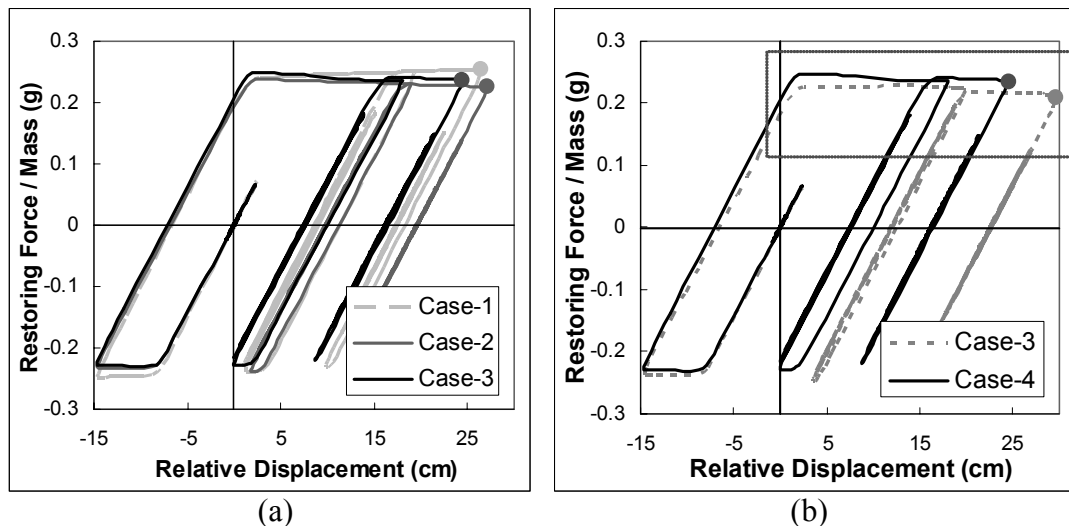


Fig. 13 Comparison of the force-deformation relations for various combinations of the horizontal and vertical components of ground motion and the P-Δ effects (Case-1: horizontal excitation without the P-Δ effects; Case-2: horizontal excitation with the P-Δ effects; Case-3: coupled horizontal and vertical excitations with the P-Δ effects)

So far, the impact of the simultaneous application of the vertical and horizontal components on the displacement and ductility demands of a bridge bent is comparatively demonstrated. In the next phase, the tilt component of the motion is incorporated in the response computations. Note that unlike the vertical motion, the tilt component affects the right side of the equation of motion by introducing additional lateral forces (see Equations (6) and (10)); yet it has no impact on the geometric-stiffness term. Figure 14 compares the inelastic displacement response of the SDOF oscillator when the three components are applied in tandem (to be referred to as Case-5). Also plotted in Figure 14 is the response from Case-3 for a direct comparison. It is evident that inclusion of the tilt motion during the response analysis results in a noticeable asymmetric deformation compared to the previous cases (Case-1 to Case-4). One of the consequences of the asymmetric deformation is a large relative displacement and the resultant higher ductility demand. The maximum ductility demand caused by the coupled motion extends to 9.1, while it remains only 3.63 when the tilt effects are excluded. Therefore, for the tall systems, the tilt component (if it reaches a few degrees) has a more pronounced impact than the vertical motion. Figure 14 suggests that the structures that would not have collapsed under a few cycles of shaking may be driven to collapse due to additional plastic cycles associated with the coupling of ground motion components (if $|\kappa - \theta|$ is large enough). In fact, coupling of the three components of motion results in numerous additional cycles of deformation that exceed the yield rotation. Since the inelastic response results in a permanent drift, it is more convenient to count the number of half-cycles wherein each half-cycle is the peak-to-peak amplitude. If the peak-to-peak amplitude exceeds twice the yield rotation, each such cycle is referred to as a “plastic cycle” (Kalkan and Kunnath, 2006). For Case-5, there were eight half-plastic cycles during the response, whereas ignoring tilt component as in Case-3 produced only three half-plastic cycles. The cumulative damage resulting from the plastic cycles in degrading systems (although not considered here) is much greater than that implied by the peak ductility demand and should not be ignored in the performance assessment of structural systems (Kunnath and Kalkan, 2004).

Another important aspect of including tilt in the analysis is the resultant maximum and residual base rotation from the design and serviceability point of view. Figure 15 compares the drift time-histories for the SDOF oscillator excited by multi-component motions (i.e., Case-5 and Case-3) and by the

translational motion alone (i.e., Case-1). Recall that the permissible column base rotation constraint by the design is 0.02 rad. Case-1 satisfies this design criterion by producing peak plastic rotation not exceeding but close to 0.02 rad. This limit is exceeded in Case-3 by 20 percent, whereas Case-5 exerts large influence on the drift demand with the system pushed to almost 8 percent plastic rotation. This is significantly (almost four times) larger than the design limit. There is also an obvious difference in the residual rotations in the coupled cases and in that caused by the translational motion alone. As the ground motion ceased, the SDOF oscillator excited by the translational component remained in the tilted position at only 0.7° (0.012 rad), while considering coupling of the three components doubled it in the opposite direction with a relative inclination of 1.4° (0.024 rad).

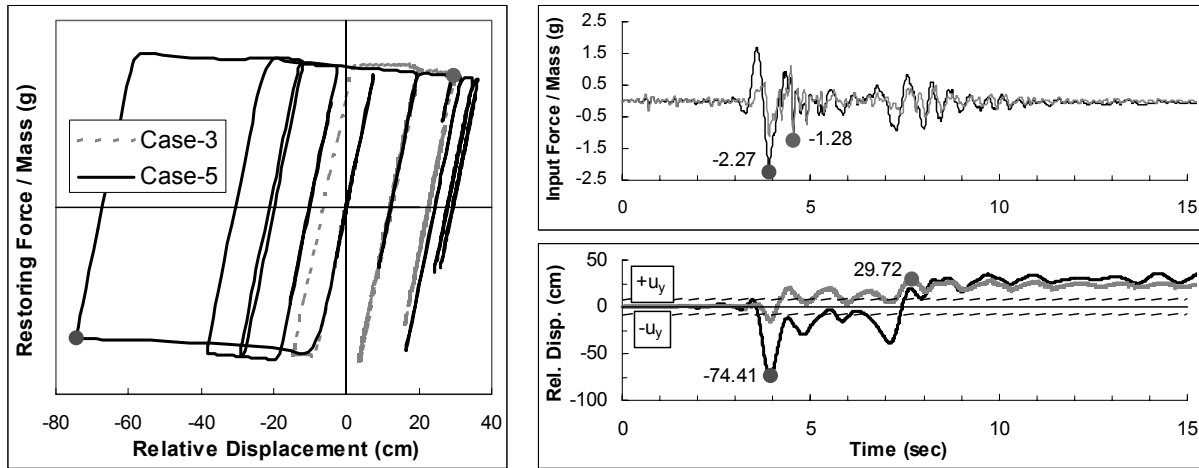


Fig. 14 Comparison of the force-deformation relations for various combinations of the horizontal and vertical components and the P- Δ effects (Case-3: coupled horizontal and vertical excitations with the P- Δ effects; Case-5: coupled horizontal, vertical and tilting excitations with the P- Δ effects)

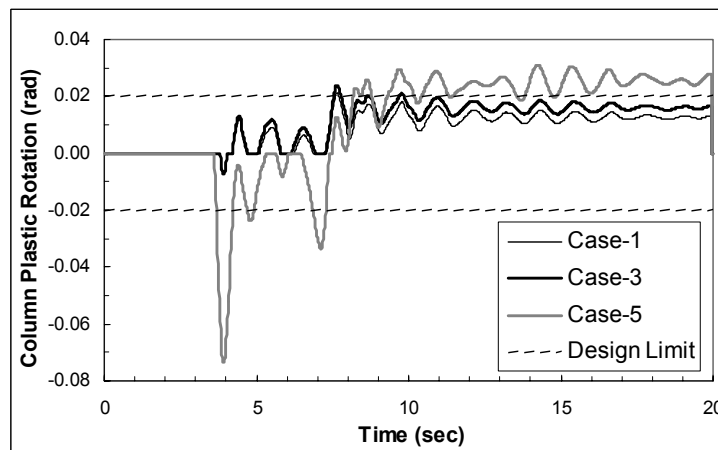


Fig. 15 Column plastic rotation demands imposed by the translational motion (Case-1), coupled translational and vertical motion (Case-3), and by the coupled translational, vertical and tilt motion (Case-5) (dashed lines indicate the permissible plastic rotation constraint by design)

Figures 14 and 15 collectively indicate that coupling of the three components leads to a radically different dynamic response as compared to the response produced by the horizontal motion alone. An eminent fact that emerges from these results is that if the maximum deformation demand is considered as a performance evaluation criterion, one neglects the big difference in the behavior that a system exhibits on considering or not considering the multi-component coupling effects. In order to systematically address this issue in the design of new structures or in the performance evaluation of existing structures, peak response values for a range of periods are computed and combined in a spectral format. The

resultant spectrum is referred to as “multi-component ground motion response spectrum”, and it is conceptually detailed in the following section.

MULTI-COMPONENT GROUND MOTION RESPONSE SPECTRA

For the design and performance assessment of structures, a ground motion spectrum is often computed considering only the horizontal component. In rare applications, the vertical ground motion spectrum is also utilized in parallel. In generating a horizontal spectrum, it is customary to characterize the P- Δ effects by the constant values of stability coefficient θ (e.g., Bernal, 1998; MacRae, 1994), although in many cases such effects are completely disregarded. As mentioned earlier, the use of θ in a spectral format is misleading since θ is a spectral-period-dependent parameter (see Equation (2)). On the other hand, the “geometric oscillation period” (T_G or T'_G) becomes a more meaningful descriptor to characterize the P- Δ effects since it is independent of the spectral period. For the bridge bent example shown in Figure 10, T_G equals 6.0 s, being much larger than $T_0 = 1.16$ s. The large difference between T_G and T_0 implies that instability is unlikely to occur as long as the system is subjected to the horizontal excitation alone. On the other hand, due to the vertical component coupling, geometric oscillation period becomes time-variant (see Equation (12)). Figure 16 shows the plot of the time-variation of T'_G when the vertical and horizontal components are simultaneously applied to the SDOF oscillator base. Also marked in this figure is the constant value of T_G as a reference to demonstrate the degree of fluctuation. Note that in the beginning and as the amplitude of the vertical component of motion diminishes, T'_G converges to T_G . Stability in the system increases as T'_G becomes larger than T_G . On the other hand, the system tends to be less stable if T'_G falls below T_G . As Figure 16 shows, the minimum value of T'_G is 4.04 s, being 30 percent smaller than T_G . If the vertical excitation effects are accounted for in the translational response computation, it is always recommended to check the variation of T'_G before starting the analysis or design process. For stable systems, T'_G should always be larger than T_0 (see Equation (14)); likewise θ' should be less than unity.

In order to identify those situations in which the overall response is likely to receive significant contributions from the vertical and tilt components of ground motion, regular response spectra (based on the translational motion only) and multi-component ground motion spectra including the three components of motion in tandem are compared. 5 percent of critical damping is used for each case, and three components of Pacoima dam record are used as the input. The P- Δ effects are represented by the “geometric oscillation period” ($T'_{G,\min} = 4.04$ s in the cases where the vertical excitation is accounted for). Figure 17 portrays the elastic (i.e., ductility = 1.0) and inelastic spectral response quantities of interest, i.e., the relative displacement of a SDOF system and its time derivatives. The inelastic spectra are generated for the constant ductility ratios of 3 and 6. As depicted, the tilt component, when it is coupled with the vertical and translational components, amplifies all response quantities regardless of the spectral period. The difference between the two cases becomes more pronounced as the spectral period increases, and is noticeable at all ductility levels. At the mid-range and longer periods, the multi-component excitation yields more than three times larger spectral displacement demand compared to the displacement demand imposed by the pure translational motion. The major contributor to the amplified seismic level is the tilt component whose adverse effects are inherently conditioned on the height of the system. Based on the difference between the spectral ordinates in Figure 17, it can be concluded that ground tilting of few degrees can be most detrimental, particularly for the long and flexible structures.

These results indicate that isolating the effects of vertical and horizontal excitations in design or assessment studies by ignoring their coupling effects could be misleading. Given a structural system and estimated yield displacement, the usual design process is to determine the associated strength value required to limit the ductility and peak displacement response within acceptable performance levels. In that respect, multi-component spectra can serve as a useful tool, since the multi-component excitation effects on the translational response of the system can be estimated accurately by using the information available in the early stage of design process (i.e., initial period, damping, and design ductility demand).

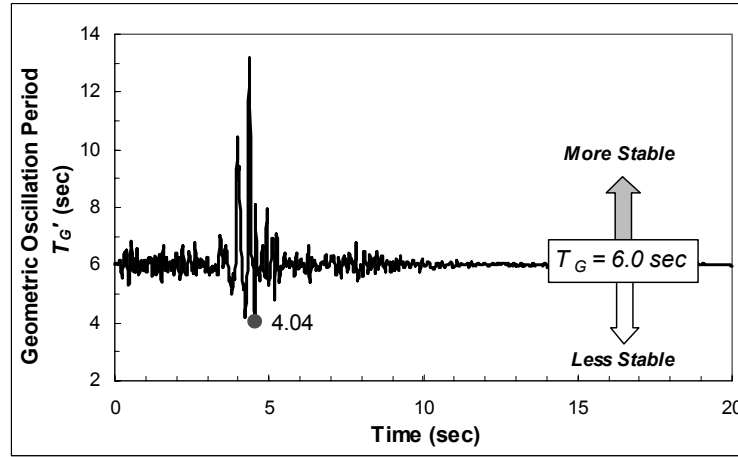


Fig. 16 Time variation of geometric oscillation period (T'_G)

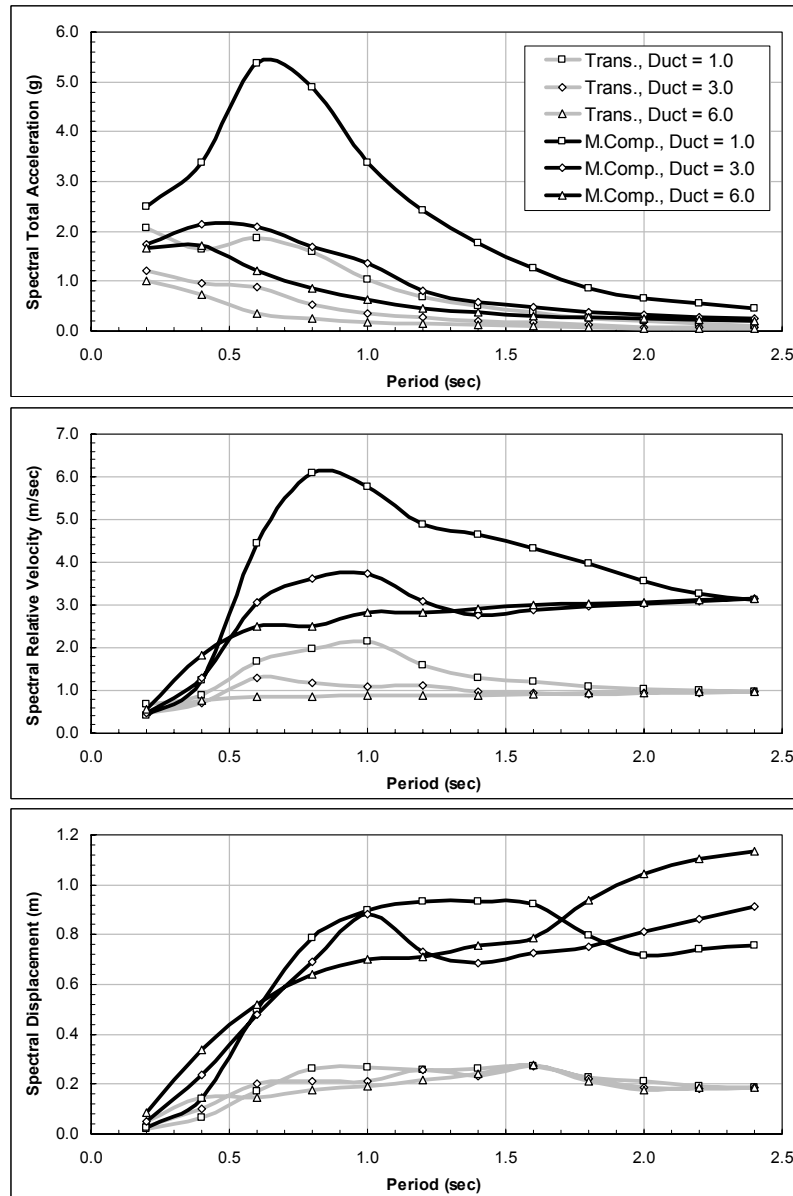


Fig. 17 Constant-ductility inelastic response spectra for acceleration, velocity and displacement (Trans.: translational motion only without the P- Δ effects; M. Comp.: multi-component excitation with the P- Δ effects)

SUMMARY AND CONCLUSIONS

In current practice, seismic demands are established based on the horizontal excitation through an uncoupled equation of motion without paying attention to the P- Δ effects. Vertical and rotational components on the other hand are almost always neglected. In reality, peak amplitude of the vertical ground motion can exceed that of the horizontal motion at short periods and near-source distances. Intensity of the rotational components may also be large in the near-field zone. For a structure to exhibit satisfactory performance, its seismic design should provide adequate stiffness and strength so that its ultimate ductility level does not exceed its maximum ductility under the design level seismic excitation. Using the above as a performance evaluation criterion, a structure exhibiting satisfactory seismic performance under a translational motion may go into large displacement demands (or even collapse) when the translational motion is coupled with intense vertical motion and/or ground tilting of a few degrees. In order to put such amplified seismic demands in proper design and performance assessment perspective, the governing equation of motion that implicitly constitutes the forcing functions associated with the multi-component excitations is postulated. The extended equation is theoretically complete for the three components of motion. Based on this equation, the multi-component spectrum is proposed for use in engineering applications. The proposed spectrum reflects the kinematic characteristics of the ground motion that are not identifiable by the conventional ground motion response spectrum alone, at least for the near-fault region where the high intensity vertical shaking and rotational excitation are likely to occur.

Based on the findings of this study, the following conclusions are made:

- Comparison of the coupled and uncoupled equations of motion used to compute the response of the SDOF oscillator clearly indicates the level of simplification that is introduced by ignoring the vertical component and the ground tilting. Results of the current work and our previous study (Kalkan and Graizer, 2007) emphasize that inclusion of vertical and tilt components in the computation of the ductility demand results in additional forcing functions and enhanced P- Δ effects. The resulting amplified seismic demand and eroded stiffness may adversely influence the displacement (ductility) demand and dynamic stability. Therefore, for structures susceptible to high-intensity vertical shaking and/or ground tilting, multi-components effects should be considered in their seismic design or performance assessment.
- Except in rare applications, P- Δ effects are practically neglected when the seismic demands are presented in a spectral format. The difference between the first-order and second-order analyses becomes evident, as the coupling of vertical and tilt components is included. In this respect, geometric-stiffness term turns out to be the controlling parameter. It is independent of both non-stationary tilting and horizontal excitations, whereas it is a function of axial load, vertical motion and length of the oscillator.
- If the direction of dominant vertical pulses is in phase with the gravity, they may diminish the overall stiffness of system by increasing the contribution of the geometric-stiffness term. The associated enhanced P- Δ effects may create negative tangent stiffness in the post-yield deformation range by offsetting the effects of kinematic strain hardening. Hence, the bias towards increasing displacements in one direction becomes increasingly larger. This may create important practical consequences, e.g., dynamic instability (or collapse) can be initiated if the energy of the multi-component excitations is large enough to carry the system inelastically in one direction. On the other hand, if the major pulses in the vertical component are out of phase with respect to the gravity, they act conversely and tend to minimize the destabilizing force. Same applies for the tilt component: depending upon its phase difference with respect to the horizontal motion, it may either remediate the system by offsetting the plastic rotations and reducing the overall inertia force, or it may act in line with the horizontal motion and amplify the total inertia force.
- Inclusion of tilt excitation in the dynamic response computations increases the individual forcing functions on the right side of the equation of motion, and its P- Δ contribution is implicitly considered within the geometric-stiffness term; therefore the only change takes place on the right side of the equation. However, including vertical component in addition to the tilt excitation results in not only an additional forcing term on the right side of the equation but also in a change on the left side of the equation within the geometric-stiffness term. The modified term becomes time-variant and vertical component may gradually modify its value. The instantaneous changes in the geometric-stiffness term

create progressive modifications in the overall stiffness. This situation can virtually be observed from the initial slope of the force-deformation curve, which may diverge, at any instant, from its initial linear elastic position (this divergence is even more pronounced in the inelastic regime). The intensity of these time-variant changes (referred to as the “wave-effect”) in the force-deformation slope depends on the amplitude of the vertical acceleration pulses. If the intensity of the vertical acceleration pulses is large enough, the oscillator period may show noticeable variations. In that case, it is not possible to retain a constant-period oscillation, and a linear-elastic oscillator may act as a nonlinear-elastic oscillator. This phenomenon may have unfavorable effects, especially on the inverted pendulums used in some old ground motion recording instruments (e.g., mechanical horizontal seismometer of Weichert).

- In this study, geometric oscillation period (T_G) (or T'_G if vertical excitation is considered) is used in lieu of the stability coefficient (θ), to represent the P- Δ effects in response spectra. Unlike the geometric oscillation period, θ is a function of the stiffness (i.e., spectral period); therefore, it cannot be a spectrum-compatible parameter (assuming that the length of the oscillator is kept invariant at each spectral period). For a stable system, geometric oscillation period should be greater than the initial elastic period. Therefore, T_G (or T'_G) can serve as a valuable tool in design to assure stability by quantifying the lower-bound limit for the lateral stiffness while considering possible intensity of the vertical shaking (to be on the conservative side, peak intensity of the vertical motion should be assumed to be in phase with the gravity).
- Compared to vertical component, tilt component of the motion has more impact on the translational response of the system. Few degrees of dynamic ground tilting can easily double the overall system response. This difference will be more pronounced for the tall structures since the inertia force due to the angular acceleration is directly proportional to the effective height.
- The governing equation of motion considering the multi-component excitation is derived based on the concept of equivalent fixed-base oscillator; hence it directly provides the relative drift associated with the exact deformation. This interpretation makes the implementation easy in a computational framework. In this study, the equations of motion were formulated in a state-space form in MATLAB, and were solved in time domain by using the stiff ordinary differential equation solver (ODE15s).

Formulations and methodology presented herein are limited to the structural systems that can be potentially idealized as a SDOF oscillator. The vertical oscillation of mass and its corresponding effects (i.e., axial force and bending moment interaction at the section level) were not accounted for. Expanding the analytical approach for including such effects requires the SDOF idealization to be violated and thus necessitates a MDOF system solution. Foundation effects and associated rocking response were also not included; readers are referred to the study by Kalkan and Graizer (2007) for including the rocking effects. Results presented here are based on three components (i.e., horizontal, vertical and tilt) of the Pacoima dam upper left abutment record. The physically measured permanent tilt at this station (few days after the earthquake) provided the opportunity to extract a realistic tilting motion. Due to the recorded rotational components during a strong ground shaking being unavailable, our results are limited to the ground motion recorded at this station only.

ACKNOWLEDGEMENTS

We would like to thank Dr. E. Erduran for compiling near-fault ground motion subset from the NGA dataset. Sincere thanks are extended to Professor M.D. Trifunac for his encouragement and valuable comments. We also acknowledge the suggestions of three anonymous reviewers, which improved the technical quality of the paper. Any opinions, findings, and conclusions or recommendations expressed in this paper are those of the authors solely and do not necessarily reflect the views of the California Geological Survey.

REFERENCES

1. Abdelkareem, K.H. and Machida, A. (2000). "Effects of Vertical Motion of Earthquake on Failure Mode and Ductility of RC Bridge Piers", Proceedings of the 12th World Conference on Earthquake Engineering, Auckland, New Zealand, Paper No. 0463 (on CD).
2. Akiyama, H. (1985). "Earthquake-Resistant Limit-State Design of Buildings", University of Tokyo Press, Tokyo, Japan.
3. Ambraseys, N.N. and Simpson, K.A. (1996). "Prediction of Vertical Response Spectra in Europe", Earthquake Engineering & Structural Dynamics, Vol. 25, No. 4, pp. 401–412.
4. Ariman, T. and Muleski, G.E. (1981). "A Review of the Response of Buried Pipelines under Seismic Excitation", Earthquake Engineering & Structural Dynamics, Vol. 9, No. 2, pp. 133–152.
5. Bernal, D. (1998). "Instability of Buildings during Seismic Response", Engineering Structures, Vol. 20, No. 4-6, pp. 496–502.
6. Biot, M.A. (1932). "Transient Oscillations in Elastic Systems", Ph.D. Thesis No. 259, Aeronautics Department, California Institute of Technology, Pasadena, U.S.A.
7. Biot, M.A. (1933). "Theory of Elastic Systems Vibrating under Transient Impulse with an Application to Earthquake-Proof Buildings", Proceedings of the National Academy of Sciences of the United States of America, Vol. 19, No. 2, pp. 262–268.
8. Biot, M.A. (1934). "Theory of Vibration of Buildings during Earthquake", Zeitschrift für Angewandte Mathematik und Mechanik, Vol. 14, No. 4, pp. 213–223.
9. Biot, M.A. (1941). "A Mechanical Analyzer for the Prediction of Earthquake Stresses", Bulletin of the Seismological Society of America, Vol. 31, No. 2, pp. 151–171.
10. Biot, M.A. (1942). "Analytical and Experimental Methods in Engineering Seismology", ASCE Transactions, Vol. 108, pp. 365–408.
11. Bouchon, M. and Aki, K. (1982). "Strain, Tilt, and Rotation Associated with Strong Ground Motion in the Vicinity of Earthquake Faults", Bulletin of the Seismological Society of America, Vol. 72, No. 5, pp. 1717–1738.
12. Bozorgnia, Y. and Campbell, K.W. (2004). "The Vertical-to-Horizontal Response Spectral Ratio and Tentative Procedures for Developing Simplified V/H and Vertical Design Spectra", Journal of Earthquake Engineering, Vol. 8, No. 2, pp. 175–207.
13. Bozorgnia, Y., Niazi, M. and Campbell, K.W. (1995). "Characteristics of Free-Field Vertical Ground Motion during the Northridge Earthquake", Earthquake Spectra, Vol. 11, No. 4, pp. 515–525.
14. Bycroft, G.N. (1980). "Soil-Foundation Interaction and Differential Ground Motions", Earthquake Engineering & Structural Dynamics, Vol. 8, No. 5, pp. 397–404.
15. Castellani, A. and Boffi, G. (1986). "Rotational Components of the Surface Ground Motion during an Earthquake", Earthquake Engineering & Structural Dynamics, Vol. 14, No. 5, pp. 751–767.
16. Chopra, A.K. (1966). "The Importance of the Vertical Component Earthquake Motions", Bulletin of the Seismological Society of America, Vol. 56, No. 5, pp. 1163–1175.
17. Chopra, A.K. and Goel, R.K. (2001). "Direct Displacement-Based Design: Use of Inelastic vs. Elastic Design Spectra", Earthquake Spectra, Vol. 17, No. 1, pp. 47–64.
18. Diotallevi, P.P. and Landi, L. (2000). "Effect of the Axial Force and of the Vertical Ground Motion Component on the Seismic Response of R/C Frames", Proceedings of the 12th World Conference on Earthquake Engineering, Auckland, New Zealand, Paper No. 1026 (on CD).
19. Elnashai, A.S. and Papazoglou, A.J. (1997). "Procedure and Spectra for Analysis of RC Structures Subjected to Strong Vertical Earthquake Loads", Journal of Earthquake Engineering, Vol. 1, No. 1, pp. 121–155.
20. Ghafory-Ashtiany, M. and Singh, M.P. (1986). "Structural Response for Six Correlated Earthquake Components", Earthquake Engineering & Structural Dynamics, Vol. 14, No. 1, pp. 103–119.
21. Graizer, V.M. (1987). "Determination of the Path of Ground Motion during Seismic Phenomena", Izvestiya, Physics of the Solid Earth, Vol. 22, No. 10, pp. 791–794.

22. Graizer, V.M. (1989). "Bearing on the Problem of Inertial Seismometry", *Izvestiya, Physics of the Solid Earth*, Vol. 25, No. 1, pp. 26–29.
23. Graizer, V.M. (1991). "Inertial Seismometry Methods", *Izvestiya, Physics of the Solid Earth*, Vol. 27, No. 1, pp. 51–61.
24. Graizer, V. (2006a). "Tilts in Strong Ground Motion", *Bulletin of the Seismological Society of America*, Vol. 96, No. 6, pp. 2090–2102.
25. Graizer, V. (2006b). "Comparison of Attenuation of Peak Ground Motion and V/H Ratios for California Earthquakes (Abstract)", *Seismological Research Letters*, Vol. 77, No. 2, p. 324.
26. Gupta, V.K. and Trifunac, M.D. (1990). "Response of Multistoried Buildings to Ground Translation and Torsion during Earthquakes", *European Earthquake Engineering*, Vol. IV, No. 1, pp. 34–42.
27. Gupta, V.K. and Trifunac, M.D. (1991). "Effects of Ground Rocking on Dynamic Response of Multistoried Buildings during Earthquakes", *Structural Engineering/Earthquake Engineering, JSCE*, Vol. 8, No. 2, pp. 87s–94s.
28. Hall, W.J., Mohraz, B. and Newmark, N.M. (1975). "Statistical Studies of Vertical and Horizontal Earthquake Spectra", Report NUREG-0003 (prepared for United States Nuclear Regulatory Commission), Newmark Consulting Engineering Services, Urbana, U.S.A.
29. Hart, G.C., Lew, M. and DiJulio, R.M. (1975). "Torsional Response of High-Rise Buildings", *Journal of the Structural Division, Proceedings of ASCE*, Vol. 101, No. ST2, pp. 397–414.
30. Housner, G.W. (1959). "Behavior of Structures during Earthquakes", *Journal of the Engineering Mechanics Division, Proceedings of ASCE*, Vol. 85, No. EM4, pp. 109–129.
31. Huang, B.S. (2003). "Ground Rotational Motions of the 1999 Chi-Chi, Taiwan Earthquake as Inferred from Dense Array Observations", *Geophysical Research Letters*, Vol. 30, No. 6, pp. 1307–1310.
32. Ishida, S. and Morisako, K. (1985). "Collapse of SDOF System to Harmonic Excitation", *Journal of Engineering Mechanics, ASCE*, Vol. 111, No. 3, pp. 431–448.
33. Jennings, P.C. and Husid, R. (1968). "Collapse of Yielding Structures during Earthquakes", *Journal of the Engineering Mechanics Division, Proceedings of ASCE*, Vol. 94, No. 5, pp. 1045–1065.
34. JSCE (1995). "Preliminary Report on the Great Hanshin Earthquake, January 17, 1995", Japan Society of Civil Engineers, Tokyo, Japan.
35. Kalkan, E. and Gülkan, P. (2004a). "Site-Dependent Spectra Derived from Ground Motion Records in Turkey", *Earthquake Spectra*, Vol. 20, No. 4, pp. 1111–1138.
36. Kalkan, E. and Gülkan, P. (2004b). "Empirical Attenuation Equations for Vertical Ground Motion in Turkey", *Earthquake Spectra*, Vol. 20, No. 3, pp. 853–882.
37. Kalkan, E. and Graizer, V. (2007). "Coupled Tilt and Translational Ground Motion Response Spectra", *Journal of Structural Engineering, ASCE*, Vol. 133, No. 5, pp. 609–619.
38. Kalkan, E. and Kunnath, S.K. (2006). "Effects of Fling Step and Forward Directivity on the Seismic Response of Buildings", *Earthquake Spectra*, Vol. 22, No. 2, pp. 367–390.
39. Kharin, D.A. and Simonov, L.I. (1969). "VBPP Seismometer for Separate Registration of Translational Motion and Rotations", *Seismic Instruments*, Vol. 5, pp. 51–66 (in Russian).
40. Kunnath, S.K. and Kalkan, E. (2004). "Evaluation of Seismic Deformation Demands Using Non-linear Procedures in Multistory Steel and Concrete Moment Frames", *ISET Journal of Earthquake Technology*, Vol. 41, No. 1, pp. 159–181.
41. Kunnath, S., Abrahamson, N., Chai, Y.H., Zong, Z. and Yilmaz, Z. (2005). "Effects of Vertical Ground Motions on Seismic Response of Highway Bridges", *Proceedings of the Bridge Research Conference 2005, Sacramento, U.S.A., Paper No. 02-504 (on CD)*.
42. Lam, N., Wilson, J., Chandler, A. and Hutchinson, G. (2000). "Response Spectrum Modeling for Rock Sites in Low and Moderate Seismicity Regions Combining Velocity, Displacement and Acceleration Predictions", *Earthquake Engineering & Structural Dynamics*, Vol. 29, No. 10, pp. 1491–1525.
43. Lee, V.W. (1979). "Investigation of Three-Dimensional Soil-Structure Interaction", Report CE 79-11, University of Southern California, Los Angeles, U.S.A.

44. Lee, V.W. and Trifunac, M.D. (1985). "Torsional Accelerograms", *International Journal of Soil Dynamics and Earthquake Engineering*, Vol. 4, No. 3, pp. 132–139.
45. Lee, V.W. and Trifunac, M.D. (1987). "Rocking Strong Earthquake Accelerations", *Soil Dynamics and Earthquake Engineering*, Vol. 6, No. 2, pp. 75–89.
46. MacRae, G.A. (1994). "P- Δ Effects on Single-Degree-of-Freedom Structures in Earthquakes", *Earthquake Spectra*, Vol. 10, No. 3, pp. 539–568.
47. Malhotra, P.K. (2006). "Smooth Spectra of Horizontal and Vertical Ground Motions", *Bulletin of the Seismological Society of America*, Vol. 96, No. 2, pp. 506–518.
48. Mohraz, B. (1976). "A Study of Earthquake Response Spectra for Different Geological Conditions", *Bulletin of the Seismological Society of America*, Vol. 66, No. 3, pp. 915–935.
49. Newmark, N.M. and Hall, W.J. (1969). "Seismic Design Criteria for Nuclear Reactor Facilities", *Proceedings of the Fourth World Conference on Earthquake Engineering*, Santiago, Chile, Vol. B-4, pp. 37–50.
50. Newmark, N.M. and Hall, W.J. (1982). "Earthquake Spectra and Design", Monograph MNO-3, Earthquake Engineering Research Institute, Berkeley, U.S.A.
51. Newmark, N.M., Blume, J.A. and Kapur, K.K. (1973). "Seismic Design Spectra for Nuclear Power Plants", *Journal of the Power Division, Proceedings of ASCE*, Vol. 99, No. PO2, pp. 287–303.
52. Niazi, M. (1986). "Inferred Displacements, Velocities and Rotations of a Long Rigid Foundation Located at El Centro Differential Array Site during the 1979 Imperial Valley, California, Earthquake", *Earthquake Engineering & Structural Dynamics*, Vol. 14, No. 4, pp. 531–542.
53. Niazi, M. and Bozorgnia, Y. (1991). "Behavior of Near-Source Peak Horizontal and Vertical Ground Motions over SMART-1 Array, Taiwan", *Bulletin of the Seismological Society of America*, Vol. 81, No. 3, pp. 715–732.
54. Nigbor, R.L. (1994). "Six-Degree-of-Freedom Ground-Motion Measurement", *Bulletin of the Seismological Society of America*, Vol. 84, No. 5, pp. 1665–1669.
55. Oliveira, C.S. and Bolt, B.A. (1989). "Rotational Components of Surface Strong Ground Motion", *Earthquake Engineering & Structural Dynamics*, Vol. 18, No. 4, pp. 517–526.
56. Ozdemir, H. (1976). "Nonlinear Transient Dynamic Analysis of Yielding Structures", Ph.D. Dissertation, Department of Civil Engineering, University of California, Berkeley, U.S.A.
57. Pamuk, A., Kalkan, E. and Ling, H.I. (2005). "Structural and Geotechnical Impacts of Surface Rupture on Highway Structures during Recent Earthquakes in Turkey", *Soil Dynamics and Earthquake Engineering*, Vol. 25, No. 7-10, pp. 581–589.
58. Papazoglou, A.J. and Elnashai, A.S. (1996). "Analytical and Field Evidence of the Damaging Effect of Vertical Earthquake Ground Motion", *Earthquake Engineering & Structural Dynamics*, Vol. 25, No. 10, pp. 1109–1137.
59. Power, M., Chiou, B., Abrahamson, N. and Roblee, C. (2006). "The Next Generation of Ground Motion Attenuation Models (NGA) Project: An Overview", *Proceedings of the Eighth U.S. National Conference on Earthquake Engineering (8NCEE)*, San Francisco, U.S.A., Paper No. 2022 (on CD).
60. Ranzo, G., Petrangeli, M. and Pinto, P.E. (1999). "Vertical Oscillations due to Axial-Bending Coupling during Seismic Response of RC Bridge Piers", *Earthquake Engineering & Structural Dynamics*, Vol. 28, No. 12, pp. 1685–1704.
61. Salazar, A.R. and Haldar, A. (2000). "Structural Responses Considering the Vertical Component of Earthquakes", *Computers & Structures*, Vol. 74, No. 2, pp. 131–145.
62. Seed, H.B., Ugas, C. and Lysmer, J. (1976). "Site-Dependent Spectra for Earthquake-Resistant Design", *Bulletin of the Seismological Society of America*, Vol. 66, No. 1, pp. 221–243.
63. Shakal, A., Cao, T. and Darragh, R. (1994). "Processing of the Upper Left Abutment Record from Pacoima Dam for the Northridge Earthquake", Report OSMS 94-13, Department of Conservation, State of California, Sacramento, U.S.A.
64. Silva, W. (1997). "Characteristics of Vertical Strong Ground Motions for Applications to Engineering Design", *Proceedings of the Workshop on National Representation of Seismic Ground Motion for New and Existing Highway Facilities*, Burlingame, U.S.A., pp. 205–252.

65. Stratta, J.L. and Griswold, T.F. (1976). "Rotation of Footings due to Surface Waves", *Bulletin of the Seismological Society of America*, Vol. 66, No. 1, pp. 105–108.
66. Sun, C.-K., Berg, G.V. and Hanson, R.D. (1973). "Gravity Effect on Single-Degree Inelastic System", *Journal of the Engineering Mechanics Division, Proceedings of ASCE*, Vol. 99, No. EM1, pp. 183–200.
67. Takeo, M. and Ito, H.M. (1997). "What Can Be Learned from Rotational Motions Excited by Earthquakes?", *Geophysical Journal International*, Vol. 129, No. 2, pp. 319–329.
68. Trifunac, M.D. and Hudson, D.E. (1971). "Analysis of the Pacoima Dam Accelerogram—San Fernando, California, Earthquake of 1971", *Bulletin of the Seismological Society of America*, Vol. 61, No. 5, pp. 1393–1411.
69. Trifunac, M.D. and Todorovska, M.I. (1998). "Nonlinear Soil Response as a Natural Passive Isolation Mechanism—The 1994 Northridge, California, Earthquake", *Soil Dynamics and Earthquake Engineering*, Vol. 17, No. 1, pp. 41–51.
70. Trifunac, M.D., Todorovska, M.I. and Ivanović, S.S. (1996). "Peak Velocities and Peak Surface Strains during Northridge, California, Earthquake of 17 January 1994", *Soil Dynamics and Earthquake Engineering*, Vol. 15, No. 5, pp. 301–310.
71. Uenishi, K. and Sakurai, S. (2000). "Characteristic of the Vertical Seismic Waves Associated with the 1995 Hyogo-Ken Nanbu (Kobe), Japan Earthquake Estimated from the Failure of the Daikai Underground Station", *Earthquake Engineering & Structural Dynamics*, Vol. 29, No. 6, pp. 813–821.
72. Weichert, D.H., Wetmiller, R.J. and Munro, P. (1986). "Vertical Earthquake Acceleration Exceeding 2 g? The Case of the Missing Peak", *Bulletin of the Seismological Society of America*, Vol. 76, No. 5, pp. 1473–1478.

STRENGTH-REDUCTION FACTORS FOR STRUCTURES SUBJECTED TO NEAR-SOURCE DIFFERENTIAL STRONG GROUND MOTIONS

Reza S. Jalali* and Mihailo D. Trifunac**

*Department of Civil Engineering

Iran University of Science & Technology, Narmak, Tehran 16846, Iran

**Department of Civil Engineering

University of Southern California, Los Angeles, CA 90089, U.S.A.

ABSTRACT

The effects of differential motions on strength-reduction factors are described for the structures subjected to propagating horizontal, vertical, and rocking near-source, fault-normal, and fault-parallel strong-motion displacements. It is shown that the common design rules for selection of the strength-reduction factors are not conservative for both fault-normal pulse and fault-parallel displacement. It is recommended that for the design of structures close to active faults the strength-reduction factors for all components of strong motion be constant and equal to $(2\mu - 1)^{1/2}$, where μ is ductility, for long periods, but only up to the collapse boundaries (where dynamic instability and gravity loads dominate). For the periods shorter than about 2 s, these strength-reduction factors should be further reduced by 30 to 50 percent.

KEYWORDS: Strength-Reduction Factors, Earthquake Differential Motions, Non-linear Earthquake Response, Near-Source Earthquake Motion, Design of Structures

INTRODUCTION

In the engineering design of earthquake-resistant structures by pushover analyses (FEMA, 1997a, 1997b, 2000; ATC, 1996), the design is governed by the target displacements determined from the inelastic response of the corresponding single-degree-of-freedom (SDOF) system. For the estimation of the maximum nonlinear response of a SDOF system, u_m , in terms of the maximum linear response, u_0 , it is necessary to specify a relation between u_m and u_0 . By defining the yield-strength reduction factor as $R_y = u_0 / u_y$, where u_y is the yielding displacement of the SDOF-system-equivalent spring, and ductility as $\mu = u_m / u_y$, for the same ground motion the ratio u_m / u_0 becomes equal to μ / R_y . Veletsos and Newmark (1960) were among the first to show that (i) for a long-period SDOF system, when its natural period T_n becomes very long, u_m / u_0 tends to 1, and R_y approaches μ (equal-deformation rule); (ii) for the response amplitudes governed mainly by the peak excitation velocities, u_m / u_0 can be approximated by $\mu / \sqrt{2\mu - 1}$ and R_y by $\sqrt{2\mu - 1}$ (equal-strain-energy rule); and (iii) for a high-frequency (stiff) system when $T_n \sim 0$, $R_y \sim 1$.

Departures from these “equal-energy and equal-displacement rules” were first noted by Riddell and Newmark (1979), and more recently by Cuesta and Aschheim (2001) and Mylonakis and Voyagaki (2006). For the model we study in this paper, of the rigid mass of length L , which experiences two translations and one rotation, as would a three-degree-of-freedom (3DOF) system when excited by propagating horizontal, vertical, and rocking ground motions, the classical equal-energy and equal-displacement rules for SDOF systems will not apply. For convenience and comparison with numerous papers written on this subject, we will nevertheless refer to these classical equal-energy and equal-displacement rules in the discussion of the results for our system.

With a gradual increase in the number of recorded strong-motion accelerograms (Trifunac and Todorovska, 2001), the researchers started to improve these rules to reflect the trends observed in the responses to the recorded data (Veletsos et al., 1965; Veletsos and Vann, 1971; Chopra and Chintanapakdee, 2001; Riddell et al., 2002) for different site conditions and ductility factors (Miranda,

1991; Ruiz-Garcia and Miranda, 2006), for rupture distance and earthquake magnitude (Miranda, 2000), and for fault-normal, near-field records in the zone affected by directivity (Baez and Miranda, 2000; MacRae et al., 2001). Ruiz-Garcia and Miranda (2003) noted that the average value of the ratio u_m/u_0 is not much influenced by the recording site classification, by earthquake magnitude when $u_0/u_y < 4$, or by the rupture distance. Tiwari and Gupta (2000) and Chakraborti and Gupta (2005) presented comprehensive regression models based on large data-sets and showed clear dependence of the strength-reduction factors on magnitude, predominant period, duration of strong motion, and geologic site conditions. Chopra and Chintanapakdee (2004) investigated the variations of inelastic deformation ratio with moment magnitude, fault-to-station distance, and site conditions for far-field and near-field recorded strong ground motions. Jalali and Trifunac (2008) found strong dependence of R_y versus T_n on the magnitude of an earthquake for the response of a SDOF system to motions at the earthquake source. They showed that for synchronous, horizontal near-source ground motions, the classical design curves are conservative for fault-normal pulse but that for fault-parallel displacements the common design rules are not conservative. They recommended that for designs near faults the strength-reduction factors for all components of synchronous motion should be constant for all periods and equal to $(2\mu - 1)^{1/2}$. For differential, horizontal near-source ground motions, they recommended that the strength-reduction factors for all components of motion should be constant for long periods and equal to $(2\mu - 1)^{1/2}$, while for the periods shorter than about 1 s these strength-reduction factors should be further reduced by 30 to 40 percent (Jalali et al., 2007).

The effects of spatial variations of motion at multiple supports of structures may be neglected in many design analyses. However, when the distance between the multiple support points is large (e.g., for bridges, dams, tunnels, long buildings), the effects of differential motions become important and should be considered (Bogdanoff et al., 1965). Spatial and temporal stochastic representations of strong earthquake motion have been investigated (Loh et al., 1982; Harichandran and Vanmarcke, 1986; Hao, 1989). Differential motion effects have been studied for the response of beams (Harichandran and Wang, 1988, 1990; Zerva, 1991), bridges (Kashefi and Trifunac, 1986; Perotti, 1990; Hyun et al., 1992), simple models of three-dimensional structures (Hao, 1991), long buildings (Todorovska and Lee, 1989; Todorovska and Trifunac, 1989, 1990a, 1990b), and dams (Kojic and Trifunac, 1991a, 1991b; Kojic et al., 1988). Okubo et al. (1984) were among the first to measure and interpret finite ground strains of recorded earthquake motions for plan dimensions representative of the intermediate and large buildings. They showed that, for short-period (stiff) structures, finite ground strains lead to increased base shears. Zembaty and Krenk (1993, 1994) studied the same model using random vibration-based shear force response spectrum.

Simple analyses of two-dimensional models of long buildings suggest that when $a/\lambda < 10^{-4}$, where a is the wave amplitude and λ is the corresponding wavelength, the wave-propagation effects on the response of simple structures can be neglected (Todorovska and Trifunac, 1990b). For shorter waves, but those still longer than the characteristic dimensions of the structure, Trifunac and Todorovska (1997) and Trifunac and Gicev (2006) showed that the common response spectrum method for synchronous ground motions can be extended to make it applicable for the earthquake response analyses of extended structures experiencing differential in-plane and out-of-plane ground motions.

The purpose of this paper is to describe the effects of differential motion on the strength-reduction factors of a simple 3DOF structure subjected to the horizontal, vertical, and rocking components of near-source ground motions and to evaluate the validity of the classical strength-reduction factors for such excitations. Analyses of the consequences of the differences in ground motion at structural supports, caused by non-uniform soil properties, soil-structure interaction, and lateral spreading, for example, are beyond the scope of this paper.

Together with several previous studies of the effects of differential strong motion on the response of simple structures (Trifunac and Todorovska, 1997; Trifunac and Gicev, 2006), and of how the strength-reduction factors are affected by the proximity to the earthquake fault (Jalali and Trifunac, 2008; Jalali et al., 2007), this paper also aims to explore how the classical response spectrum method might be extended to apply for physical conditions that are well beyond its original formulation. The original response spectrum method (Biot, 1932, 1933, 1934) has been formulated using a vibrational solution of the differential equation of a SDOF system, for excitation by a synchronous (at one point) and only horizontal

(one component) representation of the ground motion. The role of the simultaneous action by all six components of ground motion (three translations and three rotations) is still rarely considered today in engineering design (Trifunac, 2006), even though it has been 75 years since the response spectrum method was formulated and about 40 years since it became the principal tool in engineering design (Trifunac, 2003). Because the response spectrum method has become an essential part of engineering design and of the description process of how future strong motion should be specified for a broad range of applications (Todorovska et al., 1995), we hope that the present work will help in further understanding and extension of its limits of applicability.

THE MODEL

The nature of relative motion of individual column foundations or of the entire foundation system depends on the type of foundation, the characteristics of the soil surrounding the foundation, the type of incident waves, and on the direction of wave arrival, such that at the base of each column the motion has six degrees of freedom. In this paper we consider only the in-plane horizontal, vertical, and rocking components of the motion of column foundations, and the analysis will be performed for the structures on isolated foundations only. We assume that the structure is near the fault and that the longitudinal axis of the structure (X axis) coincides with the radial direction (r axis) of the propagation of waves from the earthquake source so that the displacements at the base of columns are different as a result of the wave passage. We suppose that excitations at the piers have the same amplitude with different phases. The phase difference (or time delay) will depend upon the distance between piers and the horizontal phase velocity of the incident waves.

The simple model we consider is described in Figures 1(a), 1(b), and 1(c). It represents a one-story structure consisting of a rigid mass m with length L and supported by two rigid massless columns with height h , which are connected at the top to the mass and at the bottom to the ground by rotational springs (see Figure 1(b)). The stiffness of the springs, k_ϕ , is assumed to be elastic-plastic, as shown in Figure 1(a), without hardening. The massless columns are connected to the ground and to the rigid mass by rotational dashpots, c_ϕ , providing a fraction of critical damping equal to 5 percent. Rotation of the columns, ϕ_i , $i = 1, 2$, which is assumed not to be small, leads us to consider the geometric nonlinearity. The mass is acted upon by the acceleration due to gravity, g , and is excited by the differential horizontal, vertical, and rocking ground motions, u_{g_i} , v_{g_i} , and θ_{g_i} , $i = 1, 2$ (see Figure 1c) at the two bases such that

$$u_{g_2}(t) = u_{g_1}(t - \tau); \quad v_{g_2}(t) = v_{g_1}(t - \tau); \quad \theta_{g_2}(t) = \theta_{g_1}(t - \tau); \quad \tau = L/C_x \quad (1)$$

with τ being the time delay between the motions at the two piers and C_x being the horizontal phase velocity of the incident waves. The functional forms of u_{g_i} , v_{g_i} , and θ_{g_i} are defined by the near-source ground motions d_F and d_N , which are described in the next section. The governing differential equation for the system in Figures 1(b) and 1(c) is then

$$\left\{ A + \frac{(B \cos \phi_1 - C \sin \phi_1)}{(B \cos \phi_2 - C \sin \phi_2)} D \right\} \ddot{\phi}_1(t) + \left\{ F - \frac{E}{(B \cos \phi_2 - C \sin \phi_2)} D \right\} = 0 \quad (2)$$

$$\left\{ L + u_{g_2} + h \sin \phi_2 - u_{g_1} - h \sin \phi_1 \right\}^2 + \left\{ v_{g_2} - h(1 - \cos \phi_2) - v_{g_1} + h(1 - \cos \phi_1) \right\}^2 - L^2 = 0$$

where

$$\theta_G = \sin^{-1} \left\{ \frac{v_{g_1} - v_{g_2} - h(1 - \cos \phi_1) + h(1 - \cos \phi_2)}{L} \right\} \quad (3a)$$

$$\dot{\theta}_G = \frac{\dot{v}_{g_1} - \dot{v}_{g_2} - h \sin \phi_1 \dot{\phi}_1 + h \sin \phi_2 \dot{\phi}_2}{L \cos \theta_G} \quad (3b)$$

$$A = -\frac{1}{2} + \left\{ -\frac{1}{4} \sin \phi_1 \cos(\phi_1 - \theta_G) + \frac{\sin \phi_1 \cos \phi_1}{12 \cos \theta_G} \right\} \left\{ \frac{\sin(\phi_2 - \phi_1)}{\cos \theta_G \cos \phi_1 \cos \phi_2 + \frac{1}{2} \sin \theta_G \sin(\phi_1 + \phi_2)} \right\} \quad (3c)$$

$$B = \frac{L + u_{g_2} - u_{g_1}}{h} + \sin \phi_2 - \sin \phi_1 \quad (3d)$$

$$C = \frac{v_{g_2} - v_{g_1}}{h} + \cos \phi_2 - \cos \phi_1 \quad (3e)$$

$$D = -\frac{1}{2} \cos(\phi_2 - \phi_1) + \left\{ -\frac{1}{4} \sin \phi_2 \cos(\phi_1 - \theta_G) - \frac{\sin \phi_2 \cos \phi_1}{12 \cos \theta_G} \right\} \left\{ \frac{\sin(\phi_2 - \phi_1)}{\cos \theta_G \cos \phi_1 \cos \phi_2 + \frac{1}{2} \sin \theta_G \sin(\phi_1 + \phi_2)} \right\} \quad (3f)$$

$$E = \left(\frac{\dot{u}_{g_2} - \dot{u}_{g_1}}{h} - \cos \phi_1 \dot{\phi}_1 + \cos \phi_2 \dot{\phi}_2 \right)^2 + \left(\frac{\dot{v}_{g_2} - \dot{v}_{g_1}}{h} + \sin \phi_1 \dot{\phi}_1 - \sin \phi_2 \dot{\phi}_2 \right)^2 + B \left(\frac{\ddot{u}_{g_2} - \ddot{u}_{g_1}}{h} + \sin \phi_1 \dot{\phi}_1^2 - \sin \phi_2 \dot{\phi}_2^2 \right) + C \left(\frac{\ddot{v}_{g_2} - \ddot{v}_{g_1}}{h} + \cos \phi_1 \dot{\phi}_1^2 - \cos \phi_2 \dot{\phi}_2^2 \right) \quad (3g)$$

$$F = -\frac{1}{2} \cos \phi_1 \left(\frac{\ddot{u}_{g_2} + \ddot{u}_{g_1}}{h} - \sin \phi_1 \dot{\phi}_1^2 - \sin \phi_2 \dot{\phi}_2^2 \right) + \left(\frac{g}{h} + \frac{1}{2} \left(\frac{\ddot{v}_{g_2} + \ddot{v}_{g_1}}{h} - \cos \phi_1 \dot{\phi}_1^2 - \cos \phi_2 \dot{\phi}_2^2 \right) \right) \times \left(\sin \phi_1 + \frac{1}{2} \frac{\cos(\phi_1 - \theta_G) \sin(\phi_2 - \phi_1)}{\cos \theta_G \cos \phi_1 \cos \phi_2 + \frac{1}{2} \sin \theta_G \sin(\phi_1 + \phi_2)} \right) - \frac{1}{12} \frac{L \cos \phi_1}{h \cos \theta_G} \left\{ \frac{h}{L} \left(\frac{\ddot{v}_{g_1} - \ddot{v}_{g_2}}{h} - \cos \phi_1 \dot{\phi}_1^2 + \cos \phi_2 \dot{\phi}_2^2 \right) + \sin \theta_G \dot{\theta}_G^2 \right\} \times \left\{ \frac{\sin(\phi_2 - \phi_1)}{\cos \theta_G \cos \phi_1 \cos \phi_2 + \frac{1}{2} \sin \theta_G \sin(\phi_1 + \phi_2)} \right\} + \left\{ (M_1 + M_2) \cos \phi_1 + \frac{L}{2h} \sin \theta_G \left[(M_2 + M_2') \frac{\cos \phi_1}{\cos \phi_2} - (M_1 + M_1') \right] \right\} \times \left\{ \frac{h}{L} \frac{\sin(\phi_2 - \phi_1)}{\cos \theta_G \cos \phi_1 \cos \phi_2 + \frac{1}{2} \sin \theta_G \sin(\phi_1 + \phi_2)} \right\} - \left(M_2 + M_2' \right) \frac{\cos \phi_1}{\cos \phi_2} - M_1 - M_1' \quad (3h)$$

$$M_1 = \frac{\omega_n^2}{4} \Phi(\phi_1 - \theta_G) + \frac{1}{2} \varsigma \omega_n (\dot{\phi}_1 - \dot{\theta}_G) \quad (3i)$$

$$M_2 = \frac{\omega_n^2}{4} \Phi(\phi_2 - \theta_G) + \frac{1}{2} \varsigma \omega_n (\dot{\phi}_2 - \dot{\theta}_G) \quad (3j)$$

$$M_1' = \frac{\omega_n^2}{4} \Phi(\phi_1 - \theta_{g1}) + \frac{1}{2} \zeta \omega_n (\dot{\phi}_1 - \dot{\theta}_{g1}) \quad (3k)$$

$$M_2' = \frac{\omega_n^2}{4} \Phi(\phi_2 - \theta_{g2}) + \frac{1}{2} \zeta \omega_n (\dot{\phi}_2 - \dot{\theta}_{g2}) \quad (3l)$$

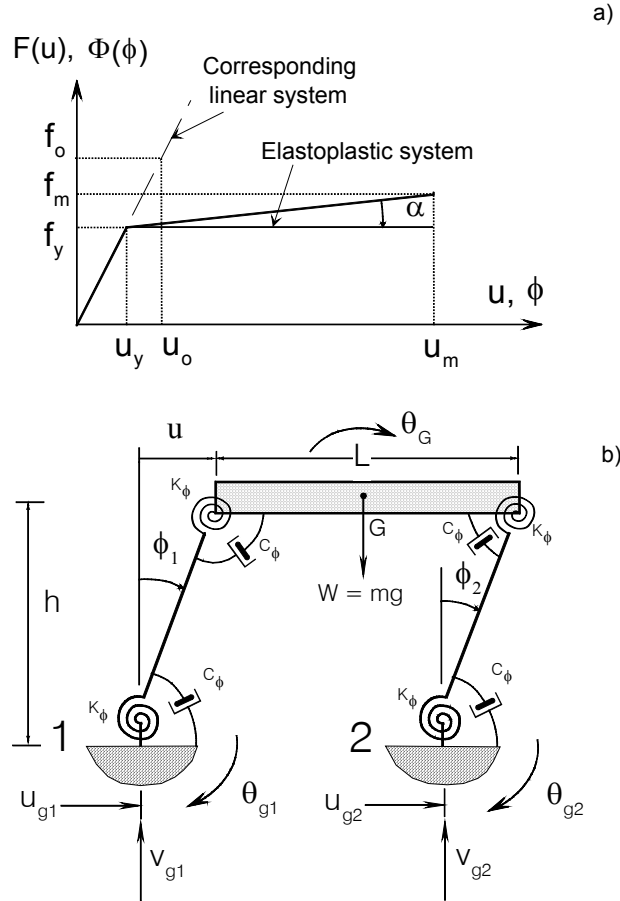


Fig. 1 (a) Force-displacement (moment-rotation) relationship for bilinear spring; (b) Relative responses of the system excited by the differential ground motions, u_{g1} , v_{g1} , θ_{g1} , u_{g2} , v_{g2} , θ_{g2} , at the base of its two columns 1 and 2

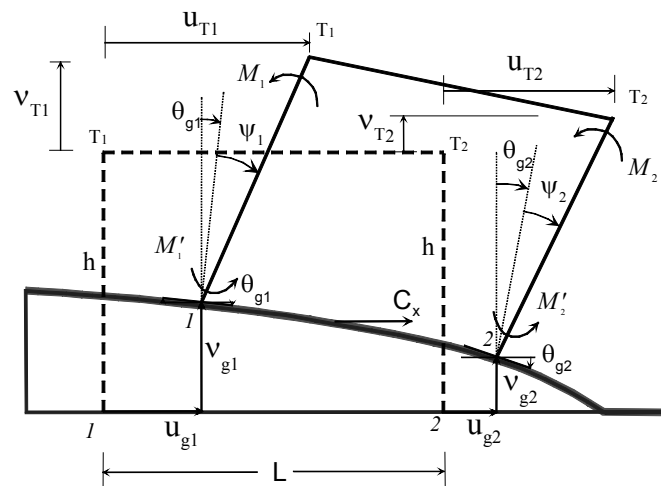


Fig. 1(c) The system deformed by the wave, propagating from left to right, with phase velocity C_x , for the case of $+v_{g_i}$ ("up" motion)

In Equation (3), when $\tau = 0$, ω_n and ζ are the circular natural frequency and damping ratio of the equivalent SDOF system, and $\Phi(\phi)$ is a nonlinear function of the type described in Figure 1(a). For $\tau \neq 0$, the mass with length L has three degrees of freedom (horizontal and vertical translations of G , and rotation θ_G ; see Figures 1(b) and 1(c)).

NEAR-SOURCE GROUND MOTION

In general, it is not possible to predict the detailed nature of the near-source ground motion and of the associated pulses due to irregular distribution of fault slip and because of non-uniform distribution of geologic rigidities surrounding the fault, non-uniform distribution of stress on the fault, and complex nonlinear processes that accompany the faulting (e.g., Trifunac, 1974; Trifunac and Udawadia, 1974; Mavroeidis et al., 2004). Thus, in this paper we adopt a simplified approach and model these motions using smooth pulses that have correct average amplitudes and durations and that have been compared to and calibrated against the observed fault slip and the recorded strong motions in terms of their peak amplitudes in time and their spectral content (Trifunac, 1993; Trifunac and Todorovska, 1994).

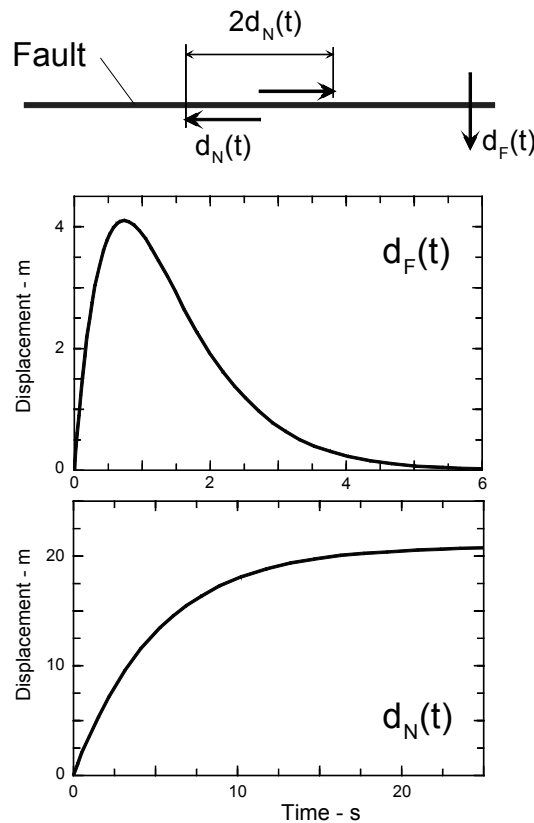


Fig. 2 Fault parallel, $d_N(t)$, and fault-normal (pulse), $d_F(t)$, displacements adopted to represent the near-source motions in this study

Figure 2 shows schematically a plan view of the vertical strike-slip fault and two characteristic simple motions, d_N and d_F , which describe the fault-parallel displacement and fault-normal pulse. For excitation by the fault-normal pulse, we choose (see Figure 2 (center); Trifunac, 1993)

$$d_F(t) = A_F t e^{-\alpha_F t} \quad (4)$$

where the typical values of A_F and α_F for different earthquake magnitudes are shown in Table 1 (Trifunac, 1993). Because the recorded strong-motion data are abundant only up to about $M = 6.5$, we place the values of α_F and A_F , for $M = 7$ and 8 , in Tables 1 and 2 in the parentheses to emphasize that

these are based on extrapolation. For the near-source permanent displacement, we consider (see Figure 2 (bottom))

$$d_N(t) = \frac{A_N}{2} \left(1 - e^{-\frac{t}{\tau_N}} \right) \quad (5)$$

The values of A_N and τ_N for different earthquake magnitudes are shown in Table 2 (Trifunac, 1993).

The amplitudes of d_F and d_N have been studied in many regression analyses of recorded peak displacements at various distances from the fault and in terms of the observed surface expressions of fault slip. In seismological papers the d_N amplitudes are traditionally presented in terms of the average dislocation amplitudes \bar{u} , which are related to d_N as $\bar{u} = 2d_N$ (see Figure 2 (top)). Figure 3 summarizes the trends of average dislocation amplitudes, $\bar{u} = 2d_N$, versus magnitude M . Average dislocation is the value of dislocation amplitudes averaged over the fault surface and is the quantity used in the spectral interpretations of near-field motions and of the body wave amplitudes in the far field. Different symbols in Figure 3 show the results extracted from the studies of selected earthquakes (Trifunac, 1972a, 1972b; Fletcher et al., 1984). The dashed line shows the amplitudes of $2d_{N,\max}$ as used in this paper (see Table 2). It is seen that the agreement is very good.

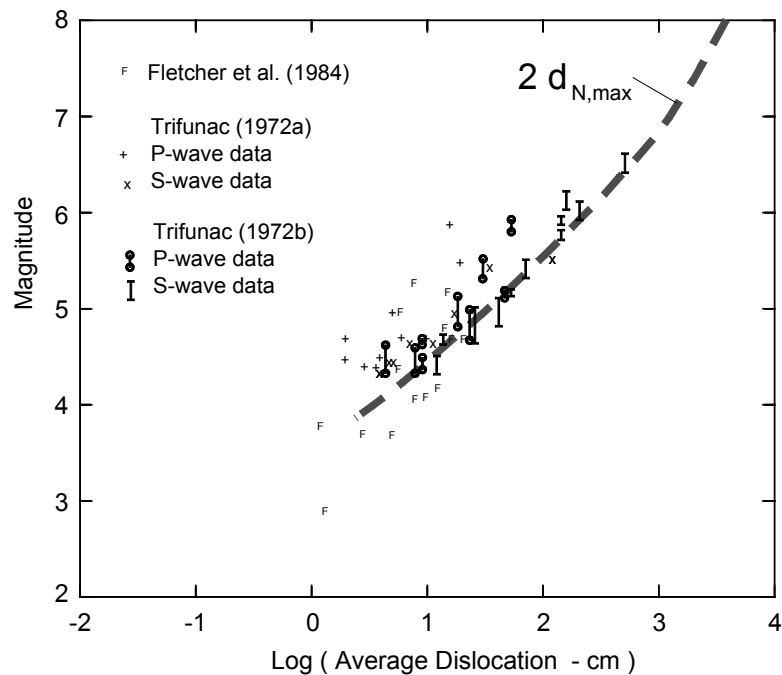


Fig. 3 Comparison of the average dislocation amplitudes on the fault, $\bar{u} = 2d_{N,\max}$, evaluated in several spectral analyses of the recorded strong ground motion (different symbols), with the amplitudes of $d_{N,\max}$ (Table 2), adopted for scaling $d_N(t)$ in this paper (dashed line)

Table 1: Characteristics of Brune's Pulse Displacement (Trifunac, 1993)

Magnitude, M	α_F (s^{-1})	A_F (cm/s)	$d_{F,\max}$ (cm)	$\dot{d}_{F,\max}$ (cm/s)
4	14.04	56.48	1.48	56.48
5	7.90	151.61	7.06	151.61
6	4.44	546.97	45.32	546.97
7	(2.50)	(860.34)	(126.6)	(860.34)
8	(1.40)	(1560.29)	(410.0)	(1560.29)

Table 2: Characteristics of Brune's Near-Field Displacement (Trifunac, 1993)

Magnitude, M	τ_N (s)	A_N (cm)	$d_{N,max}$ (cm)	$\dot{d}_{N,max}$ (cm/s)
4	0.55	4.9	2.45	4.45
5	1.2	29.2	14.6	12.17
6	1.8	245.5	122.75	68.19
7	(3.0)	(1288.0)	(644.0)	(214.7)
8	(5.0)	(4169.0)	(2084.5)	(416.9)

An important physical property of the d_F and d_N functions, as used in this paper, is their initial velocity. It can be shown that $\dot{d}_F \sim \sigma\beta/\mu$, where σ is the effective stress (\sim stress drop) on the fault surface, β is the velocity of shear waves in the fault zone, and μ is the rigidity of rocks surrounding the fault. For \dot{d}_N it can be shown that $\dot{d}_N = 0.5C_0\sigma\beta/\mu$, at $t = 0$, where typical values of C_0 are 0.6, 0.65, 1.00, 1.52, and 1.52 for $M = 4, 5, 6, 7$, and 8 (Trifunac, 1993, 1997). The largest peak velocity observed so far, 5 to 10 km above the fault, is 170 cm/s, which was recorded during the Northridge, California earthquake of 1994 (Trifunac et al., 1998). Because there are no strong-motion measurements of peak ground velocity at the fault surface, the peak velocities \dot{d}_F and \dot{d}_N can be evaluated only indirectly in terms of σ . The accuracy of the stress estimates depends upon the assumptions and methods used in the interpretation of recorded strong-motion records and is typically about one order of magnitude. Therefore, in solving the above equations, for σ we can use $\sigma \sim 2\mu\dot{d}_{N,max}/(\beta C_0)$ (see the dotted lines in Figure 4) with $\dot{d}_{N,max}$ as given in Table 2, and $\sigma \sim \mu\dot{d}_{F,max}/\beta$ (see the continuous lines in Figure 4) with $\dot{d}_{F,max}$ as given in Table 1, to check their consistency with the other published estimates of σ . Figure 4 shows this comparison for typical values of μ and β . The scatter of the reported estimates of σ is large, but the values of $\dot{d}_{F,max}$ and $\dot{d}_{N,max}$ given in Tables 1 and 2 are consistent with the observed trends.

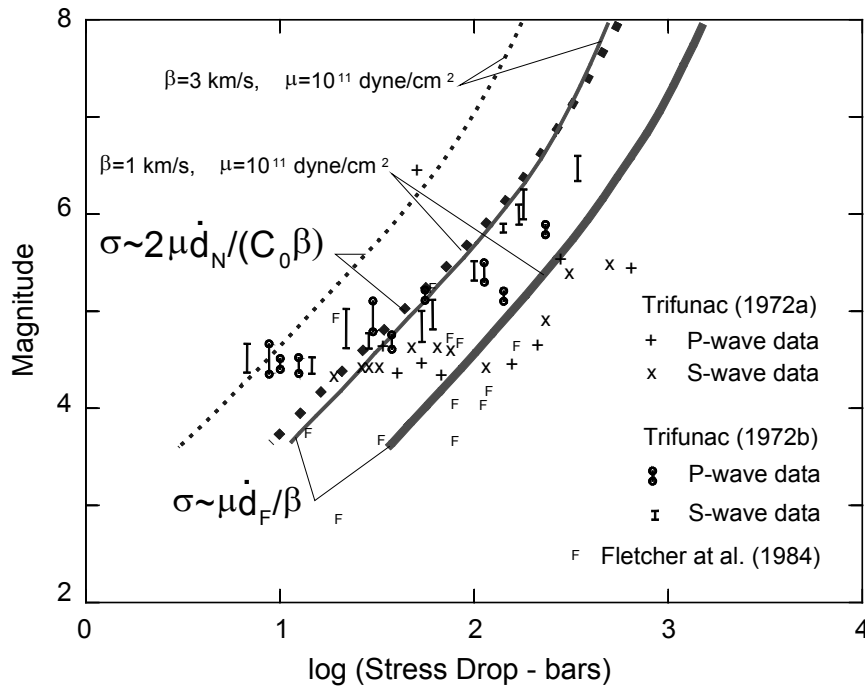


Fig. 4 Comparison of the stress drop determined from the near-field recordings of strong motion (different symbols), with the stress drop associated with the values of \dot{d}_F (solid lines; Table 1) and \dot{d}_N (dotted lines; Table 2) used in this paper

Amplitudes of the pseudo relative velocity (PSV) spectra of the linear response of the SDOF systems in the far-field can be viewed and scaled in three period ranges, where the PSV amplitudes are dominated by (1) peak ground acceleration (for short periods), (2) peak ground velocity (for intermediate periods), and (3) peak ground displacement (for long periods) (Veletsos et al., 1965). When the fault motions d_F and d_N begin with a sudden jump in the ground velocity (caused by a sudden stress drop on the fault surface), this large initial velocity will dominate the spectral amplitudes, and for the short periods of the oscillator, the “acceleration-dominated” zone of the PSV amplitudes will disappear. This will result in essentially constant PSV amplitudes in the short-period range (Jalali et al., 2007). This effect of large initial velocities, \dot{d}_F and \dot{d}_N , on the PSV spectral amplitudes in the short-period range is reminiscent of the effects of differential motions, particularly for the stiff structures, at soft soil sites, and for large plan dimensions. There, the peak strains in the soil (that are proportional to the peak ground velocity) lead to constant PSV spectral amplitudes at short periods (Trifunac and Todorovska, 1997; Trifunac and Gicev, 2006).

The presence of the motions resembling d_N in the recorded velocities and displacements filtered by data processing can be noticed by a trained eye in numerous plots of processed strong-motion records. The frequency of the occurrence and the amplitudes of such pulses are larger for the motions recorded closer to the causative faults. For the assumed motions d_F and d_N in this paper there is a Dirac delta function for the accelerations at time zero. In the observed motions, because of wave propagation through the sediments and soil, this will correspond to large but not infinite accelerations.

Figure 5 (top) shows an example of the ground displacement, perpendicular to the fault, recorded during the Parkfield, California earthquake of 1966, about 3 km above and about 10 km south-east from the principal fault slip (Trifunac and Udawadia, 1974). This displacement, computed by double integration from the recorded and band-pass filtered accelerogram, is used here to illustrate an example of a near-field (not near-fault) “pulse-like” ground motion, which may have left the fault surface as d_F (shown in Figure 2 (middle)), but was subsequently attenuated and “filtered” along its 11 km long path between the south-eastern end of the fault slip and the recording station. Figure 5 (bottom) shows the ground displacement recorded several kilometers above the fault, which slipped during the San Fernando, California earthquake of 1971. This displacement was also band-pass filtered by the routine data processing methods, and therefore does not contain periods of motion longer than 15 s and shorter than 0.04 s. However, in spite of the band-pass filtering, it suggests two episodes of permanent ground displacements, starting near 2.5 and 6 s. Further examples of how d_N for this earthquake may have appeared in the near-field can be found in Figures 6 and 10 of Trifunac (1974), which are based on synthetic computation of the fault slip during the San Fernando earthquake of 1971. The displacements shown in Figure 5 are examples of the recorded near-field (but not near-fault, or fault) motions, which lend support to our choice of the simple fault displacement functions, d_F and d_N .

The functions d_F and d_N model the displacement time histories in the fault-normal and fault-parallel directions. For the vertical strike-slip faults, d_F and d_N will also represent strike-normal and strike-parallel motions along the surface expression of the fault. For the dip-slip faults, a linear combination of d_F and d_N will contribute only to the vertical and strike-normal displacements on the ground surface. For a general fault orientation both d_F and d_N will contribute to the surface displacements, as determined by their projections onto horizontal and vertical motions on the ground surface (Mavroeidis and Papageorgiou, 2003). In the following, we will refer to d_F and d_N in the context of vertical strike-slip faults only.

In this paper, for simplicity, we assume that $v_{g_i}(t) = \pm u_{g_i}(t)$ and that the functional form of $u_{g_i}(t)$ is defined by Equations (4) and (5) for the fault-normal pulse and fault-parallel displacement, respectively. In the following plots, we label the results for $+v_{g_i}$ with “up”, and those for $-v_{g_i}$ with “down”. The rocking component of the ground motion will be approximated by (Trifunac, 1982; Lee and Trifunac, 1987)

$$\theta_{g_i}(t) = \left(-\frac{1}{C_x} \right) \dot{v}_{g_i}(t) \quad (6)$$

where $\dot{v}_{g_i}(t)$ is the vertical velocity of the ground motion at the i th column. Of course, in a more accurate modeling, the ratio of v_{g_i} to u_{g_i} amplitudes will depend on the incident angle and the character of incident waves, while the associated rocking θ_{g_i} will be described by a superposition of rocking angles associated with the incident body and dispersed surface waves (Lee and Trifunac, 1987). The sensitivity studies of how the strength-reduction factors will depend on different incident angles is beyond the scope of this paper, and will be addressed in our future work.

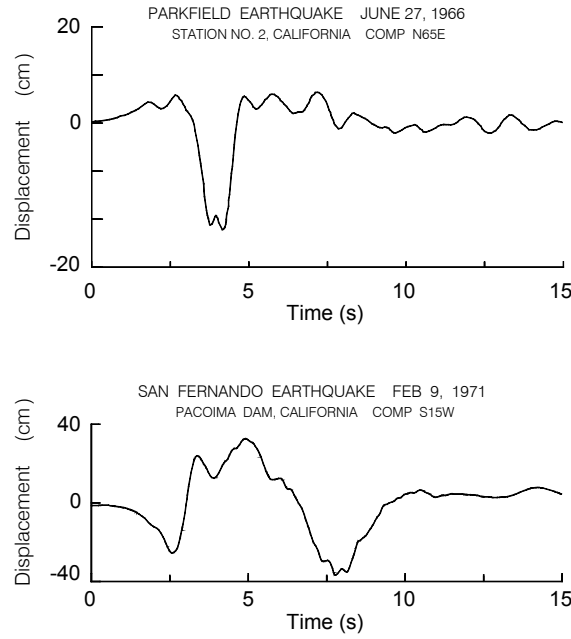


Fig. 5 Ground displacement, perpendicular to the fault strike, about 10 km south-east and 3 km above the south-eastern end of the fault slip on a vertical strike-slip fault, during the Parkfield, California, earthquake of 1966 (Trifunac and Udwadia, 1974) (top); Ground displacement recorded near the center and several kilometers above the thrust fault, which ruptured during the San Fernando, California, earthquake of 1971 (bottom)

STRENGTH-REDUCTION FACTORS OF THE SYSTEM UNDER DIFFERENTIAL GROUND MOTIONS

The yield-strength reduction factor for the system subjected to a synchronous ground motion is $R_y = f_0 / f_y = u_0 / u_y$, where all of the quantities are defined as in Figure 1(a). In this paper, for the assumed model and because of the differential ground motions and rotation of the beam, relative rotation for the two columns at their top and bottom will be different. Therefore, we define the R -factor and ductility for each corner of the system instead of one factor for the whole system: at the top of the left column,

$$R_{tl} = \frac{M_{10}}{M_y}; \quad \mu_{tl} = \frac{\phi_1 - \theta_G}{\phi_y} \quad (7)$$

at the bottom of the left column,

$$R_{bl} = \frac{M'_{10}}{M_y}; \quad \mu_{bl} = \frac{\psi_1}{\phi_y}; \quad \psi_1 = \phi_1 - \theta_{g_1} \quad (8)$$

at the top of the right column,

$$R_{tr} = \frac{M_{20}}{M_y}; \quad \mu_{tr} = \frac{\phi_2 - \theta_G}{\phi_y} \quad (9)$$

and at the bottom of the right column,

$$R_{br} = \frac{M'_{20}}{M_y}; \quad \mu_{br} = \frac{\psi_2}{\phi_y}; \quad \psi_2 = \phi_2 - \theta_{g_2} \quad (10)$$

In Equations (7)–(10), M_{10} , M'_{10} , M_{20} , and M'_{20} are the maximum linear moments, and $(\phi_1 - \theta_G)$, ψ_1 , $(\phi_2 - \theta_G)$, and ψ_2 are the maximum nonlinear relative rotations at the four corners of the system. Further, M_y and ϕ_y are the yield moment and yield rotation of the columns, respectively. Iterations are required to compute the inelastic deformation ratio for a specified ductility factor because different values of M_y may lead to the same ductility. The convention is to choose the largest M_y (Veletsos and Newmark, 1964).

RESPONSE OF THE SYSTEM SUBJECTED TO NEAR-SOURCE DIFFERENTIAL GROUND MOTIONS

In all calculations, we consider the actions of the horizontal, vertical, and rocking components of the ground motion, and the effects of the gravity force, dynamic instability, and geometric non-linearity. For the structure shown in Figures 1(b) and 1(c), we calculate the maximum linear and nonlinear relative rotations at the four corners of the system under downward ($-v_{g_i}$), radial, and rocking, and upward ($+v_{g_i}$), radial, and rocking near-source differential ground motions. The calculations are done corresponding to the earthquake magnitudes $M = 5, 6, 7$, and 8 , for ductilities $\mu = 2, 4$, and 8 , and for different time delays, $\tau = 0.001, 0.01, 0.05$, and 0.1 s. Then we plot R_y versus T_n for the four corners of the system.

Figure 6 illustrates typical results for R_y versus the oscillator period for near-source, fault-parallel displacement with downward vertical displacement, magnitude $M = 8$, ductility ratio of eight, and for time delay $\tau = 0.05$ s. It shows the results for the top-left, top-right, bottom-left, and bottom-right corners of the system, assuming wave propagation from left to right (see Figure 1(c)). For reference and for an easier comparison with the previously published results, we also plotted one of the oldest estimates of R_y versus period, using piecewise straight lines (Jalali and Trifunac, 2008; Jalali et al., 2007; Chopra, 1995). The curve $(R_y)_{\min}$ then shows the minimum values of R_y for the d_N motion with $-v_{g_i}$, $M = 8$, $\mu = 8$, and for $\tau = 0.05$.

Figures 7(a) and 7(b) illustrate the role of the vertical (up: $+v_{g_i}$, and down: $-v_{g_i}$) components of the near-fault motion. The results are shown for R_y versus the oscillator period, with $M = 5, 6, 7$, and 8 and $\tau = 0.001$, for $d_F(t)$ (i.e., the fault-normal pulse in Equation (4)), and $d_N(t)$ (the fault-parallel displacement in Equation (5)). Again, for reference and for an easier comparison with the previous results, the old estimates of R_y versus the oscillator period are shown by the piecewise straight lines. For periods longer than 5 to 10 s, R_y curves approach the “collapse boundaries” (Jalali and Trifunac, 2008; Jalali et al., 2007). At or beyond these boundaries, the nonlinear system collapses due to the action of gravity loads. The results for $\tau = 0.001$ s correspond to the nearly vertical incidence of strong-motion waves or to the motions at a site with high seismic wave velocity, or both. These conditions are physically close to a situation in which the wave propagation effects are negligible, i.e., $\tau = 0$ or when the motions at the supports 1 and 2 (see Figure 1(c)) are equal (Jalali and Trifunac, 2008). For such small values of τ , the R -factors at the four corners in our 3DOF model are approximately the same. Therefore, in Figures 7(a) and 7(b) we show the R -factor for the top-right (see solid line for the “down” and dashed line for the “up” motions) and bottom-right (see dotted line for the “down” and dash-dot line for the “up” motions) corners only. It can be seen from Figures 7(a) and 7(b) that the differences between the “up” and

“down” wave motions are more pronounced for the stiff structures and that those tend to decrease for the longer period structures.

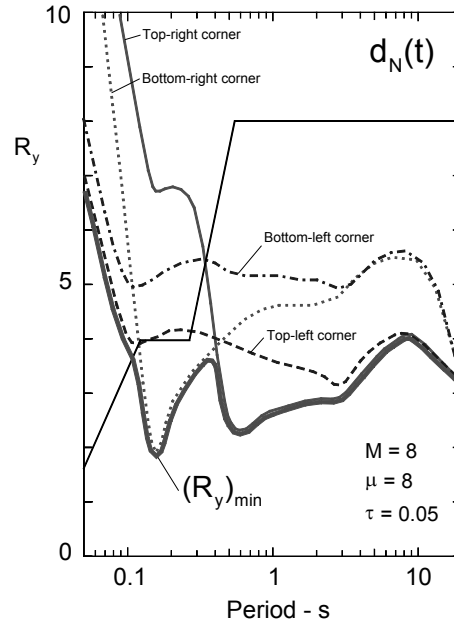


Fig. 6 Example of the effects of the differential ground motion on the strength-reduction factors at the four corners of the system, which is subjected to the horizontal, vertical, and rocking components of the fault-parallel displacement $d_N(t)$ for the downward vertical motion ($-v_{g_i}$), $M = 8$, $\mu = 8$, and for the delay at the right support, $\tau = 0.05$ s (the amplitudes of the piecewise straight representation of the classical R_y are shown for comparison; $(R_y)_{\min}$ shows the smallest values of the R -factors, which for the set of conditions considered in this example are determined by the response at the top-left corner (for the periods shorter than 0.1 s), at the bottom-right corner (for the periods between 0.1 and 0.35 s), and at the top-right corner (for the periods longer than 0.35 s))

With simultaneous consideration of the sign of the vertical motions and for larger delays ($\tau = 0.01$, 0.05 and 0.1 s), variations of R_y versus the oscillator period increase and become complicated. This is because for different conditions of excitation (i.e., different amplitudes and durations of $d_F(t)$, different amplitudes and rise time of $d_N(t)$) and larger τ , R_y amplitudes change abruptly from large to small values at different oscillator periods (e.g., as in Figure 6). Plotting all those rapid changes would clutter the figures and would not lead to simple trends, due to dependence of the results on many parameters. Since it is $(R_y)_{\min}$ (as illustrated in Figure 6) versus the period of the oscillator that is of interest for design, in Figures 8(a), 8(b), 9(a), and 9(b) we show only $(R_y)_{\min}$ versus period, for $M = 5, 6, 7$, and 8, $\mu = 2, 4$, and 8, and for $\tau = 0.01, 0.05$, and 0.1 s.

As can be seen from Figure 7, for small time delay ($\tau = 0.01$) and for very high frequencies (i.e., the acceleration-sensitive region), the R -factors of the system tend to the asymptotes with amplitudes equal to $(2\mu - 1)^{1/2}$, which are the consequence of strong initial velocity associated with a sudden onset of near-source ground motion (Jalali and Trifunac, 2008; Jalali et al., 2007). For long periods (i.e., the displacement-sensitive region), the R -factors of the system at first start to tend towards the asymptotic values for the SDOF system, i.e., equal to μ , but then decrease below the values for which the collapse occurs because of the destabilizing effect of gravity. Thus, for $\tau \rightarrow 0$ the classical design curves are approximately conservative for the fault-normal pulse (see Figure 7(a)). However, they are not conservative for the fault-parallel displacement (see Figure 7(b)).

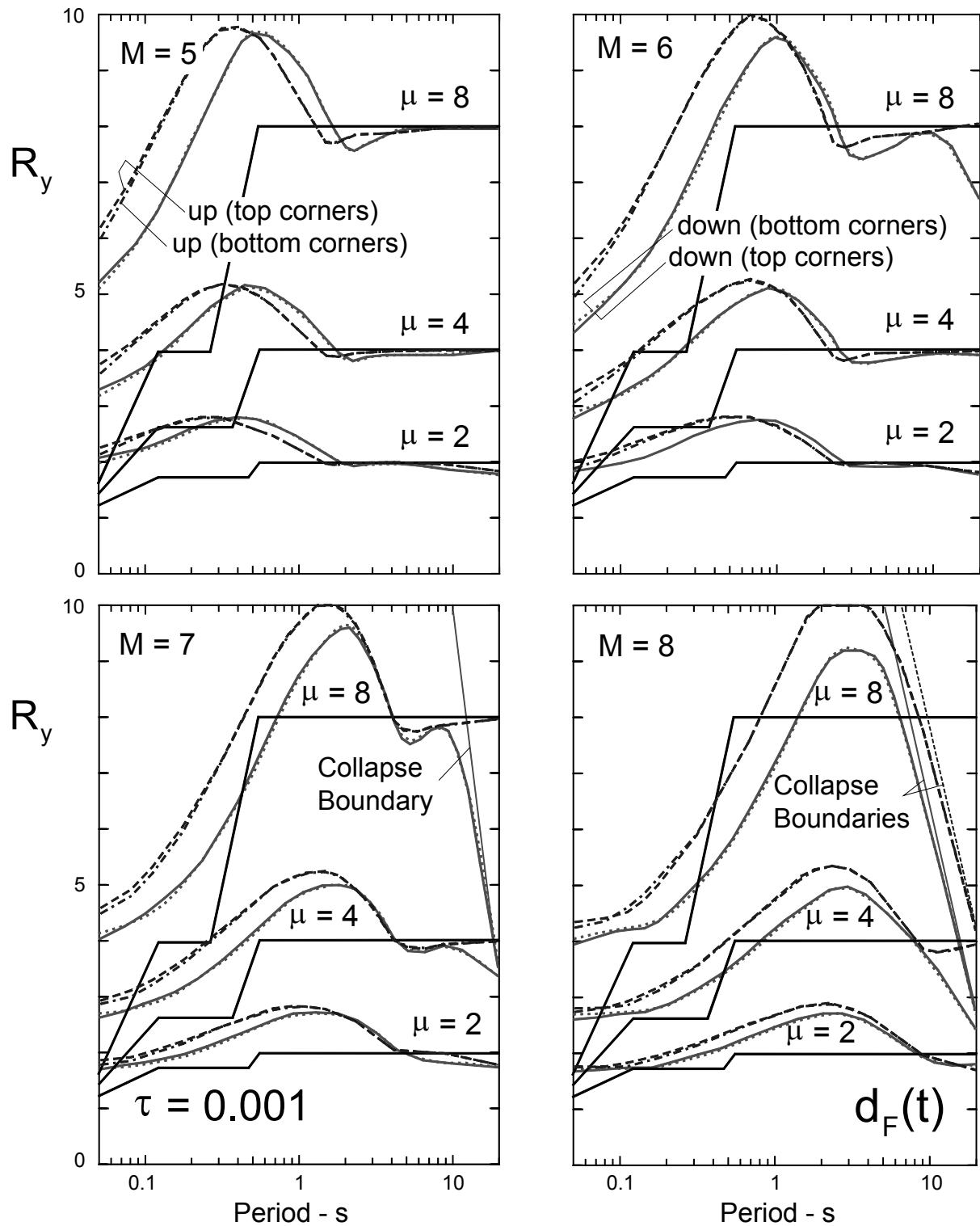
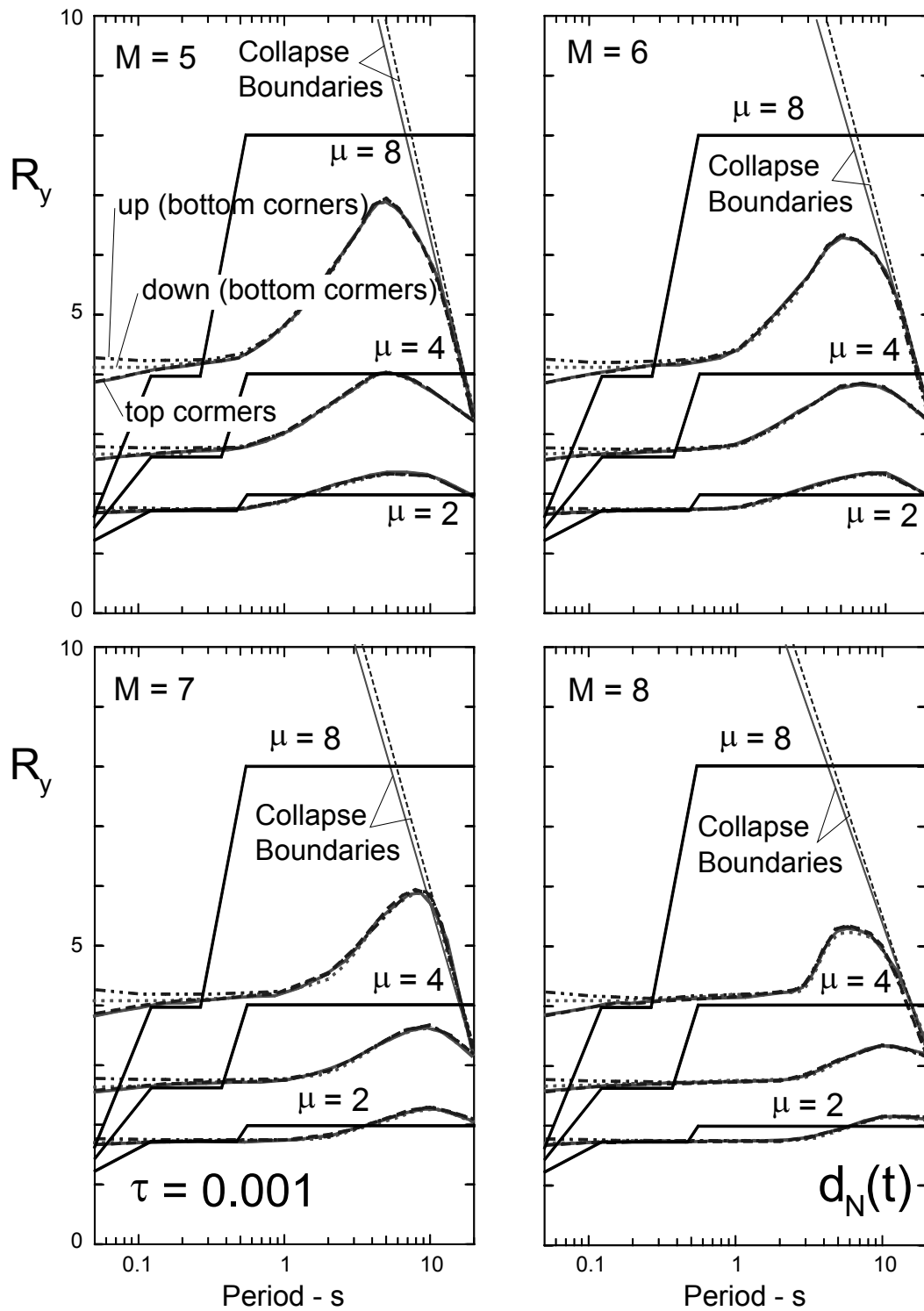


Fig. 7(a) An example of the effects of the differential ground motions on the strength-reduction factors at the corners of the system shown in Figure 1(b), which is subjected to the horizontal, vertical, and rocking components of the fault-normal pulse $d_F(t)$, for the “down” ($-v_{g_i}$) and “up” ($+v_{g_i}$) vertical components, $M=5, 6, 7$, and 8 , $\mu=2, 4$, and 8 , and for the delay time $\tau=0.001$ s (for this τ , the R -factors for the left and right columns are approximately same)

Fig. 7(b) Same as in Figure 7(a), but for $d_N(t)$

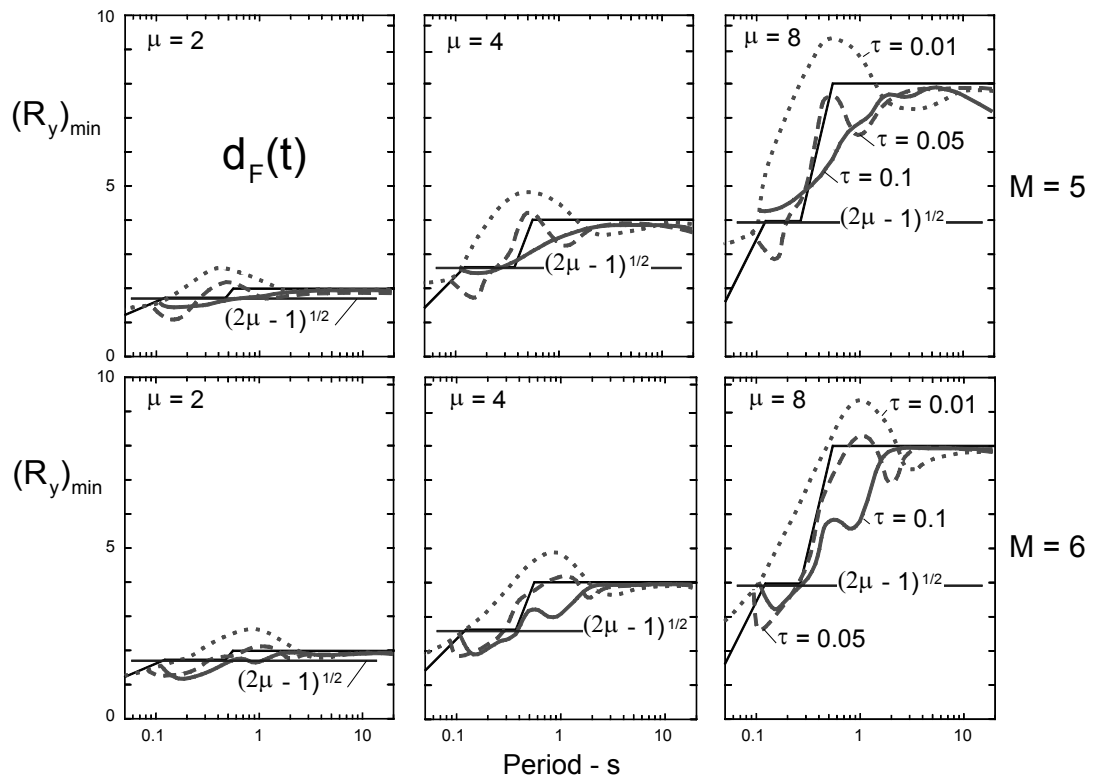


Fig. 8(a) Examples of $(R_y)_{\min}$ versus system period for the excitation by the fault-normal pulse $d_F(t)$, for $M = 5$ and 6 , $\mu = 2, 4$, and 8 , and for $\tau = 0.01, 0.05$, and 0.1 s (classical piecewise straight approximation of R_y and amplitudes equal to $(2\mu - 1)^{1/2}$ are shown for comparison)

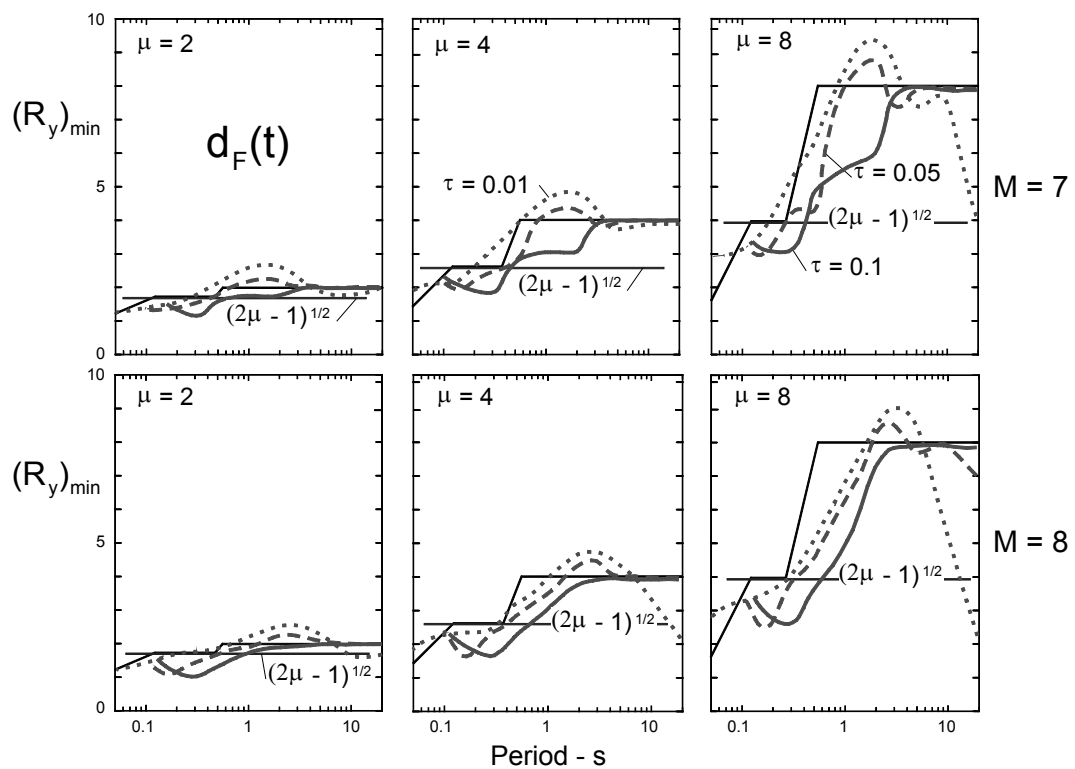
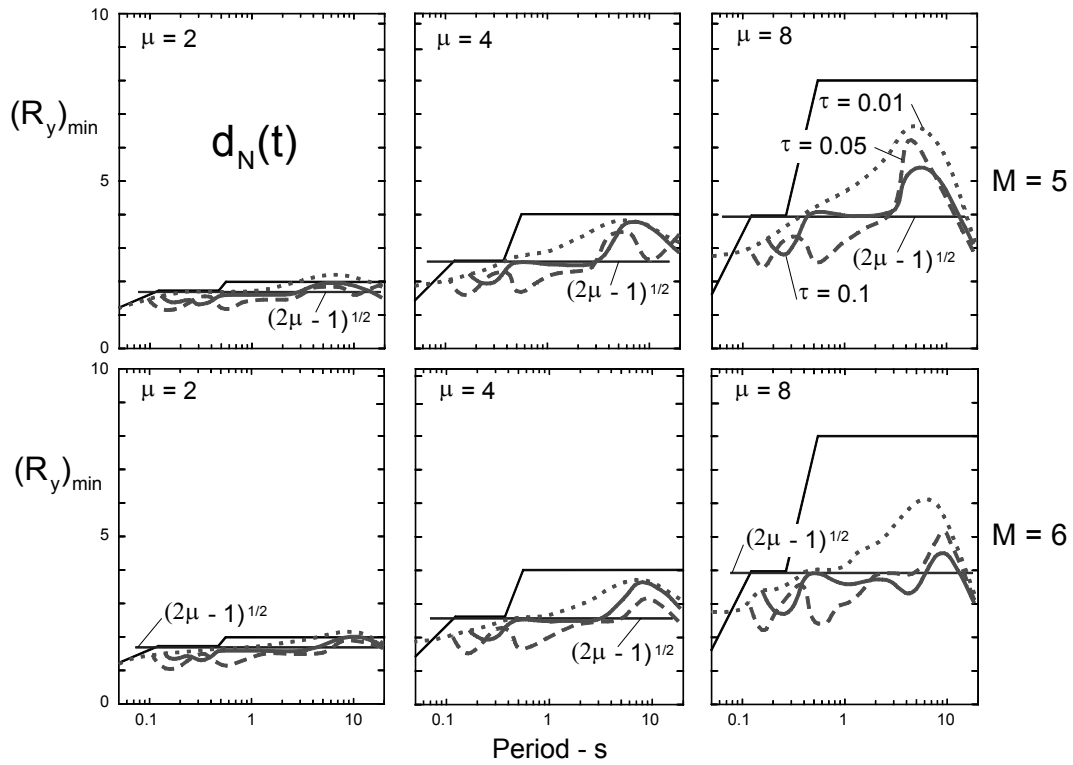
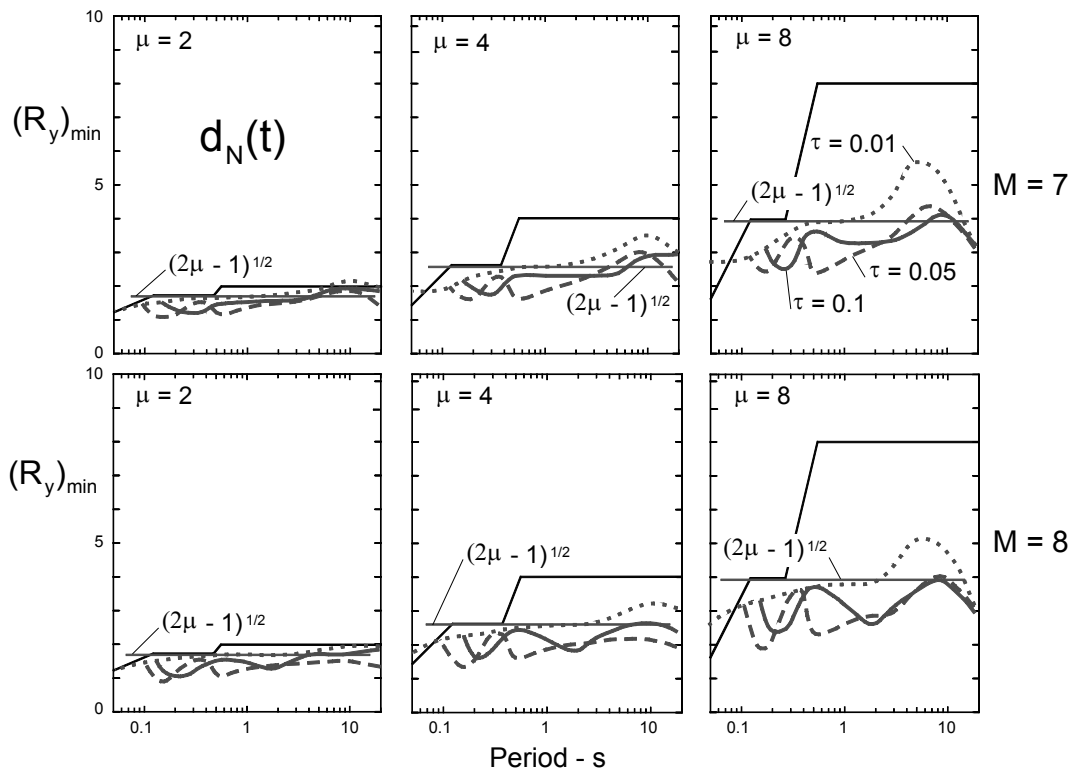


Fig. 8(b) Same as in Figure 8(a), but for $M = 7$ and 8

Fig. 9(a) Same as in Figure 8(a), but for $d_N(t)$ Fig. 9(b) Same as in Figure 9(a), but for $M = 7$ and 8

With increasing time delay, the R -factors at the four corners of the system become very different. From Figures 8(a), 8(b), 9(a), and 9(b), it can be seen that for the fault-normal pulse with increasing time delay, the R -factors of the system fall below the classical design curves for the periods between 0.1 and 2.0 s. For the fault-parallel displacement with increasing time delay, the R -factors of the system fall even

below the value of $(2\mu-1)^{1/2}$ by 30 to 50 percent for most periods, and for the cases studied in this paper, mainly for the periods between 0.1 and 2.0 s.

CONCLUSIONS

We have illustrated the effects of differential motion on the strength-reduction factors, R_y , versus T_n , for a simple 3DOF system subjected to propagating horizontal, vertical, and rocking components of near-source ground motions. For small time delays and for very-high-frequency systems, the R -factors are dominated by the initial velocity of the ground motion and those tend to the amplitudes equal to $(2\mu-1)^{1/2}$ (Jalali and Trifunac, 2008; Jalali et al., 2007). For $\tau = 0$, the classical design curves are approximately conservative for the fault-normal pulse, but they are not conservative for the fault-parallel displacement. With increasing time delay (in this paper we studied delays up to 0.1 s), the R -factors at the four corners of our model (see Figure 1(b)) become different and move below the classical design curves for the periods between 0.1 and 2.0 s for the fault-normal pulse, and essentially for all the periods for the fault-parallel displacements.

In view of these results, it is recommended that for design in the near-field, i.e., close to active faults, the strength-reduction factors for all the components of strong motion should be constant and equal to $(2\mu-1)^{1/2}$ for long periods, but only up to the collapse boundaries where dynamic instability and gravity effects become dominant. For the periods shorter than about 2 s, these strength-reduction factors should be further reduced by 30 to 50 percent.

REFERENCES

1. ATC (1996). "Seismic Evaluation and Retrofit of Concrete Buildings: Volume 1", Report ATC-40, Applied Technology Council, Redwood City, California, U.S.A.
2. Baez, J.I. and Miranda, E. (2000). "Amplification Factors to Estimate Inelastic Displacement Demands for the Design of Structures in the Near Field", Proceedings of the 12th World Conference on Earthquake Engineering, Auckland, New Zealand, Paper No. 1561 (on CD).
3. Biot, M.A. (1932). "Transient Oscillations in Elastic Systems", Ph.D. Thesis No. 259, Aeronautics Department, California Institute of Technology, Pasadena, U.S.A.
4. Biot, M.A. (1933). "Theory of Elastic Systems Vibrating under Transient Impulse with an Application to Earthquake-Proof Buildings", Proceedings of the National Academy of Sciences of the United States of America, Vol. 19, No. 2, pp. 262–268.
5. Biot, M.A. (1934). "Theory of Vibration of Buildings during Earthquake", Zeitschrift für Angewandte Mathematik und Mechanik, Vol. 14, No. 4, pp. 213–223.
6. Bogdanoff, J.L., Goldberg, J.E. and Schiff, A.J. (1965). "The Effect of Ground Transmission Time on the Response of Long Structures", Bulletin of the Seismological Society of America, Vol. 55, No. 3, pp. 627–640.
7. Chakraborti, A. and Gupta, V.K. (2005). "Scaling of Strength Reduction Factors for Degrading Elasto-Plastic Oscillators", Earthquake Engineering & Structural Dynamics, Vol. 34, No. 2, pp. 189–206.
8. Chopra, A.K. (1995). "Dynamics of Structures: Theory and Applications to Earthquake Engineering", Prentice-Hall, Englewood Cliffs, U.S.A.
9. Chopra, A.K. and Chintanapakdee, C. (2001). "Comparing Response of SDF Systems to Near-Fault and Far-Fault Earthquake Motions in the Context of Spectral Regions", Earthquake Engineering & Structural Dynamics, Vol. 30, No. 12, pp. 1769–1789.
10. Chopra, A.K. and Chintanapakdee, C. (2004). "Inelastic Deformation Ratios for Design and Evaluation of Structures: Single-Degree-of-Freedom Bilinear Systems", Journal of Structural Engineering, ASCE, Vol. 130, No. 9, pp. 1309–1319.
11. Cuesta, I. and Aschheim, M.A. (2001). "Isoductile Strengths and Strength Reduction Factors of Elasto-Plastic SDOF Systems Subjected to Simple Waveforms", Earthquake Engineering & Structural Dynamics, Vol. 30, No. 7, pp. 1043–1059.

12. FEMA (1997a). "NEHRP Guidelines for the Seismic Rehabilitation of Buildings", Report FEMA 273, Federal Emergency Management Agency, Washington, DC, U.S.A.
13. FEMA (1997b). "NEHRP Commentary on the Guidelines for the Seismic Rehabilitation of Buildings", Report FEMA 274, Federal Emergency Management Agency, Washington, DC, U.S.A.
14. FEMA (2000). "Prestandard and Commentary for the Seismic Rehabilitation of Buildings", Report FEMA 356, Federal Emergency Management Agency, Washington, DC, U.S.A.
15. Fletcher, J., Boatwright, J., Haar, L., Hanks, T. and McGarr, A. (1984). "Source Parameters for Aftershocks of the Oroville, California, Earthquake", *Bulletin of the Seismological Society of America*, Vol. 74, No. 4, pp. 1101–1123.
16. Hao, H. (1989). "Effects of Spatial Variation of Ground Motions on Large Multiply-Supported Structures", Report UCB/EERC-89/06, University of California, Berkeley, U.S.A.
17. Hao, H. (1991). "Response of Multiply Supported Rigid Plate to Spatially Correlated Seismic Excitations", *Earthquake Engineering & Structural Dynamics*, Vol. 20, No. 9, pp. 821–838.
18. Harichandran, R.S. and Vanmarcke, E.H. (1986). "Stochastic Variation of Earthquake Ground Motion in Space and Time", *Journal of Engineering Mechanics, ASCE*, Vol. 112, No. 2, pp. 154–174.
19. Harichandran, R.S. and Wang, W. (1988). "Response of Simple Beam to Spatially Varying Earthquake Excitation", *Journal of Engineering Mechanics, ASCE*, Vol. 114, No. 9, pp. 1526–1541.
20. Harichandran, R.S. and Wang, W. (1990). "Response of Intermediate Two-Span Beam to Spatially Varying Seismic Excitation", *Earthquake Engineering & Structural Dynamics*, Vol. 19, No. 2, pp. 173–187.
21. Hyun, C.H., Yun, C.B. and Lee, D.G. (1992). "Nonstationary Response Analysis of Suspension Bridges for Multiple Support Excitations", *Probabilistic Engineering Mechanics*, Vol. 7, No. 1, pp. 27–35.
22. Jalali, R.S. and Trifunac, M.D. (2008). "A Note on Strength Reduction Factors for Design of Structures near Earthquake Faults", *Soil Dynamics and Earthquake Engineering*, Vol. 28, No. 3 (in press).
23. Jalali, R.S., Trifunac, M.D., Ghodrati Amiri, G. and Zahedi, M. (2007). "Wave-Passage Effects on Strength-Reduction Factors for Design of Structures near Earthquake Faults", *Soil Dynamics and Earthquake Engineering*, Vol. 27, No. 8, pp. 703–711.
24. Kashefi, I. and Trifunac, M.D. (1986). "Investigation of Earthquake Response of Simple Bridge Structures", Report CE 86-02, University of Southern California, Los Angeles, U.S.A.
25. Kojic, S.B. and Trifunac, M.D. (1991a). "Earthquake Stresses in Arch Dams. I: Theory and Antiplane Excitation", *Journal of Engineering Mechanics, ASCE*, Vol. 117, No. 3, pp. 532–552.
26. Kojic, S.B. and Trifunac, M.D. (1991b). "Earthquake Stresses in Arch Dams. II: Excitation by SV, P, and Rayleigh Waves", *Journal of Engineering Mechanics, ASCE*, Vol. 117, No. 3, pp. 553–574.
27. Kojic, S.B., Trifunac, M.D. and Lee, V.W. (1988). "Earthquake Response of Arch Dams to Nonuniform Canyon Motion", Report CE 88-03, University of Southern California, Los Angeles, U.S.A.
28. Lee, V.W. and Trifunac, M.D. (1987). "Rocking Strong Earthquake Accelerations", *Soil Dynamics and Earthquake Engineering*, Vol. 6, No. 2, pp. 75–89.
29. Loh, C.H., Penzien, J. and Tsai, Y.B. (1982). "Engineering Analyses of SMART 1 Array Accelerograms", *Earthquake Engineering & Structural Dynamics*, Vol. 10, No. 4, pp. 575–591.
30. MacRae, G.A., Morrow, D.V. and Roeder, C.W. (2001). "Near-Fault Ground Motion Effects on Simple Structures", *Journal of Structural Engineering, ASCE*, Vol. 127, No. 9, pp. 996–1004.
31. Mavroeidis, G.P. and Papageorgiou, A.S. (2003). "A Mathematical Representation of Near-Fault Ground Motions", *Bulletin of the Seismological Society of America*, Vol. 93, No. 3, pp. 1099–1131.
32. Mavroeidis, G.P., Dong, G. and Papageorgiou, A.S. (2004). "Near-Fault Ground Motions, and the Response of Elastic and Inelastic Single-Degree-of-Freedom (SDOF) Systems", *Earthquake Engineering & Structural Dynamics*, Vol. 33, No. 9, pp. 1023–1049.
33. Miranda, E. (1991). "Seismic Evaluation and Upgrading of Existing Structures", Ph.D. Dissertation, Department of Civil Engineering, University of California, Berkeley, U.S.A.

34. Miranda, E. (2000). "Inelastic Displacement Ratios for Structures on Firm Sites", *Journal of Structural Engineering*, ASCE, Vol. 126, No. 10, pp. 1150–1159.
35. Mylonakis, G. and Voyagaki, E. (2006). "Yielding Oscillator Subjected to Simple Pulse Waveforms: Numerical Analysis & Closed-Form Solutions", *Earthquake Engineering & Structural Dynamics*, Vol. 35, No. 15, pp. 1949–1974.
36. Okubo, T., Arakawa, T. and Kawashima, K. (1984). "Dense Instrument Array Program of the Public Works Research Institute and Preliminary Analysis of the Records", *Proceedings of the Eighth World Conference on Earthquake Engineering*, San Francisco, U.S.A., Vol. II, pp. 151–158.
37. Perotti, F. (1990). "Structural Response to Non-stationary Multiple-Support Random Excitation", *Earthquake Engineering & Structural Dynamics*, Vol. 19, No. 4, pp. 513–527.
38. Riddell, R. and Newmark, N.M. (1979). "Statistical Analysis of the Response of Nonlinear Systems Subjected to Earthquakes", *Structural Research Series 468*, Department of Civil Engineering, University of Illinois at Urbana-Champaign, Urbana, U.S.A.
39. Riddell, R., Garcia, J.E. and Garces, E. (2002). "Inelastic Deformation Response of SDOF Systems Subjected to Earthquakes", *Earthquake Engineering & Structural Dynamics*, Vol. 31, No. 3, pp. 515–538.
40. Ruiz-Garcia, J. and Miranda, E. (2003). "Inelastic Displacement Ratios for Evaluation of Existing Structures", *Earthquake Engineering & Structural Dynamics*, Vol. 32, No. 8, pp. 1237–1258.
41. Ruiz-Garcia, J. and Miranda, E. (2006). "Inelastic Displacement Ratios for Evaluation of Structures Built on Soft Soil Sites", *Earthquake Engineering & Structural Dynamics*, Vol. 35, No. 6, pp. 679–694.
42. Tiwari, A.K. and Gupta, V.K. (2000). "Scaling of Ductility and Damage-Based Strength Reduction Factors for Horizontal Motions", *Earthquake Engineering & Structural Dynamics*, Vol. 29, No. 7, pp. 969–987.
43. Todorovska, M.I. and Lee, V.W. (1989). "Seismic Waves in Buildings with Shear Walls or Central Core", *Journal of Engineering Mechanics*, ASCE, Vol. 115, No. 12, pp. 2669–2686.
44. Todorovska, M.I. and Trifunac, M.D. (1989). "Antiplane Earthquake Waves in Long Structures", *Journal of Engineering Mechanics*, ASCE, Vol. 115, No. 12, pp. 2687–2708.
45. Todorovska, M.I. and Trifunac, M.D. (1990a). "A Note on the Propagation of Earthquake Waves in Buildings with Soft First Floor", *Journal of Engineering Mechanics*, ASCE, Vol. 116, No. 4, pp. 892–900.
46. Todorovska, M.I. and Trifunac, M.D. (1990b). "Note on Excitation of Long Structures by Ground Waves", *Journal of Engineering Mechanics*, ASCE, Vol. 116, No. 4, pp. 952–964.
47. Todorovska, M.I., Gupta, I.D., Gupta, V.K., Lee, V.W. and Trifunac, M.D. (1995). "Selected Topics in Probabilistic Seismic Hazard Analysis", Report CE 95-08, University of Southern California, Los Angeles, U.S.A.
48. Trifunac, M.D. (1972a). "Stress Estimates for the San Fernando, California, Earthquake of February 9, 1971: Main Event and Thirteen Aftershocks", *Bulletin of the Seismological Society of America*, Vol. 62, No. 3, pp. 721–750.
49. Trifunac, M.D. (1972b). "Tectonic Stress and the Source Mechanism of the Imperial Valley, California, Earthquake of 1940", *Bulletin of the Seismological Society of America*, Vol. 62, No. 5, pp. 1283–1302.
50. Trifunac, M.D. (1974). "A Three-Dimensional Dislocation Model for the San Fernando, California, Earthquake of February 9, 1971", *Bulletin of the Seismological Society of America*, Vol. 64, No. 1, pp. 149–172.
51. Trifunac, M.D. (1982). "A Note on Rotational Components of Earthquake Motions on Ground Surface for Incident Body Waves", *International Journal of Soil Dynamics and Earthquake Engineering*, Vol. 1, No. 1, pp. 11–19.
52. Trifunac, M.D. (1993). "Broad Band Extension of Fourier Amplitude Spectra of Strong Motion Acceleration", Report CE 93-01, University of Southern California, Los Angeles, U.S.A.
53. Trifunac, M.D. (1997). "Stresses and Intermediate Frequencies of Strong Earthquake Acceleration", *Geofizika*, Vol. 14, pp. 1–27.

54. Trifunac, M.D. (2003). "23rd ISET Annual Lecture: 70-th Anniversary of Biot Spectrum", ISET Journal of Earthquake Technology, Vol. 40, No. 1, pp. 19–50.
55. Trifunac, M.D. (2006). "Effects of Torsional and Rocking Excitations on the Response of Structures" in "Earthquake Source Asymmetry, Structural Media and Rotation Effects (edited by R. Teisseyre, M. Takeo and E. Majewski), Springer-Verlag, Heidelberg, Germany.
56. Trifunac, M.D. and Gicev, V. (2006). "Response Spectra for Differential Motion of Columns, Paper II: Out-of-Plane Response", Soil Dynamics and Earthquake Engineering, Vol. 26, No. 12, pp. 1149–1160.
57. Trifunac, M.D. and Todorovska, M.I. (1994). "Broad Band Extension of Pseudo Relative Velocity Spectra of Strong Ground Motion", Report CE 94-02, University of Southern California, Los Angeles, U.S.A.
58. Trifunac, M.D. and Todorovska, M.I. (1997). "Response Spectra for Differential Motion of Columns", Earthquake Engineering & Structural Dynamics, Vol. 26, No. 2, pp. 251–268.
59. Trifunac, M.D. and Todorovska, M.I. (2001). "Evolution of Accelerographs, Data Processing, Strong Motion Arrays and Amplitude and Spatial Resolution in Recording Strong Earthquake Motion", Soil Dynamics and Earthquake Engineering, Vol. 21, No. 6, pp. 537–555.
60. Trifunac, M.D. and Udawadia, F.E. (1974). "Parkfield, California, Earthquake of June 27, 1966: A Three-Dimensional Moving Dislocation", Bulletin of the Seismological Society of America, Vol. 64, No. 3-1, pp. 511–533.
61. Trifunac, M.D., Todorovska, M.I. and Lee, V.W. (1998). "The Rinaldi Strong Motion Accelerogram of the Northridge, California, Earthquake of 17 January, 1994", Earthquake Spectra, Vol. 14, No. 1, pp. 225–239.
62. Veletsos, A.S. and Newmark, N.M. (1960). "Effect of Inelastic Behavior on the Response of Simple Systems to Earthquake Motions", Proceedings of the Second World Conference on Earthquake Engineering, Tokyo, Japan, Vol. II, pp. 859–912.
63. Veletsos, A.S. and Newmark, N.M. (1964). "Design Procedures for Shock Isolation Systems of Underground Protective Structures. Volume III. Response Spectra of Single-Degree-of-Freedom Elastic and Inelastic Systems", Report RTD TDR 63-3096 (prepared for Air Force Weapons Laboratory, Kirtland Air Force Base, Albuquerque, New Mexico), Newmark Hansen and Associates, Urbana, U.S.A.
64. Veletsos, A.S. and Vann, W.P. (1971). "Response of Ground-Excited Elastoplastic Systems", Journal of the Structural Division, Proceedings of ASCE, Vol. 97, No. ST4, pp. 1257–1281.
65. Veletsos, A.S., Newmark, N.M. and Celapati, C.V. (1965). "Deformation Spectra for Elastic and Elastoplastic Systems Subjected to Ground Shock and Earthquake Motion", Proceedings of the Third World Conference on Earthquake Engineering, Wellington, New Zealand, Vol. II, pp. 663–682.
66. Zerva, A. (1991). "Effect of Spatial Variability and Propagation of Seismic Ground Motions on the Response of Multiply Supported Structures", Probabilistic Engineering Mechanics, Vol. 6, No. 3-4, pp. 212–221.
67. Zembaty, Z. and Krenk, S. (1993). "Spatial Seismic Excitations and Response Spectra", Journal of Engineering Mechanics, ASCE, Vol. 119, No. 12, pp. 2449–2460.
68. Zembaty, Z. and Krenk, S. (1994). "Response Spectra of Spatial Seismic Ground Motion", Proceedings of the Tenth European Conference on Earthquake Engineering, Vienna, Austria, Vol. 2, pp. 1271–1275.

ENERGY AND POWER OF NONLINEAR WAVES IN A SEVEN-STORY REINFORCED CONCRETE BUILDING

V. Gicev* and Mihailo D. Trifunac**

*Rudarsko-Geoloski Fakultet

Goce Delcev 89, 2000 Stip, Republic of Macedonia

**Department of Civil Engineering

University of Southern California, Los Angeles, CA 90089, U.S.A.

ABSTRACT

We note the limitations of the classical Response Spectrum Method (RSM) for the design of earthquake-resistant structures in the near field of strong earthquakes. The main limitation is that the RSM is based on the largest peak of the relative response and does not consider the duration of strong motion. To illustrate an alternative approach the recorded response of a seven-story reinforced concrete hotel (VN7SH) in Van Nuys, California, damaged during January 1994, Northridge earthquake is described in terms of one-dimensional layered shear beam model, undergoing nonlinear wave excitation. We use this model to show the time and space variations of wave energy and of power in the building response, and to set a physical basis for a new design method based on the power of strong motion pulses propagating through a building.

KEYWORDS: Earthquake Response Spectra, Power of Incident Waves, Power Design Method

INTRODUCTION

“The problem of designing structures to withstand destructive earthquakes is not in a very satisfactory condition. On the one hand engineers do not know what characteristics of the ground motion are responsible for destruction, and on the other hand seismologists have no measurements of seismic motion which are sufficiently adequate to serve for design, even if the destructive characteristics were known. Consequently, engineers have been forced to proceed on an empirical basis. From past experience ... it has been found that buildings, which are designed to withstand a constant horizontal acceleration of 0.1 gravity are, on the whole, fairly resistant to seismic damage. It is fortunate that such a simple formula works at all ...” (Benioff, 1934).

Modern earthquake engineering began with the formulation of the concept of response spectrum by Biot, who presented the general theory (Biot, 1932, 1933, 1934), analyzed the recorded accelerograms, and formulated the principles of response spectrum superposition (Biot, 1941, 1942). Today, three quarters of a century later, his ideas still govern the principles of earthquake-resistant design (Trifunac, 2003, 2005). Biot’s method works well for the design of structures expected to vibrate without damage. However, pragmatic considerations and optimization of cost result in the design of structures, which may experience damage from a rare and very strong earthquake shaking. Thus, during the past 40 years, many modifications and “corrections” have been introduced into the Biot’s response spectrum method to reconcile its “linear” nature with its desired “nonlinear” use in design (Veletsos and Newmark, 1960).

At present much of the earthquake-resistant design continues to be based on the linear concepts of relative response spectrum, and on mode superposition. However, as used in practice, the modal approach has a low-pass filtering effect on the end result (e.g., the computed peak relative displacement at each floor) because in design the higher modes are usually neglected. Therefore, in typical earthquake engineering applications the modal approach is not able to represent the sudden transient response. This is particularly so for the excitation by high-frequency pulses in the near-field, with large peak velocities, which are associated with high stress drop at the near asperities, and with duration that is short relative to the travel time required for an incident wave to reach the top of the building. Although, in principle, the representation of the linear response as a combination of the modal responses is mathematically complete, short “impulsive” representation would require considering infinitely many modes, which is impractical. The wave propagation methods are therefore more “natural” for representing the “early” transient response, and should be used to find solutions where the modal approach is limited.

Well-designed structures are expected to have uniformly distributed “ductile behavior” during the largest credible shaking, and “large energy reserve” to at least delay failure if it cannot be avoided. As the structure enters large nonlinear response, it absorbs the excess of the input energy by ductile deformation of its components. Thus, it is logical to formulate earthquake-resistant design procedures in terms of the energy driving this process. Benioff (1934) proposed the seismic destructiveness to be measured in terms of the response energy, which also can be related to the energy of strong motion (Arias, 1970; Trifunac and Brady, 1975). Thus an alternative to the spectral method in earthquake-resistant design is to analyze the flow of energy during the strong motion. The principal stages of this flow include the earthquake source, the propagation path, and finally the remaining energy, which leads to the response of a structure (Trifunac et al., 2001c).

The seismic energy associated with the elastic waves that radiate from the source (Gutenberg and Richter, 1956a, 1956b) can be used to compare “sizes” of different earthquakes. This energy, E_s , is attenuated along the epicentral distance r through the mechanisms of inelastic attenuation (Trifunac, 1994), scattering, and geometric spreading. The wave energy arriving towards the site is next attenuated by the nonlinear response of shallow sediments and soil in the “free-field” (Joyner, 1975; Joyner and Chen, 1975; Trifunac and Todorovska, 1996, 1998a, 1999) before it begins to excite the foundation. The incident wave energy is further reduced by the nonlinear response of soil during the soil-structure interaction (Gicev, 2005; Trifunac et al., 1999a, 1999b, 2001a, 2001b), and by the radiation damping (Luco et al., 1986; Todorovska and Trifunac, 1991, 1992; Hayir et al., 2001).

Engineering analyses of seismic energy flow and distribution among different aspects of the structural response have been carried out since the mid-1950's. A review of the subject and examples describing the “limit-state” design can be found in the book by Akiyama (Akiyama, 1985), and in the collection of papers edited by Fajfar and Krawinkler (Fajfar and Krawinkler, 1992), for example. In most engineering studies, the analysis begins by integrating the differential equation of dynamic equilibrium of an equivalent single-degree-of-freedom system with respect to displacement, which results in

$$E_I = E_K + E_\zeta + E_E + E_H \quad (1)$$

where E_I is the input energy, E_K is the kinetic energy, E_ζ is the damping energy, E_E is the elastic strain energy, and E_H is the hysteretic energy (e.g., Uang and Bertero, 1988). A typical limitation of this approach is that the computed energy is essentially converted to the peak relative velocity (Akiyama, 1985), thus using energy merely to compute the equivalent relative velocity spectra, and then the classical response spectrum superposition method is used. Further the effects of soil-structure interaction are ignored, and therefore significant mechanisms of energy loss (via nonlinear response of the soil and radiation damping) are neglected, leading to erroneous inferences about the energy available to drive the structural response. Other simplifications and important omissions in Equation (1) are that the dynamic instability and the effects of gravity on the nonlinear response are usually ignored (Husid, 1967; Lee, 1979; Todorovska and Trifunac, 1991, 1993).

Figure 1 illustrates the cumulative wave energies recorded at a building site during two hypothetical earthquakes (see the demands E1 and E2), and presents the conceptual framework for development of the power design method. E1 results in a larger total shaking energy at the site, and has long duration of shaking leading to relatively small average power, P1. E2 leads to smaller total shaking energy at the site, but has short duration and thus larger power, P2. The power capacity of a structure cannot be described by one unique cumulative curve, as this depends on the time history of shaking. For the purposes of this example, the line labeled “capacity envelope of the structure” can be thought of as an envelope of all possible cumulative energy paths for the response of this structure. Figure 1 implies that E1 will not damage this structure, but E2 will. Hence, “for a given structure, it is not the total energy of an earthquake event (and the equivalent energy compatible relative velocity spectrum), but the rate with which this energy arrives and shakes the structure, that is essential for the design of the required power capacity of the structure to withstand this shaking, and to control the level of damage” (Trifunac et al., 2001c).

In this paper elementary aspects of response, based on the energy and power of the wave motion, are illustrated. It will be shown how this power can be compared with the temporal and spatial capacity of the structure to absorb the incident wave energy.

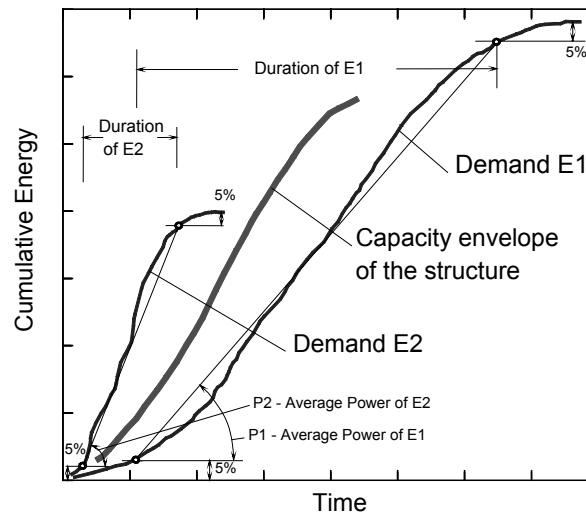


Fig. 1 Comparison of the strong motion demands E1 and E2 with an envelope of structural capacity

CASE STUDY—VAN NUYS HOTEL (VN7SH)

The example building used in this study is a seven-story hotel (VN7SH) located in Van Nuys, California. It was damaged by the 1994 Northridge, California earthquake (Ivanović et al., 1999a, 1999b; Trifunac and Hao, 2001; Trifunac et al., 1999a, 1999b). The building, designed in 1965 and constructed in 1966 (John A. Blume & Associates, 1973; Mulhern and Maley, 1973), is 18.9×45.7 m in plan, has seven stories, and is 20 m high. The typical framing consists of four rows of columns spaced at 6.1 m centers in the transverse direction and nine columns of columns at 5.7 m centers in the longitudinal direction. Spandrel beams surround the perimeter of the structure. Lateral forces in the longitudinal (EW) direction are resisted by the interior column-slab frames (B and C) and exterior column spandrel beam frames (A and D). The added stiffness in the exterior frames associated with the spandrel beams creates exterior frames that are roughly twice as stiff as the interior frames. The floor system consists of reinforced concrete flat slab, which is 25.4 cm thick at the second floor, 21.6 cm thick at the third to seventh floors, and 20.3 cm thick at the roof (Browning et al., 2000; De la Llera et al., 2001; Islam, 1996; Li and Jirsa, 1998; Trifunac and Ivanović, 2003). The building is situated on undifferentiated Holocene alluvium, uncemented and unconsolidated, with a thickness of < 30 m and an age of < 10,000 years (Trifunac and Todorovska, 1998b). The average shear-wave velocity in the top 30 m of soil is 300 m/s, and the soil-boring log shows that the underlying soil consists primarily of fine sandy silts and silty fine sands. The foundation system consists of 96.5-cm deep pile caps, supported by groups of two to four poured-in-place 61-cm-diameter reinforced concrete friction piles. These are centered under the main building columns. All of the pile caps are connected by a grid of beams. Each pile is approximately 12.2 m long and has a design capacity of over 444.82×10³ N vertical load and up to 88.96×10³ N lateral load. The structure is constructed of normal-weight reinforced concrete ((John A. Blume & Associates, 1973).

1. Earthquake Damage

The $M_L = 6.4$ Northridge earthquake of January 17, 1994 severely damaged the building. The structural damage was extensive in the exterior north (D) (see Figure 2(a)) and south (A) (see Figure 2(b)) frames that were designed to take most of the lateral load in the longitudinal (EW) direction. Severe shear cracks occurred at the middle columns of Frame A, near the contact with the spandrel beam of the 5th floor (see Figure 2(b)). Those cracks significantly decreased the axial, moment, and shear capacity of the columns. The shear cracks that appeared in the north (D) frame (see Figure 2(a)) caused minor to moderate changes in the capacities of these structural elements. No major damage to the interior longitudinal (B and C) frames was observed, and there was no visible damage to the slabs or around the foundation. The nonstructural damage was significant. Photographs and detailed descriptions of the damage from the earthquake can be found in Trifunac et al. (1999b) and Trifunac and Hao (2001). An analysis of the relationship between the observed damage and the changes in the equivalent vertical shear-

wave velocity in the building can be found in Ivanović et al. (1999b) and Todorovska and Trifunac (2006). A discussion of the extent to which this damage has contributed to the changes in the apparent period of the soil-structure system can be found in Trifunac et al. (2001a, 2001b).

2. Strong-Motion Records

The earthquake response of VN7SH was recorded by a 13-channel CR-1 central recording system, and by one tri-component SMA-1 accelerograph (see Figure 3) with an independent recording system but with common trigger time with the CR-1 recorder (Trifunac et al., 1999b). The five transducers, which recorded EW response of the building during the earthquake, were located at the ground (first), second, third, and sixth floors, and on the roof (see Figures 2(a), 2(b) and 3).

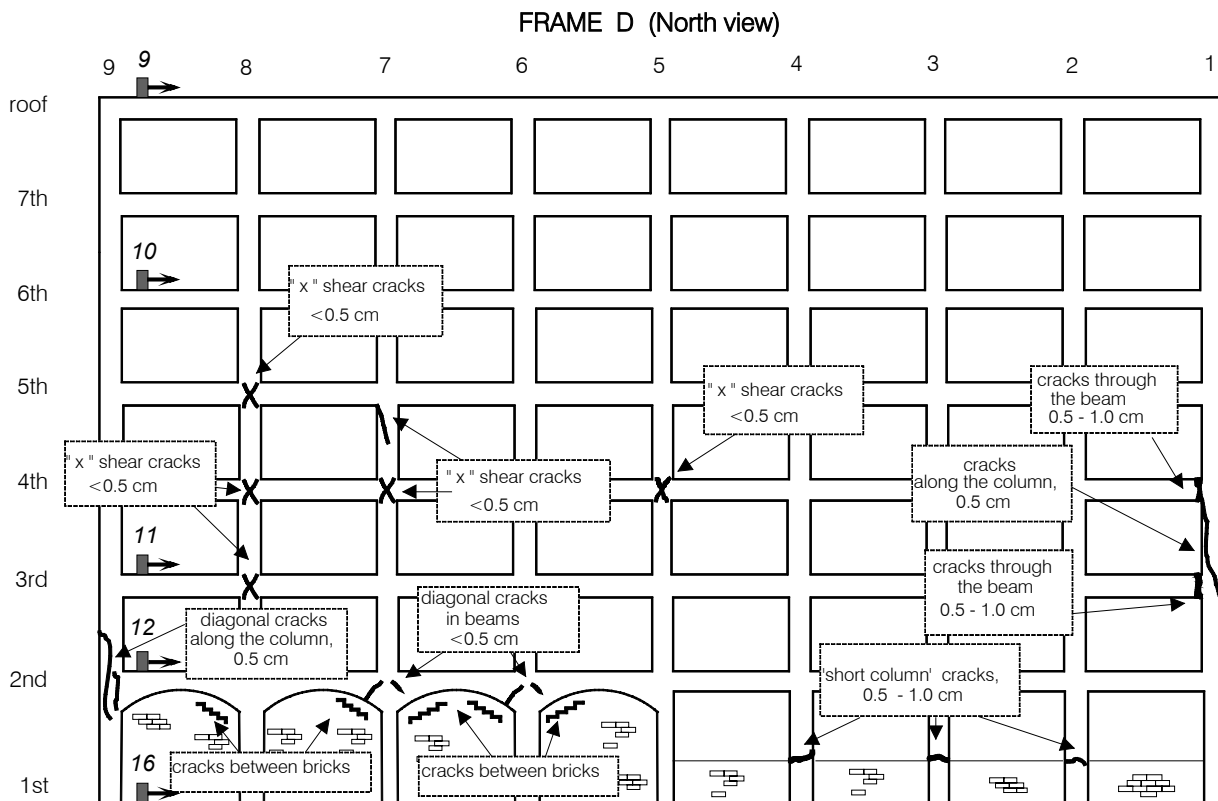


Fig. 2(a) Observed damage of Frame D

3. Previous Work

Two full-scale ambient vibration tests of VN7SH were performed (Ivanović et al., 1999a, 2000) following the earthquake. During the second ambient vibration survey, measurements of wave motion through the building foundation showed that the foundation is “flexible” and deforms with the passage of micro-tremor waves. This in turn indicated that for the studies of soil-structure interaction the rigid foundation assumption may not be appropriate (Trifunac et al., 1999a). The apparent period of the soil-structure system and its dependence upon the response amplitudes in VN7SH were described by Trifunac et al. (2001a, 2001b), and an application of off-line and on-line identification techniques to the building response data in VN7SH was presented by Loh and Lin (1996). A continuum mechanics representation of VN7SH in terms of isotropic and anisotropic two-dimensional models and their response to incident wave motion was considered by Todorovska et al. (2001a, 2001b). The feasibility of identifying the observed damage through wave propagation studies using recorded earthquake responses was explored in Ivanović et al. (1999b), Trifunac et al. (2003), and Todorovska and Trifunac (2006).

The engineering studies of VN7SH have focused mainly on its longitudinal (EW) response. Without exception, these studies have neglected the effects of soil-structure interaction and have implicitly assumed that all nonlinearities in the observed response are associated with the building structure.

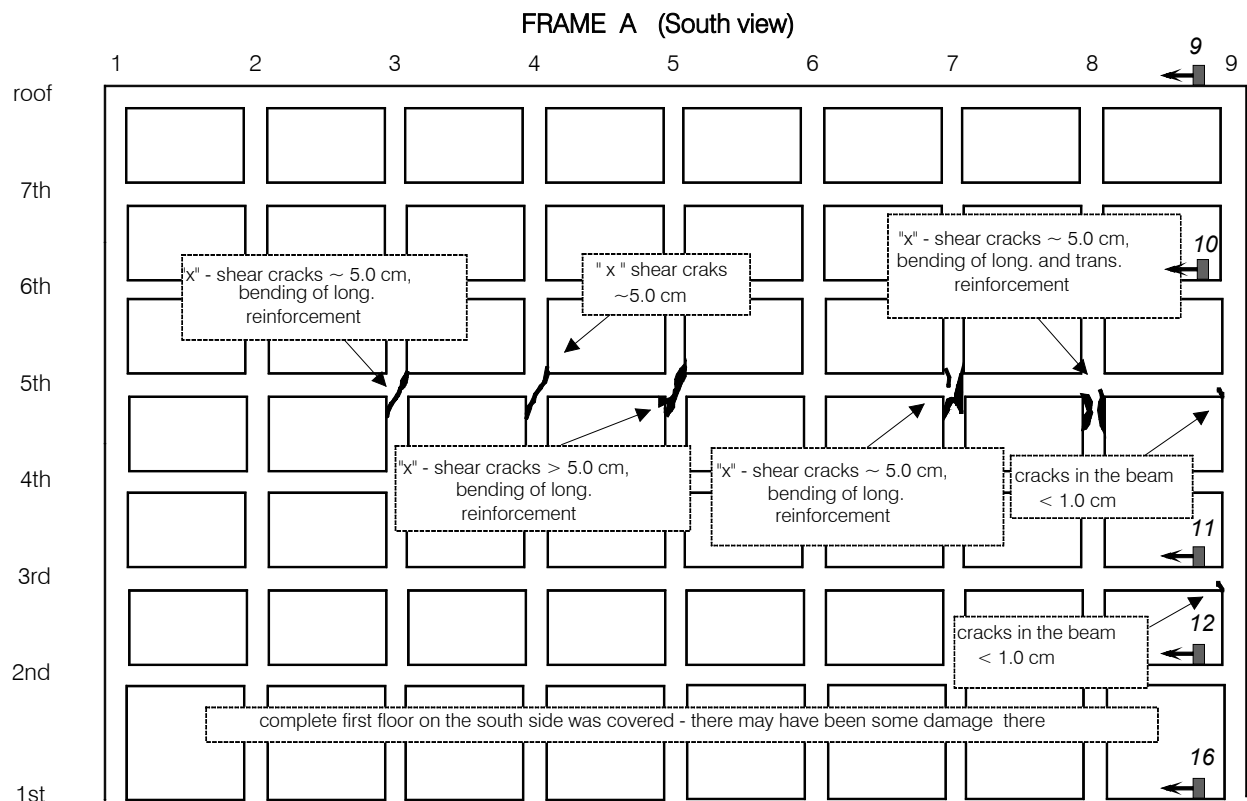


Fig. 2(b) Observed damage of Frame A

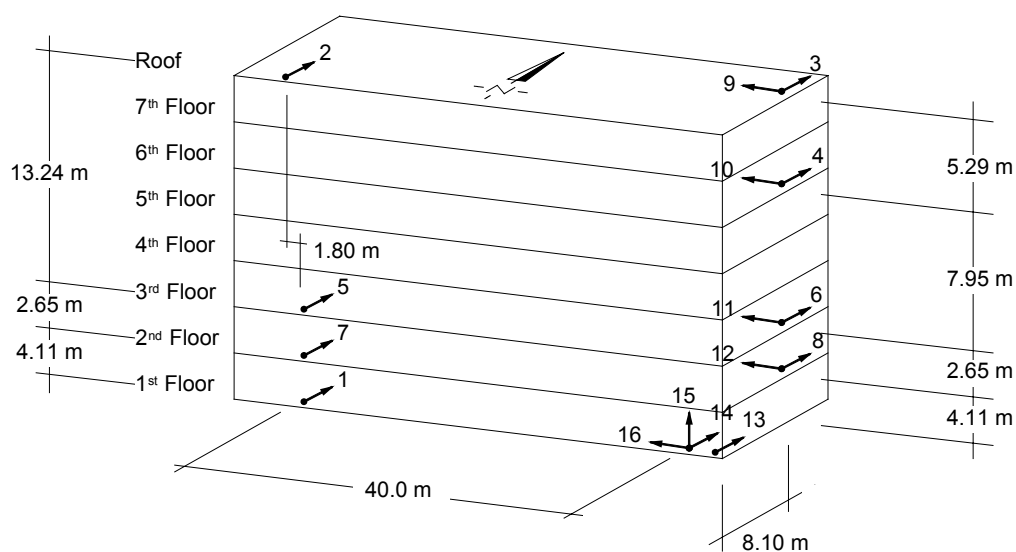


Fig. 3 Location of CR-1 channels (1-13), and of SMA-1 accelerographs (14-16)

Islam (1996) considered two two-dimensional models for EW response of the building. Assuming the building to be fixed at the ground floor level, he used the triangular distributed horizontal load to perform a push-over analysis. Figure 4 shows his results for V/W , the resulting base shear (V), normalized by the appropriate fraction of building weight (W), versus the roof displacement, assuming that the south perimeter frame (A) resists one third of the lateral load. Islam (1996) concluded, “many of the structural elements may have exceeded their elastic limit state at approximately 4 s into the earthquake. However, the most severe damage, e.g., breakdown of the entire load path in the south perimeter frame columns immediately below the 5th floor level, may have actually occurred at approximately 9 s, which coincides with the time of the peak ground acceleration in the longitudinal direction”. He also notes, “a push-over analysis performed on the longitudinal frame with a triangular load pattern was unable to predict the damage observed in the building”.

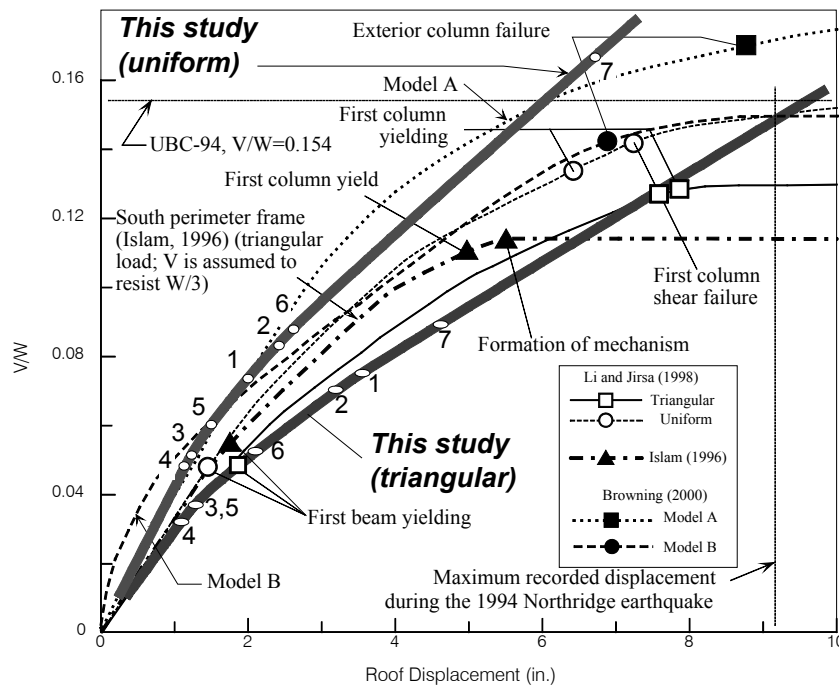


Fig. 4 Base shear (V) coefficient, normalized by total building weight W , versus EW roof displacement of VN7SH (open circles indicate the first occurrence of nonlinear strain at the floors 1 through 7 as obtained in this study)

Li and Jirsa (1998) performed a “nonlinear time history” analysis of VN7SH in the longitudinal (EW) direction “only because most of the damage occurred in this direction”. Acceleration time histories recorded at ground level were used as the input ground motion, and columns were assumed to be fixed at the base. Soil-structure interaction was not included in the models. Effective stiffness and residual lateral capacity were chosen so that the period of calculated response-time history would match the recorded time history, and $0.35EI_g$ was chosen as an effective stiffness for all beams and columns. Their analysis was two-dimensional, and therefore no torsional effects of excitation and of response could be included. Li and Jirsa stated, “push-over analysis successfully predicted that the structure almost lost its lateral load-resisting capacity, and the shear failures of columns occurred prior to reaching the maximum roof displacement the building experienced during the earthquake”.

Browning et al. (2000) compared three independent analyses, including their own results, with regard to the response of VN7SH to the Northridge earthquake: Approach A (by Lynn and Moehle); Approach B (by Browning and Sozen); and Approach C (by Li and Jirsa). Because Approach C has already been summarized, we mention briefly only the results of the analyses based on the approaches A and B. Approach A idealizes the building as a two-dimensional frame and considers only the longitudinal (interior and exterior) framing lines. A simple bi-linear relation without stiffness or strength degradation is used to describe load-deformation properties of the frames. The foundation is assumed to be rigid, i.e., no soil-structure interaction is considered, and the authors used triangular load distribution with monotonically increasing amplitude in their push-over analysis (Figure 4). Dynamic “nonlinear response histories” were computed for the motion measured at the base of the building. Approach B used geometry of the model similar to that in Approach A, but the in-fill walls were assumed not to contribute to resistance to the lateral forces. A “Takeda nonlinear model” with unloading stiffness reduction equal to 0.4 was adopted, and nonlinear static and dynamic response analyses were conducted. The results of the push-over analysis are shown in Figure 4.

De la Llera et al. (2001) noted, “planar analyses of the building reported previously are obviously not capable of predicting ... torsional motion”. They developed an idealization of the building consisting of a “single column-like element” (SEM) connecting two consecutive floors, and used this model to interpret the three-dimensional response of the VN7SH building to the earthquake. As in all previous investigations of the response of this building, De la Llera et al. (2001) ignored the soil-structure interaction effects in their analyses of translational and torsional responses.

NONLINEAR WAVES

Wave propagation models of buildings have been used for many years (Kanai, 1965), but are only recently beginning to be verified against observations (Ivanović et al., 1999b; Todorovska et al., 2001a, 2001b, 2001c; Trifunac and Todorovska, 2001; Trifunac et al., 2001c). Continuous, 2-D wave propagation models (i.e., homogeneous, horizontally layered and vertically layered shear plates) can be employed to study the effects of traveling waves on the response of long buildings (Todorovska et al., 1988; Todorovska and Trifunac, 1989, 1990a, 1990b; Todorovska and Lee, 1989). Discrete-time 1-D wave propagation models were proposed to study the response of tall buildings (Gilstrap et al., 1998), and 2-D finite difference methods were used to study linear and nonlinear soil-structure interaction (Gicev, 2005).

In the following the elementary principles of wave propagation through a layered shear beam model will be used to demonstrate the relationships between the power of incident strong ground motion and of the building response.

1. The Building Model

We consider a one-dimensional finite difference model, and use the velocity of shear waves and the density of the slabs and inter-story columns based on the analysis of the impulse response for EW recorded motions in Holiday Inn hotel (Todorovska and Trifunac, 2006). These parameters together with the inter-story heights, as adopted in this study, are summarized in Table 1. As can be seen from this table, the stiffness and the density of the floors is much larger than the stiffness of the columns. Therefore it can be expected that the floors will move essentially as rigid bodies. The yielding and the nonlinear characteristics of the material have been estimated previously from the east-west response of this model by assuming that the input ground motion can be approximated by strong motion recorded at the first (ground) floor (i.e., at the channel 16). We did this by comparing the computed motions with the recorded motions at higher floors in the building (i.e., at the channel 12 at the second floor, channel 11 at the third floor, channel 10 at the sixth floor, and at the channel 9 at the roof) (Gicev and Trifunac, 2006b). The location of the instruments in the building, which recorded the EW response, is shown in Figure 3. By varying the yielding strain and the strengthening factor γ , assuming that they are same for the whole building, and by minimizing the error between the recorded and the calculated responses, we obtained the best estimates for the yielding strain $\varepsilon_y = 0.0025$ and $\gamma = 0.44$. These two parameters together with those in Table 1 then complete the description of our finite difference bilinear model parameters (Gicev and Trifunac, 2006b).

Table 1: One-Dimensional Building Model

	Interstory Height $h_{\text{interstory}}$ (m)	Slab Thickness h_{slab} (m)	$\beta_{\text{interstory}}$ (m/s)	β_{slab} (m/s)	$\rho_{\text{interstory}}$ (kg/m ³)	ρ_{slab} (kg/m ³)
Roof Slab		0.203		2000		2384
Seventh Story	2.44		73.15		82.90	
Seventh Floor Slab		0.215		2000		2384
Sixth Story	2.44		76.20		82.90	
Sixth Floor Slab		0.216		2000		2384
Fifth Story	2.44		77.72		82.90	
Fifth Floor Slab		0.216		2000		2384
Fourth Story	2.44		79.25		82.90	
Fourth Floor Slab		0.216		2000		2384
Third Story	2.44		91.44		82.90	
Third Floor Slab		0.216		2000		2384
Second Story	2.44		129.50		82.90	
Second Floor Slab		0.254		2000		2384
First Story	3.86		140.20		76.92	

In this paper, we adopt the same model parameters but consider the one-dimensional interaction between the soil and the building by taking two more spatial points in the soil (Gicev and Trifunac, 2006a). We further assume that the soil is linear having shear wave velocity $\beta_s = 300$ m/s and density $\rho_s = 2000$ kg/m³. We assume that the horizontal wave motion in the ground propagates upward and that it is the one recorded at the channel 16 (see Figure 5). Of course, this is not the actual incident wave motion during the Northridge main event, because the record in the channel 16 resulted from the incident and reflected wave-field at the base of the building. Also this record contains the soil-structure interaction effects. Nevertheless, using this record as an approximation for the arriving waves in the ground we can approximately study the overall features of the response of the building during the main event of the Northridge earthquake from the energy point of view. In all other respects our modeling of the building by the one-dimensional finite difference model is identical to the one described in Gicev and Trifunac (2006a), and its description is, therefore, not repeated here.

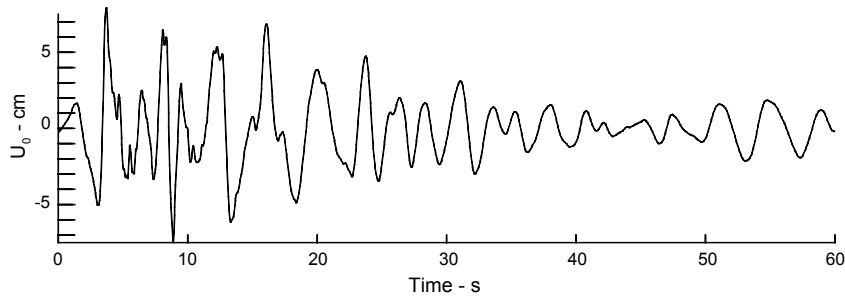


Fig. 5 Incident ground motion

2. Results

2.1 Energy Distribution in the Model

Because the model we study represents a conservative system, the kinetic and elastic parts of the potential energy, the energy that radiated out from the building into the soil, and the energy spent for development of the permanent strains in the building must add up to the incident wave energy. In Figure 6 the energy that radiated out of the building into the soil, E_{out} , and the energy spent on the work leading to the permanent strains, E_{hys} , are shown versus time. The energy is computed in kilojoules (1 kJ = 1 kN-m), while the time is shown in seconds.

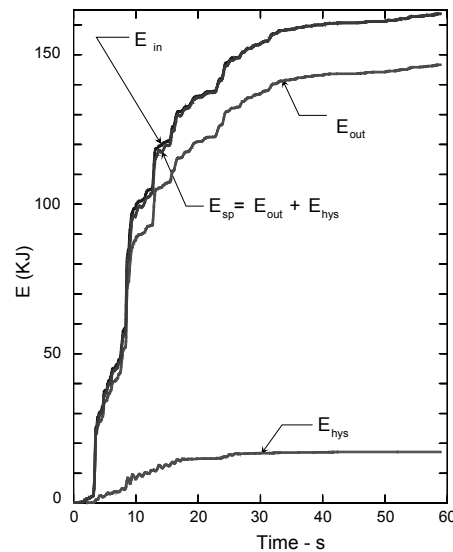


Fig. 6 Energy distribution in VN7SH during the Northridge earthquake (the spent energy consisting of the energy going out of the building and the spent hysteretic energy balance the input energy)

The input energy E_{in} is computed from the input displacement record (as in Figure 5). First, by differentiation of the displacement record with respect to time, the input particle velocity is obtained. The input energy, assuming that the cross section of the model is $A = 1 \text{ m}^2$, is computed assuming vertically propagating one-dimensional plane waves,

$$E_{in} = \rho_s \beta_s \int_0^T v^2 dt \cong \rho_s \beta_s \sum_{k=1}^M v_k^2 \Delta t \quad (2)$$

where ρ_s and β_s are the density and the shear wave velocity of the soil; $v = \partial u_0 / \partial t$ is the input particle velocity; T is the time at the end of the record; k is the order number of a time-step; $M = T / \Delta t$ is the discrete time at the end of the record; and $v_k = (u_{0,k} - u_{0,k-1}) / \Delta t$ for $k > 1$, and $v_1 = u_{0,1} / \Delta t$ for $k = 1$, are the discrete particle velocities.

The output energy E_{out} is computed from the velocity of the wave going downward, v_{out} (Gicev and Trifunac, 2006a). The cumulative output energy is then computed as

$$E_{out} = \rho_s \beta_s \int_0^T v^2 dt \cong \rho_s \beta_s \sum_{k=1}^M (v_{out}^k)^2 \Delta t \quad (3)$$

The hysteretic energy E_{hys} is the energy spent on the development of permanent strains in the building. The hysteretic loop (see Figure 7) represents the relation $\sigma(\varepsilon)$ at a point during one cycle of the response, $T_{0,i} < t < T_{0,i+1}$, where $T_{0,1} = 4 \sum_{j=1}^{14} (h_j / \beta_j) \approx 0.8 \text{ s}$ can be used to approximate the apparent period of the building. Depending upon the input ground motion and the time during the strong motion, the loop can be narrower or wider. By adding the areas of those loops, and assuming no strength reduction due to repetitive loads, we can compute the energy spent for the development of permanent strains at a point. Next, we generalize this for a layer (i.e., a continuous equivalent representation of the columns and walls at a given floor) and for the whole building. The hysteretic energy for a certain layer is obtained as the sum of the loops at the points belonging to that layer, while the hysteretic energy for the whole building is obtained as the sum of the energies in all layers. The hysteretic energy in the building in discrete time space is computed as

$$E_{hys} = \sum_{i=3}^N \Delta x_i \sum_{k=1}^M \sigma_{av}^k \Delta \varepsilon^k \quad (4)$$

where the indices i and k stand for the spatial and temporal discrete points in the model; N is the point representing the top of the building; M is the point representing the end of the record; $\sigma_{av}^k = (\sigma^k + \sigma^{k-1}) / 2$ is the average stress at a point i in the time-step k ; and $\Delta \varepsilon^k$ is the strain-increment at the point i in the k th time-step. The points in the slabs do not contribute to the hysteretic energy because those are assumed to remain linear and to only transmit the wave energy to the layers above and below. As can be seen from Figure 6, after about $t = 30 \text{ s}$, there is a negligible growth of all energies, and therefore in the following analysis we consider only the first 30 s of strong motion.

Subtracting from the input energy (see Equation (2)), the output (radiated) energy (see Equation (3)), we obtain the instantaneous energy in the building, E_b (see Figure 8). The difference,

$$E_{el}^b = E_b - E_{hys} \quad (5)$$

then represents the instantaneous elastic (linear) energy in the building. All these energies are computed in kJ. In the bottom of Figure 8, the derivatives (power) of these three energies are shown versus time. The power is shown in kilowatts ($1 \text{ kW} = 1 \text{ kJ/s} = 1 \text{ kN-m/s}$). Until the end of the record, one part of the elastic energy is radiated, contributing to the output energy E_{out} , and one part is later spent for the development of permanent strains contributing to the hysteretic energy E_{hys} . A part of the energy in the building is reversible. During the loading a fraction of the elastic energy is transformed into the hysteretic energy, and during the unloading a part of the hysteretic energy is converted back into the elastic energy.

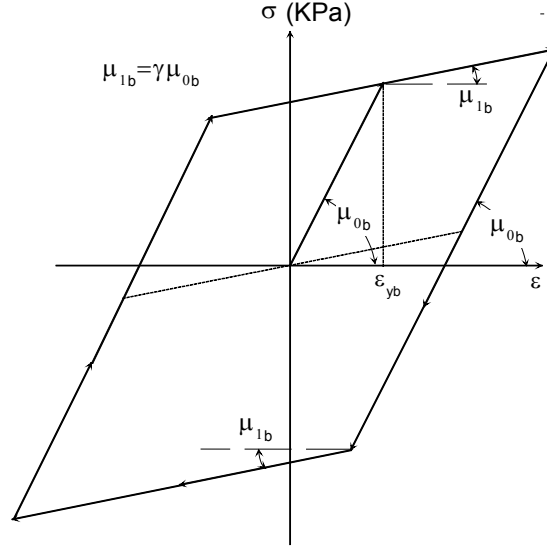


Fig. 7 Hysteresis loop representing $\sigma(\varepsilon)$ during the time $T_{0,i} < t < T_{0,i+1}$

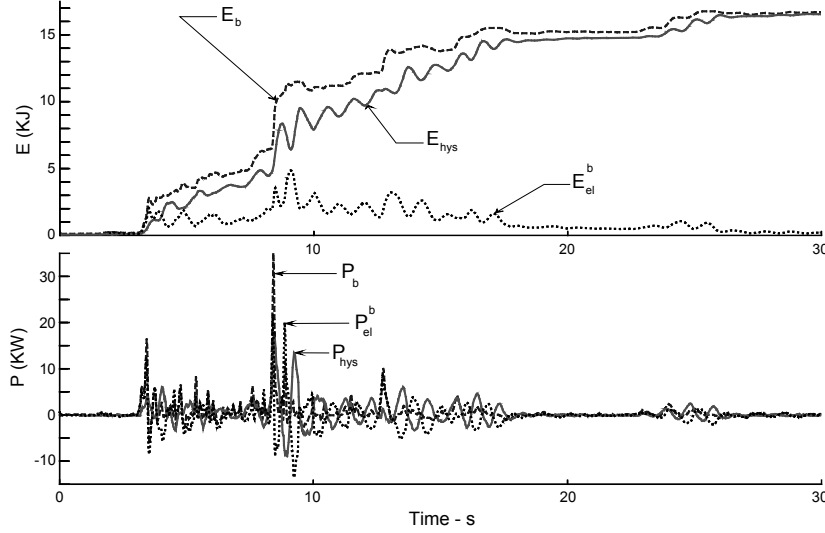


Fig. 8 Energy E_b (top) and power P_b (bottom) in the VN7SH building during the Northridge earthquake, where $E_{el}^b = E_b - E_{hys}$

2.2 Energy and Power Capacities and Demands in the Building

To study how the VN7SH building performed during the Northridge earthquake, we consider the energy and the power capacities of different floors. To determine the energy capacity for one period, E_{T_0} , we consider the hysteretic loop at a point, during which the point reaches the strain, ε_u (see Figure 9). The area of the loop A_i is the energy capacity of the floor i for that ε_u and for one period,

$$A_i = E_{T_0}^i = 4A_{OABB'} = 4 \cdot \overline{OB'} \cdot \overline{AA'} \cdot h_i \quad (6)$$

where h_i is the height of the i th floor. From Figure 9 there follows

$$\overline{AA'} = (\mu_{0i}\varepsilon_{yb} - \mu_{1i}\varepsilon_{yb}) \cos \alpha_{1i} \quad \text{and} \quad \overline{OB'} = \frac{\varepsilon_u - \varepsilon_{yb}}{\cos \alpha_{1i}} \quad (7a)$$

where $\mu_{1i} = \gamma\mu_{0i}$, and the ductility is

$$d = \frac{\varepsilon_u}{\varepsilon_{yb}} \quad (7b)$$

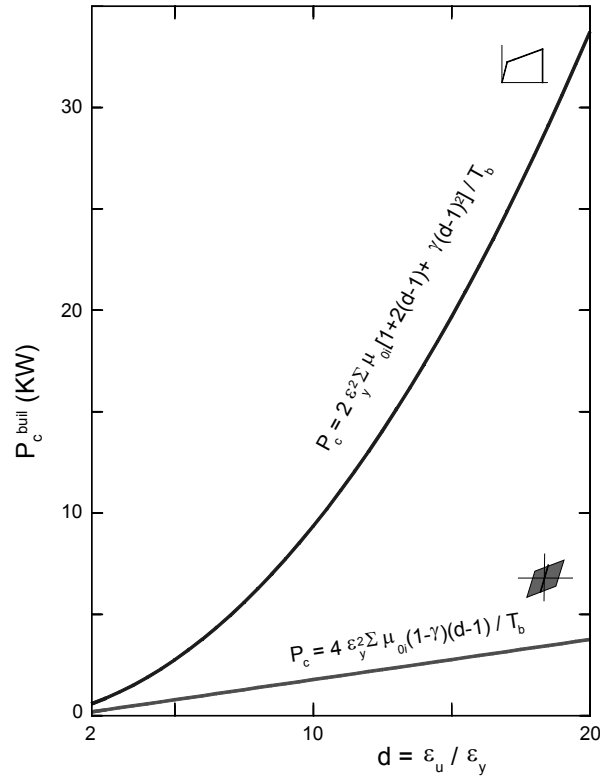


Fig. 10 Power capacities for VN7SH for one and one-quarter periods

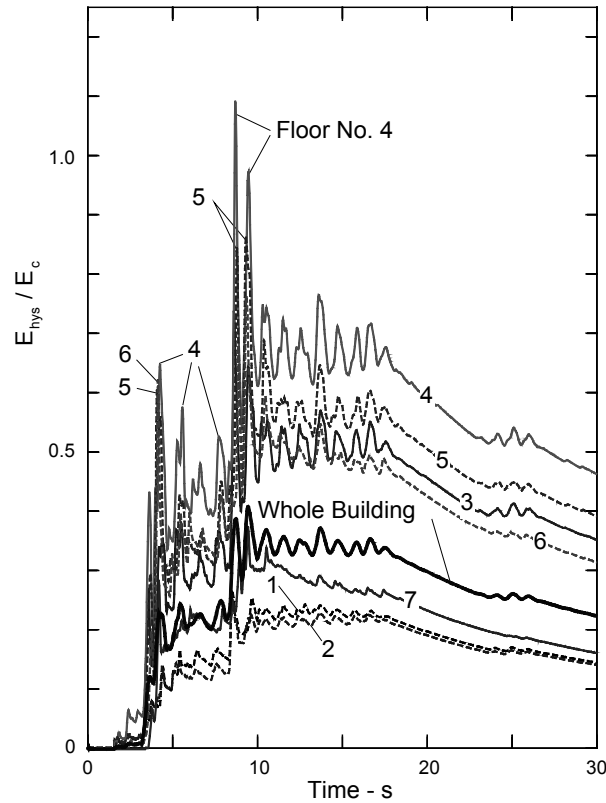


Fig. 11 Normalized cumulative hysteretic energies E_{hys} / E_c versus time in seven layers (floors) and in the whole building

Trifunac et al. (2001c) estimated input velocity in the building for the equivalent SDOF system that will cause failure, by equalizing the input power in the building and its apparent (i.e., based on actual observation of earthquake effects) power capacity. Following this approach, to understand failure, we

may compare the maximum power in the floor/building with the power capacity of the floor/building. In Figure 11 the cumulative hysteretic energies during the Northridge earthquake for all inter-story layers are presented during the first thirty seconds of strong motion, after normalization (division) by the energy capacities for the ductility $d = 10$. The cumulative energy capacities, computed from Equation (8), can be approximated by straight lines as

$$E_{cT_0}^i(t) = E_{T_0}^i \frac{t}{T_0} \quad (16)$$

where t is the time when the energy capacity of the i th column for one full period is computed, and T_0 is the period of the building. The approximation by Equation (16) is a straight line, with the slope $E_{T_0}^i / T_0$, which represents the power capacity for a full cycle of response. Figure 11 then shows the evolution of the process at each floor. For small oscillations in the beginning of the strong motion, the power demand is small and the maximum capacity of the floors is not mobilized. With the arrival of large strong motion pulses (at about 4 and 9 s after the trigger time), large nonlinear deformations occur with $E_{\text{hys}} / E_{c(d=10)}$ exceeding 1.0.

The ductility demands for this model of VN7SH have been calculated by Gicev and Trifunac (2006b), for different floors, and are summarized in Table 2. The maximum strains occurred during the time interval $8.5 \text{ s} \leq t \leq 9.5 \text{ s}$.

Table 2: Peak Ductilities $|d|_{\text{max}}$ computed by Gicev and Trifunac (2006b)

Interstory Layer, i	$ d _{\text{max}}$
1	4.10
2	3.67
3	8.64
4	9.39
5	9.39
6	6.73
7	3.71

From Figure 11 it can be seen that the cumulative hysteretic energies $E_{\text{hys}}(t)$ (see Equation (4)), normalized with respect to the energy capacities $E_c(t)$ (see Equation (16)) for ductility $d = 10$, for example, are in good agreement with the previously computed maximum ductilities for the same building and for the same excitation, as shown in Table 2 (Gicev and Trifunac, 2006b).

The hysteretic energy demand takes into account only the strains, but does not consider the time rates of change in those strains. In contrast, the power takes into account the energy rates in time, which we compute as derivatives of the energy, after normalization by the rates representing capacity (per unit time T_0 for P_{T_0}) for one hysteretic cycle, or by the rates representing capacity (per unit time $T_0/4$ for P_q) for one monotonic loading interval.

Figure 11 shows that at the fourth and the fifth floors, the hysteretic energy, starting from $t = 4 \text{ s}$, becomes larger than the energy capacity E_c for $d \sim 5$, while it exceeds the energy capacity for $d = 10$ only in a short interval around $t = 9 \text{ s}$. The energy demand for the whole building is slightly higher than the energy capacity for $d \sim 3.5$ in the interval $8.5 \text{ s} < t < 20 \text{ s}$.

Figures 12(a) and 12(b) show a more detailed view of the physical nature of the demands and of the capacities for two time windows, from 3 to 6 s and from 8 to 11 s, in terms of relative power. In these figures relative power is plotted in terms of the ratio of P_{hys} , which is the time rate of change of E_{hys} (see Equation (4)), normalized (divided) by $P_{c,\text{quart}}$ (see Equation (15)) and calculated for $d = 10$. It is seen that this power ratio approaches 2 at the 4th and 7th floors, while at the 5th and 6th floors it is near 3 around 4 s. At the 3rd, 4th, 5th and 6th floors, this ratio exceeds 1 around 5.2 s. The same ratio exceeds 5, for example, at the 3rd, 4th, 5th, and 6th floors between 8.5 and 8.8 s, and again at the 5th floor around 9.2 s.

The largest peak of the ratio $P_{\text{hys}} / P_{\text{c,quart}}$ (for $d = 10$) occurred on the 4th floor, with amplitude larger than 8, at about 8.6 s. These results are in excellent agreement with the location of the observed post-earthquake damage on the same floor (see Figures 2(a) and 2(b)), and with the analyses of the peak strains and peak drifts in the response of the one-dimensional model of VN7SH to the Northridge earthquake (Gicev and Trifunac, 2006b).

Further perusal of the largest peaks of the power ratio, $P_{\text{hys}} / P_{\text{c,quart}}$ (for $d = 10$) (see Figures 12(a) and 12(b)), will show that those occur in sequence, at progressively higher floors, and at the times following the entrance of the strong pulses from the ground motion into the building. The local peak ratios occur in Figure 12(a) around 4 s (at the floors 3, 4, 5, and 6), around 5.2 s (at the floors 1, 2, 3, 4, 5 and 6), and in Figure 12(b) around 8.4 s (at the floors 1, 2, 3, 4, 5, and 6), 9.3 s (at the floors 4, 5 and 6), and 10.3 s (at the floors 3, 4, 5, 6 and 7). As they propagated up into the building, these power pulses caused damage along their path, whenever and wherever the power ratio exceeded the value of about 2. From the time delays between these consecutive pulses in Figures 12(a) and 12(b), we can estimate the average wave speeds associated with the propagation of their energies. Around 4 and 5 s (in Figure 12(a)) this speed is about 40 m/s. Around 8.5 s and 10.2 s (in Figure 12(b)) this speed is lower, about 30 m/s. Comparing these speeds with the initial (linear) velocities in our model (see Table 1), which are in the range from 73 m/s (at the seventh story) to 91 m/s (at the third story) and 140 m/s (at the first story), it can be concluded that those lower speeds resulted from nonlinear deformations in the model. Their values and their times of occurrence are consistent with the results of other direct (see Table 2 and Figure 11 in Todorovska and Trifunac (2008a)) and indirect analyses of the nonlinear waves in VN7SH (Gicev and Trifunac, 2006b; Todorovska and Trifunac, 2006), and show trends similar to what has been seen in other buildings damaged by the strong-motion waves (Todorovska and Trifunac, 2007a, 2007b, 2008b).

SUMMARY AND CONCLUSIONS

Biot's response spectrum method uses characteristic functions (mode shapes) to represent vibrations of a multi-degree-of-freedom system via a set of equivalent single-degree-of-freedom oscillators. Superposition of modal responses is then used to compute actual system response and the peak of that response is employed in earthquake-resistant design to construct envelopes of maximum relative responses (thus defining maximum drift) or of maximum inter-story forces. Mathematically this approach is complete, and the representation in terms of modal responses converges to the exact linear response. However, the simplifications imposed by the design practice result in the use of only the lowest modes of response. The consequence is that the amplitudes of dynamic response to sudden, high-frequency excitation by a near-field pulse are seriously underestimated. For large strong-motion amplitudes the above approach breaks down as the representation in terms of a superposition of modal responses ceases to be valid for the nonlinear response.

When the motion of the structure can be approximated via one-dimensional shear beam idealization (i.e., the contribution of rotational waves can be neglected), we have shown how by comparing the power of a pulse entering the structure (i.e., the demand) with the ability of structure to absorb this power (i.e., the capacity), one can lead to simple and direct estimation of the required structural capacity.

Power (i.e., energy and its duration) of the strong near-field pulses will determine whether the wave entering the structure will continue to propagate through the structure as a linear wave, or will begin to create nonlinear zones (first near the top, and/or near the base of the structure (Gicev, 2005)). For high-frequency pulses the nonlinear zone with permanent strains can be created before the wave motion reaches the top of the structure, i.e., before the interference of waves has even started to occur leading to the formation of mode shapes. Overall duration of the strong motion (Trifunac and Novikova, 1994) will determine the number of times the structure may be able to complete full cycles of response and the associated number of "minor" excursions into the nonlinear response range, when the response is weakly nonlinear (Gupta and Trifunac, 1996), while the presence of powerful pulses of strong motion will determine the extent to which the one-directional quarter-period responses may lead to excessive ductility demand, leading to dynamic instability and failure, precipitated by the gravity loads (Husid, 1967). All these possibilities can be examined and quantified deterministically by the computation of the associated power capacities and power demands for different scenarios for given recorded or synthesized strong motion accelerograms, or probabilistically by extending the methods developed for the uniform hazard analysis (Todorovska et al., 1995).

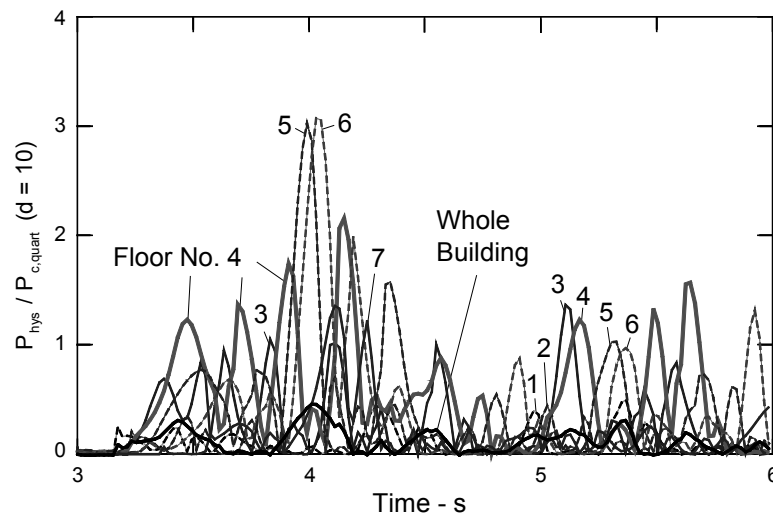


Fig. 12(a) Normalized power demands in the model of VN7SH building during excitation by the Northridge earthquake, shown separately at the seven floors and in the whole building, for $3 < t < 6$ s

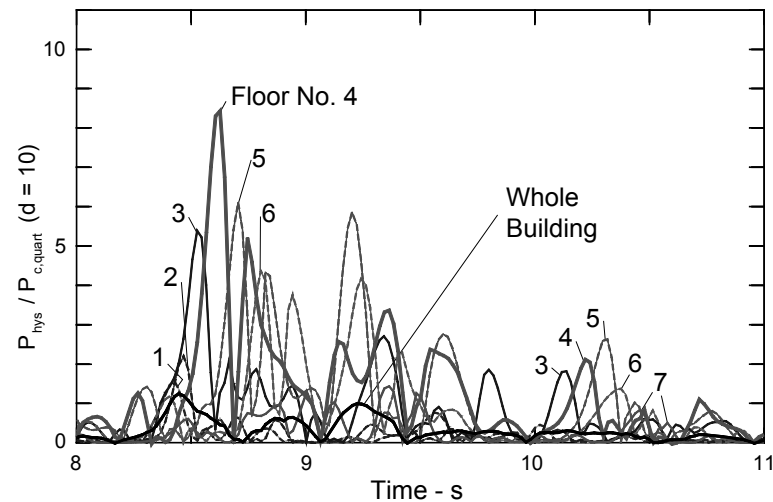


Fig. 12(b) Normalized power demands in the model of VN7SH building during excitation by the Northridge earthquake, shown separately at the seven floors and in the whole building, for $8 < t < 11$ s

REFERENCES

1. Akiyama, H. (1985). "Earthquake-Resistant Limit-State Design for Buildings", University of Tokyo Press, Tokyo, Japan.
2. Arias, A. (1970). "A Measure of Earthquake Intensity" in "Seismic Design in Nuclear Power Plants (edited by R.J. Hansen)", The MIT Press, Cambridge, U.S.A.
3. Benioff, H. (1934). "The Physical Evaluation of Seismic Destructiveness", Bulletin of the Seismological Society of America, Vol. 24, No. 4, pp. 398-403.
4. Biot, M.A. (1932). "Transient Oscillations in Elastic Systems", Ph.D. Thesis No. 259, Aeronautics Department, California Institute of Technology, Pasadena, U.S.A.
5. Biot, M.A. (1933). "Theory of Elastic Systems Vibrating under Transient Impulse with an Application to Earthquake-Proof Buildings", Proceedings of the National Academy of Sciences of the United States of America, Vol. 19, No. 2, pp. 262-268.

6. Biot, M.A. (1934). "Theory of Vibration of Buildings during Earthquake", *Zeitschrift für Angewandte Mathematik und Mechanik*, Vol. 14, No. 4, pp. 213–223.
7. Biot, M.A. (1941). "A Mechanical Analyzer for the Prediction of Earthquake Stresses", *Bulletin of the Seismological Society of America*, Vol. 31, No. 2, pp. 151–171.
8. Biot, M.A. (1942). "Analytical and Experimental Methods in Engineering Seismology", *ASCE Transactions*, Vol. 108, pp. 365–408.
9. Browning, J.A., Li, R.Y., Lynn, A. and Moehle, J.P. (2000). "Performance Assessment for a Reinforced Concrete Frame Building", *Earthquake Spectra*, Vol. 16, No. 3, pp. 541–555.
10. De la Llera, J.C., Chopra, A.K. and Almazan, J.L. (2001). "Three-Dimensional Inelastic Response of an RC Building during the Northridge Earthquake", *Journal of Structural Engineering, ASCE*, Vol. 127, No. 5, pp. 482–489.
11. Fajfar, P. and Krawinkler, H. (editors) (1992). "Nonlinear Seismic Analysis and Design of Reinforced Concrete Buildings", Elsevier Applied Science, London, U.K.
12. Gicev, V. (2005). "Investigation of Soil-Flexible Foundation-Structure Interaction for Incident Plane SH Waves", Ph.D. Dissertation, Department of Civil Engineering, University of Southern California, Los Angeles, U.S.A.
13. Gicev, V. and Trifunac, M.D. (2006a). "Rotations in the Transient Response of Nonlinear Shear Beam", Report CE 06-02, University of Southern California, Los Angeles, U.S.A.
14. Gicev, V. and Trifunac, M.D. (2006b). "Non-linear Earthquake Waves in Seven-Storey Reinforced Concrete Hotel", Report CE 06-03, University of Southern California, Los Angeles, U.S.A.
15. Gilstrap, J.M., Dolan, C.W. and Safak, E. (1998). "New Approach to Analyzing Soil-Building Systems", *Soil Dynamics and Earthquake Engineering*, Vol. 17, No. 7, pp. 509–517.
16. Gupta, I.D. and Trifunac, M.D. (1996). "Investigation of Nonstationarity in Stochastic Seismic Response of Structures", Report CE 96-01, University of Southern California, Los Angeles, U.S.A.
17. Gutenberg, B. and Richter, C.F. (1956a). "Earthquake Magnitude, Intensity, Energy, and Acceleration", *Bulletin of the Seismological Society of America*, Vol. 46, No. 2, pp. 105–145.
18. Gutenberg, B. and Richter, C.F. (1956b). "Magnitude and Energy of Earthquakes", *Annali di Geofisica*, Vol. 9, No. 1, pp. 1–15.
19. Hayir, A., Todorovska, M.I. and Trifunac, M.D. (2001). "Antiplane Response of a Dike with Flexible Soil-Structure Interface to Incident SH Waves", *Soil Dynamics and Earthquake Engineering*, Vol. 21, No. 7, pp. 603–613.
20. Husid, R. (1967). "Gravity Effects on the Earthquake Response of Yielding Structures", Ph.D. Dissertation, California Institute of Technology, Pasadena, U.S.A.
21. Islam, M.S. (1996). "Analysis of the Response of an Instrumented 7-Story Nonductile Concrete Frame Building Damaged during the Northridge Earthquake", *Proceedings of the 1996 Annual Meeting of the Los Angeles Tall Buildings Structural Design Council*, Los Angeles, U.S.A., Paper No. 96-9.
22. Ivanović, S.S., Trifunac, M.D., Novikova, E.I., Gladkov, A.A. and Todorovska, M.I. (1999a). "Instrumented 7-Storey Reinforced Concrete Building in Van Nuys, California: Ambient Vibration Surveys Following the Damage from the 1994 Northridge Earthquake", Report CE 99-03, University of Southern California, Los Angeles, U.S.A.
23. Ivanović, S.S., Trifunac, M.D. and Todorovska, M.I. (1999b). "On Identification of Damage in Structures via Wave Travel Time", *Proceedings of the NATO Advanced Research Workshop on Strong Motion Instrumentation for Civil Engineering Structures*, Istanbul, Turkey, pp. 447–468.
24. Ivanović, S.S., Trifunac, M.D., Novikova, E.I., Gladkov, A.A. and Todorovska, M.I. (2000). "Ambient Vibration Tests of a Seven-Story Reinforced Concrete Building in Van Nuys, California, Damaged by the 1994 Northridge Earthquake", *Soil Dynamics and Earthquake Engineering*, Vol. 19, No. 6, pp. 391–411.
25. John A. Blume & Associates (1973). "Holiday Inn" in "San Fernando, California, Earthquake of February 9, 1971 (edited by L.M. Murphy), Vol. I, Part A", National Oceanic and Atmospheric Administration, U.S. Department of Commerce, Washington, DC, U.S.A.

26. Joyner, W.B. (1975). "A Method for Calculating Nonlinear Seismic Response in Two Dimensions", *Bulletin of the Seismological Society of America*, Vol. 65, No. 5, pp. 1337–1357.
27. Joyner, W.B. and Chen, A.T.F. (1975). "Calculation of Nonlinear Ground Response in Earthquakes", *Bulletin of the Seismological Society of America*, Vol. 65, No. 5, pp. 1315–1336.
28. Kanai, K. (1965). "Some Problems of Seismic Vibration of Structures", *Proceedings of the Third World Conference on Earthquake Engineering*, Wellington, New Zealand, Vol. II, pp. 260–275.
29. Lee, V.W. (1979). "Investigation of Three-Dimensional Soil-Structure Interaction", Report CE 79-11, University of Southern California, Los Angeles, U.S.A.
30. Li, R.Y. and Jirsa, J.D. (1998). "Nonlinear Analyses of an Instrumented Structure Damaged in the 1994 Northridge Earthquake", *Earthquake Spectra*, Vol. 14, No. 2, pp. 265–283.
31. Loh, S.-H. and Lin, H.-M. (1996). "Application of Off-line and On-line Identification Techniques to Building Seismic Response Data", *Earthquake Engineering & Structural Dynamics*, Vol. 25, No. 3, pp. 269–290.
32. Luco, J.E., Wong, H.L. and Trifunac, M.D. (1986). "Soil-Structure Interaction Effects on Forced Vibration Tests", Report CE 86-05, University of Southern California, Los Angeles, U.S.A.
33. Mulhern, M.R. and Maley, R.P. (1973). "Building Period Measurements before, during and after the San Fernando Earthquake" in "San Fernando, California, Earthquake of February 9, 1971 (edited by L.M. Murphy), Vol. I, Part B", National Oceanic and Atmospheric Administration, U.S. Department of Commerce, Washington, DC, U.S.A.
34. Todorovska, M.I. and Lee, V.W. (1989). "Seismic Waves in Buildings with Shear Walls or Central Core", *Journal of Engineering Mechanics*, ASCE, Vol. 115, No. 12, pp. 2669–2686.
35. Todorovska, M.I. and Trifunac, M.D. (1989). "Antiplane Earthquake Waves in Long Structures", *Journal of Engineering Mechanics*, ASCE, Vol. 115, No. 12, pp. 2687–2708.
36. Todorovska, M.I. and Trifunac, M.D. (1990a). "A Note on the Propagation of Earthquake Waves in Buildings with Soft First Floor", *Journal of Engineering Mechanics*, ASCE, Vol. 116, No. 4, pp. 892–900.
37. Todorovska, M.I. and Trifunac, M.D. (1990b). "Note on Excitation of Long Structures by Ground Waves", *Journal of Engineering Mechanics*, ASCE, Vol. 116, No. 4, pp. 952–964.
38. Todorovska, M.I. and Trifunac, M.D. (1991). "Radiation Damping during Two-Dimensional In-plane Building-Soil Interaction", Report CE 91-01, University of Southern California, Los Angeles, U.S.A.
39. Todorovska, M.I. and Trifunac, M.D. (1992). "The System Damping, the System Frequency and the System Response Peak Amplitudes during In-plane Building-Soil Interaction", *Earthquake Engineering & Structural Dynamics*, Vol. 21, No. 2, pp. 127–144.
40. Todorovska, M.I. and Trifunac, M.D. (1993). "The Effects of Wave Passage on the Response of Base-Isolated Buildings on Rigid Embedded Foundations", Report CE 93-10, University of Southern California, Los Angeles, U.S.A.
41. Todorovska, M.I. and Trifunac, M.D. (2006). "Impulse Response Analysis of the Van Nuys 7-Story Hotel during 11 Earthquakes (1971–1994): One-Dimensional Wave Propagation and Inferences on Global and Local Reduction of Stiffness due to Earthquake Damage", Report CE 06-01, University of Southern California, Los Angeles, U.S.A.
42. Todorovska, M.I. and Trifunac, M.D. (2007a). "Earthquake Damage Detection in the Imperial County Services Building I: The Data and Time-Frequency Analysis", *Soil Dynamics and Earthquake Engineering*, Vol. 27, No. 6, pp. 564–576.
43. Todorovska, M.I. and Trifunac, M.D. (2007b). "Earthquake Damage Detection in the Imperial County Services Building II: Analysis of Novelties via Wavelets", *Soil Dynamics and Earthquake Engineering* (under review).
44. Todorovska, M.I. and Trifunac, M.D. (2008a). "Impulse Response Analysis of the Van Nuys 7-Storey Hotel during 11 Earthquakes and Earthquake Damage Detection", *Structural Control and Health Monitoring*, Vol. 15, No. 1 (in press).
45. Todorovska, M.I. and Trifunac, M.D. (2008b). "Earthquake Damage Detection in the Imperial County Services Building III: Analysis of Wave Travel Times via Impulse Response Functions", *Soil Dynamics and Earthquake Engineering* (in press).

46. Todorovska, M.I., Lee, V.W. and Trifunac, M.D. (1988). "Investigation of Earthquake Response of Long Buildings", Report CE 88-02, University of Southern California, Los Angeles, U.S.A.
47. Todorovska, M.I., Gupta, I.D., Gupta, V.K., Lee, V.W. and Trifunac, M.D. (1995). "Selected Topics in Probabilistic Seismic Hazard Analysis", Report CE 95-08, University of Southern California, Los Angeles, U.S.A.
48. Todorovska, M.I., Ivanović, S.S. and Trifunac, M.D. (2001a). "Wave Propagation in a Seven-Story Reinforced Concrete Building: Part I. Theoretical Models", *Soil Dynamics and Earthquake Engineering*, Vol. 21, No. 3, pp. 211–223.
49. Todorovska, M.I., Ivanović, S.S. and Trifunac, M.D. (2001b). "Wave Propagation in a Seven-Story Reinforced Concrete Building: Part II. Observed Wavenumbers", *Soil Dynamics and Earthquake Engineering*, Vol. 21, No. 3, pp. 225–236.
50. Todorovska, M.I., Hayir, A. and Trifunac, M.D. (2001c). "Antiplane Response of a Dike on Flexible Embedded Foundation to Incident SH-Waves", *Soil Dynamics and Earthquake Engineering*, Vol. 21, No. 7, pp. 593–601.
51. Trifunac, M.D. (1994). "Q and High-Frequency Strong Motion Spectra", *Soil Dynamics and Earthquake Engineering*, Vol. 13, No. 3, pp. 149–161.
52. Trifunac, M.D. (2003). "23rd ISET Annual Lecture: 70-th Anniversary of Biot Spectrum", *ISET Journal of Earthquake Technology*, Vol. 40, No. 1, pp. 19–50.
53. Trifunac, M.D. (2005). "Scientific Citations of M.A. Biot" in "Poro-Mechanics III: Biot Centennial (1905–2005) (edited by Y.N. Abousleiman, A.H.-D. Cheng and F.-J. Ulm)", A.A. Balkema, London, U.K.
54. Trifunac, M.D. and Brady, A.G. (1975). "A Study on the Duration of Strong Earthquake Ground Motion", *Bulletin of the Seismological Society of America*, Vol. 65, No. 3, pp. 581–626.
55. Trifunac, M.D. and Hao, T.Y. (2001). "7-Storey Reinforced Concrete Building in Van Nuys, California: Photographs of the Damage from the 1994 Northridge Earthquake", Report CE 01-05, University of Southern California, Los Angeles, U.S.A.
56. Trifunac, M.D. and Ivanović, S.S. (2003). "Analysis of Drifts in a Seven-Story Reinforced Concrete Structure", Report CE 03-01, University of Southern California, Los Angeles, U.S.A.
57. Trifunac, M.D. and Novikova, E.I. (1994). "State of the Art Review on Strong Motion Duration", *Proceedings of the Tenth European Conference on Earthquake Engineering*, Vienna, Austria, Vol. 1, pp. 131–140.
58. Trifunac, M.D. and Todorovska, M.I. (1996). "Nonlinear Soil Response—1994 Northridge, California, Earthquake", *Journal of Geotechnical Engineering*, ASCE, Vol. 122, No. 9, pp. 725–735.
59. Trifunac, M.D. and Todorovska, M.I. (1998a). "Nonlinear Soil Response as a Natural Passive Isolation Mechanism—The 1994 Northridge, California, Earthquake", *Soil Dynamics and Earthquake Engineering*, Vol. 17, No. 1, pp. 41–51.
60. Trifunac, M.D. and Todorovska, M.I. (1998b). "Damage Distribution during the 1994 Northridge, California, Earthquake Relative to Generalized Categories of Surficial Geology", *Soil Dynamics and Earthquake Engineering*, Vol. 17, No. 4, pp. 239–253.
61. Trifunac, M.D. and Todorovska, M.I. (1999). "Reduction of Structural Damage by Nonlinear Soil Response", *Journal of Structural Engineering*, ASCE, Vol. 125, No. 1, pp. 89–97.
62. Trifunac, M.D. and Todorovska, M.I. (2001). "Recording and Interpreting Earthquake Response of Full-Scale Structures", *Proceedings of the NATO Advanced Research Workshop on Strong Motion Instrumentation for Civil Engineering Structures*, Istanbul, Turkey, pp. 131–155.
63. Trifunac, M.D., Ivanović, S.S., Todorovska, M.I., Novikova, E.I. and Gladkov, A.A. (1999a). "Experimental Evidence for Flexibility of a Building Foundation Supported by Concrete Friction Piles", *Soil Dynamics and Earthquake Engineering*, Vol. 18, No. 3, pp. 169–187.
64. Trifunac, M.D., Ivanović, S.S. and Todorovska, M.I. (1999b). "Seven Story Reinforced Concrete Building in Van Nuys, California: Strong Motion Data Recorded between 7 February 1971 and 9 December 1994, and Description of Damage Following Northridge, 17 January 1994 Earthquake", Report CE 99-02, University of Southern California, Los Angeles, U.S.A.

65. Trifunac, M.D., Ivanović, S.S. and Todorovska, M.I. (2001a). "Apparent Periods of a Building. I: Fourier Analysis", *Journal of Structural Engineering*, ASCE, Vol. 127, No. 5, pp. 517–526.
66. Trifunac, M.D., Ivanović, S.S. and Todorovska, M.I. (2001b). "Apparent Periods of a Building. II: Time-Frequency Analysis", *Journal of Structural Engineering*, ASCE, Vol. 127, No. 5, pp. 527–537.
67. Trifunac, M.D., Hao, T.Y. and Todorovska, M.I. (2001c). "On Energy Flow in Earthquake Response", Report CE 01-03, University of Southern California, Los Angeles, U.S.A.
68. Trifunac, M.D., Ivanović, S.S. and Todorovska, M.I. (2003). "Wave Propagation in a Seven-Story Reinforced Concrete Building. III. Damage Detection via Changes in Wavenumbers", *Soil Dynamics and Earthquake Engineering*, Vol. 23, No. 1, pp. 65–75.
69. Uang, C.M. and Bertero, V.V. (1988). "Use of Energy as a Design Criterion in Earthquake-Resistant Design", Report UCB/EERC-88/18, University of California, Berkeley, U.S.A.
70. Veletsos, A.S. and Newmark, N.M. (1960). "Effect of Inelastic Behavior on the Response of Simple Systems to Earthquake Motions", *Proceedings of the Second World Conference on Earthquake Engineering*, Tokyo, Japan, Vol. II, pp. 859–912.